

Hot subdwarfs

Small stars marking important events in stellar evolution

Habilitationsschrift
der Naturwissenschaftlichen Fakultät
der Friedrich-Alexander-Universität Erlangen-Nürnberg

vorgelegt von

Stephan Geier
aus Stadtsteinach

Fachmentorat:

Prof. Dr. U. Katz (Vorsitzender)

Prof. Dr. U. Heber

Prof. Dr. K. Werner (Universität Tübingen)

Contents

- Abstract** **1**

- 1 Introduction** **3**

- 2 Analysis Methods** **6**
 - 2.1 Finding and classifying hot subdwarfs 6
 - 2.2 Quantitative spectral analysis 7
 - 2.3 Close binary analysis 9

- 2 Hot Subdwarf Atmospheres** **16**

- 3 Close hot subdwarf binaries** **20**

- 4 Substellar companions** **23**

- 5 Supernova type Ia progenitors and ejected donor remnants** **27**

- Bibliography** **30**

- Acknowledgements** **34**

- Appended papers** **35**

Abstract

This habilitation thesis consists of a number of publications aiming at understanding the formation and evolution of hot subdwarfs (sdO/Bs). I adopted different approaches to substantially increase and analyse the samples of both single stars and close binaries. Quantitative spectroscopic analyses of sdB atmospheres allowed me to uncover and study the diverse effects of diffusion on the abundance patterns of those stars. Measuring the rotation of single sdBs I put constraints on possible formation channels. In a large and ongoing international observation project led by myself we search for the close binary sdBs with the most and the least massive companions. Significantly enhancing the known sample of close binary sdBs we performed the first comprehensive study of this population. Triggered by the discovery of two sdB binaries with close brown dwarf companions in the course of this project, we were able to show that the interaction of stars with substellar companions is an important channel to form sdB stars. Finally, we discovered a unique and very compact binary system consisting of an sdB and a massive white dwarf, which qualifies as progenitor candidate for a supernova type Ia. In addition to that, we could connect those explosions to the class of hypervelocity hot subdwarf stars, which we consider as the surviving companions of such events. Being the stripped cores of red giants, hot subdwarfs turned out to be important markers of peculiar events in stellar evolution ranging all the way from star-planet interactions to the progenitors of stellar explosion used to measure the expansion of our Universe.

1 Introduction

Looking into standard astronomy textbooks, stellar evolution appears to be quite well understood and based on established theories. That our Sun will expand to become a red giant and will eventually end her life cooling down as white dwarf tends to become common knowledge. However, this is in part a misconception, because certain phases of stellar evolution are not only less elaborated in detail, but are in fact hardly understood at all. The problem becomes even more severe, as soon as stars evolve in binary systems, which is by no means an exception but rather the rule.

Mass transfer, either stable or unstable, can alter stellar evolution and form objects, which cannot be understood in a different way. Especially in the late stages of stellar evolution, where compact objects like white dwarfs and their direct precursors in very close binaries are involved, the underlying physical mechanisms can only be crudely parametrised. Among those mysterious objects, the hot subdwarf stars (sdO/Bs) stick out, because they constitute a prominent population of faint blue stars at high Galactic latitudes. With masses around $0.5 M_{\odot}$ and radii between $0.1 R_{\odot}$ and $0.3 R_{\odot}$ they are much smaller and of lower mass than hot main sequence stars of similar spectral types. Hot subdwarfs have been studied extensively for several reasons: They are common enough to account for the UV excess observed in early-type galaxies (O’Connell, 1999). Pulsating sdB stars became an important tool for asteroseismology (Charpinet et al., 2010). SdB stars in close binaries qualify as type Ia supernova progenitors (Maxted et al., 2000). And substellar companions like brown dwarfs and planets have been discovered as well (Silvotti et al., 2007). The state-of-the-art in hot subdwarf research has been reviewed by Heber (2009).

Main sequence stars burn hydrogen in their cores until this nuclear fuel reservoir is exhausted. In the next stage of evolution the stars expand and become red giants. This expansion stops as soon as helium burning starts in the red-giant cores. Depending on the amount of hydrogen envelope left after the red-giant phase, the stars in this phase occupy a region of roughly constant luminosity, but quite diverse temperatures in the Hertzsprung-Russell diagram, which is called the horizontal branch (HB, see Fig. 1.1). Subluminous B stars (sdBs) have been identified as extreme horizontal branch (EHB) stars (Heber, 1986); i.e. they are core helium-burning stars with very thin hydrogen envelopes and therefore high temperatures. Unlike normal HB stars, which reascend the giant branch, EHB stars evolve directly to the white-dwarf cooling sequence. While the sdB stars spectroscopically form a homogeneous class, a large variety of spectra is observed among their hotter siblings, the subluminous O stars (for a detailed classification scheme of hot subdwarfs see Drilling et al., 2013).

The formation of hot subdwarf stars in general is still unclear (Geier et al., 2012). SdB stars can only be formed, if the progenitor loses its envelope almost entirely after passing the red-giant branch. While single-star scenarios are discussed, the focus shifted to binary evolution, when systematic surveys for radial velocity (RV) variable stars revealed that a large fraction of the sdB stars (40 – 70 %) are members of close binaries with orbital periods ranging from $\simeq 0.05$ d to $\simeq 30$ d (e.g. Maxted et

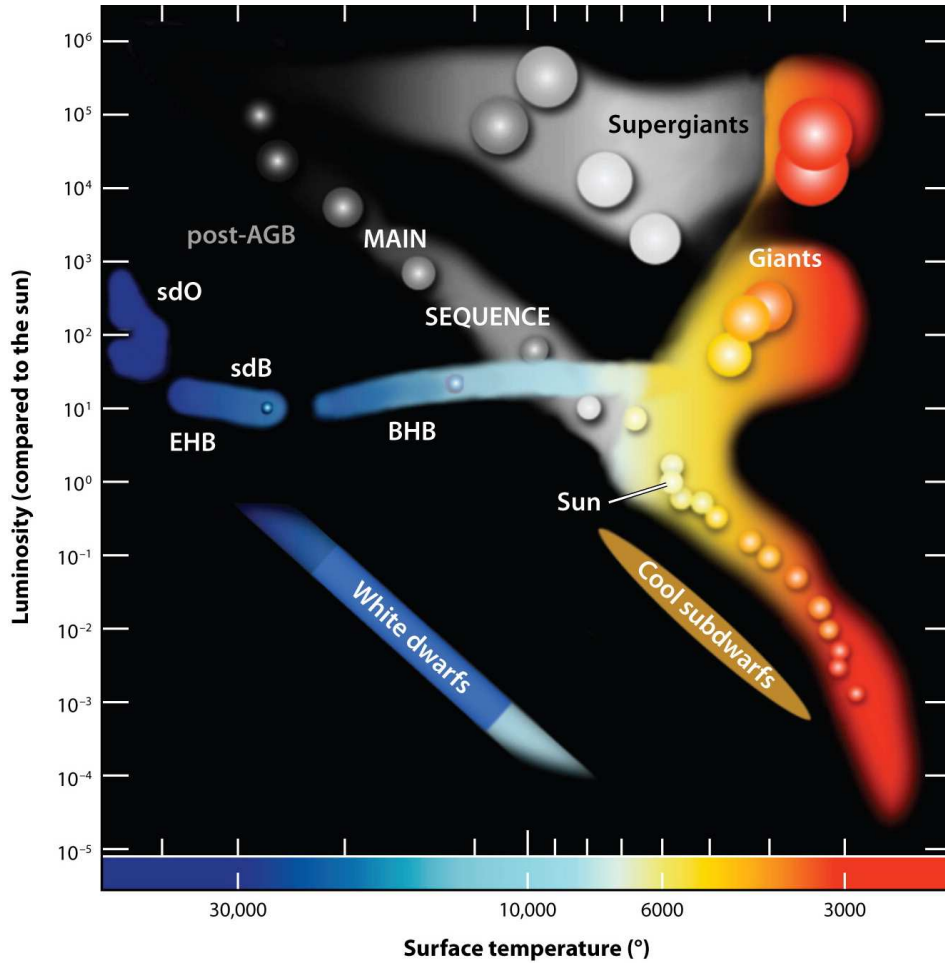


Figure 1.1: Hertzsprung-Russell diagram. The location of the extreme horizontal branch, where the sdO/Bs are located, is indicated (Heber, 2009).

al., 2001). While such close binaries are formed most likely after a common envelope phase, where the companion becomes completely immersed in the red-giant envelopment, stable mass transfer to a main sequence companion and the merger of two helium white dwarfs have been proposed as possible formation channels as well (see Fig. 1.2, Han et al., 2002, 2003, and references therein).

Most companions have been identified in the shortest period systems. Amongst them white dwarfs prevail, but main sequence stars of low mass are also quite common. However, the mass spectrum of sdB companions widened significantly in the last couple of years. A planetary companion to a pulsating sdB star has been discovered from sinusoidal variations of its pulsation frequencies (Silvotti et al., 2007). More such substellar companions in wide orbits with periods of a few hundred days have been discovered in a similar way orbiting eclipsing sdB binaries (e.g. Beuermann et al., 2012). The discovery of potential close earth-size planets (Charpinet et al., 2011) on the other hand showed that such objects might play a role for the formation of sdBs as well. At the other end of the mass scale, massive and

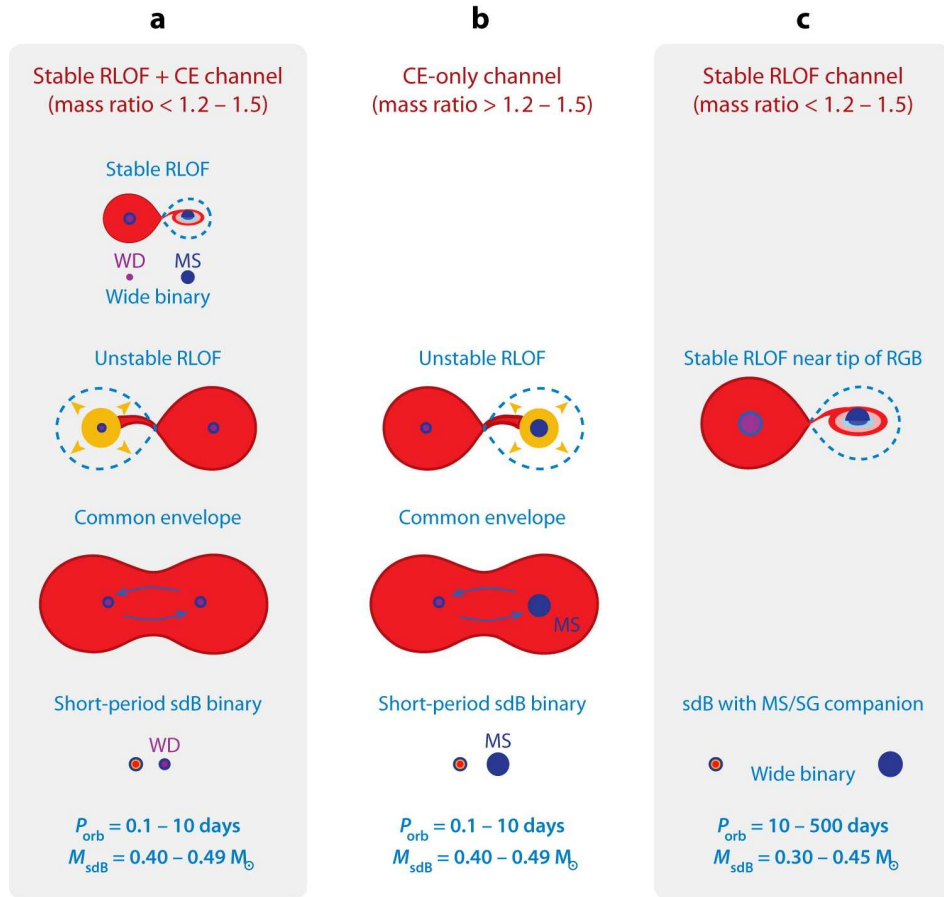


Figure 1.2: Binary formation channels for single and binary hot subdwarf stars (Podsiadlowski et al., 2008; Heber, 2009).

compact companions like massive white dwarfs, candidate neutron stars or even black holes have been found as well (Geier et al., 2010; Mereghetti et al., 2011). And recently, the theoretically predicted sdBs with main-sequence companions in wide binary systems have finally been discovered (Vos et al., 2013; Barlow et al., 2013b).

The formation of the subclass of helium-rich sdOs (He-sdOs) is even more enigmatic than the one of hydrogen-rich sdB stars. Most He-sdOs are concentrated in a very small region in the HRD, slightly blueward of the EHB (Ströer et al., 2007) and the population of He-sdOs observed so far seems to consist mostly of single stars (Napiwotzki, 2008). A way of forming such objects and explaining their helium-rich composition might be the merger of two helium white dwarfs (Webbink, 1984) or the delayed helium flash of a WD (Lanz et al., 2004).

2 Analysis Methods

2.1 Finding and classifying hot subdwarfs

The colours and magnitudes of celestial objects can be used to classify them. To first order the colour of a star depends on the effective temperature on its surface. While cool stars are red, hot stars emit most of their radiation in blue and ultraviolet (UV) light. Photometric surveys in different bands ranging from the UV to the infrared (IR) are regularly conducted to map the entire sky. Those surveys are the starting point when searching for certain classes of stars.

Hot subdwarfs are most easily selected by applying colour cuts to photometric surveys at high Galactic latitude, because they stick out as UV-excess objects in the old and predominantly red thick disc or Galactic halo environment and dominate the population of faint blue stars down to a limiting visual magnitude of about 18 mag. UV-excess surveys like the Palomar Green survey (Green et al., 1986) applied a limit of $U - B < -0.57$ in the Johnson photometric system. The corresponding effective temperature of a star according to models by Castelli & Kurucz (2003) is $\simeq 15000$ K, well below the observed range for sdB stars (> 20000 K). In addition, a limit of $B - V < +0.3$ is applied to include sdBs in spectroscopic binaries, if the main sequence companion is of spectral type F or later. We studied a sample of bright hot subdwarf stars from the literature. Most of those stars have been selected in a similar way. To select the much larger and fainter sample from the Sloan Digital Sky Survey (SDSS), we transformed those colour cuts to the SDSS photometric system ($u - g < 0.4$ and $g - r < 0.1$, Jester et al., 2005, see Fig. 2.1). Those criteria also exclude the large number of extragalactic objects, which were the priority targets of SDSS in the first place.

Since colour selection just provides constraints on the stellar temperature, spectroscopic follow-up observations are necessary to distinguish hot subdwarfs from other types of faint blue stars (mostly hot white dwarfs). To cover and resolve the distinctive spectral features of hot subdwarf stars, it is necessary to obtain medium to high resolution spectra ($\Delta\lambda < 5.0 \text{ \AA}$) with a wavelength coverage ideally ranging from the near-UV to the near infrared ($\sim 3700 - 7000 \text{ \AA}$). Depending on quality and resolution of the spectra as well as on the faintness of the targets (typically $V = 10 - 18$ mag for the objects studied here) 2m- to 8m-class telescopes have to be used. Since most radiation is emitted in the UV, the coverage of this wavelength range would be highly desirable, but due to atmospheric absorption it is only accessible with space-based telescopes. After the decommissioning of smaller UV-satellites like IUE and FUSE, today only the Hubble Space Telescope provides the necessary instrumentation.

Existence, width, and depth of helium and hydrogen absorption lines as well as the flux distribution are used as criteria to identify and classify hot subdwarfs. Subdwarf B stars show broadened hydrogen Balmer and He I lines, sdOB stars He II lines in addition, while the spectra of sdO stars are dominated by weak Balmer and strong He II lines depending on the He abundance. A flux excess in the red compared to a reference spectrum as well as the presence of certain spectral features are revealing a late

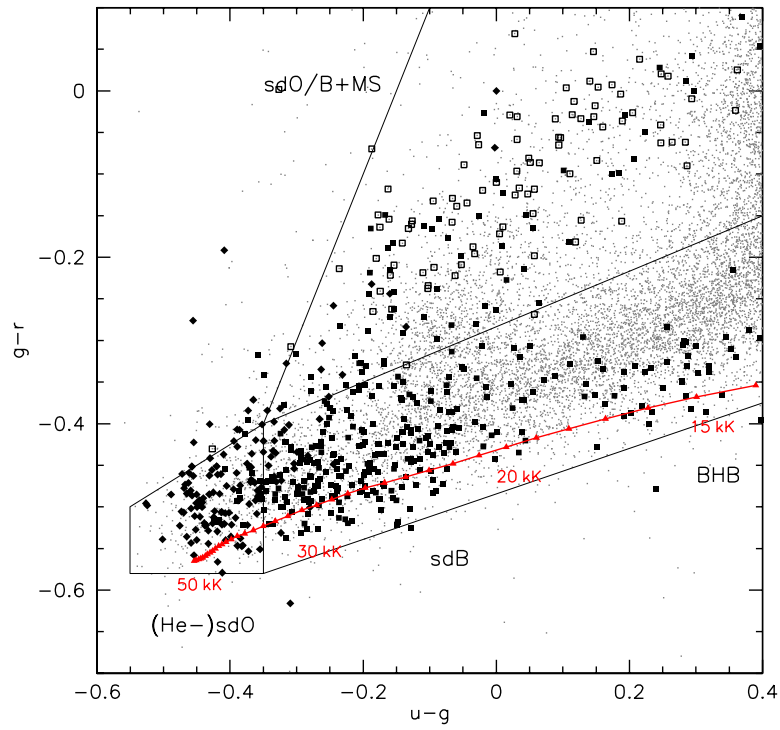


Figure 2.1: SDSS $g - r$ -colours plotted against $u - g$ of subdwarfs with $g < 18$ mag. The grey dots mark all stellar objects with spectra available in the SDSS database. Most of them are classified as white dwarfs. The solid diamonds mark (He-)sdO stars, the solid squares sdB and sdOB stars. Open squares mark hot subdwarfs with main sequence companions visible in the spectra. The sequence of composite objects is clearly separated from the single-lined stars. Synthetic colours from Castelli & Kurucz (2003) for stars with temperatures ranging from 14 000 K to 50 000 K ($\log g = 5.0$) are marked with upward triangles and connected. The stepsize of the colour grid is 1000 K. The labels mark models of certain temperatures (Geier et al., 2011b).

type companion star (for a few examples see Fig. 2.2, for a more detailed spectral classification of hot subdwarf stars see Drilling et al., 2013).

2.2 Quantitative spectral analysis

The analysis of stellar spectra allows us to determine the properties of stellar atmospheres. To first order, the continuum flux depends on the effective temperature of the atmosphere and follows the Maxwell-Boltzmann distribution. However, each stellar atmosphere has a certain structure and chemical composition with elements in different ionization stages. Those ions absorb radiation at wavelengths where transitions in their electron shells can be excited. In this way, the continuum spectrum is superimposed by absorption lines. These patterns of absorption lines depend on the chemical composition, but also

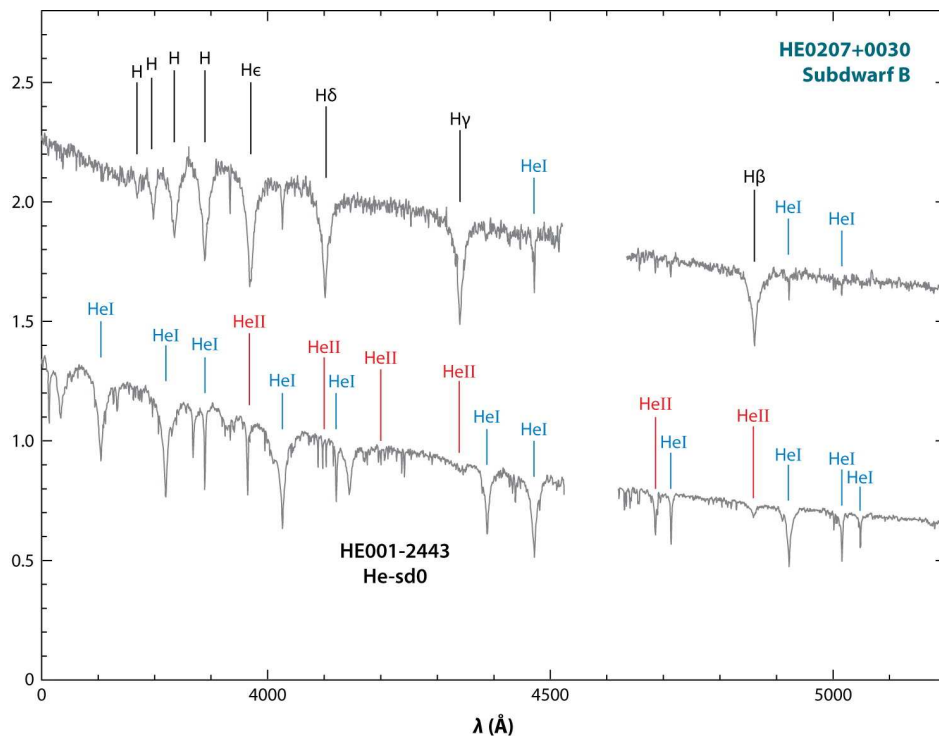


Figure 2.2: High-resolution spectra of a typical hydrogen-rich sdB and a helium-rich sdO star. The most important hydrogen and helium lines are marked. The unmarked small and sharp absorption lines are originating from metals (Heber, 2009).

on the temperature and surface gravity. The shape of the spectral lines is affected by the conditions in the different layers of the stellar atmosphere. The lines are broadened by quantum mechanical effects, temperature and pressure.

Since stars are point sources, we only see the integrated spectrum of the actual stellar disc. The Doppler effect leads to a shift in the wavelength of the spectral lines depending on the radial velocity of the star with respect to the observer. Furthermore, rotation introduces a blueshift of the stellar hemisphere approaching us and a redshift of the hemisphere receding. Integrated over the stellar disc those effects lead to a characteristic broadening of the spectral lines. Asymmetric effects like star spots or pulsations can cause more complicated deformations of the lines in the integrated spectrum.

To determine the most important atmospheric parameters in hot subdwarf atmospheres, which are the effective temperature T_{eff} , the surface gravity $\log g$ and the helium abundance $\log n(\text{He})/n(\text{H})$ ($\log y$) we fit synthetic models to the hydrogen and helium lines of the observed spectra. Depending on effective temperature and composition of the atmospheres, different models are used. For hydrogen-rich sdBs with temperatures up to 30 000 K, simple models calculated in local thermodynamic equilibrium (LTE) are sufficient. For higher temperatures, deviations from LTE have to be taken into account using models in non-local thermodynamic equilibrium (NLTE). Depending on the chemical compositions of the atmospheres, the opacities of metals have to be included as well. Since we were analysing different classes of hot subdwarfs, we used a variety of appropriate model grids (e.g. Geier et al., 2011b).

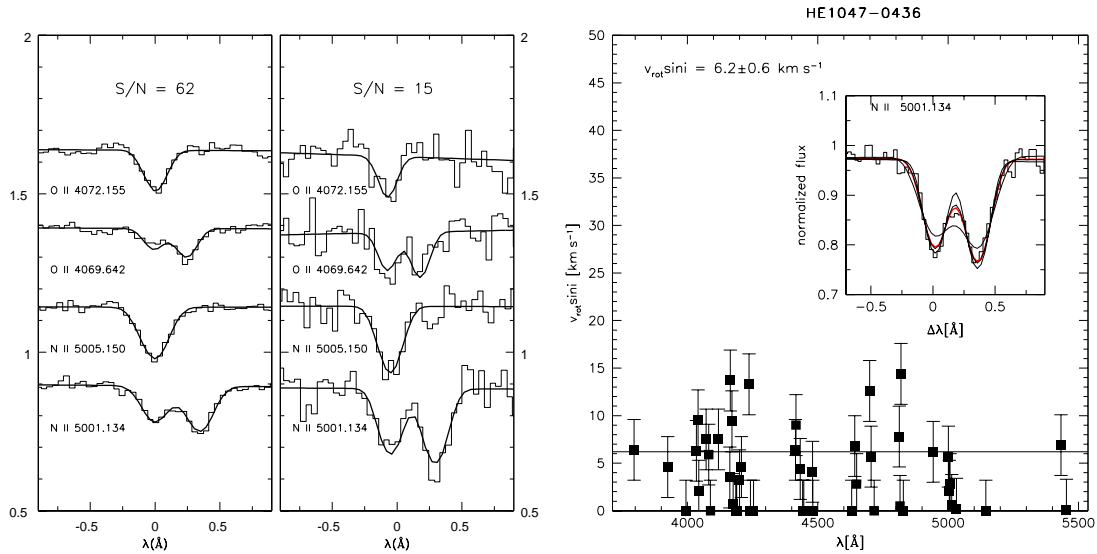


Figure 2.3: *Left panel:* Example fits of common oxygen and nitrogen lines for two sdB spectra with different quality (Geier, 2013). *Right panel:* Rotational broadening fit result for an sdB star. The measured $v_{\text{rot}} \sin i$ is plotted against the wavelength of the analysed lines. The solid line corresponds to the average. The inset shows an example fit of a line doublet. The thick solid line is the best fit $v_{\text{rot}} \sin i$. The three thin lines correspond to fixed rotational broadenings of 0, 5, 10 km s^{-1} (Geier et al., 2010).

When determining the metal abundances for all the different elements in the stellar atmospheres of our sdB sample, the number of adjustable parameters becomes so high, that simultaneous fitting in a model grid is not feasible any more. To simplify this approach, we computed metal line-blanketed LTE model atmospheres (Heber et al., 2000) for the atmospheric parameters already determined from the hydrogen and helium lines using the LINFOR program (developed by Holweger, Steffen and Steenbock at Kiel university, modified by Lemke, Lemke, 1997). For a given effective temperature and surface gravity, the abundance of an ion scales with the equivalent width of the spectral lines.

A standard set of 182 metal lines from 24 different ions was chosen and a simultaneous fit of elemental abundance, projected rotational velocity ($v_{\text{rot}} \sin i$) and radial velocity (RV) was performed for each identified line (see Fig. 2.3) using the FITSB2 routine (Napiwotzki et al., 2004). Mean value and standard deviation were calculated from all abundance measurements of each ion and the mean $v_{\text{rot}} \sin i$ with associated uncertainty has been calculated from all suitable metal lines (Geier et al., 2010; Geier & Heber, 2012; Geier, 2013).

2.3 Close binary analysis

Most stars in our Galaxy are members of binary or multiple systems. In a binary star, the two components are revolving around their common centre of gravity on Keplerian orbits. The orbital periods of known binaries range from a few minutes to thousands of years. A significant fraction of the hot subdwarf stars is found in close binary systems with periods ranging from a few hours to a few days. In such systems the two stars are only separated by a few solar radii and do not behave as point sources

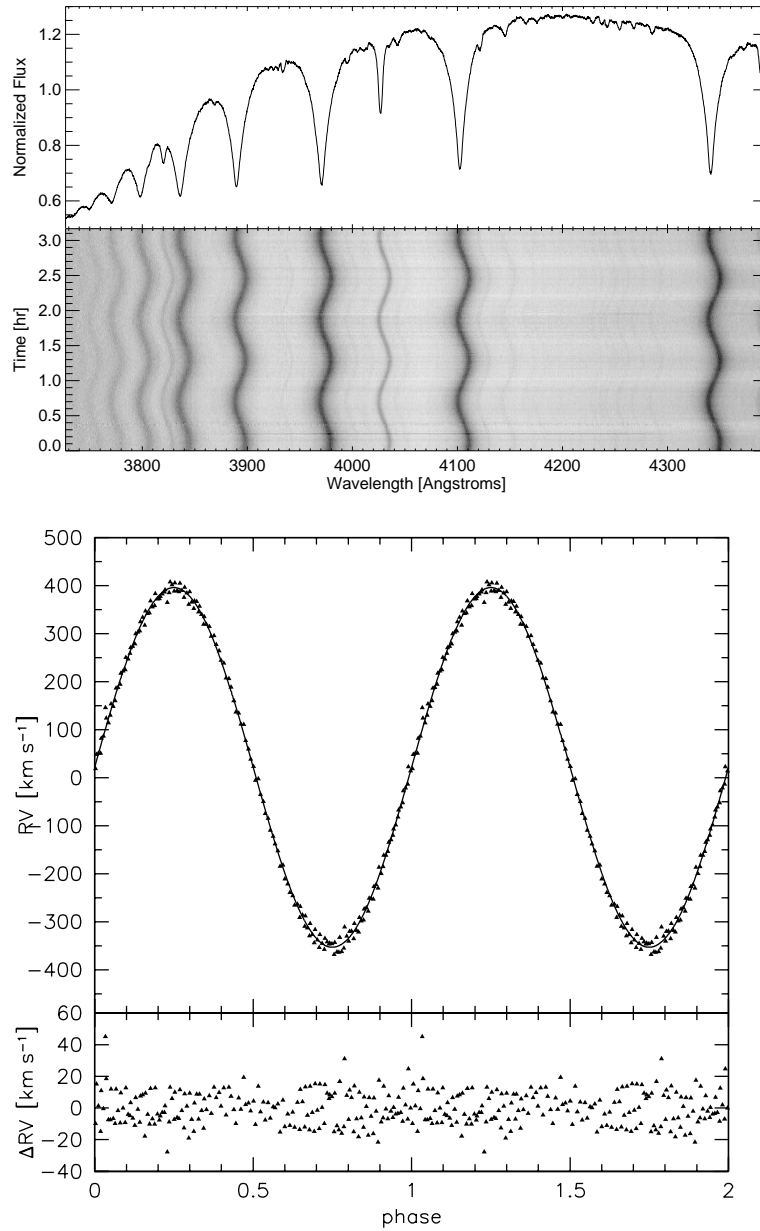


Figure 2.4: *Upper panel:* Spectrum of the sdB binary CD-30°11223 coadded from 175 single spectra taken with SOAR/Goodman. The hydrogen Balmer series is clearly visible as well as a prominent helium line at 4026 Å. *Middle panel:* Single spectra of the same binary plotted against time. The short-period sinusoidal variations of the Doppler-shifted spectral lines is caused by the motion of the visible sdB star Geier et al. (2013c). *Lower panel:* Radial velocity curve plotted against orbital phase for the most likely period derived from those data.

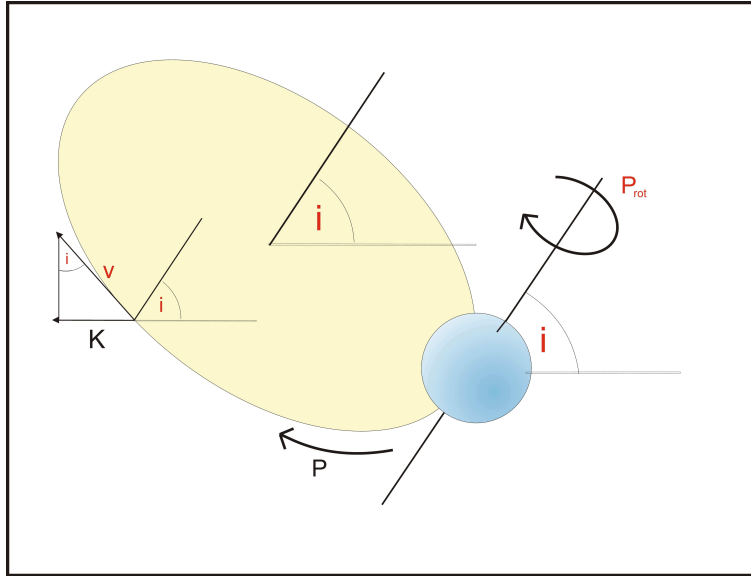


Figure 2.5: Schematic view of a single-lined close binary system. Measured quantities are written in black, free parameters in red.

any more. Tidal interactions between the stars lead to an exchange of energy and angular momentum. The most important consequences of those effects are the circularisation of the orbits and the synchronisation of the stars' rotation periods with the orbital period.

Close binary stars cannot be resolved with telescopes. To study them, we have to measure time-dependent features in their spectra and light curves. Due to the Doppler effect, the spectral lines become blue- or redshifted depending on whether the star approaches us or recedes from us. For a close binary star on a circular orbit, this variation is time dependent and follows a characteristic sine curve (see Fig. 2.4). To derive the radial velocity curves of our sdB binaries (e.g. Fig. 2.4 lower panel), we measured the radial velocities by fitting a set of mathematical functions (Gaussians, Lorentzians and polynomials) to the individual hydrogen Balmer as well as helium lines using the FITSB2 routine (Napiwotzki et al., 2004). Three functions are used to match the continuum, the line and the line core, respectively and mimic the typical profile of spectral lines. The profiles are fitted to all suitable lines simultaneously using χ^2 -minimization and the RV shift with respect to the rest wavelengths is measured. To achieve the necessary accuracy of the single RV measurements, medium-resolution spectra ($\Delta\lambda < 3 \text{ \AA}$) are necessary. Due to the short periods of the variations, the single exposure times have to be limited from a few minutes up to an hour at most. Otherwise the spectral lines would move considerably during the exposure and cause what is called orbital smearing. For most stars in our samples at least 4m-class telescopes are required to fulfill both criteria.

Assuming circular orbits sine curves with time at phase zero T_0 , orbital period P , RV-semi-amplitude K and system velocity of the binary system γ as free parameters were then fitted to the RV data points in fine steps over a range of test periods. For each period the χ^2 of the best fitting sine curve was determined. In order to estimate the significance of the orbital solutions and the contributions of systematic effects to the error budget, we normalised the χ^2 of the most probable solution by adding systematic er-

rors in quadrature until the reduced χ^2 reached $\simeq 1.0$. Using these modified uncertainties we performed Monte Carlo simulations for the most likely periods. For each simulation a randomised set of RVs was drawn from Gaussian distributions with central value and width corresponding to the RV measurements and the analysis repeated. From these simulations the probabilities for the orbital periods to deviate from our best solution by more than 1% or 10% were calculated.

In order to derive most conservative errors for K and γ we fixed the most likely period and created new RV datasets with a bootstrapping algorithm. Ten thousand RV datasets were obtained by random sampling with replacement from the original dataset. In each case an orbital solution was calculated in the way described above. The standard deviation of these results was adopted as error estimate. The accuracy of this methods is limited by the resolution of the spectra and their signal-to-noise. Combining data obtained with different instruments is also expected to contribute to the systematic error (for details of our methods see Geier et al., 2011c).

Close hot subdwarf binaries are single-lined systems, meaning that only the sdB star is visible in the spectrum, because the companion is much less luminous. Furthermore, we can only measure the radial component of the sdBs orbital velocity and in general do not know the orientation of the binary in space with respect to us. In the case of circular orbits this orientation can be parameterized by just one additional parameter, the inclination angle i (see Fig. 2.5). Although the problem seems to be under-determined, it is still possible to gain some important information from the available data. The binary mass function f_m , which relates the measured quantities K and P to the other binary parameters, can be derived from Keplers laws:

$$f_m = \frac{M_{\text{comp}}^3 \sin^3 i}{(M_{\text{comp}} + M_{\text{sdB}})^2} = \frac{PK^3}{2\pi G}$$

In this equation the sdB mass M_{sdB} , the companion mass M_{comp} and the inclination angle i remain free parameters. Based on models for single-star evolution the sdB mass is expected to be close to the mass of the degenerate red-giant core in the moment when the helium flash is triggered. This so-called canonical mass of $\sim 0.47 M_{\odot}$ is in reasonable agreement with masses derived from observations (e.g. Fontaine et al., 2012) and is adopted to constrain the binary parameters. Furthermore, by definition the inclination angle cannot become higher than 90° , which means that we see the binary face-on. Adopting $M_{\text{sdB}} = 0.47 M_{\odot}$ and $i < 90^\circ$ we can therefore derive a lower limit for the companion mass.

This lower limit can be used to put constraints on the nature of the companion. If only the sdB is contributing to the measured spectral energy distribution from the optical to the infrared, an upper limit for the luminosity of the companion is given (for details see Kupfer et al., 2015). For minimum companion masses lower than $\sim 0.4 M_{\odot}$ the companion may be a late-type main sequence star or a compact object like a WD. Main sequence stars in this mass range are outshined by the sdBs. If on the other hand the minimum companion mass exceeds $\sim 0.4 M_{\odot}$, the contribution of a main sequence companion becomes detectable in the IR and the optical. The non-detection of this contribution therefore allows us to exclude a main sequence star. The companion must then be a compact object. More massive compact companions like massive WDs, neutron stars or black holes are more likely as soon as the minimum mass exceeds $1.0 M_{\odot}$ or even the Chandrasekhar limit $1.4 M_{\odot}$. Studying sufficiently large samples of sdB binaries, a random distribution of inclination angles (taking into account selection effects) can be assumed and the companion mass distribution constrained (Kupfer et al., 2015).

To measure the binary properties more accurately, it is necessary to put stricter constraints on the inclination angle. This can be done in an indirect way by measuring the projected rotational velocity of the sdB primary (see Sect. 2.1) and assuming its rotation period to be synchronised to its orbital period.

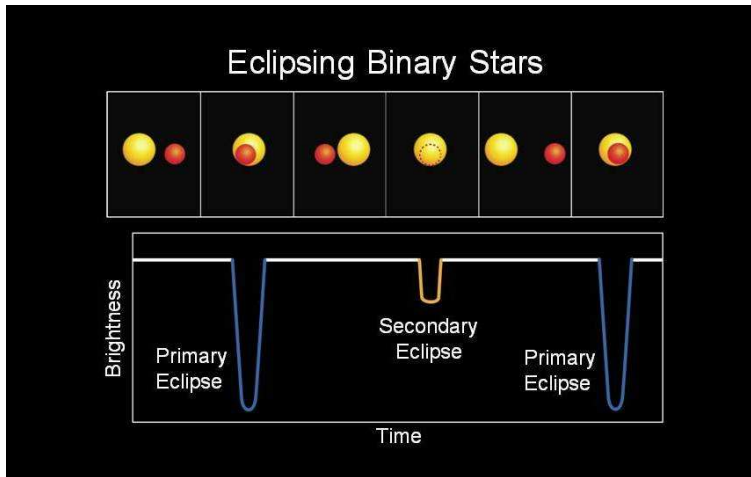


Figure 2.6: Schematic view of an eclipsing binary system and its characteristic light curve (taken from NASA).

We applied this method to a sample of sdB binaries (for details see Geier et al., 2007, 2010). However, we found that orbital synchronisation seems to be only valid for close sdB binaries with relatively massive companions, while sdBs with low-mass companions seem to rotate significantly slower than predicted (Schaffenroth et al., 2014a,b).

Eclipsing binaries provide the most direct way to constrain the inclination angle, because to show eclipses in the light curve, the orientation of the binary must be more or less face-on (see Fig. 2.6). Furthermore, fitting the observed light curve to models, the relative radii of the two components can be measured from the eclipse depth and all other parameters derived. In close sdB binaries other effects are usually superimposed on the light curve. If the companion is a cool object of similar radius as the sdB itself (e.g. a low-mass M star), the hemisphere facing the hot sdB is irradiated and heated. Since the projected area of this irradiated hemisphere changes, while the companion orbits the sdB, it causes a sinusoidal variation of the light curve, which is known as reflection effect (e.g. see Fig. 4.1 right panel). If the companion is a compact object like a WD and the orbital period is sufficiently short, the sdB can become distorted by the tidal influence of the companion. This leads to a small sinusoidal variation of a few percent with exactly half the orbital period. Finally, relativistic effects like Doppler boosting or microlensing can slightly modify the light curves as well (e.g. see Fig. 5.1 Bloemen et al., 2011; Geier et al., 2013c). Light curves of sufficient quality and short single exposure times can be taken with 1m to 2m-class telescopes ideally using different filters, because especially the amplitude of the reflection effect is highly dependent on the wavelength. To study the more subtle relativistic effects, space-based lightcurves as provided by the Kepler and CoRoT missions are needed (e.g. Bloemen et al., 2011).

The light curves of sdBs with cool companions were analysed using the MORO code, which is based on the Wilson-Devinney approach (Wilson & Devinney, 1971) but takes into account radiative interaction between the components of hot, close binaries (Drechsel et al., 1995). Models of the binary components are calculated taking into account deformations caused by the tidal influence on each other as well as the irradiation of the cool companion by the sdB. The models are calculated for different orbital phases as well as the emitted radiation (see Fig. 2.7). In this way, model lightcurves are

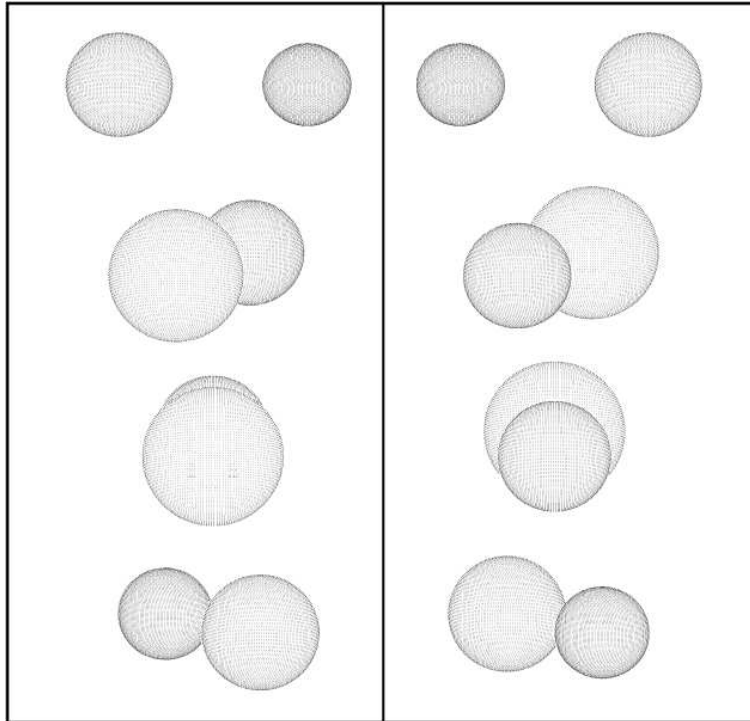


Figure 2.7: Models of the eclipsing sdB+dM binary HS 0705+6700 for different orbital phases (Drechsel et al., 2001).

constructed.

After fixing parameters like limb darkening and gravity darkening exponents, which depend on the stellar type, to literature values, the remaining adjustable parameters are the inclination, the temperature of the second component, the Roche potentials, the bolometric albedo of the secondary, the radiation pressure parameter and the luminosity of the hot component. The fractional Roche radii in units of the orbital separation are calculated using the Roche potentials and the mass ratio. We used the binary mass function derived from spectroscopy to calculate possible mass ratios for a range of primary masses. Grids of light curve solutions with different mass ratios were calculated. To derive errors we created 500 new datasets with a bootstrapping algorithm by random sampling with replacement from the original dataset. In each case a light curve solution was calculated in the way described above. The standard deviations of these results were adopted as the error estimates for the parameters (Geier et al., 2011e). Similar light curve codes like LCURVE developed by T. Marsh also take into account relativistic effects and have been used to model them appropriately (e.g. Geier et al., 2013c). It has to be pointed out that the light curve solutions are usually degenerate with respect to the adopted radius ratio of the binary components. To find consistent solutions, assumptions about the mass and radius of the primary or the secondary based on theoretical models have to be made.

Several sdB binaries show reflection effects and ellipsoidal deformation without being eclipsing. Especially the amplitude of the ellipsoidal variation can be used as diagnostic tool, because it depends on the mass of the unseen companion (e.g. Geier et al., 2007). The reflection effect on the other hand

is ill-suited to constrain the binary inclination. Modelling the irradiation of the cool companion as pure reflection is an oversimplification of the problem. Furthermore, the amplitude of the variation depends on several degenerate parameters. However, the presence or absence of a reflection effect can still be used to constrain the nature of the companion (Schaffenroth et al., 2014a).

2 Hot subdwarf atmospheres

Spectra allow us to determine the properties of stellar atmospheres. Besides the effective temperature and the surface gravity, the abundance patterns can be measured. Those patterns are usually compared to stellar evolution models and used to determine the ages of stellar populations or the evolutionary stages of the stars. However, certain classes of hot stars like blue horizontal branch (BHB) stars, B/Am stars, HgMn stars, hot white dwarfs and others show peculiarities in their abundances, which are caused by physical processes in the atmospheres themselves rather than different population ages or evolutionary histories. The outer envelopes of hot stars are radiative, which implies that they are not constantly mixed by convection. In the stellar atmospheres two main mechanisms are invoked, which can affect the chemical composition in a process called diffusion. Due to their higher masses, ions of heavier elements sink into deeper regions of the radiative envelope, while the lighter elements float on top. This gravitational settling leads to a depletion of heavy elements with respect to their lighter counterparts. Radiative levitation on the other hand can lead to an enrichment especially of heavy metals. The reason is the much higher number of transitions and absorption lines of those elements. Similar to sailing boats with large sails the radiation pressure preferentially pushes those ions outwards despite their relatively high masses. Both mechanisms are at work at the same time and are far from understood in a quantitative way. Hot subdwarfs belong to the class of chemically peculiar stars and the abundance anomalies found in those stars are important to understand the physical properties of hot stellar atmospheres in general.

Sargent & Searle (1966) discovered the helium deficiency of sdB stars for the first time and Greenstein & Sargent (1974) suggested that diffusion in the hot atmosphere of sdBs may cause this deficiency. Peculiar metal abundances were first reported by Baschek et al. (1972). While some metals show solar abundances, others are depleted or even enriched. Radiative levitation of heavy elements and mass loss caused by stellar winds (Vink & Cassisi, 2002) have been invoked to counteract the gravitational settling as well as extra mixing at the surface (Michaud et al., 2011; Hu et al., 2011). Although more recent abundance studies of individual sdB stars have been performed using optical and UV spectra, the consistent analysis of a large sample of such stars spanning the full range of atmospheric parameters and allowing to search for patterns and correlations was missing.

To study the atmospheric peculiarities of such a large sample of sdB stars in detail, I analysed high-resolution spectra of 106 stars by fitting appropriate model spectra to the observed line profiles (Geier, 2013, appended). A general trend of enrichment was found with increasing temperature for most of the heavier elements. The lighter elements like carbon, oxygen and nitrogen are depleted and less affected by temperature (see Fig. 2.1). Those patterns are similar for both pulsating and non-pulsating sdBs. State-of-the-art diffusion models predict such patterns and are in qualitative agreement with our results (Michaud et al., 2011). However, the highest enrichments measured cannot be explained with these models. Peculiar line shapes of the strongest metal lines in some stars indicate vertical stratification to be present in the atmospheres. Such effects are not accounted for in current diffusion models and may

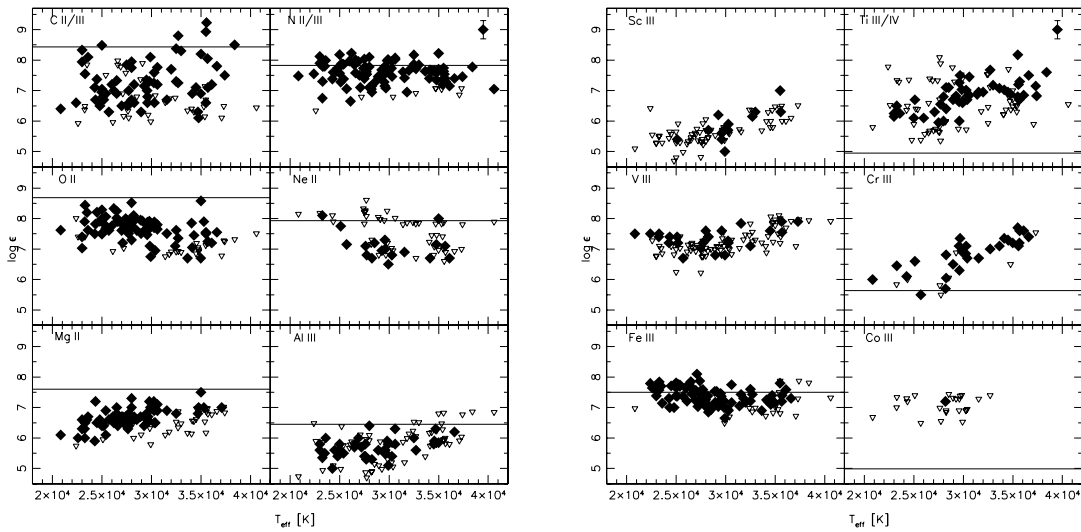


Figure 2.1: Elemental abundances plotted against effective temperature. The filled diamonds mark measured abundances while the open triangles mark upper limits. Typical error bars are given in the upper right corner. The solid horizontal lines mark solar abundances. In some cases (scandium, vanadium) the solar abundances are lower than covered by the plotted area (Geier, 2013).

be responsible for some of the yet unexplained abundance anomalies.

Furthermore, I measured the atmospheric parameters and helium abundances of 44 sdBs and confirmed a correlation of helium abundance with temperature and the existence of two distinct sequences in helium abundance found previously (see Fig. 2.2 right panel). I focused on isotopic shifts of helium lines and found ^3He to be strongly enriched in 8 of the programme stars. Most of these stars cluster in a small temperature range between 27 000 K and 31 000 K (see Fig. 2.2 left panel) very similar to the known ^3He -rich main sequence B stars, which cluster at somewhat lower temperatures. This phenomenon is most probably also related to diffusion processes in the atmosphere, but still poses a challenge to diffusion models (Geier et al., 2013b, appended).

Another important hint for the formation history of sdB stars is their rotation. Therefore I studied 105 sdB stars, which are either single stars or in wide binaries where tidal interactions become negligible. The projected rotational velocities have been determined by measuring the broadening of metal lines using high resolution optical spectra. All stars in our sample are slow rotators ($v_{\text{rot}} \sin i < 10 \text{ km s}^{-1}$). We show that blue horizontal and extreme horizontal branch stars are related in terms of surface rotation and angular momentum (see Fig. 2.3) suggesting a similar formation scenario. Hot blue horizontal branch stars ($T_{\text{eff}} > 11\,500 \text{ K}$) with diffusion-dominated atmospheres are slow rotators like the hot subdwarf stars located on the extreme horizontal branch, which lost more envelope and therefore angular momentum in the red-giant phase. The uniform rotation of single and wide binary sdBs we found poses a challenge to our understanding of hot subdwarf formation. Especially the high fraction of helium white dwarf mergers predicted by theory, which are expected to spin faster, seems to be inconsistent with the results (Geier & Heber, 2012, appended).

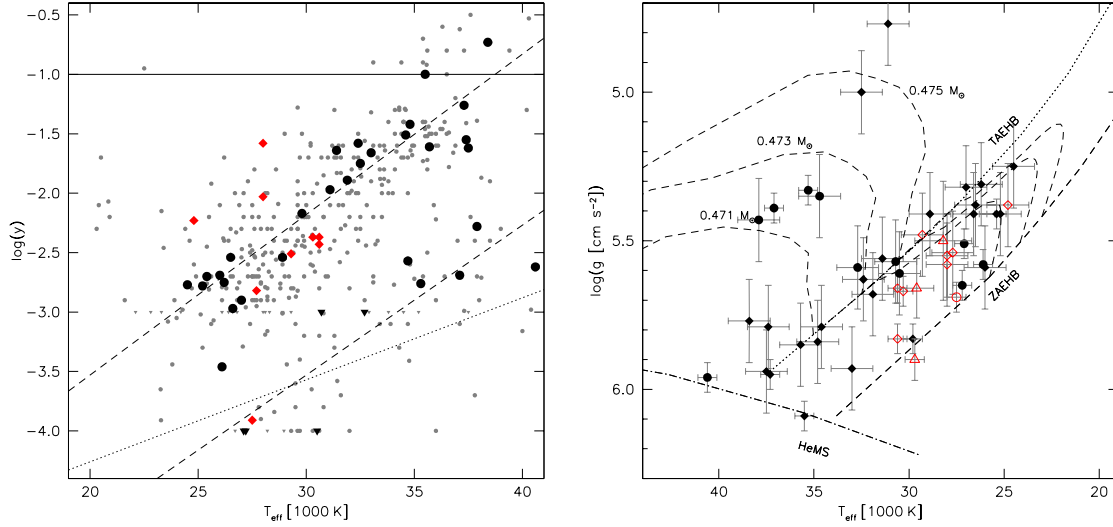


Figure 2.2: *Left panel:* Helium abundance $\log y$ plotted against effective temperature. The filled symbols mark the results from my study. Filled diamonds mark objects where isotopic shifts due to an enrichment of ^3He were detected, filled circles objects with atmospheres dominated by ^4He . Upper limits are marked with triangles. The solid horizontal line is drawn at solar helium abundance. The two dashed lines are regression lines for the two distinct helium sequences taken from Edelmann et al. (2003). The dotted regression line for the lower sequence is taken from Németh et al. (2012). Measurements taken from literature are plotted as grey symbols. *Right panel:* $T_{\text{eff}} - \log g$ -diagram of a sample of bright sdB stars. The helium main sequence (HeMS) and the EHB band (limited by the zero-age EHB, ZAEHB, and the terminal-age EHB, TAEHB) are superimposed with EHB evolutionary tracks for solar metallicity taken from Dorman et al. (1993) labelled with their masses. Open symbols mark objects where isotopic shifts due to an enrichment of ^3He were detected, filled symbols objects with atmospheres dominated by ^4He . The diamonds mark stars belonging to the upper helium sequence, the circles stars belonging to the lower sequence. The triangles mark three sdBs with enriched ^3He from literature (Geier et al., 2013b).

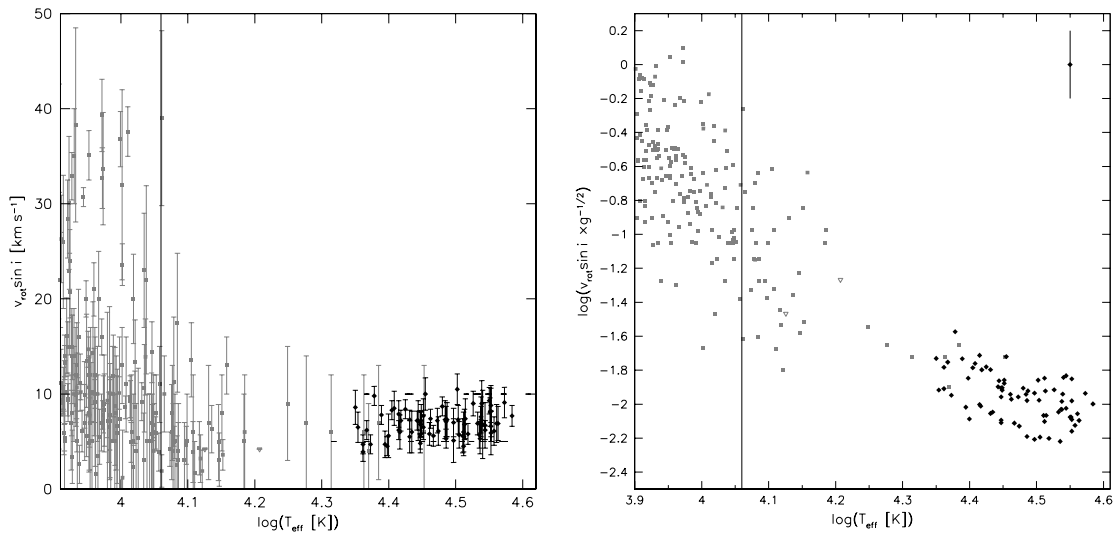


Figure 2.3: *Left panel:* Projected rotational velocity plotted against effective temperature. The grey squares mark BHB and some sdB stars from literature. The black diamonds mark the sdBs from my sample. The vertical line marks the jump temperature of 11 500 K. *Right panel:* $v_{\text{rot}} \sin i \times g^{-1/2}$ (proportional to the angular momentum) plotted against effective temperature for the same objects (Geier & Heber, 2012).

3 Close hot subdwarf binaries

Most stars are not formed alone, but as members of binary or multiple systems. If the separation between the companions is sufficiently large and the orbital period therefore long enough, there will be no interaction and both stars will evolve independent from each. However, if the initial orbital period of a binary is smaller than a few hundred days, the two components will interact in the later stages of stellar evolution as soon as the more massive star evolves away from the main sequence and becomes a giant. Several different types of interactions are possible. Mass can be transferred in a stable fashion from one star to the other, close-by stars can form overcontact systems or merge. Depending on the detailed configuration, a binary can also undergo several distinct episodes of mass-transfer during its lifetime.

To form close sdB binaries with periods down to a few hours and separations down to less than the radius of the Sun, there is only one feasible scenario. To end up with a binary that is much more compact than the initial system has been on the main sequence, common envelope (CE) ejection is the only likely channel. Initially, two main sequence stars evolve independently in a binary system. The more massive one will evolve faster to become a red giant. Unstable mass transfer from the red giant to the companion will lead to a CE phase. Due to friction and gravitational drag the two stellar cores lose orbital energy and angular momentum, which leads to a shrinkage of the orbit. This energy is deposited in the envelope which will finally become unbound. If the core reaches the mass required for the core-helium flash before the envelope is lost, a binary consisting of a core-helium burning sdB star and a main sequence companion is formed. In another possible scenario the more massive star evolves to become a WD either through a CE phase or stable mass transfer onto the less massive companion. After that the less massive star evolves to become a red giant. Unstable mass transfer will lead to a CE, and once the envelope is ejected the red giant remnant starts burning helium, and a system consisting of an sdB and a WD companion is formed (Han et al., 2002, 2003). The details of the CE phase are only poorly understood (Ivanova et al., 2013) and observations of significant samples of post-CE binaries are necessary to understand this important process.

It is difficult to determine the nature of the close companions in sdB binaries, because they are single-lined system, where the sdB is the only component visible in the spectra. The lower mass limits derived from the binary mass functions are in general compatible with late-type main sequence stars of spectral type M or compact objects like white dwarfs. Only in some cases (e.g. eclipsing systems) it is possible to distinguish between those two options. In a project done for my PhD thesis (Geier et al., 2010) I found that a sizeable fraction of the sdB binary population might harbour massive compact companions, i.e. massive white dwarfs, neutron stars or even black holes. The existence of such systems is actually predicted by binary evolution theory (Podsiadlowski et al., 2002; Pfahl et al., 2003; Nelemans, 2010). The formation channel includes two phases of unstable mass transfer and one supernova explosion. The fraction of those systems is consistently predicted to be about 1 – 2%. I determined

high-precision projected rotational velocities and gravities of 40 sdB stars by assuming that the rotation of the sdB primary is tidally locked to its orbit. However, the synchronisation timescales as well as the sdB ages are quite uncertain. Hence, there was a need to determine companion masses for sdB stars without having to call for synchronisation.

Motivated by this issue I initiated a radial velocity survey (Massive Unseen Companions to Hot Faint Underluminous Stars from SDSS¹, MUCHFUSS) to find sdBs with compact companions like massive white dwarfs, neutron stars or black holes (Geier et al., 2011b, appended), which should show very high RV variability. We used the SDSS spectroscopic database as the starting point for our survey and obtained follow-up observations of the stars that showed the most significant RV shifts. Conducting more than 200 nights of spectroscopic and photometric follow-up, we constrained the orbits and companion types of 30 newly discovered sdB binaries up to now (Geier et al., 2011c,d, 2013c; Østensen et al., 2013; Geier et al., 2014; Schaffneroth et al., 2014b; Kupfer et al., 2015, papers appended).

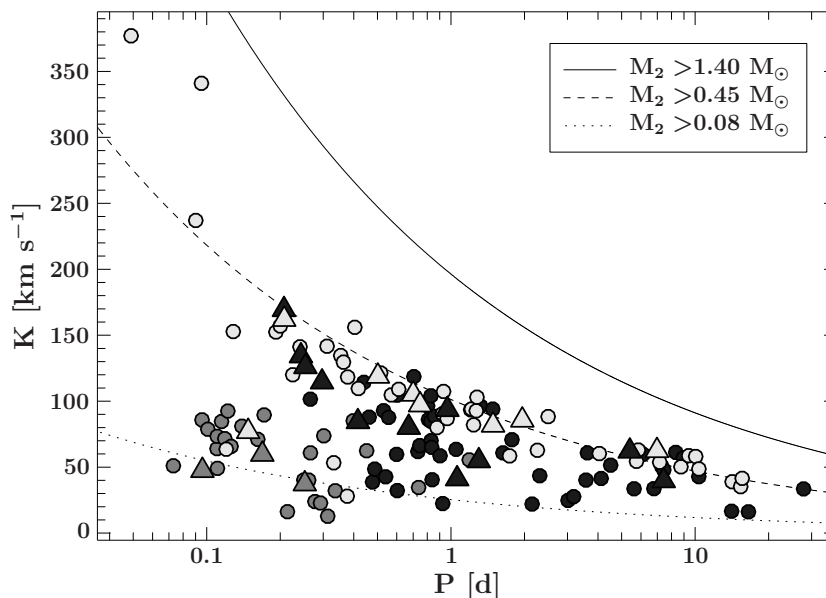


Figure 3.1: The RV semiamplitudes of all known sdB binaries with spectroscopic solutions plotted against their orbital periods (open symbols). The dashed, dotted and solid lines mark the regions to the right where the minimum companion masses derived from the binary mass function (assuming $0.47 M_{\odot}$ for the sdBs) exceed $0.08 M_{\odot}$, $0.45 M_{\odot}$, and $1.40 M_{\odot}$. The white symbols mark sdBs with known WD companions, the grey symbols sdBs with low-mass M-star or brown dwarf companions and the black symbols sdBs with unknown companion type (for details see Kupfer et al., 2015).

Combining our new discoveries with the known close sdB binaries we performed the first comprehensive study of this population (see Fig. 3.1, Kupfer et al., 2015). This work was led by Thomas Kupfer as part of his PhD thesis at the University of Nijmegen under my co-supervision. The minimum companion mass distribution of this sample of 142 solved close sdB binaries is bimodal. One peak around $0.1 M_{\odot}$ corresponds to the low-mass main sequence and substellar companions. The other peak around $0.4 M_{\odot}$ corresponds to the white dwarf companions. The derived masses for the white dwarf

¹Sloan Digital Sky Survey

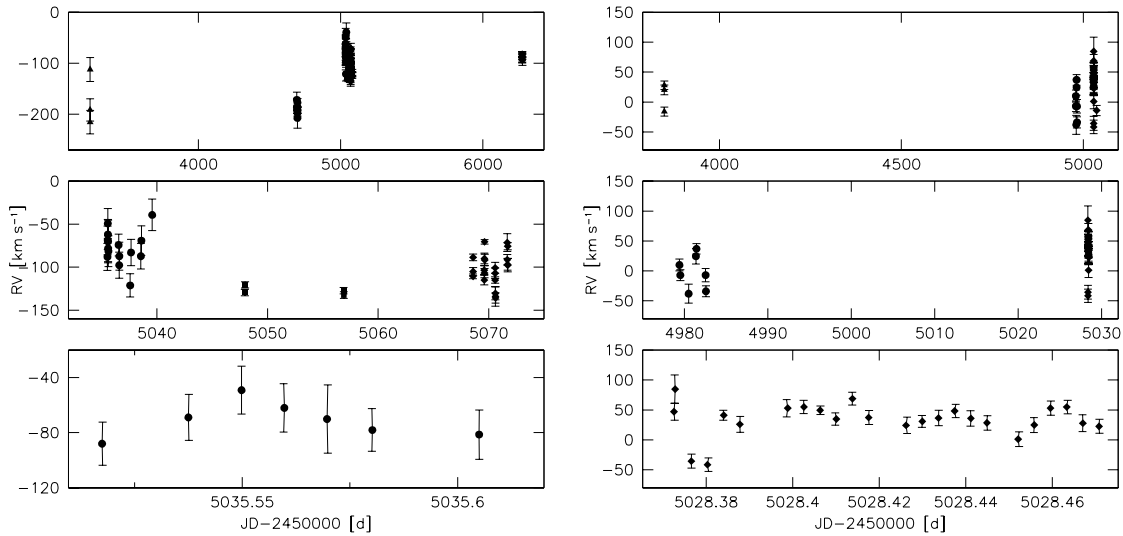


Figure 3.2: Radial velocities of the He-sdOs J232757.46+483755.2 (left panels) and J141549.05+111213.9 (right panels) against Julian date (Geier et al., 2015b). Significant variations are present on timescales of years (upper panels), days (middle panels) and hours (lower panels).

companions are significantly lower than the average mass for single carbon-oxygen white dwarfs, which might be an indication, that those objects are actually helium white dwarfs. We compared the sample to the populations of extremely low-mass helium white dwarf binaries as well as short period white dwarfs with main sequence companions. Both samples show a significantly different companion mass distribution indicating either different selection effects or different evolutionary paths. The sdB binaries with the shortest periods are predicted to evolve to become cataclysmic variables, stable AM CVn type binaries or to merge and form massive C/O WDs, RCrB stars or even to explode as supernovae type Ia.

We also published a catalogue with 1914 radial velocity measurements of the 177 RV variable hot subluminous star we found in SDSS Data Release 7. So far, we did not find an sdB binary with a compact companion exceeding $1.0 M_{\odot}$. Based on this non-detection we constrain the fraction of close massive compact companions in our sample to be smaller than $\sim 1.3\%$, which is already close to the theoretical predictions. However, the sample might still contain such binaries with moderate RV-shifts and periods exceeding ~ 8 d.

Surprisingly, irregular RV variations of unknown origin with amplitudes of up to $\sim 180 \text{ km s}^{-1}$ on timescales of years, days and even hours have been detected in some He-sdO stars (see Fig. 3.2). They might be connected to irregular photometric variations in some cases. Variable magnetic fields might be responsible, but no strong conclusions can be drawn yet (Geier et al., 2015b, appended). Another very interesting byproduct of our project is the discovery of new classes of RV variable stars in the Galactic halo. Among them the first RV variable BHB stars, three candidate runaway main-sequence type B binaries (Geier et al., 2015c) and some rare hydrogen- and helium-rich post-AGB stars (Reindl et al., 2015).

4 Substellar companions

Since the discovery of the first exoplanets more than 20 years ago, a whole new and very dynamic field of research emerged. Based on data from several ground- and space-based transit and RV surveys we now know more than 2000 exoplanets and at least as many candidates. Besides the characterisation of those objects and the hunt for habitable planets, research focuses on the formation and evolution of planetary systems. The relation between gas giant planets and the other type of substellar objects, the more massive brown dwarfs (BDs), plays a key role in this respect. Recently, more attention has been devoted to the interactions between stars and substellar objects and a series of workshops has been held (the first one being organized by our group in Bamberg 2010). The question, whether the interaction with close substellar companions might affect or even substantially change the evolution of their host stars, becomes more and more relevant. Our discoveries in the last couple of years provide strong evidence, that hot subdwarf stars might be key objects to address this question.

Soker (1998) suggested that substellar objects like brown dwarfs and planets may also be swallowed by their host star and that common envelope ejection could form hot subdwarfs. Substellar objects with masses higher than about $10 M_J$ were predicted to survive the common envelope phase and end up in a close orbit around the stellar remnant, while planets with lower masses would entirely evaporate or merge with the stellar core. The stellar remnant is predicted to lose most of its envelope and evolve towards the EHB. A similar scenario has been proposed to explain the formation of apparently single low-mass white dwarfs (Nelemans & Tauris, 1998). The discovery of a brown dwarf in close orbit around such a white dwarf supported this scenario and shows that substellar companions can influence the outcome of stellar evolution (Maxted et al., 2006).

The fact that substellar companions in wide orbits around sdBs seem to be common suggests that similar objects closer to their host stars might exist as well (Silvotti et al., 2007; Beuermann et al., 2012). Possible signatures of earth-sized planets closely orbiting two pulsating sdB stars have been found in high-precision Kepler light curves (Charpinet et al., 2011; Silvotti et al., 2014). These findings indicate that planets and brown dwarf companions can survive common envelope phases. The two earth-size planets reported by Charpinet et al. (2011) have been explained either as the stripped cores of two previously more massive planets or as the tidally disrupted core fragments of one massive planet (Bear & Soker, 2012).

Based on high-resolution spectra we discovered a sinusoidal variation with very small amplitude of less than 3 km s^{-1} in the RV-curve of the bright sdOB HD 149382 and concluded that it might be orbited by a planetary companion with a period of 2.39 d (Geier et al., 2009, appended). Although this early result could not be confirmed by other groups (Norris et al., 2011), we soon found much better candidates. The selection criteria of the MUCHFUSS project not only single out massive companions, but also companions with very low masses in extremely short orbits. Initially, we discovered two short-period systems (0.069 and 0.095 d) and time-resolved photometry revealed eclipses, which allowed us

to constrain the companion masses. The companion mass of the eclipsing sdB binary J082053+000843 ($0.045 - 0.068 M_{\odot}$) turned out to be lower than the hydrogen-burning limit ($0.07 - 0.08 M_{\odot}$), which separates stars from brown dwarfs without nuclear fusion in their cores. This system therefore hosts a brown dwarf companion and was the first such system discovered (see Fig. 4.1, Geier et al., 2011e, appended). The sdB in the very similar eclipsing binary system J162256+473051 is also orbited by a brown dwarf companion (Schaffenroth et al., 2014b, appended). On the topic of eclipsing sdB binaries with low-mass companions I co-supervised the PhD student Veronika Schaffenroth and the diploma students Lew Classen and Kathrin Nagel from the Remeis observatory of the University of Erlangen.

These results, which showed that brown dwarfs can trigger and survive a common envelope phase, provided the best evidence so far that substellar companions play an important role in the formation of sdB stars. We therefore searched for more sdB binaries with low-mass companions and found two close reflection effect binaries with grazing eclipses and low-mass stellar companions (Kupfer et al., 2015; Schaffenroth et al., 2013, appended). In addition to a reflection effect, which signals the presence of a cool, low-mass stellar companion, we detected p-mode pulsations in the light curve of the sdB binary FBS 0117+396. Only a few of the known short-period sdB pulsators are in close binary systems (Østensen et al., 2013). Furthermore, I became involved in several other studies of sdB binaries with low-mass stellar companions (Geier et al., 2011d; Naslim et al., 2012; Barlow et al., 2013a; Telting et al., 2014).

Our goal is to increase the sample of sdB binaries with substellar companions and to check, whether there is a lower mass limit for the surviving companion as suggested by Soker (1998). Recently, we found two new reflection effect binaries with cool companions and very small minimum companion masses down to $0.027 M_{\odot}$. We also studied the known sample of sdBs with low-mass stellar companions (Schaffenroth et al., 2014a, appended) and conclude that the fraction of sdBs formed after an interaction with low-mass stars is comparable to the fraction of sdBs formed after an interaction with substellar objects. Furthermore, we do not find any binaries with both orbital periods shorter than ~ 0.2 d and minimum masses below $\sim 0.06 M_{\odot}$ and argue that substellar companions in this range might not survive the common envelope phase. Instead they might either merge with the core of the red giant or evaporate in its envelope as suggested by Soker (1998).

Independently, we found more evidence backing this scenario. Among our sample of bright sdBs, we discovered two single stars, which are fast rotators. We showed that the large majority of single sdBs are slow rotators (Fig. 2.3, Geier & Heber, 2012) and since tidal forces spin up the rotation in close binary stars, we initially took rapid rotation as indication for close binary stars (Geier et al., 2010). We found EC 22081–1916 to show strongly rotationally broadened line profiles (Geier et al., 2011a, appended). However, time-resolved spectroscopy did not show any RV variations leading to the conclusion that the star was formed by a common envelope merger of a low-mass, possibly substellar object with a red-giant core just as proposed by Soker (1998) and further elaborated by Politano et al. (2008). Subsequently, we found the single sdB SB 290 to behave in a similar way (Geier et al., 2013a, appended).

While a common envelope merger event is predicted to form a fast rotating sdB (Politano et al., 2008), it is much harder to prove the evaporation of a low-mass companion just before common envelope ejection, because the companion does not survive the interaction and should not have any measurable influence on the formed sdB. However, the mere existence of single sdB stars might already be an indication for such a process. Based on the very slow rotation of apparently single sdBs we showed that the merger of two He-WDs is an unlikely formation scenario for sdB stars (see Sect. 2, Geier & Heber, 2012). The merger scenario is also not consistent with the very narrow mass distribution of sdB stars

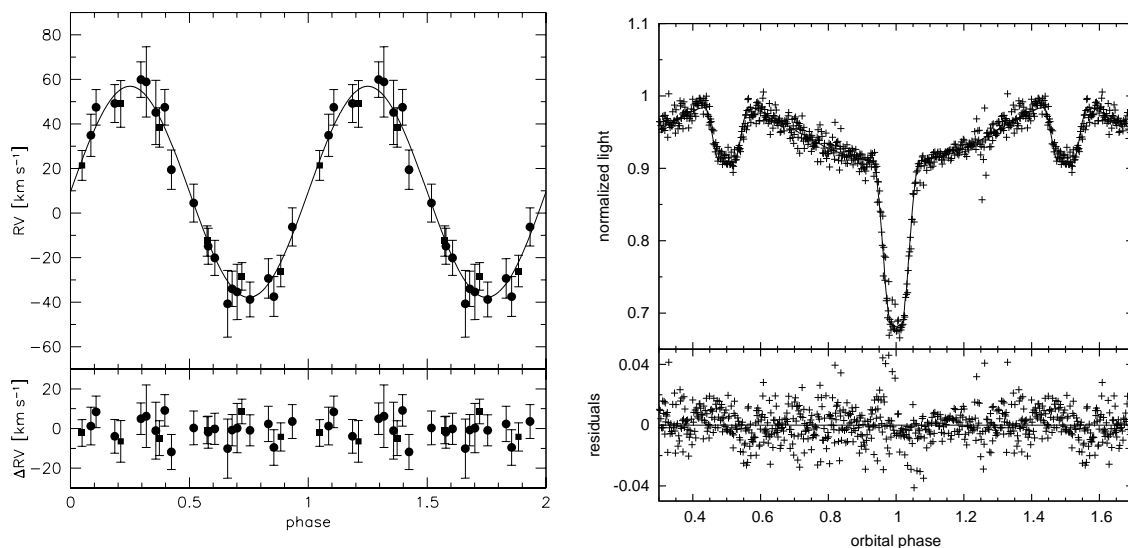


Figure 4.1: *Left panel:* Radial velocity plotted against orbital phase of the sdB+BD binary J08205+0008. *Right panel:* Phased R-band light curve of J08205+0008. A model is overlotted as solid line (Geier et al., 2011e).

determined from asteroseismic and close binary analyses (Fontaine et al., 2012). While the formation of sdBs in binaries can be explained, we are lacking such a scenario for single sdBs.

One possible way out might be that there are no single sdBs, because the least massive companions just remained undetected so far. Because previous searches for RV-variability have been done using medium-resolution spectra, which only allowed us to measure RV shifts higher than $\sim 10 \text{ km s}^{-1}$, we measured RVs from our high-resolution spectra with an accuracy down to less than $\sim 1.0 \text{ km s}^{-1}$ to check whether a yet undetected population of sdB binaries with small RV amplitudes (see Fig. 4.2) might be present. Preliminary results show that companions in close orbits with masses down to $0.01 M_{\odot}$ can be excluded in more than half of our sample meaning that single sdBs indeed exist (Classen et al., 2011). One possible way to explain their existence might be the interaction with a close companion, which has been evaporated.

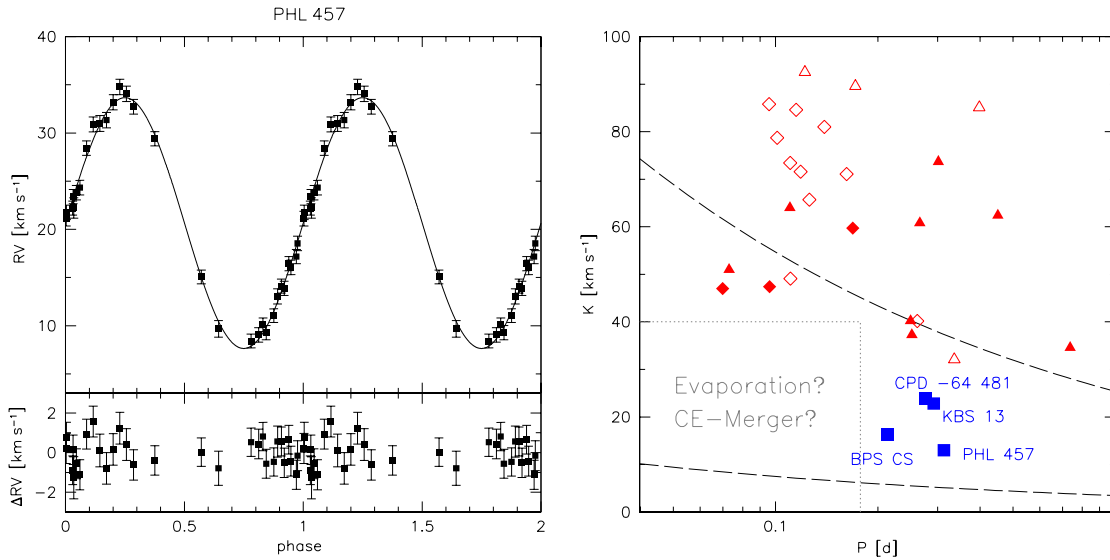


Figure 4.2: *Left panel:* Radial velocity plotted against orbital phase for PHL 457, the sdB binary with the smallest confirmed RV variation. *Right panel:* The RV semiamplitudes of all known sdB binaries with reflection effects and spectroscopic solutions plotted against their orbital periods (Schaffenroth et al., 2014a). Diamonds mark eclipsing sdB binaries where the companion masses are well constrained, triangles systems without eclipses, where only lower limits can be derived for the companion masses. Squares mark candidate sdB+BD systems. Open symbols mark systems that have been discovered based on photometry, filled symbols have been discovered based on spectroscopy. The dashed lines mark the regions to the right where the minimum companion masses derived from the binary mass function (assuming $0.47 M_{\odot}$ for the sdBs) exceed $0.01 M_{\odot}$ (lower curve) and $0.08 M_{\odot}$ (upper curve).

5 Supernova type Ia progenitors and ejected donor remnants

The accelerated expansion of the universe was one of the most unexpected discoveries in astronomy. It is attributed to a form of energy which counteracts gravitation and dominates the energy budget of the universe. However, the properties of this so-called dark energy are basically unknown. Deriving those properties therefore became one of the key unsolved problems in astronomy today. Using supernovae type Ia (SN Ia) as cosmological standard candles provided the first and still most direct evidence for the accelerated expansion of the universe (Riess et al., 1998; Perlmutter et al., 1999, Nobel prize 2011). If a SN Ia is detected in another galaxy, its distance can be measured by comparing its apparent brightness with its known absolute brightness. However, the accuracy of this method is limited, because the progenitors of SN Ia explosions are still unknown.

There is consensus that the observed features of SN Ia can only be conclusively explained by the thermonuclear explosion of a white dwarf consisting of carbon and oxygen. To reach the critical mass for the ignition, matter must be transferred from a close companion star. Only if the progenitor systems of SN Ia are properly understood, we can hope to use these tools to gain a deeper insight into the nature of the dark energy and the evolution of our universe (for a review see Wang & Han, 2012).

Close subdwarf binaries with massive WD companions turned out to be candidates for SN Ia progenitors because those systems shrink further due to the emission of gravitational waves and merge. One of the best known candidate systems for this double-degenerate merger scenario is the sdB+WD binary KPD 1930+2752 (Maxted et al., 2000; Geier et al., 2007). Another possible channel for SN Ia is the single-degenerate scenario where a supermassive white dwarf accretes matter from a close companion until it reaches the critical mass and explodes. Mereghetti et al. (2009) showed that in the X-ray binary HD 49798 a supermassive ($> 1.2 M_{\odot}$) white dwarf accretes matter from a closely orbiting subdwarf O companion.

In the course of the MUCHFUSS project we discovered the extremely close ($P = 0.04987$ d), eclipsing binary system CD-30°11223, which fulfills all requirements for the progenitor of an SN Ia via the so-called sub-Chandrasekhar double-detonation scenario (Fink et al., 2010). In this system a white dwarf ($\sim 0.8 M_{\odot}$) is orbited by a core-helium burning compact hot subdwarf star, which will start to transfer helium-rich material on short timescales. The ignition of He-burning in the newly formed envelope ($\simeq 0.1 M_{\odot}$) is predicted to trigger carbon-burning in the core although the WD is less massive than the Chandrasekhar limit (see Figs. 2.4, 5.1). Furthermore, we argued that the hypervelocity sdO US 708 is likely to be the surviving donor remnant of such an event (Geier et al., 2013b, appended).

This connection between SN Ia and surviving helium stars, that are ejected from the very close progenitor binaries at high velocities, has been predicted by theory (Justham et al., 2009; Wang & Han, 2009). In a follow-up study of US 708 we were able to strengthen this connection further. This star

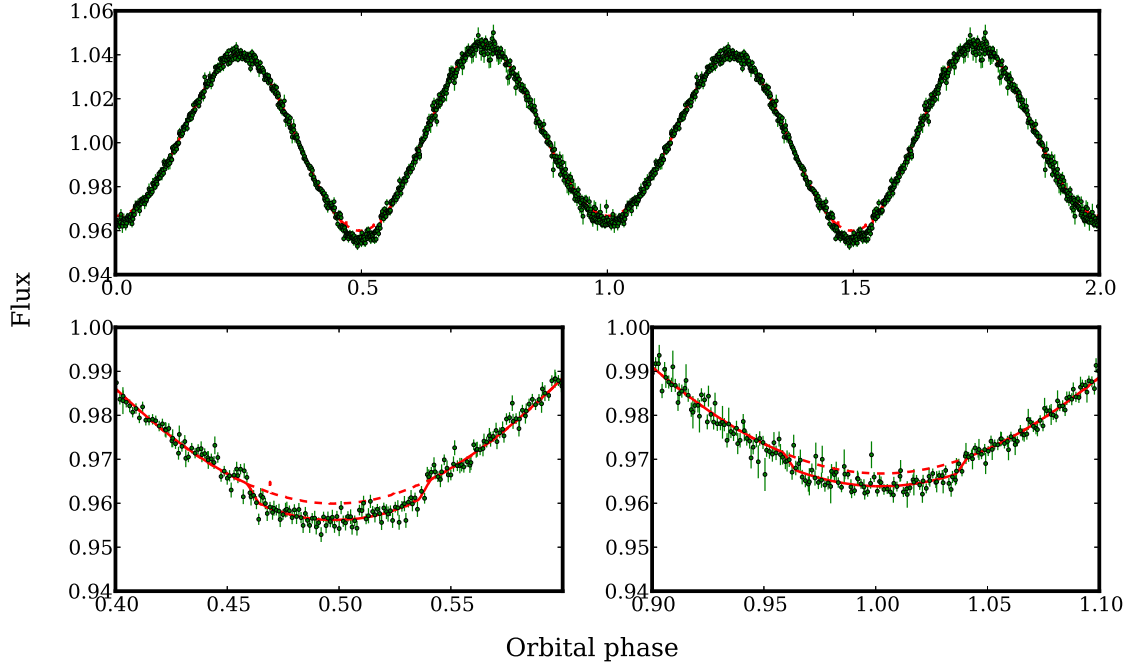


Figure 5.1: *Upper panel:* V-band light curve of CD-30°11223 taken with SOAR/Goodman (green) with superimposed model (red) plotted twice against orbital phase for better visualisation. The dashed red curve marks the same model without transits and eclipses. The sinusoidal variation is caused by the ellipsoidal deformation of the hot subdwarf due to the tidal drag of the compact white dwarf. The difference in amplitude between phase 0.25 and 0.75 originates from the relativistic Doppler beaming effect, which is usually not detectable with ground-based telescopes. *Lower panels:* Close-up on the transit of the WD in front of the sdB (left). The WD companion is comparable in size to Earth. The detection of transits is essential to determine the fundamental parameters of the binary using model light curves. It is even possible to detect the eclipse of the WD by the sdB (right), which tells us that the WD is still young and therefore hot enough to contribute significant flux (Geier et al., 2013c).

is not only a fast rotator as expected because it must have been spun-up in the close binary before. Its origin can also be traced back to the Galactic disc rather than the Galactic centre (Fig. 5.2, Geier et al., 2015a, appended). In this way, essentially all other proposed acceleration scenarios for this star can be excluded (e.g. Hills, 1988). Measuring all velocity components of US 708 for the first time, we find it to be the fastest unbound star in our Galaxy. If it can be shown, that high velocity sdO/B stars are indeed the ejected donor remnants, it would be a direct proof that the double-detonation scenario leads to SN Ia explosions. The first type of SN Ia progenitors would then be unambiguously identified.

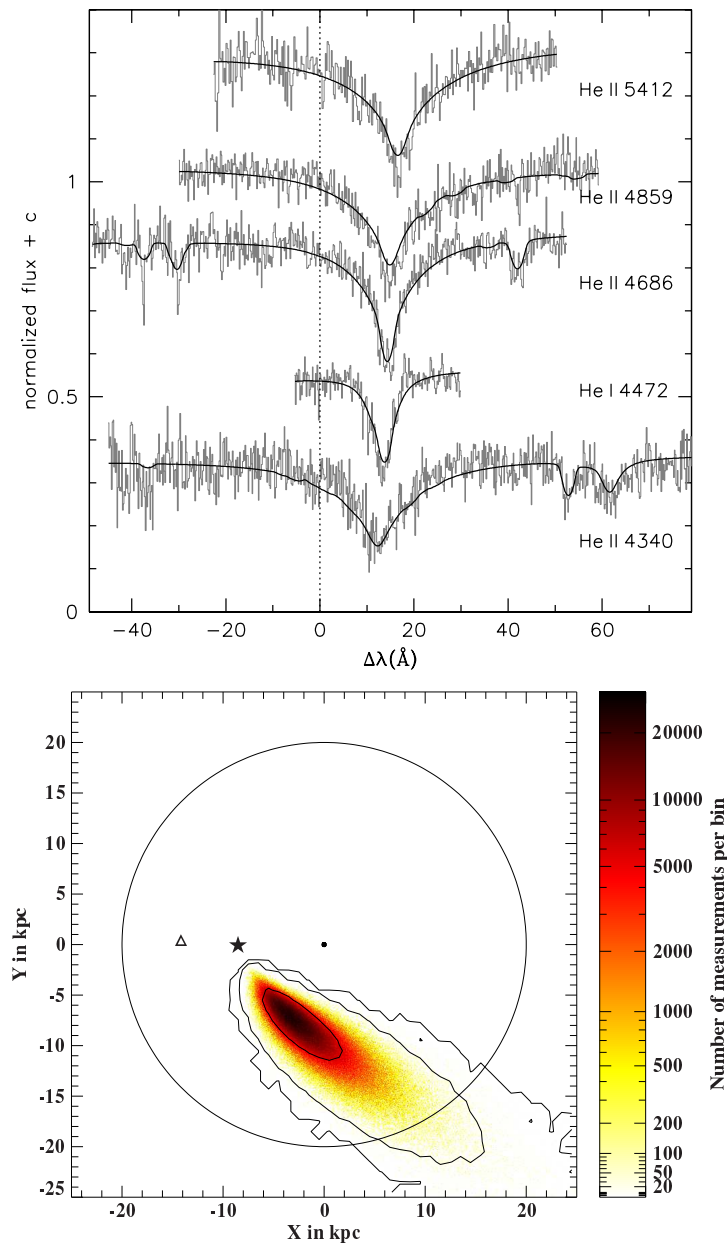


Figure 5.2: *Left panel:* Fit of model spectrum. Fit of synthetic NLTE models to the helium and nitrogen lines of a Keck/ESI spectrum of US 708. The normalized fluxes of the single lines are shifted for better visualisation and the most prominent lines are labeled. The dashed vertical line marks the rest wavelengths of the lines. The high radial velocity shift as well as the significant broadening of the lines are clearly visible. *Right panel:* Origin of US 708. Monte Carlo simulation (10^8 iterations) of the past trajectory of US 708. The colour-coded bins mark the positions, where the star crossed the Galactic disc, which is shown pole-on. The contours correspond to the 1σ , 3σ and 5σ confidence limits. The position of the Galactic centre is marked by the black dot, the position of the Sun with the star symbol. The current position of US 708 is marked by a triangle (Geier et al., 2015a).

Bibliography

- Barlow, B. N., Kilkenny, D., Drechsel, H., ... (**Geier, S.**), et al. 2013a, MNRAS, 430, 22
- Barlow, B. N., Liss, S. E., Wade, R. A., & Green, E. M. 2013b, ApJ, 771, 23
- Baschek, B., Sargent, W. L. W., & Searle, L. 1972, AJ, 173, 611
- Bear, E., & Soker, N. 2012, ApJL, 749, L14
- Beuermann, K., Dreizler, S., Hessman, F. V., & Deller, J. 2012, A&A, 543, A138
- Bloemen, S., Marsh, T. R., Østensen, R. H., et al. 2011, MNRAS, 410, 1787
- Castelli, F., & Kurucz, R. L. 2003, IAU Symposium, 210, 20
- Charpinet, S., Green, E. M., Baglin, A., et al. 2010, A&A, 516, 6
- Charpinet, S., Fontaine, G., Brassard, P., et al. 2011, Nature, 480, 496
- Classen, L., **Geier, S.**, Heber, U., & O'Toole, S. J. 2011, AIP Conf. Ser., 1331, 297
- Dorman, B., Rood, R. T., & O'Connell, R. W. 1993, ApJ, 419, 596
- Drechsel, H., Haas, S., Lorenz, R., & Gayler, S. 1995, A&A, 294, 723
- Drechsel, H., Heber, U., Napiwotzki, R., et al. 2001, A&A, 397, 893
- Drilling, J. S., Jeffery, C. S., Heber, U., Moehler, S., & Napiwotzki, R. 2013, A&A, 551, 31
- Edelmann, H., Heber, U., Hagen, H.-J., et al. 2003, A&A, 400, 939
- Fink, M., Röpke, F. K., Hillebrandt, W., et al. 2010, A&A, 514, A53
- Fontaine, G., Brassard, P., Charpinet, S., et al. 2012, A&A, 539, 12
- Geier, S.**, Nesslinger, S., Heber, U., et al. 2007, A&A, 464, 299
- Geier, S.**, Edelmann, H., Heber, U., & Morales-Rueda, L. 2009, ApJ, 702, L96
- Geier, S.**, Heber, U., Podsiadlowski, P., et al. 2010, A&A, 519, A25
- Geier, S.**, Classen, L., & Heber, U. 2011a, ApJ, 733, L13
- Geier, S.**, Hirsch, H., Tillich, A., et al. 2011b, A&A 530, A28
- Geier, S.**, Maxted, P. F. L., Napiwotzki, R., et al. 2011c, A&A, 526, 39

- Geier, S., Napiwotzki, R., Heber, U., & Nelemans, G. 2011d, *A&A*, 528, L16
- Geier, S., Schaffenroth, V., Drechsel, H., et al. 2011e, *ApJ*, 731, L22
- Geier, S., & Heber, U. 2012, *A&A*, 543, 149
- Geier, S., Schaffenroth, V., Hirsch, H., et al. 2012b, *AN*, 333, 431
- Geier, S. 2013, 549, 110
- Geier, S., Heber, U., Heuser, C., et al. 2013a, *A&A*, 551, L4
- Geier, S., Heber, U., Edelmann, H., et al. 2013b, *A&A*, 557, 122
- Geier, S., Marsh, T. R., Wang, B., et al. 2013c, *A&A*, 554, 54
- Geier, S., Østensen, R. H., Heber, U., et al. 2014, *A&A*, 526, 95
- Geier, S., Fürst, F., Ziegerer, E., et al. 2015a, *Science*, 347, 1126
- Geier, S., Kupfer, T., Heber, U., et al. 2015b, *A&A*, in press (arXiv:1502.04086)
- Geier, S., Kupfer, T., Schaffenroth, V., et al. 2015c, *A&A*, in prep.
- Green, R. F., Schmidt, M., & Liebert, J. 1986, *ApJS*, 61, 305
- Greenstein, J. L., & Sargent, A. I. 1974, *ApJS*, 28, 157
- Han, Z., Podsiadlowski, P., Maxted, P. F. L., Marsh, T. R., & Ivanova, N. 2002, *MNRAS*, 336, 449
- Han, Z., Podsiadlowski, P., Maxted, P. F. L., & Marsh, T. R. 2003, *MNRAS*, 341, 669
- Heber, U. 1986, *A&A*, 155, 33
- Heber, U. 2009, *ARA&A*, 47, 211
- Heber, U., Reid, I. N., & Werner, K. 2000, *A&A*, 363, 198
- Hills, J. G. 1988, *Nature*, 331, 687
- Hu, H., Tout, C. A., Glebbeek, E., & Dupret, M.-A. 2011, *MNRAS*, 418, 195
- Iben, I., & Tutukov, A. V. 1984, *ApJ*, 284, 719
- Ivanova, N., Justham, S., Chen, X., et al. 2013, *A&ARv*, 21, 59
- Jeffery, C. S., *ASP Conf. Ser.* 2008, 391, 3
- Jester, S., Schneider, D. P., Richards, G. T., et al. 2005, *AJ*, 130, 873
- Justham, S., Wolf, C., Podsiadlowski, P., & Han, Z. 2009, *A&A*, 493, 1081
- Kupfer, T., Geier, S., Heber, U., et al. 2015, *A&A*, in press (arXiv:1501.03692)
- Lanz, T., Brown, T. M., Sweigart, A. V., Hubeny, I., & Landsman, W. B. 2004, *ApJ*, 602, 342
- Lemke, M. 1997, *A&AS*, 122, 285
- Maxted, P.F.L., Marsh, T.R., & North, R.C. 2000, *MNRAS*, 317, L41

- Maxted, P.F.L., Heber, U., Marsh, T.R., & North, R.C. 2001, MNRAS, 326, 1391
- Maxted, P. F. L., Napiwotzki, R., Dobbie, P. D., & Burleigh, M. R. 2006, Nature, 442, 543
- Mereghetti, S., Tiengo, A., Esposito, P., et al. 2009, Science, 325, 1222
- Mereghetti, S., La Palombara, N., Tiengo, A., et al. 2011, ApJ, 737, 51
- Michaud, G., Richer, J., & Richard, O. 2011, A&A, 529, 60
- vNapiwotzki, R., Yungelson, L., Nelemans, G. et al. 2004, ASP Conf. Ser., 318, 402
- Napiwotzki, R. 2008, ASP Conf. Ser. 392, 139
- Naslim, N., **Geier, S.**, Jeffery, C. S., et al. 2012, MNRAS, 423, 3031
- Nelemans, G., & Tauris, T. M. 1998, A&A, 335, L85
- Nelemans, G. 2010, ApSS, 329, 25
- Németh, P., Kawka, A., & Vennes, S. 2012, MNRAS, 427, 2180
- Norris, J. M., Wright, J. T., Wade, R. A., Mahadevan, S., & Gettel, S. 2011, ApJ, 743, 88
- O'Connell, R. W. 1999, ARA&A, 37, 603
- Østensen, R. H., **Geier, S.**, Schaffenroth, V., et al. 2013, A&A, 559, 35
- Perlmutter, S., Aldering, G., Goldhaber, G., et al. 1999, ApJ, 517, 565
- Pfahl, E., Rappaport, S., & Podsiadlowski, P. 2003, ApJ, 597, 1036
- Podsiadlowski, P., Han, Z., Lynas-Gray, A. E., & Brown, D. 2008, APS Conf. Ser., 392, 15
- Podsiadlowski, P., Rappaport, S., & Pfahl, E. D. 2002, ApJ, 565, 1107
- Politano, M., Taam, R. E., van der Sluys, M., & Willems, B. 2008, ApJ, 687, L99
- Reindl, N., **Geier, S.**, Kupfer, T., et al. 2015, A&A, in prep.
- Riess, A., Filippenko, A. V., Challis, P., et al. 1998, AJ, 116, 1009
- Sargent, W. L. W., & Searle, L. 1966, ApJ, 145, 652
- Schaffenroth, V., **Geier, S.**, Drechsel, H., et al. 2013, A&A, 553, 18
- Schaffenroth, V., Classen, L., Nagel, K., **Geier, S.**, et al. 2014a, A&A, 570, 70
- Schaffenroth, V., **Geier, S.**, Heber, U. et al. 2014b, A&A, 564, 98
- Silvotti, R., et al. 2007, Nature, 449, 189
- Silvotti, R., et al. 2014, A&A, 570, 130
- Soker, N. 1998, AJ, 116, 1308
- Ströer, A., Heber, U., Lisker, T., et al. 2007, A&A, 462, 269
- Teltung, J. H., Baran, A. S., Nemeth, P., ... (**Geier, S.**), et al. 2014, A&A, 570, 129

-
- Vink, J. S., & Cassisi, S. 2002, *A&A*, 392, 553
- Vos, J., Østensen, R. H., Degroote, P., et al. 2012, *A&A*, 548, 6
- Vos, J., Østensen, R. H., Nemeth, P., et al. 2013, *A&A*, 559, 54
- Wang, B. & Han, Z. 2009, *A&A*, 508, L27
- Wang, B. & Han, Z. 2012, *New. A. Rev*, 56, 122
- Webbink, R. F. 1984, *ApJ*, 277, 355
- Wilson, R. E., & Devinney, E. J. 1971, *ApJ*, 166, 605
- Zhang, X., & Jeffery, C. S. 2012, *MNRAS*, 419, 452

Acknowledgements

It's my pleasure to thank Uli Katz, Klaus Werner and especially Uli Heber for their willingness to accompany the progress of this work as mentors. I am deeply grateful to my collaborators and friends all over the world, especially the students from Bamberg, who supported this project enthusiastically and volunteered to travel to remote places for observations.

Special thanks go to my hosts at ESO, who gave me the great opportunity to spend three years as a fellow in the vibrant and inspiring environment of the headquarter in Garching, supported my scientific work, and allowed me to fulfill the teaching duties that came with this habilitation in Erlangen.

I also want to thank my family and friends for their constant support in all those years.

Appended papers

Published papers

Hot subdwarf atmospheres

Geier, S., Heber, U., Edelmann, H., Morales-Rueda, L., Kilkenny, D., O'Donoghue, D., Marsh, T. R., Copperwheat, C.; *Hot subdwarf stars in close-up view IV. Helium abundances and the 3He isotopic anomaly of subdwarf B star*, 2013, A&A, 557, 122

Geier, S.; *Hot subdwarf stars in close-up view – III. Metal abundances of subdwarf B stars*, 2013, A&A, 549, 110

Geier, S., Heber, U.; *Hot subdwarf stars in close-up view. II. Rotational properties of single and wide binary subdwarf B stars*, 2012, A&A, 543, 149

Close hot subdwarf binaries

Geier, S., Østensen, R. H., Heber, U., Kupfer, T., Maxted, P. F. L., Barlow, B. N., Vuckovic, M., Tillich, A., Miller, S., Edelmann, H., Classen, L., McLeod, A. F.; *Orbital solutions of eight close sdB binaries and constraints on the nature of the unseen companions*, 2014, A&A, 526, 95

Geier, S., Schaffenroth, V., Hirsch, H., Tillich, A., Heber, U., Maxted, P. F. L., Østensen, R. H., Barlow, B. N., O'Toole, S. J., Kupfer, T., Marsh, T. R., Gänsicke, B. T., Napiwotzki, R., Cordes, O., Müller, S., Classen, L., Ziegerer, E., Drechsel, H.; *MUCHFUSS – Massive Unseen Companions to Hot Faint Underluminous Stars from SDSS*, 2012, AN, 333, 431

Geier, S., Napiwotzki, R., Heber, U., Nelemans, G.; *Binaries discovered by the SPY survey. VI. Discovery of a low mass companion to the hot subluminous planetary nebula central star EGB 5 – a recently ejected common envelope?*, 2011, A&A, 528, L16

Geier, S., Maxted, P. F. L., Napiwotzki, R., Østensen, R. H., Heber, U., Hirsch, H., Kupfer, T., Müller, S., Tillich, A., Barlow, B. N., Oreiro, R., Ottosen, T. A., Gänsicke, B. T., Marsh, T. R.; *Massive unseen companions to hot faint underluminous stars from SDSS (MUCHFUSS). Analysis of seven close subdwarf B binaries*, 2011, A&A, 526, 39

Geier, S., Hirsch, H., Tillich, A., Maxted, P. F. L., Bentley, S. J., Østensen, R. H., Heber, U., Gänsicke, B. T., Marsh, T. R., Napiwotzki, R., Barlow, B. N., O’Toole, S. J.; *The MUCHFUSS project – Searching for hot subdwarf binaries with massive unseen companions. Survey and target selection for follow-up*, 2011, A&A, 530, 28

Substellar companions

Schaffenroth, V., Classen, L., Nagel, K., **Geier, S.**, Koen, C., Heber, U., Edelmann, H.; *Two candidate brown dwarf companions around core helium-burning stars*, 2014, A&A, 570, 70

Schaffenroth, V., **Geier, S.**, Heber, U., Kupfer, T., Ziegerer, E., Heuser, C., Classen, L., Cordes, O.; *Binaries discovered by the MUCHFUSS project: SDSS J162256.66+473051.1 – An eclipsing subdwarf B binary with a brown dwarf companion*, 2014, A&A, 564, 98

Schaffenroth, V., **Geier, S.**, Drechsel, H., Heber, U., Wils, P., Østensen, R. H., Maxted, P. F. L., di Scala, G.; *A new bright eclipsing hot subdwarf binary from the ASAS and SuperWASP surveys*, 2013, A&A, 553, 18

Geier, S., Heber, U., Heuser, C., Classen, L., O’Toole, S. J., Edelmann, H.; *The subdwarf B star SB 290 – A fast rotator on the extreme horizontal branch*, 2013, A&A, 551, L4

Geier, S., Classen, L., Heber, U.; *The Fast-Rotating, Low-gravity Subdwarf B Star EC 22081-1916: Remnant of a Common Envelope Merger Event*, 2011, ApJ, 733, L13

Geier, S., Schaffenroth, V., Drechsel, H., Heber, U., Kupfer, T., Tillich, A., Østensen, R. H., Smolders, K., Degroote, P., Maxted, P. F. L., Barlow, B. N., Gänsicke, B. T., Marsh, T. R., Napiwotzki, R.; *Binaries Discovered by the MUCHFUSS Project: SDSS J08205+0008 – An Eclipsing Subdwarf B Binary with a Brown Dwarf Companion*, 2011, ApJ, 731, L22

Geier, S., Edelmann, H. and Heber, U., Morales-Rueda, L.; *Discovery of a close substellar companion to the hot subdwarf star HD149382 – The decisive influence of substellar objects on late stellar evolution*, 2009, ApJ, 702, L96

Supernova type Ia progenitors and ejected donor remnants

Geier, S., Marsh, T. R., Wang, B., Dunlap, B., Barlow, B. N., Schaffenroth, V., Chen, X., Irrgang, A., Maxted, P. F. L., Ziegerer, E., Kupfer, T., Miszalski, B., Heber, U., Han, Z., Shporer, A., Telting, J. H., Gnsicke, B. T., Østensen, R. H., O’Toole, S. J., Napiwotzki, R.; *A progenitor binary and an ejected mass donor remnant of faint type Ia supernovae*, 2013, A&A, 554, 54

Geier, S., Fürst, F., Ziegerer, E., Kupfer, T., Heber, U., Irrgang, A., Wang, B., Liu, Z., Han, Z., Sesar, B., Levitan, D., Kotak, R., Magnier, E., Smith, K., Burgett, W. S., Chambers, K., Flewelling, H., Kaiser, N., Wainscoat, R., Waters, C.; *The fastest unbound star in our Galaxy ejected by a thermonuclear supernova*, 2015, Science, 347, 1126

Papers accepted for publication

Close hot subdwarf binaries

Kupfer, T., **Geier, S.**, Heber, U., Østensen, R. H., Barlow, B. N., Maxted, P. F. L., Heuser, C., Schaffenroth, V., Gänsicke, B. T.; *Hot subdwarf binaries from the MUCHFUSS project – Analysis of 12 new systems and a study of the short period binary population*, 2015, A&A, in press (arXiv:1501.03692)

Geier, S., Kupfer, T., Heber, U., Schaffenroth, V., Barlow, B. N., Østensen, R. H., O’Toole, S. J., Ziegerer, E., Heuser, C., Maxted, P. F. L., Gänsicke, B. T., Marsh, T. R., Napiwotzki, R., Brünner, P., Schindewolf, M., Niederhofer, F.; *The catalogue of radial velocity variable hot subluminous stars from the MUCHFUSS project*, 2015, A&A, in press (arXiv:1502.04086)

Hot subdwarf stars in close-up view

IV. Helium abundances and the ^3He isotopic anomaly of subdwarf B stars[★]

S. Geier^{1,2}, U. Heber¹, H. Edelmann¹, L. Morales-Rueda³, D. Kilkenny⁴, D. O'Donoghue^{5,6},
T. R. Marsh⁷, and C. Copperwheat^{8,7}

¹ Dr. Karl Remeis-Observatory & ECAP, Astronomical Institute, Friedrich-Alexander University Erlangen-Nuremberg, Sternwartstr. 7, 96049 Bamberg, Germany
e-mail: sgeier@eso.org

² European Southern Observatory, Karl-Schwarzschild-Str. 2, 85748 Garching, Germany

³ Department of Astrophysics, Faculty of Science, Radboud University Nijmegen, PO Box 9010, 6500 GL Nijmegen, The Netherlands

⁴ Department of Physics, University of Western Cape, Private Bag X17, 7535 Bellville, South Africa

⁵ South African Astronomical Observatory, PO Box 9, 7935 Observatory Cape Town, South Africa

⁶ Southern African Large Telescope Foundation, PO Box 9, 7935 Observatory Cape Town, South Africa

⁷ Department of Physics, University of Warwick, Coventry CV4 7AL, UK

⁸ Astrophysics Research Institute, Liverpool John Moores University, Twelve Quays House, Egerton Wharf, Birkenhead CH 41 1LD, UK

Received 11 June 2013 / Accepted 22 July 2013

ABSTRACT

Atmospheric parameters and helium abundances of 44 bright subdwarf B stars have been determined. More than half of our sample consists of newly discovered stars from the Edinburgh Cape survey. We showed that effective temperatures and surface gravities can be derived from high resolution echelle spectra with sufficient accuracy. Systematic uncertainties have been determined by comparing the parameters derived from the high resolution data with the ones derived from medium resolution spectra. Helium abundances have been measured with high accuracy. Besides the known correlation of helium abundance with temperature, two distinct sequences in helium abundance have been confirmed. Significant isotopic shifts of helium lines due to an enrichment in ^3He have been found in the spectra of 8 subluminous B stars (sdBs). Most of these stars cluster in a small temperature range between 27 000 K and 31 000 K very similar to the known ^3He -rich main sequence B stars, which also cluster in such a small strip, but at different temperatures. Both the helium sequences and the isotopic anomaly are discussed.

Key words. subdwarfs – stars: atmospheres – stars: abundances – stars: fundamental parameters

1. Introduction

Subluminous B stars (sdBs) have similar colours and spectral characteristics to main sequence stars of spectral type B, but are much less luminous. Strong line broadening and the early confluence of the Balmer series is caused by the high surface gravities ($\log g \approx 5.0\text{--}6.0$) of these compact stars ($R_{\text{sdB}} \approx 0.1\text{--}0.3 R_{\odot}$). SdBs are considered to be core helium-burning stars with very thin hydrogen envelopes and masses of about half a solar mass (Heber 1986) located at the extreme end of the horizontal branch (EHB).

The origin of these stars is unclear. A mass loss mechanism must manage to remove all but a tiny fraction of the hydrogen envelope at about the same time as the helium core has attained the mass ($\approx 0.5 M_{\odot}$) required for the helium flash. The reason for this mass loss is still unknown. Several single star scenarios invoke enhanced stellar winds or interaction with the stellar environment (see Heber 2009 for a review).

However, Mengel et al. (1976) showed that the required strong mass loss can occur in a close-binary system. The progenitor of the sdB star has to fill its Roche lobe near the tip of

the red-giant branch (RGB) to lose most of its hydrogen-rich envelope. The merger of binary white dwarfs (WDs) was investigated by Webbink (1984) who showed that an EHB star can form when two helium core white dwarfs merge and the product is sufficiently massive to ignite helium.

Maxted et al. (2001) determined a very high fraction of radial velocity variable sdB stars (see also Morales-Rueda et al. 2003; Napiwotzki et al. 2004a; Copperwheat et al. 2011). Han et al. (2002, 2003) used binary population synthesis models and studied the stable Roche lobe overflow (RLOF) channel, the common envelope ejection (CE) channel, where the mass transfer to the companion is dynamically unstable, and the He-WD merger channel.

The formation of sdBs has also been related to the origin of the even more enigmatic He-sdO/Bs (Ahmad & Jeffery 2003; Naslim et al. 2010; Ströer et al. 2007; Hirsch & Heber 2009). The so-called late hot flasher scenario was proposed to form these objects (Lanz et al. 2004; Miller-Bertolami et al. 2008).

At first glance, determining the helium abundance in sdB atmospheres seems to be the best diagnostic tool to distinguish between the different formation channels. While the merger of two He-WDs would form a pure He-star, a wide range of helium abundances is predicted by the late hot flasher scenario. Different

[★] Tables 1 and 2 and Appendix A are available in electronic form at <http://www.aanda.org>

mass-loss on the RGB, either triggered via single-star or binary evolution, may also leave an imprint on the helium abundance of the formed sdB.

Unfortunately, the primordial helium abundance of sdB stars is significantly affected by processes in the hot and very dense atmospheres of these stars. Sargent & Searle (1966) found sdB stars to be helium deficient for the first time. Greenstein et al. (1967) suggested that diffusion might cause the observed helium deficiency. However, theoretical diffusion models yielded only little success (e.g. Michaud et al. 1983), since the timescales for the gravitational settling were predicted to be too short. The atmospheres of sdBs should not only be depleted in helium, but essentially helium-free. Several attempts have been made to model the atmospheres of sdBs by invoking radiative levitation and mass loss caused by stellar winds to counteract the gravitational settling (Bergeron et al. 1988; Michaud et al. 1989; Fontaine & Chayer 1997; Ohl et al. 2000; Unglaub & Bues 2001).

Diffusion not only affects the elemental abundances, but can also lead to a separation of different isotopes. When a heavier isotope is significantly affected by gravitational settling, the lighter one appears to be enriched in the atmosphere. An enrichment of ^3He has initially been found in main sequence B stars with subsolar helium abundance (Sargent & Jugaku 1961; Hartoog & Cowley 1979) and explained by diffusion processes (Vauclair et al. 1974). Feige 86 was the first horizontal branch star showing this anomaly (Hartoog 1979). Eventually Heber (1987) detected strong line shifts in the sdB star SB 290 and the blue horizontal branch star PHL 25 indicating that basically the whole helium content of the atmosphere consists of ^3He . Later, Edelmann et al. (2001) and Heber & Edelmann (2004) found another three sdBs (Feige 36, BD +48 2721, PG 0133+114) where ^3He is enriched in the atmosphere.

Finally, diffusion may change the atmospheres of hot subdwarfs in an even more substantial way. Miller-Bertolami et al. (2008) argued that due to diffusion processes He-sdOs will turn into hydrogen rich subdwarfs before they evolve towards the white dwarf graveyard. The discovery of sdBs with He abundances between the normal sdBs and the He-rich ones seems to be consistent with this scenario (Ahmad et al. 2007; Vennes et al. 2007; Naslim et al. 2011, 2012).

In this paper, we determine the helium abundances and isotopic shifts caused by enrichment of ^3He of 44 sdBs from high-resolution spectroscopy. Previous papers of this series dealt with the rotational properties of sdB binaries (Geier et al. 2010, Paper I), the rotational properties of single sdBs (Geier & Heber 2012, Paper II) and the metal abundances of sdBs in the context of diffusion (Geier 2013, Paper III).

In Sect. 2 we give an overview of the observations taken with different instruments. The determination of the atmospheric parameters and helium abundances as well as an evaluation of the uncertainties are described in Sect. 3. In Sects. 4–6 we present our results regarding the atmospheric parameters, helium abundances and isotopic shifts, which are discussed further in Sect. 7. Finally, a summary is given in Sect. 8.

2. Observations and data reduction

39 bright subdwarf B stars were observed with the FEROS spectrograph ($R = 48\,000$, 3750–9200 Å) mounted at the ESO/MPG 2.2 m telescope in La Silla. The spectra were downloaded from the ESO science archive and reduced with the FEROS-DRS pipeline under the ESO MIDAS context in optimum extraction mode. The single spectra of all programme stars were

RV-corrected and co-added in order to achieve higher signal-to-noise.

Five stars were observed with the FOCES spectrograph ($R = 30\,000$, 3800–7000 Å) mounted at the CAHA 2.2 m telescope and the spectra were also reduced with the MIDAS package.

Medium resolution spectra of 12 stars were obtained with the ISIS spectrograph ($R \approx 4000$, $\lambda = 3440\text{--}5270$ Å) mounted at the WHT. Nine sdBs discovered in the course of the Edinburgh-Cape blue object survey (Stobie et al. 1997; Kilkenny et al. 1997; O’Donoghue et al. 2013) have been observed with the grating spectrograph and intensified Reticon Photon Counting System on the 1.9 m telescope of the SAAO ($R \approx 1300$, $\lambda = 3300\text{--}5600$ Å). Spectra of five sdBs have been taken with the CAFOS spectrograph mounted at the CAHA 2.2 m telescope ($R \approx 1000$, $\lambda = 3500\text{--}5800$ Å). Table 1 provides a detailed overview of the observed sample and the data.

3. Atmospheric parameter determination and systematic effects

3.1. High-resolution echelle spectra – known issues

Most spectroscopic studies of sdB stars have relied on low and medium-resolution data ($R \approx 500\text{--}4000$). Fitting model atmospheres to high signal-to-noise ratio (S/N) data allows us to determine T_{eff} and $\log g$ with formal uncertainties lower than the systematic effects between different model grids (Green et al. 2008; Heber et al. 2000). This standard technique yielded key results on which our current understanding of sdB formation and evolution is founded (e.g. Heber 1986; Heber & Langhans 1986; Saffer et al. 1994; Maxted et al. 2001; Edelmann et al. 2003; Green et al. 2008; Østensen et al. 2010; Copperwheat et al. 2011; Vennes et al. 2011; Geier et al. 2011b; Németh et al. 2012).

On the other hand, high resolution echelle spectrographs ($R > 10\,000$) are widely used in astronomy today. However, data reduction and analysis of echelle spectra is difficult. Even if sophisticated data reduction pipelines are available, issues such as fringing, extraction errors, insufficient order merging and normalisation remain. Due to the low luminosity of sdBs, echelle spectroscopy of these objects is rather challenging, as only a few of them have magnitudes brighter than 10th. Furthermore, sdBs are hot stars and the most important lines for their analysis are found in the bluest parts of optical spectra; unfortunately, echelle spectrographs are often not very sensitive in the blue, particularly where fibre-feeds are used.

The spectra of sdBs are dominated by strong and broad hydrogen Balmer lines, which are the key to deriving their atmospheric parameters. Since these lines are usually broader than the single echelle orders, merging errors can severely affect the parameter determination and suspicious features can be hard to spot, particularly in low S/N data. However, Lisker et al. (2005) successfully analysed high resolution spectra of sdBs observed in the course of the ESO-SPY project (Napiwotzki et al. 2003). In this case, the UVES spectrograph at the ESO-VLT was used, which is very sensitive in the blue wavelength range. Furthermore, rectification of the data was done by dividing by the featureless spectra of DC-type white dwarfs. However, most of the known DC white dwarfs are too faint to be observed with 2 m-class telescopes and it is therefore not clear, in general, whether reliable atmospheric parameters of sdBs can be derived from medium S/N (30–50), high resolution echelle spectra.

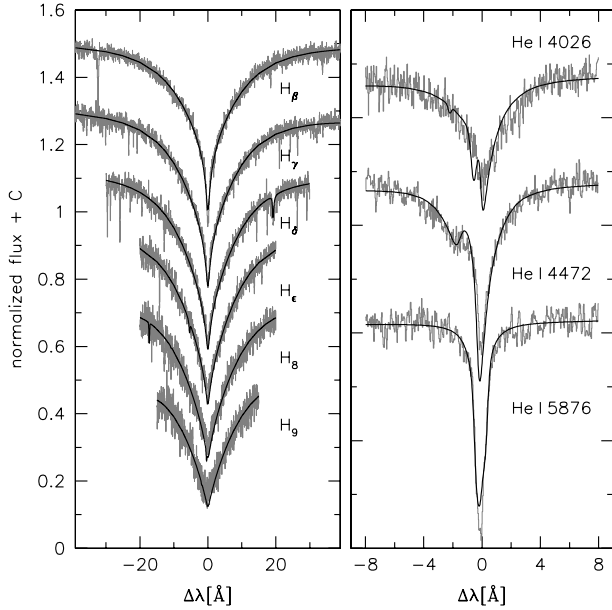


Fig. 1. Example fit of LTE models to the Balmer and selected He I lines in the FEROS spectrum of EC 03591–3232.

3.2. Determination of atmospheric parameters

Atmospheric parameters and helium abundances of our sample have been determined by fitting model spectra to the hydrogen Balmer and helium lines of the high-resolution spectra using the SPAS routine developed by H. Hirsch (see Fig. 1). The method is described in Copperwheat et al. (2011). To derive the atmospheric parameters we used local thermodynamic equilibrium (LTE) model with solar metallicity for stars with effective temperatures between 24 000 K and 30 000 K. The hottest stars with $T_{\text{eff}} > 30\,000$ K have been fitted with LTE models with supersolar metallicity (see Copperwheat et al. 2011).

Due to the high resolution of the spectra the formal errors derived with a bootstrapping algorithm are much smaller than the typical systematic offsets between different model grids ($\Delta T_{\text{eff}} \approx 500$ K, $\Delta \log g \approx 0.05$). However, these formal uncertainties must not be adopted as error estimates, because systematic shifts are the dominant error source in this case.

3.3. Comparison with medium resolution data

Due to the caveats discussed in Sect. 3.1, the parameter determination from the high-resolution spectra needs to be checked and systematic effects have to be quantified properly. We used medium-resolution spectra obtained with the ISIS, the SAAO-Reticon and the CAFOS spectrograph and analysed them in the same way as the high-resolution data.

The ISIS and CAFOS spectra have a very high S/N (>100) and cover the blue spectral range down to the Balmer jump. These spectra are perfectly suited for the determination of atmospheric parameters. Again, formal errors are much smaller than the typical systematic offsets between different model grids, which are adopted as error estimates in this case. The SAAO-Reticon spectra also cover the higher Balmer lines, but their quality is inhomogeneous. Although the formal fitting errors can be large – ranging from 700 K to 2000 K in T_{eff} and from 0.12 to 0.28 in $\log g$ – they provide a valuable consistency check for the results derived from the high-resolution data.

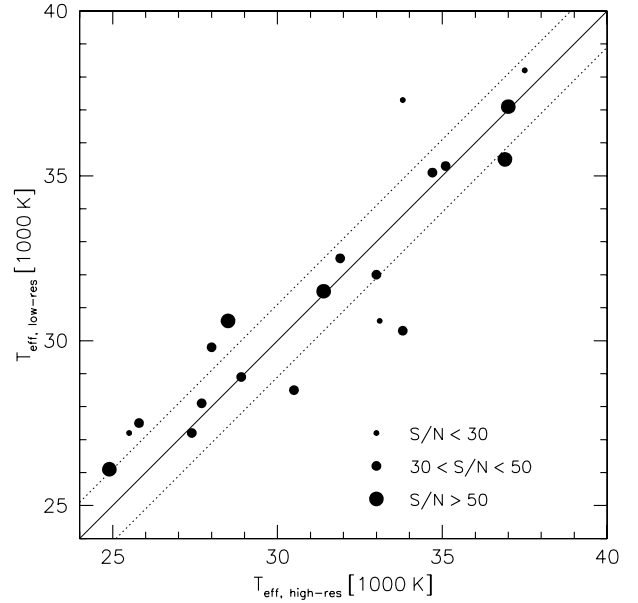


Fig. 2. Effective temperature derived from high-resolution spectra plotted against effective temperature derived from medium resolution spectra (ISIS, SAAO-Reticon, CAFOS). The dotted lines mark the average deviation between the two datasets. The size of the points scales with the data quality of the high-resolution spectra.

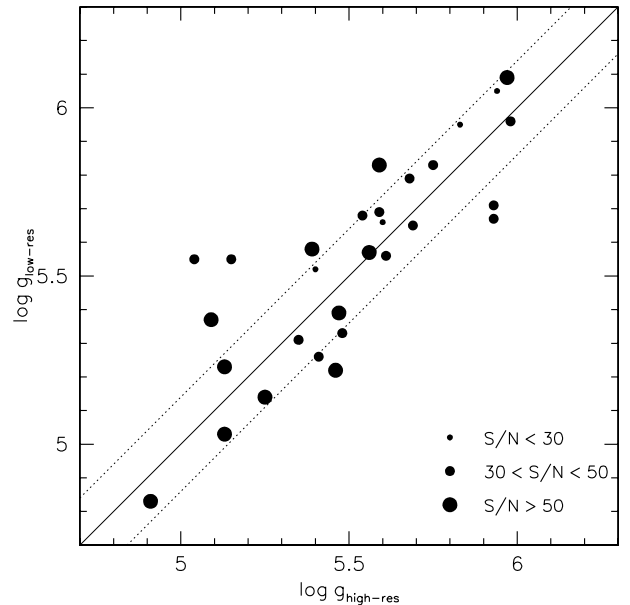


Fig. 3. Surface gravity derived from high-resolution spectra plotted against surface gravity derived from medium-resolution spectra (see Fig. 2).

Figures 2 and 3 show the comparison between the high-resolution and the medium-resolution parameters. In general, the consistency between the parameters derived from high- and medium-resolution data is reasonable.

In order to quantify the uncertainties in the parameter determination, the averages of the shifts with respect to the parameters derived from medium-resolution spectra have been calculated; these are $\Delta T_{\text{eff}} \approx 1100$ K and $\Delta \log g \approx 0.12$. The high resolution spectra of PG 1616+144, PG 1710+490 and PG 2205+023 have S/N values below 30 and hence show large deviations especially in T_{eff} (up to 3500 K). These stars have been excluded before calculating the average. Although not

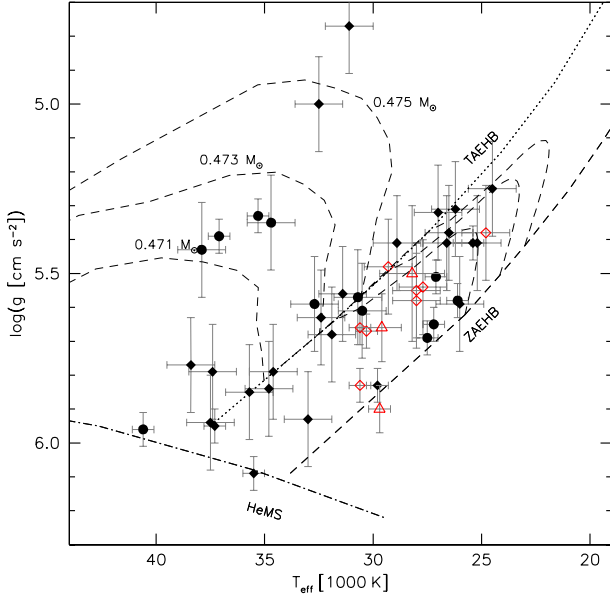


Fig. 4. $T_{\text{eff}} - \log g$ -diagram for the entire sample under study. The helium main sequence (HeMS) and the EHB band (limited by the zero-age EHB, ZAEHB, and the terminal-age EHB, TAEHB) are superimposed with EHB evolutionary tracks for solar metallicity taken from Dorman et al. (1993) labelled with their masses. Open symbols mark objects where isotopic shifts due to an enrichment of ^3He were detected, filled symbols objects with atmospheres dominated by ^4He . The diamonds mark stars belonging to the upper helium sequence, the circles stars belonging to the lower sequence (see Fig. 5). The triangles mark the three sdBs with enriched ^3He from literature (Heber et al. 1984; Edelman et al. 1999; Morales-Rueda et al. 2003).

perfect, the above uncertainties are consistent with values found in the literature (see Appendix A).

4. Atmospheric parameters

The atmospheric parameters of all 44 programme stars are shown in Table 2. The final parameters are derived either from high S/N ISIS and CAFOS spectra, if available, or from high-resolution spectra obtained with FEROS and FOCES. The $T_{\text{eff}} - \log g$ -diagram of the whole sample under study is shown in Fig. 4. All stars are concentrated on or above the EHB, fully consistent with theory, and we therefore conclude that the atmospheric parameter determination is of sufficient quality (see also the comparison with independent determinations from the literature given in Table A.1).

5. Helium abundances

High resolution spectra are very well suited for measuring accurate elemental abundances of sdBs, because the rather weak lines of helium and metals are fully resolved. We therefore used the FEROS and FOCES spectra to determine the helium abundances of our programme stars. The formal uncertainties are very small ($\Delta \log y = 0.01-0.07$) and comparable to the deviations measured when analysing several single spectra of one object. Taking systematic effects into account the helium abundances should therefore be accurate to ≈ 0.1 dex. The results are given in Table 2.

Figure 5 shows the helium abundances of our sample plotted against effective temperature. All but two of our programme stars have the subsolar helium abundances typical of sdB stars.

Edelmann et al. (2003) reported a correlation of helium abundance with temperature, which was subsequently confirmed by Lisker et al. (2005) and Németh et al. (2012). This correlation can be clearly seen in our sample as well.

Edelmann et al. (2003) also reported the discovery of two distinct sequences showing a similar correlation with temperature. The “low sequence” is offset by about 2 dex from the “high sequence”. Lisker et al. (2005) and Geier et al. (2011b) could not confirm this finding, but the sample size of these studies was smaller than that of Edelmann et al. (2003). Németh et al. (2012) studied a sample of bright hot sdwarfs spanning the whole temperature and helium abundance range from sdBs to He-sdOs and found indications for the two distinct sequences although, in their sample, the lower sequence appears to be less steep than reported by Edelmann et al. (2003).

The two distinct sequences are also visible in our data and combining these with the results of other studies (Saffer et al. 1994; Maxted et al. 2001; Edelmann et al. 2003; Morales-Rueda et al. 2003; Lisker et al. 2005; Østensen et al. 2010; Geier et al. 2011b; Németh et al. 2012) the underlying pattern becomes more apparent. In Fig. 5, all of these results are over-plotted with the two regression lines calculated by Edelmann et al. (2003) as well as the regression line for the lower sequence calculated by Németh et al. (2012) based on their results spanning a larger range in effective temperatures and helium abundances. The two lines by Edelmann et al. (2003) match very well with the sequences seen in our sample, while the line by Németh et al. (2012) is slightly different. However, as has been correctly pointed out by Németh et al. (2012), those lines are only very crude tentative models, which certainly do not reflect the real complexity of the underlying data.

Defining a dividing line between the two helium sequences by eye, which follows the relation $\log y = 0.127 T_{\text{eff}}/1000 \text{ K} - 6.718$, the numbers of stars belonging to the different sequences can be counted. From our sample of 44 stars, 31 of them (70%) are associated with the upper sequence while 13 (30%) belong to the lower one. The respective fractions of the full sample of 383 sdBs are 82% and 18%, but the full sample is likely to be biased against low helium abundances because most analyses are based on low- and medium-resolution spectra where weak He lines are often not detectable. We therefore regard the respective fractions derived from our sample to be more reliable.

6. The ^3He isotopic anomaly

The high-resolution spectra are also perfectly suited to search for small shifts in the rest wavelengths of the helium lines due to the enrichment of ^3He . Wavelength shifts can be caused by different effects (for example, the presence of magnetic fields or pressure shifts in high density environments), but the helium line shifts caused by the enrichment of ^3He can be modelled quite accurately and show a typical pattern. While some lines like He I 5876 are only shifted by 0.04 \AA towards redder wavelengths, the shifts of He I 4922 and He I 6678 are significant (0.33 and 0.50 \AA respectively; Fred et al. 1951; given in Hartoog & Cowley 1979). Displacements of this order can be easily detected in high resolution spectra.

All of the stars in our sample have been examined and in 8 cases, isotopic shifts due to the presence of ^3He are clearly visible (Figs. 6, 7). One of these (BD+48 2721) has already been discovered by Edelmann et al. (2001).

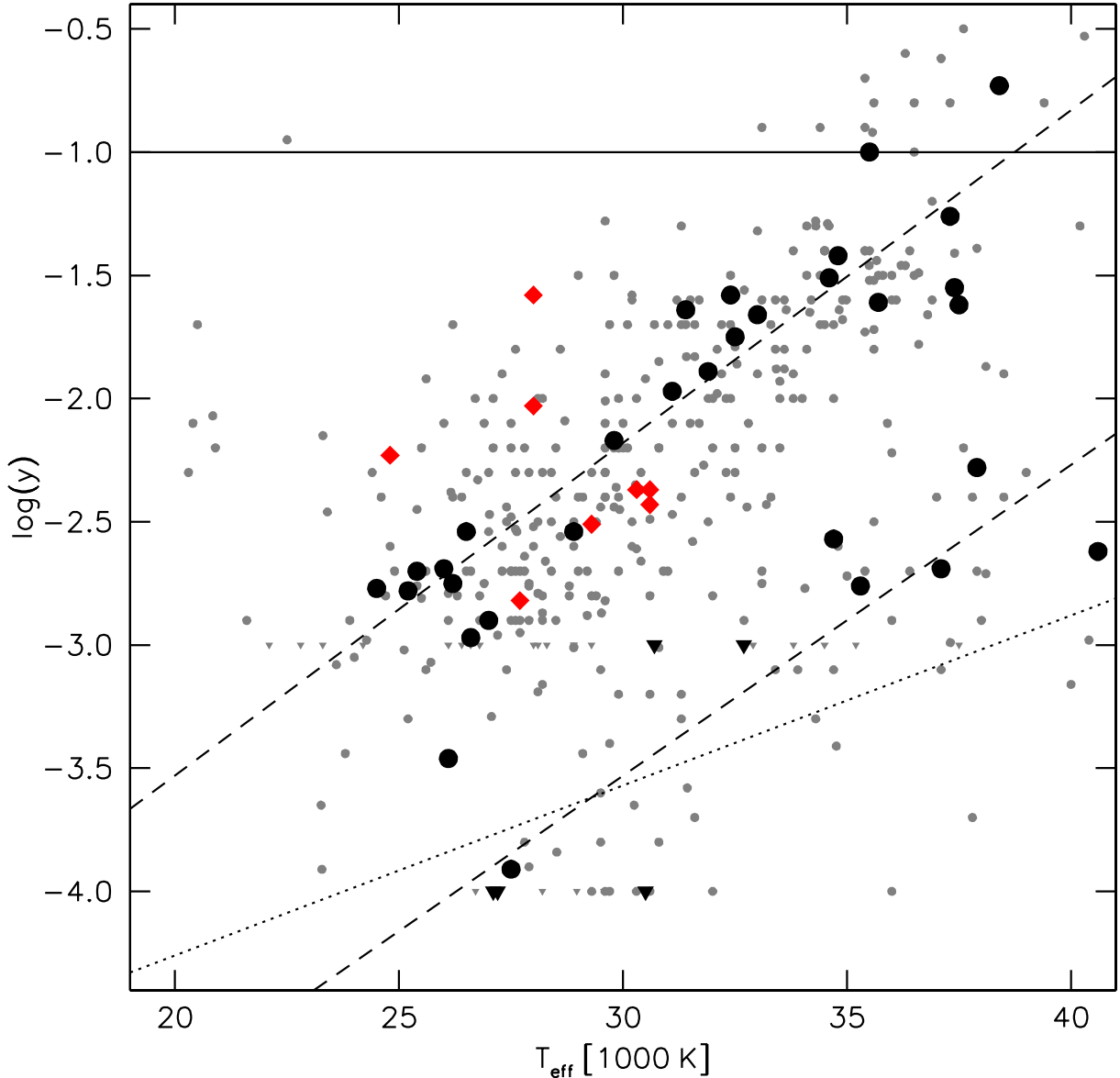


Fig. 5. Helium abundance $\log y$ plotted against effective temperature. The filled symbols mark the results from our study. Filled diamonds mark objects where isotopic shifts due to an enrichment of ^3He were detected, filled circles objects with atmospheres dominated by ^4He . Upper limits are marked with triangles. The solid horizontal line is drawn at solar helium abundance. The two dashed lines are regression lines for the two distinct helium sequences taken from Edelmann et al. (2003). The dotted regression line for the lower sequence is taken from Németh et al. (2012). Measurements taken from literature are plotted as grey symbols.

7. Discussion

7.1. Helium sequences

The reasons for the correlation of the helium abundance with temperature and the bimodal structure in the $T_{\text{eff}} - \log y$ diagram are unknown, although several suggestions have been made and are discussed briefly below.

Photospheric convection has been proposed as the cause of the relative enrichment of helium in sdB atmospheres towards higher temperature. Greenstein & Sargent (1974) suggested that a $\text{He}^+/\text{He}^{2+}$ convection zone could transport helium from deeper layers into the photosphere of subdwarfs hotter than 30 000 K (but see also Groth et al. 1985). However, Michaud et al. (2011) calculated complete stellar evolution models, including the effects of atomic diffusion and radiative acceleration, to study the abundance anomalies observed on the hot end of the HB.

Their models, which assume extra mixing but no stellar-wind mass loss, are in general agreement with the observed metal abundances of sdB stars (Geier 2013) as well as the helium abundances for $T_{\text{eff}} > 25\,000$ K. Furthermore, they show that diffusion effects reach far deeper than the stellar atmospheres themselves and should also be dominant in the $\text{He}^+/\text{He}^{2+}$ convection zone (Moehler, Michaud, priv. comm.).

According to the Michaud et al. (2011) models, the observed scatter in helium abundance is caused by different HB ages and differences in the initial metallicity of the progenitor populations, but these models predict neither the observed correlation with temperature nor the two helium sequences. If the helium abundance does depend on the age of the sdB, one would expect to see a continuous distribution and not a concentration in distinct sequences.

Aznar Cuadrado & Jeffery (2002) argued that, due to tidal effects, sdBs residing in short-period binaries might have higher

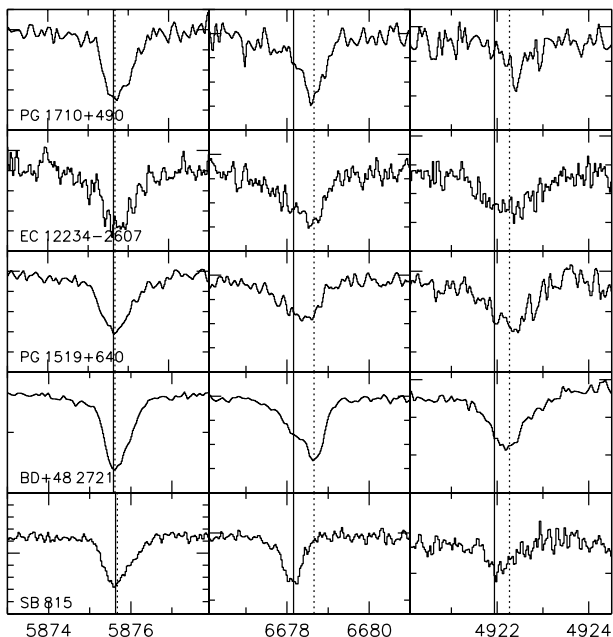


Fig. 6. Helium lines of sdB stars. The rest wavelengths of the ^4He (solid) and ^3He lines (dotted) are plotted as vertical lines. The rest wavelengths of the ^3He lines have been taken from Hartoog & Cowley (1979). The stars are highly enriched in ^3He , but also show a component of ^4He . For comparison, the He lines of SB 815 are plotted in the lowest panel. This star does not show line shifts due to enrichment of ^3He .

photospheric helium content than long-period systems or single stars. Edelmann et al. (2003) suggested that this effect could be responsible for the two helium sequences – and this can be directly tested with the available data. Our current sample of bright sdBs consists mostly of stars in which no radial velocity shifts have been detected and so these sdBs are not in close binaries with stellar mass companions. On the other hand, the target sample for the MUCHFUSS project (Geier et al. 2011b), which aims at finding sdBs with massive compact companions in close orbits, consists only of RV variable stars. From the 51 sdBs drawn from the MUCHFUSS sample, 15 belong to the lower helium sequence, so the fraction of these stars is almost exactly the same as in the sample presented here. The close binary hypothesis can therefore be excluded as an explanation of the helium sequences.

O’Toole (2008) proposed another possibility: whilst the stars belonging to the upper sequence might be core helium-burning (post-)EHB stars evolving in the way modelled by, for example, Dorman et al. (1993), the sdBs forming the lower sequence could be post-RGB objects without helium burning in their cores. The latter objects are direct progenitors of He-WDs with masses ranging from $\sim 0.2 M_{\odot}$ to $0.33 M_{\odot}$ and are crossing the EHB on cooling tracks (e.g. Driebe et al. 1998). The only sdB for which the post-RGB nature could be proven unambiguously (using a trigonometric parallax) is HD 188112 (Heber et al. 2003) which also has the lowest helium abundance ($\log y = -5$) ever measured for an sdB. Two candidates of similar low mass have been discovered by Vennes et al. (2011) and Silvotti et al. (2012) but, even though these sdBs also show no detectable helium lines, their post-RGB nature is less well established than in the case of HD 188112. Observational evidence for particularly low helium abundance in post-RGB objects therefore remains weak.

Another way to probe the post-RGB scenario is the comparison of both helium populations in the $T_{\text{eff}} - \log g$ diagram (O’Toole 2008). In Fig. 8, the stars associated with the upper sequence are plotted. Most sdBs are situated within or close to

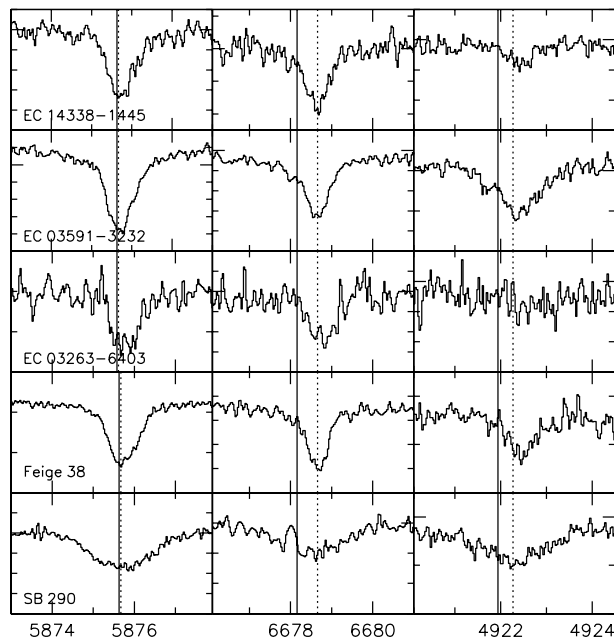


Fig. 7. Comments are as for Fig. 6 except that in these stars, the helium lines are entirely shifted to the ^3He rest wavelength and no traces of ^4He are visible. For comparison, the He lines of SB 290 are plotted in the lowest panel. This star is the prototype of sdBs enriched in ^3He (Heber 1987) but note that the lines show significant rotational broadening (Geier et al. 2013).

the EHB band but about 10% are above the EHB – consistent with the standard scenario in which most stars are core helium-burning and therefore residing on the EHB and only a minority are more evolved shell helium-burning objects (Dorman et al. 1993).

The distribution of the helium-poor sdBs is different (see Fig. 9) in that the number density of stars on and above the EHB is similar. In the classical picture, sdBs evolve from the EHB but such an even distribution is not expected because the evolutionary time on the EHB is significantly longer than that for post-EHB evolution (~ 10 times as long).

Comparing the distribution of the helium-poor sdBs with post-RGB tracks calculated by Driebe et al. (1998), one would expect these objects to be the progenitors of He-WDs with masses between $0.25 M_{\odot}$ and $0.3 M_{\odot}$. The evolutionary timescales on these tracks scale strongly with mass; while the evolution of a $0.25 M_{\odot}$ object takes of the order of 100 Myr, it shortens to only a few million years if the object is more massive ($0.3 M_{\odot}$). Accordingly, one would expect a higher density of objects with low masses in the $T_{\text{eff}} - \log g$ diagram (if the formation rate of post-RGB objects does not depend on the mass) but this is not the case – most objects are evenly distributed between the $\sim 0.25 M_{\odot}$ and $0.3 M_{\odot}$ evolutionary tracks (see Fig. 9).

Being aware of this problem, O’Toole (2008) argued that many more He-WDs with masses close to $0.3 M_{\odot}$ are formed than objects with even lower masses (e.g. Liebert et al. 2005; De Gennaro et al. 2008) which could compensate for the difference in evolutionary timescales. Given that the 18–29% of the sdB population belonging to the helium poor sequence are all direct He-WD progenitors with an evolution about 100 times shorter than the lifetime on the EHB (≈ 100 Myr), the formation rate of these objects (neglecting selection effects) would be more than ~ 20 times higher than the formation rate of core

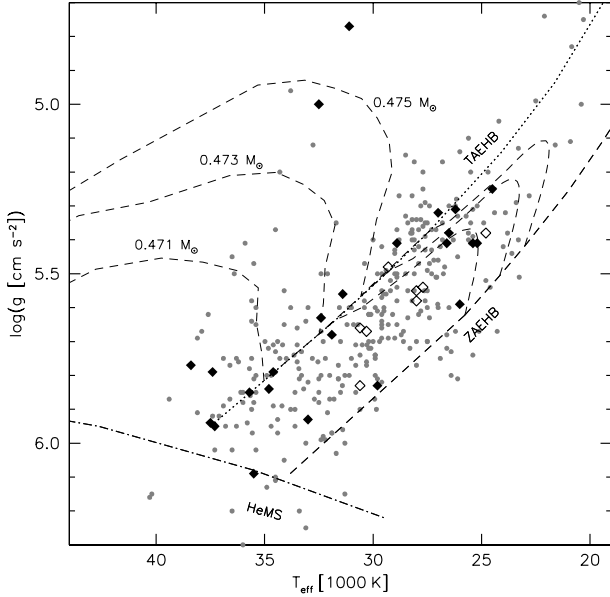


Fig. 8. $T_{\text{eff}} - \log g$ -diagram for the sDBs associated with the upper helium sequence (see Fig. 4).

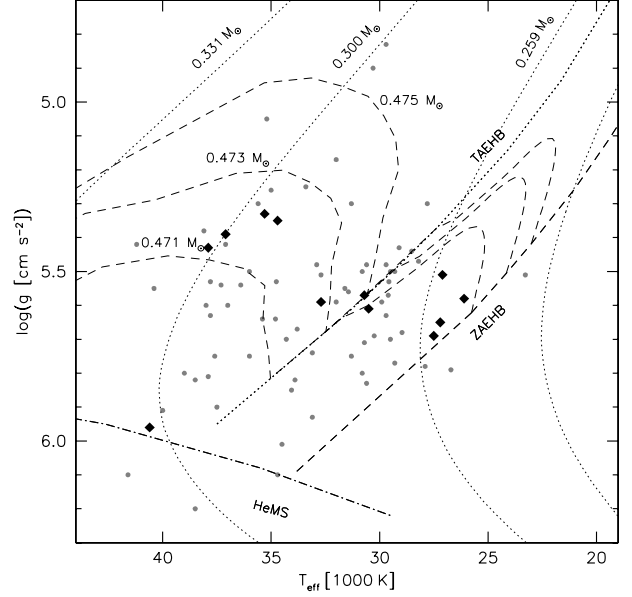


Fig. 9. $T_{\text{eff}} - \log g$ -diagram for the sDBs associated with the lower helium sequence. The figure is similar to Fig. 4 with additional evolutionary tracks for post-RGB objects plotted as dotted lines (Driebe et al. 1998).

helium-burning sDBs. Even so, the distribution of objects seen in Fig. 9 is still hard to explain with the post-RGB scenario. The crowding near the EHB remains especially suspicious, because evolution should be more or less uniform along the tracks given by Driebe et al. (1998). The lack of objects below the EHB poses a particular problem in this respect. In contrast, a significant number of He-WD progenitors with masses between $0.16 M_{\odot}$ and $0.4 M_{\odot}$ have been discovered at temperatures below $\approx 25\,000$ K and well below the HB (see Kilic et al. 2012 and references therein). We therefore conclude that post-RGB evolution, despite being a very interesting option, is not able to explain all of the observations in a conclusive way.

7.2. Isotopic anomaly

The enrichment of ^3He in around 18% of our programme stars also remains unexplained. Figure 4 shows the distribution of these stars in the $T_{\text{eff}} - \log g$ -diagram, including the three sDBs with isotopic shifts taken from the literature. It can be clearly seen that they cluster in a narrow temperature range between $27\,000$ K and $31\,000$ K, with BD+48 2721 ($T_{\text{eff}} = 24\,800$ K) being the only exception and – given the uncertainties – this ^3He -strip could be pure. The fact that all ^3He enriched sDBs belong to the upper helium sequence (Fig. 5) might be a selection effect, because the diagnostic helium lines are too weak to measure the isotopic shifts in the helium-poor stars.

Most ^3He sDB stars show clear shifts of the He I line at 6678 \AA , indicating that almost all the helium in the atmosphere is ^3He . BD+48 2721, EC 12234–2607 and PG 1519+640 show strong lines of ^3He blended with weak components of ^4He (see Fig. 6) and these three stars cover the whole ^3He temperature strip. The isotope ratio is therefore not correlated with effective temperature.

Michaud et al. (2011) predict a mild enrichment of ^3He but, due to gravitational settling of the heavier isotope, this should be the case in all sDBs. Hartoog & Cowley (1979) studied the enrichment of ^3He in main sequence B stars and discovered a pattern strikingly similar to our results: stars enriched in ^3He were found at effective temperatures between $18\,000$ K and $21\,000$ K;

stars with lower temperatures down to $\sim 13\,000$ K show slight underabundances in helium with respect to the Sun, while the hotter stars up to $\sim 32\,000$ K are slightly overabundant in helium. The two known BHB stars with detected ^3He isotopic shifts (Feige 86, $T_{\text{eff}} = 16\,400$ K; Bonifacio et al. 1995; PHL 25, $T_{\text{eff}} = 19\,500$ K; Heber & Langhans 1986) have temperatures close to the strip detected by Hartoog & Cowley (1979).

In Figs. 4 and 5 a similar pattern can be seen. The sDBs enriched in ^3He occupy a small strip in T_{eff} , within which the helium abundance decreases towards lower temperatures and increases towards higher temperatures.

Hartoog & Cowley (1979) argued that diffusion is responsible for this effect. At low temperatures, the radiation pressure is not strong enough to support helium in the atmosphere. As soon as the temperature reaches a certain threshold value, the less massive ^3He can be supported, but not the more abundant ^4He , which leads to an enrichment of ^3He in the atmosphere. At even higher temperatures, both isotopes are enriched and the isotopic anomaly vanishes as the helium abundance rises (see also Vauclair et al. 1974).

A similar scenario might explain the more compact sDB stars. Focusing on the upper helium sequence in Fig. 5 one can see that the helium abundance is scattering around $\log y \approx -2.5$ for temperatures below $31\,000$ K. ^3He is enriched at the border region. For temperatures higher than $\approx 31\,000$ K the helium abundance is rising.

Finally, radiatively driven stellar wind mass loss might play a role (see, for example, Babel 1996 and references therein), but Hu et al. (2011) derived upper limits for this mass loss to be of the order of $10^{-15} M_{\odot} \text{ yr}^{-1}$ to allow sDBs to pulsate. However, even weak and fractionated winds might already affect the abundances in the atmospheres of sDB stars (Unglaub 2008).

8. Summary

Atmospheric parameters and helium abundances of 44 bright sDBs have been determined. We have shown that effective temperatures and surface gravities can be derived from high

resolution echelle spectra with sufficient accuracy. Systematic uncertainties have been determined by comparing the parameters derived from the high resolution data with the ones derived from medium resolution spectra. Most stars are core helium-burning, but some sdBs are already in the shell helium-burning phase.

Helium abundances have been measured with high accuracy. Besides the known correlation of helium abundance with temperature, two distinct sequences in helium abundance have been confirmed. The reasons for both the increasing helium abundance with temperature and the bimodal distribution have been discussed, but we are left without a strong conclusion.

Significant isotopic shifts of helium lines due to an enrichment in ^3He have been found in the spectra of 8 sdBs. Most of these stars cluster in a small temperature range between 27 000 K and 31 000 K very similar to the known ^3He -rich main sequence B stars, which cluster at somewhat lower temperatures. This phenomenon is most probably related to diffusion processes in the atmosphere.

Acknowledgements. S.G. was supported by the Deutsche Forschungsgemeinschaft under grant He 1356/49-1. D.K. thanks the University of the Western Cape and the South African National Research Foundation for financial support. We thank R. A. Saffer for sharing his data with us as well as N. Hambly and H. McGillivray for their contributions to the EC survey. We also thank S. J. O'Toole, S. Moehler and N. Reindl for fruitful discussions. Finally, we want to thank the referee S. Vennes for helpful comments and suggestions. Based on observations at the La Silla Observatory of the European Southern Observatory for programmes number 073.D-0495(A), 074.B-0455(A), 076.D-0355(A), 077.D-0515(A) and 078.D-0098(A). Based on observations with the William Herschel Telescope and the *Isaac Newton* Telescope operated both by the Isaac Newton Group at the Observatorio del Roque de los Muchachos of the Instituto de Astrofísica de Canarias on the island of La Palma, Spain. This paper uses observations made at the South African Astronomical Observatory (SAAO). Based on observations collected at the Centro Astronómico Hispano Alemán (CAHA) at Calar Alto, operated jointly by the Max-Planck Institut für Astronomie and the Instituto de Astrofísica de Andalucía (CSIC).

References

- Ahmad, A., & Jeffery, C. S. 2003, *A&A*, 402, 335
 Ahmad, A., Behara, N. T., Jeffery, C. S., Sahin, T., & Woolf, V. M. 2007, *A&A*, 465, 541
 Aznar Cuadrado, R., & Jeffery, C. S. 2001, *A&A*, 368, 994
 Aznar Cuadrado, R., & Jeffery, C. S. 2002, *A&A*, 385, 131
 Babel, J. 1996, *A&A*, 309, 867
 Bergeron, P., Wesemael, F., Michaud, G., & Fontaine, G. 1988, *ApJ*, 332, 964
 Blanchette, J.-P., Chayer, P., Wesemael, F., et al. 2008, *ApJ*, 678, 1329
 Bonifacio, P., Castelli, F., & Hack, M. 1995, *A&AS*, 110, 441
 Chayer, P., Fontaine, M., Fontaine, G., Wesemael, F., & Dupuis, J. 2006, *Balt. Astron.*, 15, 131
 Copperwheat, C. M., Morales-Rueda, L., Marsh, T. R., Maxted, P. F. L., & Heber, U. 2011, *MNRAS*, 415, 1381
 De Gennaro, S., von Hippel, T., Winget, D. E., et al. 2008, *AJ*, 135, 1
 Dorman, B., Rood, R. T., & O'Connell, R. W. 1993, *ApJ*, 419, 596
 Driebe, T., Schönberner, D., Bloeker, T., & Herwig, F. 1998, *A&A*, 339, 123
 Edelmann, H., Heber, U., & Napiwotzki, R. 1999, *ASP Conf. Ser.*, 169, 546
 Edelmann, H., Heber, U., & Napiwotzki, R. 2001, *Astron. Nachr.*, 322, 401
 Edelmann, H., Heber, U., Hagen, H.-J., et al. 2003, *A&A*, 400, 939
 Edelmann, H., Heber, U., Altmann, M., Karl, C., & Lisker, T. 2005, *A&A* 442, 1023
 Fontaine, G., & Chayer, P. 1997, in *Proc. of Conference on Faint Blue Stars*, eds. A. G. D., Philip, J., Liebert, R. A., Saffer, & D. S., Hayes, 169
 Fred, M., Tomkins, F. S., Brody, J. K., & Hameremesh, M. 1951, *Phys. Rev.*, 82, 406
 Geier, S. 2013, *A&A*, 549, A110
 Geier, S., & Heber, U. 2012, *A&A*, 543, A149
 Geier, S., Nesslinger, S., Heber, U., et al. 2007, *A&A*, 464, 299
 Geier, S., Heber, U., Podsiadlowski, Ph., et al. 2010, *A&A*, 519, A25
 Geier, S., Classen, L., & Heber, U. 2011a, *ApJ*, 733, L13
 Geier, S., Hirsch, H., Tillich, A., et al. 2011b, *A&A*, 530, A28
 Geier, S., Heber, U., Heuser, C., et al. 2013, *A&A*, 551, A4
 Green, E. M., Fontaine, G., Hyde, E. A., For, B.-Q., & Chayer, P. 2008, *ASP Conf. Ser.*, 392, 75
 Greenstein, J. L., & Sargent, A. I. 1974, *ApJS*, 28, 157
 Greenstein, J. L., Truran, J. W., & Cameron, A. G. W. 1967, *Nature*, 213, 871
 Groth, H. G., Kudritzki, R.-P., & Heber, U. 1985, *A&A*, 152, 107
 Han, Z., Podsiadlowski, P., Maxted, P. F. L., Marsh, T. R., & Ivanova, N. 2002, *MNRAS*, 336, 449
 Han, Z., Podsiadlowski, P., Maxted, P. F. L., & Marsh, T. R. 2003, *MNRAS*, 341, 669
 Hartoog, M. R. 1979, *ApJ*, 231, 161
 Hartoog, M. R., & Cowley, A. P. 1979, *ApJ*, 228, 229
 Heber, U. 1986, *A&A*, 155, 33
 Heber, U. 1987, *MitAG*, 70, 79
 Heber, U. 2009, *ARA&A*, 47, 211
 Heber, U., & Edelmann, H. 2004, *Ap&SS*, 291, 341
 Heber, U., & Langhans, G. 1986, in *Proc. New insights in astrophysics*, ESA SP, 263, 279
 Heber, U., Hunger, K., Jonas, G., & Kudritzki, R. P. 1984, *A&A*, 130, 119
 Heber, U., Reid, I. N., & Werner, K. 2000, *A&A*, 363, 198
 Heber, U., Edelmann, H., Lisker, T., & Napiwotzki, R. 2003, *A&A*, 411, 477
 Hirsch, H. A., & Heber, U. 2009, *JPh Conf. Ser.*, 172, 012015
 Hu, H., Tout, C. A., Glebbeek, E., & Dupret, M.-A. 2011, *MNRAS*, 418, 195
 Kilic, M., Brown, W. R., Allende Prieto, C., et al. 2012, *ApJ*, 751, 141
 Kilkenny, D., O'Donoghue, D., Koen, C., Stobie, R. S., & Chen, A. 1997, *MNRAS*, 287, 867
 Lamontagne, R., Wesemael, F., & Fontaine, G. 1987, *ApJ*, 318, 844
 Lanz, T., Brown, T. M., Sweigart, A. V., Hubeny, I., & Landsman, W. B. 2004, *ApJ*, 602, 342
 Liebert, J., Bergeron, P., & Holberg, J. B. 2005, *ApJS*, 156, 47
 Lisker, T., Heber, U., Napiwotzki, R., et al. 2005, *A&A*, 430, 223
 Maxted, P. F. L., Marsh, T. R., & North, R. C. 2000, *MNRAS*, 317, L41
 Maxted, P. F. L., Heber, U., Marsh, T. R., & North, R. C. 2001, *MNRAS*, 326, 139
 Mengel, J. G., Norris, J., & Gross, P. G. 1976, *ApJ*, 204, 488
 Michaud, G., Vauclair, G., & Vauclair, S. 1983, *ApJ*, 267, 256
 Michaud, G., Bergeron, P., Heber, U., & Wesemael, F. 1989, *ApJ*, 338, 417
 Michaud, G., Richer, J., & Richard, O. 2011, *A&A*, 529, 60
 Miller Bertolami, M. M., Althaus, L. G., Unglaub, K., & Weiss, A. 2008, *A&A*, 491, 253
 Morales-Rueda, L., Maxted, P. F. L., Marsh, T. R., North, R. C., & Heber, U. 2003, *MNRAS*, 338, 752
 Napiwotzki, R., Christlieb, N., Drechsel, H., et al. 2003, *ESO Msng*, 112, 25
 Napiwotzki, R., Karl, C. A., Lisker, T., et al. 2004a, *Ap&SS*, 291, 321
 Napiwotzki, R., Yungelson, L., Nelemans, G., et al. 2004b, *ASP Conf. Ser.*, 318, 402
 Naslim, N., Jeffery, C. S., Ahmad, A., Behara, N. T., & Sahin, T. 2010, *MNRAS*, 409, 582
 Naslim, N., Jeffery, C. S., Behara, N. T., & Hibbert, A. 2011, *MNRAS*, 412, 363
 Naslim, N., Geier, S., Jeffery, C. S., et al. 2012, *MNRAS*, 423, 3031
 Németh, P., Kawka, A., & Vennes, S. 2012, *MNRAS*, 427, 2180
 O'Donoghue, D., Kilkenny, D., Koen, C., et al. 2013, *MNRAS*, 431, 240
 Østensen, R. H., Silvotti, R., Charpinet, S., et al. 2010, *MNRAS*, 409, 1470
 Ohl, R. G., Chayer, P., & Moos, H. W. 2000, *ApJ*, 538, L95
 O'Toole, S. J. 2008, *ASP Conf. Ser.*, 392, 67
 O'Toole, S. J., & Heber, U. 2006, *A&A*, 452, 579
 Saffer, R. A., Bergeron, P., Koester, D., & Liebert, J. 1994, *ApJ*, 432, 351
 Sargent, A. W. L. W., & Jugaku, J. 1961, *ApJ*, 134, 777
 Sargent, A. W. L. W., & Searle, L. 1966, *ApJ*, 145, 652
 Silvotti, R., Østensen, R. H., Bloemen, S., et al. 2012, *MNRAS*, 424, 1752
 Stobie, R. S., Kilkenny, D., O'Donoghue, D., et al. 1997, *MNRAS*, 287, 848
 Ströer, A., Heber, U., Lisker, T., et al. 2007, *A&A*, 462, 269
 Theissen, A., Moehler, S., Heber, U., Schmidt, J. H. K., & de Boer, K. S. 1995, *A&A*, 298, 577
 Unglaub, K. 2008, *A&A*, 486, 923
 Unglaub, K., & Bues, I. 2001, *A&A*, 374, 570
 Vauclair, S., Michaud, G., & Charland, Y. 1974, *A&A*, 31, 381
 Vennes, S., Kawka, A., & Smith, J. A. 2007, *ApJ*, 668, L59
 Vennes, S., Kawka, A., & Németh, P. 2011, *MNRAS*, 410, 2095
 Webbink, R. F. 1984, *ApJ*, 277, 355

Table 1. Target sample and data.

Object	Other names	m [mag]	Instrument	No. spec	S/N	ISIS	SAAO-Reticon	CAFOS
BD+48 2721		10.7 ^V	FOCES	1	84			
[CW83] 0512–08		11.3 ^V	FEROS	2	66			
[CW83] 1758+36	PG 1758+364	11.4 ^V	FOCES	1	41			
EC 00042–2737		14.0 ^V	FEROS	2	21		+	
EC 01120–5259		13.5 ^V	FEROS	2	45		+	
EC 02542–3019		12.8 ^B	FEROS	2	39		+	
EC 03263–6403		13.2 ^V	FEROS	1	17			
EC 03408–1315		13.6 ^V	FEROS	3	29			
EC 03470–5039 ^{ir}		13.6 ^V	FEROS	2	31		+	
EC 03591–3232	CD –32 1567	11.2 ^V	FEROS	2	73			
EC 05479–5818		13.1 ^V	FEROS	3	47		+	
EC 10189–1502		13.8 ^V	FEROS	2	35			
EC 12234–2607		13.8 ^V	FEROS	3	26			
EC 13047–3049		12.8 ^V	FEROS	2	47		+	
EC 14248–2647		12.0 ^V	FEROS	1	60		+	
EC 14338–1445 ^{rv}		13.5 ^V	FEROS	3	37		+	
EC 20106–5248		12.6 ^V	FEROS	4	60		+	
EC 20229–3716		11.4 ^V	FEROS	3	69			
EC 21043–4017		13.1 ^V	FEROS	2	37			
EC 22081–1916		12.9 ^V	FEROS	3	40			
Feige 38	PG 1114+072	12.8 ^B	FEROS	5	89	+		+
Feige 65	PG 1233+426	11.8 ^B	FOCES	1	54			
GD 108	PG 0958–072	13.3 ^B	FEROS	3	61			+
HE 0447–3654		14.6 ^V	FEROS	1	26			
LB 1516 ^{l,rv}		12.7 ^B	FEROS	2	35			
PB 5333		12.5 ^B	FEROS	1	42	+		+
PG 0342+026		11.1 ^B	FEROS	4	106			
PG 0909+164 ^s		13.9 ^B	FEROS	2	33	+		
PG 0909+276		13.9 ^B	FEROS	2	52			+
PG 1303+097		14.3 ^B	FEROS	3	31	+		
PG 1505+074		12.2 ^B	FEROS	3	102	+		+
PG 1519+640 ^{rv}		12.1 ^B	FOCES	1	39	+		
PG 1616+144		13.5 ^B	FEROS	1	24	+		
PG 1653+131		14.1 ^B	FEROS	3	40	+		
PG 1710+490		12.1 ^B	FOCES	1	27	+		
PG 2151+100		12.9 ^B	FEROS	3	39			
PG 2205+023		12.9 ^B	FEROS	2	19	+		
PG 2314+076 ^{rv}		13.9 ^B	FEROS	2	41	+		
PG 2349+002		12.0 ^B	FEROS	2	50	+		
PHL 44 ^l	EC 21324–1346	13.0 ^B	FEROS	3	44			
PHL 334	TONS 61	12.5 ^B	FEROS	3	48			
	BPS CS 23431–0044							
PHL 457 ^{l,rv}	GD 1110	13.0 ^B	FEROS	2	50			
PHL 1548		12.5 ^B	FEROS	3	42			
SB 815	CD –35 15910	10.6 ^B	FEROS	2	50			

Notes. ^(s) Pulsating subdwarf of V 361 Hya type (sdBV_r). ^(l) Pulsating subdwarf of V 1093 Her type (sdBV_s). ^(rv) Radial velocity variable star in a close binary (PHL 457, LB 1516, Edelman et al. 2005; PG 1519+640, PG 2314+076, Copperwheat et al. 2011). A maximum RV shift of $54.0 \pm 1.4 \text{ km s}^{-1}$ has been detected between the three FEROS spectra of EC 14338–1445 analysed in this work. ^(ir) An excess in the infrared 2MASS colours has been reported by Copperwheat et al. (2011), which may be due to a late main sequence companion.

Table 2. Atmospheric parameters.

System	Instrument	T_{eff} [K]	$\log g$	$\log y$	
EC 20106–5248	FEROS	24 500	5.25	–2.77	
BD+48 2721	FOCES	24 800	5.38	–2.23	³ He
LB 1516	FEROS	25 200	5.41	–2.78	
PG 1653+131	ISIS	25 400	5.41	–2.70	
PG 0342+026	FEROS	26 000	5.59	–2.69	
GD 108	CAFOS	26 100	5.58	–3.46	
Feige 65	FOCES	26 200	5.31	–2.75	
PHL 457	FEROS	26 500	5.38	–2.54	
PHL 44	FEROS	26 600	5.41	–2.97	
SB 815	FEROS	27 000	5.32	–2.90	
PG 2205+023	ISIS	27 100	5.51	<–4.0	
PG 2314+076	ISIS	27 200	5.65	<–4.0	
EC 14338–1445	FEROS	27 700	5.54	–2.82	³ He
EC 03591–3232	FEROS	28 000	5.55	–2.03	³ He
EC 12234–2607	FEROS	28 000	5.58	–1.58	³ He
PG 2349+002	ISIS	28 000	5.73	–3.45	
EC 01120–5259	FEROS	28 900	5.41	–2.54	
EC 03263–6403	FEROS	29 300	5.48	–2.51	³ He
PG 1303+097	ISIS	29 800	5.83	–2.17	
PG 1519+640	ISIS	30 300	5.67	–2.37	³ He
EC 03470–5039	FEROS	30 500	5.61	<–4.0	
PG 1710+490	ISIS	30 600	5.66	–2.43	³ He
Feige 38	ISIS	30 600	5.83	–2.37	³ He
HE 0447–3656	FEROS	30 700	5.57	<–3.0	
EC 22081–1916	FEROS	31 100	4.77	–1.97	
EC 14248–2647	FEROS	31 400	5.56	–1.64	
EC 02542–3019	FEROS	31 900	5.68	–1.89	
EC 21043–4017	FEROS	32 400	5.63	–1.58	
EC 20229–3716	FEROS	32 500	5.00	–1.75	
PG 2151+100	FEROS	32 700	5.59	<–3.0	
EC 05479–5818	FEROS	33 000	5.93	–1.66	
EC 13047–3049	FEROS	34 700	5.35	–2.57	
[CW83] 1758+36	FOCES	34 600	5.79	–1.51	
PHL 334	FEROS	34 800	5.84	–1.42	
PG 0909+164	ISIS	35 300	5.33	–2.76	
PG 0909+276	CAFOS	35 500	6.09	–1.00	
EC 03408–1315	FEROS	35 700	5.85	–1.61	
PG 1505+074	ISIS	37 100	5.39	–2.69	
PG 1616+144	ISIS	37 300	5.95	–1.26	
PHL 1548	FEROS	37 400	5.79	–1.55	
EC 00042–2737	FEROS	37 500	5.94	–1.62	
EC 10189–1502	FEROS	37 900	5.43	–2.28	
[CW83] 0512–08	FEROS	38 400	5.77	–0.73	
PB 5333	ISIS	40 600	5.96	–2.62	

Appendix A: Comparison of atmospheric parameters with the literature

Atmospheric parameters of 20 of the sdBs analysed here have also been found in the literature. All parameters derived from model fits to the spectral lines are listed in Table A.1. Given the fact that different methods, models and data were used to determine these parameters, our new results are in general agreement with the literature values. The lower temperature (-2600 K) Saffer et al. (1994) derived for [CW83] 1758+36 may be more accurate, because our analysis is based on only one FOCES spectrum of mediocre quality, while the spectra used by Saffer et al. (1994) cover the Balmer jump. We reanalysed the spectrum used by Saffer et al. (1994) with our method and confirmed the parameters given in this study (Saffer refit).

The atmospheric parameters of the bright sdB, PG 0342+026, have been determined from its spectral energy distribution by Lamontagne et al. (1987), Theissen et al. (1995) and Aznar Cuadrado & Jeffery (2001). Given the higher uncertainties of this method the derived parameters are consistent with our results within the error limits.

Table A.1. Atmospheric parameters from the literature.

System	Other names	T_{eff} [K]	$\log g$	$\log y$	Reference
[CW83]0512-08		38400	5.77	-0.73	
		38000	5.6		Edelmann et al. (2001)
[CW83] 1758+36	PG 1758+364	34 600	5.79	-1.51	
		32 100	5.91	-1.82	Saffer et al. (1994)
		32 500	5.73	-1.85	Saffer refit
EC 03591-3232	CD -32 1567	28 000	5.55	-2.03	
		$27\,000 \pm 1300$	5.36 ± 0.19	-1.63 ± 0.21	Vennes et al. (2011)
		$30\,490 \pm 240$	5.71 ± 0.05	-1.92 ± 0.05	Németh et al. (2012)
EC 14248-2647		31 400	5.56	-1.64	
		$31\,880 \pm 300$	5.70 ± 0.07	-1.71 ± 0.08	Németh et al. (2012)
EC 22081-1916		31 100	4.77	-1.97	see also Geier et al. (2011a)
Feige 38	PG 1114+072	30 600	5.83	-2.37	
		29 800	5.81	-2.22	Saffer et al. (1994)
Feige 65	PG 1233+426	26 200	5.31	-2.75	
		26 500	5.60	-2.3	Saffer et al. (1994)
LB 1516		25 200	5.41	-2.78	
		26 300	5.7	-2.5	Heber (1986)
		26 100	5.4		Chayer et al. (2006)
PB 5333		40 600	5.96	-2.62	
		37 900	5.81	-2.70	Saffer et al. (1994)
PG 0342+026		26 000	5.59	-2.69	
		26 200	5.67	-2.4	Saffer et al. (1994)
PG 0909+164		35 300	5.33	-2.76	
		35 400	5.64	-2.70	Saffer (priv. comm.), Maxted et al. (2001)
PG 0909+276		35 500	6.09	-1.00	
		35 400	6.02	-0.92	Saffer et al. (1994)
PG 1303+097		29 800	5.83	-2.17	
		30 300	5.76	-1.96	Saffer (priv. comm.), Maxted et al. (2001)
PG 1505+074		37 100	5.39	-2.69	
		37 100	5.42	-3.1	NLTE, Maxted et al. (2001)
PG 1616+144		37 300	5.95	-1.26	
		36 500	6.02	-1.51	NLTE, Maxted et al. (2001)
PG 1710+490		30 600	5.66	-2.43	
		29 900	5.74	-2.22	Saffer et al. (1994)
		30 300	5.7		Chayer et al. (2006)
PG 2314+076		27 200	5.65	<-4.0	
		28 600	5.75	<-4.0	Saffer (priv. comm. refit)
PG 2349+002		28 000	5.73	-3.45	
		29 300	5.77		Saffer et al. (1994)
PHL 457	GD 1110	26 500	5.38	-2.54	
		25 000	5.3	-2.44	Heber (1986)
		28 200	5.5	-2.5	NLTE, Blanchette et al. (2008)
		29 300	5.6	-2.4	LTE, Blanchette et al. (2008)
SB 815	CD -35 15910	27 000	5.32	-2.90	
		28 800	5.4	-2.44	Heber et al. (1984)
		$28\,390 \pm 300$	5.39 ± 0.04	-3.07 ± 0.2	Németh et al. (2012)

Notes. The first lines refer to the results derived in this paper.

Hot subdwarf stars in close-up view

III. Metal abundances of subdwarf B stars^{*}

S. Geier

Dr. Karl Remis-Observatory & ECAP, Astronomical Institute, Friedrich-Alexander University Erlangen-Nuremberg, Sternwartstr. 7, 96049 Bamberg, Germany
e-mail: geier@sternwarte.uni-erlangen.de

Received 12 October 2012 / Accepted 8 November 2012

ABSTRACT

Context. Hot subdwarf B stars (sdBs) are considered to be core helium-burning stars with very thin hydrogen envelopes situated on or near the extreme horizontal branch. The formation of sdBs is still unclear as well as the chemical composition of their atmospheres. The observed helium depletion is attributed to atmospheric diffusion. Metal abundances have been determined for about a dozen sdBs only resulting in puzzling patterns with enrichment of heavy metals and depletion of lighter ones.

Aims. We present a detailed metal abundance analysis of 106 sdBs.

Methods. From high resolution spectra we measured elemental abundances of up to 24 different ions per star. A semi-automatic analysis pipeline was developed to calculate and fit LTE models to a standard set of spectral lines.

Results. A general trend of enrichment was found with increasing temperature for most of the heavier elements. The lighter elements like carbon, oxygen, and nitrogen are depleted and less affected by temperature. Although there is considerable scatter from star to star, the general abundance patterns in most sdBs are similar. State-of-the-art diffusion models predict such patterns and are in qualitative agreement with our results. However, the highest enrichments measured cannot be explained with these models. Peculiar line shapes of the strongest metal lines in some stars indicate vertical stratification to be present in the atmospheres. Such effects are not accounted for in current diffusion models and may be responsible for some of the yet unexplained abundance anomalies.

Key words. stars: atmospheres – subdwarfs

1. Introduction

Subluminous B (sdB) stars are considered to be core helium-burning stars with very thin hydrogen envelopes and masses around $0.5 M_{\odot}$ (Heber et al. 1986; Heber 2009). The formation of these objects is still unclear. SdB stars can only be formed, if the progenitor loses its envelope almost entirely after passing the red-giant stage and the remaining hydrogen-rich envelope has not retained enough mass to sustain a hydrogen-burning shell. The star cannot ascend the asymptotic giant branch, but remains on the extreme horizontal branch (EHB) until the core helium-burning stops and eventually evolves to become a white dwarf. The reason for this very high mass loss near the core helium flash is still unclear. Several single star and close binary scenarios are currently under discussion (see Han et al. 2002, 2003; Yi 2008, and references therein). Close binary evolution is a promising option, because the envelope can be lost through common envelope ejection or stable Roche lobe overflow. An alternative way of forming a single sdB is the merger of two helium white dwarfs (Webbink 1984; Iben & Tutukov 1984).

The abundance anomalies of hot subdwarf stars are very important to understand the physical properties of hot stellar atmospheres. Sargent & Searle (1966) discovered the helium deficiency of sdB stars for the first time. This finding seemed to be at variance with the big-bang theory of nucleosynthesis. Greenstein, Truran & Cameron (1974) suggested that diffusion

in the hot atmosphere of sdBs could cause the helium deficiency. Peculiar metal abundances were first reported by Baschek et al. (1972) for HD 4539. While some metals show solar abundances, others are depleted or even enriched.

Studies of optical spectra remained scarce. Heber et al. (1999, 2000) analysed high resolution spectra of four pulsating sdB stars taken with *Keck/HIRES*. Napiwotzki et al. (2001) and Telting et al. (2008) derived metal abundances of the sdB binary HE 1047–0436 and the hybrid sdB pulsator Balloon 090100001 from optical spectra, respectively. Finally, Edelmann et al. (1999, 2001), Przybilla et al. (2006) as well as Pereira & Jeffery (2008) published some preliminary results of their analysis of high resolution spectra.

Hot stars display a much larger number of spectral lines in the ultraviolet (UV) than in the optical. With the advent of the IUE satellite it became possible to determine abundances of C, N and Si from strong UV resonance lines for nine sdB stars (Lamontagne et al. 1987 and references therein). Lines of heavier metal have been analysed from IUE spectra of two stars (Baschek et al. 1982a,b). The most detailed analysis of UV spectra has been carried out by O’Toole & Heber (2006) based on spectra obtained with STIS onboard *Hubble* Space Telescope (HST). The FUSE satellite opened up the far UV (FUV) regime for abundance studies. Many sdBs have been observed, but only some have been analysed (Fontaine et al. 2006; Chayer et al. 2006; Blanchette et al. 2008; Pereira & Jeffery 2008).

Due to their faintness, quantitative analyses of hot subdwarfs in globular clusters (GCs) are restricted to low-resolution

^{*} Tables A.1–A.3 are only available at the CDS via anonymous ftp to cdsarc.u-strasbg.fr (130.79.128.5) or via <http://cdsarc.u-strasbg.fr/viz-bin/qcat?J/A+A/549/A110>

spectroscopy. Therefore constraints can only be put on the helium abundances and the analysis of metal abundances remains coarse (Heber et al. 1986; Moni Bidin et al. 2007; Moehler et al. 2007; Brown et al. 2011).

The blue horizontal branch (BHB) stars are the cooler siblings of the EHB stars ($T_{\text{eff}} < 20\,000$ K; for a review see Behr 2003a). Their chemical composition is of interest especially in GC research. Since the morphology of the HB in GCs still remains unclear, different explanations for the shape of and the apparent gaps along the HB have been proposed. In GCs all stars belong to the same population and should therefore have similar primordial chemical compositions.

Glaspey et al. (1989) were the first to discover a significant change of chemical abundances as function of the position on the HB. While a BHB star with $T_{\text{eff}} \approx 10\,000$ K in NGC 6752 showed helium and iron abundances similar to the cluster composition (which is usually derived from abundance studies of red giants), a hotter one ($T_{\text{eff}} \approx 16\,000$ K) turned out to show depletion of helium and strong enrichment of iron. Further abundance studies of BHB stars in several GCs revealed a general pattern (Moehler et al. 1999; Behr et al. 2003a; Fabbian et al. 2005; Pace et al. 2006), which can also be observed in field BHB stars (Behr et al. 2003b; For & Sneden 2010). Stars cooler than about 11 500 K show the typical abundances of their parent population, while stars hotter than that are in general depleted in helium and strongly enriched in iron and other heavy elements like titanium or chromium. Lighter elements like magnesium and silicon on the other hand have normal abundances.

Diffusion processes in the stellar atmosphere are responsible for this effect. Michaud et al. (1989) predicted such abundance patterns even before the anomalies were observed. Caloi (1999) explained the sharp transition between the two abundance patterns as disappearance of subsurface convection layers at a critical temperature. Modelling BHB stars Sweigart (1997b) indeed found that thin convective layers below the surface driven by hydrogen ionisation should exist and move closer to the surface, as soon as the temperature increases. At about 12 000 K the convection zone reaches the surface and the outer layer of the star becomes fully radiative. Since convection is very efficient in mixing the envelope, diffusion processes cannot set in below this limit. In hotter stars with radiative atmospheres helium is expected to diffuse downward, since its mean molecular weight is higher than the one of hydrogen. Heavier elements on the other hand present sufficiently large cross sections to the outgoing radiation field and experience radiative accelerations greater than gravity. Hence these elements become enriched in the atmosphere. If the radiative acceleration almost equals gravity, the diffusion timescales get very long and the element is not significantly affected by diffusion. Michaud et al. (2008) modelled these effects and reproduced for the first time the observed abundance patterns of BHB stars.

Atmospheric diffusion processes have also been invoked to explain abundance peculiarities in a wide range of stars including white dwarfs, luminous blue variables, low mass halo stars, Ap and Am stars, and HgMn stars (see Vauclair & Vauclair 1982, for a review). For sdB stars the first theoretical diffusion models met with little success only (e.g. Michaud et al. 1983). Since then several attempts have been made to model the atmospheres of sdBs (Bergeron et al. 1988; Michaud et al. 1989; Fontaine & Chayer 1997; Ohl et al. 2000; Unglaub & Bues 2001). Radiative levitation and mass loss caused by stellar winds (Vink & Cassisi 2002) have been invoked to counteract the gravitational settling as well as extra mixing at the surface (Michaud et al. 2011; Hu et al. 2011).

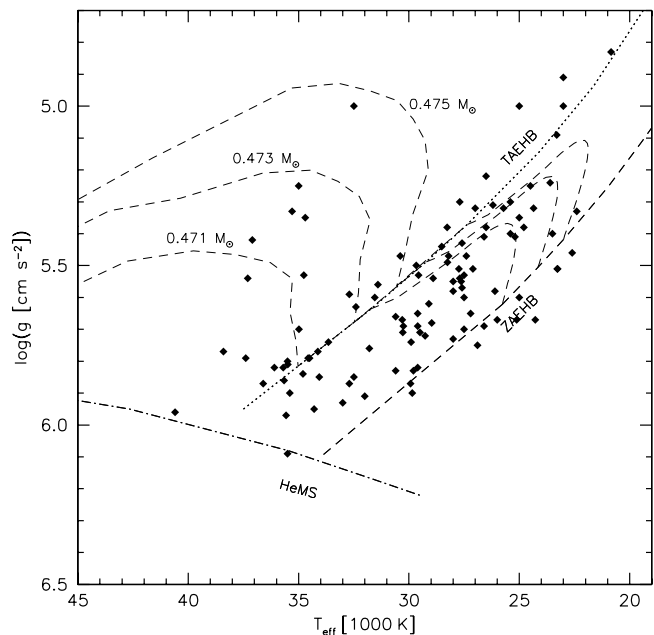


Fig. 1. Surface gravity is plotted against effective temperature. The diamonds mark the programme stars from our sample. Zero age extreme horizontal branch (ZAEHB) and terminal age extreme horizontal branch (TAEHB) are plotted as well as the helium main sequence (HeMS). Tracks for canonical EHB stars are taken from Dorman et al. (1993). The sample covers the whole parameter range on the EHB and also subdwarfs that already evolved away from the EHB.

Here we present a metal abundance analysis of 106 sdB stars, by far the largest sample to date. Previous papers of this series dealt with the rotational properties of sdB binaries (Geier et al. 2010, Paper I) and the rotational properties of single sdBs (Geier & Heber 2012, Paper II).

In Sect. 2 the dataset is described. Section 3 introduces the semi-automatic analysis pipeline used to measure elemental abundances. In Sect. 4 our results are compared with the literature and systematic uncertainties are discussed. The metal abundances, general trends as well as details for individual elements, are presented in Sect. 5. The abundance patterns of different sdB sub-populations (e.g. pulsators vs. non-pulsators) are discussed in Sects. 6–8, while Sect. 9 contains a comparison of our results with the abundance patterns on the BHB. State-of-the-art diffusion models are compared to our results in Sect. 10. Remaining abundance anomalies and peculiar shapes of metal lines are discussed in (Sect. 11). Finally, conclusions are drawn in Sect. 12.

2. Sample of sdBs with high resolution spectra

We selected a large sample of 106 sdB stars for which high resolution spectroscopy ($R = 20\,000$ – $48\,000$) suitable for the analysis of weak and sharp metal lines is available. Observations and data reduction are described in Lisker et al. (2005), Geier et al. (2012) and the Papers I and II of this series.

Our sample contains 38 radial velocity (RV) variable systems in close binary systems. The remaining 68 are apparently single stars. Eleven sdBs in our sample are known pulsators. Four of them belong to the class of short-period pulsators (V361 Hya, sdBV_r), seven are long-period pulsators (V1093 Her, sdBV_s). Our programme stars cover the entire parameter range in the $T_{\text{eff}} - \log g$ -diagram (see Fig. 1).

3. Semi-automatic abundance analysis

To derive the metal abundances we compared the observed spectra with synthetic line profiles. Metal line-blanketed LTE (local thermodynamic equilibrium) model atmospheres (Heber et al. 2000) were computed for the atmospheric parameters given in Lisker et al. (2005), Geier et al. (2012) and Papers I and II using the LINFOR Program (developed by Holweger, Steffen and Steenbock at Kiel university, modified by Lemke 1997).

A standard set of lines was chosen taking several criteria into account. First of all the lines had to be strong enough to be detectable in noisy spectra. Blends with lines of different ions were not used. Only line blends of the same ion could be handled because only one abundance was fitted to individual lines or multiplets. We selected a set of 182 metal lines from 24 different ions (see Table 1) and used atomic data from the lists of Kurucz (1992), Wiese et al. (1996), Ekberg (1993), and Hirata & Horaguchi (1995). For carbon, nitrogen, oxygen and silicon, the NIST database was used to obtain state-of-the-art atomic data.

A simultaneous fit of elemental abundance, projected rotational velocity ($v_{\text{rot}} \sin i$) and RV was then performed for each identified line using the FITSB2 routine (Napiwotzki et al. 2004). Inappropriate lines were neglected. This rejection procedure included several criteria. Equivalent width and depth of the fitted line was measured and compared to the noise level to distinguish between lines and noise features. The resulting individual RV had to be low, because all spectra were corrected to zero RV before. Otherwise the lines were considered as misidentifications or noise features. Then the fit quality given by the χ^2 had to be comparable to the average value to sort out lines contaminated by blends or artifacts caused by cosmic rays. Mean value and standard deviation were calculated from all abundance measurements of each ion. Because not all lines were present or suitable for fits in each star, the number of fitted lines differs. Upper limits were calculated by comparing the depth of the rotationally broadened synthetic spectral lines with the noise level. If only one line was found suitable for determining the abundance, the upper limits derived for the other lines of the same element where compared to this abundance. Only consistent results (within the error margins) were considered reliable, lowering the probability of misidentifications.

The accuracy of our results is limited by the quality of the spectra. Figure 2 shows two examples of spectra with highly different quality. The errors given in Table A.1 are the standard deviations of the individual line measurements. Numerical experiments were carried out to quantify the impact of noise on the result (see Paper I). We therefore regard 0.3 dex as typical statistical uncertainty of our abundance analysis. Some lines have peculiar profiles (see Sect. 11), which cannot be matched with the synthetic models. However, the equivalent widths are similar to the models and the abundance determination should therefore be correct to within ± 0.5 dex.

4. Comparison with literature and systematic uncertainties

Important sources of systematic errors are discussed in Przybilla et al. (2006) and references therein. Enhanced metal abundances can cause significant line blanketing (e.g. O'Toole & Heber 2006; Geier et al. 2007), which can affect the temperature-pressure stratification of the atmosphere and therefore the atmospheric parameter determination. However, these parameters are used to construct the model spectra for measuring the metal abundances. Some lines are much more sensitive to a change in

Table 1. Standard line list.

Ion	λ [Å]	Ion	λ [Å]	Ion	λ [Å]
Ne II	3694.212	V III	4274.417	S II	4815.552
Ne II	3713.080	Ti III	4281.555	Si III	4828.951
Si III	3796.124	S III	4284.979		4829.030
	3796.203	Fe III	4286.091		4829.111
Si III	3806.562		4286.128	Ar II	4879.863
	3806.700		4286.164	O II	4890.858
O II	3850.799	V III	4294.919	O II	4906.833
	3851.033	O II	4303.615	O II	4941.069
O II	3911.959		4303.833	O II	4943.003
	3912.107	Fe III	4304.748	N II	4994.353
C II	3920.681		4304.767		4994.360
O II	3945.038	O II	4342.009		4994.370
N II	3994.997	O II	4349.426	N II	5001.134
N II	4035.081	O II	4351.262	O II	5001.474
N II	4041.310	Fe III	4352.577	N II	5005.150
N II	4043.532	Fe III	4371.337	N II	5007.328
C III	4056.061	V III	4383.391	Sc III	5032.072
P III	4059.312	Ne II	4391.991	Fe III	5063.421
O II	4060.526	O II	4414.905	Si III	5091.250
Sc III	4061.210	O II	4416.974		5091.364
O II	4069.623	Fe III	4419.596		5091.455
	4069.886	Mg II	4481.126		5091.543
O II	4072.157		4481.325	Fe III	5127.387
P III	4080.089	O II	4452.375		5127.631
N II	4082.270	Al III	4528.945	C II	5132.947
Si IV	4088.862		4529.189		5133.281
O II	4097.258	N II	4530.410	C II	5143.495
Si IV	4116.104	Si III	4552.622	C II	5145.165
O II	4119.215	Si III	4567.840	C II	5151.085
Fe III	4122.780	Si III	4574.757	Fe III	5156.111
K II	4134.723	O II	4590.972	N II	5175.896
Fe III	4137.764	O II	4596.175	N II	5179.521
Fe III	4139.350	C II	4618.559	Fe III	5193.909
Al III	4149.913		4619.249	S II	5212.267
	4149.968	N II	4630.539		5212.620
	4150.173	N III	4634.126	Fe III	5235.658
C III	4162.877	N III	4640.644	Fe III	5276.476
Fe III	4164.731	O II	4641.810	Fe III	5282.297
	4164.916	C III	4647.418		5282.579
Fe III	4166.840	O II	4649.134	Fe III	5299.926
N II	4171.595	C III	4650.246	Fe III	5302.602
S II	4174.265		4651.016	S II	5320.723
N II	4176.195		4651.473	C II	5342.376
K II	4186.162	Si IV	4654.312	S II	5345.712
O II	4189.789	O II	4661.633		5346.084
N III	4195.760	O II	4676.235	Ti IV	5398.930
Ti III	4207.491	N II	4678.135	S II	5432.797
Ti III	4215.525	N II	4694.642	Ti IV	5492.512
Fe III	4222.271	O II	4699.003	N II	5535.346
Ca III	4233.713		4699.220	S II	5606.151
	4233.736	O II	4701.184	N II	5679.558
N II	4236.927		4701.708	N II	5686.213
	4237.047	O II	4703.163	N II	5710.766
Ca III	4240.742	O II	4705.352	Si III	5739.734
N II	4241.755	Si III	4716.654	Fe III	5833.938
	4241.786	Ar II	4735.906	N II	5893.147
S III	4253.589	C II	4737.966	N II	5931.782
K II	4263.447	C II	4744.766	N II	5941.654
C II	4267.001	C II	4747.279	Fe III	6032.604
	4267.261	Ar II	4806.021	N II	6167.755
V III	4268.183	Si III	4813.333		

the atmospheric parameters than others. Especially for the heavier elements there is a severe lack of adequate atomic data, which may introduce systematic shifts of the derived abundances.

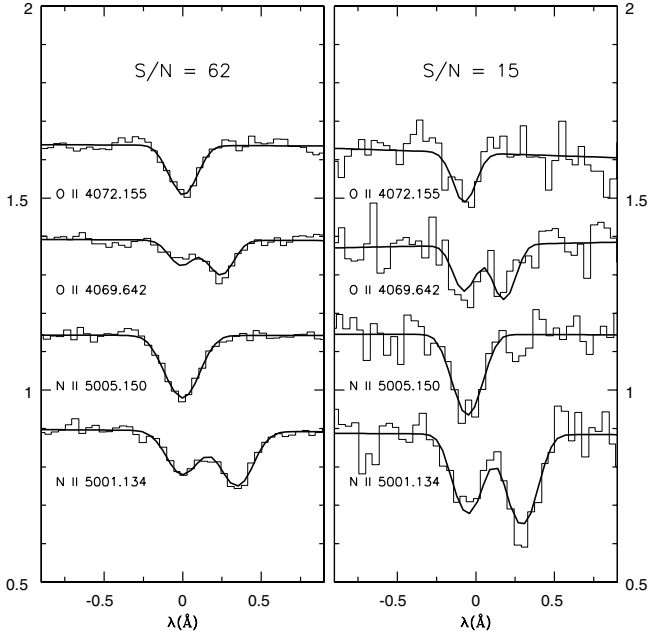


Fig. 2. Example fits of common oxygen and nitrogen lines for two spectra with different quality. Although the fit quality deteriorates, it is still possible to fit models with reasonable equivalent widths.

NLTE (non-local thermodynamic equilibrium) effects which are neglected in this analysis become important especially at higher temperatures. But not all lines are equally affected by NLTE effects. In detailed analyses of main sequence B stars, some lines were found to behave well in LTE, while others can deviate in abundance by orders of magnitude when NLTE effects are taken into account (Nieva & Przybilla 2008). Finally, microturbulence may lead to systematic trends in the abundances derived from single lines dependent on the line-strength. Due to the limited number of lines used in this study, it is not possible to measure this effect directly. However, more detailed analyses of a few stars in literature showed that in most cases microturbulence in sdB atmospheres is either negligible or small (e.g. Heber et al. 2000; Edelmann 2003; Przybilla et al. 2006).

To check whether the abundances determined with the pipeline approach are consistent with those derived by more detailed studies, we compared our results with independent determinations from literature. While we restrict ourselves to a limited set of pre-selected metal lines, other studies usually use all suitable lines in the spectra. The latter approach is more challenging and time consuming.

Metal abundances of HD 4539, PG 1710+490, PG 1627+027, PG 1716+426, PHL 457 and PG 0101+039 have been determined by Fontaine et al. (2006) and Blanchette et al. (2008) using FUV-spectra obtained with the FUSE satellite. O’Toole & Heber (2006) performed a detail analysis of UV-spectra obtained with the HST/STIS spectrograph for Feige 48, CD-24°731 and CPD-64°481. Optical high-resolution spectra were used to determine the abundances of PG 1101+249 (Feige 36, Edelmann et al. 1999), HE 1047-0436 (Napiwotzki et al. 2001), TONS 183 (Pereira & Jeffery 2008), KPD 2109+440, PG 1219+534 (Heber et al. 2000), HD 205805 and Feige 49 (Przybilla et al. 2006).

Figure 3 shows the differences of our abundances and the results from literature. Despite different wavelength ranges of the spectra, different atomic data and different methods to calculate the models (LTE or NLTE) the average scatter (± 0.2 dex) is consistent with our estimate of the statistical uncertainties. In

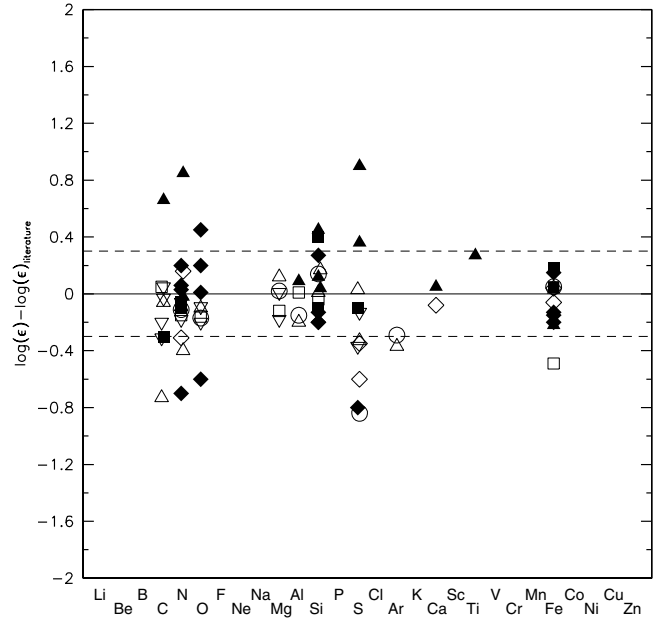


Fig. 3. Residuals between the metal abundances determined here and from literature are plotted against the chemical elements. Filled symbols mark results derived from UV-spectroscopy (squares, Fontaine et al. 2006; diamonds, Blanchette et al. 2008; triangles, O’Toole & Heber 2006), open symbols results derived from optical high-resolution spectra (circles, Edelmann et al. 1999; upward triangles, Napiwotzki et al. 2001; squares, Pereira & Jeffery 2008; diamonds, Heber et al. 2000; downward triangles, Przybilla et al. 2006). The dashed horizontal lines mark our statistical uncertainty estimate (± 0.3 dex).

conclusion, the metal abundances determined using the pipeline method are in general consistent with the ones determined by more detailed approaches.

However, in a few cases the differences between our results and the results from literature are more significant (>0.5 dex). The same holds for the ionisation equilibria of some elements, which are very sensitive to the atmospheric parameters, especially the effective temperature. In most cases such mismatches can be explained and a few of them are discussed now.

The abundances of C II and C III differ by more than 0.6 dex in some stars (CPD-64°481, HE 1047-0436) while the abundances of other elements in different ionisation stages are consistent within the error margins. Since the C II/C III abundances given in literature (Napiwotzki et al. 2001; O’Toole & Heber 2006) do not show such high deviations, we conclude that the limited number of lines used in our study leads to those systematic shifts. Especially the C II lines at 4267 Å are known to be very sensitive to NLTE effects (Nieva & Przybilla 2008). In a pilot study, Przybilla et al. (2006) derived the carbon abundance from the C II and C III lines of HD 205805 using LTE and NLTE models. The mismatch of 0.43 dex using the LTE approach consistent with our results could be significantly reduced to 0.17 dex using NLTE models. However, the similar difference between the abundances derived from C II and C III lines in the hotter sdB Feige 49, which is measured here as well, could not be reduced in this way.

The most significant differences in the carbon ionisation equilibrium are seen in HE 0101-2707 (0.9 dex) and HS 2033+0821 (1.2 dex), where the abundances derived from the C III lines are much higher than the ones derived from the C II lines. The most likely explanation for these mismatches are peculiarities in the line profiles discussed in Sect. 11.

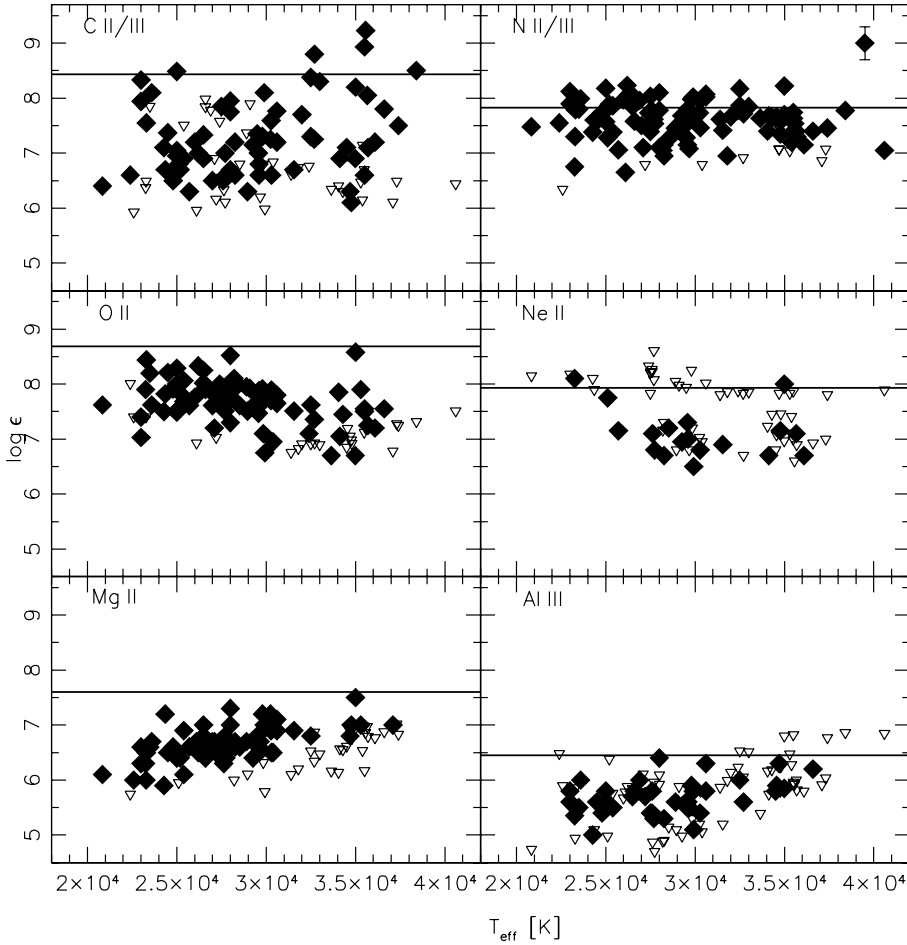


Fig. 4. Elemental abundances from carbon to aluminium plotted against effective temperature. If two ionisation stages are present, the average abundance is given. The filled diamonds mark measured abundances while the open triangles mark upper limits. Typical error bars are given in the upper right corner. The solid horizontal lines mark solar abundances (Asplund et al. 2009).

The abundances derived from N II/N III lines, Si III/Si IV lines and S II/S III lines agree within the given error margins for most stars where both ionisation stages are present. Although the abundances of Ti III and Ti IV agree within the given error margins in most stars, in some cases the difference can be as high as 1.4 dex. NLTE effects or insufficient atomic data are the most likely reasons for these discrepancies.

5. Metal abundances

Metal abundances of all stars are given in Table A.1 and are plotted against effective temperature in Figs. 4–6. Atmospheric parameters and helium abundances are published in Lisker et al. (2005), Geier et al. (2012) and Paper I, the projected rotational velocities in Papers I and II.

5.1. Carbon

The observed C abundances derived from C II/III lines scatter from -2.5 dex subsolar to solar (solar abundance 8.43 dex). Three sdBs with $T_{\text{eff}} > 32\,000$ K show supersolar abundances up to more than $+1.0$ dex.

5.2. Nitrogen and oxygen

The N II abundances (solar abundance 7.83 dex) range from -1.0 dex to $+0.5$ dex and do not show any trend with temperature. The O II abundances (solar abundance 8.69 dex) range from -2.0 dex to solar. At a temperature of $\approx 30\,000$ K the average abundance is shifted by -0.5 with respect to the cooler stars in the sample.

5.3. Neon and magnesium

The Ne II abundance scatters from -1.5 dex to $+0.1$ dex (solar abundance 7.93 dex). A slight trend can be seen with temperature in the magnesium abundance (solar abundance 7.60 dex), which ranges from -1.5 dex to -0.2 dex.

5.4. Aluminium and silicon

A slight trend with temperature is present in the Al III abundance (solar abundance 6.45 dex). Aluminium is enriched from -1.5 dex to 0.0 dex. The abundances from Si III as well as from Si IV (solar abundance 7.51 dex) show a large scatter between -2.0 dex and 0.0 dex w. r. t. solar. Subdwarfs with strong silicon lines are present in the same temperature range as sdBs where only low upper limits can be given. At temperatures higher than $\approx 35\,000$ K the mean silicon abundance drops by about -1.0 dex.

5.5. Phosphorus and sulfur

A trend with temperature is present in the P III abundance (solar abundance 5.41 dex). Phosphorus is enriched starting at a temperature of $T_{\text{eff}} > 28\,000$ K from -0.5 dex to $+1.0$ dex. The two stars HE 2307–0340 and HE 0539–4246 with temperatures of $\approx 23\,000$ K show lines at a wavelength of P III 4080.089 Å. Although no possible blends were found in line lists, these lines may be misidentifications since the derived abundances (5.90 dex) seem to be too high to fit in the overall trend. The S II and especially S III abundances (solar abundance 7.12 dex) scatter between -1.5 dex and $+1.0$ dex.

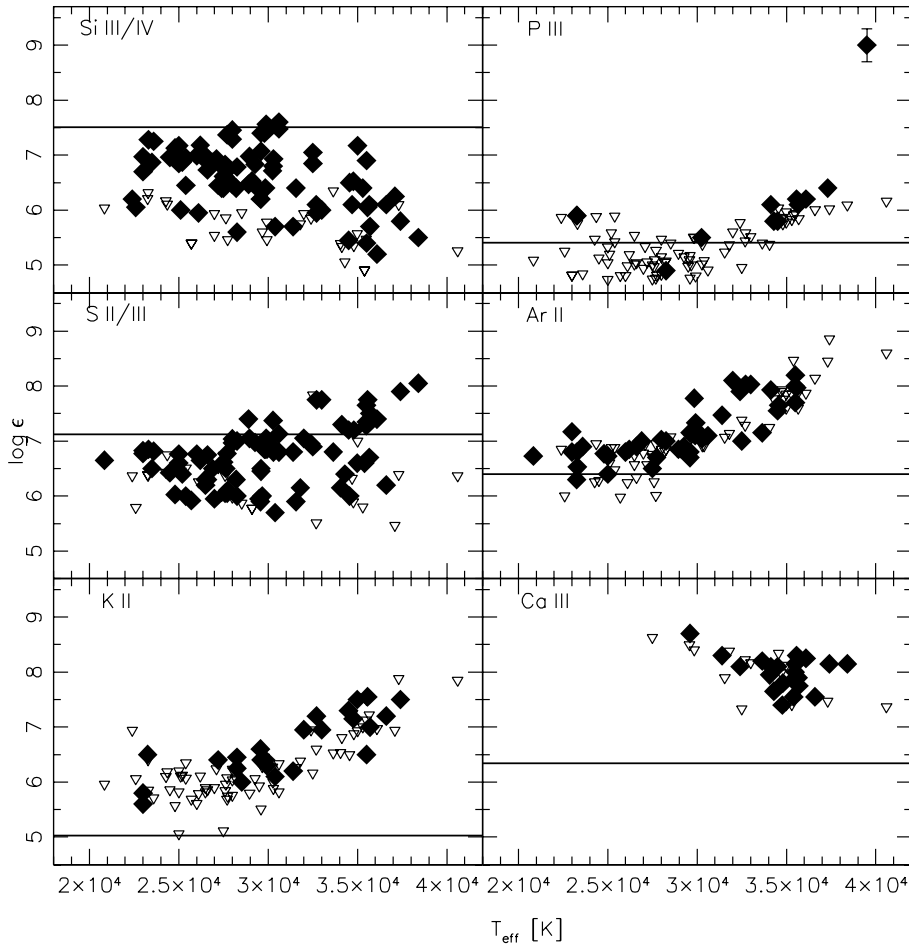


Fig. 5. Elemental abundances from silicon to calcium plotted against effective temperature (see Fig. 4).

5.6. Argon, potassium, and calcium

The Ar abundance increases with temperature from solar to +1.8 dex (solar abundance 6.40 dex). This trend has not been reported in prior analyses. Potassium has not been discovered in sdB atmospheres so far (solar abundance 5.03 dex). Similar to argon, the K abundance increases with temperature from +0.7 dex to +3.0 dex. Ca III (solar abundance 6.34 dex) is present at temperatures higher than $T_{\text{eff}} > 29\,000$ K. The abundances scatter from +1.0 dex to +2.5 dex. Ca II was not included in our analysis because the most prominent lines are usually blended with interstellar lines.

5.7. Scandium, titanium, vanadium and chromium

Sc III (solar abundance 3.15 dex) is strongly enriched and its abundance increases with temperature from +2.0 dex to +4.0 dex. Ti III (solar abundance 4.95 dex) is enriched and scatters from +1.0 dex to +3.0 dex. V III (solar abundance 3.93 dex) is highly enriched independent of the temperature ranging from +2.0 dex to almost +4.0 dex. The Cr III abundance (solar abundance 5.64 dex) increases with temperature from +0.0 dex to +2.0 dex.

5.8. Iron, cobalt and zinc

The Fe III abundance (solar abundance 7.50 dex) is constant ranging from -0.7 dex to $+0.5$ dex. For cobalt (solar abundance 4.99 dex) and zinc (solar abundance 4.56 dex) only upper limits could be given (zinc is not shown in Fig. 6 because upper limits could be derived from a single line only). These limits allow

high enrichments of these elements up to +2.0 dex, which is consistent with the results from UV-spectroscopy (O'Toole & Heber 2006; Chayer et al. 2006; Blanchette et al. 2008).

6. Abundance patterns of sdB sub-populations

Besides apparently single sdB stars our sample contains several pulsating sdBs and RV-variable systems in close binaries. These stars may have formed differently or – in the case of the pulsating sdBs – may be in a distinct evolutionary phase. It is instructive to compare the metal abundance patterns of these sub-populations and search for differences, which may help to clarify these issues.

Our sample contains 38 RV-variable sdBs in single-lined, close spectroscopic binary systems. Aznar Cuadrado & Jeffery (2002) argued that the helium content in such close binary sdBs may be higher than in single stars, because tidal effects might lead to mixing in the stellar atmosphere. According to this scenario, the metal abundances should be affected as well. However, we showed that the helium content in sdB atmospheres is not affected in this way (Geier et al. 2012).

There is also no significant difference between the metal abundance patterns of sdBs in close binaries and apparently single stars. In conclusion, moderate tidal influence of close companions does not change the abundances in sdB atmospheres. In the most extreme cases, where the sdB has been spun up to very high rotational velocities of the order of 100 km s^{-1} (e.g. KPD 1930+2752, Geier et al. 2007; EC 22081–1916, Geier et al. 2011a), it was not yet possible to determine the metal abundances, because the broadening of the spectral lines is too strong. Such objects may still show peculiar abundance patterns.

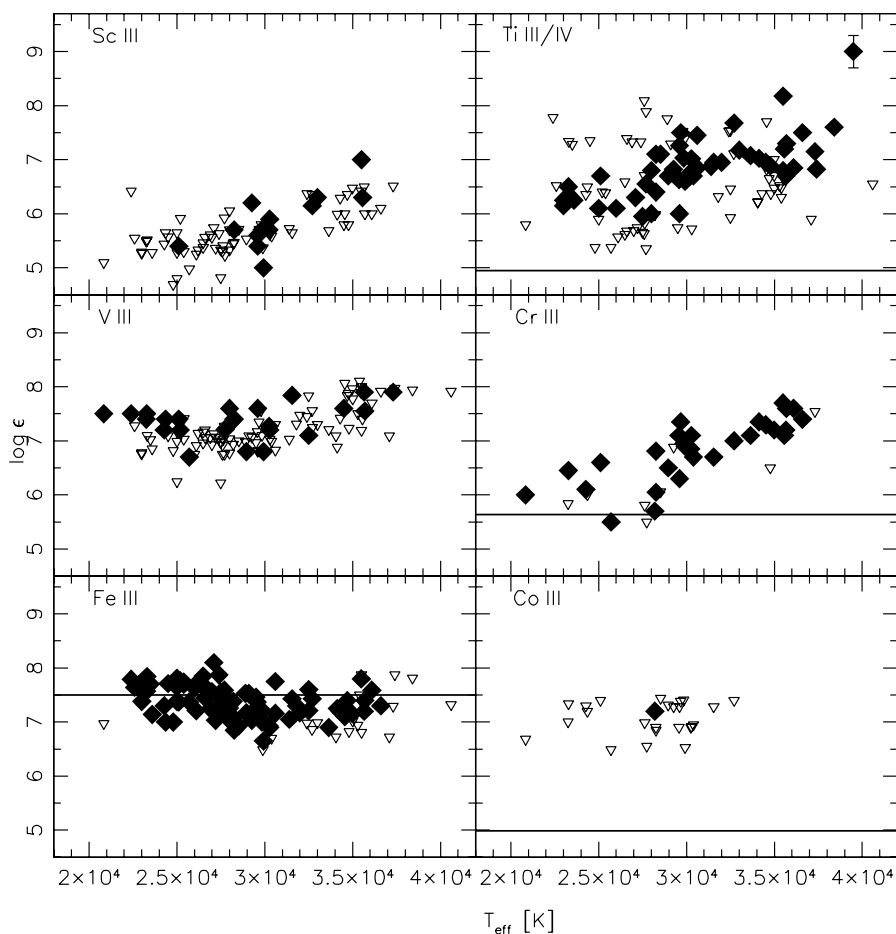


Fig. 6. Elemental abundances from scandium to cobalt plotted against effective temperature (see Fig. 4). In the case of scandium and vanadium the solar abundances are lower than 4.5 dex (see text).

Since the driving mechanism of pulsations in sdB stars is thought to be an enrichment of iron in the outer layers of the star (Charpinet et al. 1997), the metal abundances of pulsating sdBs have been determined to search for peculiarities. However, the abundance patterns of pulsating sdBs turned out to be the same as the ones of non-pulsating comparison stars with similar atmospheric parameters (Heber et al. 2000; O’Toole & Heber 2006; Blanchette et al. 2008).

Our sample includes the short-period pulsators Feige 48 (Koen et al. 1998), KPD 2109+440 (Billères et al. 1998), PG 1219+534 (O’Donoghue et al. 1999) and HE 0230–4323 (Kilkenny et al. 2010) as well as the long-period pulsators PG 1627+017 (Green et al. 2003), LB 1516 (Koen et al. 2010), JL 82 (Koen 2009), PHL 44 (Kilkenny et al. 2007), PHL 457 (Blanchette et al. 2008), PG 1716+426 (Green et al. 2003) and PG 0101+039 (Randall et al. 2005). Consistent with the results of Heber et al. (2000), O’Toole & Heber (2006) and Blanchette et al. (2008) no differences have been found in the metal abundance patterns of these stars with respect to the rest of the sample.

7. Helium and metal abundances

Edelmann et al. (2003) discovered a correlation between the effective temperatures of sdB stars and their helium abundances. Hotter sdB stars tend to show higher enrichments of helium in some cases reaching or even exceeding the solar abundance. However, the scatter in helium abundance is high and two distinct sequences appear in the $T_{\text{eff}} - \log y$ -diagram. These results have been confirmed by Geier et al. (2012). About 75% of the field sdB population belongs to the upper sequence, while $\approx 25\%$ form the lower sequence, which is offset by about 2 dex.

It is instructive to compare the metal abundances of sdBs belonging to the two helium sequences (see Fig. 7). Most species are not significantly affected by the difference in helium abundance. For nitrogen, oxygen, iron and all other metals not shown in Fig. 7 there are no obvious differences between the two subsamples. The silicon abundances of the helium-poor stars seem to be somewhat lower than for the helium-rich ones. However, this impression is most likely created by the different sizes of the samples.

In contrast, significant differences are visible for the carbon and sulfur abundances. All sdBs on the lower helium sequence have carbon abundances of -1.0 or less with respect to the solar value, while the stars with more helium show a large scatter in carbon abundance up to supersolar values. The sulfur abundances behave in a similar way. While the helium-poor sample shows subsolar abundances, sulfur can be enriched to supersolar values in the helium-rich sample.

8. Other trends

It has been noted by several authors (e.g. Lamontagne et al. 1985, 1987; O’Toole & Heber 2006) that the silicon abundance in sdB stars appears to drop sharply at $T_{\text{eff}} > 32\,000$ K. Fractionated winds have been invoked to explain this strange observation (Ungraub 2008). The aluminium abundance were proposed to behave in a similar way. As can be clearly seen in Figs. 4 and 5, this assumption has to be dropped. Silicon as well as aluminium are present all over the temperature range of sdBs.

O’Toole & Heber (2006) also reported a possible anti-correlation between iron and the other heavy elements. In our sample no such trend is visible for the Ti and Ca abundances.

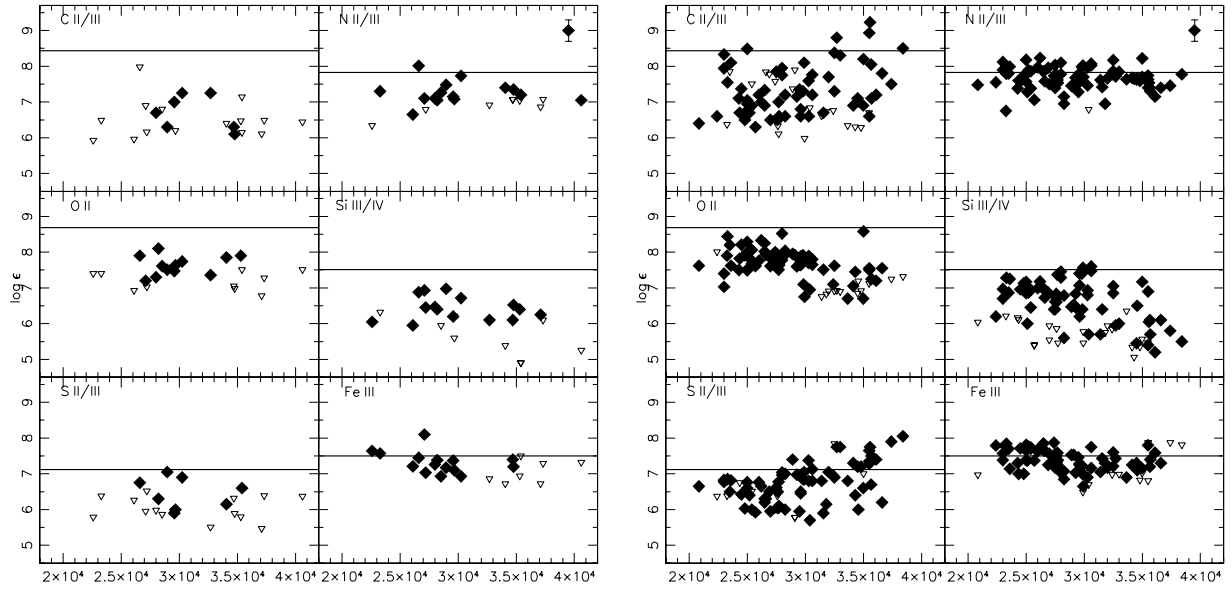


Fig. 7. Abundances of selected elements plotted against effective temperature (see Fig. 4). *Left panel:* only sdBs belonging to the lower He-sequence are plotted. *Right panel:* only sdBs belonging to the upper He-sequence are plotted.

Looking at high resolution spectra of a sample of sdBs it is striking that most of them show a lot of metal lines, while some don't show any metal lines at all. At first instance one could argue, that there exist two different populations of sdBs with different metallicities. Heber & Edlmann (2004) discovered three hot sdBs showing lots of metal lines (e.g. PG 0909+276). They were subsequently named “super-metal-rich” sdBs because their metal abundances seemed to be exceptionally high.

Our results provide a natural explanation for this effect, since such an enrichment is found to be quite normal for sdBs in the high temperature range. All stars with no metal lines are lying at the hot end of the EHB with temperatures higher than $T_{\text{eff}} > 33\,000$ K. Although they show no lines, the derived upper limits are consistent with the abundance measurements of hot sdBs with metal lines. At these temperatures the optical lines are becoming so weak that they are only observable in high signal to noise ratio (S/N) spectra. The effect can be seen in Fig. 4, where the oxygen and magnesium abundance measurements partly turn into upper limit estimates at high temperatures. Spectra of slightly poorer quality appear to be metal free, but they are not. This selection effect illustrates the limitation of optical spectroscopy for metal abundance analyses in hot stars. Therefore UV spectra are needed to study the strong metal lines of higher ionisation stages in hotter sdO/B or sdO stars.

9. Extreme horizontal branch versus blue horizontal branch

Quantitative spectral analyses of BHB stars have been published by Behr et al. (2003a,b), Fabbian et al. (2005) and Pace et al. (2006) and it is worthwhile to compare them to our results for EHB stars. In Fig. 8 the abundances of iron and titanium are plotted against effective temperature. Abundances of all BHB stars are plotted together, although they are derived from stars coming from very different populations. Eight different GCs as well as field stars are put together here¹. At first glance this makes

¹ The gap in temperature between the BHB and EHB stars is a known, but yet unexplained feature, which is also observed in two-colour diagrams of field blue halo stars and GCs (Newell 1973; Geier et al. 2011b, and references therein).

absolutely no sense, because stars from different chemical environments should have different abundances. This would result in a scattered plot from which no relevant information could be derived.

However, Fig. 8 proves that this is not the case. Although there is a high scatter in the iron abundance at low temperatures, all stars hotter than about 11 500 K end up at almost solar abundance with a significantly lower scatter (Fig. 8, upper panel). As soon as diffusion sets in, the atmospheres of stars from different populations become similar regardless of the primordial abundances. The distribution of sdBs now shows that the iron abundance remains indeed saturated at this value up to temperatures of 40 000 K. This plot clearly illustrates that the abundance of iron in EHB and the hottest BHB stars is not “solar” for reasons of star formation and stellar evolution. This abundance reflects the surface concentration of iron caused by an interplay of gravitational settling and radiative levitation, which becomes saturated in stars hotter than 11 500 K, and is just by chance “solar”. This result is in perfect agreement with diffusion models (Michaud et al. 2008, 2011).

A similar behaviour is predicted by Michaud et al. (2008) for the titanium abundance. In BHB stars only a rise of the titanium abundance can be observed, which is more continuous than in the case of iron. Adding the sdBs one can see that the abundance becomes saturated at an effective temperature of about 30 000 K and an abundance of roughly 100 times solar (Fig. 8, lower panel). This behaviour proves in a most convincing way, that heavy elements in EHB and hot BHB stars are enriched by radiative levitation.

10. Diffusion at work along the horizontal branch

The metal abundances of the sdBs in our sample show a pattern, which could not be seen that clearly before. While the light elements carbon, nitrogen, oxygen and neon are not affected by higher temperatures, most heavier elements from aluminium to chromium become enriched in hotter atmospheres, the high scatters in the silicon and sulfur abundance being interesting exceptions. Iron, on the other hand, becomes saturated at solar abundance in HB star atmospheres as soon as the effective

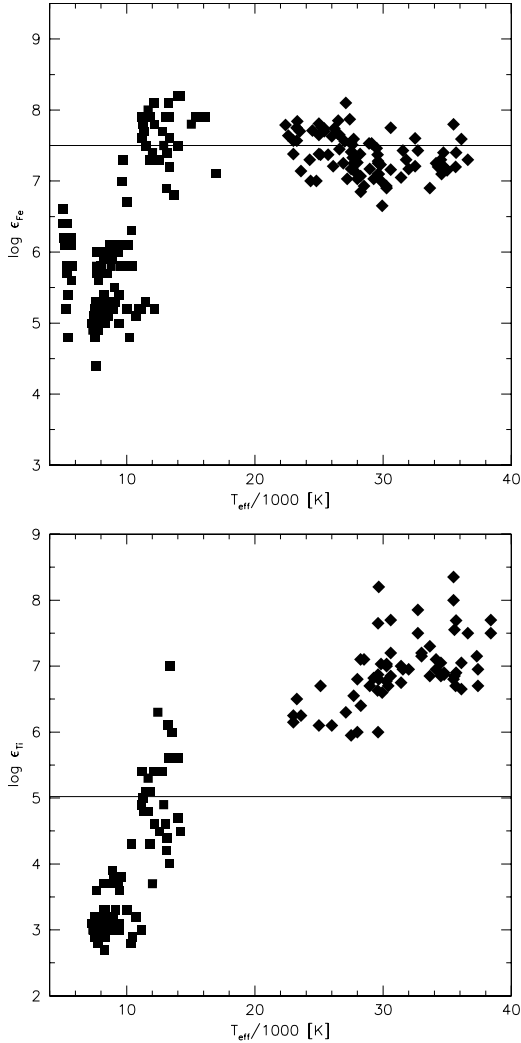


Fig. 8. *Left panel:* iron abundance is plotted against effective temperature. The filled diamonds mark the results from the sdBs. The filled rectangles mark the combined results for BHB stars from seven GCs and the field (Behr et al. 2003a,b; Fabbian et al. 2005). *Right panel:* titanium abundance is plotted against effective temperature. The filled diamonds mark the results from the sdBs. The filled rectangles mark the combined results for BHB stars from eight GCs and the field (Behr et al. 2003a,b; Fabbian et al. 2005; Pace et al. 2006).

temperature exceeds 11 500 K. Consistent with that the hotter sdB stars all have “solar” iron abundances.

These results are in reasonable agreement with theoretical calculations performed by Michaud et al. (2008, 2011). The authors calculated full evolutionary models, including the effects of diffusion and radiative acceleration for different primordial metallicities. The evolution on the HB was followed for the first 32 Myr, which is about one third of the typical lifetime of core helium-burning stars. Their calculations of the abundance anomalies only depend on the mass mixed by turbulence at the surface. Other effects like mass-loss via stellar winds have not been taken into account. Michaud et al. (2011) used the observed iron abundances in sdB stars mostly taken from a preliminary version of the dataset presented here to fix the mixed surface mass to $\approx 10^{-7} M_{\odot}$.

The time evolution of the surface abundances was then calculated for the elements C, N, O, Ne, Mg, Al, Si, P, S, Ar, K, Ca, Ti, Cr and Fe. To compare our measurements with these curves, we can restrict ourselves to models with solar metallicity on the

main sequence (Michaud et al. 2011). Since the sdBs in our sample are rather bright field stars, we can assume that most of them originate from the Galactic thin disc with only minor contributions from the thick disc or the halo (e.g. Altmann & de Boer 2000).

In general, the models of Michaud et al. (2011) match the observations quite well. The predicted enrichments or depletions are mostly of the same order as the observations. This is the first time that the complete abundance patterns of sdB stars could be modelled in a quantitative way. However, the models do neither predict the highly supersolar enrichments of C, S, P, K and Ar with temperature nor the large scatter in the C, Si and S abundances.

Both the high enrichments and the large scatter of certain abundances may partly be caused by age effects. Michaud et al. (2011) pointed out that their evolutionary calculations only cover a part of the lifetime on the EHB. There are no clear correlations between the metal abundances and the ages of the stars derived from their position in the $T_{\text{eff}} - \log g$ -diagram. However, such a trend may be washed out by the uncertainties in the atmospheric parameters and the abundances. Furthermore, mass loss via stellar winds, which was not accounted for, might play a role as well (e.g. Unglaub 2008, and references therein). However, a closer inspection of the data makes an alternative explanation more likely.

11. Peculiar line profiles and stratification

While the enrichments of P, K, Ar (and maybe also S at the hot end) follow a general trend with temperature, which seems to be an indicator of radiative levitation, the supersolar enrichment of some stars in C is hard to explain in this framework, because the other light elements N, O, Ne and Al are depleted with respect to their solar abundances.

Since carbon enrichment is also common in the helium-rich sdBs (Ahmad & Jeffery 2003; Naslim et al. 2010) and sdOs (Ströer et al. 2007; Hirsch & Heber 2009) and the helium abundances of hot sdBs with carbon enrichment are among the highest in our sample, a connection seems to be likely. Alternative formation scenarios like the late hot flasher (Sweigart 1997b; Lanz et al. 2004) do indeed predict an enrichment of helium and carbon.

In the case of helium enrichment prior to the subdwarf stage Groth et al. (1985) predict a broad subsurface convection zone, which should be able to mix nuclear processed material in the atmosphere and therefore counteract gravitational settling. Of course, this mechanism would have to ensure the enrichment of He and C without destroying the general abundance pattern caused by diffusion, which might require some finetuning. Diffusion might also lead to a slow transformation of He-rich subdwarfs into He-deficient ones (Miller Bertolami et al. 2008). The discovery of sdBs with intermediate He abundances right in between the normal sdBs and the He-rich ones may be consistent with such a scenario (Ahmad et al. 2007; Naslim et al. 2011; Naslim et al. 2012).

However, we found observational evidence that yet another unaccounted effect may be responsible for the most extreme chemical peculiarities in sdB atmospheres. Looking at the spectra of our sample in detail, the shape of the strongest metal lines in some stars (CPD-64°481, EC 03591-3232, EC 05479-5818, Feige 38, HD 205805, HE 0101-2707, PG 0133+144, PG 1303+097, PG 1710+490, PG 1743+477) was found to be peculiar (see Fig. 9). The lines are too sharp to be fitted with synthetic models even if the rotational broadening is set to zero.

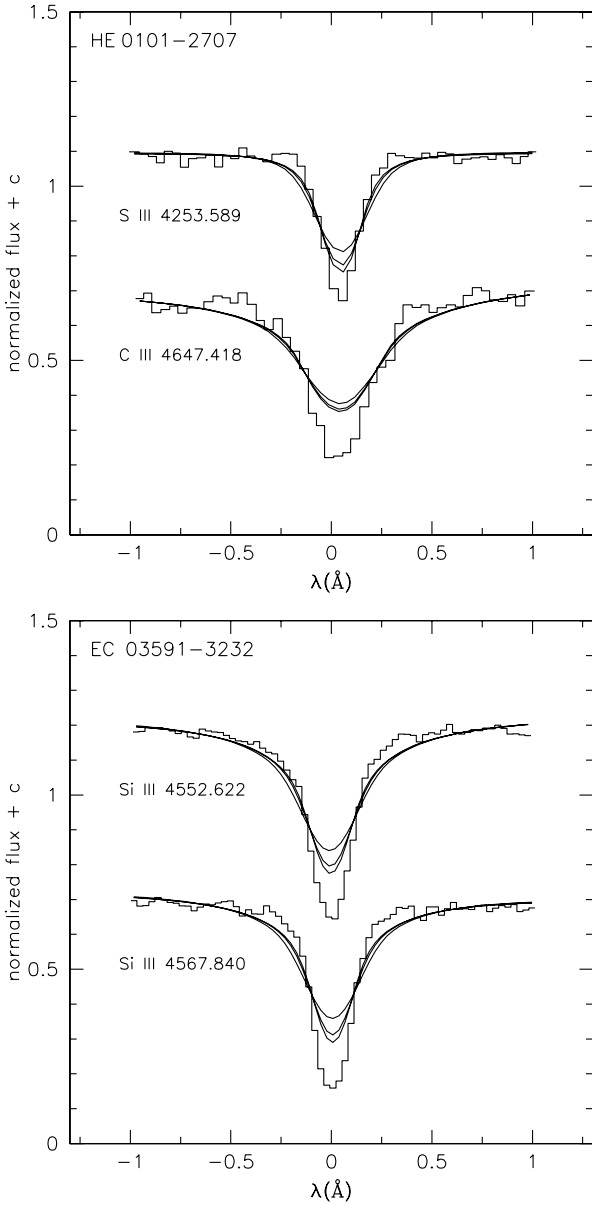


Fig. 9. *Upper panel:* fits of models with different rotational broadening (solid lines, 0, 5, 10 km s⁻¹ respectively) to an S III and a C III line (solid histograms) of HE 0101–2707. *Lower panel:* similar fits of models to Si III-lines of EC 03591–3232. It can be clearly seen that the synthetic line profiles do not match the observed ones at all. Examples for normal fits to metal lines are given in Fig. 2.

Especially the line wings are much too weak with respect to the depths of the cores. NLTE effects cannot cause such line shapes and the weaker metal lines don't show similar profiles.

Using five spectra of Feige 38 taken within a timespan of 1.8 yr we checked whether the shape of the peculiar lines changes. The lines do not show any significant differences in depth and shape. Time dependent effects like star spots can therefore be excluded.

The most significant peculiarities are seen in the strongest Si III lines of EC 03591–3232 (see Fig. 9, lower panel), PG 0133+114, Feige 38 and PG 1710+490. Most remarkably all of these stars belong to the rare class of sdBs that also show an enrichment in ³He (Geier et al. 2012).

Michaud et al. (2011) pointed out that additional element separation may occur in the stellar atmosphere between the bottom of the mixed mass ($\approx 10^{-7} M_{\odot}$) and the surface. Such effects

are not included in their models. The ³He anomaly observed in sdB stars with temperatures around 30 000 K is not predicted by the model of Michaud et al. (2011) either and should therefore not be present in the mixed zone. Nevertheless, it is clear that the settling of almost all ⁴He must be caused by diffusion, which can then only happen in the outermost atmosphere.

Diffusion in the photosphere should lead to vertical stratification of the metal abundances. Observational evidence for such a stratification of Fe in the atmospheres of BHB stars has been found (Khalack et al. 2007, 2010; LeBlanc et al. 2009, 2010). How is the shape of the spectral lines affected by vertical stratification? If radiative levitation leads to an abundance gradient in the atmosphere, the wings of a spectral line should become weaker, because of less absorption at the bottom of the atmosphere. This not only explains the peculiar shape of the lines, but also the fact that the weak lines are not affected. Those lines originate from deeper layers, where the gradient is less pronounced. Together with the ³He anomaly the peculiar line shapes provide evidence for diffusion processes above the mixed zone in the atmospheres of sdBs.

Such effects may also provide a reasonable explanation for the high scatter of the C, Si and S abundances as well as mismatches in the ionisation equilibria (see Sect. 4), since peculiar line shapes have also been found for strong C III and S III lines in the spectra of hot sdBs (e.g. HE 0101–2707, see Fig. 9). Given that these peculiarities are only detectable in the most extreme cases or in data of high quality, stratification may be rather common in sdB atmospheres. It is therefore possible that the highest enrichments not predicted by the models of Michaud et al. (2011) are caused by radiative levitation in the stellar atmosphere rather than the mixed zone beneath. Of course, this hypothesis needs to be tested further.

12. Conclusion

A combination of diffusion both in a mixed zone close to the surface and in the stellar atmosphere on top of it seem to be sufficient to explain most of the results presented here. However, different formation scenarios, which lead to different amounts of helium in the atmosphere may still leave some imprint on the final abundance patterns. The connection between sdBs with hydrogen-rich atmospheres, He-sdBs and intermediate objects remains as unclear as the reason for the differences in the abundance patterns of the two distinct helium populations (see Sect. 7). Our lack of understanding the details of diffusion in sdBs is very well illustrated by the extremely peculiar intermediate He-sdB LS IV–14°116, whose atmosphere is highly enriched in strontium, yttrium and zirconium (Naslim et al. 2011). The reason for this is unclear and the very well detected spectral lines of these elements are not present in any of the sdBs of our sample.

Furthermore, as pointed out by Hu et al. (2011), the physical mechanism necessary to mix the surface in the way needed to reproduce the observed abundances is still unknown. Mass loss through stellar winds may play a role, but Hu et al. (2011) also showed that the mass loss rates must be lower than $\approx 10^{-15} M_{\odot} \text{ yr}^{-1}$ to allow sdBs to pulsate. Since the abundance patterns of sdB pulsators do not differ from the ones of stable sdBs, one would expect similar mass loss rates. But even very weak and fractionated winds might affect the atmospheric abundances (Ungraub 2008).

Although in most cases unstratified photospheres reproduce the observed line profiles well, the discovery of spectral lines with peculiar shapes possibly caused by vertical stratification might pose a new challenge for atmospheric models of sdB stars.

Besides NLTE effects (Przybilla et al. 2006) and enhanced line blanketing by metals enriched due to diffusion (O'Toole & Heber 2006), next generation models might have to take vertical stratification into account. Especially the strong resonance lines in the UV should be affected and due to crowding and blending in this region such effects might not be obvious.

Acknowledgements. Based on observations at the Paranal Observatory of the European Southern Observatory for programmes number 165.H-0588(A), 167.D-0407(A), 071.D-0380(A) and 072.D-0487(A). Based on observations at the La Silla Observatory of the European Southern Observatory for programmes number 073.D-0495(A), 074.B-0455(A), 076.D-0355(A), 077.D-0515(A) and 078.D-0098(A). Based on observations collected at the Centro Astronómico Hispano Alemán (CAHA) at Calar Alto, operated jointly by the Max-Planck Institut für Astronomie and the Instituto de Astrofísica de Andalucía (CSIC). Some of the data used in this work were obtained at the Hobby-Eberly Telescope (HET), which is a joint project of the University of Texas at Austin, the Pennsylvania State University, Stanford University, Ludwig-Maximilians-Universität München, and Georg-August-Universität Göttingen, for programmes number UT07-2-004 and UT07-3-005. Some of the data presented here were obtained at the *W.M. Keck* Observatory, which is operated as a scientific partnership among the California Institute of Technology, the University of California, and the National Aeronautics and Space Administration. The Observatory was made possible by the generous financial support of the W.M. Keck Foundation. S.G. was supported by the Deutsche Forschungsgemeinschaft under grant He 1356/49-1. I would like to thank U. Heber, H. Edelmann, N. Przybilla, M. F. Nieva, K. Unglaub and I. Bues for their comments and fruitful discussions.

References

- Ahmad, A., & Jeffery, C. S. 2003, *A&A*, 402, 335
 Ahmad, A., Behara, N. T., Jeffery, C. S., Sahin, T., & Woolf, V. M. 2007, *A&A*, 465, 541
 Altmann, M., & de Boer, K. S. 2000, *A&A*, 353, 135
 Asplund, M., Grevesse, N., Sauval, A. J., & Scott, P. 2009, *ARA&A*, 47, 481
 Aznar Cuadrado, R., & Jeffery, C. S. 2002, *A&A*, 385, 131
 Baschek, B., Sargent, W. L. W., & Searle, L. 1972, *AJ*, 173, 611
 Baschek, B., Hoeflich, P., & Scholz, M. 1982a, *A&A*, 112, 76
 Baschek, B., Scholz, M., Kudritzki, R.-P., & Simon, K. P. 1982b, *A&A*, 108, 387
 Behr, B. B. 2003a, *ApJS*, 149, 67
 Behr, B. B. 2003b, *ApJS*, 149, 101
 Bergeron, P., Wesemael, F., Michaud, G., & Fontaine, G. 1988, *ApJ*, 332, 964
 Billères, M., Fontaine, G., Brassard, P., et al. 1998, *ApJ*, 494, L75
 Blanchette, J.-P., Chayer, P., Wesemael, F. et al. 2008, *ApJ*, 678, 1329
 Brown, T. M., Lanz, T., Sweigart, A. V., et al. 2011, *ASP Conf. Ser.*, 452, 23
 Caloi, V. 1999, *A&A*, 343, 904
 Charpinet, S., Fontaine, G., Brassard, P., et al. 1997, *ApJ*, 483, 123
 Chayer, P., Fontaine, M., Fontaine, G., Wesemael, F., & Dupuis, J. 2006, *Baltic Astron.*, 15, 131
 Dorman, B., Rood, R. T., & O'Connell, R. W. 1993, *ApJ*, 419, 596
 Edelmann, H. 2003, Ph.D. Thesis, Univ. Erlangen-Nuremberg
 Edelmann, H., Heber, U., Napiwotzki, R., Reid, I. N., & Saffer, R. A. 1999, *ASP Conf. Ser.*, 169, 546
 Edelmann, H., Heber, U., & Napiwotzki, R. 2001, *AN*, 322, 401
 Edelmann, H., Heber, U., Hagen, H.-J., et al. 2003, *A&A*, 400, 939
 Ekberg, J. O. 1993, *A&AS*, 101, 1
 Fabbian, D., Recio-Blanco, A., Gratton, R. G., & Piotto, G. 2005, *A&A*, 434, 235
 Fontaine, G., & Chayer, P. 1997, in *Proc. Conf. Faint Blue Stars*, eds. A. G. D. Philip, J. Liebert, R. A. Saffer, & D. S. Hayes, 169
 Fontaine, M., Chayer, P., Wesemael, F., et al. 2006, *ASP Conf. Ser.*, 348, 224
 For, B.-Q., & Sneden, C. 2010, *AJ*, 140, 1694
 Geier, S., & Heber, U. 2012, *A&A*, 543, A149
 Geier, S., Nesslinger, S., Heber, U., et al. 2007, *A&A*, 464, 299
 Geier, S., Heber, U., Podsiadlowski, Ph., et al. 2010, *A&A*, 519, A25
 Geier, S., Classen, L., & Heber, U. 2011a, *ApJ*, 733, L13
 Geier, S., Hirsch, H., Tillich, A., et al. 2011b, *A&A*, 530, A28
 Geier, S., Heber, U., Edelmann, H., et al. 2012, *ASP Conf. Ser.*, 452, 57
 Glaspey, J. W., Michaud, G., Moffat, A. F., & Demers, S. 1989, *ApJ*, 339, 926
 Green, E. M., Fontaine, G., Reed, M. D., et al. 2003, *ApJ*, 583, L31
 Greenstein, J. L., & Sargent, A. I. 1974, *ApJS*, 28, 157
 Groth, H. G., Kudritzki, R.-P., & Heber, U. 1985, *A&A*, 152, 107
 Han, Z., Podsiadlowski, P., Maxted, P. F. L., Marsh, T. R., & Ivanova, N. 2002, *MNRAS*, 336, 449
 Han, Z., Podsiadlowski, P., Maxted, P. F. L., & Marsh, T. R. 2003, *MNRAS*, 341, 669
 Heber, U. 1986, *A&A*, 155, 33
 Heber, U. 2009, *ARA&A*, 47, 211
 Heber, U., & Edelmann, H. 2004, *Ap&SS*, 291, 341
 Heber, U., Kudritzki, R. P., Caloi, V., Castellani, V., & Danziger, J. 1986, *A&A*, 162, 171
 Heber, U., Reid, I. N., & Werner, K. 1999, *A&A*, 348, L25
 Heber, U., Reid, I. N., & Werner, K. 2000, *A&A*, 363, 198
 Hirata, R., Horaguchi, T. 1995, *Atomic spectral line list*, Department of Astronomy, Kyoto University and National Science Museum
 Hirsch, H. A., & Heber, U. 2009, *JPh Conf. Ser.*, 172, 012015
 Hu, H., Tout, C. A., Glebbeek, E., & Dupret, M.-A. 2011, *MNRAS*, 418, 195
 Iben, I., & Tutukov, A. V. 1984, *ApJ*, 284, 719
 Khalack, V. R., LeBlanc, F., Bohlender, D., Wade, G. A., & Behr, B. B. 2007, *A&A*, 466, 667
 Khalack, V. R., LeBlanc, F., & Behr, B. B. 2010, *MNRAS*, 407, 1767
 Kilkenny, D., Copley, C., Zietsman, E., & Worters, H. 2007, *MNRAS*, 375, 1325
 Kilkenny, D., Koen, C., & Worters, H. 2010, *MNRAS*, 404, 376
 Koen, C. 2009, *MNRAS*, 395, 979
 Koen, C., O'Donoghue, D., Pollacco, D. L., & Nitta, A. 1998, *MNRAS*, 300, 1105
 Koen, C., Kilkenny, D., Pretorius, M. L., & Frew, D. J. 2010, *MNRAS*, 401, 1850
 Kurucz, R. L. 1992, in *Proc. 149th Symp. IAU*, eds. B. Barbuy, & A. Renzini (Kluwer Academic Publishers: Dordrecht), 225
 Lamontagne, R., Wesemael, F., Fontaine, G., & Sion, E. M. 1985, *ApJ*, 299, 496
 Lamontagne, R., Wesemael, F., & Fontaine, G. 1987, *ApJ*, 318, 844
 Lanz, T., Brown, T. M., Sweigart, A. V., Hubeny, I., & Landsman, W. B. 2004, *ApJ*, 602, 342
 LeBlanc, F., Monin, D., Hui-Bon-Hoa, A., & Hauschildt, P. H. 2009, *A&A*, 495, 937
 LeBlanc, F., Hui-Bon-Hoa, A., & Khalack, V. R. 2010, *MNRAS*, 409, 1606
 Lemke, M. 1997, *A&AS*, 122, 285
 Lisker, T., Heber, U., Napiwotzki, R., et al. 2005, *A&A*, 430, 223
 Michaud, G., Vauclair, G., & Vauclair, S. 1983, *ApJ*, 267, 256
 Michaud, G., Bergeron, P., Heber, U., & Wesemael, F. 1989, *ApJ*, 338, 417
 Michaud, G., Richer, J., & Richard, O. 2008, *ApJ*, 675, 1223
 Michaud, G., Richer, J., & Richard, O. 2011, *A&A*, 529, A60
 Miller Bertolami, M. M., Althaus, L. G., Unglaub, K., & Weiss, A. 2008, *A&A*, 491, 253
 Moehler, S., Sweigart, A. V., Landsmann, W. B., Heber, U., & Catelan, M. 1999, *A&A*, 346, 1
 Moehler, S., Dreizler, S., Lanz, T., et al. 2007, *A&A*, 475, 5
 Moni Bidin, C., Moehler, S., Piotto, G., Momany, Y., & Recio-Blanco, A. 2007, *A&A*, 474, 505
 Napiwotzki, R., Edelmann, H., Heber, U., et al. 2001, *A&A*, 378, L17
 Napiwotzki, R., Yungelson, L., Nelemans, G., et al. 2004, *ASP Conf. Ser.*, 318, 402
 Naslim, N., Jeffery, C. S., Ahmad, A., Behara, N. T., & Sahin, T. 2010, *MNRAS*, 409, 582
 Naslim, N., Jeffery, C. S., Behara, N. T., & Hibbert, A. 2011, *MNRAS*, 412, 363
 Naslim, N., Geier, S., Jeffery, C. S., et al. 2012, *MNRAS*, 423, 3031
 Newell, E. B. 1973, *ApJS*, 26, 37
 Nieva, M. F., & Przybilla, N. 2008, *A&A*, 481, 199
 O'Donoghue, D., Koen, C., Kilkenny, D., & Stobie, R. S. 1999, *ASP Conf. Ser.*, 169, 149
 Ohl, R. G., Chayer, P., & Moos, H. W. 2000, *ApJ*, 538, L95
 O'Toole, S. J., & Heber, U. 2006, *A&A*, 452, 579
 Pace, G., Recio-Blanco, A., Piotto, G., & Momany, Y. 2006, *A&A*, 452, 493
 Pereira, C., & Jeffery, C. S. 2008, *ASP Conf. Ser.*, 392, 123
 Przybilla, N., Nieva, M. F., & Edelmann, H. 2006, *Baltic Astron.*, 15, 107
 Randall, S. K., Matthews, J. M., Fontaine, G., et al. 2005, *ApJ*, 633, 460
 Sargent, W. L. W., & Searle, L. 1966, *ApJ*, 145, 652
 Ströer, A., Heber, U., Lisker, T., et al. 2007, *A&A*, 462, 269
 Sweigart, A. V. 1997a, in *Proc. Third Conf. Faint Blue Stars*, eds. A. G. D. Philip et al., 3
 Sweigart, A. V. 1997b, *ApJ*, 474, L23
 Telting, J. H., Geier, S., Østensen, R. H., et al. 2008, *A&A*, 492, 815
 Vauclair, S., & Vauclair, G. 1982, *ARA&A*, 20, 37
 Wiese, W. L., Fuhr, J. L., & Deters, T. M. 1996, *Atomic transition probabilities of carbon, nitrogen and oxygen: a critical data compilation*, American Chemical Society for the National Institute of Standards and Technology, Washington DC
 Unglaub, K. 2008, *A&A*, 486, 923
 Unglaub, K., & Bues, I. 2001, *A&A*, 374, 570
 Vink, J. S., & Cassisi, S. 2002, *A&A*, 392, 553
 Webbink, R. F. 1984, *ApJ*, 277, 355
 Yi, S. K. 2008, *ASP Conf. Ser.*, 392, 3

Hot subdwarf stars in close-up view

II. Rotational properties of single and wide binary subdwarf B stars[★]

S. Geier and U. Heber

Dr. Karl Remeis-Observatory & ECAP, Astronomical Institute, Friedrich-Alexander University Erlangen-Nuremberg, Sternwartstr. 7, 96049 Bamberg, Germany
e-mail: geier@sternwarte.uni-erlangen.de

Received 23 April 2012 / Accepted 7 June 2012

ABSTRACT

Subluminous B stars (sdBs) form the extremely hot end of the horizontal branch and are therefore related to the blue horizontal branch (BHB) stars. While the rotational properties of BHB stars have been investigated extensively, studies of sdB stars have concentrated on close binaries that are influenced by tidal interactions between their components. Here we present a study of 105 sdB stars, which are either single stars or in wide binaries where tidal effects become negligible. The projected rotational velocities have been determined by measuring the broadening of metal lines using high-resolution optical spectra. All stars in our sample are slow rotators ($v_{\text{rot}} \sin i < 10 \text{ km s}^{-1}$). Furthermore, the $v_{\text{rot}} \sin i$ -distributions of single sdBs are similar to those of hot subdwarfs in wide binaries with main-sequence companions as well as close binary systems with unseen companions and periods exceeding $\approx 1.2 \text{ d}$. We show that blue horizontal and extreme horizontal branch stars are also related in terms of surface rotation and angular momentum. Hot BHB stars ($T_{\text{eff}} > 11\,500 \text{ K}$) with diffusion-dominated atmospheres are slow rotators like the hot subdwarf stars located on the extreme horizontal branch, which lost more envelope and therefore angular momentum in the red-giant phase. The uniform rotation distributions of single and wide binary sdBs pose a challenge to our understanding of hot subdwarf formation. Especially the high fraction of helium white dwarf mergers predicted by theory seems to be inconsistent with the results presented here.

Key words. binaries: spectroscopic – subdwarfs – stars: rotation

1. Introduction

Subluminous B stars (sdBs) show similar colours and spectral characteristics to main sequence stars of spectral type B, but are less luminous. Compared to main sequence B stars, the hydrogen Balmer lines in the spectra of sdBs are stronger while the helium lines are much weaker. The strong line broadening and the early confluence of the Balmer series is caused by the high surface gravities ($\log g \approx 5.0\text{--}6.0$) of these compact stars ($R_{\text{sdB}} \approx 0.1\text{--}0.3 R_{\odot}$). Subluminous B stars are considered to be core helium-burning stars with very thin hydrogen envelopes and masses of about half a solar mass (Heber 1986) located at the extreme end of the horizontal branch (EHB).

[★] Based on observations at the Paranal Observatory of the European Southern Observatory for programmes number 165.H-0588(A), 167.D-0407(A), 071.D-0380(A) and 072.D-0487(A). Based on observations at the La Silla Observatory of the European Southern Observatory for programmes number 073.D-0495(A), 074.B-0455(A), 076.D-0355(A), 077.D-0515(A) and 078.D-0098(A). Based on observations collected at the Centro Astronómico Hispano Alemán (CAHA) at Calar Alto, operated jointly by the Max-Planck Institut für Astronomie and the Instituto de Astrofísica de Andalucía (CSIC). Some of the data presented here were obtained at the W. M. Keck Observatory, which is operated as a scientific partnership among the California Institute of Technology, the University of California, and the National Aeronautics and Space Administration. The Observatory was made possible by the generous financial support of the W. M. Keck Foundation. Based on data obtained with the Hobby-Eberly Telescope (HET), which is a joint project of the University of Texas at Austin, the Pennsylvania State University, Stanford University, Ludwig-Maximilians-Universität München, and Georg-August-Universität Göttingen.

1.1. Hot subdwarf formation

The origin of EHB stars is still unknown (see Heber 2009, for a review). The key question is how all but a tiny fraction of the red-giant progenitor's hydrogen envelope was removed at the same time at which the helium core has attained the mass ($\approx 0.5 M_{\odot}$) to ignite the helium flash. The reason for this high mass loss at the tip of the red giant branch (RGB) is unclear. Several single-star scenarios are under discussion (D'Cruz et al. 1996; Sweigart 1997; De Marchi & Paresce 1996; Marietta et al. 2000), which require either a fine-tuning of parameters or extreme environmental conditions that are unlikely to be met for the bulk of the observed subdwarfs in the field.

According to Mengel et al. (1976), the required strong mass loss can occur in a close-binary system. The progenitor of the sdB star has to fill its Roche lobe near the tip of the RGB to lose a large part of its hydrogen envelope. The merger of close binary white dwarfs was investigated by Webbink (1984) and Iben & Tutukov (1984), who showed that an EHB star can form when two helium core white dwarfs (WDs) merge and the product is sufficiently massive to ignite helium. Politano et al. (2008) proposed that the merger of a red giant and a low-mass main-sequence star during a common envelope (CE) phase may lead to the formation of a rapidly rotating single hot subdwarf star.

Maxted et al. (2001) determined a very high fraction of radial velocity variable sdB stars, indicating that about two thirds of the sdB stars in the field are in close binaries with periods of less than 30 days (see also Morales-Rueda et al. 2003; Napiwotzki et al. 2004a; Copperwheat et al. 2011). Han et al. (2002, 2003) used binary population synthesis models to study

the stable Roche lobe overflow (RLOF) channel, the common envelope ejection channel, where the mass transfer to the companion is dynamically unstable, and the He-WD merger channel.

The companions are mostly main sequence stars or white dwarfs. If the white dwarf companion is sufficiently massive, the merger of the binary system might exceed the Chandrasekhar mass and explode as a type Ia supernova. Indeed, Maxted et al. (2000) found the sdB+WD binary KPD 1930+2752 to be a system that might qualify as a supernova Ia progenitor (see also Geier et al. 2007). In Paper I of this series (Geier et al. 2010b) more candidate systems with massive compact companions, either massive white dwarfs or even neutron stars and black holes, have been found. Furthermore, Geier et al. (2011d) reported the discovery of an eclipsing sdB binary with a brown dwarf companion.

1.2. Rotation on the horizontal branch

The rotational properties of horizontal branch (HB) stars both in globular clusters and in the field all the way from the red to the blue end have been studied extensively in the last decades (Peterson 1983, 1985; Peterson et al. 1983, 1995; Behr et al. 2000a,b; Kinman et al. 2000; Recio-Blanco et al. 2002, 2004; Behr 2003a,b; Carney et al. 2003, 2008). Most of these investigations were motivated by the puzzling HB morphologies in some globular clusters and the search for second or third parameters responsible for this phenomenon. The most interesting result of these studies is the discovery of a significant change in the rotational velocities of blue horizontal branch (BHB) stars when their effective temperatures exceed $\approx 11\,500$ K. HB stars cooler than this threshold value show $v_{\text{rot}} \sin i$ values up to 40 km s^{-1} , while the hotter stars rotate with velocities lower than $\approx 10 \text{ km s}^{-1}$.

The transition in rotational velocity is accompanied by a jump towards brighter magnitudes in the colour-magnitude diagram (Grundahl et al. 1999) and a change in the atmospheric abundance pattern. Stars cooler than $\approx 11\,500$ K show the typical abundances of their parent population (e.g. For & Sneden 2010), while stars hotter than that are in general depleted in helium and strongly enriched in iron and other heavy elements such as titanium or chromium. Lighter elements such as magnesium and silicon on the other hand have normal abundances (Behr et al. 2003a,b; Fabbian et al. 2005; Pace et al. 2006). Diffusion processes in the stellar atmosphere are most likely responsible for this effect. Michaud et al. (1983) predicted such abundance patterns before the anomalies were observed (see also Michaud et al. 2008). Caloi (1999) explained the sharp transition between the two abundance patterns as the disappearance of subsurface convection layers at a critical temperature. Sweigart (2002) indeed found that thin convective layers below the surface driven by hydrogen ionization should exist and shift closer to the surface when the effective temperature increases. At about $12\,000$ K the convection zone reaches the surface and the outer layer of the star becomes fully radiative. Since convection is very efficient in mixing the envelope, diffusion processes do not operate in HB star atmospheres of less than $12\,000$ K.

Slow rotation is considered as a prerequisite for diffusion. Michaud (1983) was the first to show that meridional circulation stops the diffusion process as soon as the rotational velocity reaches a critical value and could explain the chemical peculiarity of HgMn stars in this way. Quievy et al. (2009) performed similar calculations for BHB stars and showed that the critical rotational velocity is somewhere near $\approx 20 \text{ km s}^{-1}$ at the transition temperature of $11\,500$ K. This means that the atmospheric

abundances of stars with lower $v_{\text{rot}} \sin i$ should be affected by diffusion processes.

What causes the slow rotation that allows diffusion to happen, is still unclear. Sills & Pinsonneault (2000) used a standard stellar evolution code and modelled the distribution of rotational velocities on the BHB. In order to reproduce the two populations of fast and slow rotators they assumed two distinct main sequence progenitor populations with different rotational velocities. In their picture the slowly rotating BHBs originate from slowly rotating main sequence stars.

Another possible explanation is the spin-down of the surface layers by diffusion itself. Sweigart (2002) argued that the radiative levitation of iron triggers a weak stellar wind that carries away angular momentum. Vink & Cassisi (2002) showed that such winds are radiatively driven.

Brown (2007) used a stellar evolution code including rotation and modelled the distribution of rotational velocities on the BHB. This code allows one to follow the evolution of the progenitor star through the He-flash. Brown (2007) argues that no significant angular momentum is exchanged between the stellar core and stellar envelope during the flash. The surface rotation of their models highly depends on the rotation of the surface convection zone, which contains most of the outer envelope's angular momentum. Hot BHB stars without surface convection zone rotate slower than the cooler ones with convection zone. This approach allows one to reproduce the observed $v_{\text{rot}} \sin i$ -distribution of BHB stars without assuming bimodal stellar populations (Brown et al. 2008).

While the rotational properties of HB stars both in globular clusters and in the field are thoroughly examined, the investigation of EHB stars has mostly been restricted to close binary systems, where tidal interaction plays a major role (Geier et al. 2010b). Very few apparently single EHB stars have been studied so far, all of which are slow rotators ($< 10 \text{ km s}^{-1}$, e.g. Heber et al. 2000; Edelmann 2001).

In this paper we determine the projected rotational velocities of more than a hundred sdB stars by measuring the broadening of metal lines. In Paper I (Geier et al. 2010b) the rotational properties of sdBs in close binary system were derived and used to clarify the nature of their unseen companions. Here we focus on the rotational properties of apparently single sdBs and wide binary systems, for which tidal interactions become negligible.

In Sect. 2 we give an overview of the observations of high-resolution spectra and the atmospheric parameters of our sample. The determination of the rotational properties of 105 sdB stars are described in Sect. 3, the results are interpreted in Sect. 4 and compared to the corresponding results for BHB stars in Sect. 5. The implications for the sdB formation scenarios and the further evolution to the white dwarf cooling tracks are discussed in Sects. 6 and 7, respectively. Finally, a summary is given in Sect. 8.

2. Observations and atmospheric parameters

ESO-VLT/UVES spectra were obtained in the course of the ESO Supernovae Ia Progenitor Survey (SPY, Napiwotzki et al. 2001, 2003) at spectral resolution $R \approx 20\,000$ – $40\,000$ covering 3200 – 6650 \AA with two small gaps at 4580 \AA and 5640 \AA . Each of the 50 stars was observed at least twice (Lisker et al. 2005).

Another sample of 46 known bright subdwarfs was observed with the FEROS spectrograph ($R = 48\,000$, 3750 – 9200 \AA) mounted at the ESO/MPG 2.2 m telescope (Geier et al. 2012).

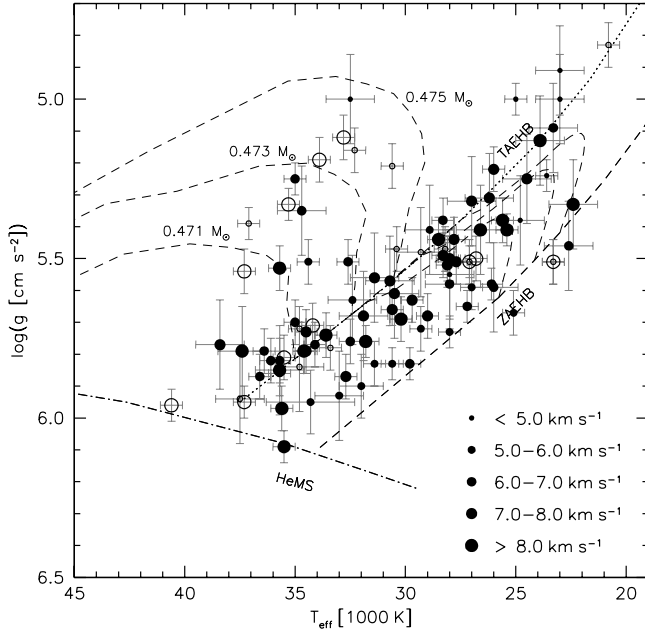


Fig. 1. $T_{\text{eff}} - \log g$ -diagram for the entire sample (not RV-variable) under study. The helium main sequence (HeMS) and the EHB band (limited by the zero-age EHB, ZAEHB, and the terminal-age EHB, TAEHB) are superimposed with EHB evolutionary tracks for solar metallicity taken from Dorman et al. (1993) labelled with their masses. Open circles mark objects where only upper limits could be derived for $v_{\text{rot}} \sin i$, filled circles objects with significant $v_{\text{rot}} \sin i$. The size of the symbols scales with the value of $v_{\text{rot}} \sin i$.

Six stars were observed with the FOCES spectrograph ($R = 30\,000$, $3800\text{--}7000\text{ \AA}$) mounted at the CAHA 2.2 m telescope (Geier et al. 2012). Two stars were observed with the HIRES instrument ($R = 45\,000$, $3600\text{--}5120\text{ \AA}$) mounted at the Keck telescope (Heber et al. 2000). One star was observed with the HRS fiber spectrograph at the Hobby Eberly Telescope ($R = 30\,000$, $4260\text{--}6290\text{ \AA}$, Geier et al. 2010b).

Because a wide slit was used in the SPY survey and the seeing disk did not always fill the slit, the instrumental profile of some of the UVES spectra was seeing-dependent. This has to be accounted for to estimate the instrumental resolution (see Paper I). The resolution of the spectra taken with the fiber spectrographs FEROS and FOCES was assumed to be constant.

The single spectra of all programme stars were radial-velocity (RV) corrected and co-added in order to achieve higher signal-to-noise.

Atmospheric parameters of the stars observed with UVES have been determined by Lisker et al. (2005). HD 205805 and Feige 49 have been analysed by Przybilla et al. (2006), the two sdB pulsators KPD 2109+4401 and PG 1219+534 by Heber et al. (2000), and the sdB binaries PG 1725+252 and TONS 135 by Maxted et al. (2001) and Heber (1986), respectively. The rest of the sample was analysed in Geier et al. (2012) and a more detailed publication of these results is in preparation. We adopted the atmospheric parameters given in Saffer et al. (1994) for [CW83] 1758+36.

The whole sample under study is listed in Tables 1 and 2 and the effective temperatures are plotted versus the surface gravities in Fig. 1. Comparing the positions of our sample stars to evolutionary tracks, we conclude that all stars are concentrated on or above the EHB, which is fully consistent with the theory. We

point out that the inaccuracies in the atmospheric parameters do not significantly affect the derived projected rotational velocities.

3. Projected rotational velocities from metal lines

To derive $v_{\text{rot}} \sin i$, we compared the observed spectra with rotationally broadened, synthetic line profiles using a semi-automatic analysis pipeline. The profiles were computed for the appropriate atmospheric parameters using the LINFOR program (developed by Holweber, Steffen and Steenbock at Kiel university, modified by Lemke 1997).

For a standard set of up to 187 unblended metal lines from 24 different ions and with wavelengths ranging from 3700 to 6000 \AA , a model grid with appropriate atmospheric parameters and different elemental abundances was automatically generated with LINFOR. The actual number of lines used as input for an individual star depends on the wavelength coverage. Owing to the insufficient quality of the spectra and the pollution with telluric features in the regions blueward of 3700 \AA and redward of 6000 \AA we excluded them from our analysis. A simultaneous fit of elemental abundance, projected rotational velocity and radial velocity was then performed separately for each identified line using the FITSB2 routine (Napiwotzki et al. 2004b). A detailed investigation of statistical and systematic uncertainties of the techniques applied is presented in Paper I. Depending on the quality of the data and the number of metal lines used, an accuracy of about 1.0 km s^{-1} can be achieved. For the best spectra with highest resolution the detection limit is about 5.0 km s^{-1} .

Projected rotational velocities of 105 sdBs have been measured (see Tables 1, 2). Ninety-eight sdBs do not show any RV variability. In addition, seven are radial velocity variable systems with orbital periods of about a few days (see Table 2).

For eleven stars of our sample upper limits for the projected rotational velocities have already been published (Heber et al. 2000; Edelmann et al. 2001) based on the same spectra as used here (see Table 3). Only for PHL 932 and PG 0909+276 our measured $v_{\text{rot}} \sin i$ deviate significantly from the results of Edelmann et al. (2001). This is most likely because they used fewer metal lines in their study.

Przybilla et al. (2006) performed an NLTE analysis of Feige 49 and HD 205805 using the same FEROS spectra as we do here and derived a $v_{\text{rot}} \sin i$ below the detection limit. Again our measurements are consistent with their results, because they are very close to the detection limit we derived for FEROS spectra of sdBs ($\approx 5\text{ km s}^{-1}$, see Paper I).

4. Projected rotational velocity distributions

The projected rotational velocities of our full sample of 98 stars without radial velocity variations are all low ($< 10\text{ km s}^{-1}$, see Table 1). Taking into account the uncertainties, one can see that there is no obvious trend with the atmospheric parameters (see Fig. 1).

Figure 2 shows the distribution of $v_{\text{rot}} \sin i$ binned to the average measurement error (1.5 km s^{-1}). Eleven stars that had only fairly weak upper limits of 10 km s^{-1} , were sorted out. The distribution is very uniform and shows a prominent peak at $6\text{--}8\text{ km s}^{-1}$. Because we can only determine the projected rotation, the true rotational velocities of most stars in the sample should be about $7\text{--}8\text{ km s}^{-1}$.

Table 1. Projected rotational velocities of single sdBs and sdBs with visible companions.

System	T_{eff} [K]	$m_{B/V}$ [mag]	S/N	Seeing [arcsec]	N_{lines}	$v_{\text{rot}} \sin i$ [km s $^{-1}$]	Instrument
HE 0151–3919	20 800	14.3 ^B	66	1.06	27	<5.0	UVES
EC 21494–7018	22 400	11.2 ^V	85		16	8.6 ± 1.8	FEROS
EC 15103–1557	22 600	12.9 ^V	163		8	6.5 ± 1.6	FEROS
HD 4539	23 000	10.1 ^B	112		21	3.9 ± 1.0	FEROS
EC 11349–2753	23 000	12.5 ^B	185		49	4.7 ± 1.0	FEROS
EC 14345–1729	23 300	13.1 ^V	117		40	6.2 ± 1.0	FEROS
HE 0539–4246	23 300	14.5 ^B	40	0.87	19	<10.0	UVES
HE 2307–0340 ^{no}	23 300	15.8 ^B	61	0.89	17	<5.0	UVES
PG 1432+004 ^{nr}	23 600	12.0 ^B	170		13	4.7 ± 1.0	FEROS
EC 19563–7205 ^c	23 900	12.8 ^B	85		34	9.8 ± 1.0	FEROS
EC 20106–5248	24 500	12.6 ^V	114		47	7.8 ± 1.0	FEROS
BD+48° 2721	24 800	10.5 ^B	326		10	4.7 ± 1.4	FOCES
HD 205805	25 000	9.9 ^B	255		20	4.5 ± 1.0	FEROS
HE 0321–0918 ^{no}	25 100	14.7 ^B	37	1.22	7	5.6 ± 2.3	UVES
PG 1653+131	25 400	14.1 ^B	68		32	8.3 ± 1.0	FEROS
HE 2237+0150	25 600	15.8 ^B	40	0.78	11	8.5 ± 1.8	UVES
PG 0342+026	26 000	11.1 ^B	190		54	6.2 ± 1.0	FEROS
PG 2122+157 ^c	26 000	15.0 ^B	67	0.78	13	7.9 ± 1.4	UVES
GD 108	26 100	13.3 ^B	97		6	6.0 ± 1.8	FEROS
Feige 65	26 200	11.8 ^B	150		18	7.2 ± 1.1	FOCES
PHL 44 ^l	26 600	13.0 ^B	85		31	8.4 ± 1.0	FEROS
HE 0513–2354	26 800	15.8 ^B	21	0.99	18	<10.0	UVES
HE 0135–6150	27 000	16.3 ^B	37	0.71	13	5.5 ± 1.7	UVES
SB 815	27 000	10.6 ^B	85		48	7.3 ± 1.0	FEROS
HE 2201–0001	27 100	16.0 ^B	35	1.10	28	<5.0	UVES
PG 2205+023	27 100	12.9 ^B	36		9	<10.0	FEROS
PG 2314+076 ^{nb}	27 200	13.9 ^B	71		6	6.0 ± 2.2	FEROS
SB 485	27 700	13.0 ^B	112	0.71	24	7.2 ± 1.0	UVES
KUV 01542–0710 ^c	27 800	16.3 ^B	58	0.92	8	7.2 ± 2.1	UVES
HE 2156–3927 ^c	28 000	14.1 ^B	62	0.61	16	7.0 ± 1.2	UVES
EC 03591–3232	28 000	11.2 ^V	131		34	4.8 ± 1.0	FEROS
EC 12234–2607	28 000	13.8 ^B	60		19	6.8 ± 1.4	FEROS
PG 2349+002	28 000	12.0 ^B	68		11	5.7 ± 1.5	FEROS
HE 2322–0617 ^{c,no}	28 100	15.7 ^B	62	0.70	15	6.8 ± 1.3	UVES
PG 0258+184 ^{c,no}	28 100	15.2 ^B	48	0.99	12	7.2 ± 1.7	UVES
HE 0136–2758 ^{no}	28 200	16.2 ^B	29	1.20	27	<5.0	UVES
HE 0016+0044 ^{no}	28 300	13.1 ^B	58	0.67	14	6.5 ± 1.3	UVES
PG 1549–001 ^{no}	28 300	14.8 ^B	45	1.16	20	5.6 ± 1.1	UVES
HE 2349–3135	28 500	15.6 ^B	53	1.13	13	10.0 ± 1.7	UVES
EC 01120–5259	28 900	13.5 ^V	73		19	5.8 ± 1.2	FEROS
HE 0007–2212 ^{no}	29 000	14.8 ^B	53	0.64	21	7.4 ± 1.0	UVES
LB 275*	29 300	14.9 ^B	48	1.16	20	5.6 ± 1.1	UVES
EC 03263–6403	29 300	13.2 ^V	32		40	<5.0	FEROS
HE 1254–1540 ^{c,no}	29 700	15.2 ^B	54	0.75	20	7.2 ± 1.3	UVES
PG 1303+097	29 800	14.3 ^B	51		18	6.1 ± 1.5	FEROS
HE 2222–3738	30 200	14.2 ^B	61	0.83	28	8.7 ± 1.0	UVES
HE 2238–1455	30 400	16.0 ^B	48	0.80	14	<5.0	UVES
EC 03470–5039	30 500	13.6 ^V	53		9	7.3 ± 2.0	FEROS
Feige 38	30 600	12.8 ^B	148		34	5.3 ± 1.0	FEROS
HE 1038–2326 ^c	30 600	15.8 ^B	34	1.27	28	<5.0	UVES
PG 1710+490	30 600	12.1 ^B	80		11	7.1 ± 1.6	FOCES
HE 0447–3654	30 700	14.6 ^V	44		11	7.3 ± 1.8	FEROS
EC 14248–2647	31 400	12.0 ^V	104		14	7.0 ± 1.5	FEROS
HE 0207+0030 ^{no}	31 400	14.7 ^B	27	1.30	7	5.1 ± 2.3	UVES
KPD 2109+4401 ^s	31 800	13.2 ^B	136		9	10.5 ± 1.6	HIRES
EC 02542–3019	31 900	12.8 ^B	65		13	7.3 ± 1.5	FEROS
[CW83] 1758+36 ^{nb}	32 000	11.1 ^B	110		5	5.7 ± 1.4	FOCES
TON S 155 ^c	32 300	14.9 ^B	35	0.85	14	<5.0	UVES
EC 21043–4017	32 400	13.1 ^V	65		8	5.6 ± 1.8	FEROS
EC 20229–3716	32 500	11.4 ^V	153		29	4.5 ± 1.0	FEROS
HS 2125+1105 ^c	32 500	16.4 ^B	29	0.80	8	6.0 ± 2.4	UVES
HE 1221–2618 ^c	32 600	14.9 ^B	35	1.06	11	6.8 ± 1.6	UVES
HS 2033+0821 ^{no}	32 700	14.4 ^B	43	1.14	37	<5.0	UVES

Table 1. continued.

System	T_{eff} [K]	m_B [mag]	S/N	Seeing [arcsec]	N_{lines}	$v_{\text{rot}} \sin i$ [km s $^{-1}$]	Instrument
HE 0415–2417 ^{no}	32 800	16.2 ^B	34	0.83	10	<10.0	UVES
EC 05479–5818	33 000	13.1 ^V	81		20	5.8 ± 1.1	FEROS
HE 1200–0931 ^{c,no}	33 400	16.2 ^B	30	0.86	12	<5.0	UVES
PHL 932	33 600	12.0 ^B	102	1.10	12	9.0 ± 1.3	UVES
HE 1422–1851 ^{c,no}	33 900	16.3 ^B	14	0.58	10	<10.0	UVES
PHL 555	34 100	13.8 ^B	56	0.88	17	6.9 ± 1.2	UVES
HE 1419–1205 ^c	34 200	16.2 ^B	28	0.69	16	<10.0	UVES
PG 1219+534 ^s	34 300	12.4 ^B	140		11	5.7 ± 1.4	HIRES
HS 2216+1833 ^c	34 400	13.8 ^B	54	0.90	11	5.3 ± 1.6	UVES
HE 1050–0630 ^{no}	34 500	14.0 ^B	59	1.20	28	7.3 ± 1.4	UVES
HE 1519–0708 ^{no}	34 500	15.6 ^B	20	0.84	8	9.0 ± 2.4	UVES
HE 1450–0957	34 600	15.1 ^B	32	0.71	6	9.0 ± 2.4	UVES
EC 13047–3049	34 700	12.8 ^V	68		5	6.8 ± 3.6	FEROS
HS 1710+1614 ^{no}	34 800	15.7 ^B	38	1.30	13	<5.0	UVES
PHL 334	34 800	12.5 ^B	87		13	<5.0	FEROS
Feige 49	35 000	13.2 ^B	119		40	6.2 ± 1.0	FEROS
HE 2151–1001 ^s	35 000	15.6 ^B	42	0.66	6	6.7 ± 2.4	UVES
PG 0909+164 ^s	35 300	13.9 ^B	52		4	<10.0	FEROS
HE 1021–0255 ^{no}	35 500	15.3 ^B	40	1.61	11	<10.0	UVES
PG 0909+276 ^{nb}	35 500	13.9 ^B	82		13	9.3 ± 1.4	FOCES
HE 0101–2707	35 600	15.0 ^B	67	0.85	12	8.1 ± 1.5	UVES
EC 03408–1315	35 700	13.6 ^V	66		11	8.8 ± 1.8	FEROS
HE 1352–1827 ^c	35 700	16.2 ^B	24	0.85	5	8.2 ± 2.7	UVES
PG 1207–032 ^{no}	35 700	13.1 ^B	50	0.64	9	6.6 ± 1.6	UVES
HE 0019–5545	35 700	15.8 ^B	38	0.76	7	5.9 ± 2.3	UVES
GD 619	36 100	13.9 ^B	96	0.81	10	6.1 ± 1.5	UVES
HE 1441–0558 ^{c,no}	36 400	14.4 ^B	30	0.70	8	6.9 ± 2.0	UVES
HE 0123–3330	36 600	15.2 ^B	48	0.66	8	6.9 ± 1.8	UVES
PG 1505+074	37 100	12.2 ^B	153		4	<5.0	FEROS
HE 1407+0033 ^{no}	37 300	15.5 ^B	35	0.72	9	<10.0	UVES
PG 1616+144 ^{nb}	37 300	13.5 ^B	44		4	<10.0	FEROS
EC 00042–2737 ^c	37 500	13.9 ^B	37		9	<10.0	FEROS
PHL 1548	37 400	12.5 ^B	90		10	9.1 ± 1.6	FEROS
PB 5333 ^{nb}	40 600	12.5 ^B	66		2	<10.0	FEROS
[CW83] 0512–08	38 400	11.3 ^B	124		14	7.7 ± 1.1	FEROS

Notes. The average seeing is only given if the spectra were obtained with a wide slit in the course of the SPY survey. In all other cases the seeing should not influence the measurements. ^(c) Main sequence companion visible in the spectrum (Lisker et al. 2005). ^(s) Pulsating subdwarf of V 361 Hya type. ^(l) Pulsating subdwarf of V 1093 Her type. No short-period pulsations have been detected either by ^(nb) Billères et al. (2002), ^(mr) Randall et al. (2006) or ^(no) Østensen et al. (2010). ^(*) Misidentified as CBS 275 in Lisker et al. (2005).

Table 2. Projected rotational velocities of radial velocity variable sdBs.

System	T_{eff} [K]	$m_{B/V}$ [mag]	S/N	N_{lines}	$v_{\text{rot}} \sin i$ [km s $^{-1}$]	Instrument
TONS 135	25 000	13.1 ^B	45	35	6.4 ± 1.0	FEROS
LB 1516 ^l	25 200	12.7 ^B	58	23	6.0 ± 1.3	FEROS
PHL 457 ^l	26 500	13.0 ^B	59	47	6.1 ± 1.0	FEROS
EC 14338–1445	27 700	13.5 ^V	71	39	8.9 ± 1.0	FEROS
PG 1725+252	28 900	11.5 ^B	45	11	7.4 ± 1.1	HRS
PG 1519+640	30 300	12.1 ^B	104	11	9.4 ± 1.4	FOCES
PG 2151+100	32 700	12.9 ^B	69	9	9.0 ± 1.7	FEROS

Notes. ^(l) Pulsating subdwarf of V 1093 Her type.

4.1. Single-lined sdBs

Our sample contains 71 single-lined sdBs, of which the $v_{\text{rot}} \sin i$ could be constrained. Ten stars of which we were only able to derive upper limits of 10 km s $^{-1}$ were sorted out. Figure 3 shows the $v_{\text{rot}} \sin i$ distribution of this subsample. Most remarkably,

the distribution is almost identical to that of the full sample. Adopting a random distribution of inclination angles and a constant v_{rot} of ≈ 8 km s $^{-1}$, the observed $v_{\text{rot}} \sin i$ -distribution can indeed be well reproduced (see Fig. 2). We therefore conclude that most single sdBs in our sample have very similar rotation velocities.

4.2. Double-lined sdB binaries

Our sample contains 18 sdBs with visible spectral signatures of cooler main sequence (MS) companions (e.g. MgI, Lisker et al. 2005). Again, two stars with upper limits of 10 km s $^{-1}$ were excluded.

The orbital periods of these systems are long. Green et al. (2006) have argued that such systems should have periods of many months or years. Recently, Deca et al. (2012) were able to determine the orbital period $P \approx 760$ d of the sdB+K binary PG 1018–047. Similar periods were reported by Østensen & van Winckel (2012) for eight such binaries. The separations of the components are so wide that tidal interaction is negligible.

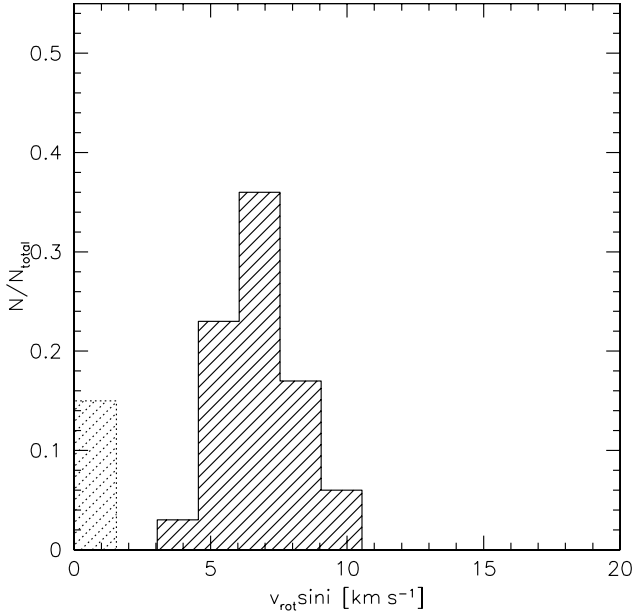


Fig. 2. Distribution of $v_{\text{rot}} \sin i$ for the full sample. Objects with limits below the detection limit have been stacked into the first dotted bin.

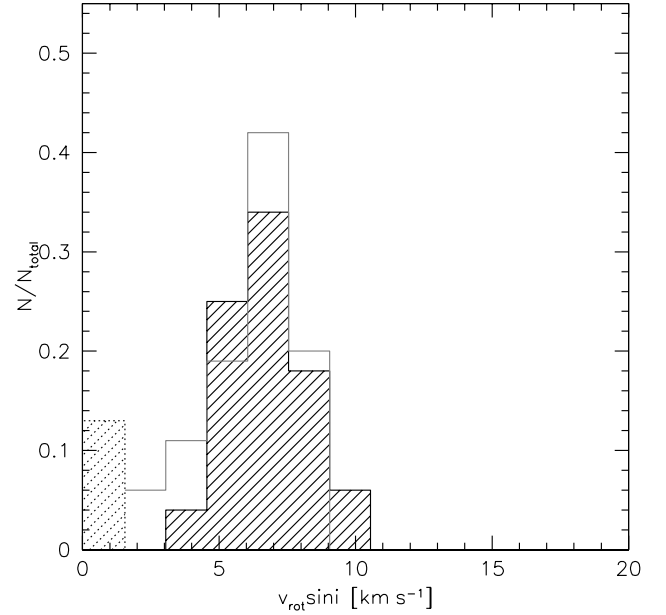


Fig. 3. Distribution of $v_{\text{rot}} \sin i$ for 71 single stars from our sample using the same binning as in Fig. 2. The solid grey line marks the distribution of $v_{\text{rot}} \sin i$ under the assumption of randomly oriented rotation axes and a constant $v_{\text{rot}} = 7.65 \text{ km s}^{-1}$, which matches the observed distribution very well.

Table 3. Comparison with literature.

System	This work $v_{\text{rot}} \sin i$ [km s^{-1}]	Literature $v_{\text{rot}} \sin i$ [km s^{-1}]	Reference
KPD 2109+4401	10.5 ± 1.6	<10.0	Heber
PG 1219+534	5.7 ± 1.4	<10.0	et al. (2000)
BD+48° 2721	4.7 ± 1.4	<5.0	Edelmann
Feige 65	7.2 ± 1.1	<5.0	et al. (2001)
HD 205805	4.5 ± 1.0	<5.0	
HD 4539	3.9 ± 1.0	<5.0	
LB 1516	6.0 ± 1.3	<5.0	
PG 0342+026	6.2 ± 1.0	<5.0	
PG 0909+276	9.3 ± 1.4	<5.0	
PHL 932	9.0 ± 1.3	<5.0	
Feige 49	6.2 ± 1.0	0.0^*	Przybilla
HD 205805	4.5 ± 1.0	0.0^*	et al. (2006)

Notes. (*) Adopted value for line fits is below the detection limit.

Main-sequence companions do therefore not affect the rotational properties of the sdB stars in this type of binaries.

The distribution for sdBs with composite spectra is displayed in Fig. 4. Taking into account the much smaller sample size, the result is again similar. We therefore conclude that the rotational properties of sdBs in wide binaries with MS companions are the same as those of single sdBs, although they have probably formed in a very different way (see Sect. 6).

4.3. Pulsating sdBs

Two types of sdB pulsators are known. The slow pulsations of the V 1093 Her stars (sdBV_s, Green et al. 2003) are not expected to influence the line broadening significantly (see Geier et al. 2010b). For the short-period pulsators (V 361 Hya type, sdBV_r, Charpinet et al. 1997; Kilkenny et al. 1997) unresolved pulsations can severely affect or even dominate the broadening of the metal lines and therefore fake high $v_{\text{rot}} \sin i$. Telting et al. (2008) showed that this happens in the case of the hybrid pulsator

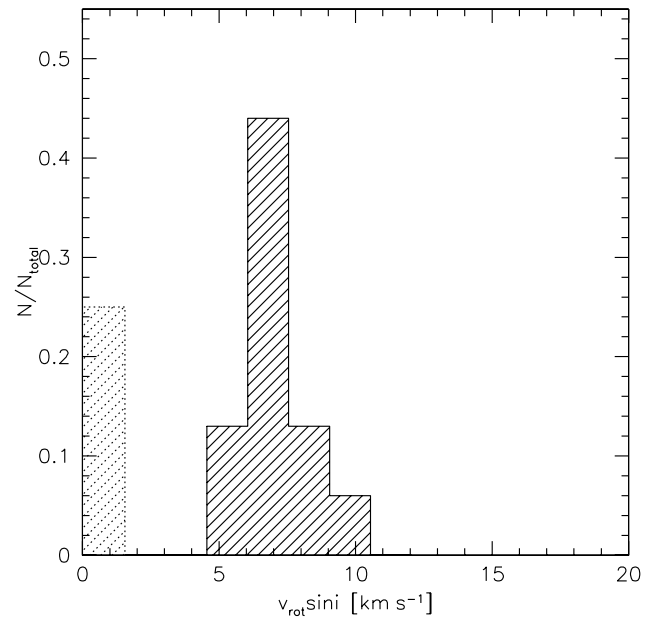


Fig. 4. Distribution of $v_{\text{rot}} \sin i$ for 16 sdBs with companions visible in the spectra using the same binning as in Fig. 2.

Balloon090100001 using the same method as in this work. Unresolved pulsations are also most likely responsible for the high line broadening (39 km s^{-1}) measured for the strong pulsator PG 1605+072 (Heber et al. 1999, 2000).

Our sample contains three known long-period pulsators (PHL 44, Kilkenny et al. 2007; PHL 457, Blanchette et al. 2008; LB 1516, Koen et al. 2010) and two short-period ones (KPD 2109+4401, Billères et al. 1998; PG 1219+534, O'Donoghue et al. 1999). The $v_{\text{rot}} \sin i$ of KPD 2109+4401 is indeed among the highest of all sdBs in our sample ($10.5 \pm 1.6 \text{ km s}^{-1}$), but it is unclear if this might not be partly due to unresolved pulsations. Jeffery & Pollacco (2000) measured

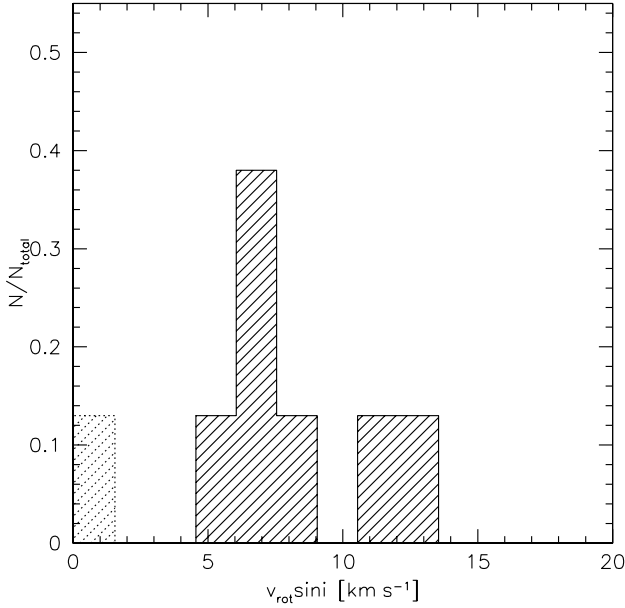


Fig. 5. Distribution of $v_{\text{rot}} \sin i$ for 8 radial velocity variable sdBs with orbital periods exceeding ≈ 1.2 d using the same binning as in Fig. 2.

RV variations of 2 km s^{-1} for KPD 2109+4401. Taking this into account, the sdBs rotational velocity may be slightly lower than measured. The $v_{\text{rot}} \sin i$ of the other pulsators are not peculiar.

For most stars in our sample it is not clear whether they are pulsators or not, because no light curves of sufficient quality are available. Because only about 5% of all sdBs show pulsations detectable from the ground, one may conclude that the contamination by pulsators should be quite low. Thanks to the extensive photometric surveys for sdB pulsators conducted by Billères et al. (2002), Randall et al. (2006) and Østensen et al. (2010), we know that 27 stars from our sample do not show short-period pulsations.

Restricting ourselves to these objects and again excluding those with visible companions, we constructed a “pure” sample of 16 single sdBs, for which the rotational broadening is proven to be disturbed neither by the presence of a companion nor by pulsations. The associated $v_{\text{rot}} \sin i$ distribution does not differ from the other distributions (see Figs. 2–4). We therefore conclude that unresolved pulsations do not significantly affect our results.

4.4. Radial velocity variable sdBs

In Paper I we showed that the $v_{\text{rot}} \sin i$ distribution of sdBs in close binary systems is strongly affected by the tidal interaction with their companions, but that this influence becomes negligible if the orbital periods of the binaries become longer than ≈ 1.2 d. It is instructive to have a look at the $v_{\text{rot}} \sin i$ -distribution of these long-period radial velocity variable systems. From Paper I we selected all seven binaries with periods longer than 1.2 d, for which tidal synchronisation is not established. We added the system LB 1516, a binary with yet unknown orbital parameters, but for which Edelmann et al. (2005) provided a lower limit for the period of the order of days¹.

Figure 5 shows the associated distribution. Given the small sample size and although two stars have somewhat

¹ TONS 135 was not included because the orbital period of ≈ 4 d given in Edelmann et al. (2005) is not very significant and shorter periods cannot be excluded yet.

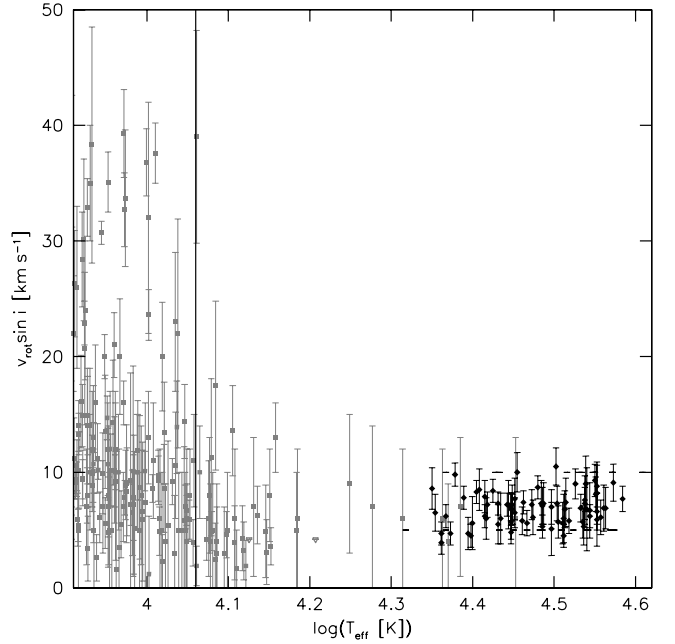


Fig. 6. Projected rotational velocity plotted against effective temperature. The grey squares mark BHB and some sdB stars taken from Peterson et al. (1995), Behr (2003a,b), Kinman et al. (2000), and Recio-Blanco et al. (2004). Upper limits are marked with grey triangles. The black diamonds mark the sdBs from our sample. The vertical line marks the jump temperature of 11 500 K.

higher $v_{\text{rot}} \sin i = 10\text{--}12 \text{ km s}^{-1}$, the distribution is again very similar to the distributions shown before (see Figs. 2–4). Subdwarf B stars in close binaries obviously rotate in the same way as single stars or sdBs with visible companions if the orbital period is sufficiently long.

5. Comparison with BHB stars

Projected rotational velocities of BHB stars have been determined for many globular cluster and field stars (Peterson et al. 1995; Behr 2003a,b; Kinman et al. 2000; Recio-Blanco et al. 2004). The results are plotted against the effective temperature in Fig. 6. The characteristic jump in $v_{\text{rot}} \sin i$ at a temperature of about $\approx 11\,500$ K can be clearly seen. The sdB sequence basically extends the BHB trend to higher temperatures. The $v_{\text{rot}} \sin i$ values remain at the same level as observed in hot BHB stars.

Comparing the $v_{\text{rot}} \sin i$ of BHB and EHB stars, one has to take into account that the radii of both types of HB stars are quite different, which translates directly into very different angular momenta. While sdBs have surface gravities $\log g$ between 5.0 and 6.0, the surface gravities of BHB stars range from $\log g = 3.0$ to 4.0. The BHB stars with the same rotational velocities as EHB stars have higher angular momenta. Assuming rigid rotation, the same inclination angle of the rotation axis, and the same mass of $\approx 0.5 M_{\odot}$ for BHB and EHB stars, one can calculate the quantity $v_{\text{rot}} \sin i \times g^{-1/2}$, which is directly proportional to the angular momentum. The surface gravities of the sdBs were taken from the literature (see Sect. 2), those for the BHB stars from Behr (2003a,b) and Kinman et al. (2000). Since Peterson et al. (1995) and Recio-Blanco et al. (2004) did not determine surface gravities for their BHB sample, we adopted a $\log g$ of 3.0 for stars with temperatures below $\approx 10\,000$ K and 3.5 for the hotter ones as suggested by the results of Behr (2003a,b) and Kinman et al. (2000).

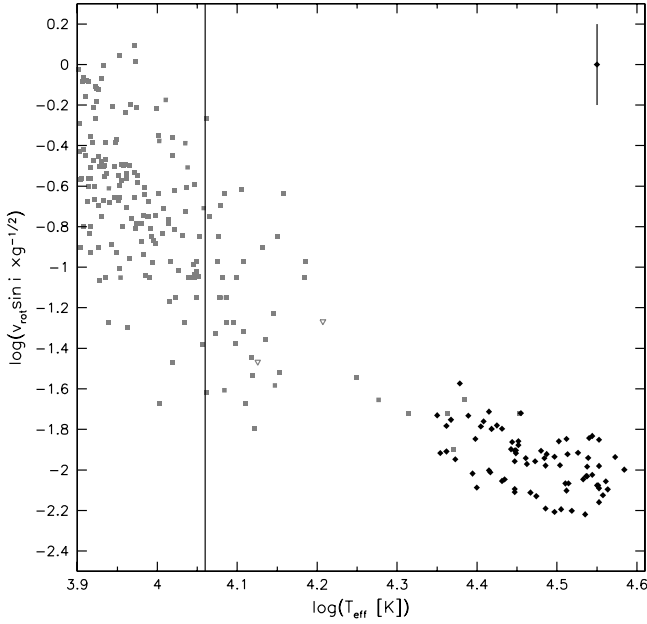


Fig. 7. $v_{\text{rot}} \sin i \times g^{-1/2}$ plotted against effective temperature. The grey squares mark BHB and some sdB stars taken from Peterson et al. (1995), Behr (2003a,b), Kinman et al. (2000), and Recio-Blanco et al. (2004). Upper limits are marked with grey triangles. The black diamonds mark the sdBs from our sample. The vertical line marks the jump temperature of 11 500 K. Typical uncertainties for the sdBs are given in the upper right corner.

In Fig. 7 $v_{\text{rot}} \sin i \times g^{-1/2}$ is plotted against T_{eff} . The transition between BHB and EHB stars is smooth. Since the progenitors of the EHB stars lost more envelope material on the RGB, the EHB stars are expected to have lower angular momenta than the BHB stars. This is consistent with what can be seen in Fig. 7.

6. Implications for hot subdwarf formation

The uniform distribution of low projected rotational velocities in single and wide binary sdBs has consequences for the open question of hot subdwarf formation. As shown in this study, sdBs appear to rotate at low but spectroscopically detectable velocities of $8\text{--}10 \text{ km s}^{-1}$. These results are remarkably similar to those derived for their cooler relatives, the BHB stars. Hot subdwarfs are likely formed through binary interaction or merging, which is also accompanied by a transfer of angular momentum. The rotational properties of sdB stars therefore allow one to constrain possible formation scenarios.

6.1. Uniform rotation of EHB stars and mass loss on the RGB

The rotational properties of sdBs residing on the EHB are very similar to those of hot BHB stars. The only exception is that the EHB stars obviously lost more envelope in the red-giant phase and therefore retained less angular momentum. How the envelope is lost does not affect the rotational velocities of sdB stars, since the $v_{\text{rot}} \sin i$ -distribution of RV variable systems with orbital periods sufficiently long to neglect the tidal influence of the companion (Fig. 5) is similar to those of apparently single sdB stars (Fig. 3) and for sdB stars with visible main sequence companions (Fig. 4).

The abundance patterns of sdBs are dominated by diffusion processes very similar to those of the hot BHB stars

(Geier et al. 2010a). No surface convection zone should be present, and according to the model of Brown (2007) the angular momentum of the outer layers should be low. Stellar winds and magnetic fields may help to slow down the upper layers of the star. However, Unglaub (2008) showed that the weak winds predicted for sdB stars are most likely fractionated and are therefore not able to carry away the most abundant elements hydrogen and helium.

Angular momentum gained or retained from the formation process may also be stored in the stellar core, which may be rapidly rotating. Kawaler & Hostler (2005) proposed such a scenario and suggested an asteroseismic approach to probe the rotation of the inner regions of sdBs. Van Grootel et al. (2008) and Charpinet et al. (2008) performed such an analysis for the two short-period sdB pulsators Feige 48 and PG 1336–018, respectively, and found no deviation from rigid rotation at least in the outer layers of these stars down to about half the stellar radius. But these results may not be representative, because both stars are in close binary systems and are synchronised by the tidal influence of their companions (Geier et al. 2010b). The rigid body rotation may have been caused by this effect and may not be a general feature of sdBs. Another setback of these analyses is the problem that p-mode pulsations are not suited to probe the innermost regions of sdBs. In contrast to that, g-mode pulsations reach the stellar core and it should be possible to measure the rotational properties of the whole stellar interior with asteroseismic methods. With the availability of high-precision light curves from the Kepler and CoRoT missions, the analysis of g-mode pulsators became possible and first results have been published by van Grootel et al. (2010) and Charpinet et al. (2011b).

For the RV variable systems CE ejection is the only feasible formation channel. The systems with visible companions may have lost their envelopes via stable RLOF. Very recently, Østensen et al. (2012) and Deca et al. (2012) reported the discovery of sdB+MS binaries with orbital periods up to $\approx 1200 \text{ d}$, which may have been sufficiently close for mass transfer. However, the visible companions to the sdBs may still have been separated by too much for an interaction with the subdwarf progenitors. More detailed binary evolution calculations are needed to solve this problem. Common envelope ejection and stable RLOF form similar sdB stars, because in both cases the hydrogen envelope is removed and the helium burning should start under similar conditions. It would therefore not be surprising if their $v_{\text{rot}} \sin i$ -distributions were to look similar.

6.2. Where are the He-WD merger products?

The $v_{\text{rot}} \sin i$ -distribution of the single sdB stars (Fig. 3) is particularly hard to understand in the context of the WD merger scenario. If a certain fraction or even all of the apparently single sdBs would have been formed in this way, one would not expect a $v_{\text{rot}} \sin i$ -distribution that resembles that of the post-CE or post-RLOF sdBs. Gourgouliatos & Jeffery (2006) showed that the merger product of two WDs would rotate faster than break-up velocity, if angular momentum were conserved. These authors concluded that angular momentum must be lost during the merger process. One way to lose angular momentum are stellar winds and magnetic fields. Another explanation may be the interaction with the accretion disc during the merger. If the less massive object is disrupted, it should form an accretion disc around the more massive component. The WD can only gain mass if angular momentum is transported outward in the disc. This process is expected to spin down the merger product (Gourgouliatos & Jeffery 2006). According to a model

proposed by Podsiadlowski (priv. comm.), the merger is accompanied by a series of outbursts caused by the ignition of helium. These flashes remove angular momentum from the merged remnant and should slow it down to rotational velocities of less than 20 km s^{-1} .

However, even if it is possible to slow down the merged remnant of two He-WDs, it is very unlikely that the merger products would have a $v_{\text{rot}} \sin i$ -distribution almost identical to sdBs, of which we know that they were formed via CE-ejection or maybe stable RLOF. This would require an extreme fine-tuning of parameters, unless there is an as yet unknown mechanism at work, which leads to uniform rotation of the radiative, diffusion-dominated atmospheres. It is therefore questionable whether our sample contains stars that were formed by an He-WD merger or a CE-merger event. If this is not the case and because of the size of our sample, it would be safe to conclude that the merger channel does not contribute significantly to the observed population of single hydrogen-rich sdO/Bs in contrast to the models of Han et al. (2002, 2003).

This conclusion is consistent with the most recent results by Fontaine et al. (2012), who studied the empirical mass distribution of sdB stars derived from eclipsing binary systems and asteroseismic analyses. The lack of sdB stars more massive than $\approx 0.5 M_{\odot}$, which would be the outcome of the merger channel, led to the conclusion that mergers are less frequent in the formation process of isolated sdB stars than predicted by theory.

The only known single and fast rotating hot subdwarf star EC 22081–1916 (Geier et al. 2011a) may be the rare outcome of a CE merger event as suggested by Politano et al. (2008). It is unique among ≈ 100 sdBs of our sample.

Possible candidates for WD-merger products are the helium rich sdOs (He-sdOs, Ströer et al. 2007), since Hirsch et al. (2009) measured $v_{\text{rot}} \sin i$ values of $20\text{--}30 \text{ km s}^{-1}$ for some of those stars. Although their velocities are not particularly high, they are significantly different from the typical $v_{\text{rot}} \sin i$ of sdBs. However, while the He-sdOs were first considered as single stars (Napiwotzki et al. 2008), evidence grows that a fraction of them resides in close binaries (Green et al. 2008; Geier et al. 2011c). At least those He-sdOs could not have been formed by a He-WD merger.

6.3. Alternative formation scenarios

Because the canonical binary scenario for sdB formation, which rests on the three pillars CE ejection, stable RLOF and He-WD merger, turned out to be very successful not only in explaining the properties of sdBs in the field (Han et al. 2002, 2003), but also in globular clusters (Han 2008) and the UV-upturn phenomenon in old galaxies (Han et al. 2007), the possible lack of merger candidates poses a problem.

Alternative formation scenarios such as CE ejection triggered by substellar companions (Soker 1998; Bear & Soker 2012) may be responsible for the formation of apparently single sdBs. Evidence grows that such objects are quite common around sdB stars (e.g. Silvotti et al. 2007; Geier et al. 2011d; Charpinet et al. 2011a). In the light of the results presented here and other recent observational evidence, the conclusion has to be drawn that the question of sdB formation is still far from settled.

7. Connection to white dwarfs

Owing to their thin hydrogen envelopes, hot subdwarf stars will not evolve to the asymptotic giant branch

(AGB-manqué, Dorman et al. 1993). After about 100 Myr of core He-burning on the EHB and a shorter episode of He-shell burning, these objects will join the WD cooling sequence.

The rotational properties of single WDs are difficult to determine. Owing to the high pressure in the dense WD atmospheres, the spectral lines of WDs are strongly broadened and hence do not appear to be suitable to measure $v_{\text{rot}} \sin i$. However, the H_{α} line often displays a sharp line core, which is caused by NLTE effects. In a small fraction of the WD-population metal lines are visible. However, excellent high-resolution spectra are necessary to constrain the projected rotational velocity (Berger et al. 2005).

The derived upper limits ($\approx 10\text{--}50 \text{ km s}^{-1}$) are consistent with the much lower rotational velocities of pulsating WDs derived with asteroseismic methods ($\approx 0.2\text{--}3.5 \text{ km s}^{-1}$, Kawaler 2003). Most single WDs are therefore obviously rather slow rotators. The reason for this is most likely a significant loss of mass and angular momentum due to stellar winds and thermal pulses in the AGB-phase, as has been shown by Charpinet et al. (2009).

The properties of WDs evolved from sdB progenitors on the other hand should be very different. Since the hot subdwarfs bypass the AGB-phase, both their masses and their angular momenta are expected to remain more or less constant when evolving to become WDs.

The average mass of these sdB remnants ($\approx 0.47 M_{\odot}$) is expected to be significantly lower than the average mass of normal WDs ($\approx 0.6 M_{\odot}$). But more importantly, the rotational velocities of these WDs must be very high. We have shown that single sdBs have small, but still detectable $v_{\text{rot}} \sin i$. Assuming rigid rotation and conservation of mass and angular momentum, the rotational velocity at the surface scales with the stellar radius. Because the radius decreases by a factor of about 10, the rotational velocity should increase by a factor of about 100. Assuming an average $v_{\text{rot}} \approx 8 \text{ km s}^{-1}$ for single sdBs, WDs evolved through an EHB-phase should therefore have an average $v_{\text{rot}} \approx 800 \text{ km s}^{-1}$. Because about 1% of all WDs are expected to have evolved through an EHB-phase, we expect a similar fraction of extremely fast rotating, low-mass WDs. These high $v_{\text{rot}} \sin i$ -values should be easily detectable even in medium-resolution spectra. The sample of WDs with observed spectra from the Sloan Digital Sky Survey (Eisenstein et al. 2006) for example should contain more than 100 of these objects.

8. Summary

We extended a project to derive the rotational properties of sdB stars and determined the projected rotational velocities of 105 sdB stars by measuring the broadening of metal lines using high-resolution spectra. All stars in our sample have low $v_{\text{rot}} \sin i < 10 \text{ km s}^{-1}$. For $\approx 75\%$ of the sample we were able to determine significant rotation. The distribution of projected rotational velocities is consistent with an average rotation of $\approx 8 \text{ km s}^{-1}$ for the sample. Furthermore, the $v_{\text{rot}} \sin i$ -distributions of single sdBs, hot subdwarfs with main sequence companions visible in the spectra and close binary systems with periods exceeding 1.2 d are similar. The BHB and EHB stars are related in terms of surface rotation and angular momentum. Hot BHBs with diffusion-dominated atmospheres are slow rotators like the EHB stars, which lost more envelope and therefore angular momentum on the RGB. The uniform rotation distributions of single and wide binary sdBs pose a challenge to our understanding of hot subdwarf formation. Especially the high fraction of He-WD mergers predicted by theory seems to be inconsistent with our results. We predict

that the evolutionary channel of single sdB stars gives birth to a small population of rapidly rotating WDs with masses lower than average.

Acknowledgements. S.G. was supported by the Deutsche Forschungsgemeinschaft under grant He 1354/49-1. The authors thank N. Reid, R. Napiwotzki, L. Morales-Rueda and H. Edelmann for providing their data. Furthermore, we would like to thank the referee G. Fontaine for his comments and suggestions.

References

- Bear, E., & Soker, N. 2012, *ApJ*, 749, L14
- Behr, B. B. 2003a, *ApJS*, 149, 67
- Behr, B. B. 2003b, *ApJS*, 149, 101
- Behr, B. B., Cohen, J. G., & McCarthy, J. K. 2000a, *ApJ*, 531, L57
- Behr, B. B., Djorgovski, S. G., Cohen, J. G., et al. 2000b, *ApJ*, 528, 849
- Berger, L., Koester, D., Napiwotzki, R., Reid, I. N., & Zuckerman, B. 2005, *A&A*, 444, 565
- Billères, M., Fontaine, G., Brassard, P., et al. 1998, *ApJ*, 494, L75
- Billères, M., Fontaine, G., Brassard, P., & Liebert, J. 2002, *ApJ*, 578, 515
- Blanchette, J.-P., Chayer, P., Wesemael, F., et al. 2008, *ApJ*, 678, 1329
- Brown, D. 2007, Ph.D. Thesis, Liverpool John Moores University
- Brown, D., Salaris, M., Cassisi, S., & Pietrinfermi, A. 2008, *Mem. Soc. Astron. It.*, 79, 579
- Caloi, V. 1999, *A&A*, 343, 904
- Carney, B. W., Latham, D. W., Stefanik, R. P., Laird, J. B., & Morse, J. A. 2003, *AJ*, 125, 293
- Carney, B. W., Gray, D. F., Yong, D., et al. 2008, *ApJ*, 135, 892
- Charpinet, S., Fontaine, G., Brassard, P., et al. 1997, *ApJ*, 483, 123
- Charpinet, S., van Grootel, V., Reese, D., et al. 2008, *A&A*, 489, 377
- Charpinet, S., Fontaine, G., & Brassard, P. 2009, *Nature*, 461, 501
- Charpinet, S., Fontaine, G., Brassard, P., et al. 2011a, *Nature*, 480, 496
- Charpinet, S., van Grootel, V., Fontaine, G., et al. 2011b, *A&A*, 530, A3
- Copperwheat, C. M., Morales-Rueda, L., Marsh, T. R., Maxted, P. F. L., & Heber, U. 2011, *MNRAS*, 415, 1381
- de Marchi, G., & Paresce, F. 1996, *ApJ*, 467, 658
- D’Cruz, N. L., Dorman, B., Rood, R. T., & O’Connell, R. W. 1996, *ApJ*, 466, 359
- Deca, J., Marsh, T. R., Østensen, R. H., et al. 2012, *MNRAS*, 421, 2798
- Dorman, B., Rood, R. T., & O’Connell, R. W. 1993, *ApJ*, 419, 596
- Edelmann, H., Heber, U., & Napiwotzki, R. 2001, *Astron. Nachr.*, 322, 401
- Edelmann, H., Heber, U., Altmann, M., Karl, C., & Lisker, T. 2005, *A&A*, 442, 1023
- Eisenstein, D. J., Liebert, J., Harris, H. C., et al. 2006, *ApJS*, 167, 40
- Fabbian, D., Recio-Blanco, A., Gratton, R. G., & Piotto, G. 2005, *A&A*, 434, 235
- Fontaine, G., Brassard, P., Charpinet, S., et al. 2012, *A&A*, 539, A12
- For, B.-Q., & Sneden, C. 2010, *AJ*, 140, 1694
- Geier, S., Nesslinger, S., Heber, U., et al. 2007, *A&A*, 464, 299
- Geier, S., Heber, U., Edelmann, H., Morales-Rueda, L., & Napiwotzki, R. 2010a, *Ap&SS*, 329, 127
- Geier, S., Heber, U., Podsiadlowski, Ph., et al. 2010b, *A&A*, 519, A25
- Geier, S., Classen, L., & Heber, U. 2011a, *ApJ*, 733, L13
- Geier, S., Hirsch, H., Tillich, A., et al. 2011b, *A&A*, 530, A28
- Geier, S., Schaffenroth, V., Drechsel, H., et al. 2011c, *ApJ*, 731, L22
- Geier, S., Heber, U., Edelmann, H., et al. 2012, *ASP Conf. Ser.*, 452, 57
- Gourgouliatos, K. N., & Jeffery, C. S. 2006, *MNRAS*, 371, 1381
- Green, E. M., Fontaine, G., Reed, M. D., et al. 2003, *ApJ*, 583, L31
- Green, E. M., Fontaine, G., Hyde, E. A., Charpinet, S., & Chayer, P. 2006, *Baltic Astron.*, 15, 167
- Green, E. M., Fontaine, G., Hyde, E. A., For, B.-Q., & Chayer, P. 2008, *ASP Conf. Ser.*, 392, 75
- Grundahl, F., Catelan, M., Landsman, W. B., et al. 1999, *ApJ*, 524, 242
- Han, Z. 2008, *A&A*, 484, 31
- Han, Z., Podsiadlowski, P., Maxted, P. F. L., Marsh, T. R., & Ivanova, N. 2002, *MNRAS*, 336, 449
- Han, Z., Podsiadlowski, P., Maxted, P. F. L., & Marsh, T. R. 2003, *MNRAS*, 341, 669
- Han, Z., Podsiadlowski, P., & Lynas-Gray, A. E. 2007, *MNRAS*, 380, 1098
- Heber, U. 1986, *A&A*, 155, 33
- Heber, U. 2009, *ARA&A*, 47, 211
- Heber, U., Reid, I. N., & Werner, K. 1999, *A&A*, 348, L25
- Heber, U., Reid, I. N., & Werner, K. 2000, *A&A*, 363, 198
- Hirsch, H., & Heber, U. 2009, *JPhCS*, 172, 2015
- Iben, I., & Tutukov, A. V. 1984, *ApJ*, 284, 719
- Jeffery, C. S., & Pollacco, D. 2000, *MNRAS*, 318, 974
- Kawaler, S. D. 2003, in *Proc. IAU Symp.* 215, eds. A. Maeder, & P. Eenens
- Kawaler, S. D., & Hostler, S. R. 2005, *ApJ*, 621, 432
- Kilkenny, D., Koen, C., O’Donoghue, D., & Stobie, R. S. 1997, *MNRAS*, 285, 640
- Kilkenny, D., Copley, C., Zietsman, E., & Worters, H. 2007, *MNRAS*, 375, 1325
- Kinman, T. D., Castelli, F., Cacciari, C., et al. 2000, *A&A*, 364, 102
- Koen, C., Kilkenny, D., Pretorius, M. L., & Frew, D. J. 2010, *MNRAS*, 401, 1850
- Lemke, M. 1997, *A&AS*, 122, 285
- Lisker, T., Heber, U., Napiwotzki, R., Christlieb, N., Han, Z., et al. 2005, *A&A*, 430, 223
- Marietta, E., Burrows, A., & Fryxell, B. 2000, *ApJS*, 128, 615
- Maxted, P. F. L., Marsh, T. R., & North, R. C. 2000, *MNRAS*, 317, L41
- Maxted, P. F. L., Heber, U., Marsh, T. R., & North, R. C. 2001, *MNRAS*, 326, 139
- Mengel, J. G., Norris, J., & Gross, P. G. 1976, *ApJ*, 204, 488
- Michaud, G., Vauclair, G., & Vauclair, S. 1983, *ApJ*, 267, 256
- Michaud, G., Richer, J., & Richard, O. 2008, *ApJ*, 675, 1223
- Morales-Rueda, L., Maxted, P. F. L., Marsh, T. R., North, R. C., & Heber, U. 2003, *MNRAS*, 338, 752
- Napiwotzki, R. 2008, *ASP Conf. Ser.*, 392, 139
- Napiwotzki, R., Christlieb, N., Drechsel, H., et al. 2001, *Astron. Nachr.*, 322, 411
- Napiwotzki, R., Christlieb, N., Drechsel, H., et al. 2003, *ESO Msngr*, 112, 25
- Napiwotzki, R., Karl, C. A., Lisker, T., et al. 2004a, *Ap&SS*, 291, 321
- Napiwotzki, R., Yungelson, L., Nelemans, G., et al. 2004b, *ASP Conf. Ser.*, 318, 402
- O’Donoghue, D., Koen, C., Kilkenny, D., & Stobie, R. S. 1999, *ASP Conf. Ser.*, 169, 149
- Østensen, R. H., & van Winckel, H. 2012, *ASP Conf. Ser.*, 452, 163
- Østensen, R. H., Oreiro, R., Solheim, J.-E., et al. 2010, *A&A*, 513, A6
- Pace, G., Recio-Blanco, A., Piotto, G., & Momany, Y. 2006, *A&A*, 452, 493
- Peterson, R. C. 1983, *ApJ*, 275, 737
- Peterson, R. C. 1985, *ApJ*, 294, L35
- Peterson, R. C., Tarbell, T. D., & Carney, B. W. 1983, *ApJ*, 265, 972
- Peterson, R. C., Rood, R. T., & Crocker, D. A. 1995, *ApJ*, 453, 214
- Politano, M., Taam, R. E., van der Sluys, M., & Willems, B. 2008, *ApJ*, 687, L99
- Przybilla, N., Nieva, M. F., & Edelmann, H. 2006, *Baltic Astron.*, 15, 107
- Quievy, D., Charbonneau, P., Michaud, G., & Richer, J. 2009, *A&A*, 500, 1163
- Randall, S. K., Fontaine, G., Green, E. M., et al. 2006, *ApJ*, 643, 1198
- Recio-Blanco, A., Piotto, G., Aparicio, A., & Renzini, A. 2002, *ApJ*, 572, L71
- Recio-Blanco, A., Piotto, G., Aparicio, A., & Renzini, A. 2004, *A&A*, 452, 875
- Saffer, R. A., Bergeron, P., Koester, D., & Liebert, J. 1994, *ApJ*, 432, 351
- Sills, A., & Pinsonneault, M. H. 2000, *ApJ*, 540, 489
- Silvotti, R., Schuh, S., Janulis, R., et al. 2007, *Nature*, 449, 189
- Soker, N. 1998, *AJ*, 116, 1308
- Ströer, A., Heber, U., Lisker, T., et al. 2007, *A&A*, 462, 269
- Sweigart, A. V. 1997a, in *Third Conference on Faint Blue Stars*, eds. A. G. D. Philip, J. Liebert, R. Saffer, & D. S. Hayes (Schenectady: L. Davis Press), 3
- Sweigart, A. V. 2002, *Highlights of Astronomy*, 12, 292
- Telting, J. H., Geier, S., Østensen, R. H., et al. 2008, *A&A*, 492, 815
- Unglaub, K. 2008, *A&A*, 486, 923
- van Grootel, V., Charpinet, S., Fontaine, G., & Brassard, P. 2008, *A&A*, 483, 875
- van Grootel, V., Charpinet, S., Fontaine, G., Green, E. M., & Brassard, P. 2010, *A&A*, 524, A63
- Vink, J. S., & Cassisi, S. 2002, *A&A*, 392, 553
- Webbink, R. F. 1984, *ApJ*, 277, 355

Orbital solutions of eight close sdB binaries and constraints on the nature of the unseen companions[★]

S. Geier¹, R. H. Østensen², U. Heber³, T. Kupfer⁴, P. F. L. Maxted⁵, B. N. Barlow⁶, M. Vučković⁷, A. Tillich³, S. Müller³, H. Edelmann³, L. Classen³, and A. F. McLeod^{2,4}

¹ European Southern Observatory, Karl-Schwarzschild-Str. 2, 85748 Garching, Germany
e-mail: geier@sternwarte.uni-erlangen.de

² Institute of Astronomy, KU Leuven, Celestijnenlaan 200D, 3001 Heverlee, Belgium

³ Dr. Karl Remeis-Observatory & ECAP, Astronomical Institute, Friedrich-Alexander University Erlangen-Nuremberg, Sternwartstr. 7, 96049 Bamberg, Germany

⁴ Department of Astrophysics/IMAPP, Radboud University Nijmegen, PO Box 9010, 6500 GL Nijmegen, The Netherlands

⁵ Astrophysics Group, Keele University, Staffordshire, ST5 5BG, UK

⁶ Department of Physics, High Point University, 833 Montlieu Avenue, High Point, NC 27262, USA

⁷ European Southern Observatory, Alonso de Cordova 3107, Vitacura, Casilla 19001, Santiago, Chile

Received 22 November 2013 / Accepted 13 December 2013

ABSTRACT

The project Massive Unseen Companions to Hot Faint Underluminous Stars from SDSS (MUCHFUSS) aims at finding hot subdwarf stars (sdBs) with massive compact companions such as white dwarfs, neutron stars, or stellar-mass black holes. In a supplementary programme we obtained time-resolved spectroscopy of known hot subdwarf binary candidates. Here we present orbital solutions of eight close sdB binaries with orbital periods ranging from ~ 0.1 d to 10 d, which allow us to derive lower limits on the masses of their companions. Additionally, a dedicated photometric follow-up campaign was conducted to obtain light curves of the reflection-effect binary HS 2043+0615. We are able to constrain the most likely nature of the companions in all cases but one, making use of information derived from photometry and spectroscopy. Four sdBs have white dwarf companions, while another three are orbited by low-mass main sequence stars of spectral type M.

Key words. binaries: spectroscopic – subdwarfs

1. Introduction

Subluminous B stars or hot subdwarfs (sdBs) are core helium-burning stars with thin hydrogen envelopes and masses around $0.5 M_{\odot}$ (Heber 1986; see Heber 2009, for a review). A large proportion of the sdB stars (40% to 80%) are members of short-period binaries (Maxted et al. 2001; Napiwotzki et al. 2004a). Several studies aimed at determining the orbital parameters of short-period subdwarf binaries and have found periods ranging from 0.05 d to more than 10 d with a peak around 0.5 to 1.0 d (e.g. Morales-Rueda et al. 2003; Edelmann et al. 2005; Copperwheat et al. 2010). For these close binary sdBs, common envelope (CE) ejection is the only feasible formation channel. At first, two main sequence stars evolve in a binary system. The more massive one will then enter the red-giant phase and eventually fill its Roche lobe. Triggered by dynamically unstable mass transfer, a common envelope is formed. Owing to friction the two stellar cores lose orbital energy, which is deposited within the envelope and leads to a shrinking of the binary orbit. Eventually, the common envelope is ejected and a close binary system is formed, which contains a core helium-burning sdB and a main sequence companion. A close sdB binary with

white dwarf (WD) companion is formed after two consecutive phases of mass-transfer (Han et al. 2002, 2003).

The nature of the close companions to sdB stars is hard to constrain in general, since most of those binaries are single-lined with the hot subdwarf being the only star detectable in the spectrum. Measuring the Doppler reflex motion of this star from time-resolved spectra, the radial velocity (RV) curve can be derived and a lower limit can be given for the mass of the companion from the binary mass function. These lower limits are in general compatible with main sequence stars of spectral type M or compact objects such as white dwarfs.

Subdwarf binaries with massive WD companions are candidates for supernova type Ia (SN Ia) progenitors because these systems lose angular momentum through the emission of gravitational waves and start mass transfer. This mass transfer, either from accretion of helium onto the WD during the sdB phase (see Wang et al. 2013, and references therein), or the subsequent merger of the system (Tutukov & Yungelson 1981; Webbink 1984), may cause the companion to explode as SN Ia. Two of the best known candidate systems for SN Ia are sdB+WD binaries (Maxted et al. 2000; Geier et al. 2007, 2013; Vennes et al. 2012). More candidates, some of which might even have more massive compact companions (i.e. neutron stars or black holes), have been found as well (Geier et al. 2008, 2010a,b). Such systems are also predicted by binary evolution theory (Podsiadlowski et al. 2002; Pfahl et al. 2003; Yungelson & Tutukov 2005; Nelemans 2010).

[★] Radial velocities are available in electronic form at <http://www.aanda.org> and at the CDS via anonymous ftp to cdsarc.u-strasbg.fr (130.79.128.5) or via <http://cdsarc.u-strasbg.fr/viz-bin/qcat?J/A+A/562/A95>

The project Massive Unseen Companions to Hot Faint Underluminous Stars from SDSS (MUCHFUSS) aims at finding sdBs with such massive compact companions. We selected and classified hot subdwarf stars from the Sloan Digital Sky Survey (SDSS, Data Release 7, Abazajian et al. 2009) by colour selection and visual inspection of their spectra. Radial velocity variable subdwarfs with high shifts were selected as candidates for time-resolved spectroscopy to derive their orbital parameters and follow-up photometry to search for features such as eclipses in their light curves.

Target selection and follow-up strategy were presented in Geier et al. (2011a, 2012). In a spin-off project the kinematics of fast-moving sdBs in the halo have been studied (Tillich et al. 2011). The spectroscopic and photometric follow-up campaigns of the binary candidates are described in Geier et al. (2011b), Kupfer et al. (in prep.), and Schaffenroth et al. (in prep.). We discovered three eclipsing binary systems, two of them with brown dwarf companions (Geier et al. 2011c; Schaffenroth et al., in prep.), and one hybrid sdB pulsator with reflection effect (Østensen et al. 2013). Here we report on our supplementary programme that investigates known hot subdwarf binaries.

2. MUCHFUSS supplementary programme

In addition to the priority objects, the MUCHFUSS project targeted known sdB binaries of special importance, whenever scheduling constraints or weather conditions were unsuitable to execute the main programme. In particular, objects were included for which light variations either caused by eclipses, by the reflection effect, or by stellar oscillations have been reported in the literature, because this complementary information is of great value for understanding their nature and evolutionary history.

Providing sufficient RV information is therefore rewarding. We also keep a list of targets, that have insufficient RV coverage, mostly from the SPY survey (Lisker et al. 2005) and Copperwheat et al. (2010). The highlight of our supplementary programme so far was the discovery of the ultracompact sdB+WD binary CD-30°11223. It is not only the shortest-period ($P \simeq 0.049$ d) hot subdwarf binary known, but also an excellent progenitor candidate for an underluminous SN Ia (Geier et al. 2013).

Here we present orbital solutions of eight close hot subdwarf binaries, which allow us to derive lower limits on the masses of their companions. Furthermore, we are able to constrain the most likely nature of the companions in all cases but one, making use of additional information derived from photometry and spectroscopy.

3. Observations and data reduction

3.1. Spectroscopic observations

Follow-up medium resolution spectra were taken during dedicated MUCHFUSS follow-up runs (Geier et al. 2011a,b; Kupfer et al., in prep.) with the EFOSC2 spectrograph ($R \simeq 2200, \lambda = 4450\text{--}5110 \text{ \AA}$) mounted at the ESO-NTT, the ISIS spectrograph ($R \simeq 4000, \lambda = 3440\text{--}5270 \text{ \AA}$) mounted at the WHT, the TWIN spectrograph mounted at the CAHA-3.5 m telescope ($R \simeq 4000, \lambda = 3460\text{--}5630 \text{ \AA}$), and the Goodman spectrograph mounted at the SOAR telescope ($R \simeq 2500, \lambda = 3500\text{--}6160 \text{ \AA}$).

In addition to this we used spectra taken with the EMMI instrument ($R \simeq 3400, \lambda = 3900\text{--}4400 \text{ \AA}$) mounted at the

ESO-NTT and the UVES spectrograph ($R \simeq 20\,000, \lambda = 3300\text{--}6600 \text{ \AA}$) mounted at the ESO-VLT in the course of the ESO Supernova Ia Progenitor Survey (SPY, Napiwotzki et al. 2003). Data taken for studies of sdB binaries at high resolution (Edelmann et al. 2005; Classen et al. 2011) both with the FEROS spectrograph ($R \simeq 48\,000, \lambda = 3800\text{--}9200 \text{ \AA}$) mounted at the ESO/MPG-2.2 m telescope and with the Cross-Dispersed Echelle Spectrograph ($R \simeq 60\,000, \lambda = 3700\text{--}10\,000 \text{ \AA}$) mounted at the McDonald observatory 2.7 m telescope were used as well. Reduction was made either with the MIDAS, IRAF or PAMELA and MOLLY¹ packages.

3.2. Photometry of HS 2043+0615

HS 2043+0615 was extensively observed with the MEROPE camera at the Mercator telescope during the 2007 observing season. In total we used R_C -band photometry from 16 different nights, the first from April 22 and the last from November 15. The exposure time for these observations was 300 s, and we collected in total 516 useful observations. Most of these runs spanned only a fraction of an orbit, and the photometric reduction was complicated because different setups and windows were used during the different runs, forcing us to use different reference stars for different runs. No standards were observed for these runs either, so to calibrate the photometry we made a catalogue of 22 stars in the field, starting by assigning R -band magnitudes from the NOMAD survey to each of the stars. These were then iteratively corrected until consistent values were achieved. The corrected magnitudes were then used to calibrate the differential photometry of HS 2043+0615 to a common scale.

Recently, HS 2043+0615 was reobserved with the three-channel MAIA camera on the Mercator telescope (Raskin et al. 2013). MAIA splits the incoming light into three beams with dichroics to produce simultaneous photometry in a red, green, and UV channel, using three cameras equipped with large-format frame-transfer CCDs. We used an observing mode in which the R and G channels were read out every 120 s and the U channel only every second cycle to increase the signal-to-noise ratio. A run of 7 h duration, almost a complete orbital cycle, was obtained on the night of September 3, 2013.

4. Orbital and atmospheric parameters

The radial velocities were measured by fitting a set of mathematical functions to all suitable hydrogen Balmer as well as helium lines simultaneously, using χ^2 -minimization and the RV shift with respect to the rest wavelengths was measured (FITSB2, Napiwotzki et al. 2004b). Gaussians were used to match the line cores, Lorentzians to match the line wings, and polynomials to match the continua. The RVs and formal 1σ -errors are given in Appendix A.

For four binaries of our sample (HE 1415-0309, HS 2359+1942, LB 1516, and BPS CS 22879-149) the orbital parameters T_0 , period P , system velocity γ , and RV-semiamplitude K as well as their uncertainties and associated false-alarm probabilities ($p_{\text{false}}[1\%]$, $p_{\text{false}}[10\%]$) were determined as described in Geier et al. (2011b). To estimate the significance of the orbital solutions and the contributions of systematic effects to the error budget, we normalised the χ^2 of the most probable solution by adding systematic errors e_{norm} in quadrature until the reduced χ^2 reached $\simeq 1.0$. The phased RV

¹ <http://www2.warwick.ac.uk/fac/sci/physics/research/astro/people/marsh/software>

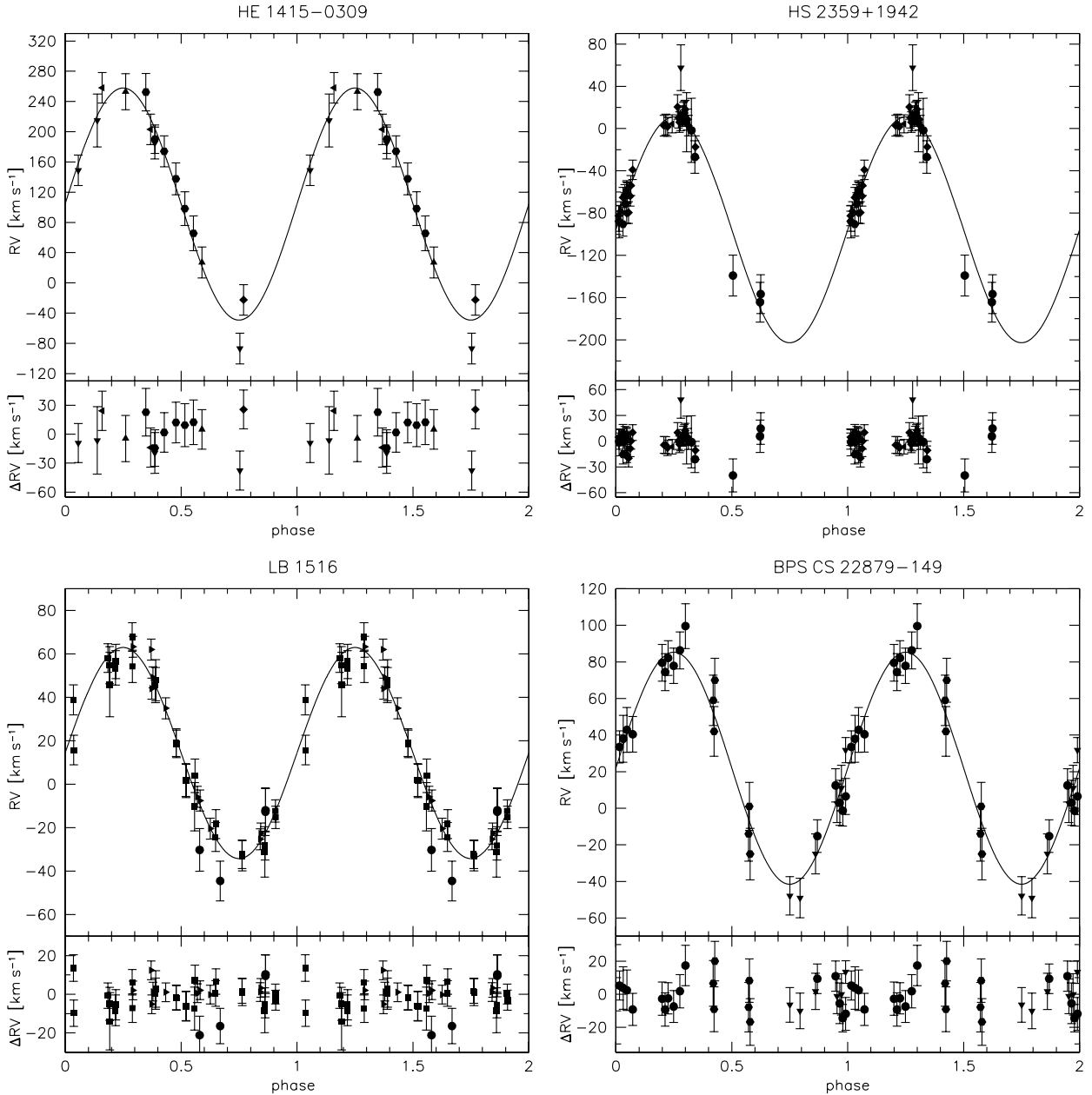


Fig. 1. Radial velocity plotted against orbital phase. The RV data were phase folded with the most likely orbital periods. The residuals are plotted below. The RVs were measured from spectra obtained with CAHA-3.5 m/TWIN (upward triangles), WHT/ISIS (diamonds), ESO-NTT/EMMI (downward triangles), ESO-VLT/UVES (triangles turned to the left), ESO-MPG2.2 m/FEROS (triangles turned to the right), ESO-NTT/EFOSC2 (circles) and SOAR/Goodman (hexagons). RVs of LB 1516 taken from Copperwheat et al. (2010) are marked with rectangles. The RV data of BPS CS 22879–149 was folded to the period alias at 0.478 d.

curves for the best solutions are given in Fig. 1, the χ^2 -values plotted against orbital period in Fig. 2. The minimum in χ^2 corresponds to the most likely solution. The adopted systematic errors and false-alarm probabilities are given in Table 1. The probabilities that the adopted orbital periods are correct to within 10% range from 90% to more than 99.99%. For BPS CS 22879–149, no unique solution was found. The two possible solutions are discussed in Sect. 5.4.

For OGLE BUL–SC16335 and V 1405 Ori the orbital period was independently determined from the variations seen in their light curves. These periods were kept fixed, but the other orbital parameters were determined in the way described above. The likely period of the eclipsing sdB+WD PG 0941+280 was estimated from a light curve plotted in

Green et al. (2004) and compared with the period aliases derived from the RV measurements. The alias closest to the estimate from the light curve was identified as solution. A similar approach was chosen for the reflection effect binary HS 2043+0615, for which the most likely period of the light curve was compared with the corresponding alias periods of the radial velocity curve. The phased radial velocity curves of those binaries are shown in Fig. 3.

The atmospheric parameters effective temperature T_{eff} , surface gravity $\log g$ and helium abundance $\log y$ of PG 0941+280, V 1405 Ori and OGLE BUL–SC16335 were determined as described in Geier et al. (2011a) by fitting model atmospheres with local thermodynamic equilibrium and supersolar metallicity (O’Toole & Heber 2006) to the hydrogen and helium lines of

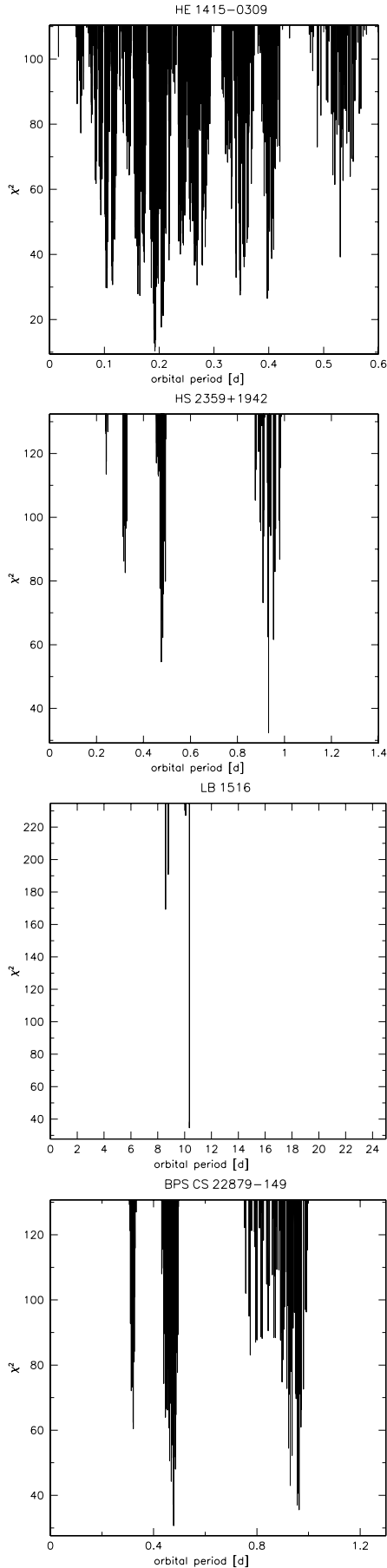


Fig. 2. χ^2 plotted against orbital period. The lowest peak corresponds to the most likely solution.

a coadded spectrum. For PG 0941+280 and V 1405 Ori we used a TWIN spectrum, whereas an EFOSC2 spectrum was used for OGLE BUL-SC16 335.

5. Nature of the unseen companions

5.1. Methods to constrain the nature of the companion

All spectroscopic binaries in our sample are single-lined and their binary mass functions can be determined from

$$f_m = \frac{M_{\text{comp}}^3 \sin^3 i}{(M_{\text{comp}} + M_{\text{sdb}})^2} = \frac{PK^3}{2\pi G}. \quad (1)$$

The RV semi-amplitude and the orbital period can be derived from the RV curve, but the sdb mass M_{sdb} , the companion mass M_{comp} and the inclination angle i remain free parameters. Adopting the canonical sdb mass $M_{\text{sdb}} = 0.47 M_{\odot}$ (see discussion in Fontaine et al. 2012) and $i < 90^\circ$, we derive a lower limit for the companion masses (see Table 2). For minimum companion masses lower than $\sim 0.45 M_{\odot}$ the companion may be a late-type main sequence star or a compact object such as a WD. Main sequence stars in this mass range are outshone by the sdb and are not visible in optical spectra (Lisker et al. 2005). If on the other hand the minimum companion mass exceeds $0.45 M_{\odot}$, spectral features of a main sequence companion become visible in the optical. The non-detection of such features therefore allows us to exclude a main sequence star.

Indicative features in the light curves constrain the nature of the companions further in some cases. A sinusoidal variation with orbital period originates from the irradiation of a cool companion by the hot subdwarf primary. The projected area of the companion's heated hemisphere changes while it orbits the primary. The detection of this so-called reflection effect indicates a cool companion with a size similar to the hot subdwarf primary, either a low-mass main sequence star of spectral type M or a substellar object such as a brown dwarf. If eclipses are present as well, the inclination angle can be measured and the mass of the companion can be constrained. Such eclipsing sdb binaries with reflection effect are also known as HW Vir-type binaries.

The lack of variations in the light curve, on the other hand, can be used to exclude a cool companion, when the orbital period of the binary is sufficiently short. In this case a reflection effect would be easily detectable and a non-detection implies that the companion must be a compact object. The detection of the very shallow eclipses from a compact WD companion also allows us to constrain its mass. Smaller variations indicative of a massive compact companion, which are caused by the ellipsoidal deformation and the relativistic Doppler beaming of the sdb primary, can only be detected from the ground in the most extreme cases (e.g. Geier et al. 2007, 2013). However, using high-precision space-based photometry, these variations can be detected and used to constrain the binary parameters (Geier et al. 2008; Bloemen et al. 2011; Telting et al. 2012).

5.2. White dwarf companions

HE 1415-0309 has been identified as a single-lined sdb star in the course of the SPY project (Lisker et al. 2005). A significant shift in radial velocity ($\sim 130 \text{ km s}^{-1}$), indicating a close binary, has been measured from two UVES spectra (Napiwotzki, priv. comm.). The minimum mass of the companion is too low ($0.37 M_{\odot}$) to exclude a main sequence star. However, a light curve of this star ($\sim 1 \text{ h}$) was taken with the Nordic Optical

Table 1. Derived orbital solutions.

Object	T_0 [HJD-2 450 000]	P [d]	γ [km s ⁻¹]	K [km s ⁻¹]	e_{norm} [km s ⁻¹]	$\log p_{\text{false}}[10\%]$	$\log p_{\text{false}}[1\%]$
HE 1415-0309	5240.909 ± 0.002	0.192 ± 0.004	104.7 ± 9.5	152.4 ± 11.2	18.6	-1.0	-0.4
HS 2359+1942	6279.221 ± 0.007	0.93261 ± 0.00005	-96.1 ± 6.0	107.4 ± 6.8	8.3	-1.2	-1.1
LB 1516	5495.73 ± 0.05	10.3598 ± 0.0005	14.3 ± 1.1	48.6 ± 1.4	4.4	<-4.0	<-4.0
BPS CS 22879-149	5413.102	0.478	21.9 ± 2.5	63.5 ± 2.8	5.4
	5412.448	0.964	-25.5 ± 5.3	121.7 ± 6.3	6.2
OGLE BUL-SC16335	4758.614	0.122	36.4 ± 19.6	92.5 ± 26.2	25.1
HS 2043+0615	4254.610 ± 0.003	0.3015 ± 0.0003	-43.5 ± 3.4	73.7 ± 4.3	8.3
PG 0941+280	4476.185	0.311	73.0 ± 4.9	141.7 ± 6.3	19.4
V 1405 Ori	4477.362	0.398	-33.6 ± 5.5	85.1 ± 8.6	15.2

Notes. The systematic error adopted to normalise the reduced χ^2 (e_{norm}) is given for each case. The probabilities for the orbital period to deviate from our best solution by more than 10% ($p_{\text{false}}[10\%]$) or 1% ($p_{\text{false}}[1\%]$) are given in the last columns. The last four lines show the binaries, where the orbital period has been determined from photometry.

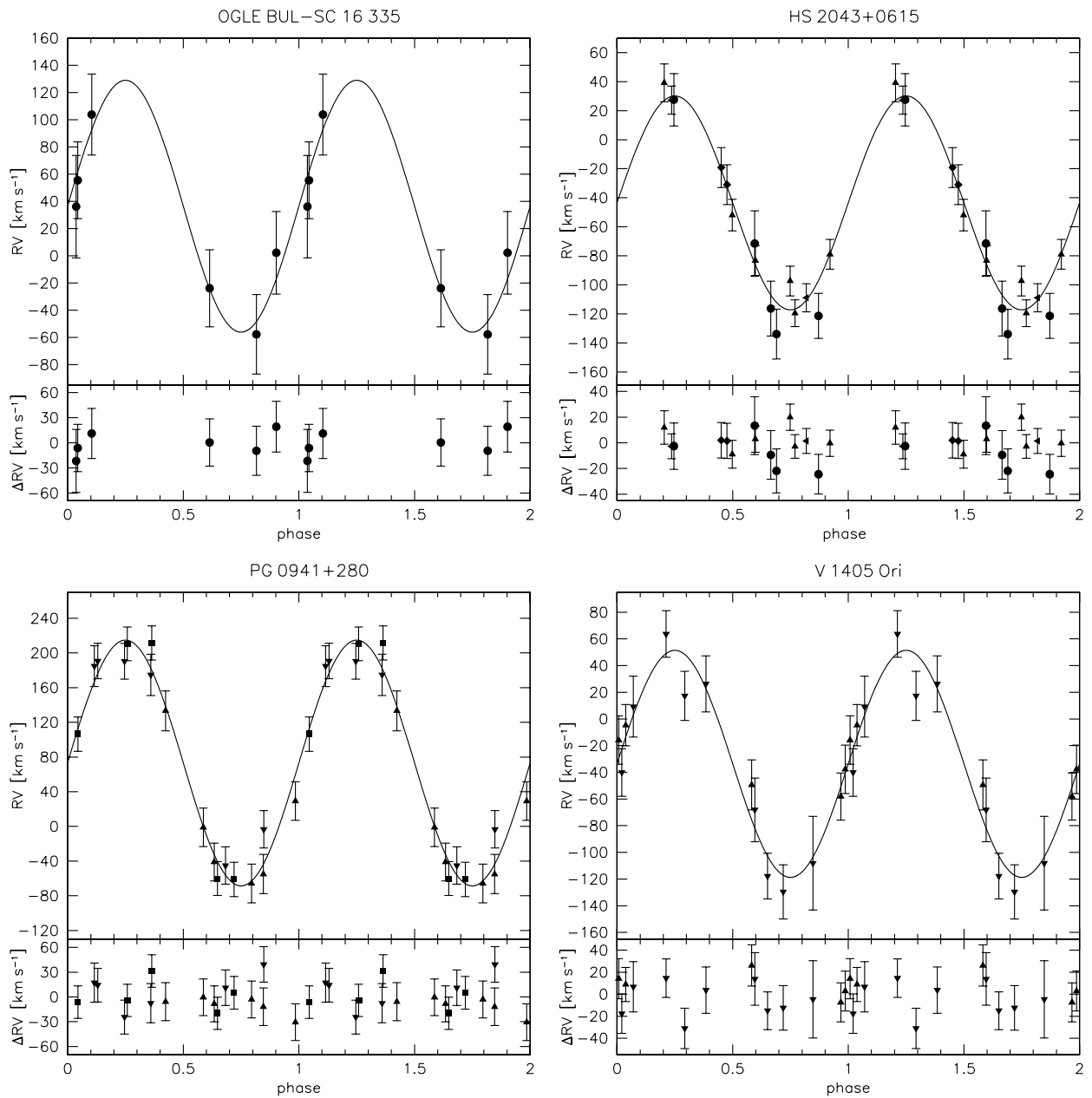


Fig. 3. Phased radial velocity curves plotted twice for visualisation. The rectangles mark RVs measured from spectra obtained with McDonald-2.7 m/Coude. The other symbols are the same as in Fig. 1.

Table 2. Derived masses and most probable nature of the companions.

Object	$f(M)$ [M_{\odot}]	M_2 [M_{\odot}]	Companion
HE 1415–0309	0.07	>0.37	WD
PG 0941+280	0.092	0.42 ± 0.03	WD
HS 2359+1942	0.12	>0.47	WD
LB 1516	0.12	>0.48	WD
OGLE BUL–SC16 335	0.01	0.16 ± 0.05	MS
HS 2043+0615	0.013	0.18–0.34	MS
V 1405 Ori	0.034	>0.26	MS
BPS CS 22879–149	0.013	>0.18	MS/WD
	0.17	>0.57	WD

Telescope on La Palma to search for pulsations and no variations have been reported (Østensen et al. 2010b). Due to the short orbital period of only 4.6 h, a reflection effect would have been easily detectable. We therefore conclude that the unseen companion of HE 1415–0309 must be a compact object, most likely a WD.

HS 2359+1942 (PG 2359+197) was drawn from the SPY sample and analysed by Lisker et al. (2005). We detected an RV shift of an EMMI spectrum with respect to the survey spectrum taken with UVES. The minimum companion mass is $0.47 M_{\odot}$, similar to the adopted mass of the sdB itself. Since no spectral features of a cool MS companion have been found, we conclude that the companion must be a compact object, presumably a WD.

LB 1516 (EC 22590–4819) has been discovered to be an sdB binary with a period of a few days by Edelmann et al. (2005), but no unambiguous solution was found. Koen et al. (2010) identified the sdB to be a g-mode pulsator. Subsequently, Copperwheat et al. (2010) obtained an orbital solution of this system ($P = 10.3592$, $K = 46.8 \pm 1.8 \text{ km s}^{-1}$). We combined the RV measurements from Edelmann et al. (2005) and Copperwheat et al. (2010) with additional RVs measured from FEROS spectra and our new measurements to obtain a more accurate solution. The rather long period of 10.3958 d leads to a minimum companion mass of $0.48 M_{\odot}$. Since no spectral features of the companion are detectable, the companion is likely to be a WD.

PG 0941+280 (HX Leo) has been identified as an sdB star by Saffer et al. (1994). The effective temperature $T_{\text{eff}} = 29\,400 \pm 500$ K, surface gravity $\log g = 5.43 \pm 0.05$ and helium abundance $\log y = -3.0 \pm 0.1$ are consistent with the results ($T_{\text{eff}} = 29\,000 \pm 1000$ K, $\log g = 5.58 \pm 0.15$, $\log y = -3.0$) of Saffer et al. (1994), who used pure hydrogen models.

Green et al. (2004) detected shallow eclipses of an earth-sized WD companion in the light curve. The orbital period estimated from these eclipses is around 0.3 d. We adopted the period alias of our RV analysis closest to this result as the most likely orbital period. The derived mass of the companion assuming $i = 1$ is $0.42 \pm 0.03 M_{\odot}$.

5.3. M-dwarf companions

OGLEBUL–SC16 335 was identified as an HW Vir system by Polubek et al. (2007). Since this analysis was based on photometry alone, the sdB nature of the primary could not be proven unambiguously. We constrained the atmospheric parameters of *OGLEBUL–SC16 335* by fitting model spectra. Due to the limited wavelength range we were only able to use H_{β} and the two He I lines at 4472 Å and 4922 Å. However, within the uncertainties the resulting effective temperature $T_{\text{eff}} = 31\,500 \pm 1800$ K, surface gravity $\log g = 5.7 \pm 0.2$,

Table 3. Photometric amplitudes from three-channel photometry.

Band	A	B
R	0.0660(6)	0.0119(6)
G	0.0416(6)	0.0084(6)
U	0.0307(14)	0.0041(14)

and helium abundance $\log y = -1.8 \pm 0.1$ are perfectly consistent with an sdB primary.

Adopting the orbital period derived from the light curve by Polubek et al. (2007), we determined the RV semiamplitude and the mass of the companion ($0.16 \pm 0.05 M_{\odot}$). A substellar companion can be excluded and the companion is a low-mass M-dwarf.

HS 2043+0615 was again drawn from the SPY sample and analysed by Lisker et al. (2005). A shift in radial velocity ($\sim 135 \text{ km s}^{-1}$) has been measured from two UVES spectra (Napiwotzki, priv. comm.). As mentioned by Østensen et al. (2010b), it was observed on two consecutive nights in June 2005 with the NOT, and found to have a strong variability with a period of several hours, presumably due to a reflection effect. An extensive photometric follow-up has then been conducted with the Mercator telescope.

To determine the ephemeris we phase-folded the seven months of MEROPE photometry on different trial periods and selected that with the lowest variance. The resulting light curve after folding into 50 phase bins is shown in Fig. 4. There are no significant competing aliases in the periodogram. As there are no sharp eclipses that can be used to accurately phase observations at different epochs, the error on the period is quite large. We estimate that we can phase our data to a precision of 1/10 of a cycle, and since our useful observations span $206.8 \text{ d} \approx 686$ cycles, the phase error would be $\sim 0.3/10/686$. We thus state the ephemeris as $T_0 = 2454\,213.70 \pm 0.03$ and $P = 0.30156 \pm 0.00005$ d, perfectly consistent with the corresponding alias of the RV periodogram. The MAIA multiband light curves are plotted in Fig. 5. We fitted the light curves with a pair of phase-locked cosine functions as in Østensen et al. (2013), Eq. (1), and these are plotted with solid lines in Fig. 5. The semi-amplitudes for the orbital period, A , and for the first harmonic, B , are given in Table 3.

From the orbital solution we derive a minimum companion mass of $0.17 M_{\odot}$ consistent with an M-dwarf companion. Following the simple modelling approach described in Østensen et al. (2013) and adopting the atmospheric parameters of *HS 2043+0615* given in Lisker et al. (2005) as well as the theoretical mass-radius relation for M-dwarfs from Baraffe et al. (1998), we constrain the likely range of orbital inclinations to $30^{\circ} < i < 75^{\circ}$ and the companion mass range to $0.18 M_{\odot} < M_{\text{comp}} < 0.34 M_{\odot}$ (see Fig. 6).

V 1405 Ori was discovered to be a short-period sdB pulsator (Koen et al. 1999) with a reflection effect (Reed et al. 2010). We phased our RVs to the orbital period determined from the light curve (0.398 d) and derived a minimum mass of $0.26 M_{\odot}$ for the M-dwarf companion. The effective temperature $T_{\text{eff}} = 35\,100 \pm 800$ K, surface gravity $\log g = 5.66 \pm 0.11$, and helium abundance $\log y = -2.5 \pm 0.2$ are quite typical for short-period sdB pulsators of V 361 Hya type (see Østensen 2010, and references therein).

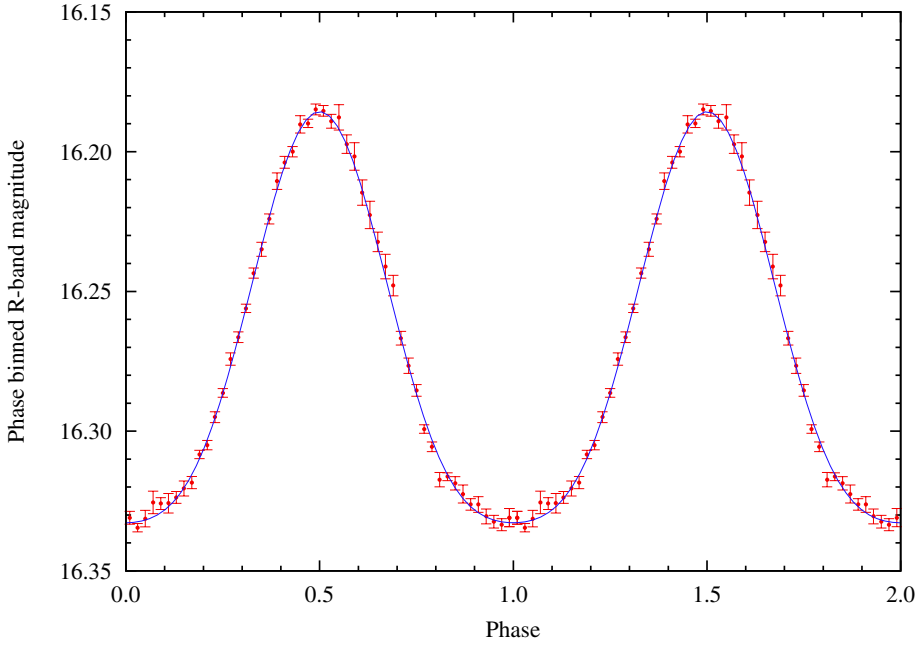


Fig. 4. Phase-binned light curve of HS 2043+0615. The 516 MEROPE data points from 2007 were phase-folded on $P = 0.30156$ day using 50 bins, and are plotted twice to better visualise the difference in width of the peaks and troughs. The error bars indicate the rms for each phase bin.

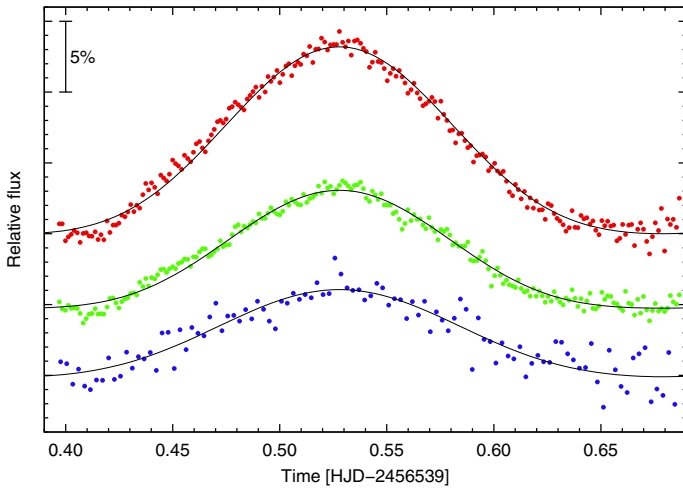


Fig. 5. Multiband light curve of HS 2043+0615 taken with the MAIA camera (R , G , U -bands from top to bottom).

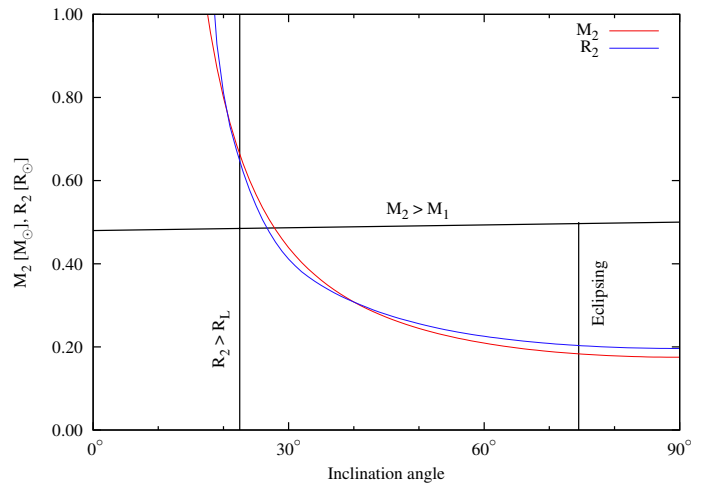


Fig. 6. Mass and radius of the M-dwarf companion to HS 2043+0615 as a function of inclination angle, as indicated by the mass function and the mass-radius relation for M-dwarfs. The box limited by the three solid lines marks the possible parameter range. The companion cannot fill its Roche lobe R_L , the binary is not eclipsing, and the companion mass cannot be higher than the mass of the subdwarf, because it would then be visible in the optical spectrum (for details see Østensen et al. 2013).

5.4. Unconstrained companion type

BPS CS 22879–149 was identified as an sdB star by Beers et al. (1992) and chosen as a bright backup target for the southern sky. Since no unique orbital solution could be found, the minimum mass of the companion is either constrained to $0.18 M_{\odot}$ or to $0.57 M_{\odot}$. While in the latter case a WD companion would be most likely, a compact object of low mass is possible as well as an M dwarf in the former case. Comparing the two orbital solutions with the sample of known sdB binaries, the long-period solution appears to be more likely, because the number of known sdB binaries with such orbital parameters is higher than the number of binaries with the short-period parameters (see Fig. 7). However, selection effects also favour the detection of higher RV-shifts. We conclude that the nature of the companion cannot be firmly constrained at this point.

6. Discussion

We derived orbital solutions of eight close hot subdwarf binaries and constrained the most likely nature of the unseen companions in all cases but one, using additional information derived from photometry and spectroscopy. These binaries cover the full parameter range of the known close binary sdB population (see Fig. 7). Their companion types are also consistent with the apparent split between M-dwarf and substellar companions on one hand and WD companions on the other hand, especially at short orbital periods < 0.3 d. Furthermore, our sample contains some peculiar binaries that deserve a more detailed analysis in the future.

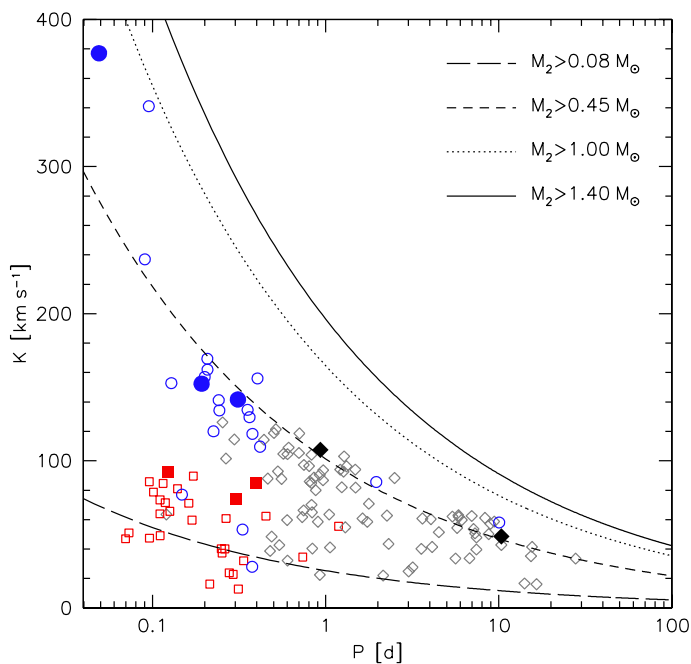


Fig. 7. RV semiamplitudes of all known sdB binaries with spectroscopic solutions plotted against their orbital periods (Kupfer et al., in prep.). Circles mark sdB binaries with compact companions, squares systems with M-dwarf or substellar companions, and diamonds binaries where the nature of the companion cannot be further constrained by photometry. The lines mark the regions to the right where the minimum companion masses derived from the binary mass function (assuming $0.47 M_{\odot}$ for the sdBs) exceed certain values. The binaries from the MUCHFUSS supplementary programme including CD-30°11223 (Geier et al. 2013) are marked with filled symbols, binaries taken from the literature with open symbols.

PG 0941+280 is one of only five sdB+WD binaries, where the shallow eclipses of the white dwarf have been detected in the light curves (the others are KPD 0422+5421, Orosz & Wade 1999; PG 2345+318, Green et al. 2004; KPD 1946+4340, Bloemen et al. 2011; CD-30°11223, Geier et al. 2013). Its mass of $0.42 M_{\odot}$ is significantly smaller than the average mass of single CO-WDs ($\sim 0.6 M_{\odot}$, Liebert et al. 2005) and very close to the tentative upper mass limit for WD companions to sdB stars seen in the sdB binary sample (Fig. 7, see discussion in Kupfer et al., in prep). Time-resolved photometry is needed to obtain a high-quality light curve of this system, perform a detailed analysis, and derive observational constraints on the mass-radius relation of the WD. Furthermore, sdB+WD binaries are important laboratories for studying relativistic effects such as Doppler boosting and microlensing (Geier et al. 2008, 2013; Bloemen et al. 2011).

OGLE BUL-SC16 335 is the faintest HW Vir system known ($V \approx 16.5$ mag). It is located in the Galactic disc at a Galactic latitude of only $b = -3.5^{\circ}$. Studying sdB binaries in different stellar populations is important for understanding their formation. Different metallicities and especially different ages are expected to influence the properties of the progenitor binaries. Time-resolved spectroscopy and multicolour photometry are needed to perform a full analysis of OGLE BUL-SC16 335, which was formed in the young disc population, and compare the results with the HW Vir systems found in the course of the MUCHFUSS project that originate from older populations like the thick disc or the halo.

V 1405 Ori is one of only four short-period pulsators in a reflection effect binary (the others are NY Vir, Kilkenney et al. 1998; HE 0230-4323, Kilkenney et al. 2010; 2M1938+4603,

Østensen et al. 2010a; and FBS 0117+396, Østensen et al. 2013). Such binaries are important as observational calibrators for current asteroseismic models of pulsating sdBs (e.g. van Grootel et al. 2013). Furthermore, the tidal influence of close companions might also influence the pulsational properties of the sdBs and should therefore be taken into account in the next generation of these models.

Acknowledgements. A.T. was supported by the Deutsche Forschungsgemeinschaft (DFG) through grant HE1356/45-1. The research leading to these results has received funding from the European Research Council under the European Community's Seventh Framework Programme (FP7/2007–2013)/ERC grant agreement N° 227224 (PROSPERITY), from the Research Council of KU Leuven grant agreement GOA/2008/04. We thank the referee Dave Kilkenney for his constructive report. Based on observations at the Paranal Observatory of the European Southern Observatory for programmes number 165.H-0588(A) and 167.H-0407(A). Based on observations at the La Silla Observatory of the European Southern Observatory for programmes number 073.D-0495(A), 079.D-0288(A), 080.D-0685(A), 082.D-0649(A) and 086.D-0714(A). Based on observations collected at the Centro Astronómico Hispano Alemán (CAHA) at Calar Alto, operated jointly by the Max-Planck-Institut für Astronomie and the Instituto de Astrofísica de Andalucía (CSIC). Based on observations with the *William Herschel* Telescope operated by the Isaac Newton Group at the Observatorio del Roque de los Muchachos of the Instituto de Astrofísica de Canarias on the island of La Palma, Spain. Based on observations with the Southern Astrophysical Research (SOAR) telescope operated by the US National Optical Astronomy Observatory (NOAO), the Ministério da Ciência e Tecnologia of the Federal Republic of Brazil (MCT), the University of North Carolina at Chapel Hill (UNC), and Michigan State University (MSU). Based on observations at the McDonald observatory operated by the University of Texas in Austin. Based on observations made with the Mercator Telescope, operated on the island of La Palma by the Flemish Community, at the Spanish Observatorio del Roque de los Muchachos of the Instituto de Astrofísica de Canarias.

References

- Abazajian, K. N., Adelman-McCarthy, J. K., Agüeros, M. A., et al. 2009, *ApJS*, 182, 543
- Baraffe, I., Chabrier, G., Allard, F., & Haunschildt, P. H. 1998, *A&A*, 337, 403
- Beers, T. C., Preston, G. W., Shectman, S. A., Doinidis, S. P., & Griffin, K. E. 1992, *AJ*, 103, 267
- Bloemen, S., Marsh, T. R., Østensen, R. H., et al. 2011, *MNRAS*, 410, 1787
- Classen, L., Geier, S., Heber, U., & O'Toole, S. J. 2011, *AIP Conf. Ser.*, 1331, 297
- Copperwheat, C., Morales-Rueda, L., Marsh, T. R., et al. 2011, *MNRAS*, 415, 1381
- Edelmann, H., Heber, U., Altmann, M., Karl, C., & Lisker, T. 2005, *A&A*, 442, 1023
- Fontaine, G., Brassard, P., Charpinet, S., et al. 2012, *A&A*, 539, A12
- Geier, S., Nesslinger, S., Heber, U., et al. 2007, *A&A*, 464, 299
- Geier, S., Nesslinger, S., Heber, U., et al. 2008, *A&A*, 477, L13
- Geier, S., Heber, U., Kupfer, T., & Napiwotzki, R. 2010a, *A&A*, 515, A37
- Geier, S., Heber, U., Podsiadlowski, Ph., et al. 2010b, *A&A*, 519, A25
- Geier, S., Hirsch, H., Tillich, A., et al. 2011a, *A&A*, 530, A28
- Geier, S., Maxted, P. F. L., Napiwotzki, R., et al. 2011b, *A&A*, 526, A39
- Geier, S., Schaffneroth, V., Drechsel, H., et al. 2011c, *ApJ*, 731, L22
- Geier, S., Schaffneroth, V., Hirsch, H., et al. 2012, *ASP Conf. Ser.*, 452, 129
- Geier, S., Marsh, T. R., Wang, B., et al. 2013, *A&A*, 554, A54
- Green, E. M., For, B., Hyde, E. A., et al. 2004, *Ap&SS*, 291, 267
- Han, Z., Podsiadlowski, P., Maxted, P. F. L., Marsh, T. R., & Ivanova N. 2002, *MNRAS*, 336, 449
- Han, Z., Podsiadlowski, P., Maxted, P. F. L., & Marsh, T. R. 2003, *MNRAS*, 341, 669
- Heber, U. 1986, *A&A*, 155, 33
- Heber, U. 2009, *ARA&A*, 47, 211
- Kilkenney, D., O'Donoghue, D., Koen, C., Lynas-Gray, A. E., & van Wyk, F. 1998, *MNRAS*, 296, 329
- Kilkenney, D., Koen, C., & Worters, H. 2010, *MNRAS*, 404, 376
- Koen, C., O'Donoghue, D., Kilkenney, D., Stobie, R. S., & Saffer, R. A. 1999, *MNRAS*, 306, 213
- Koen, C., Kilkenney, D., Pretorius, M. L., & Frew, D. J. 2010, *MNRAS*, 401, 1850
- Liebert, J., Bergeron, P., & Holberg, J. B. 2005, *ApJS*, 156, 47

- Lisker, T., Heber, U., Napiwotzki, R., et al. 2005, *A&A*, 430, 223
Maxted, P. F. L., Marsh, T. R., & North, R. C. 2000, *MNRAS*, 317, L41
Maxted, P. F. L., Heber, U., Marsh, T. R., & North, R. C. 2001, *MNRAS*, 326, 139
Morales-Rueda, L., Maxted, P. F. L., Marsh, T. R., North, R. C., & Heber, U. 2003, *MNRAS*, 338, 752
Napiwotzki, R., Christlieb, N., Drechsel, H., et al. 2003, *ESO Msgr*, 112, 25
Napiwotzki, R., Karl, C., Lisker, T., et al. 2004a, *Ap&SS*, 291, 321
Napiwotzki, R., Yungelson, L., Nelemans, G. et al. 2004b, *ASP Conf. Ser.*, 318, 402
Nelemans, G. 2010, *Ap&SS*, 329, 25
Østensen, R. H. 2010, *Astron. Nachr.*, 331, 1026
Østensen, R. H., Green, E. M., Bloemen, S., et al. 2010a, *MNRAS*, 408, L51
Østensen, R. H., Oreiro, R., Solheim, J.-E., et al. 2010b, *A&A*, 513, A6
Østensen, R. H., Geier, S., Schaffenroth, V., et al. 2013, *A&A*, 559, A35
Orosz, J. A., & Wade, R. A. 1999, *MNRAS*, 310, 773
O'Toole, S. J., & Heber, U. 2006, *A&A*, 452, 579
Pfahl, E., Rappaport, S., & Podsiadlowski, Ph. 2003, *ApJ*, 597, 1036
Podsiadlowski, Ph., Rappaport, S., & Pfahl, E. D. 2002, *ApJ*, 565, 1107
Polubek, G., Pigulski, A., Baran, A., & Udalski, A. 2007, *ASP Conf. Ser.*, 372, 487
Raskin, G., Bloemen, S., Morren, J., et al. 2013, *A&A*, 559, A26
Reed, M. D., Terndrup, D. M., Østensen, R. H., et al. 2010, *Ap&SS*, 329, 83
Saffer, R. A., Bergeron, P., Koester, D., & Liebert, J. 1994, *ApJ*, 432, 351
Telting, J. H., Østensen, R. H., Baran, A. S., et al. 2012, *A&A*, 544, A1
Tillich, A., Heber, U., Geier, S., et al. 2011, *A&A*, 527, A137
Tutukov, A. V., & Yungelson, L. R. 1981, *Nauchnye Informatsii*, 49, 3
van Grootel, V., Charpinet, S., Brassard, P., Fontaine, G., & Green, E. M. 2013, *A&A*, 553, A97
Vennes, S., Kawka, A., O'Toole, S. J., Németh, P., & Burton, D. 2012, *ApJ*, 759, L25
Yungelson, L. R., & Tutukov, A. V. 2005, *Astron. Rep.*, 49, 871
Wang, B., Justham, S., & Han, Z. 2013, *A&A*, 559, A94
Webbink, R. F. 1984, *ApJ*, 277, 355

Appendix A: Radial velocities

Table A.1. BPS CS 22879–149.

Mid–HJD –2 450 000	RV [km s ⁻¹]	Instrument
4252.43920	2.6 ± 9.0	EMMI
4253.31834	–49.0 ± 9.4	
4253.40334	11.1 ± 11.2	
4254.25248	–47.9 ± 9.0	
4254.30548	–24.9 ± 9.5	
4254.36750	31.8 ± 4.2	
<hr/>		
4756.50430	99.6 ± 11.0	EFOSC2
5146.52218	–15.2 ± 7.1	
5147.51507	12.5 ± 7.3	
5147.52352	3.0 ± 11.1	
5147.52970	–1.3 ± 6.3	
5147.53589	6.5 ± 8.3	
5147.54742	33.6 ± 7.0	
5147.55499	37.9 ± 11.6	
5147.56256	42.8 ± 11.0	
5147.57460	40.4 ± 8.1	
5148.59060	79.5 ± 8.5	
5148.59678	74.4 ± 8.5	
5148.60296	82.1 ± 7.7	
5148.61428	77.9 ± 8.0	
5148.62717	86.3 ± 8.5	
<hr/>		
5412.82527	59.0 ± 12.7	Goodman
5412.82707	42.0 ± 12.4	
5412.82867	70.0 ± 10.7	
5412.89817	–14.0 ± 13.9	
5412.89977	1.0 ± 12.0	
5412.90137	–25.0 ± 13.0	

Table A.2. HE 1415–0309.

Mid–HJD –2 450 000	RV [km s ⁻¹]	Instrument
1740.63899	258.2 ± 8.0	UVES
1755.48571	203.1 ± 8.0	
<hr/>		
4253.49757	149.0 ± 7.9	EMMI
4253.63156	–86.9 ± 8.0	
4253.70556	214.9 ± 29.6	
4254.52251	185.0 ± 10.0	
<hr/>		
4476.85174	27.0 ± 8.6	TWIN
4479.86504	253.0 ± 15.0	
<hr/>		
4587.64673	–22.5 ± 7.8	ISIS
<hr/>		
5240.78331	252.4 ± 16.3	Goodman
5240.79081	190.1 ± 3.0	
5240.79851	174.1 ± 8.7	
5240.80821	137.6 ± 9.9	
5240.81561	98.3 ± 12.3	
5240.82282	65.6 ± 13.6	

Table A.3. HS 2043+0615.

Mid–HJD –2 450 000	RV [km s ⁻¹]	Instrument
2387.90703	27.2 ± 5.0	UVES
2521.66074	–108.9 ± 5.0	
<hr/>		
4586.73051	–19.2 ± 11.0	ISIS
4586.73799	–31.0 ± 10.9	
<hr/>		
4692.49332	39.2 ± 10.0	TWIN
4693.48658	–51.9 ± 7.0	
4693.51664	–83.2 ± 6.0	
4694.47290	–119.5 ± 4.0	
4696.57722	–97.3 ± 6.0	
4696.62917	–78.9 ± 6.0	
<hr/>		
4756.53557	–71.6 ± 21.0	EFOSC2
4757.52335	–121.4 ± 13.0	
4757.63634	27.6 ± 16.0	
4758.66733	–116.3 ± 17.0	
4758.67470	–133.9 ± 15.0	

Table A.4. HS 2359+1942.

Mid–HJD –2 450 000	RV [km s ⁻¹]	Instrument
2610.54512	4.4 ± 2.0	UVES
<hr/>		
4252.91279	57.6 ± 20.0	EMMI
<hr/>		
5068.69977	–87.7 ± 4.5	ISIS
5068.70011	–82.6 ± 4.5	
5068.70725	–78.3 ± 3.8	
5068.71712	–65.2 ± 4.6	
5068.72433	–62.6 ± 5.0	
5068.73153	–60.0 ± 4.4	
5068.74844	–53.9 ± 4.6	
5068.75565	–39.0 ± 4.0	
5069.66466	–80.2 ± 4.8	
5069.67188	–79.5 ± 6.0	
5069.67909	–63.9 ± 4.4	
5070.74702	2.7 ± 5.3	
5070.75423	3.8 ± 5.2	
5070.76144	1.7 ± 3.3	
<hr/>		
4755.63418	–1.7 ± 29.2	EFOSC2
4755.64807	–27.0 ± 13.0	
4756.73373	–139.1 ± 17.5	
4758.70798	–164.3 ± 16.9	
4758.71068	–156.7 ± 16.4	
<hr/>		
5412.83585	–88.1 ± 12.9	Goodman
5412.85165	–90.6 ± 7.5	
<hr/>		
6277.39152	–71.1 ± 6.2	ISIS
6277.39885	–57.8 ± 2.1	
6277.40252	–60.9 ± 5.0	
6279.48917	11.8 ± 5.1	
6279.49283	14.4 ± 6.2	
6279.49650	14.7 ± 7.8	
6279.50016	18.2 ± 2.1	
6280.40209	20.5 ± 8.0	
6280.40576	10.4 ± 5.3	
6280.40942	6.1 ± 5.0	
6280.41309	7.8 ± 5.0	
6280.43805	6.0 ± 26.7	
6280.44171	8.6 ± 5.5	
6280.44538	2.8 ± 5.0	
6280.47358	–17.4 ± 6.5	

Table A.5. LB 1516.

Mid–HJD –2 450 000	RV [km s ^{–1}]	Instrument
1795.62809	–25.3 ± 2.0	FEROS
1795.65378	–22.7 ± 2.0	
2495.87673	35.0 ± 2.0	
2497.86693	–20.4 ± 2.0	
3250.67647	63.3 ± 2.0	
3251.57092	49.2 ± 2.0	
3253.55317	–5.8 ± 2.0	
3253.67530	–7.5 ± 2.0	
4755.83240	–30.2 ± 8.8	EFOOSC2
4756.74952	–44.5 ± 8.0	
4758.77238	–12.7 ± 10.0	
4758.77510	–11.9 ± 9.0	
5499.57381	62.0 ± 2.0	FEROS
5499.59649	44.0 ± 2.0	

Table A.8. V 1405 Ori.

Mid–HJD –2 450 000	RV [km s ^{–1}]	Instrument
4476.68258	17.3 ± 10.3	EMMI
4477.59921	–68.1 ± 18.4	
4477.64791	–129.6 ± 13.4	
4477.69907	–108.1 ± 31.6	
4478.58382	9.3 ± 17.0	
4478.64047	63.7 ± 8.6	
4478.70892	26.3 ± 14.5	
4479.61084	–117.8 ± 7.9	
4479.75802	–40.1 ± 9.3	
4692.65549	–58.1 ± 9.0	
4692.66317	–37.8 ± 10.0	
4692.67134	–15.8 ± 10.0	
4692.67896	94.1 ± 12.0	
4693.69611	–49.5 ± 11.0	
4696.66314	–4.6 ± 3.0	

Table A.6. OGLE BUL–SC16335.

Mid–HJD –2 450 000	RV [km s ^{–1}]	Instrument
4757.58903	–23.9 ± 13.0	EFOOSC2
4758.49724	55.5 ± 13.0	
4758.50460	103.8 ± 16.0	
4758.59169	–57.8 ± 15.0	
4758.60219	2.2 ± 17.0	
4758.61866	36.1 ± 28.0	

Table A.7. PG 0941+280.

Mid–HJD –2 450 000	RV [km s ^{–1}]	Instrument
3715.01112	210.4 ± 1.9	McDonald
3716.99883	–60.2 ± 2.3	
3717.02115	–61.1 ± 4.1	
3766.89779	106.3 ± 3.7	
3768.86376	211.5 ± 3.2	
4476.76052	–3.3 ± 9.2	EMMI
4476.84388	184.8 ± 13.5	
4477.78158	190.7 ± 6.5	
4478.75103	190.3 ± 6.8	
4479.71960	174.8 ± 13.8	
4479.82016	–45.1 ± 9.2	
4979.36163	133.3 ± 12.3	TWIN
4979.41243	–1.0 ± 10.9	
4980.36049	–41.0 ± 10.0	
4980.41073	–65.8 ± 11.2	
4980.42660	–55.0 ± 11.7	
4981.40285	29.2 ± 10.7	

MUCHFUSS – Massive Unseen Companions to Hot Faint Underluminous Stars from SDSS

S. Geier^{1,*}, V. Schaffenroth¹, H. Hirsch¹, A. Tillich¹, U. Heber¹, P.F.L. Maxted², R.H. Østensen³, B.N. Barlow^{4,5}, S.J. O’Toole⁶, T. Kupfer^{1,7}, T. Marsh⁸, B. Gänsicke⁸, R. Napiwotzki⁹, O. Cordes¹⁰, S. Müller¹, L. Classen¹, E. Ziegerer¹, and H. Drechsel¹

¹ Dr. Karl Remeis-Observatory & ECAP, Astronomical Institute, Friedrich-Alexander University Erlangen-Nürnberg, Sternwartstr. 7, D-96049 Bamberg, Germany

² Astrophysics Group, Keele University, Staffordshire, ST5 5BG, UK

³ Institute of Astronomy, K.U.Leuven, Celestijnenlaan 200D, B-3001 Heverlee, Belgium

⁴ Department of Physics and Astronomy, University of North Carolina, Chapel Hill, NC 27599-3255, USA

⁵ Department of Astronomy & Astrophysics, Eberly College of Science, The Pennsylvania State University, 525 Davey Lab, University Park, PA 16802, USA

⁶ Australian Astronomical Observatory, PO Box 296, Epping, NSW, 1710, Australia

⁷ Department of Astrophysics, Faculty of Science, Radboud University Nijmegen, P.O. Box 9010, 6500 GL Nijmegen, NE

⁸ Department of Physics, University of Warwick, Coventry CV4 7AL, UK

⁹ Centre of Astrophysics Research, University of Hertfordshire, College Lane, Hatfield AL10 9AB, UK

¹⁰ Argelander-Institut für Astronomie, Auf dem Hügel 71, D-53121 Bonn, Germany

Received 2012 Jan 13, accepted 2012 Mar 19

Published online 2012 Jun 15

Key words binaries: spectroscopic – subdwarfs

The project Massive Unseen Companions to Hot Faint Underluminous Stars from SDSS (MUCHFUSS) aims at finding hot subdwarf stars with massive compact companions (white dwarfs with masses $M > 1.0 M_{\odot}$, neutron stars or black holes). The existence of such systems is predicted by binary evolution calculations and some candidate systems have been found. We identified $\simeq 1100$ hot subdwarf stars from the Sloan Digital Sky Survey (SDSS). Stars with high velocities have been reobserved and individual SDSS spectra have been analysed. About 70 radial velocity variable subdwarfs have been selected as good candidates for follow-up time resolved spectroscopy to derive orbital parameters and photometric follow-up to search for features like eclipses in the light curves. Up to now we found nine close binary sdBs with short orbital periods ranging from $\simeq 0.07$ d to 1.5 d. Two of them are eclipsing binaries with companions that are most likely of substellar nature.

© 2012 WILEY-VCH Verlag GmbH & Co. KGaA, Weinheim

1 Introduction

Hot subdwarf stars (sdO/B) are core-helium burning stars located at the extreme blue end of the horizontal branch (see Heber 2009 for a review). These stars with masses of about half solar consist almost entirely of helium surrounded by a very thin hydrogen envelope only. The cause of the extreme mass-loss in the red-giant phase necessary to form hot subdwarfs remains unclear.

A significant fraction ($\simeq 50\%$) of the sdBs stars are in short period binaries (Maxted et al. 2001; Napiwotzki et al. 2004) with periods ranging from only 0.07 d to more than 10 d. These close binary sdBs are most likely formed by common envelope (CE) ejection (Han et al. 2002, 2003). Because most of them are single-lined, only lower mass limits have been derived from the binary mass functions consistent with late main sequence stars of spectral type M or compact objects like white dwarfs (WDs).

Subdwarf binaries with massive WD companions may be candidates for supernova type Ia (SN Ia) progenitors because these systems lose angular momentum due to the emission of gravitational waves and shrink. Mass transfer or the subsequent merger of the system may cause the WD to reach the Chandrasekhar limit and explode as a SN Ia. One of the best known candidate systems for the double degenerate merger scenario is the sdB + WD binary KPD 1930+2752 (Maxted et al. 2000; Geier et al. 2007).

Geier et al. (2010a, 2010b) analysed high resolution spectra of single-lined sdB binaries. Because the inclinations of these systems are not known, additional information is needed to derive companion masses. Accordingly, Geier et al. (2010a, 2010b) performed a quantitative spectral analysis and determined surface gravities and projected rotational velocities. Assuming synchronised orbits the masses and the nature of the unseen companions were constrained. Surprisingly, the masses of some companions are only consistent with either massive white dwarfs ($M > 1.0 M_{\odot}$),

* Corresponding author: geier@sternwarte.uni-erlangen.de

neutron stars (NS) or stellar mass black holes (BH). However, the assumption of orbital synchronisation in close sdB binaries was shown to be not always justified and the analysis suffers from selection effects (Geier et al. 2010b). On the other hand, the existence of sdB + NS/BH systems is predicted by binary evolution theory (Podsiadlowski et al. 2002; Pfahl et al. 2003; Yungelson & Tutukov 2005; Nelemans 2010). The formation channel includes two phases of unstable mass transfer and one supernova explosion, while the fraction of systems formed in this way is predicted to be about 1–2% of all sdBs.

If the companion were a neutron star, it could be detectable by radio observations as a pulsar. Coenen et al. (2011) searched for pulsed radio emission at the positions of four candidate systems from Geier et al. (2010b) using the Green Bank radio telescope, but did not detect any signals. Most recently, Mereghetti et al. (2011) searched for X-ray signatures of mass transfer driven by weak stellar winds from the sdBs. Using the XRT instrument on board of the SWIFT satellite and targeting twelve binaries from the sample of Geier et al. (2010b), Mereghetti et al. (2011) did not detect any X-ray emission.

In order to find sdBs with compact companions like massive white dwarfs ($M > 1.0 M_{\odot}$), neutron stars or black holes we started a radial velocity (RV) survey (Massive Unseen Companions to Hot Faint Underluminous Stars from SDSS¹, MUCHFUSS, Geier et al. 2011a, 2011b).

The same selection criteria that we applied to find such binaries are also well suited to single out hot subdwarf stars with constant high radial velocities in the Galactic halo like extreme population II and hypervelocity stars and led to a very interesting spin-off project (Tillich et al. 2011).

2 Target selection

2.1 Colour and RV selection

The target selection is optimised to find close massive compact companions to sdB stars. The SDSS spectroscopic database (Data Release 6) is the starting point for our survey. SdO/B candidates were selected by applying a colour cut to SDSS photometry. All point source spectra within the colours $u - g < 0.4$ and $g - r < 0.1$ were downloaded from the SDSS Data Archive Server². About 10 000 hot stars were classified by visual inspection. The sample contains 1100 hot subdwarfs (for details see Geier et al. 2011a).

SdBs with radial velocities (RVs) lower than $\pm 100 \text{ km s}^{-1}$ have been excluded to filter out such binaries with normal disc kinematics, by far the majority of the sample. Another selection criterion is the brightness of the stars since the quality of the spectra is not sufficient for faint stars. Because of that most objects much fainter than $g = 19 \text{ mag}$ have been excluded.

2.2 Survey for RV variable stars

Second epoch medium resolution spectroscopy ($R = 1800\text{--}4000$) was obtained for 88 stars using ESO-VLT/FORS1, WHT/ISIS, CAHA-3.5 m/TWIN and ESO-NTT/EFOSC2. Second epoch observations by SDSS have been used as well. We discovered 46 RV variable systems in this way.

The SDSS spectra are co-added from at least three individual “sub-spectra” with typical exposure times of 15 min, which are normally taken consecutively. Hence, those spectra can be used to probe for radial velocity variations on short timescales. We have obtained the sub-spectra for all sdBs brighter than $g = 18.5 \text{ mag}$ and discovered 81 new sdB binaries with radial velocity variations on short time scales ($\approx 0.03 \text{ d}$) in this way. In total we found 127 new RV variable hot subdwarf stars (see Fig. 1).

In addition, 20 helium-rich sdOs (He-sdOs) show RV variability. This fraction was unexpectedly high since in the SPY sample only 4% of these stars turned out to be RV variable (Napiwotzki et al. 2008). However, it is not yet clear what causes this RV variability, since the orbital parameters of any such object couldn’t be derived yet. This would be necessary to prove, that these He-sdOs are in close binaries.

2.3 Selection of candidates with massive companions

Numerical simulations were carried out to select the most promising targets for follow-up and estimate the probability for a subdwarf binary with known RV shift to host a massive compact companion. We created a mock sample of sdBs with a close binary fraction of 50% and adopted the distribution of orbital periods of the known sdB binaries. Two RVs were taken from the model RV curves at random times and the RV difference was calculated for each of the 10^6 binaries in the simulation sample. To account for the fact that the individual SDSS spectra were taken within short time spans, another simulation was carried out, where the first RV was taken at a random time, but the second one just 0.03 d later (for details see Geier et al. 2011a).

The sample of promising targets consists of 69 objects in total. These objects either show significant RV shifts ($> 30 \text{ km s}^{-1}$) within 0.03 d (52 stars) or high RV shifts ($100\text{--}300 \text{ km s}^{-1}$) within more than one day (17 stars). An extension of our target selection to SDSS Data Release 7 is in progress.

3 Sample statistics

The classification of the hot subdwarf sample is based on existence, width, and depth of helium and hydrogen absorption lines as well as the flux distribution between 4000 and 6000 Å. Subdwarf B stars show broadened hydrogen Balmer and He I lines, sdOB stars He II lines in addition, while the spectra of sdO stars are dominated by weak Balmer and strong He II lines depending on the He abundance. A flux excess in the red compared to the reference

¹ Sloan Digital Sky Survey

² das.sdss.org

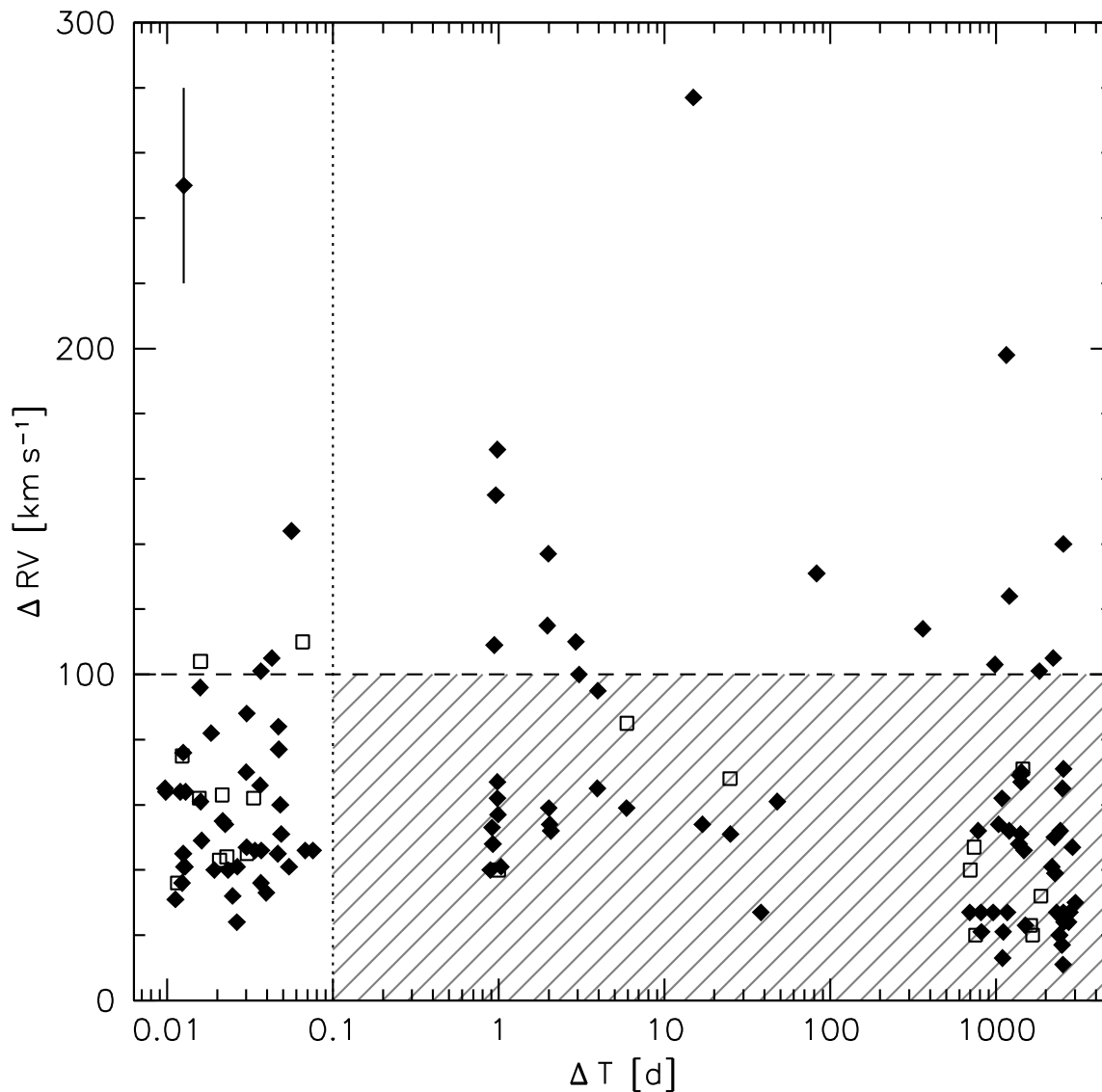


Fig. 1 Highest radial velocity shift between individual spectra (ΔRV) plotted against time difference between the corresponding observing epochs (ΔT). The dashed horizontal line marks the selection criterion $\Delta RV > 100 \text{ km s}^{-1}$, the dotted vertical line the selection criterion $\Delta T < 0.1 \text{ d}$. All objects fulfilling at least one of these criteria lie outside the shaded area and belong to the top candidate list for the follow-up campaign. The filled diamonds mark sdBs, while the open squares mark He-sdOs (Geier et al. 2011a).

spectrum as well as the presence of spectral features such as the Mg I triplet at 5170 \AA or the Ca II triplet at 8650 \AA are taken as indications of a late type companion.

In total we found 1100 hot subdwarfs. 725 belong to the class of single-lined sdBs and sdOBs. Features indicative of a cool companion were found for 89 of the sdBs and sdOBs. 9 sdOs have main sequence companions, while 198 sdOs, most of which show helium enrichment, are single-lined (Geier et al. 2011a).

4 Spectroscopy follow-up

Follow-up medium resolution ($R = 1200\text{--}4000$) spectra were taken during dedicated follow-up runs with ESO-

NTT/EFOSC2, WHT/ISIS, CAHA-3.5 m/TWIN, INT/IDS, SOAR/Goodman and Gemini-N/GMOS. Orbital parameters of eight sdB binaries discovered in the course of the MUCHFUSS project have been determined so far (Geier et al. 2011b, 2011c).

Because we deal with single-lined spectroscopic binaries, only their mass functions

$$f_m = M_{\text{comp}}^3 \sin^3 i / (M_{\text{comp}} + M_{\text{sdB}})^2 = PK^3 / 2\pi G$$

can be calculated. Although the RV semi-amplitude K and the period P can be derived from the RV curve, the sdB mass M_{sdB} , the companion mass M_{comp} and the inclination angle i remain free parameters. Adopting the canonical mass for core helium-burning stars $M_{\text{sdB}} = 0.47 M_{\odot}$ and $i < 90^\circ$ we derive a lower limit for the companion mass.

With this minimum mass a qualitative classification of the companions' nature is possible in certain cases. For minimum companion masses lower than $0.45 M_{\odot}$ a main sequence companion can not be excluded because its luminosity would be too low to be detectable in the optical spectra (Lisker et al. 2005). The companion could therefore be a compact object like a WD or a late main sequence star. If the minimum companion mass exceeds $0.45 M_{\odot}$ and no spectral signatures of the companion are visible, it has to be a compact object. If the mass limit exceeds $1.00 M_{\odot}$ or even the Chandrasekhar limit ($1.40 M_{\odot}$) the existence of a massive WD or even an NS or BH companion is proven.

The derived minimum companion masses of seven binaries from our sample are similar ($0.32\text{--}0.41 M_{\odot}$). From these minimum masses alone the nature of the companions cannot be constrained unambiguously. However, the fact that all seven objects belong to the sdB binary population with the highest minimum masses illustrates that our target selection is efficient and singles out sdB binaries with massive companions (see Geier et al. 2011b).

5 Photometry follow-up

Photometric follow-up helps to clarify the nature of the companions. Short period sdB binaries with late main sequence or substellar companions show variations in their light curves caused by the irradiated surfaces of the cool companions facing the hot subdwarf stars. If this so-called reflection effect is present, the companion is most likely a main sequence star. If not, the companion is most likely a compact object. In the case of the short period system J1138–0035 a light curve taken by the SuperWASP project (Pollacco et al. 2006) shows no variation exceeding $\simeq 1\%$. The companion is therefore most likely a white dwarf (Geier et al. 2011b).

We obtained follow-up photometry with the Mercator telescope and the BUSCA instrument mounted on the CAHA-2.2 m telescope. In this way we discovered the first eclipsing sdB binary J0820+0008 to host a brown dwarf companion with a mass ranging from 0.045 to $0.068 M_{\odot}$ (Fig. 2, Geier et al. 2011c).

A very similar eclipsing system (J1622+4730) was discovered serendipitously (see Fig. 3). A preliminary analysis shows that the orbital period is very short ($\simeq 0.07$ d) and the RV semi-amplitude quite low ($\simeq 47$ km s $^{-1}$). The companion is most likely a substellar object as well. The high success rate in finding these objects shows that our target selection not only singles out sdB binaries with high RV-amplitudes, but also systems with very short orbital periods and moderate RV-amplitudes.

Most recently, we detected p-mode pulsations in the sdB J0120+3950 (FBS 0117+396, Geier et al. 2011a) as well as a longer trend indicative of a reflection effect in a light curve taken with BUSCA. Only a few of the known short-period sdB pulsators (sdBV $_r$) are in close binary systems.

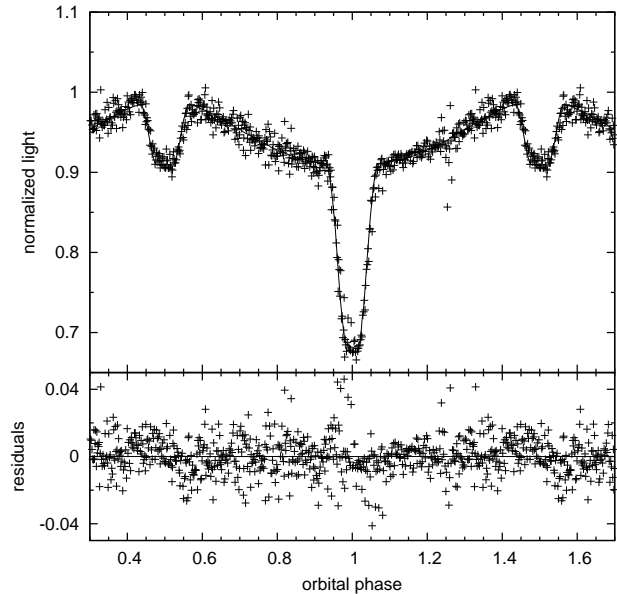


Fig. 2 Phased *R*-band light curve of J0820+0008 taken with the Mercator telescope. A light curve model is fitted to the data and residuals are given below. Primary and secondary eclipses can be clearly seen as well as the sinusoidal shape caused by the reflection effect (Geier et al. 2011c).

6 Substellar companions

The existence of eclipsing sdB + late dM binaries of HW Vir type with short orbital periods ($0.1\text{--}0.26$ d) and companion masses between $0.1 M_{\odot}$ and $0.2 M_{\odot}$ (For et al. 2010; Østensen et al. 2010 and references therein) shows that stars close to the nuclear burning limit of $\simeq 0.08 M_{\odot}$ are able to help eject a common envelope and form a hot subdwarf. Substellar companions to sdB stars have been found using the light travel time technique (Schuh 2010 and references therein). However, these systems have wide orbits and none of these companions influenced the evolution of its host star.

In the course of the MUCHFUSS project we discovered two sdBs with most likely substellar companions in close orbits. These companions evidently interacted with the sdB progenitor stars and caused the ejection of the common envelopes. Some theoretical models indeed predict such an interaction between planets or brown dwarf companions and their nearby host stars to be a possible formation channel for hot subdwarfs and helium white dwarfs (Soker 1998; Nelemans & Tauris 1998). Our finding can be used to constrain such models and learn more about the role substellar companions play in the formation of single and close binary sdBs.

7 Summary

The MUCHFUSS project aims at finding hot subdwarf stars with massive compact companions. We identified 1100 hot subdwarfs by colour selection and visual inspection of the SDSS-DR6 spectra. The best candidates for massive

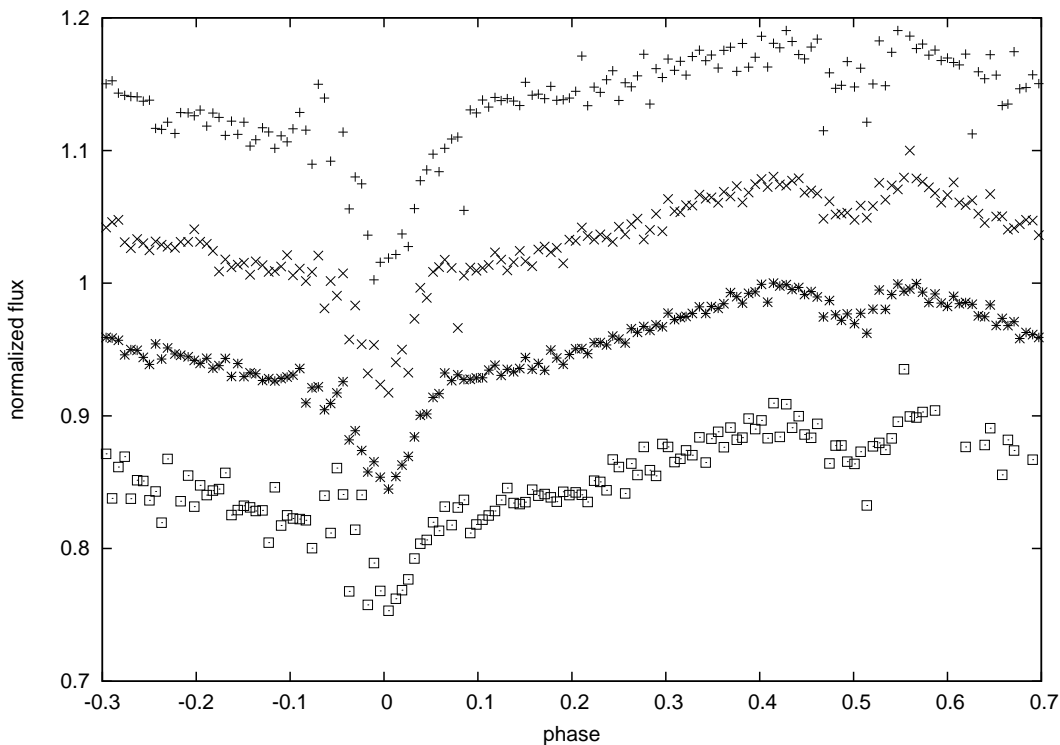


Fig. 3 Phased light curves of J1622+4730 taken with BUSCA (UV, *B*, *R*, IR-band). Although the eclipses are not total, the light curve looks very similar to the one of J0820+0008 (see Fig. 2).

compact companions are followed up with time resolved medium resolution spectroscopy. Up to now orbital solutions have been found for eight single-lined binaries. Seven of them have large minimum companion masses compared to the sample of known close binaries, which shows that our target selection works quite well. However, it turns out that our selection strategy also allows us to detect low-mass companions to sdBs in very close orbits. We discovered an eclipsing sdB with a brown dwarf companion and a very similar candidate system in the course of our photometric follow-up campaign. These early results encourage us to go on, because they demonstrate that MUCHFUSS will find both the most massive and the least massive companions to sdB stars.

References

- Abazajian, K.N., Adelman-McCarthy, J.K., Agüeros, M.A., et al.: 2009, *ApJS* 182, 543
- Coenen, T., van Leeuwen, J., Stairs, I.H.: 2011, *A&A* 531, 125
- For, B.-Q., Green, E.M., Fontaine, G., et al.: 2010, *ApJ* 708, 253
- Geier, S., Nesslinger, S., Heber, U., et al.: 2007, *A&A* 464, 299
- Geier, S., Heber, U., Kupfer, T., Napiwotzki, R.: 2010a, *A&A* 515, 37
- Geier, S., Heber, U., Podsiadlowski, Ph., et al.: 2010b, *A&A* 519, 25
- Geier, S., Hirsch, H., Tillich, A., et al.: 2011a, *A&A*, 530, 28
- Geier, S., Maxted, P.F.L., Napiwotzki, R., et al.: 2011b, *A&A* 526, 39
- Geier, S., Schaffenroth, V., Drechsel, H., et al.: 2011c, *ApJ* 731, L22
- Han, Z., Podsiadlowski, P., Maxted, P.F.L., Marsh, T.R., Ivanova, N.: 2002, *MNRAS* 336, 449
- Han, Z., Podsiadlowski, P., Maxted, P.F.L., Marsh, T.R.: 2003, *MNRAS* 341, 669
- Heber, U.: 2009, *ARA&A* 47, 211
- Kleinman, S.J.: 2010, in: K. Werner, T. Rauch (eds.), *White dwarf*, AIP Conf. Ser. 1273, p. 156
- Lisker, T., Heber, U., Napiwotzki, R., Christlieb, N., Han, Z., et al.: 2005, *A&A* 430, 223
- Maxted, P.F.L., Marsh, T.R., North, R.C.: 2000, *MNRAS* 317, L41
- Maxted, P.F.L., Heber, U., Marsh, T.R., North, R.C.: 2001, *MNRAS* 326, 139
- Mereghetti, S., Campana, S., Esposito, P., La Palombara, N., Tiengo, A.: 2011, *A&A* 536, 69
- Napiwotzki, R.: 2008, in: U. Heber, C.S. Jeffery, R. Napiwotzki (eds.), *Hot subdwarf stars and related objects*, ASPC 392, p. 139
- Napiwotzki, R., Karl, C., Lisker, T., et al.: 2004, *Ap&SS* 291, 321
- Nelemans, G.: 2010, *Ap&SS* 329, 25
- Nelemans, G., Tauris, T.M.: 1998, *A&A* 335, L85
- Østensen, R.H., Green, E.M., Bloemen, S., et al.: 2010, *MNRAS* 408, 51
- Pfahl, E., Rappaport, S., Podsiadlowski, Ph.: 2003, *ApJ* 597, 1036
- Podsiadlowski, Ph., Rappaport, S., Pfahl, E.D.: 2002, *ApJ* 565, 1107
- Pollacco, D.L., Skillen, I., Collier Cameron, A., et al.: 2006, *PASP* 118, 1407
- Schuh, S.: 2010, *AN* 331, 489
- Soker, N.: 1998, *AJ* 116, 1308
- Tillich, A., Heber, U., Geier, S., et al.: 2011, *A&A* 527, 137
- Yungelson, L.R., Tutukov, A.V.: 2005, *Astronomy Reports* 49, 871

LETTER TO THE EDITOR

Binaries discovered by the SPY survey

VI. Discovery of a low mass companion to the hot subluminous planetary nebula central star EGB 5 – a recently ejected common envelope?*

S. Geier¹, R. Napiwotzki², U. Heber¹, and G. Nelemans³

¹ Dr. Karl Remeis-Observatory & ECAP, Astronomical Institute, Friedrich-Alexander University Erlangen-Nuremberg, Sternwartstr. 7, 96049 Bamberg, Germany

e-mail: geier@sternwarte.uni-erlangen.de

² Centre of Astrophysics Research, University of Hertfordshire, College Lane, Hatfield AL10 9AB, UK

³ Department of Astrophysics, Radboud University Nijmegen, PO Box 9010, 6500 GL Nijmegen, The Netherlands

Received 3 February 2011 / Accepted 21 February 2011

ABSTRACT

Hot subdwarf B stars (sdBs) in close binary systems are assumed to be formed via common envelope ejection. According to theoretical models, the amount of energy and angular momentum deposited in the common envelope scales with the mass of the companion. That low mass companions near or below the core hydrogen-burning limit are able to trigger the ejection of this envelope is well known. The currently known systems have very short periods ≈ 0.1 – 0.3 d. Here we report the discovery of a low mass companion ($M_2 > 0.14 M_\odot$) orbiting the sdB star and central star of a planetary nebula EGB 5 with an orbital period of 16.5 d at a minimum separation of $23 R_\odot$. Its long period is only just consistent with the energy balance prescription of the common envelope. The marked difference between the short and long period systems will provide strong constraints on the common envelope phase, in particular if the masses of the sdB stars can be measured accurately. Due to selection effects, the fraction of sdBs with low mass companions and similar or longer periods may be quite high. Low mass stellar and substellar companions may therefore play a significant role for the still unclear formation of hot subdwarf stars. Furthermore, the nebula around EGB 5 may be the remnant of the ejected common envelope making this binary a unique system to study this short and poorly understood phase of binary evolution.

Key words. binaries: spectroscopic – subdwarfs

1. Introduction

The ESO SN Ia Progenitor Survey (SPY) was developed to identify double degenerate progenitor candidates to SN Ia. More than 1000 white dwarfs (WDs) and pre-WDs were checked for radial velocity (RV) variations using high resolution spectra obtained with the UVES instrument at the ESO-VLT (e.g. Napiwotzki et al. 2003). Results for nine binaries discovered in the SPY survey were presented in Papers I–V (Napiwotzki et al. 2001, 2002; Karl et al. 2003; Nelemans et al. 2005; Geier et al. 2010a).

Subluminous B stars, which are also known as hot subdwarf stars, display the same spectral characteristics as main-sequence stars of spectral type B, but are much less luminous. They are assumed to be core helium-burning stars with very thin hydrogen envelopes and masses around $0.5 M_\odot$ (Heber 1986). The formation of these objects is still unclear. Different formation channels have been discussed (see Han et al. 2002, 2003). It is found that a large fraction of sdB stars are members of short period binaries (Maxted et al. 2001; Napiwotzki et al. 2004a). For these

systems, common envelope (CE) ejection is the most probable formation channel (Paczynski 1976). In this scenario, two main-sequence stars of different masses evolve in a binary system. The heavier one will reach the red giant phase first and fill its Roche lobe. If the mass transfer to the companion is dynamically unstable, a common envelope is formed. Owing to gravitational drag, the two stellar cores lose orbital energy, which is deposited within the envelope and leads to a shortening of the binary period (e.g. Ricker & Taam 2008). Eventually the common envelope is ejected and a close binary system is formed, which contains a core helium-burning sdB and a main-sequence companion. If the second star reaches the red giant branch, another common envelope phase is possible and can lead to a close binary with a white dwarf companion and an sdB.

EGB 5 was discovered to be the blue central star of a faint elliptical planetary nebula (PN G 211.9+22.6) by Ellis et al. (1984). Méndez et al. (1988a) derived the atmospheric parameters of this star by fitting model spectra. The resulting parameters $T_{\text{eff}} = 42\,000 \pm 5\,000$ K and $\log g = 5.8 \pm 0.2$ were neither consistent with canonical post-asymptotic giant branch (post-AGB) evolutionary tracks nor the parameters of all other known central stars of planetary nebulae (CSPN, Drilling & Schönberner 1985). Méndez et al. (1988a) recognized that these parameters are typical of a hot subdwarf star rather than a post-AGB object and speculated that this is a close binary that experienced non-conservative mass exchange during the first giant phase.

* Based on observations at the Paranal Observatory of the European Southern Observatory for programmes No. 167.H-0407(A) and 71.D-0383(A). Based on observations collected at the Centro Astronómico Hispano Alemán (CAHA) at Calar Alto, operated jointly by the Max-Planck Institut für Astronomie and the Instituto de Astrofísica de Andalucía (CSIC). Some of the data used in this work were obtained at the William Herschel Telescope (WHT) operated by the Isaac Newton Group of Telescopes (ING).

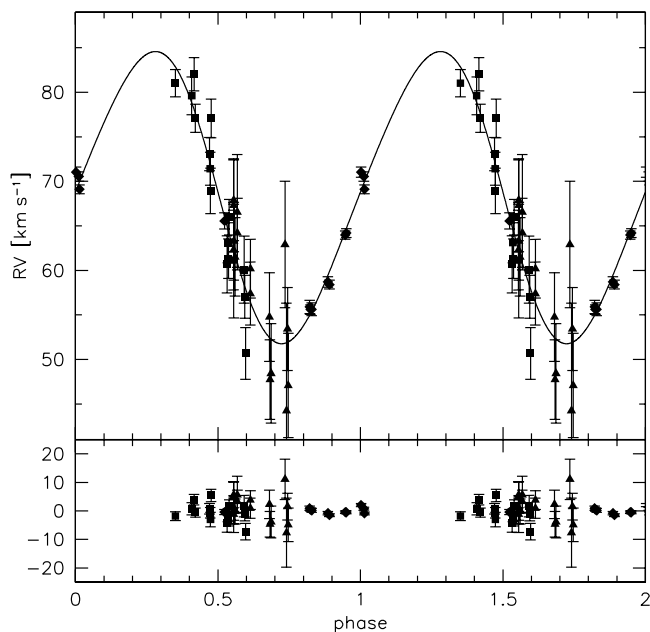


Fig. 1. Radial velocities of the subdwarf primary measured from spectra obtained with UVES (rectangles), ISIS (upward triangles), and TWIN (diamonds) plotted against orbital phase ($P = 16.537$ d). The residuals are plotted below.

Lisker et al. (2005) derived more accurate atmospheric parameters of EGB 5 from high resolution spectra obtained in the course of the SPY survey, which are perfectly consistent with a core helium-burning sdB star ($T_{\text{eff}} = 34\,000 \pm 400$ K, $\log g = 5.85 \pm 0.05$, $\log y = -2.77 \pm 0.04$).

Only one CSPN candidate with similar parameters is known so far (PHL 932, Méndez et al. 1988b; Napiwotzki 1999; Lisker et al. 2005). Whether this star has a close companion remains disputed, because several searches for RV variations yielded inconsistent results (Wade 2001; de Marco et al. 2004; Afşar & Bond 2005). It is therefore unclear whether this star experienced a common envelope phase. Furthermore, Frew et al. (2010) convincingly demonstrated that the nebula around PHL 932 is not a planetary nebula, but rather a Strömgren sphere.

Here we report the discovery of a close companion to EGB 5.

2. Orbital parameters

EGB 5 was observed twice in the course of the SPY project with the high resolution echelle spectrograph UVES at the ESO-VLT. Follow-up high resolution spectra were obtained with UVES, medium resolution spectra were taken with the ISIS spectrograph at the WHT, and the TWIN spectrograph mounted at the CAHA 3.5 m telescope. The RVs were measured by fitting a set of mathematical functions (Gaussians, Lorentzians, and polynomials) to the hydrogen Balmer and helium lines using the FITSB2 routine (Napiwotzki et al. 2004b). Errors were calculated with a bootstrapping algorithm. The RV measurements are given in Table 1.

To determine the orbital parameters and estimate the significance of the solution, sine curves were fitted to 43 RV data points using a χ^2 -minimising method (SVD). The χ^2 against orbital period is given in Fig. 2. Two peaks are present at $P \approx 16.53$ d and $P \approx 25.39$ d with the former one being the most probable solution. We performed Monte Carlo simulations (10 000 iterations)

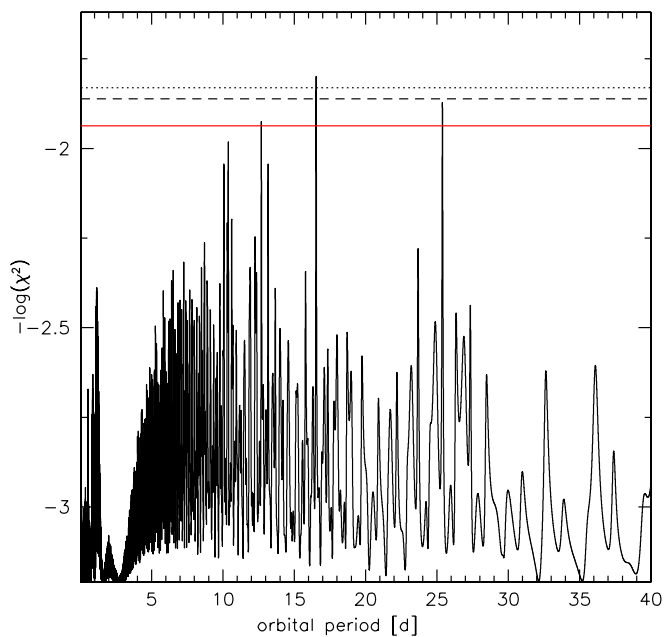


Fig. 2. In this power spectrum $-\log \chi^2$ of the best sine fits is plotted against the orbital periods. The dotted horizontal line marks the 1σ confidence limit, the dashed the 3σ , and the solid line the 6σ limit.

to estimate the significance of the solution. For each simulation, a randomised set of RVs was drawn from Gaussian distributions with central values and widths corresponding to the RV measurements and the analysis repeated. In 82% of the trials, the most likely solution was fitted, the next best solution being chosen in 12% of the iterations.

Since the RV variation in EGB 5 is very small, we used FITSB2 to perform a simultaneous fit of Keplerian orbits to all 169 lines in the 43 spectra covering different orbital phases, i.e., all available information is combined into the parameter determination procedure. Motivated by the discovery of eccentric orbits in close sdB binaries (Edelmann et al. 2005; Napiwotzki et al., in prep.), we did not restrict our fitting to circular orbits. The best-fit orbital solution is shown in Table 2. The errors were determined by bootstrapping and the reduced χ^2 of the best-fit solution is 0.97. For comparison, a sine curve was fitted to the single RV points in the way described in Geier et al. (2011), and our derived orbital parameters ($P = 16.532$ d, $\gamma = 68.8$ km s $^{-1}$, $K = 16.1$ km s $^{-1}$) are consistent with the results given in Table 2.

We are reluctant to claim orbital eccentricity in the case of EGB 5 despite the formal eccentricity being found to be 0.098 ± 0.048 . An F-test indicates a borderline significance of 87% compared to a circular solution. Systematic errors introduced by combining datasets taken with different instruments can easily mimic small eccentricities. High-resolution, time-resolved spectroscopy with a better coverage of the whole orbit would be necessary to solve this issue. Since the formal eccentricity is low, it does not significantly affect the derived minimum companion mass.

3. Atmospheric parameters

The atmospheric parameters of EGB 5 were determined by fitting LTE models with enhanced UV metal line blanketing to the coadded high S/N UVES spectrum. Using models with solar metallicity, the Balmer lines and the He II line at 4686 Å cannot

Table 1. Radial velocities of EGB 5.

Mid-HJD-2 450 000	RV [km s ⁻¹]	Instrument
2008.58634	69.1 ± 0.5	UVES
2033.54169	65.6 ± 0.9	
2716.50684	55.9 ± 0.7	
2716.55553	55.6 ± 0.5	
2716.63020	55.6 ± 0.7	
2717.57133	58.7 ± 0.6	
2717.65759	58.4 ± 0.5	
2718.57307	64.0 ± 0.5	
2718.63521	64.2 ± 0.5	
2719.49370	71.0 ± 0.6	
2719.65305	70.6 ± 0.5	
2328.35974	81.0 ± 1.5	TWIN
2329.30317	79.6 ± 2.1	
2329.44255	82.0 ± 1.9	
2329.52035	77.1 ± 1.6	
2330.33790	73.1 ± 1.9	
2330.38145	71.4 ± 1.9	
2330.39448	68.9 ± 2.6	
2330.43186	77.1 ± 2.2	
2331.35629	60.7 ± 3.2	
2331.40692	63.1 ± 2.3	
2331.43920	61.3 ± 2.2	
2331.48586	66.0 ± 2.0	
2332.34960	60.1 ± 3.8	
2332.38591	57.1 ± 2.4	
2332.42981	50.7 ± 2.9	
2662.47992	62.3 ± 4.5	ISIS
2662.48416	67.9 ± 4.5	
2662.48781	67.3 ± 5.2	
2662.49147	61.1 ± 6.4	
2662.49513	63.3 ± 4.4	
2662.57002	61.5 ± 4.4	
2662.69661	66.5 ± 6.5	
2662.70027	64.2 ± 3.9	
2663.45598	57.4 ± 3.5	
2663.45964	60.2 ± 3.3	
2664.56672	54.8 ± 5.0	
2664.59451	47.7 ± 4.5	
2664.65670	48.4 ± 5.6	
2665.46532	62.9 ± 7.1	
2665.54901	44.3 ± 12.1	
2665.61243	53.4 ± 4.7	
2665.65533	47.1 ± 5.9	

be fitted simultaneously. We choose ten times solar metallicity models to mimic strong UV line blanketing. This is motivated by the strong enrichment of heavy elements produced by radiative levitation in sdB stars with similar parameters (O’Toole & Heber 2006; Geier et al. 2007). The atmospheric parameters (see Table 2) are similar to the ones derived by Lisker et al. (2005).

4. Nature of the unseen companion

Adopting the canonical sdB mass of $0.47 M_{\odot}$, the minimum mass of the unseen companion ($0.14 M_{\odot}$) is consistent with either a late main-sequence star of spectral type M or a low-mass white dwarf. Since no spectral features of the companion are visible in the optical spectra, a main-sequence companion with a mass higher than $\approx 0.45 M_{\odot}$ can be excluded (Lisker et al. 2005). A white dwarf companion of similar or more mass would require the binary inclination to be lower than 24° . Assuming randomly distributed inclinations, the probability for such a low inclination in the case of EGB 5 is less than 9%.

Table 2. Binary parameters of EGB 5.

Orbital parameters	
T_0 [HJD]	$2\,452\,719.457 \pm 0.055$
P	16.537 ± 0.003 d
γ	68.5 ± 0.7 km s ⁻¹
K	16.1 ± 0.8 km s ⁻¹
e	0.098 ± 0.048
Ω	$102 \pm 59^{\circ}$
$f(M)$	$0.0072 \pm 0.0011 M_{\odot}$
Atmospheric parameters	
T_{eff}	$34\,500 \pm 500$ K
$\log g$	5.85 ± 0.05
$\log y$	-2.9 ± 0.09
Derived binary parameters	
M_1 (adopted)	$0.47 M_{\odot}$
R_1	$0.13 R_{\odot}$
$M_{2,\text{min}}$	$0.14 M_{\odot}$
a_{min}	$23 R_{\odot}$

Owing to its long orbital period it is rather unlikely that the system is eclipsing or that it shows other detectable features (e.g. reflection effects) in its light curve. It is therefore not possible to constrain the nature of the companion further. The low mass indicates that it is either a late M dwarf or a low mass WD with a He core.

For the most likely companion mass range of $0.14\text{--}0.45 M_{\odot}$, the separation between sdB and companion is constrained to be $23\text{--}27 R_{\odot}$. All relevant measurements and parameters of the EGB 5 system are summarized in Table 2.

5. Discussion

EGB 5 has the second longest period of all known sdBs in close binary systems. Morales-Rueda et al. (2003) discovered three binaries with periods near or exceeding 10 d and unseen companions (PG 0850+170, 27.815 d; PG 1619+522, 15.3578 d; PG 1110+294, 9.4152 d). In all these cases, the derived minimum companion masses exceed $0.45 M_{\odot}$ consistent with WD companions. The low minimum companion mass of EGB 5 is therefore rather unusual.

Close binaries with sdB primaries and M dwarf companions have been discovered by means of variations in their light curves caused by light originating in the heated surface of the cool companion and often accompanied by eclipses (see e.g. For et al. 2010; Østensen et al. 2010). The orbital periods of these binaries are very short ($\approx 0.1\text{--}0.3$ d), because these so-called reflection effects can only be detected in such cases. The longest period systems, where a reflection effect was detected, is the binary JL 82 (0.7371 d, Edelmann et al. 2005; Koen 2009; Geier et al. 2010b).

With an orbital period of 16.537 days, EGB 5 would have by far the longest period of all sdB+dM binaries known. The M-dwarf companion must have been engulfed by the giant progenitor of the sdB star and the common envelope ejected. According to theoretical models, the change in orbital energy must be at least as large as the binding energy of the giant (see Paczynski 1976; Han et al. 2002, 2003). Detailed models of giants at the tip of the red-giant branch that will form sdB stars after the common envelope are given in Hu et al. (2007). For a $1 M_{\odot}$ progenitor, even a low mass companion of $0.14 M_{\odot}$ in principle could eject the envelope, at least if the thermal energy of the envelope can be used. For more massive companions, the envelope could even be ejected without the thermal energy. However,

in any case it implies that the efficiency of the common envelope (α) is high. Assuming that the efficiency is a universal parameter, this means that the much closer HW Vir binaries should have formed from more massive sdB progenitors and thus should have lower masses (see Hu et al. 2007, Fig. 3) than EGB 5. In contrast, the masses of most sdB primaries in HW Vir systems constrained by observations seem to be close to the canonical value. However, we point out that reliable mass determinations in such systems are still hampered by severe issues (see e.g. For et al. 2010; Østensen et al. 2010). de Marco et al. (2011) suggested that low mass companions may have higher common envelope efficiencies, possibly because of their longer in-spiral timescales.

While close binary sdB+dM systems of HW Vir type are easy to find from their characteristic light curves, it is much harder to discover these systems in wider orbits and at lower inclination. Were the companion of EGB 5 to be an M dwarf, these systems might be very common and that $\approx 10\%$ of all known sdB binaries are of HW Vir type just a selection effect. Barlow et al. (2010) found a sinusoidal variation in the O–C-diagram of the pulsating sdB CS 1246, which is most likely caused by a low mass companion in a 14.1 d orbit very similar to EGB 5.

The period distribution of sdBs with confirmed WD companions is much wider (Morales-Rueda et al. 2003; Geier et al. 2010b), but the combination of low mass and long period make EGB 5 peculiar. All known detached double-degenerate systems with very low-mass WDs have much shorter periods (Steinfadt et al. 2010, and references therein), which may again be caused by selection effects.

Furthermore, EGB 5 may be the first very young post-CE system, where the ejected envelope is still visible (Méndez et al. 1988a) and may provide direct evidence of this sdB formation channel. This would make this binary a unique system to study this short and poorly understood phase of binary evolution.

PHL 932 has been regarded as a similar object. However, evidence that it has a close companion is not compelling. In addition, Frew et al. (2010) showed that the nebulous structure around PHL 932 is not a planetary nebula, but rather a Strömgren sphere created by the hot sdB in the surrounding interstellar medium. Since EGB 5 is located at relatively low Galactic latitude ($+22.6^\circ$) this possibility should be seriously investigated.

Acknowledgements. S.G. is supported by the Deutsche Forschungsgemeinschaft under grant HE1356/49-1.

References

- Afşar, M., & Bond, H. E. 2005, *MmSAI*, 76, 608
 Barlow, B. N., Dunlap, B. H., & Clemens, J. C. 2010, *AIP Conf. Proc.*, 1273, 548
 de Marco, O., Bond, H. E., Harmer, D., & Fleming, A. J. 2004, *ApJ*, 602, L93
 de Marco, O., Passy, J.-C., Moe, M., et al. 2011, *MNRAS*, 411, 2277
 Drilling, J., & Schönberner, D. 1985, *A&A*, 146, L23
 Edelmann, H., Heber, U., Altmann, M., Karl, C., & Lisker, T. 2005, *A&A*, 442, 1023
 Ellis, G. L., Grayson, E. T., & Bond, H. E. 1984, *PASP*, 96, 283
 Frew, D. J., Madsen, G. J., O’Toole, S. J., & Parker, Q. A. 2010, *PASA*, 27, 203
 For, B.-Q., Green, E. M., Fontaine, G., et al. 2010, *ApJ*, 708, 253
 Geier, S., Nesslinger, S., Heber, U., et al. 2007, *A&A*, 464, 299
 Geier, S., Heber, U., Kupfer, T., & Napiwotzki, R. 2010a, *A&A*, 515, A37
 Geier, S., Heber, U., Podsiadlowski, Ph., et al. 2010b, *A&A*, 519, A25
 Geier, S., Maxted, P. F. L., Napiwotzki, R., et al., 2011, *A&A*, 526, A39
 Han, Z., Podsiadlowski, P., Maxted, P. F. L., Marsh, T. R., & Ivanova, N. 2002, *MNRAS*, 336, 449
 Han, Z., Podsiadlowski, P., Maxted, P. F. L., & Marsh, T. R. 2003, *MNRAS*, 341, 669
 Heber, U. 1986, *A&A*, 155, 33
 Hu, H., Nelemans, G., Østensen, R. H., et al. 2007, *A&A*, 473, 569
 Karl, C., Napiwotzki, R., Nelemans, G., et al. 2003, *A&A*, 410, 663
 Koen, C. 2009, *MNRAS*, 395, 979
 Lisker, T., Heber, U., Napiwotzki, R., et al. 2005, *A&A*, 430, 223
 Maxted, P. F. L., Heber, U., Marsh, T. R., & North, R. C. 2001, *MNRAS*, 326, 139
 Méndez, R. H., Kudritzki, R. P., Herrero, A., Husfeld, S., & Groth, H. G. 1988a, *A&A*, 190, 113
 Méndez, R. H., Groth, H. G., Husfeld, D., Kudritzki, R. P., & Herrero, A. 1988b, *A&A*, 197, L25
 Morales-Rueda, L., Maxted, P. F. L., Marsh, T. R., North, R. C., & Heber, U. 2003, *MNRAS*, 338, 752
 Napiwotzki, R. 1999, *A&A*, 350, 101
 Napiwotzki, R., Edelmann H., Heber U., et al. 2001, *A&A*, 378, L17
 Napiwotzki, R., Koester, D., Nelemans, G., et al. 2002, *A&A*, 386, 957
 Napiwotzki, R., Christlieb, N., Drechsel, H., et al. 2003, *ESO Msngr*, 112, 25
 Napiwotzki, R., Karl, C., Lisker, T., et al. 2004a, *Ap&SS*, 291, 321
 Napiwotzki, R., Yungelson, L., Nelemans, G., et al. 2004b, *ASP Conf. Ser.*, 318, 402
 Napiwotzki, R., Karl, C., Nelemans, G., et al. 2007, *ASP Conf. Ser.*, 372, 387
 Nelemans, G., Napiwotzki, R., Karl, C., et al. 2005, *A&A*, 440, 1087
 Østensen, R. H., Green, E. M., Bloemen, S., et al. 2010, *MNRAS*, 408, 51
 O’Toole, S. J., & Heber, U. 2006, *A&A*, 452, 579
 Paczyński, B. 1976, in *Structure and Evolution of Close Binaries*, ed. P. P. Eggleton, S. Mitton, & J. Whelan (Dordrecht: Kluwer), 75
 Ricker, P. M., & Taam, R. E. 2008, *ApJ*, 672, L41
 Steinfadt, J. D. R., Kaplan, D. L., Shporer, A., Bildsten, L., & Howell, S. B. 2010, *ApJ*, 716, L146
 Wade, R. A. 2001, *ASP Conf. Ser.*, 226, 199

Massive unseen companions to hot faint underluminous stars from SDSS (MUCHFUSS)

Analysis of seven close subdwarf B binaries^{*,**}

S. Geier¹, P. F. L. Maxted², R. Napiwotzki³, R. H. Østensen⁴, U. Heber¹, H. Hirsch¹, T. Kupfer¹, S. Müller¹, A. Tillich¹, B. N. Barlow⁵, R. Oreiro^{4,6}, T. A. Ottosen^{7,8}, C. Copperwheat⁹, B. T. Gänsicke⁹, and T. R. Marsh⁹

¹ Dr. Karl Remeis-Observatory & ECAP, Astronomical Institute, Friedrich-Alexander University Erlangen-Nuremberg, Sternwartstr. 7, 96049 Bamberg, Germany

e-mail: geier@sternwarte.uni-erlangen.de

² Astrophysics Group, Keele University, Staffordshire, ST5 5BG, UK

³ Centre of Astrophysics Research, University of Hertfordshire, College Lane, Hatfield AL10 9AB, UK

⁴ Institute of Astronomy, K.U. Leuven, Celestijnenlaan 200D, 3001 Heverlee, Belgium

⁵ Department of Physics and Astronomy, University of North Carolina, Chapel Hill, NC 27599-3255, USA

⁶ Instituto de Astrofísica de Andalucía Glorieta de la Astronomía s/n 18008 Granada, Spain

⁷ Department of Physics and Astronomy, Aarhus University, 8000 Aarhus C, Denmark

⁸ Nordic Optical Telescope, Apartado 474, 38700 Santa Cruz de La Palma, Santa Cruz de Tenerife, Spain

⁹ Department of Physics, University of Warwick, Coventry CV4 7AL, UK

Received 20 September 2010 / Accepted 15 November 2010

ABSTRACT

The project Massive Unseen Companions to Hot Faint Underluminous Stars from SDSS (MUCHFUSS) aims at finding hot subdwarf stars with massive compact companions like massive white dwarfs ($M > 1.0 M_{\odot}$), neutron stars or stellar mass black holes. The existence of such systems is predicted by binary evolution theory and recent discoveries indicate that they exist in our Galaxy. First results are presented for seven close binary sdBs with short orbital periods ranging from ≈ 0.21 d to 1.5 d. The atmospheric parameters of all objects are compatible with core helium-burning stars. The companions are most likely white dwarfs. In one case the companion could be shown to be a white dwarf by the absence of light-curve variations. However, in most cases late type main sequence stars cannot be firmly excluded. Comparing our small sample with the known population of close sdB binaries we show that our target selection method aiming at massive companions is efficient. The minimum companion masses of all binaries in our sample are high compared to the reference sample of known sdB binaries.

Key words. subdwarfs – binaries: spectroscopic – binaries: close – white dwarfs

* Based on observations at the Paranal Observatory of the European Southern Observatory for programme number 081.D-0819. Based on observations at the La Silla Observatory of the European Southern Observatory for programmes number 082.D-0649 and 084.D-0348. Based on observations collected at the Centro Astronómico Hispano Alemán (CAHA) at Calar Alto, operated jointly by the Max-Planck Institut für Astronomie and the Instituto de Astrofísica de Andalucía (CSIC). Based on observations with the William Herschel Telescope and the Isaac Newton Telescope operated both by the Isaac Newton Group at the Observatorio del Roque de los Muchachos of the Instituto de Astrofísica de Canarias on the island of La Palma, Spain. Based on observations with the Southern Astrophysical Research (SOAR) telescope operated by the U.S. National Optical Astronomy Observatory (NOAO), the Ministerio da Ciência e Tecnologia of the Federal Republic of Brazil (MCT), the University of North Carolina at Chapel Hill (UNC), and Michigan State University (MSU). Based on observations obtained at the Gemini Observatory, which is operated by the Association of Universities for Research in Astronomy, Inc., under a cooperative agreement with the NSF on behalf of the Gemini partnership: the National Science Foundation (United States), the Science and Technology Facilities Council (United Kingdom), the National Research Council (Canada), CONICYT (Chile), the Australian Research Council (Australia), Ministerio da Ciência e Tecnologia (Brazil) and Ministerio de Ciencia, Tecnología e Innovación Productiva (Argentina). This paper uses observations made at the South African Astronomical Observatory (SAAO).

** Appendices are only available in electronic form at

<http://www.aanda.org>

1. Introduction

Subluminous B stars (sdBs) are core helium-burning stars with very thin hydrogen envelopes and masses around $0.5 M_{\odot}$ (Heber 1986, see Heber 2009, for a review). A large fraction of the sdB stars (40% to 80%) are members of short period binaries (Maxted et al. 2001; Napiwotzki et al. 2004a). Several studies were undertaken to determine the orbital parameters of subdwarf binaries, and found periods ranging from 0.07 to more than 10 d with a peak at 0.5 to 1.0 d (e.g. Edelmann et al. 2005; Morales-Rueda et al. 2003). For close binary sdBs, common envelope (CE) ejection is the most probable formation channel. In this scenario two main sequence stars of different masses evolve in a binary system. The heavier one will reach the red giant phase first and fill its Roche lobe. If the mass transfer to the companion is dynamically unstable, a common envelope is formed. Due to friction the two stellar cores lose orbital energy, which is deposited within the envelope and leads to a shortening of the binary period. Eventually the common envelope is ejected and a close binary system is formed, which contains a core helium-burning sdB and a main sequence companion. If the companion has already evolved to a white dwarf (WD) when the red giant fills its Roche lobe, a close sdB+WD binary is formed (Han et al. 2002, 2003). Under certain conditions, two consecutive CE phases are possible as well.

In general it is difficult to put constraints on the nature of the close companions to sdB stars. Since most of the binaries are single-lined, only lower limits have been derived from the binary mass functions, which are in general compatible with main sequence stars of spectral type M or compact objects like white dwarfs. Only in special and hence rare cases can tighter constraints be put on the nature of the companions.

Subdwarf binaries with massive WD companions turned out to be candidates for supernova type Ia (SN Ia) progenitors because these systems lose angular momentum due to the emission of gravitational waves and start mass transfer. This mass transfer, either from accretion of He onto the WD during the sdB phase (e.g. Yoon & Langer 2004, and references therein), or the subsequent merger of the system after the sdB star itself has turned into a WD (Tutukov & Yungelson 1981; Webbink 1984) may cause the companion to approach the Chandrasekhar limit and explode as SN Ia.

SN Ia play a key role in the study of cosmic evolution (e.g. Riess et al. 1998; Leibundgut 2001; Perlmutter et al. 1999). One of the best known candidate systems for the double degenerate merger scenario is the sdB+WD binary KPD 1930+2752 (Maxted et al. 2000a; Geier et al. 2007). Mereghetti et al. (2009) showed that in the X-ray binary HD 49798 a massive ($>1.2 M_{\odot}$) white dwarf accretes matter from a closely orbiting subdwarf O companion. The predicted amount of accreted material is sufficient for the WD to reach the Chandrasekhar limit. This makes HD 49798 another candidate for SN Ia progenitor. Furthermore, Perets et al. (2010) showed that helium accretion onto a white dwarf may be responsible for a subclass of faint and calcium-rich SN Ib events.

Geier et al. (2008, 2010a,b) analysed high resolution spectra of sdB stars in close binaries. Assuming synchronised rotation they constrained the masses and the nature of the unseen companions in 31 cases. While most of the derived companion masses were consistent with either late type main sequence stars or white dwarfs, the compact companions of some sdBs may be either massive white dwarfs, neutron stars (NS) or stellar mass black holes (BH). However, Geier et al. (2010b) also showed that the assumption of orbital synchronisation in close sdB binaries is not always justified and that their analysis suffers from huge selection effects.

The existence of sdB+NS/BH systems is predicted by binary evolution theory (Podsiadlowski et al. 2002; Pfahl et al. 2003). The formation channel includes two phases of unstable mass transfer and one supernova explosion. The fraction of sdB+NS/BH systems is predicted to be about 2% of the close sdB binaries (Geier et al. 2010b). Yungelson & Tutukov (2005) and Nelemans (2010) performed independent binary evolution calculations and confirm that sdB+NS/BH systems should exist. According to the results of Nelemans (2010) about 1% of the subdwarfs in close binaries should have a neutron star companion, whereas only 0.01% should be orbited by a black hole. Yungelson & Tutukov (2005) predict the sdB+NS fraction to be of the order of 0.8%.

Since sdB stars eventually evolve to WDs there should also exist a population of white dwarfs with massive compact companions. Badenes et al. (2009) reported the discovery of a close binary consisting of a massive white dwarf and an unseen neutron star or black hole companion, but Marsh et al. (2010) most recently showed that the system is double-lined and consists of a massive white dwarf orbited by a low mass white dwarf. The system mass is below the Chandrasekhar limit. Their results were confirmed by Kulkarni & van Kerkwijk (2010). Common envelope ejection was proposed as the most likely formation channel

Table 1. Solved binary systems.

SDSS name	Short name	Other names
SDSS J002323.99–002953.2	J0023–0029	PB 5916
SDSS J113840.68–003531.7	J1138–0035	PG 1136–003
SDSS J150513.52+110836.6	J1505+1108	PG 1502+113
SDSS J165404.25+303701.7	J1654+3037	PG 1652+307
SDSS J172624.09+274419.3	J1726+2744	PG 1724+278
SDSS J204613.40–045418.7	J2046–0454	–
SDSS J225638.34+065651.0	J2256+0656	PG 2254+067

for the binary PSR J1802–2124, which consists of a millisecond pulsar and a CO white dwarf in close orbit ($P = 0.7$ d, Ferdman et al. 2010). This peculiar system may have evolved through an earlier sdB+NS phase.

2. The MUCHFUSS project

The discovery of sdB binary candidates with massive compact companions provides a first hint that a whole population of non-interacting binaries with such companions may be present in our Galaxy. The known candidate sdB+NS/BH binaries have low orbital inclinations (15–30°, Geier et al. 2010b). High inclination systems must exist as well and should be more numerous. In this case a determination of the orbital parameters is sufficient to put a lower limit to the companion mass by calculating the binary mass function. If this lower limit exceeds the Chandrasekhar mass and no sign of a companion is visible in the spectra, the existence of a massive compact companion is proven without the need for any additional assumptions.

The project Massive Unseen Companions to Hot Faint Underluminous Stars from SDSS¹ (MUCHFUSS) aims at finding sdBs with compact companions like massive white dwarfs ($M > 1.0 M_{\odot}$), neutron stars or black holes. About 70 binaries have been selected for follow-up. Survey and target selection are described in detail in Geier et al. (2010c). The same selection criteria that we applied to find such binaries are also well suited to single out hot subdwarf stars with constant high radial velocities (RV) in the Galactic halo and search for hypervelocity stars. First results of this second part of the project (Hyper-MUCHFUSS) are presented in Tillich et al. (2010).

Here we present the spectroscopic analysis of the first sdB binaries discovered in the course of the MUCHFUSS project (see Table 1). In Sect. 3 the observations and the data reduction are described. Sections 4 and 5 deal with the determination of the orbital and atmospheric parameters of the sdB stars. Section 6 explains the way the minimum masses of the unseen companions are constrained, while results are presented in Sect. 7. The efficiency of our target selection is discussed in Sect. 8, a short summary and an outlook are eventually given in Sect. 9.

3. Multi-site observations and data reduction

Follow-up medium resolution spectra were taken during dedicated follow-up runs (see Table 2) with the EFOSC2 spectrograph ($R \approx 2200$, $\lambda = 4450–5110 \text{ \AA}$) mounted at the ESO NTT,

¹ Sloan Digital Sky Survey.

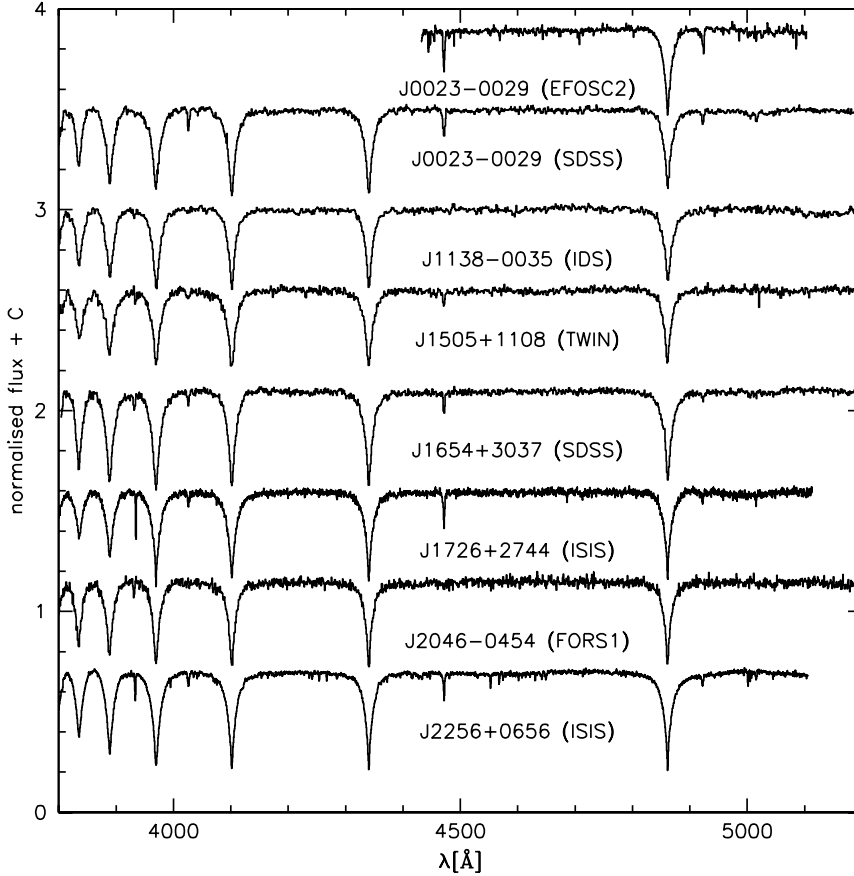


Fig. 1. Medium resolution spectra of the programme stars taken with different instruments. Multiple observations of the same target have been shifted to rest wavelength and coadded.

Table 2. Follow-up observations 2009/2010.

Date	Telescope & Instrument	Observer
2009/06/05–2009/06/09	ING-INT/IDS	R. Ø., R. O., T. O.
2009/07/22–2009/07/26	CAHA-3.5m/TWIN	T. K.
2009/08/24–2009/08/27	ING-WHT/ISIS	S. G.
2009/11/08–2009/11/12	ESO-NTT/EFOSC2	T. K.
April/August 2009	Gemini-North/GMOS	Service
2010/02/12–2010/02/15	SOAR/Goodman	B. B.

Notes. The first column lists the date of observation, while in the second the used telescope and instrumentation is shown. In the third column the observers are listed.

the ISIS spectrograph ($R \approx 4000$, $\lambda = 3440\text{--}5270 \text{ \AA}$) mounted at the WHT, the TWIN spectrograph mounted at the CAHA-3.5 m telescope ($R \approx 4000$, $\lambda = 3460\text{--}5630 \text{ \AA}$), the Goodman spectrograph mounted at the SOAR telescope ($R \approx 2500$, $\lambda = 3500\text{--}6160 \text{ \AA}$), the GMOS spectrograph ($R \approx 1200$, $\lambda = 3770\text{--}4240 \text{ \AA}$) mounted at the Gemini North telescope and the IDS spectrograph mounted at the Isaac Newton Telescope ($R \approx 1400$, $\lambda = 3000\text{--}6800 \text{ \AA}$). Informations about data taken in the course of our survey are provided in Geier et al. (2010c). Additional data could be gathered, when our targets were observed with the IDS spectrograph (March 2007, observer: T. M., C. C.; $R \approx 4000$, $\lambda = 3930\text{--}5100 \text{ \AA}$) and the grating spectrograph (March 2003, April 2004, observer: T. M.; $R \approx 4600$, $\lambda = 4170\text{--}5030 \text{ \AA}$) mounted at the 1.9 m Radcliffe Telescope. Example spectra are shown in Fig. 1.

In order to obtain a good wavelength calibration, arc lamp exposures have been taken before or after the single exposures.

In addition to that bright single sdBs have been taken as RV standards in most of the runs. In some cases the RVs of certain instruments (TWIN, GMOS) had to be corrected by a constant offset of up to $\approx 50 \text{ km s}^{-1}$, which was derived from the RV measurements of the standard stars. The slit width was always chosen to be smaller than the size of the seeing discs to minimize systematic errors due to movement of the objects within the slit. Reduction was done either with the MIDAS, IRAF or PAMELA² and MOLLY² packages.

4. Orbital parameters

The radial velocities were measured by fitting a set of mathematical functions (Gaussians, Lorentzians and polynomials) to the hydrogen Balmer lines as well as helium lines if present using the FITSB2 routine (Napiwotzki et al. 2004b). The RVs of the GMOS spectra have been measured by fitting three Gaussians to the H_γ line. Three functions are used to match the continuum, the line and the line core, respectively and mimic the typical Voigt profile of spectral lines. The profiles are fitted to all suitable lines simultaneously using χ^2 -minimization and the RV shift with respect to the rest wavelengths is measured. The RVs and formal 1σ -errors are given in Appendix B. Assuming circular orbits sine curves were fitted to the RV data points in fine steps over a range of test periods. For each period the χ^2 of the best fitting sine curve was determined. The result is similar to a power spectrum with the lowest χ^2 indicating the most likely period (see Fig. 4). In order to estimate the significance of the orbital solutions and the contributions of systematic effects to the

² <http://www2.warwick.ac.uk/fac/sci/physics/research/astro/people/marsh/software>

Table 3. Derived orbital parameters.

Object	T_0 [−2 450 000]	P [d]	γ [km s ^{−1}]	K [km s ^{−1}]
J0023–0029	5069.850 ± 0.008	1.4876 ± 0.0001	16.4 ± 2.1	81.8 ± 2.9
J1138–0035	4991.388 ± 0.001	0.207536 ± 0.000002	23.3 ± 3.7	162.0 ± 3.8
J1505+1108	4938.867 ± 0.002	0.74773 ± 0.00005	−77.1 ± 1.2	97.2 ± 1.8
J1654+3037	4991.5322 ± 0.0008	0.25357 ± 0.00001	40.5 ± 2.2	126.1 ± 2.6
J1726+2744	4981.667 ± 0.005	0.50198 ± 0.00005	−36.7 ± 4.8	118.9 ± 3.7
J2046–0454	4693.352 ± 0.002	0.24311 ± 0.00001	87.6 ± 5.7	134.3 ± 7.8
J2256+0656	5070.662 ± 0.002	0.7004 ± 0.0001	−7.3 ± 2.1	105.3 ± 3.4

Table 4. Significance of the circular orbital solutions.

Object	Best solution [d]	χ^2	χ^2_{reduced}	2nd best alias [d]	$\Delta\chi^2$	n	e_{norm} [km s ^{−1}]	log $p_{\text{false}}[1\%]$	log $p_{\text{false}}[10\%]$
J0023–0029	1.4876	157	3.74	0.5976	130	47	8.0	−3.0	−3.4
J1138–0035	0.207536	213	5.33	0.260192	426	45	16.0	−3.5	−3.5
J1505+1108	0.74773	155	4.30	0.75709	679	41	7.0	<−4.0	<−4.0
J1654+3037	0.25357	18	0.54	0.20397	64	38	–	<−4.0	<−4.0
J1726+2744	0.50198	82	2.48	1.00998	77	38	12.0	−1.2	−1.9
J2046–0454	0.24311	52	3.05	0.31971	39	22	17.0	−1.1	−1.1
J2256+0656	0.7004	276	6.13	2.1903	976	50	13.0	<−4.0	<−4.0

Notes. The best solutions for the orbital periods are given together with their minimum χ^2 and reduced χ^2 values as well as the number n of RVs. The second best aliases (further than 1% away from the best solution) and the $\Delta\chi^2$ -values with respect to the best solutions are given as well. The systematic error adopted to normalise the reduced χ^2 (e_{norm}) is given for each case. The probabilities for the orbital period to deviate from our best solution by more than 1% ($p_{\text{false}}[1\%]$) or 10% ($p_{\text{false}}[10\%]$) are given in the last columns.

error budget, we normalised the χ^2 of the most probable solution by adding systematic errors in quadrature until the reduced χ^2 reached ≈ 1.0 . Using these modified uncertainties we performed Monte Carlo simulations for the most likely periods. For each simulation a randomised set of RVs was drawn from Gaussian distributions with central value and width corresponding to the RV measurements and the analysis repeated. From these simulations the probabilities for the orbital periods to deviate from our best solution by more than 1% or 10% were calculated.

In order to derive most conservative errors for the RV semi-amplitude K and the system velocity γ we fixed the most likely period and created new RV datasets with a bootstrapping algorithm. Ten thousand RV datasets were obtained by random sampling with replacement from the original dataset. In each case an orbital solution was calculated in the way described above. The standard deviation of these results was adopted as error estimate. The RV curves are given in Figs. 2 and 3. The residuals of the RV curves after subtracting the best orbital solution are of the same order in all cases (see Figs. 2, 3). The accuracy is limited by the resolution of the spectra and their signal-to-noise. Combining data obtained with different instruments is also expected to contribute to the systematic error. Nevertheless, we found that all orbital solutions given here are significant (see Tables 3, 4).

Edelmann et al. (2005) reported the discovery of small eccentricities ($e < 0.06$) in the orbital solutions of five close hot subdwarf binaries. All of these binaries are expected to have formed via common envelope ejection. Although the CE phase is very short, it should nevertheless be very efficient in circularising the binary orbits. That is why the discovery of Edelmann et al. (2005) came as a surprise. Napiwotzki et al. (in prep.) found more such systems with even shorter periods.

In order to investigate whether the orbital solutions of our programme binaries can be improved by allowing for eccentricity, we fitted eccentric orbits to our radial velocity data and

performed statistical tests (F-test, see Pringle 1975, and the Bayesian information criterion BIC) to check whether eccentric solutions are significant or not. In all cases the circular solutions were preferred. However, the derived upper limits for the orbital eccentricities range from 0.15 to 0.3, which means that low eccentricities as the ones reported by Edelmann et al. (2005) cannot be firmly excluded.

5. Atmospheric parameters

Atmospheric parameters have been determined by fitting model spectra to the hydrogen Balmer and helium lines in the way described in Geier et al. (2007). The single spectra have been corrected for their orbital motion and coadded. Depending on the effective temperature of the stars, LTE models with solar metallicity ($T_{\text{eff}} < 30\,000$ K) or ten times solar metallicity ($T_{\text{eff}} > 30\,000$ K) have been used. The enhanced metallicity models account for the radiative levitation of heavy elements in the diffusion dominated atmospheres (for a detailed discussion see O’Toole & Heber 2006).

In order to investigate systematic effects introduced by the individual instruments, especially the different resolutions and wavelength coverages, the parameters have been derived separately from spectra taken with different instruments. As can be seen in Table A.1 no constant systematic shifts are present. The weighted means have been calculated and adopted as final solutions. Typical systematic errors introduced by different model grids are of the order of ± 0.05 in $\log g$ and 500 K in T_{eff} (e.g. Lisker et al. 2005; Geier et al. 2007). These uncertainties were added in quadrature to the statistical errors.

Three of our programme stars have been classified as hot subdwarfs by Eisenstein et al. (2006), but the authors pointed out that the atmospheric parameters of the sdO/Bs given in their catalogue are not accurate.

All stars of our sample are situated on or near the Extreme Horizontal Branch (EHB) and are most likely core-helium burning stars (see Fig. 5). Since the orbital periods of these binaries

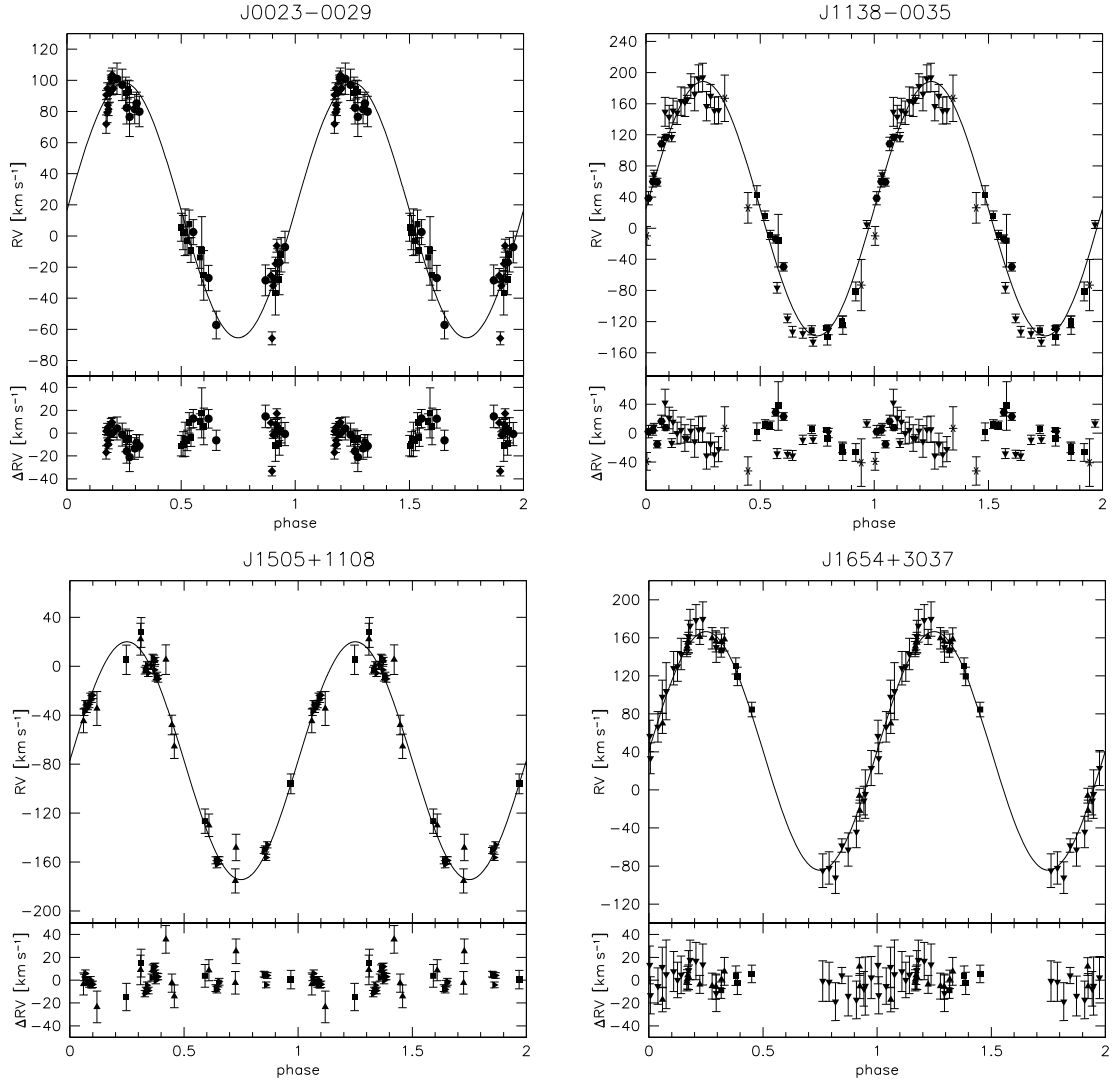


Fig. 2. Radial velocity plotted against orbital phase. The RV data were phase folded with the most likely orbital periods. The residuals are plotted below. The RVs were measured from spectra obtained with SDSS (rectangles), CAHA3.5 m/TWIN (upward triangles), WHT/ISIS (diamonds), INT/IDS (downward triangles), ESO-VLT/FORS1 (triangles turned to the left), Gemini/GMOS (triangles turned to the right), ESO-NTT/EFOSC2 (circles), SOAR/Goodman (hexagons) and SAAO-1.9 m/Grating (stars).

are short, they can only have formed via common envelope ejection. Population synthesis models (Han et al. 2002, 2003) predict a mass range of $M_{\text{sdB}} = 0.37\text{--}0.48 M_{\odot}$ for sdBs in binaries formed in this way. The mass distribution shows a sharp peak at a mass of about $0.47 M_{\odot}$. This theoretical mass distribution is consistent with analyses of close binary systems (e.g. Geier et al. 2007; For et al. 2010) as well as asteroseismic analyses of pulsating sdBs (see Charpinet et al. 2008, and references therein). If the progenitor star was massive enough on the main sequence to ignite core helium-burning under non-degenerate conditions, the sdB mass may be as low as $0.3 M_{\odot}$. A small fraction of the sdB population is predicted to be formed in that way (Han et al. 2002, 2003). Especially for sdB binaries with massive companions this formation scenario may become important.

6. Constraining the nature of the unseen companions

Since the programme stars are single-lined spectroscopic binaries, only their mass functions can be calculated.

$$f_m = \frac{M_{\text{comp}}^3 \sin^3 i}{(M_{\text{comp}} + M_{\text{sdB}})^2} = \frac{PK^3}{2\pi G}. \quad (1)$$

Although the RV semi-amplitude K and the period P can be derived from the RV curve, the sdB mass M_{sdB} , the companion mass M_{comp} and the inclination angle i remain free parameters. Adopting $M_{\text{sdB}} = 0.47 M_{\odot}$ and $i < 90^\circ$ we derive a lower limit for the companion mass (see Table 5).

For minimum companion masses lower than $0.45 M_{\odot}$ the companion may be a late type main sequence star or a compact object like a WD. Main sequence stars in this mass range are outshined by the sdBs and not visible in optical spectra (Lisker et al. 2005). That is the reason why the companions' nature still remains unknown for most of the ≈ 80 known sdB systems with low minimum companion masses (see Fig. 7). If on the other hand the minimum companion mass exceeds $0.45 M_{\odot}$, spectral features of a main sequence companion become visible in the optical. The non-detection of such features therefore allows us to exclude a main sequence star. The companion must then be a compact object. More massive compact companions like massive WDs, neutron stars or black holes are more likely as soon as the minimum mass exceeds $1.00 M_{\odot}$ or even the Chandrasekhar limit $1.40 M_{\odot}$.

Due to the fact that we selected targets with high RV shifts, the distribution of orbital inclinations in our target sample is

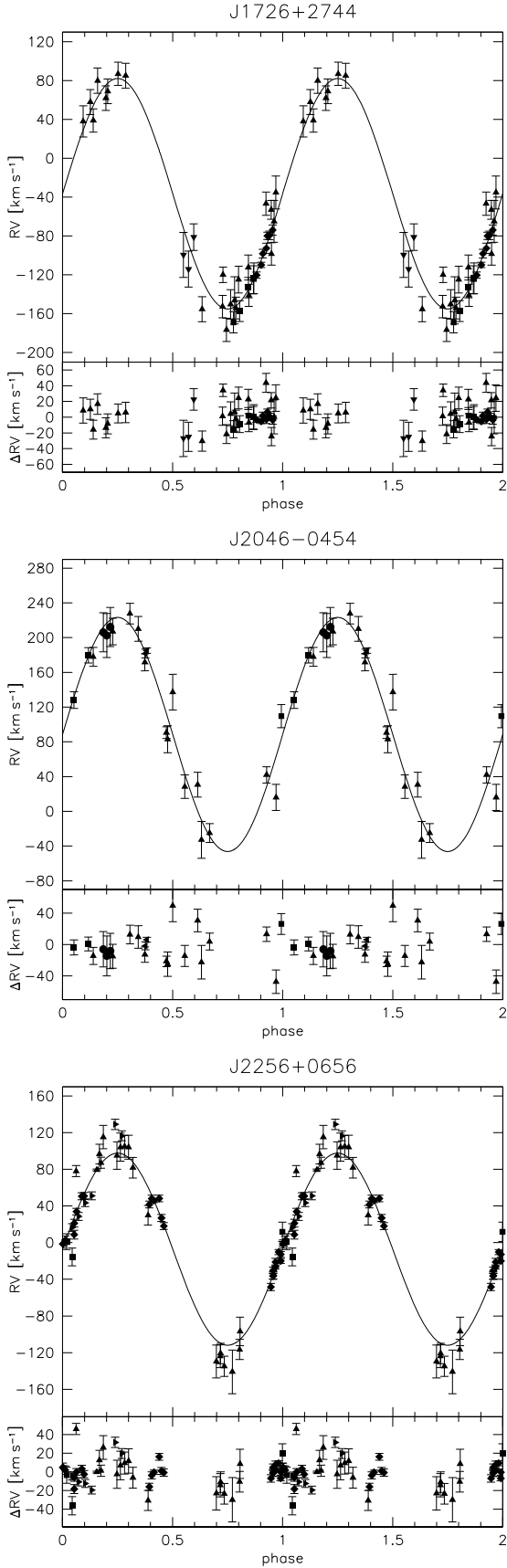


Fig. 3. Radial velocity curves (see Fig. 2).

not random any more. Our selection strategy strongly favours high inclination angles, and therefore the companion masses are

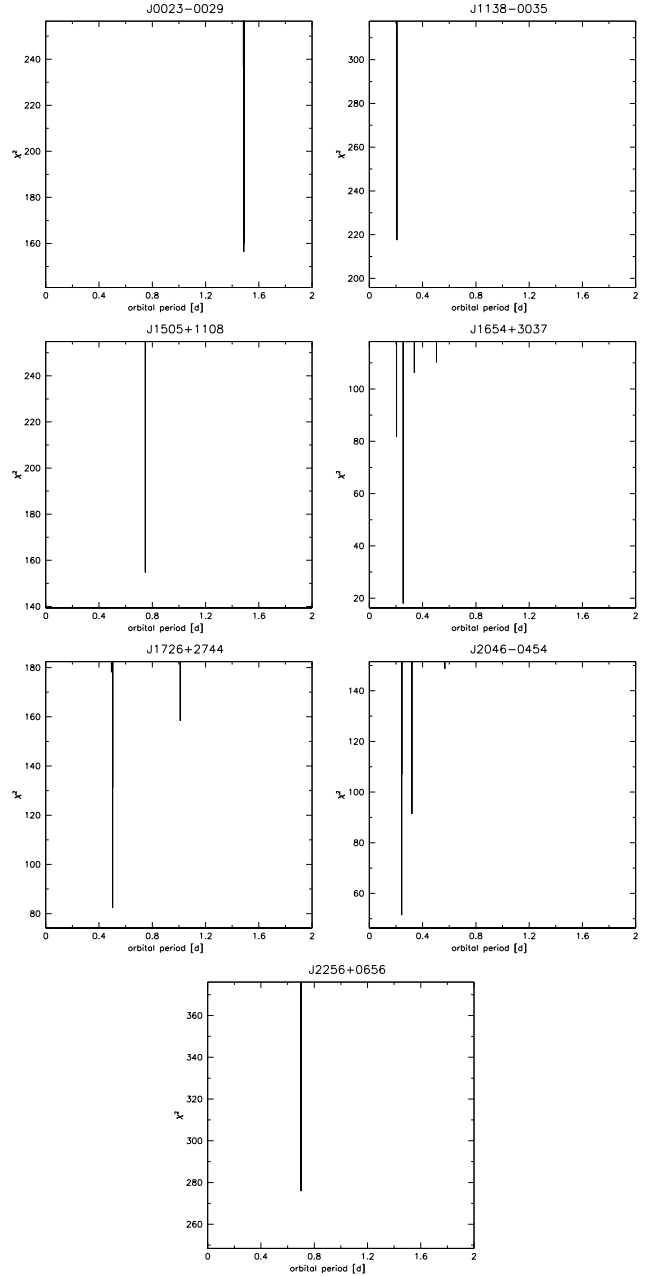


Fig. 4. χ^2 plotted against orbital period. The lowest peak corresponds to the most likely solution.

Table 5. Derived minimum masses and most probable nature of the companions.

Object	$f(M)$ [M_{\odot}]	$M_{2\min}$ [M_{\odot}]	Companion
J0023-0029	0.084	0.40	MS/WD
J1138-0035	0.091	0.42	WD
J1505+1108	0.071	0.37	MS/WD
J1654+3037	0.053	0.32	MS/WD
J1726+2744	0.087	0.41	MS/WD
J2046-0454	0.061	0.34	MS/WD
J2256+0656	0.085	0.40	MS/WD

likely to be close to their minimum values. The probability of detecting eclipses, reflection effects or variations caused by ellipsoidal deformation in the light curves of systems with short orbital periods should therefore be significantly higher than in an unbiased sample.

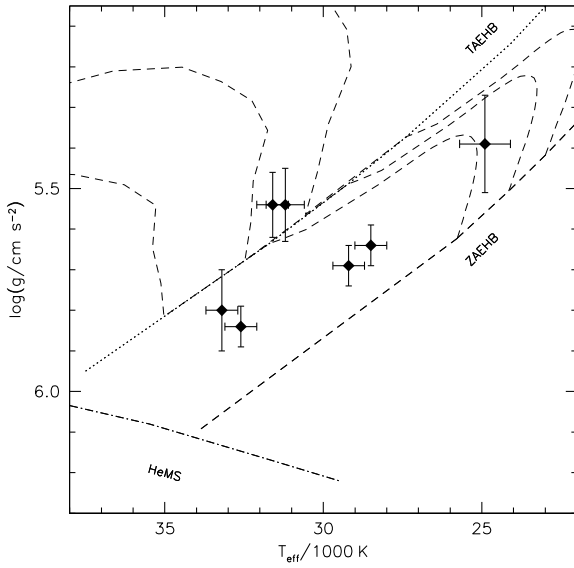


Fig. 5. $T_{\text{eff}} - \log g$ -diagram. The helium main sequence (HeMS) and the EHB band (limited by the zero-age EHB, ZAEHB, and the terminal-age EHB, TAEHB) are superimposed with EHB evolutionary tracks from Dorman et al. (1993).

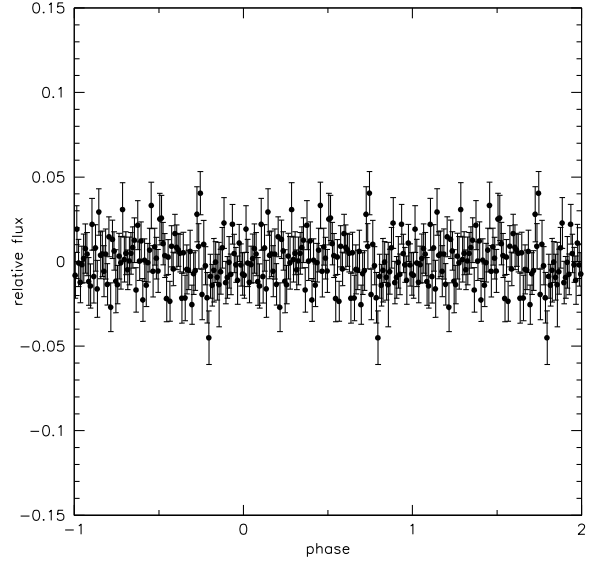


Fig. 6. SuperWASP light curve of J1138–0035 folded to the orbital phase. The 11213 data points taken between 2006/07/05 and 2009/07/02 are binned to 100 phase bins. Relative flux is plotted against the orbital phase.

7. Results

The spectra of all stars in our sample have been checked for spectral features of their companions. Hot subdwarfs with faint main sequence companions usually show spectral lines of the Mg I triplet at $\approx 5170 \text{ \AA}$ (Lisker et al. 2005) and the Ca II triplet at $\approx 8650 \text{ \AA}$. No such features are visible in the spectra of our programme stars (see e.g. Fig. 1). Stark & Wade (2003) analysed optical and IR photometry (2MASS) and found no indication of an IR-excess caused by a cool companion in the case of J1654+3037. According to the catalogue of Reed & Stiening (2004), who performed a similar analysis, J1505+1108 shows signs of an IR-excess in the H and K -bands, but the large errors of these measurements and the missing spectral signatures of a cool companion in the SDSS spectra are strong indications, that no visible companion is present.

J1654+3037 and J2046–0454 have very similar orbital parameters. The periods are short (0.25 d) and the minimum companion masses are constrained to $0.32 M_{\odot}$ and $0.34 M_{\odot}$. Whether the companions are M dwarfs or WDs is therefore not yet clear. In the former case a reflection effect should be easily detectable in the light curves. Photometric follow-up will allow us to clarify the nature of the companions.

The companion of the short period (0.2 d) system J1138–0035 is most likely a white dwarf. The minimum companion mass is constrained to $0.42 M_{\odot}$ and no sign of a companion is seen in the spectra. A light curve taken by the SuperWASP project (Pollacco et al. 2006) shows no variation exceeding $\approx 1\%$ (see Fig. 6). Due to the short period of this system a reflection effect should be visible, if the companion should be a cool main sequence star. The absence of such a variation leads to the conclusion that the companion is most likely a white dwarf.

The orbital periods of J1726+2744 (0.5 d), J2256+0656 (0.7 d) and J1505+1108 (0.75 d) are longer. Their minimum companion masses are similar ($0.37\text{--}0.41 M_{\odot}$) and close to the border between main sequence stars and white dwarfs. The companions of J1726+2744 and J2256+0656 are most likely WDs. Koen (2009) and Shimanskii et al. (2008) recently showed that

reflection effects can still be detected in the light curves of sdB binaries with similar orbital periods. A reflection effect in J0023–0029 on the other hand is most likely not detectable, because the orbital period is too long (1.5 d).

8. Efficiency of target selection

The goal of the MUCHFUSS project is to find sdB binaries with massive compact companions and study this population of close binaries. We tried to optimise our target selection to achieve this goal. Figure 7 illustrates the efficiency of our target selection. The RV semiamplitudes of all known sdB binaries with spectroscopic solutions (open symbols) are plotted against their orbital periods (Geier et al. 2010c). Binaries which have initially been discovered in photometric surveys due to indicative features in their light curves (eclipses, reflection effects, ellipsoidal variations) are marked with open circles. Binaries discovered by RV variations from time resolved spectroscopy are marked with open diamonds. The dashed, dotted and solid lines mark the regions to the right where the minimum companion masses derived from the binary mass function (assuming $0.47 M_{\odot}$ for the sdBs) exceed $0.45 M_{\odot}$, $1.00 M_{\odot}$ and $1.40 M_{\odot}$.

Most of the known sdB binaries are situated beneath the $0.45 M_{\odot}$ line, which means that the companion type cannot be constrained from the mass function alone. Photometry is necessary to clarify the companions' nature in these cases. The most massive sdB binary known to date is KPD 1930+2752 with a WD companion of $0.9 M_{\odot}$. This short period system has been discovered based on indicative features in its light curve (upper left corner in Fig. 7; Billères et al. 2000).

The seven binaries from the MUCHFUSS project are marked with filled diamonds. It can be clearly seen that they belong to the sdB binary population with the largest minimum masses close to $0.45 M_{\odot}$. We therefore conclude that our target selection is efficient and singles out sdB binaries with massive companions.

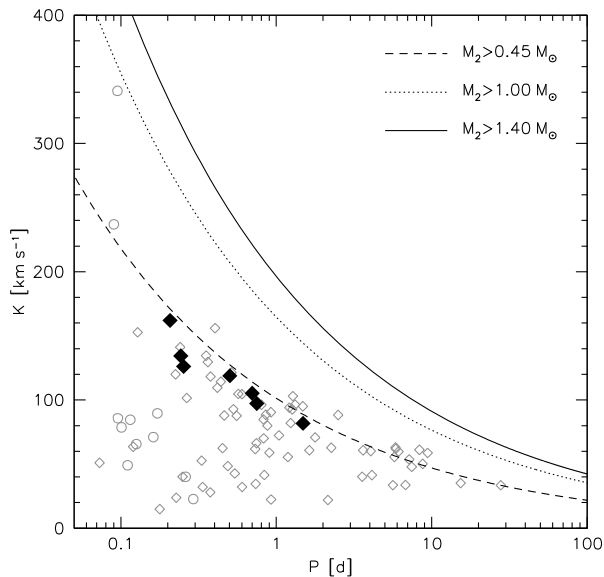


Fig. 7. The RV semi-amplitudes of all known sdB binaries with spectroscopic solutions plotted against their orbital periods (Geier et al. 2010c). Binaries which have initially been discovered in photometric surveys due to indicative features in their light curves (eclipses, reflection effects, ellipsoidal variations) are marked with open circles. Binaries discovered by detection of RV variations from time resolved spectroscopy are marked with open diamonds. The dashed, dotted and solid lines mark the regions to the right where the minimum companion masses derived from the binary mass function (assuming $0.47 M_{\odot}$ for the sdBs) exceed $0.45 M_{\odot}$, $1.00 M_{\odot}$ and $1.40 M_{\odot}$. The seven binaries from the MUCHFUSS project are marked with filled diamonds.

9. Summary and outlook

A multi-site follow-up campaign is being conducted with medium resolution spectrographs mounted at several different telescopes of mostly 2 m to 4 m-class. First results were presented for seven close binary sdBs with short orbital periods ranging from ≈ 0.21 d to 1.5 d and most likely compact companions. The atmospheric parameters of all objects are compatible with core helium-burning stars on the EHB. Comparing our small sample with the known population of close sdB binaries we are able to show that our target selection method is efficient. All binaries solved up to now have high minimum companion masses compared to the rest of the sdB binary population.

Up to now we have found significant orbital solutions for about 10% of our target sample. Photometric follow-up observations will allow us to clarify the nature of the companions in most cases. A database of more than 700 spectra has been built up and some binaries will be solvable with only a few additional RV points.

Acknowledgements. A.T., S.G. and H.H. are supported by the Deutsche Forschungsgemeinschaft (DFG) through grants HE1356/45-1, HE1356/49-1, and HE1356/44-1, respectively. R.Ø. acknowledges funding from the European Research Council under the European Community's Seventh Framework Programme (FP7/2007–2013)/ERC grant agreement N°227224 (PROSPERITY), as well as from the Research Council of K.U. Leuven grant agreement GOA/2008/04. Travel to the DSAZ (Calar Alto, Spain) was supported by DFG under grants HE1356/48-1 and HE1356/50-1. Travel to La Palma for the observing run at the WHT was funded by DFG through grant He 1356/53-1. Funding for the SDSS and SDSS-II has been provided by

the Alfred P. Sloan Foundation, the Participating Institutions, the National Science Foundation, the U.S. Department of Energy, the National Aeronautics and Space Administration, the Japanese Monbukagakusho, the Max Planck Society, and the Higher Education Funding Council for England. The SDSS Web Site is <http://www.sdss.org/>. The SDSS is managed by the Astrophysical Research Consortium for the Participating Institutions. The Participating Institutions are the American Museum of Natural History, Astrophysical Institute Potsdam, University of Basel, University of Cambridge, Case Western Reserve University, University of Chicago, Drexel University, Fermilab, the Institute for Advanced Study, the Japan Participation Group, Johns Hopkins University, the Joint Institute for Nuclear Astrophysics, the Kavli Institute for Particle Astrophysics and Cosmology, the Korean Scientist Group, the Chinese Academy of Sciences (LAMOST), Los Alamos National Laboratory, the Max-Planck-Institute for Astronomy (MPIA), the Max-Planck-Institute for Astrophysics (MPA), New Mexico State University, Ohio State University, University of Pittsburgh, University of Portsmouth, Princeton University, the United States Naval Observatory, and the University of Washington.

References

- Badenes, C., Mullally, F., Thompson, S. E., & Lupton, R. H. 2009, *ApJ*, 707, 971
- Billères, M., Fontaine, G., Brassard, P., et al. 2000, *ApJ*, 530, 441
- Charpinet, S., van Grootel, V., Reese, D., et al. 2008, *A&A*, 489, 377
- Dorman, B., Rood, R. T., & O'Connell, R. W. 1993, *ApJ*, 419, 596
- Edelmann, H., Heber, U., Altmann, M., Karl, C., & Lisker, T. 2005a, *A&A*, 442, 1023
- Eisenstein, D. J., Liebert, J. L., Harris, H. C., et al. 2006, *ApJS*, 167, 40
- Ferdman, R. D., Stairs, I. H., Kramer, M., et al. 2010, *ApJ*, 711, 764
- For, B.-Q., Green, E. M., Fontaine, G., et al. 2010, *ApJ*, 708, 253
- Geier, S., Heber, U., Kupfer, T., & Napiwotzki, R. 2010a, *A&A*, 515, A37
- Geier, S., Heber, U., Podsiadlowski, Ph., et al. 2010b, *A&A*, 519, A25
- Geier, S., Hirsch, H., Tillich, A., et al. 2010c, *A&A*, submitted
- Geier, S., Nesslinger, S., Heber, U., et al. 2007, *A&A*, 464, 299
- Geier, S., Nesslinger, S., Heber, U., et al. 2008, *A&A*, 477, L13
- Han, Z., Podsiadlowski, P., Maxted, P. F. L., Marsh, T. R., & Ivanova, N. 2002, *MNRAS*, 336, 449
- Han, Z., Podsiadlowski, P., Maxted, P. F. L., & Marsh, T. R. 2003, *MNRAS*, 341, 669
- Heber, U. 1986, *A&A*, 155, 33
- Heber, U. 2009, *ARA&A*, 47, 211
- Koen, C. 2009, *MNRAS*, 393, 1370
- Kulkarni, S. R., & van Kerkwijk, M. H. 2010, *ApJ*, 719, 1123
- Leibundgut, B. 2001, *ARA&A*, 39, 67
- Lisker, T., Heber, U., Napiwotzki, R., et al. 2005, *A&A*, 430, 223
- Marsh, T. R., Gaensicke, B. T., Steeghs, D., et al. 2010, *ApJL*, submitted [arXiv:1002.4677]
- Maxted, P. F. L., Marsh, T. R., & North, R. C. 2000, *MNRAS*, 317, L41
- Maxted, P. F. L., Heber, U., Marsh, T. R., & North, R. C. 2001, *MNRAS*, 326, 139
- Mereghetti, S., Tiengo, A., Esposito, P., et al. 2009, *Science*, 325, 1222
- Morales-Rueda, L., Maxted, P. F. L., Marsh, T. R., North, R. C., & Heber, U. 2003, *MNRAS*, 338, 752
- Napiwotzki, R., Karl, C., Lisker, T., et al. 2004a, *Ap&SS*, 291, 321
- Napiwotzki, R., Yungelson, L., Nelemans, G., et al. 2004b, *ASP Conf. Ser.*, 318, 402
- Nelemans, G. 2010, *Ap&SS*, 329, 25
- O'Toole, S. J., & Heber, U. 2006, *A&A*, 452, 579
- Perets, H. B., Gal-Yam, A., Mazzali, P. A., et al. 2010, *Nature*, 465, 322
- Perlmutter, S., Aldering, G., Goldhaber, G., et al. 1999, *ApJ*, 517, 565
- Pfahl, E., Rappaport, S., & Podsiadlowski, Ph. 2003, *ApJ*, 597, 1036
- Podsiadlowski, Ph., Rappaport, S., & Pfahl, E. D. 2002, *ApJ*, 565, 1107
- Pollacco, D. L., Skillen, I., Cameron, A. C., et al. 2006, *PASP*, 118, 1407
- Pringle, J. E. 1975, *MNRAS*, 170, 633
- Reed, M. D., & Stiening, R. 2004, *PASP*, 116, 506
- Riess, A. G., Filippenko, A. V., Challis, P., et al. 1998, *AJ*, 116, 1009
- Shimanskii, V. V., Bikmaev, I. F., Borisov, N. V., et al. 2008, *ARep*, 52, 729
- Stark, M. A., & Wade, R. A. 2003, *AJ*, 126, 1455
- Tillich, A., Heber, U., Geier, S., et al. 2010, *A&A*, accepted
- Tutukov, A. V., & Yungelson, L. R. 1981, *Nauchnye Informatsii*, 49, 3
- Yoon, S.-C., & Langer, N. 2004, *A&A*, 419, 645
- Yungelson, L. R., & Tutukov, A. V. 2005, *ARep*, 49, 871
- Webbink, R. F. 1984, *ApJ*, 277, 355

Appendix A: Atmospheric parameters**Table A.1.** Atmospheric parameters.

Object	T_{eff} [K]	$\log g$	$\log y$	Instrument
J0023–0029	30100 ± 500	5.62 ± 0.08	–2.0	SDSS
	29000 ± 100	5.71 ± 0.02	–2.0	ISIS
	29200 ± 500	5.69 ± 0.05	–2.0	adopted
J1138–0035	30800 ± 500	5.50 ± 0.09	–3.0	SDSS
	31700 ± 700	5.59 ± 0.10	–3.0	IDS
	31200 ± 600	5.54 ± 0.09	–3.0	adopted
J1505+1108	33300 ± 500	5.80 ± 0.10	–2.4	SDSS
	33000 ± 600	5.80 ± 0.11	–2.2	TWIN
	33200 ± 500	5.80 ± 0.10	–2.3	adopted
J1654+3037	24400 ± 800	5.32 ± 0.11	–2.3	SDSS
	25500 ± 900	5.47 ± 0.13	–2.5	IDS
	24900 ± 800	5.39 ± 0.12	–2.4	adopted
J1726+2744	33500 ± 400	5.71 ± 0.09	–2.2	SDSS
	33300 ± 400	5.91 ± 0.06	–2.2	TWIN
	32300 ± 100	5.87 ± 0.02	–2.2	ISIS
	32400 ± 700	5.73 ± 0.12	–2.1	IDS
	32600 ± 500	5.84 ± 0.05	–2.2	adopted
J2046–0454	31600 ± 600	5.55 ± 0.10	–3.0	SDSS
	32100 ± 500	5.57 ± 0.09	–3.0	TWIN
	31100 ± 400	5.52 ± 0.06	–3.0	FORS1
	31600 ± 500	5.54 ± 0.08	–3.0	adopted
J2256+0656	28900 ± 600	5.58 ± 0.11	–3.0	SDSS
	29200 ± 900	5.74 ± 0.09	–2.2	TWIN
	28400 ± 100	5.63 ± 0.02	–2.2	ISIS
	28500 ± 500	5.64 ± 0.05	–2.3	adopted

Appendix B: Radial velocities.

Table B.2. J1138–0035.

Table B.1. J0023–0029.

Mid–HJD –2 450 000	RV [km s ^{–1}]	Instrument	Mid–HJD –2 450 000	RV [km s ^{–1}]	Instrument	
1816.782390	92.0 ± 10.0	SDSS	1629.831447	–16.0 ± 33.7	SDSS	
1816.794497	94.1 ± 6.0		1629.861748	–131.2 ± 5.8		
1816.806476	92.7 ± 7.0		1629.875990	–139.6 ± 10.5		
1885.575567	5.6 ± 9.0		1629.890197	–124.6 ± 11.9		
1885.587847	2.2 ± 11.0		1630.849549	42.3 ± 12.3		
1885.600718	2.4 ± 15.0		1630.861782	–8.6 ± 5.8		
1885.614294	–3.1 ± 9.0		1658.666991	16.0 ± 6.1		
1885.627153	7.7 ± 9.0		1658.723102	–127.9 ± 2.4		
1885.639444	–9.0 ± 8.0		1658.737309	–120.4 ± 7.4		
1899.578750	–36.7 ± 14.0		1658.749439	–81.3 ± 12.2		
1899.590972	–17.2 ± 9.0		2720.30421	–73.0 ± 32.8		SAAO
1899.603316	–27.7 ± 10.0		2720.31674	–9.9 ± 12.2		
1899.615509	–12.1 ± 11.0		3101.42483	166.9 ± 29.9		
1900.573652	–13.8 ± 7.0		3101.44590	26.1 ± 19.6		
1900.585712	–9.6 ± 22.0		4186.50643	–146.0 ± 5.5		IDS
1900.599109	–25.3 ± 16.0		4186.52047	–130.5 ± 6.5		
5068.61892	90.6 ± 3.0	4187.51138	–76.5 ± 6.8			
5068.62614	94.8 ± 3.7	4187.52540	–133.0 ± 6.8			
5068.63335	81.4 ± 4.0	4188.55849	–115.9 ± 5.6			
5068.65013	102.0 ± 4.0	4188.57251	–135.0 ± 6.5			
5068.65736	103.5 ± 4.4	4189.46081	4.8 ± 5.2			
5068.66457	94.9 ± 3.7	4189.47485	69.2 ± 5.2			
5069.69141	–25.4 ± 4.6	4190.52859	117.1 ± 6.0			
5069.69862	–65.8 ± 4.1	4190.54262	165.7 ± 5.1			
5069.70585	–32.1 ± 2.9	4991.40638	149.6 ± 18.6	IDS		
5069.71578	–28.2 ± 2.6	4991.40999	143.0 ± 15.0			
5069.72300	–17.9 ± 4.3	4991.41360	151.1 ± 15.8			
5069.73023	–6.2 ± 4.1	4991.41722	148.4 ± 15.0			
5071.59347	71.9 ± 5.9	4991.42083	163.3 ± 18.2			
5071.60068	79.3 ± 6.4	4991.42444	162.0 ± 18.4			
5071.60442	84.1 ± 4.2	4991.42964	182.6 ± 15.9			
5071.61757	91.7 ± 5.8	4991.43325	172.7 ± 21.8			
5071.62478	100.7 ± 2.6	4991.43687	192.4 ± 17.6			
5071.63199	93.9 ± 3.2	4991.44048	193.8 ± 18.3			
5144.55811	101.0 ± 10.1	4991.44409	156.9 ± 18.8	EFOSC2		
5144.59234	97.1 ± 10.1	4991.44770	169.9 ± 15.0			
5144.63989	76.5 ± 12.6	4991.45131	151.1 ± 17.2			
5145.52594	–28.5 ± 9.9	4991.45492	151.7 ± 17.4			
5145.61524	–16.9 ± 7.8	5240.64268	38.5 ± 8.5		Goodman	
5145.65247	–7.1 ± 10.2	5240.64678	59.9 ± 7.0			
5146.54220	2.5 ± 8.0	5240.65068	59.2 ± 5.1			
5146.64161	–27.0 ± 8.1	5240.65448	108.3 ± 8.6			
5146.69219	–57.2 ± 8.9	5240.65828	116.8 ± 3.6			
5147.59722	82.4 ± 10.4	5240.75829	–13.8 ± 5.3			
5147.64906	81.5 ± 9.5	5240.76549	–49.6 ± 5.5			
5147.66103	85.2 ± 7.2					
5147.67897	80.0 ± 9.8					

Table B.3. J1505+1108.

Mid-HJD -2 450 000	RV [km s ⁻¹]	Instrument
3848.858414	5.3 ± 12.0	SDSS
3848.906794	27.7 ± 12.2	
3849.863669	-126.6 ± 10.0	
3850.893113	-96.1 ± 8.1	
4600.479632	-48.0 ± 8.0	TWIN
4600.487332	-65.4 ± 10.0	
4692.348022	22.2 ± 13.0	
4694.404665	-44.7 ± 9.7	
4696.399472	-148.2 ± 10.8	
4980.44927	-130.0 ± 9.2	
4980.53561	-175.5 ± 9.9	
4981.57813	-34.5 ± 13.8	
4982.55136	5.4 ± 12.1	
4936.672663	-37.3 ± 2.8	
4936.676403	-31.0 ± 3.0	
4936.680142	-34.7 ± 3.0	
4936.683881	-32.5 ± 3.1	
4936.871029	-3.5 ± 2.8	
4936.874768	-2.1 ± 2.8	
4936.878512	0.9 ± 2.8	
4936.882253	-5.5 ± 2.9	
4937.64103	0.8 ± 3.1	
4937.64477	7.0 ± 2.9	
4937.64852	6.1 ± 3.0	
4937.65226	4.4 ± 2.9	
4937.85083	-158.7 ± 2.9	
4937.85457	-161.9 ± 2.9	
4937.85831	-158.5 ± 2.9	
4937.86206	-158.7 ± 3.0	
4938.75627	-150.6 ± 2.5	
4938.76001	-149.4 ± 2.5	
4938.76375	-156.3 ± 2.5	
4938.76749	-146.0 ± 2.5	
4939.67990	-31.1 ± 2.8	
4939.68364	-24.8 ± 2.9	
4939.68738	-26.7 ± 2.8	
4939.69112	-23.6 ± 2.8	
4943.63233	-2.9 ± 3.0	
4943.63607	-9.2 ± 2.9	
4943.63981	-7.8 ± 2.9	
4943.64355	-10.3 ± 2.7	

Table B.4. J1654+3037.

Mid-HJD -2 450 000	RV [km s ⁻¹]	Instrument
2789.917095	119.4 ± 9.7	SDSS
2789.933032	84.5 ± 7.7	
2790.913235	146.7 ± 7.2	
2790.929502	130.3 ± 8.5	
4586.567656	-6.0 ± 7.8	TWIN
4692.367579	155.2 ± 8.0	
4693.380826	148.1 ± 8.1	
4694.433521	155.9 ± 8.0	
5037.44285	70.1 ± 10.6	
5037.47019	150.9 ± 8.4	
5037.50213	156.2 ± 11.1	
5038.42271	-21.8 ± 11.0	
5038.48616	155.0 ± 10.8	
5038.49857	161.0 ± 7.9	
4988.47623	-4.3 ± 25.5	IDS
4988.49036	56.8 ± 16.6	
4988.50437	97.9 ± 17.5	
4988.52125	129.9 ± 15.6	
4988.53530	172.6 ± 17.3	
4988.54942	179.7 ± 18.0	
4988.56430	150.0 ± 16.0	
4991.47179	-84.8 ± 17.7	
4991.47888	-82.0 ± 17.1	
4991.48596	-92.2 ± 16.6	
4991.49305	-58.5 ± 7.1	
4991.50013	-62.6 ± 17.5	
4991.50927	-44.1 ± 16.5	
4991.51753	-11.2 ± 15.1	
4991.52577	23.0 ± 18.4	
4991.53402	33.3 ± 16.2	
4991.54224	66.3 ± 16.0	
4991.55155	103.8 ± 30.1	
4991.55981	128.0 ± 17.6	
4991.56805	142.9 ± 16.5	
4991.57629	161.2 ± 17.1	
4991.58453	178.5 ± 16.4	

Table B.5. J1726+2744.

Mid-HJD -2 450 000	RV [km s ⁻¹]	Instrument
3905.819525	-168.9 ± 10.9	SDSS
3905.833513	-157.3 ± 10.7	
3905.853553	-133.2 ± 10.5	
3905.866007	-123.5 ± 15.8	
4979.59252	-125.2 ± 14.4	TWIN
4979.63382	-98.5 ± 11.6	
4980.47951	-155.4 ± 12.9	
4980.58604	-141.2 ± 11.4	
4981.53132	-120.0 ± 8.0	
4981.58892	-112.5 ± 12.9	
4981.62939	-46.7 ± 12.0	
4981.64123	-53.1 ± 9.7	
4981.65164	-35.2 ± 16.9	
4982.56453	-154.2 ± 11.2	
4982.65151	-65.0 ± 21.6	
4983.53806	-152.7 ± 11.5	
4983.54720	-176.7 ± 12.0	
4983.55638	-150.5 ± 15.2	
4983.56557	-146.3 ± 24.3	
4983.57468	-124.9 ± 13.8	
5037.45679	39.0 ± 12.0	
5037.48545	62.0 ± 12.7	
5038.43771	38.0 ± 16.1	
5038.45381	58.0 ± 12.9	
5038.47045	80.0 ± 13.0	
5039.49762	69.0 ± 12.7	
5039.52128	87.0 ± 12.0	
5039.53838	85.0 ± 12.9	
4992.48445	-99.5 ± 23.1	IDS
4992.49617	-114.1 ± 18.5	
4992.50788	-81.2 ± 13.7	
5068.47186	-92.7 ± 5.2	ISIS
5068.47906	-79.4 ± 4.4	
5068.48628	-73.9 ± 5.3	
5069.45355	-120.3 ± 3.2	
5069.46426	-109.9 ± 2.7	
5069.46786	-98.2 ± 4.5	
5069.47855	-79.9 ± 3.8	

Table B.6. J2046-0454.

Mid-HJD -2 450 000	RV [km s ⁻¹]	Instrument
3269.661429	109.6 ± 13.3	SDSS
3269.675556	128.1 ± 9.6	
3269.691435	179.6 ± 8.8	
4645.79103	181.6 ± 5.0	FORS1
4645.79259	185.0 ± 3.1	
4692.51274	28.4 ± 13.4	TWIN
4692.52696	30.7 ± 14.3	
4693.42472	227.7 ± 11.9	
4693.47199	137.2 ± 20.6	
4696.49294	42.0 ± 9.3	
4696.54469	177.8 ± 10.9	
4696.60171	171.6 ± 9.8	
4979.61251	90.6 ± 6.8	
4979.65127	-32.8 ± 21.3	
5035.46989	207.0 ± 15.3	
5035.49811	210.0 ± 14.3	
5036.50301	83.0 ± 15.5	
5037.52184	-25.0 ± 10.8	
5037.59514	16.0 ± 15.0	
4758.55029	206.1 ± 22.5	EFOSC2
4758.55416	202.4 ± 25.3	
4758.55803	212.2 ± 22.5	

Table B.7. J2256+0656.

Mid–HJD –2 450 000	RV [km s ^{–1}]	Instrument	
3710.557488	11.8 ± 10.5	SDSS	
3710.571464	1.1 ± 8.6		
3710.588935	–15.5 ± 9.7		
4694.610760	78.0 ± 6.0	TWIN	
4694.676593	79.3 ± 1.0		
4694.689883	87.1 ± 6.0		
5035.48389	–140.9 ± 23.8		
5035.50848	–96.8 ± 15.6		
5036.51782	95.0 ± 15.0		
5036.61657	29.9 ± 10.7		
5036.56824	81.7 ± 11.2		
5037.53430	–129.6 ± 17.9		
5037.54784	–120.8 ± 11.1		
5037.55965	–134.9 ± 11.0		
5037.60833	–116.5 ± 11.0		
5038.56302	96.6 ± 10.6		
5038.57506	115.1 ± 12.7		
5038.62975	104.1 ± 15.3		
5038.64304	105.0 ± 11.8		
5038.65573	104.1 ± 13.1		
5039.64785	–123.9 ± 12.5		
5048.981437	16.4 ± 4.2		GMOS
5049.002417	28.5 ± 4.3		
5049.023396	43.5 ± 4.2		
5049.044376	51.0 ± 4.3		
5077.83332	129.0 ± 5.6		
5077.85483	116.5 ± 5.3		
5068.53076	–36.5 ± 3.4	ISIS	
5068.53111	–30.2 ± 3.5		
5068.53826	–26.5 ± 2.3		
5068.54815	–10.3 ± 2.7		
5068.55536	–12.8 ± 3.2		
5068.56257	–1.5 ± 2.3		
5069.53785	41.6 ± 3.7		
5069.54507	48.0 ± 3.8		
5069.55228	45.8 ± 2.3		
5069.56913	48.2 ± 3.6		
5069.57635	26.9 ± 3.8		
5069.58358	18.2 ± 3.8		
5070.62493	–48.4 ± 4.0		
5070.63214	–35.8 ± 4.0		
5070.63942	–21.1 ± 4.1		
5070.65603	–20.0 ± 2.6		
5070.66324	–1.5 ± 4.5		
5070.67045	2.6 ± 4.6		
5071.39970	8.8 ± 4.8		
5071.39997	21.3 ± 4.2		
5071.40718	33.8 ± 3.6		
5071.42392	50.5 ± 3.8		
5071.43114	50.8 ± 3.9		

The MUCHFUSS project – searching for hot subdwarf binaries with massive unseen companions

Survey, target selection and atmospheric parameters^{*,**}

S. Geier¹, H. Hirsch¹, A. Tillich¹, P. F. L. Maxted², S. J. Bentley², R. H. Østensen³, U. Heber¹, B. T. Gänsicke⁴, T. R. Marsh⁴, R. Napiwotzki⁵, B. N. Barlow⁶, and S. J. O’Toole^{1,7}

¹ Dr. Karl Remeis-Observatory & ECAP, Astronomical Institute, Friedrich-Alexander University Erlangen-Nuremberg, Sternwartstr. 7, 96049 Bamberg, Germany

e-mail: geier@sternwarte.uni-erlangen.de

² Astrophysics Group, Keele University, Staffordshire, ST5 5BG, UK

³ Institute of Astronomy, K.U.Leuven, Celestijnenlaan 200D, 3001 Heverlee, Belgium

⁴ Department of Physics, University of Warwick, Coventry CV4 7AL, UK

⁵ Centre of Astrophysics Research, University of Hertfordshire, College Lane, Hatfield AL10 9AB, UK

⁶ Department of Physics and Astronomy, University of North Carolina, Chapel Hill, NC 27599-3255, USA

⁷ Australian Astronomical Observatory, PO Box 296, Epping, NSW, 1710, Australia

Received 1 July 2010 / Accepted 19 March 2011

ABSTRACT

The project Massive Unseen Companions to Hot Faint Underluminous Stars from SDSS (MUCHFUSS) aims at finding sdBs with compact companions like supermassive white dwarfs ($M > 1.0 M_{\odot}$), neutron stars or black holes. The existence of such systems is predicted by binary evolution theory and recent discoveries indicate that they are likely to exist in our Galaxy.

A determination of the orbital parameters is sufficient to put a lower limit on the companion mass by calculating the binary mass function. If this lower limit exceeds the Chandrasekhar mass and no sign of a companion is visible in the spectra, the existence of a massive compact companion is proven without the need for any additional assumptions. We identified about 1100 hot subdwarf stars from the SDSS by colour selection and visual inspection of their spectra. Stars with high velocities have been reobserved and individual SDSS spectra have been analysed. In total 127 radial velocity variable subdwarfs have been discovered. Binaries with high RV shifts and binaries with moderate shifts within short timespans have the highest probability of hosting massive compact companions. Atmospheric parameters of 69 hot subdwarfs in these binary systems have been determined by means of a quantitative spectral analysis. The atmospheric parameter distribution of the selected sample does not differ from previously studied samples of hot subdwarfs. The systems are considered the best candidates to search for massive compact companions by follow-up time resolved spectroscopy.

Key words. binaries: spectroscopic – subdwarfs

1. Introduction

Subluminous B stars (sdBs) are core helium-burning stars with very thin hydrogen envelopes and masses around $0.5 M_{\odot}$ (Heber 1986). A large fraction of the sdB stars are members of short period binaries (Maxted et al. 2001; Napiwotzki et al. 2004a). After the discovery of close binary subdwarfs, several studies aimed at determining the fraction of hot subdwarfs residing in such systems. Samples of hot subdwarfs checked for radial velocity (RV)

variations imply the binary fraction ranges from 39% to 78% (e.g. Maxted et al. 2001; Napiwotzki et al. 2004a). The orbital periods of subdwarf binaries for which orbital parameters could be determined range from 0.07 to >10 d with a peak at 0.5–1.0 d (e.g. Edelman et al. 2005; Morales-Rueda et al. 2003a).

For close binary sdBs common envelope ejection is the most probable formation channel (Han et al. 2002, 2003). In this scenario two main sequence stars of different masses evolve in a binary system. The more massive one will reach the red giant phase first and fill its Roche lobe near the tip of the red-giant branch. If the mass transfer to the companion is dynamically unstable, a common envelope is formed. Friction causes the two stellar cores to lose orbital energy, which is deposited within the envelope, and the period of the binary decreases. Eventually, the common envelope is ejected, and a close binary system is formed containing a core helium-burning sdB and a main sequence companion. A binary consisting of a main sequence star and a white dwarf (WD) may evolve to a close binary sdB with a white dwarf companion in a similar way. Tight constraints can be placed on the nature of the sdB companions only in the rare cases where the systems show eclipses or other features indicative

* Based on observations at the Paranal Observatory of the European Southern Observatory for programme number 081.D-0819. Based on observations at the La Silla Observatory of the European Southern Observatory for programme number 082.D-0649. Based on observations collected at the Centro Astronómico Hispano Alemán (CAHA) at Calar Alto, operated jointly by the Max-Planck Institut für Astronomie and the Instituto de Astrofísica de Andalucía (CSIC). Based on observations with the William Herschel Telescope operated by the Isaac Newton Group at the Observatorio del Roque de los Muchachos of the Instituto de Astrofísica de Canarias on the island of La Palma, Spain.

** Tables 2–4 and Appendix A are available in electronic form at <http://www.aanda.org>

of a companion in their light curves (see the catalogue of Ritter & Kolb 2009, and references therein).

Subdwarf binaries with massive WD companions are candidates for SN Ia progenitors because these systems lose angular momentum due to the emission of gravitational waves and start mass transfer. Transfer of mass or the subsequent merger of the system may cause the WD to approach the Chandrasekhar limit, ignite carbon under degenerate conditions, and explode as a SN Ia (Webbink 1984; Iben & Tutukov 1984). One of the best-known candidate systems for this double degenerate merger scenario is the sdB+WD binary KPD 1930+2752 (Maxted et al. 2000a; Geier et al. 2007). Mereghetti et al. (2009) showed that in the X-ray binary HD 49798 a massive ($>1.2 M_{\odot}$) white dwarf accretes matter from a closely orbiting subdwarf O companion. The predicted amount of accreted material is sufficient for the WD to reach the Chandrasekhar limit. This makes HD 49798 another candidate SN Ia progenitor, should the companion be a C/O white dwarf (Wang et al. 2009). SN Ia play a key role in the study of cosmic evolution since they are utilised as standard candles for determining the cosmological parameters (e.g. Riess et al. 1998; Leibundgut 2001; Perlmutter et al. 1999). Most recently Perets et al. (2010) showed that helium accretion onto a white dwarf may be responsible for a subclass of faint and calcium-rich SN Ib events.

Due to the tidal influence of the companion in close binary systems, the rotation of the primary¹ becomes synchronised to its orbital motion. In this case it is possible to constrain the mass of the companion, if mass, projected rotational velocity and surface gravity of the sdB are known. Geier et al. (2008, 2010a,b) analysed high resolution spectra of 41 sdB stars in close binaries, half of all systems with known orbital parameters. In 31 cases, the mass and nature of the unseen companions could be constrained. While most of the derived companion masses were consistent with either late main sequence stars or white dwarfs, the compact companions of some sdBs may be either massive white dwarfs, neutron stars (NS) or stellar mass black holes (BH). However, Geier et al. (2010b) also showed that the assumption of orbital synchronisation in close sdB binaries is not always justified and that their sample suffers from huge selection effects.

Binary evolution theory (Podsiadlowski et al. 2002; Pfahl et al. 2003) predicts the existence of sdB+NS/BH systems formed after two phases of unstable mass transfer and one supernova explosion. The predicted fraction of sdB+NS/BH systems ranges from about 1% to 2% of the close sdB binaries (Geier et al. 2010b; Yungelson & Tutukov 2005; Nelemans 2010).

2. Project overview

The work of Geier et al. (2010b) indicates that a population of non-interacting binaries with massive compact companions may be present in our Galaxy. The candidate sdB+NS/BH binaries have low orbital inclinations (15–30°, Geier et al. 2010b), but high inclination systems must exist as well. A lower limit can be placed on the companion mass by determining the orbital parameters and calculating the binary mass function.

$$f_m = \frac{M_{\text{comp}}^3 \sin^3 i}{(M_{\text{comp}} + M_{\text{sdB}})^2} = \frac{PK^3}{2\pi G}. \quad (1)$$

¹ The more massive component of a binary is usually defined as the primary. However, in most close sdB binaries with unseen companions the masses are unknown and it is not possible to decide a priori which component is the most massive one. For this reason we call the visible sdB component of the binaries the primary throughout this paper.

The RV semi-amplitude K and the period P can be derived from the RV curve; the sdB mass M_{sdB} , the companion mass M_{comp} and the inclination angle i remain free parameters. We adopt $M_{\text{sdB}} = 0.47 M_{\odot}$ and $i < 90^\circ$ to derive a lower limit for the companion mass. Depending on this minimum mass a qualitative classification of the companions' nature is possible in certain cases. For minimum companion masses lower than $0.45 M_{\odot}$ a main sequence companion can not be excluded because its luminosity would be too low to be detectable in the spectra (Lisker et al. 2005). If the minimum companion mass exceeds $0.45 M_{\odot}$ and no spectral signatures of the companion are visible, it must be a compact object. If it exceeds the Chandrasekhar mass and no sign of a companion is visible in the spectra, the existence of a massive compact companion is proven without the need for any additional assumptions. This is possible if such a binary is seen at high inclination. The project Massive Unseen Companions to Hot Faint Underluminous Stars from SDSS² (MUCHFUSS) aims at finding sdBs with compact companions like supermassive white dwarfs ($M > 1.0 M_{\odot}$), neutron stars or black holes. First results of our follow-up campaign are published in Geier et al. (2011).

There is an interesting spin-off from this project: the same selection criteria we applied to find binaries with massive compact companions are also well-suited to single out hot subdwarf stars with constant high radial velocities in the Galactic halo, which may be extreme population II or even hypervelocity stars. We have coined the term Hyper-MUCHFUSS to refer to this extended project, the first results of which are presented in Tillich et al. (2011).

3. Target selection

The high fraction of sdB stars in close binary systems was initially discovered by the detection of RV shifts using time resolved spectroscopy (Maxted et al. 2001). In the past decade, orbital parameters for about 80 of these systems have been determined. We summarize the orbital parameters of all known sdB binaries and give references in Table A.1 (see also Fig. 1).

To the extent that the companion masses of the known sdB binaries could be constrained, it turned out that most companions should be either late main sequence stars with masses lower than half a solar mass or compact objects like white dwarfs. Targets for spectroscopic follow-up were selected in different ways depending on the specific aims of each project.

For the MUCHFUSS project the target selection is optimised to find massive compact companions in close orbits around sdB stars. In order to discover rare objects applying the selection criteria explained in the forthcoming sections, a huge initial dataset is necessary. The enormous SDSS database (Data Release 6, DR6) is therefore the starting point for our survey. Best sky coverage is reached in the Northern hemisphere close to the galactic poles. SDSS data are widely used and therefore also well evaluated in terms of errors and accuracy (York et al. 2000; Abazajian et al. 2009). Moreover, they are supplemented by additional spectroscopic observations of appropriate quality from other sources.

3.1. Colour selection and visual classification

Hot subdwarfs are found most easily by applying a colour cut to Sloan photometry. All spectra of point sources with colours

² Sloan Digital Sky Survey.

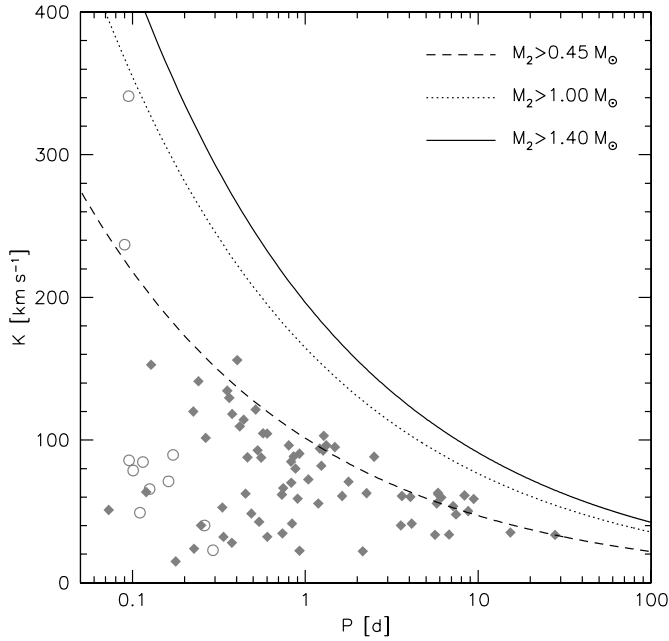


Fig. 1. The RV semiamplitudes of all known sdB binaries with spectroscopic solutions plotted against their orbital periods (see Table A.1). Binaries which were initially discovered in photometric surveys due to indicative features in their light curves (eclipses, reflection effects, ellipsoidal variations) are marked with open circles. Binaries discovered by detection of RV variation from time resolved spectroscopy are marked with filled diamonds. The dashed, dotted and solid lines mark the regions to the right where the minimum companion masses derived from the binary mass function (assuming $0.47 M_{\odot}$ for the sdBs) exceed $0.45 M_{\odot}$, $1.00 M_{\odot}$ and $1.40 M_{\odot}$. The two post-RGB objects in the sample have been excluded, because their primary masses are much lower.

$u - g < 0.4$ and $g - r < 0.1$ were selected. This colour criterion corresponds to a limit in the Johnson photometric system of $U - B < -0.57$ (Jester et al. 2005), similar to the cut-off chosen by UV excess surveys, such as the Palomar Green survey (Green et al. 1986). The corresponding effective temperature of a BHB star is $\approx 15\,000$ K (Castelli & Kurucz 2003), well below the observed range for sdB stars ($> 20\,000$ K). The limit of $g - r = +0.1$ corresponds to $B - V = +0.3$ (Jester et al. 2005). This ensures that sdBs in spectroscopic binaries are included if the dwarf companion is of spectral type F or later, e.g. the sdB+F system PB 8783 at $B - V = +0.13$ and $U - B = -0.65$ (Koen et al. 1997). On the other hand the colour criteria exclude the huge number of QSOs (quasi stellar objects) which were the priority objects of SDSS in the first place. We selected 48 267 point sources with spectra in this way.

The spectra from SDSS are flux calibrated and cover the wavelength range from 3800 \AA to 9200 \AA with a resolution of $R = 1800$. Rebassa-Mansergas et al. (2007) verified the wavelength stability to be $< 14.5 \text{ km s}^{-1}$ from repeat sub-spectra using SDSS observations of F-stars. We obtained the spectra of our targets from the SDSS Data Archive Server³ and converted the wavelength scale from vacuum to air. The spectra were classified by visual inspection.

First, we excluded spectra of extragalactic objects and spectra with low quality ($S/N < 5$) or unknown features, leaving us with 10 811 spectra of 10 153 stars. Figure 2 (left panel) shows

a two-colour plot of all selected objects. To classify the selected spectra, we compared them visually to reference spectra of hot subdwarfs and white dwarfs. Existence, width, and depth of helium and hydrogen absorption lines as well as the flux distribution between 4000 and 6000 \AA were used as criteria. Subdwarf B stars show broadened hydrogen Balmer and He I lines, sdOB stars He II lines in addition, while the spectra of sdO stars are dominated by weak Balmer and strong He II lines depending on the He abundance. A flux excess in the red compared to the reference spectrum as well as the presence of spectral features such as the Mg I triplet at 5170 \AA or the Ca II triplet at 8650 \AA were taken as indications of a late type companion (for a few examples see Fig. 3, for spectral classification of hot subdwarf stars see the review by Heber 2009).

Our selection criteria led to a sample containing a total of 1100 hot subdwarfs. 725 belong to the class of single-lined sdBs and sdOBs. Because distinguishing between these two subtypes from their spectral appearances alone can be difficult, we decided to treat them as one class. Features indicative of a cool companion were found for 89 of the sdBs. 9 sdOs have main sequence companions, while 198 of them, most of which show helium enrichment, are single-lined. A unique classification was not possible for 79 objects in our sample. Most of these stars are considered candidate sdBs with low temperatures, which cannot be distinguished clearly from blue horizontal branch (BHB) stars or low-mass DA or DB white dwarfs.

Eisenstein et al. (2006) used a semi-automatic method for the spectral classification of white dwarfs and hot subdwarfs from the SDSS DR4, and it is instructive to compare their sample to ours. Our colour cut-off is more restrictive and the confusion limit ($S/N > 5$) is brighter than that of Eisenstein et al. (2006). Due to the redder colour cuts, blue horizontal branch stars enter the Eisenstein et al. sample, which we do not consider as hot subdwarf stars (see Heber 2009). Applying our colour cuts to the hot subdwarf sample of Eisenstein et al. (2006) yields 691 objects. The stars missing in our sample are mostly fainter than $g = 19$ mag as expected. Most recently, Kleinman (2010) extended the classifications to the SDSS DR7 and found 1409 hot subdwarf stars. Since no details are published, the sample can not be compared to ours yet. Considering our more restrictive colour cuts and confusion limit, the numbers compare very well with ours. This gives us confidence that our selection method is efficient.

In Fig. 2 (right panel) only the subdwarf stars brighter than $g = 18$ mag are plotted. With less pollution by poor spectra, two sequences become clearly visible. The solid symbols mark single-lined sdBs and sdOs, while the open squares mark binaries with late type companions of most likely K and G type visible in the spectra. The contribution of the cool companions shifts the colours of the stars to the red. As can be seen in Fig. 2 the upper sequence also contains apparently single stars. Since the spectra are not corrected for interstellar reddening, some of these objects may show an excess in the red not due to the presence of a cool companion. Spectral features indicative of a late-type companion and small excesses in the red may have been missed for the faintest targets with the noisiest data.

In Fig. 2 (right panel) we also compare the sample to synthetic colours suitable for hot subdwarf stars. We chose the grid of Castelli & Kurucz (2003)⁴ and selected models with high gravity ($\log g = 5.0$). The models reproduce the lower envelope of the targets in the colour-colour-diagram very well for effective

³ das.sdss.org

⁴ <http://wwwuser.oat.ts.astro.it/castelli/colors/sloan.html>

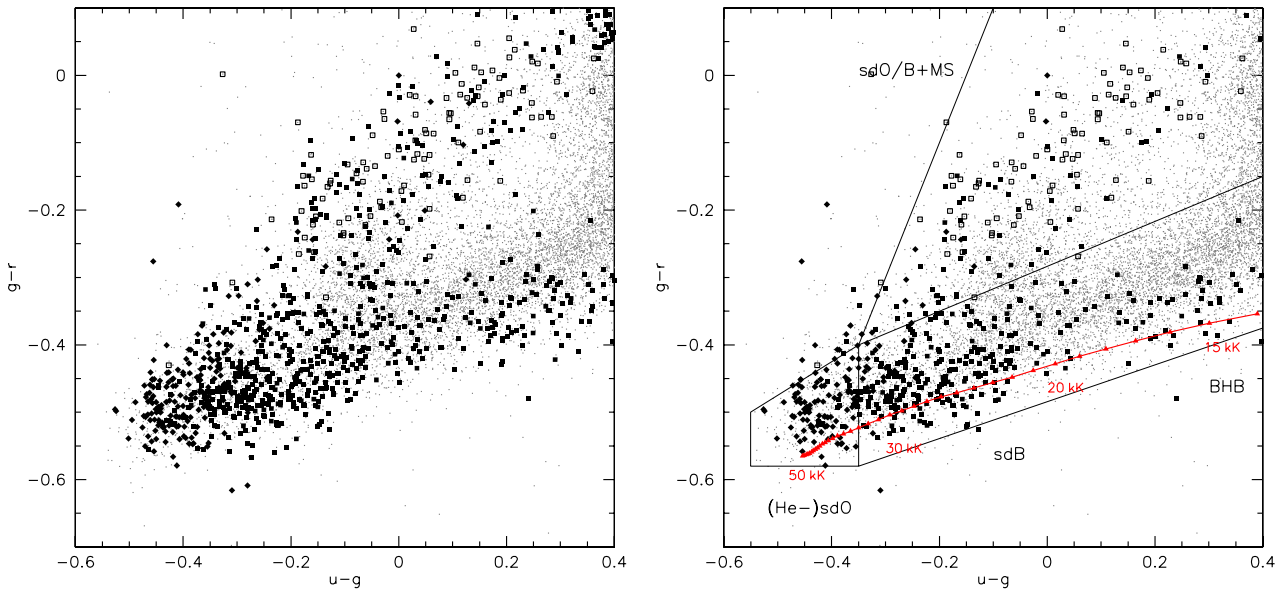


Fig. 2. *Left panel.* SDSS $g - r$ -colours plotted against $u - g$ of all stars. The grey dots mark all stellar objects with spectra available in the SDSS database. Most of them are classified as DA white dwarfs. The solid diamonds mark (He-)sdO stars, the solid squares sdB and sdOB stars. Open squares mark hot subdwarfs with main sequence companions visible in the spectra. Most of these objects are white dwarfs of DA type. *Right panel.* Only subdwarfs with $g < 18$ mag are plotted. The sequence of composite objects is clearly separated from the single-lined stars. Synthetic colours from Castelli & Kurucz (2003) for stars with temperatures ranging from 14 000 K to 50 000 K ($\log g = 5.0$) are marked with upward triangles and connected. The stepsize of the colour grid is 1000 K. The labels mark models of certain temperatures.

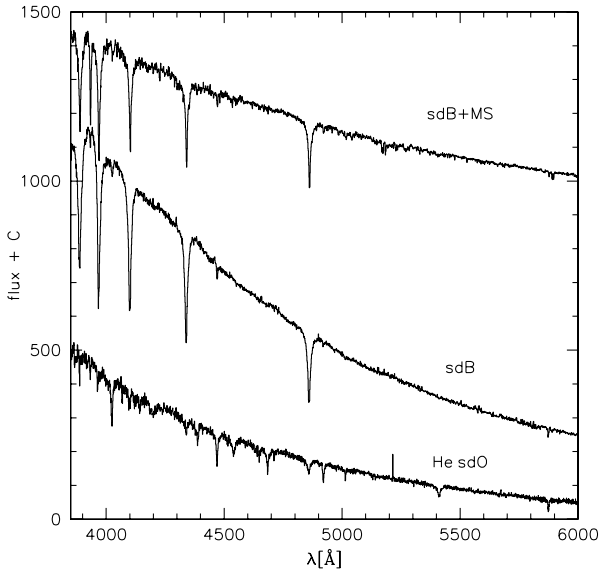


Fig. 3. Flux calibrated SDSS spectra of a single-lined sdB, a helium rich sdO and an sdB with main sequence companion visible in the spectrum. Note the different slopes of the sdB and the sdB+MS spectra.

temperatures ranging from 20 000 to 50 000 K as expected for hot subdwarf stars. Different surface gravities, chemical compositions and interstellar reddening are not accounted for but would explain the observed scatter of the stars.

It is interesting to note that there is an obvious lack of blue horizontal branch (BHB) stars with effective temperatures below

20 000 K compared to the sdBs with higher temperatures. This gap is not a result of selection effects because the BHB stars are brighter than the sdBs at optical wavelengths. We conclude that the number density of BHB stars in the analysed temperature range must be much smaller than that of sdBs. Newell (1973) was the first to report the existence of such a gap in the two-colour diagram of field blue halo stars, which was subsequently also found in some globular clusters (Momány et al. 2004). The reason for this gap remains unclear (see the review by Catelan 2009).

3.2. High radial velocity sample (HRV)

The radial velocities of all identified hot subdwarf stars (both single- and double-lined) were measured by fitting a set of mathematical functions (Gaussians, Lorentzians and polynomials) to the hydrogen Balmer lines as well as helium lines, if present, using the FITSB2 routine (Napiwotzki et al. 2004a) and the Spectrum Plotting and Analysis Suite (SPAS) developed by Hirsch. Figure 4 shows the RVs of 1002 hot subdwarf stars.

Most of the known sdB binaries are bright objects ($V \approx 10 - 14$ mag), and the vast majority of them belong to the Galactic disk population (Altmann et al. 2004). Due to the fact that these binary systems are close to the Sun they rotate around the Galactic centre with approximately the same velocity. For this reason, the system velocities of most sdB binaries are low relative to the Sun. One quarter of the known systems have $|\gamma| < 10 \text{ km s}^{-1}$, 85% have $|\gamma| < 50 \text{ km s}^{-1}$ (see Table A.1). In order to filter out normal thin-disk binaries, which in most cases have RV semiamplitudes less than 100 km s^{-1} (see Fig. 1), we excluded sdBs with RVs lower than $\pm 100 \text{ km s}^{-1}$.

Typical hot subdwarf stars fainter than $g \approx 17$ mag have distances exceeding 4 kpc and therefore likely belong to the

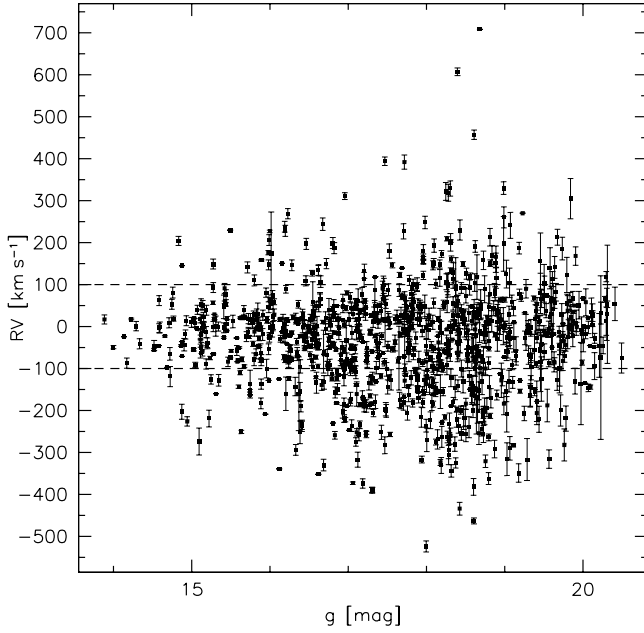


Fig. 4. Heliocentric radial velocities of 1002 subdwarfs plotted against g -magnitude. The two dashed lines mark the RV cut of $\pm 100 \text{ km s}^{-1}$.

Table 1. Survey observations.

Date	Telescope & Instrument	Observers
January–June 2008	CAHA-3.5 m/TWIN	Service
2008/04/29–2008/05/01	ING-WHT/ISIS	P. M., S. G., S. B.
2008/08/13–2008/08/17	CAHA-3.5 m/TWIN	H. H.
2008/10/15–2008/10/19	ESO-NTT/EFOSC2	A. T.
April–July 2008	ESO-VLT/FORS1	Service

Notes. The first column lists the date of observation, while in the second the used telescope and instrumentation is shown. In the third column the initials of the observers are given.

Galactic halo population. Most of the stars in our sample are fainter than that (see Fig. 4). The velocity distribution in the halo is roughly consistent with a Gaussian of 120 km s^{-1} dispersion (Brown et al. 2005). Figure 5 shows the velocity distributions of our selected objects when separated into bright and faint subsamples. The distribution of the bright subsample ($g < 16.5 \text{ mag}$) is roughly similar to the one of the faint subsample ($g > 16.5 \text{ mag}$), the latter extending to more extreme velocities and being somewhat asymmetric. Selecting objects with heliocentric radial velocities exceeding $\pm 100 \text{ km s}^{-1}$ we aim to find halo stars with extreme kinematics as well as close binaries with high RV amplitudes.

Another selection criterion is the brightness of the stars. The accuracy of the RV measurements depends on the S/N of the spectra and the existence and strength of the spectral lines. Furthermore, the classification becomes more and more uncertain as soon as the S/N drops below ≈ 10 and the probability of including DAs rises. Objects of uncertain type and RV (errors larger than 50 km s^{-1}) have therefore been excluded. Most of the excluded objects are fainter than $g = 19 \text{ mag}$. Altogether the target sample consists of 258 stars.

Second epoch medium resolution spectroscopy was obtained starting in 2008 using ESO-VLT/FORS1 ($R \approx 1800$,

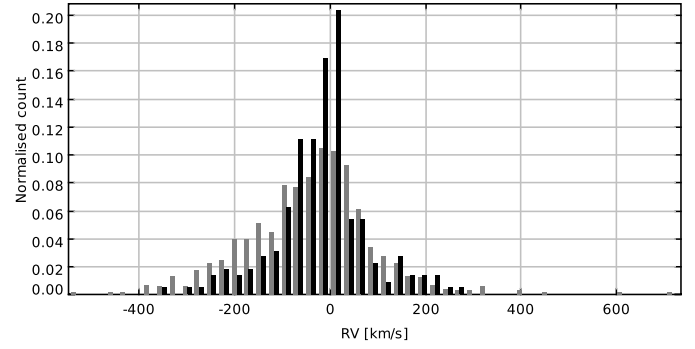


Fig. 5. Radial velocity distribution of the hot subdwarf stars (see Fig. 4). The bright sample ($g < 16.5 \text{ mag}$, black histogram) contains a mixture of stars from the disk and the halo population. The faint sample ($g > 16.5 \text{ mag}$, grey histogram) contains the halo population. The peak in the bright subsample around zero RV is caused by the thin disk population. The asymmetry in the faint subsample where negative RVs are more numerous than positive ones may be due to the presence of large structures in the halo and the movement of the solar system relative to the halo.

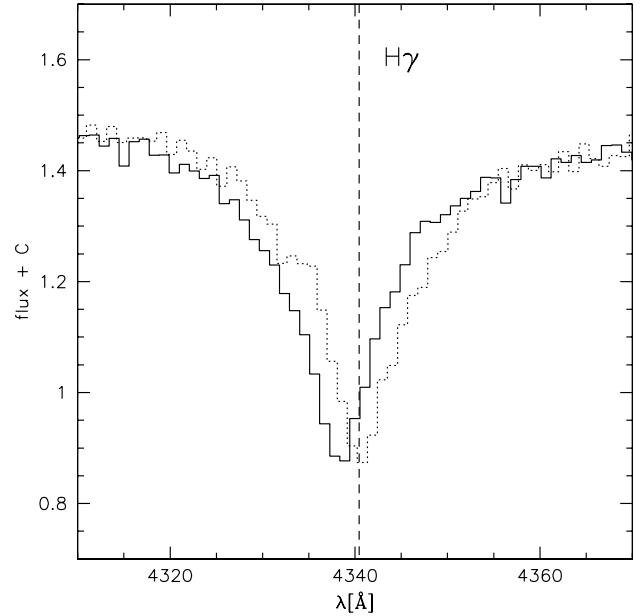


Fig. 6. $H\gamma$ -line of two consecutively taken individual SDSS spectra ($\Delta t = 0.056 \text{ d}$) of the sdB binary J113840.68–003531.7. The shift in RV ($\approx 140 \text{ km s}^{-1}$) between the two exposures is clearly visible.

$\lambda = 3730\text{--}5200 \text{ \AA}$), WHT/ISIS ($R \approx 4000$, $\lambda = 3440\text{--}5270 \text{ \AA}$), CAHA-3.5m/TWIN ($R \approx 4000$, $\lambda = 3460\text{--}5630 \text{ \AA}$) and ESO-NTT/EFOSC2 ($R \approx 2200$, $\lambda = 4450\text{--}5110 \text{ \AA}$). A log of our observations is given in Table 1. Up to now we have reobserved 88 stars. We discovered ≈ 30 halo star candidates with constant high radial velocity (see Tillich et al. 2011) as well as 46 systems with radial velocities that were most likely variable.

3.3. Rapid radial velocity variable sample (RRV)

All SDSS spectra are co-added from at least three individual “sub-spectra” with typical exposure times of 15 min. In most cases, the sub-spectra are taken consecutively; however, they may be split occasionally over several nights.

Several SDSS objects are observed more than once, either because the entire spectroscopic plate is re-observed, or because they are in the overlap area between adjacent spectroscopic plates; up to 30 sub-spectra are available for some objects. Consequently, SDSS spectroscopy can be used to probe for radial velocity variations, a method pioneered by Rebassa-Mansergas et al. (2007) to identify close white dwarf plus main-sequence binaries. We have obtained the sub-spectra for all sdBs brighter than $g = 18.5$ mag from the SDSS Data Archive Server. The quality of individual spectra of stars fainter than this is not sufficient for our analysis. The object spectra were extracted from the FITS files for the blue and red spectrographs, and merged into a single spectrum using MIDAS. From the inspection of these data, we discovered 81 new candidate sdB binaries with radial velocity variations on short time scales, ≈ 0.02 – 0.07 d (see Fig. 6 for an example).

The individual SDSS spectra are perfectly suited to search for close double degenerate binaries. Ongoing projects like SWARMS (Badenes et al. 2009; Mullally et al. 2009) focus on binaries with white dwarf primaries (see also Kilic et al. 2010; Marsh et al. 2010) and use a similar method.

3.4. Selecting high mass companions

Time resolved follow-up spectroscopy with a good phase coverage is needed to determine the orbital solutions of the RV variable systems. In order to select the most promising targets for follow-up, we carried out numerical simulations and estimated the probability for a subdwarf binary with known RV shift to host a massive compact companion. We created a mock sample of sdBs with a close binary fraction of 50%.

We adopted the distribution of orbital periods of all known sdB binaries (see Table A.1) approximated by two Gaussians centered at 0.7 d (width 0.3 d) and 5.0 d (width 3.0 d) and assumed that 82% of the binaries belong to the short period population. The short period Gaussian was truncated at 0.05 d, which is considered the minimum period for an sdB binary, because the subdwarf primary starts filling its Roche lobe for shorter periods and typical companion masses. Since stable Roche lobe overflow and the accretion onto the companion would dramatically change the spectra of these stars, we can safely presume that our sample does not contain such objects.

The orbital inclination angles are assumed to be randomly distributed, but for geometrical reasons binaries at high inclinations are more likely to be observed than binaries at low inclinations. To account for this, we used the method described in Gray (1992) and adopted a realistic distribution of inclination angles.

We assumed the canonical value of $0.47 M_{\odot}$ for the sdB masses. The distribution of companion masses was based on the results of Geier et al. (2010b). The distribution of the low mass companions was approximated by a Gaussian centered at $0.4 M_{\odot}$ (width $0.3 M_{\odot}$). The fraction of massive compact companions is estimated as 2% of the close binary population based on binary population synthesis models (Geier et al. 2010b). The mass distribution of these companions was approximated by a Gaussian centered at $2.0 M_{\odot}$ (width $1.0 M_{\odot}$).

We adopted a Gaussian distribution for the system velocities with a dispersion of 120 km s^{-1} , a typical value for halo stars (Brown et al. 2005). Two RVs were taken from the model RV curves at random times and the RV difference was calculated for each of the 10^6 binaries in the simulation sample. This selection criterion corresponds to the HRV sample. For given RV difference and timespan between the measurements the fraction

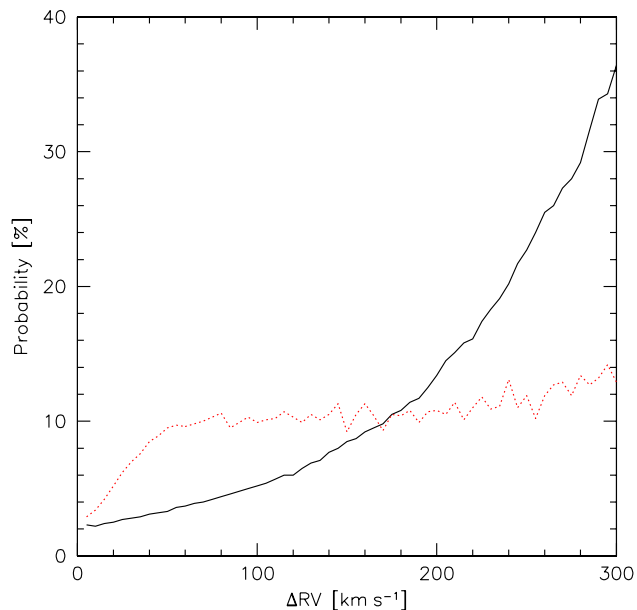


Fig. 7. Probability for an sdB binary to host a massive compact companion and to be seen at sufficiently high inclination to unambiguously identify it from its binary mass function plotted against the RV shift within random times (solid curves, HRV sample) or on short timescales (dotted curve, RRV sample).

of systems with minimum companion masses exceeding $1 M_{\odot}$ was computed.

Figure 7 shows the fraction of massive compact companions with unambiguous mass functions plotted against the RV shift between two measurements taken at random times (solid curve). It is quite obvious that binaries with high RV shifts are more likely to host massive companions. The probability for a high mass companion ($>1 M_{\odot}$) at high inclination is raised by a factor of ten as soon as the RV shift exceeds 200 km s^{-1} .

In order to check whether the selection of high velocities rather than high velocity shifts has an impact on the probability of finding sdB binaries with massive compact companions we used the same simulation. In Fig. 8 the fraction of these binaries is plotted against only one RV measurement taken at a random time. It can be clearly seen that the detection probability rises significantly for stars with high RVs. Selecting the fastest stars in the halo therefore makes sense when searching for massive compact companions to sdBs.

Since the individual SDSS spectra were taken within short timespans, another simulation was performed corresponding to the RRV sample. The first RV was taken at a random time, but the second one just 0.03 d later. The dotted curve in Fig. 7 illustrates the outcome of this simulation. As soon as the RV shift exceeds 30 km s^{-1} within 0.03 d, the probability that the companion is massive rises to $\approx 10\%$. The reason the probability does not increase significantly with increasing RV shift is that the most massive companions in our simulation have maximum RV shifts as high as 1000 km s^{-1} . At the most common periods (≈ 0.5 d), the maximum RV shift within 0.03 d is then of the order of 100 km s^{-1} . RV shifts higher than this within comparable time intervals are not physically plausible.

Our simulation provides quantitative estimates based on our current knowledge of the sdB binary populations. We note that these numbers should be considered as rough estimates only. The

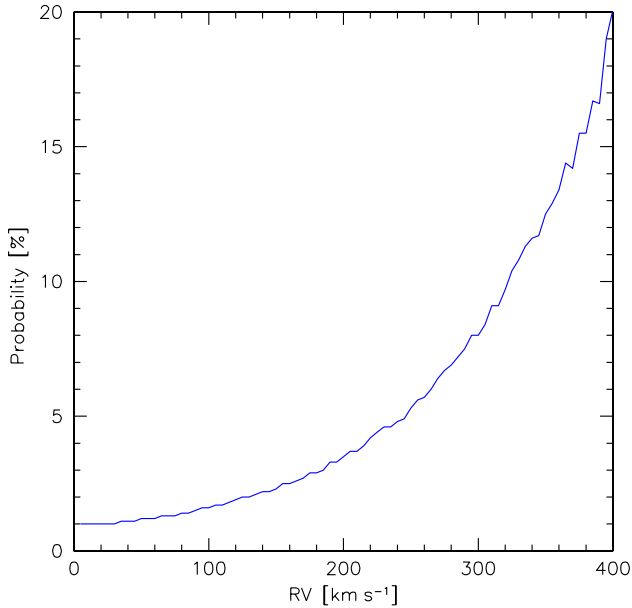


Fig. 8. Same as Fig. 7 except that the probability is plotted against RV at random time.

observed period and companion mass distributions, for example, are highly susceptible to selection effects. The derived numbers are therefore only used to create a priority list and select the best targets for follow-up.

3.5. Final target sample

Our sample of promising targets consists of 69 objects in total. 52 stars show significant RV shifts ($>30 \text{ km s}^{-1}$) within 0.02–0.07 d and are selected from the RRV sample, while 17 stars show high RV shifts ($100\text{--}300 \text{ km s}^{-1}$) within more than one day and are selected from the HRV sample (see Fig. 9).

In Geier et al. (2011) we showed that the SDSS spectra are well suited to determine atmospheric parameters by fitting synthetic line profiles to the hydrogen Balmer lines (H_β to H_9) as well as He I and He II lines. In order to maximize the quality of the data the single spectra were shifted to rest wavelength and coadded. The quality of the averaged spectra is quite inhomogeneous ($S/N \approx 20\text{--}180$, see Table 2), which affects the accuracy of the parameter determination.

A quantitative spectral analysis was performed in the way described in Lisker et al. (2005) and Ströer et al. (2007). Due to the fact that our sample consists of different subdwarf classes, we used appropriate model grids in each case. For the hydrogen-rich and helium-poor ($\log y < -1.0$) sdBs with effective temperatures below 30 000 K a grid of metal line blanketed LTE atmospheres with solar metallicity was used. Helium-poor sdBs and sdOBs with temperatures ranging from 30 000 K to 40 000 K were analysed using LTE models with enhanced metal line blanketing (O’Toole & Heber 2006). Metal-free NLTE models (Ströer et al. 2007) were used for hydrogen-rich sdOBs with temperatures below 40 000 K showing moderate He-enrichment ($\log y = -1.0\text{...}0.0$) and for hydrogen-rich sdOs. Finally, the He-sdOs were analysed with NLTE models taking into account the line-blanketing caused by nitrogen and carbon (Hirsch & Heber 2009).

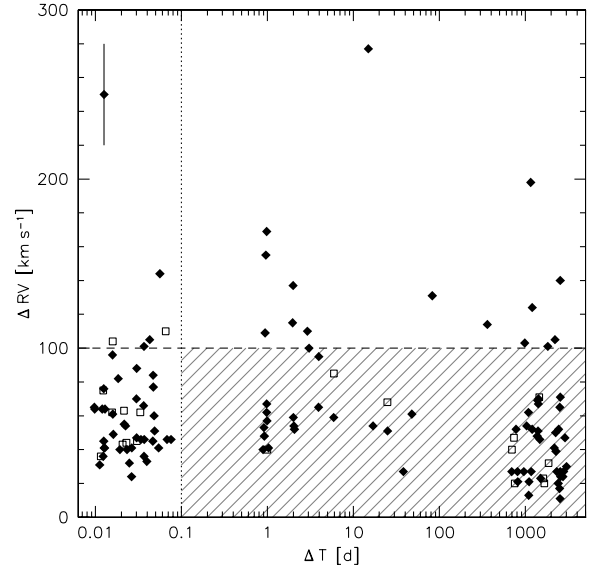


Fig. 9. Highest radial velocity shift between individual spectra plotted against time difference between the corresponding observing epochs. The dashed horizontal line marks the selection criterion $\Delta RV > 100 \text{ km s}^{-1}$, the dotted vertical line the selection criterion $\Delta T < 0.1 \text{ d}$. All objects fulfilling at least one of these criteria lie outside the shaded area and belong to the top candidate list for the follow-up campaign. The filled diamonds mark sdBs, while the blank squares mark He-sdOs.

Spectral lines of hydrogen and helium were fitted by means of chi-squared minimization using SPAS, and statistical errors were calculated with a bootstrapping algorithm. Minimum errors reflecting systematic shifts when using different model grids ($\Delta T_{\text{eff}} = 500 \text{ K}$; $\Delta \log g = 0.05$; $\Delta \log y = 0.1$, for a discussion see Geier et al. 2007) have been adopted in cases where the statistical errors were lower. Example fits for a typical sdB, an sdOB and a He-sdO star are shown in Fig. 10.

In addition to statistical uncertainties, systematic effects have to be taken into account in particular for sdB stars. The higher Balmer lines (H_ϵ and higher) at the blue end of the spectral range are very sensitive to changes in the atmospheric parameters. However, the SDSS spectral range restricts our analysis to the Balmer lines from H_β to H_9 . In high S/N data these lines are sufficient to measure accurate parameters as has been shown in Geier et al. (2011). In spectra of lower quality the bluest lines (H_9 and H_8) are dominated by noise and cannot be used any more. In order to check whether this leads to systematic shifts in the parameters as reported in Geier et al. (2010b) we made use of the individual SDSS spectra. We chose objects with multiple spectra, which have a S/N comparable to the lowest quality data in our sample (≈ 20). The atmospheric parameters were obtained from each individual spectrum. Average values of T_{eff} and $\log g$ were calculated and compared to the atmospheric parameters derived from the analysis of the appropriate coadded spectrum. For effective temperatures ranging from 27 000 K and 39 000 K no significant systematic shifts were found. This means that the error is dominated by statistical noise. However, for temperatures as low as 25 000 K systematic shifts of the order of -2500 K in T_{eff} and -0.35 in $\log g$ are present. For sdBs with low effective temperatures and signal-to-noise, the atmospheric parameters are therefore systematically underestimated. Only three stars in our sample have temperatures in this range. Since their

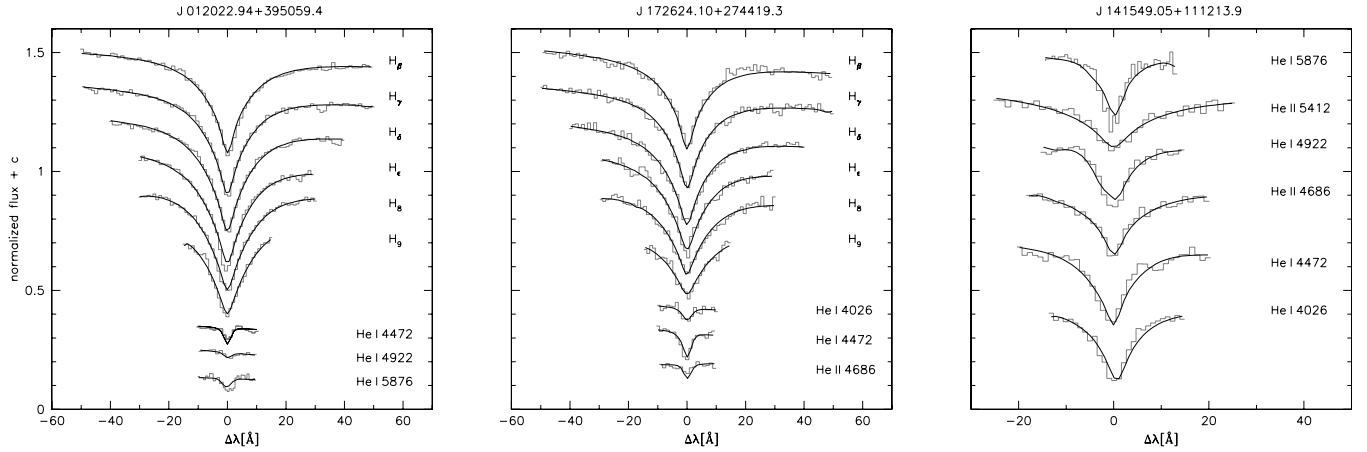


Fig. 10. Example fits of hydrogen and helium lines with model spectra for an sdB (left panel), an sdOB (middle panel) and a He-sdO star (right panel). The atmospheric parameters of these stars are given in Tables 3 and 4.

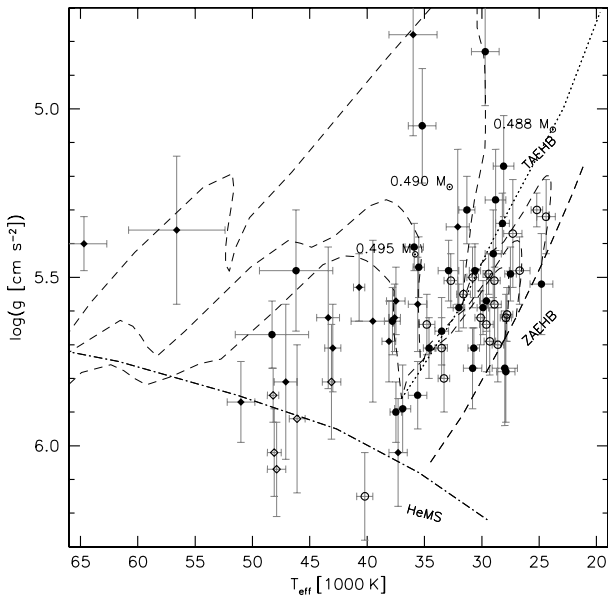


Fig. 11. $T_{\text{eff}} - \log g$ diagram of our target sample. The helium main sequence (HeMS) and the EHB band (limited by the zero-age EHB, ZAEHB, and the terminal-age EHB, TAEHB) are superimposed with EHB evolutionary tracks for subsolar metallicity ($\log z = -1.48$) from Dorman et al. (1993).

coadded spectra are of reasonable quality ($S/N = 34-167$), systematic shifts should be negligible in these cases. Because all important lines of He I and He II are well covered by the SDSS spectral range, systematic effects should be negligible in the case of He-rich sdO/Bs as well.

The parameters of the sample are given in Tables 3 and 4. Seven stars have already been analysed in Geier et al. (2011). The sample consists of 38 hydrogen rich sdBs, 13 sdOBs and 3 hydrogen rich sdOs. Thirteen stars are helium rich sdOs (He-sdOs) and J134352.14+394008.3 belongs to the rare class of helium rich sdBs.

Our SDSS sample reaches down to fainter magnitudes and hence, larger distances than any previous survey. In an ongoing

project Green et al. (2008) analyse all hot subdwarfs from the PG survey down to ≈ 14.0 mag. The sample of hot subdwarf stars analysed in the course of the SPY survey reaches down to ≈ 16.5 mag (Lisker et al. 2005; Ströer et al. 2007), quite similar to the sample of sdBs from the Hamburg Quasar Survey analysed by Edelmann et al. (2003).

Spectroscopic distances to our stars have been calculated as described in Ramspeck et al. (2001) assuming the canonical mass of $0.47 M_{\odot}$ for the subdwarfs and using the formula given by Lupton⁵ to convert SDSS- g and r magnitudes to Johnson V magnitudes. Interstellar reddening was once again neglected in these calculations, too. The distances range from 1 kpc to >16 kpc. Since the SDSS footprint is roughly perpendicular to the Galactic disk, these distances tell us something about the population membership of our stars. These subdwarfs most likely belong to the thick disk or the halo with small contributions of thin disk stars.

Figure 11 shows a $T_{\text{eff}} - \log g$ diagram of the top target sample. Most of our stars were born in an environment of low metallicity (thick disk or halo). Dorman et al. (1993) calculated evolutionary tracks for different metallicities of the subdwarf progenitor stars. For lower metallicities, the evolutionary tracks (and with them, the location of the EHB) are shifted towards higher temperatures and lower surface gravities. In Fig. 11 the $T_{\text{eff}} - \log g$ diagram is superimposed with evolutionary tracks and an EHB calculated for a subsolar metallicity of $\log z = -1.48$, which is consistent with a mixture between thick disk and halo population. Evolutionary tracks for solar metallicity are given in Fig. 12 for comparison.

Most of the sdB stars with hydrogen-rich atmospheres are found on or slightly above the EHB band implying an evolutionary status as core helium-burning EHB or shell helium-burning post-EHB stars. The sample contains only three hydrogen rich sdOs, which are thought to be evolved post-EHB stars in a transition state. The He-sdOs cluster near the HeMS at temperatures of ≈ 45 000 K. This is fully consistent with the results from the PG and the SPY surveys (Green et al. 2008; Lisker et al. 2005; Ströer et al. 2007) and illustrates that our sample is not biased (see Fig. 12).

Compared to other studies, we find only a few stars with temperatures lower than 27 000 K. Furthermore, the scatter around

⁵ <http://www.sdss.org/dr6/algorithms/sdssUBVRITransform.html>

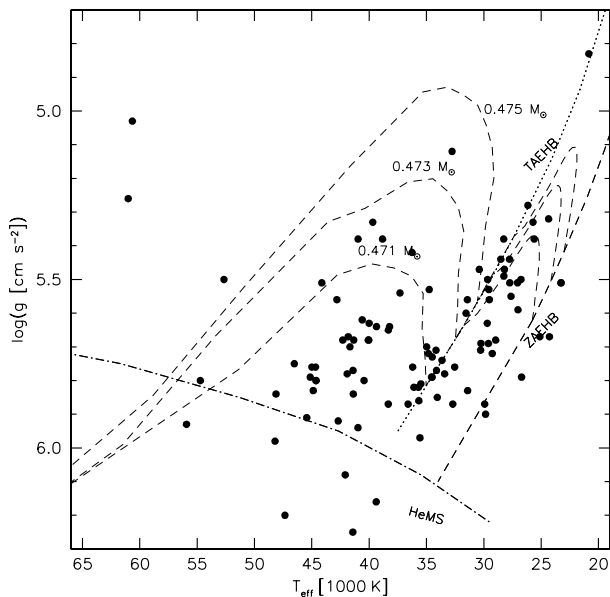


Fig. 12. $T_{\text{eff}} - \log g$ diagram of the hot subdwarfs from the SPY project (Lisker et al. 2005; Ströer et al. 2007). The helium main sequence (HeMS) and the EHB band (limited by the zero-age EHB, ZAEHB, and the terminal-age EHB, TAEHB) are superimposed with EHB evolutionary tracks for solar metallicity from Dorman et al. (1993).

the EHB seems to be systematically shifted towards higher temperatures and lower surface gravities. According to our study of systematic errors in the parameter determination, it is unlikely that this causes the effect. However, higher quality data would be necessary to verify this. Another possible explanation might be related to the volume of the sample. Since hot subdwarfs of lower temperature are brighter in the optical range because of the lower bolometric correction, we may already see all of them in a fixed volume, while the fraction of hot stars is still rising at fainter magnitudes.

In Fig. 13 the helium abundance is plotted against effective temperature. The general correlation of helium abundance with effective temperature and the large scatter in the region of the sdB stars have been observed in previous studies as well. Two sequences of helium abundance among the sdB stars as reported by Edelmann et al. (2003) could not be identified.

One has to keep in mind that our sample consists of RV variable stars only. In Fig. 11 a lack of such stars at the hot end of the EHB is visible. Green et al. (2008) reported similar systematics in their bright PG sample. The reason for this behaviour is not fully understood yet. According to the model of Han et al. (2002, 2003) and Han (2008) sdBs with thin hydrogen envelopes situated at the hot end of the EHB may be formed after the merger of two helium WDs. Since merger remnants are single stars, they are not RV variable.

The top target sample includes 13 He-sdOs for which RV shifts of up to 100 km s^{-1} have been detected within short timespans of 0.01–0.1 d. In total 20 He-sdOs show signs of RV variability. This fraction was unexpected since the fraction of close binary He-sdOs from the SPY sample turned out to be 4% at most (Napiwotzki 2008)⁶.

⁶ Green et al. (2008) suggested that the binary fraction of He-sdO stars may be comparable to the binary fraction of sdBs.

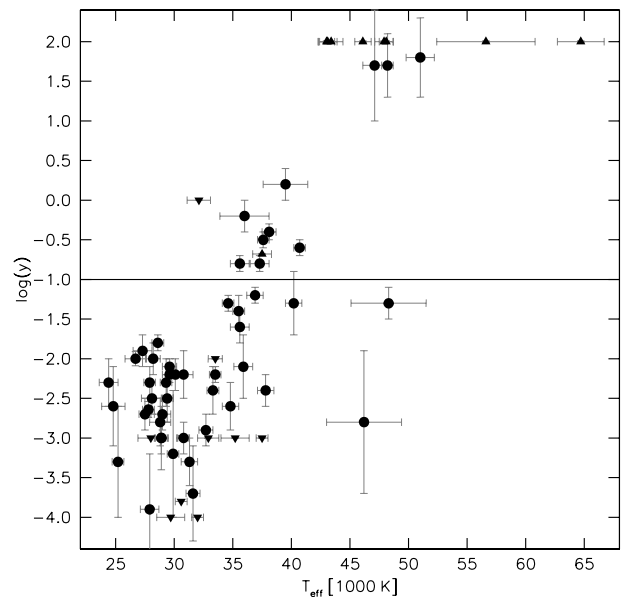


Fig. 13. Helium abundance $\log y$ plotted against effective temperature (see Tables 3, 4). The solid horizontal line marks the solar value. Lower and upper limits are marked with upward and downward triangles.

4. Summary and outlook

In this paper we introduced the MUCHFUSS project, which aims at finding sdBs in close binaries with massive compact companions. We identified 1100 hot subdwarf stars from the SDSS by colour selection and visual inspection of their spectra. Stars with high absolute radial velocities have been selected to efficiently remove normal sdB binaries from the thin disk population and were reobserved. We have found 46 binary candidates with significant RV shifts. Additionally, 81 stars with RV shifts on short timescales were found from the analysis of individual SDSS spectra.

Targets for follow-up spectroscopy were chosen using numerical simulations based on the properties of the known sdB close binary population and theoretical predictions about the relative fraction of massive compact companions. We selected 69 binaries with high RV shifts as well as significant RV shifts on short timescales as good candidates for massive compact companions and have determined their atmospheric parameters, spectroscopic distances, and population memberships.

The multi-site follow-up campaign started in 2009 and is being conducted with medium resolution spectrographs mounted on several different telescopes, most of which are 4-m class. First results are presented in Geier et al. (2011).

Acknowledgements. A.T., S.G. and H.H. are supported by the Deutsche Forschungsgemeinschaft (DFG) through grants HE1356/45-1, HE1356/49-1, and HE1356/44-1, respectively. R.Ø. acknowledges funding from the European Research Council under the European Community's Seventh Framework Programme (FP7/2007–2013)/ERC grant agreement No. 227224 (PROSPERITY), as well as from the Research Council of K.U.Leuven grant agreement GOA/2008/04. B.N.B. acknowledges the support of the National Science Foundation, under award AST-0707381.

Funding for the SDSS and SDSS-II has been provided by the Alfred P. Sloan Foundation, the Participating Institutions, the National Science Foundation, the US Department of Energy, the National Aeronautics and Space Administration, the Japanese Monbukagakusho, the Max Planck Society, and the Higher Education Funding Council for England. The SDSS Web Site is <http://www.sdss.org/>.

The SDSS is managed by the Astrophysical Research Consortium for the Participating Institutions. The Participating Institutions are the American Museum of Natural History, Astrophysical Institute Potsdam, University of Basel, University of Cambridge, Case Western Reserve University, University of Chicago, Drexel University, Fermilab, the Institute for Advanced Study, the Japan Participation Group, Johns Hopkins University, the Joint Institute for Nuclear Astrophysics, the Kavli Institute for Particle Astrophysics and Cosmology, the Korean Scientist Group, the Chinese Academy of Sciences (LAMOST), Los Alamos National Laboratory, the Max-Planck-Institute for Astronomy (MPIA), the Max-Planck-Institute for Astrophysics (MPA), New Mexico State University, Ohio State University, University of Pittsburgh, University of Portsmouth, Princeton University, the United States Naval Observatory, and the University of Washington.

References

- Abazajian, K., Adelman-McCarthy, J. K., Agüeros, M. A., et al. 2009, *ApJS*, 182, 543
- Ahmad, A., Jeffery, C. S., & Fullerton, A. W. 2004, *A&A*, 418, 275
- Altmann, M., Edelmann, H., & de Boer, K. S. 2004, *A&A*, 414, 181
- Badenes, C., Mullally, F., Thompson, S. E., & Lupton, R. H. 2009, *ApJ*, 707, 971
- Bloemen, S., Marsh, T. R., Østensen, R. H., et al. 2011, *MNRAS*, 410, 1787
- Brown, W. R., Geller, M. J., Kenyon, S. J., et al. 2005, *AJ*, 130, 109
- Castelli, F., & Kurucz, R. L. 2003, *IAU Symp.*, 210, 20
- Catelan, M. 2009, *Ap&SS*, 320, 261
- Dorman, B., Rood, R. T., & O'Connell, R. W. 1993, *ApJ*, 419, 596
- Drechsel, H., Heber, U., Napiwotzki, R., et al. 2001, *A&A*, 379, 893
- Edelmann, H. 2008, *ASP Conf. Ser.*, 392, 187
- Edelmann, H., Heber, U., Hagen, H.-J., et al. 2003, *A&A*, 400, 939
- Edelmann, H., Heber, U., Lisker, T., & Green, E. M. 2004, *Ap&SS*, 291, 315
- Edelmann, H., Heber, U., Altmann, M., Karl, C., & Lisker, T. 2005, *A&A*, 442, 1023
- Eisenstein, D. J., Liebert, J., Harris, H. C., et al. 2006, *ApJS*, 167, 40
- For, B.-Q., Green, E. M., O'Donoghue, D., et al. 2006, *ApJ*, 642, 1117
- For, B.-Q., Edelmann, H., Green, E. M., et al. 2008, *ASP Conf. Ser.*, 392, 203
- For, B.-Q., Green, E. M., Fontaine, G., et al. 2010, *ApJ*, 708, 253
- Geier, S., Nesslinger, S., Heber, U., et al. 2007, *A&A*, 464, 299
- Geier, S., Nesslinger, S., Heber, U., et al. 2008, *A&A*, 477, L13
- Geier, S., Heber, U., Kupfer, T., & Napiwotzki, R. 2010a, *A&A*, 515, A37
- Geier, S., Heber, U., Podsiadlowski, Ph., et al. 2010b, *A&A*, 519, A25
- Geier, S., Maxted, P. F. L., Napiwotzki, R., et al., 2011, *A&A*, 526, A39
- Gray, D. F. 1992, *The observation and analysis of stellar photospheres*, 2nd edn. (Cambridge: University Press)
- Green, E. M., Fontaine, G., Hyde, E. A., For, B.-Q., & Chayer, P. 2008, *ASP Conf. Ser.*, 392, 75
- Green, R. F., Schmidt, M., & Liebert, J. 1986, *ApJS*, 61, 305
- Green, E. M., For, B., Hyde, E. A., et al. 2004, *Ap&SS*, 291, 267
- Green, E. M., For, B., Hyde, E. A., et al. 2005, *ASP Conf. Ser.*, 334, 363
- Han, Z. 2008, *A&A*, 484, L31
- Han, Z., Podsiadlowski, P., Maxted, P. F. L., Marsh, T. R., & Ivanova, N. 2002, *MNRAS*, 336, 449
- Han, Z., Podsiadlowski, P., Maxted, P. F. L., & Marsh, T. R. 2003, *MNRAS*, 341, 669
- Heber, U. 1986, *A&A*, 155, 33
- Heber, U. 2009, *ARA&A*, 47, 211
- Heber, U., Drechsel, H., Østensen, R., et al. 2004, *A&A*, 420, 251
- Hirsch, H., & Heber, U. 2009, *JPhCS*, 172, 2015
- Iben, I., & Tutukov, A. V. 1984, *ApJ*, 284, 719
- Jester, S., Schneider, D. P., Richards, G. T., et al. 2005, *AJ*, 130, 873
- Karl, C., Heber, U., Napiwotzki, R., & Geier, S. 2006, *Baltic Astron.*, 15, 151
- Kawka, A., Vennes, S., Németh, P., Kraus, M., & Kubát, J. 2010, *MNRAS*, 408, 992
- Kilic, M., Brown, W. E., Allende Prieto, C., & Kenyon, S. J. 2010, *ApJ*, 716, 122
- Kleinman, S. J. 2010, *AIP Conf. Ser.*, 1237, 156
- Koen, C. 2009, *MNRAS*, 393, 1370
- Koen, C., Kilkenny, D., O'Donoghue, D., van Wyk, F., & Stobie, R. S. 1997, *MNRAS*, 285, 645
- Koen, C., Kilkenny, D., Pretorius, M. L., & Frew, D. J. 2010, *MNRAS*, 401, 1850
- Leibundgut, B. 2001, *ARA&A*, 39, 67
- Lisker, T., Heber, U., Napiwotzki, R., et al. 2005, *A&A*, 430, 223
- Marsh, T. R., Gaensicke, B. T., Steeghs, D., et al. 2010, *ApJL*, submitted [arXiv:1002.4677]
- Maxted, P. F. L., Marsh, T. R., & North, R. C. 2000a, *MNRAS*, 317, L41
- Maxted, P. F. L., Moran, C. K. J., Marsh, T. R., & Gatti, A. A. 2000b, *MNRAS*, 311, 877
- Maxted, P. F. L., Heber, U., Marsh, T. R., & North, R. C. 2001, *MNRAS*, 326, 139
- Maxted, P. F. L., Marsh, T. R., Heber, U., et al. 2002, *MNRAS*, 333, 231
- Maxted, P. F. L., Morales-Rueda, L., & Marsh, T. 2004, *Ap&SS*, 291, 307
- Mereghetti, S., Tiengo, A., Esposito, P., et al. 2009, *Science*, 325, 1222
- Momany, Y., Bedin, L. R., Cassisi, S., et al. 2004, *A&A*, 420, 605
- Morales-Rueda, L., Maxted, P. F. L., Marsh, T. R., North, R. C., & Heber, U. 2003a, *MNRAS*, 338, 752
- Morales-Rueda, L., Marsh, T. R., North, R. C., & Maxted, P. F. L. 2003b, in *White Dwarfs*, ed. D. de Martino, R. Silvotti, J.-E. Solheim, & R. Kalytis, 57
- Morales-Rueda, L., Maxted, P. F. L., Marsh, T. R., Kilkenny, D., & O'Donoghue, D. 2005, *ASP Conf. Ser.*, 334, 333
- Morales-Rueda, L., Maxted, P. F. L., Marsh, T. R., Kilkenny, D., & O'Donoghue, D. 2006, *Baltic Astron.*, 15, 187
- Moran, C., Maxted, P. F. L., Marsh, T. R., Saffer, R. A., & Livio, M. 1999, *MNRAS*, 304, 535
- Müller, S., Geier, S., & Heber, U. 2010, unpublished [arXiv:1012.3908]
- Mullally, F., Badenes, C., Thompson, S. E., & Lupton, R. 2009, *ApJ*, 707, 51
- Napiwotzki, R. 2008, *ASP Conf. Ser.*, 392, 139
- Napiwotzki, R., Edelmann, H., Heber, U., et al. 2001, *A&A*, 378, L17
- Napiwotzki, R., Karl, C., Lisker, T., et al. 2004a, *Ap&SS*, 291, 321
- Napiwotzki, R., Yungelson, L., Nelemans, G., et al. 2004b, *ASP Conf. Ser.*, 318, 402
- Nelemans, G. 2010, *Ap&SS*, 329, 25
- Newell, E. B. 1973, *ApJS*, 26, 37
- Østensen, R., Oreiro, R., Drechsel, H., et al. 2007, *ASP Conf. Ser.*, 372, 483
- Østensen, R., Green, E. M., Bloemen, S., et al. 2010, *MNRAS*, 408, 51
- Orosz, J. A., & Wade, R. A. 1999, *MNRAS*, 310, 773
- O'Toole, S. J., Heber, U., & Benjamin, R. A. 2004, *A&A*, 422, 1053
- O'Toole, S. J., Napiwotzki, R., Heber, U., et al. 2006, *Baltic Astron.*, 15, 61
- Perets, H. B., Gal-Yam, A., Mazzali, P. A., et al. 2010, *Nature*, 465, 322
- Perlmutter, S., Aldering, G., Goldhaber, G., et al. 1999, *ApJ*, 517, 565
- Pfahl, E., Rappaport, S., & Podsiadlowski, Ph. 2003, *ApJ*, 597, 1036
- Podsiadlowski, Ph., Rappaport, S., & Pfahl, E. D. 2002, *ApJ*, 565, 1107
- Polubek, G., Pigulski, A., Baran, A., & Udalski, A. 2007, *ASP Conf. Ser.*, 372, 487
- Ramspeck, M., Heber, U., & Edelmann, H. 2001, *A&A*, 379, 235
- Rebassa-Mansergas, A., Gänsicke, B. T., Rodríguez-Gil, P., Schreiber, M. R., & Koester, D. 2007, *MNRAS*, 382, 1377
- Reed, M., Terndrup, D. N., Østensen, R. H., et al. 2010, *Ap&SS*, 329, 83
- Riess, A. G., Filippenko, A. V., Challis, P., et al. 1998, *AJ*, 116, 1009
- Ritter, H., & Kolb, U. 2009, *VizieR Online Data Catalog*, 1, 2018
- Shimanskii, V. V., Bikmaev, I. F., Borisov, N. V., et al. 2008, *ARep*, 52, 729
- Ströer, A., Heber, U., Lisker, T., et al. 2007, *A&A*, 462, 269
- Tillich, A., Heber, U., Geier, S., et al. 2011, *A&A*, 527, A137
- Vučković, M., Aerts, C., Østensen, R., et al. 2007, *A&A*, 471, 605
- Vučković, M., Østensen, R., Bloemen, S., Decoster, I., & Aerts, C. 2008, *ASP Conf. Ser.*, 392, 199
- Webbink, R. F. 1984, *ApJ*, 277, 355
- Wils, P., di Scala, G., & Otero, S. 2007, *IBVS*, 5800, 1
- York, D. G., Adelman, J., Anderson, J. E., et al. 2000, *AJ*, 120, 1579
- Yungelson, L. R., & Tutukov, A. V. 2005, *ARep*, 49, 871
- Wang, B., Meng, X., Chen, X., & Han, Z. 2009, *MNRAS*, 395, 847

Table 2. Priority targets for follow-up.

Object		g	No.	S/N	Object		g	No.	S/N
J002323.99–002953.2	PB 5916	15.3	16	116	J150513.52+110836.6	PG 1502+113	15.1	4	90
J012022.94+395059.4	FBS 0117+396	15.2	8	100	J150829.02+494050.9		17.3	3	50
J012739.35+404357.8		16.5	8	59	J151415.66–012925.2		16.8	5	48
J052544.93+630726.0		17.6	3	35	J152222.15–013018.3		17.7	5	28
J074534.16+372718.5		17.6	5	26	J152705.03+110843.9		17.1	5	39
J075937.15+541022.2		17.5	3	27	J153411.10+543345.2	WD 1532+547	16.7	8	52
J082053.53+000843.4		14.9	6	103	J155628.34+011335.0		16.0	8	92
J083006.17+475150.4		15.8	5	95	J161140.50+201857.0		18.2	5	20
J085727.65+424215.4	US 1993	18.3	4	21	J161817.65+120159.6		17.8	4	18
J092520.70+470330.6		17.4	3	33	J162256.66+473051.1		16.0	4	72
J094856.95+334151.0	KUV 09460+3356	17.4	3	46	J163702.78–011351.7		17.1	12	46
J095229.62+301553.6		18.2	3	20	J164326.04+330113.1	PG 1641+331	16.1	3	55
J095238.93+625818.9		14.5	4	113	J165404.26+303701.8	PG 1652+307	15.1	4	167
J100535.76+223952.1		18.1	4	28	J170645.57+243208.6		17.5	3	39
J102151.64+301011.9		18.0	12	34	J170810.97+244341.6		18.2	3	16
J103549.68+092551.9		16.0	3	59	J171617.33+553446.7	SBSS 1715+556	16.9	8	39
J110215.97+521858.1		17.2	3	44	J171629.92+575121.2		17.9	4	21
J110445.01+092530.9		16.0	4	40	J172624.10+274419.3	PG 1724+278	15.7	4	107
J112242.69+613758.5	PG 1119+619	15.1	3	87	J174516.32+244348.3		17.4	3	22
J112414.45+402637.1		17.7	3	21	J175125.67+255003.5		17.2	4	50
J113303.70+290223.0		17.4	3	34	J202313.83+131254.9		17.0	3	33
J113418.00+015322.1	LBQS 1131+0209	17.7	6	30	J202758.63+773924.5		17.7	3	22
J113840.68–003531.7	PG 1136–003	14.2	10	174	J204300.90+002145.0		17.6	9	50
J113935.45+614953.9	FBS 1136+621	16.8	3	34	J204448.63+153638.8		17.7	7	50
J115358.81+353929.0	FBS 1151+359	16.3	3	48	J204546.81–054355.6		17.8	4	29
J115716.37+612410.7	FBS 1154+617	16.9	5	34	J204613.40–045418.7		16.0	3	120
J125702.30+435245.8		17.9	3	18	J204940.85+165003.6		17.7	7	35
J130059.20+005711.7	PG 1258+012	16.3	3	47	J210454.89+110645.5		17.2	4	37
J130439.57+312904.8	LB 28	16.8	3	42	J211651.96+003328.5		17.7	3	19
J133638.81+111949.4		17.0	3	32	J215648.71+003620.7	PB 5010	17.7	3	22
J134352.14+394008.3		18.1	3	19	J225638.34+065651.1	PG 2254+067	15.1	3	86
J135807.96+261215.5		17.7	4	23	J232757.46+483755.2		15.6	3	92
J140545.25+014419.0	PG 1403+019	15.6	3	81	J233406.11+462249.3		17.4	3	35
J141549.05+111213.9		15.8	3	82	J234528.85+393505.2		17.3	3	37
J143153.05–002824.3	LBQS 1429–0015	17.8	8	34					

Notes. Besides the names, the g magnitudes, the number of individual spectra and the S/N of the coadded spectra at $\approx 4100 \text{ \AA}$ are given.

Table 3. Priority targets for follow-up (HRV subsample).

Object	Class	T_{eff} [K]	$\log g$	$\log y$	d [kpc]	ΔRV [km s $^{-1}$]	Δt [d]
J102151.64+301011.9	sdB	30700 ± 500	5.71 ± 0.06	< -3.0	$5.8^{+0.5}_{-0.5}$	277 ± 51	14.936
J150829.02+494050.9	sdB	28200 ± 600	5.34 ± 0.09	-2.0 ± 0.2	$6.4^{+0.8}_{-0.7}$	211 ± 18	2161.429
J095229.62+301553.6	sdB	35200 ± 1200	5.05 ± 0.17	< -3.0	$16.0^{+3.8}_{-3.3}$	198 ± 40	1155.766
J113840.68–003531.7†	sdB	30800 ± 500	5.50 ± 0.09	-3.0 ± 0.2	$1.3^{+0.2}_{-0.1}$	182 ± 12	0.973
J165404.26+303701.8†	sdB	24400 ± 800	5.32 ± 0.11	-2.3 ± 0.3	$1.9^{+0.3}_{-0.3}$	181 ± 9	1795.144
J152222.15–013018.3	sdB	24800 ± 1000	5.52 ± 0.15	-2.6 ± 0.5	$4.8^{+1.1}_{-0.9}$	173 ± 36	3.001
J150513.52+110836.6†	sdB	33300 ± 500	5.80 ± 0.10	-2.4 ± 0.3	$1.5^{+0.2}_{-0.2}$	154 ± 12	0.957
J002323.99–002953.2†	sdB	30100 ± 500	5.62 ± 0.08	-2.2 ± 0.2	$1.8^{+0.2}_{-0.2}$	130 ± 14	82.784
J202313.83+131254.9	sdB	29600 ± 600	5.64 ± 0.14	-2.1 ± 0.1	$3.8^{+0.7}_{-0.6}$	124 ± 21	1202.795
J012022.94+395059.4	sdB	28900 ± 500	5.51 ± 0.08	-3.0 ± 0.4	$1.9^{+0.2}_{-0.2}$	114 ± 11	360.973
J202758.63+773924.5	sdO	46200 ± 3200	5.48 ± 0.18	-2.8 ± 0.9	$8.2^{+2.2}_{-1.8}$	114 ± 48	1.960
J095238.93+625818.9	sdB	27800 ± 500	5.61 ± 0.08	-2.64 ± 0.1	$1.2^{+0.1}_{-0.1}$	111 ± 10	2.918
J161140.50+201857.0	sdOB	36900 ± 700	5.89 ± 0.13	-1.2 ± 0.1	$6.1^{+1.1}_{-0.9}$	108 ± 36	0.947
J164326.04+330113.1	sdB	27900 ± 500	5.62 ± 0.07	-2.3 ± 0.2	$2.4^{+0.2}_{-0.2}$	108 ± 11	1.990
J204448.63+153638.8	sdB	29600 ± 600	5.57 ± 0.09	-2.2 ± 0.1	$5.7^{+0.7}_{-0.7}$	101 ± 19	3.049
J083006.17+475150.4	sdB	25200 ± 500	5.30 ± 0.05	-3.3 ± 0.7	$2.8^{+0.2}_{-0.2}$	95 ± 14	3.961
J204940.85+165003.6	He-sdO	43000 ± 700	5.71 ± 0.13	$> +2.0$	$6.2^{+1.1}_{-0.9}$	85 ± 19	5.932

Notes. † The binary system has been analysed in Geier et al. (2011).

Table 4. Priority targets for follow-up (RRV subsample).

Object	Class	T_{eff} [K]	$\log g$	$\log y$	d [kpc]	ΔRV [km s ⁻¹]	Δt [d]
J085727.65+424215.4	He-sdO	39500 ± 1900	5.63 ± 0.24	+0.2 ± 0.2	8.7 ^{+3.0} _{-2.2}	111 ± 46	0.066
J161817.65+120159.6	sdB	32100 ± 1000	5.35 ± 0.23	–	8.1 ^{+2.8} _{-2.1}	105 ± 31	0.043
J232757.46+483755.2	He-sdO	64700 ± 2000	5.40 ± 0.08	>+2.0	4.2 ^{+0.5} _{-0.4}	105 ± 24	0.016
J162256.66+473051.1	sdB	28600 ± 500	5.70 ± 0.11	-1.81 ± 0.1	2.2 ^{+0.3} _{-0.3}	101 ± 15	0.037
J163702.78-011351.7	He-sdO	46100 ± 700	5.92 ± 0.22	>+2.0	3.8 ^{+1.1} _{-0.9}	101 ± 55	0.085
J113303.70+290223.0	sdB/DA	–	–	–	–	95 ± 35	0.016
J135807.96+261215.5	sdB	33500 ± 600	5.66 ± 0.10	<-2.0	5.8 ^{+0.8} _{-0.7}	87 ± 29	0.030
J112242.69+613758.5	sdB	29300 ± 500	5.69 ± 0.10	-2.3 ± 0.3	1.5 ^{+0.2} _{-0.2}	83 ± 20	0.047
J153411.10+543345.2	sdOB	34800 ± 700	5.64 ± 0.09	-2.6 ± 0.3	3.8 ^{+0.5} _{-0.4}	83 ± 29	0.018
J082053.53+000843.4	sdB	26700 ± 900	5.48 ± 0.10	-2.0 ± 0.09	1.6 ^{+0.3} _{-0.2}	77 ± 11	0.047
J170810.97+244341.6	sdOB	35600 ± 800	5.58 ± 0.14	-0.8 ± 0.1	8.5 ^{+1.6} _{-1.4}	76 ± 33	0.013
J094856.95+334151.0	He-sdO	51000 ± 1200	5.87 ± 0.12	+1.8 ± 0.5	5.1 ^{+0.8} _{-0.7}	75 ± 17	0.012
J204613.40-045418.7†	sdB	31600 ± 600	5.55 ± 0.10	-3.7 ± 0.6	2.8 ^{+0.4} _{-0.4}	70 ± 13	0.030
J215648.71+003620.7	sdB	30800 ± 800	5.77 ± 0.12	-2.2 ± 0.3	4.7 ^{+0.8} _{-0.7}	69 ± 21	0.011
J074534.16+372718.5	sdB	37500 ± 500	5.90 ± 0.09	<-3.0	4.6 ^{+0.5} _{-0.5}	65 ± 19	0.036
J143153.05-002824.3	sdOB	37300 ± 800	6.02 ± 0.16	-0.8 ± 0.1	4.4 ^{+0.9} _{-0.8}	65 ± 22	0.012
J171629.92+575121.2	sdOB	35400 ± 1000	5.60 ± 0.18	-0.7 ± 0.1	7.8 ^{+1.0} _{-0.9}	65 ± 16	0.013
J112414.45+402637.1	He-sdO	47100 ± 1000	5.81 ± 0.23	+1.7 ± 0.7	5.9 ^{+1.9} _{-1.4}	63 ± 22	0.021
J125702.30+435245.8	sdB	28000 ± 1100	5.77 ± 0.17	<-3.0	4.9 ^{+1.3} _{-1.0}	63 ± 28	0.010
J110215.97+521858.1	He-sdO	56600 ± 4200	5.36 ± 0.22	>+2.0	8.9 ^{+3.0} _{-2.2}	62 ± 11	0.033
J151415.66-012925.2	He-sdO	48200 ± 500	5.85 ± 0.08	+1.7 ± 0.4	3.6 ^{+0.4} _{-0.3}	62 ± 22	0.016
J204300.90+002145.0	sdO	40200 ± 700	6.15 ± 0.13	-1.3 ± 0.4	3.6 ^{+0.6} _{-0.5}	61 ± 13	0.016
J171617.33+553446.7	sdB	32900 ± 900	5.48 ± 0.09	<-3.0	4.9 ^{+0.7} _{-0.6}	60 ± 24	0.048
J210454.89+110645.5	sdOB	37800 ± 700	5.63 ± 0.10	-2.4 ± 0.2	4.9 ^{+0.6} _{-0.6}	58 ± 19	0.023
J115358.81+353929.0	sdOB	29400 ± 500	5.49 ± 0.06	-2.5 ± 0.3	3.3 ^{+0.3} _{-0.3}	56 ± 12	0.022
J174516.32+244348.3	He-sdO	43400 ± 1000	5.62 ± 0.21	>+2.0	6.2 ^{+1.8} _{-1.4}	55 ± 28	0.016
J134352.14+394008.3	He-sdB	36000 ± 2100	4.78 ± 0.30	-0.2 ± 0.2	8.8 ^{+8.5} _{-6.1}	52 ± 34	0.022
J115716.37+612410.7	sdB	29900 ± 500	5.59 ± 0.08	-3.2 ± 0.8	4.0 ^{+0.5} _{-0.4}	51 ± 34	0.049
J133638.81+111949.4	sdB	27500 ± 500	5.49 ± 0.08	-2.7 ± 0.2	4.4 ^{+0.5} _{-0.5}	48 ± 17	0.030
J211651.96+003328.5	sdB	27900 ± 800	5.78 ± 0.15	-3.9 ± 0.7	4.3 ^{+0.9} _{-0.8}	48 ± 23	0.016
J170645.57+243208.6	sdB	32000 ± 500	5.59 ± 0.07	<-4.0	5.5 ^{+0.6} _{-0.5}	46 ± 14	0.013
J175125.67+255003.5	sdB	30600 ± 500	5.48 ± 0.08	<-3.8	5.0 ^{+0.6} _{-0.5}	46 ± 14	0.034
J012739.35+404357.8	sdO	48300 ± 3200	5.67 ± 0.10	-1.3 ± 0.2	4.1 ^{+0.7} _{-0.6}	45 ± 17	0.037
J113418.00+015322.1	sdB	29700 ± 1200	4.83 ± 0.16	<-4.0	1.8 ^{+2.9} _{-2.4}	45 ± 24	0.076
J172624.10+274419.3†	sdOB	33500 ± 500	5.71 ± 0.09	-2.2 ± 0.1	2.2 ^{+0.3} _{-0.2}	45 ± 16	0.047
J155628.34+011335.0	sdB	32700 ± 600	5.51 ± 0.08	-2.9 ± 0.2	3.1 ^{+0.4} _{-0.3}	44 ± 15	0.068
J103549.68+092551.9	He-sdO	48100 ± 600	6.02 ± 0.13	>+2.0	2.2 ^{+0.4} _{-0.3}	43 ± 12	0.021
J141549.05+111213.9	He-sdO	43100 ± 800	5.81 ± 0.17	>+2.0	2.4 ^{+0.5} _{-0.4}	43 ± 7	0.023
J152705.03+110843.9	sdOB	37600 ± 500	5.62 ± 0.10	-0.5 ± 0.1	4.8 ^{+0.6} _{-0.5}	43 ± 14	0.054
J052544.93+630726.0	sdOB	35600 ± 800	5.85 ± 0.10	-1.6 ± 0.2	4.3 ^{+0.6} _{-0.5}	42 ± 17	0.026
J100535.76+223952.1	sdB	29000 ± 700	5.43 ± 0.13	-2.7 ± 0.2	7.9 ^{+1.5} _{-1.3}	41 ± 18	0.019
J204546.81-054355.6	sdB	35500 ± 500	5.47 ± 0.09	-1.4 ± 0.2	7.3 ^{+0.9} _{-0.8}	41 ± 18	0.013
J092520.70+470330.6	sdB	28100 ± 900	5.17 ± 0.15	-2.5 ± 0.2	7.5 ^{+1.7} _{-1.4}	40 ± 13	0.012
J075937.15+541022.2	sdB	31300 ± 700	5.30 ± 0.10	-3.3 ± 0.3	7.6 ^{+1.1} _{-1.0}	38 ± 13	0.012
J234528.85+393505.2	He-sdO	47900 ± 800	6.07 ± 0.14	>+2.0	3.5 ^{+0.6} _{-0.5}	37 ± 14	0.012
J130439.57+312904.8	sdOB	38100 ± 600	5.69 ± 0.12	-0.4 ± 0.1	4.1 ^{+0.6} _{-0.6}	36 ± 12	0.037
J130059.20+005711.7‡	He-sdO	40700 ± 500	5.53 ± 0.10	-0.6 ± 0.1	3.9 ^{+0.5} _{-0.4}	36 ± 16	0.012
J110445.01+092530.9	sdOB	35900 ± 800	5.41 ± 0.07	-2.1 ± 0.4	3.8 ^{+0.4} _{-0.3}	34 ± 14	0.040
J113935.45+614953.9	sdB	28800 ± 900	5.27 ± 0.15	-2.8 ± 0.3	4.9 ^{+1.1} _{-0.9}	31 ± 14	0.011
J233406.11+462249.3	sdOB	34600 ± 500	5.71 ± 0.09	-1.3 ± 0.1	4.9 ^{+0.6} _{-0.6}	31 ± 14	0.025
J225638.34+065651.1†	sdB	28900 ± 600	5.58 ± 0.11	-3.0 ± 0.2	1.6 ^{+0.3} _{-0.2}	27 ± 11	0.031
J140545.25+014419.0	sdB	27300 ± 800	5.37 ± 0.16	-1.9 ± 0.2	2.5 ^{+0.6} _{-0.5}	25 ± 10	0.026

Notes. † The binary system has been analysed in Geier et al. (2011). ‡ Atmospheric parameters ($T_{\text{eff}} = 39\,400$ K, $\log g = 5.64$, $\log y = -0.55$) have been determined by Ströer et al. (2007).

Appendix A: Close binary subdwarfs from literature**Table A.1.** Orbital parameters of all known hot subdwarf binaries from literature.

Object	P [d]	γ [km s ⁻¹]	K [km s ⁻¹]	Reference
PG 0850+170	27.815	32.2 ± 2.8	33.5 ± 3.3	Morales-Rueda et al. (2003a)
PG 1619+522	15.3578	-52.5 ± 1.1	35.2 ± 1.1	Morales-Rueda et al. (2003a)
PG 1110+294	9.4152	-15.2 ± 0.9	58.7 ± 1.2	Morales-Rueda et al. (2003a)
Feige 108	8.7465	45.8 ± 0.6	50.2 ± 1.0	Edelmann et al. (2004)
PG 0940+068	8.330	-16.7 ± 1.4	61.2 ± 1.4	Maxted et al. (2000b)
PHL 861	7.44	-26.5 ± 0.4	47.9 ± 0.4	Karl et al. (2006)
HE 1448-0510	7.159	-45.5 ± 0.8	53.7 ± 1.1	Karl et al. (2006)
PG 1032+406	6.7791	24.5 ± 0.5	33.7 ± 0.5	Morales-Rueda et al. (2003a)
PG 0907+123	6.11636	56.3 ± 1.1	59.8 ± 0.9	Morales-Rueda et al. (2003a)
HE 1115-0631	5.87	87.1 ± 1.3	61.9 ± 1.1	Napiwotzki et al. (in prep.)
CD -24 731	5.85	20.0 ± 5.0	63.0 ± 3.0	Edelmann et al. (2005)
PG 1244+113	5.75207	9.8 ± 1.2	55.6 ± 1.8	Morales-Rueda et al. (2003b)
PG 0839+399	5.6222	23.2 ± 1.1	33.6 ± 1.5	Morales-Rueda et al. (2003a)
TON S 135	4.1228	-3.7 ± 1.1	41.4 ± 1.5	Edelmann et al. (2005)
PG 0934+186	4.051	7.4 ± 2.9	60.2 ± 2.0	Morales-Rueda et al. (2003b)
PB 7352	3.62166	-2.1 ± 0.3	60.8 ± 0.3	Edelmann et al. (2005)
KPD 0025+5402	3.5711	-7.8 ± 0.7	40.2 ± 1.1	Morales-Rueda et al. (2003a)
TON 245	2.501	-	88.3	Morales-Rueda et al. (2003a)
PG 1300+2756	2.25931	-3.1 ± 0.9	62.8 ± 1.6	Morales-Rueda et al. (2003a)
NGC 188/II-91	2.15	-	22.0	Green et al. (2004)
V 1093 Her ^p	1.77732	-3.9 ± 0.8	70.8 ± 1.0	Morales-Rueda et al. (2003a)
HD 171858	1.63280	62.5 ± 0.1	60.8 ± 0.3	Edelmann et al. (2005)
KPD 2040+3954	1.48291	-11.5 ± 1.0	95.1 ± 1.7	Morales-Rueda et al. (2003b)
HE 2150-0238	1.321	-32.5 ± 0.9	96.3 ± 1.4	Karl et al. (2006)
[CW83] 1735+22	1.278	20.6 ± 0.4	103.0 ± 1.5	Edelmann et al. (2005)
PG 1512+244	1.26978	-2.9 ± 1.0	92.7 ± 1.5	Morales-Rueda et al. (2003a)
PG 0133+114	1.23787	-0.3 ± 0.2	82.0 ± 0.3	Edelmann et al. (2005)
HE 1047-0436	1.21325	25.0 ± 3.0	94.0 ± 3.0	Napiwotzki et al. (2001)
HE 1421-1206	1.188	-86.2 ± 1.1	55.5 ± 2.0	Napiwotzki et al. (in prep.)
PG 1000+408	1.041145	41.9	72.4	Shimanskii et al. (2008)
PB 5333	0.92560	-95.3 ± 1.3	22.4 ± 0.8	Edelmann et al. (2004)
HE 2135-3749	0.9240	45.0 ± 0.5	90.5 ± 0.6	Karl et al. (2006)
EC 12408-1427	0.90243	-52.0 ± 1.2	58.9 ± 1.6	Morales-Rueda et al. (2006)
PG 0918+0258	0.87679	104.4 ± 1.7	80.0 ± 2.6	Morales-Rueda et al. (2003a)
PG 1116+301	0.85621	-0.2 ± 1.1	88.5 ± 2.1	Morales-Rueda et al. (2003a)
PG 1230+052	0.8372	-43.4 ± 0.8	41.5 ± 1.3	Morales-Rueda et al. (2003b)
V 2579 Oph ^p	0.8292056	-54.16 ± 0.27	70.10 ± 0.13	For et al. (2006)
TON S 183	0.8277	50.5 ± 0.8	84.8 ± 1.0	Edelmann et al. (2005)
EC 02200-2338	0.8022	20.7 ± 2.3	96.3 ± 1.4	Morales-Rueda et al. (2005)
PG 0849+319	0.74507	64.0 ± 1.5	66.3 ± 2.1	Morales-Rueda et al. (2003a)
JL 82 ^r	0.73710	-1.6 ± 0.8	34.6 ± 1.0	Edelmann et al. (2005)
PG 1248+164	0.73232	-16.2 ± 1.3	61.8 ± 1.1	Morales-Rueda et al. (2003a)
HD 188112 [†]	0.60658125	26.6 ± 0.3	188.4 ± 0.2	Edelmann et al. (2005)
PG 1247+554	0.602740	13.8 ± 0.6	32.2 ± 1.0	Maxted et al. (2000b)
PG 1725+252	0.601507	-60.0 ± 0.6	104.5 ± 0.7	Morales-Rueda et al. (2003a)
PG 0101+039 ^{sl,p}	0.569899	7.3 ± 0.2	104.7 ± 0.4	Geier et al. (2008)
HE 1059-2735	0.555624	-44.7 ± 0.6	87.7 ± 0.8	Napiwotzki et al. (in prep.)
PG 1519+640	0.54029143	0.1 ± 0.4	42.7 ± 0.6	Edelmann et al. (2004)
PG 0001+275	0.529842	-44.7 ± 0.5	92.8 ± 0.7	Edelmann et al. (2005)
PG 1743+477	0.515561	-65.8 ± 0.8	121.4 ± 1.0	Morales-Rueda et al. (2003a)
HE 1318-2111	0.487502	48.9 ± 0.7	48.5 ± 1.2	Napiwotzki et al. (in prep.)
PG 1544+488 [‡]	0.48	-23 ± 4	57 ± 4/97 ± 10	Ahmad et al. (2004)
GALEX J234947.7+384440	0.46249	2.0 ± 1.0	87.9 ± 2.2	Kawka et al. (2010)
HE 0230-4323 ^{r,p}	0.45152	16.6 ± 1.0	62.4 ± 1.6	Edelmann et al. (2005)
HE 0929-0424	0.4400	41.4 ± 1.0	114.3 ± 1.4	Karl et al. (2006)

Table A.1. continued.

Object	P [d]	γ [km s ⁻¹]	K [km s ⁻¹]	Reference
[CW83] 1419-09	0.4178	42.3 ± 0.3	109.6 ± 0.4	Edelmann et al. (2005)
KPD 1946+4340 ^{ec,el}	0.403739	-5.5 ± 1.0	167.0 ± 2.4	Morales-Rueda et al. (2003a)
KUV 04421+1416 ^{r,p}	0.398	33 ± 3	90 ± 5	Reed et al. (2010)
Feige 48 ^p	0.376	-47.9 ± 0.1	28.0 ± 0.2	O'Toole et al. (2004)
GD 687	0.37765	32.3 ± 3.0	118.3 ± 3.4	Geier et al. (2010a)
PG 1232-136	0.3630	4.1 ± 0.3	129.6 ± 0.04	Edelmann et al. (2005)
PG 1101+249	0.35386	-0.8 ± 0.9	134.6 ± 1.3	Moran et al. (1999)
PG 1438-029 ^f	0.336	-	32.1	Green et al. (2005)
PG 1528+104	0.331	-49.9 ± 0.8	52.7 ± 1.3	Morales-Rueda et al. (2003b)
PG 0941+280 ^{ec}	0.315	-	-	Green et al. (2004)
KBS 13 ^r	0.2923	7.53 ± 0.08	22.82 ± 0.23	For et al. (2008)
CPD-64 481	0.2772	94.1 ± 0.3	23.8 ± 0.4	Edelmann et al. (2005)
GALEX J032139.8+472716	0.26584	70.5 ± 2.2	59.8 ± 4.5	Kawka et al. (2010)
HE 0532-4503	0.2656	8.5 ± 0.1	101.5 ± 0.2	Karl et al. (2006)
AA Dor ^{ec,r}	0.2614	1.57 ± 0.09	40.15 ± 0.11	Müller et al. (2010)
PG 1329+159 ^f	0.249699	-22.0 ± 1.2	40.2 ± 1.1	Morales-Rueda et al. (2003a)
PG 2345+318 ^{ec}	0.2409458	-10.6 ± 1.4	141.2 ± 1.1	Moran et al. (1999)
PG 1432+159	0.22489	-16.0 ± 1.1	120.0 ± 1.4	Moran et al. (1999)
BPS CS 22169-0001 ^r	0.1780	2.8 ± 0.3	14.9 ± 0.4	Edelmann et al. (2005)
HS 2333+3927 ^r	0.1718023	-31.4 ± 2.1	89.6 ± 3.2	Heber et al. (2004)
2M 1533+3759 ^{ec,r}	0.16177042	-3.4 ± 5.2	71.1 ± 1.0	For et al. (2010)
EC 00404-4429	0.12834	33.0 ± 2.9	152.8 ± 3.4	Morales-Rueda et al. (2005)
2M 1938+4603 ^{ec,r}	0.1257653	20.1 ± 0.3	65.7 ± 0.6	Østensen et al. (2010)
BUL-SC 16 335 ^{ec,r}	0.125050278	-	-	Polubek et al. (2007)
PG 1043+760	0.1201506	24.8 ± 1.4	63.6 ± 1.4	Morales-Rueda et al. (2003a)
HW Vir ^{ec,r}	0.115	-13.0 ± 0.8	84.6 ± 1.1	Edelmann (2008)
HS 2231+2441 ^{ec,r}	0.1105880	-	49.1 ± 3.2	Østensen et al. (2007)
NSVS 14256825 ^{ec,r}	0.110374102	-	-	Wils et al. (2007)
PG 1336-018 ^{ec,r,p}	0.101015999	-25.0	78.7 ± 0.6	Vučković et al. (2007)
HS 0705+6700 ^{ec,r}	0.09564665	-36.4 ± 2.9	85.8 ± 3.6	Drechsel et al. (2001)
KPD 1930+2752 ^{el,p}	0.0950933	5.0 ± 1.0	341.0 ± 1.0	Geier et al. (2007)
KPD 0422+5421 ^{ec,el}	0.09017945	-57.0 ± 12.0	237.0 ± 18.0	Orosz & Wade (1999)
NGC 6121-V46 ^{el,†}	0.087159	31.3 ± 1.6	211.6 ± 2.3	O'Toole et al. (2006)
PG 1017-086 ^r	0.0729938	-9.1 ± 1.3	51.0 ± 1.7	Maxted et al. (2002)

Notes. The superscript p denotes sdB pulsators, r binaries where with reflection effect, ec eclipsing systems and el systems with light variations caused by ellipsoidal deformation. † Post-RGB stars without core helium-burning. ‡ Double-lined binary consisting of two helium rich sdBs. The RV semi-amplitudes of both components are given.

Two candidate brown dwarf companions around core helium-burning stars[★]

V. Schaffenroth^{1,2}, L. Classen¹, K. Nagel¹, S. Geier³, C. Koen⁴, U. Heber¹, and H. Edelmann¹

¹ Dr. Karl Remeis-Observatory & ECAP, Astronomical Institute, Friedrich-Alexander University Erlangen-Nuremberg, Sternwartstr. 7, 96049 Bamberg, Germany

e-mail: veronika.schaffenroth@sternwarte.uni-erlangen.de

² Institute for Astro- and Particle Physics, University of Innsbruck, Technikerstr. 25/8, 6020 Innsbruck, Austria

³ European Southern Observatory, Karl-Schwarzschild-Str. 2, 85748 Garching, Germany

⁴ Department of Statistics, University of the Western Cape, Private Bag X17, 7535 Bellville, South Africa

Received 16 July 2014 / Accepted 15 September 2014

ABSTRACT

Hot subdwarf stars of spectral type B (sdBs) are evolved, core helium-burning objects. The formation of those objects is puzzling, because the progenitor star has to lose almost its entire hydrogen envelope in the red-giant phase. Binary interactions have been invoked, but single sdBs exist as well. We report the discovery of two close hot subdwarf binaries with small radial velocity amplitudes. Follow-up photometry revealed reflection effects originating from cool irradiated companions, but no eclipses. The lower mass limits for the companions of CPD-64°481 ($0.048 M_{\odot}$) and PHL 457 ($0.027 M_{\odot}$) are significantly below the stellar mass limit. Hence they could be brown dwarfs unless the inclination is unfavourable. Two very similar systems have already been reported. The probability that none of them is a brown dwarf is very small, 0.02%. Hence we provide further evidence that substellar companions with masses that low are able to eject a common envelope and form an sdB star. Furthermore, we find that the properties of the observed sample of hot subdwarfs in reflection effect binaries is consistent with a scenario where single sdBs can still be formed via common envelope events, but their low-mass substellar companions do not survive.

Key words. binaries: spectroscopic – subdwarfs – brown dwarfs

1. Introduction

Hot subdwarf B stars (sdBs) are evolved, core helium-burning objects with only thin hydrogen envelopes and masses around $0.5 M_{\odot}$ (Heber 1986; see Heber 2009, for a review). To form such objects, the progenitor star has to lose almost its entire hydrogen envelope in the red-giant phase.

About half of the sdB stars are in close binaries with short periods from just a few hours to a few days (Maxted et al. 2001; Napiwotzki et al. 2004a). Because the separation in these systems is much smaller than the size of the red-giant progenitor star, these binaries must have experienced a common-envelope and spiral-in phase (Han et al. 2002, 2003). Although the common-envelope ejection channel is not properly understood (see Ivanova et al. 2013, for a review), it provides a reasonable explanation for the strong mass loss required to form sdB stars. However, for the other half of the known single-lined hot subdwarfs there is no evidence for close stellar companions as no radial velocity (RV) variations are found (Classen et al. 2011).

Soker (1998) proposed that substellar objects like brown dwarfs (BDs) and planets, which enter the envelope of a red giant, might be able to trigger its ejection. Substellar objects with masses higher than $\approx 10 M_J$ were predicted to survive the common envelope phase and end up in a close orbit around the stellar remnant, while planets with lower masses would evaporate or merge with the stellar core. The stellar remnant is predicted to lose most of its envelope and settle on the extreme horizontal

branch (EHB). Such a scenario has also been proposed to explain the formation of single low-mass white dwarfs (Nelemans & Tauris 1998).

The discovery of a brown dwarf ($M_{BD} = 0.053 \pm 0.006 M_{\odot}$) in close orbit (0.08 d) around such a white dwarf supports this scenario and shows that substellar companions can influence late stellar evolution (Maxted et al. 2006). With the discovery of the eclipsing sdB+BD binaries SDSS J0820+0008 and SDSS J1622+4730 in the course of the MUCHFUSS project (Geier et al. 2011a), it was shown observationally that substellar companions are also able to form sdBs (Geier et al. 2011c; Schaffenroth et al. 2014).

We now have to address the question, how massive the companion must be to survive the CE-phase. It might also be possible to form an sdB and either evaporate the substellar companion or merge it with the red-giant core. Substellar companions of brown dwarf and even planetary mass in wide orbits have been detected around pulsating sdBs (Silvotti et al. 2007; Lutz et al. 2012) and eclipsing sdB binaries using the timing method (see Zorotovic & Schreiber 2013, and references therein for a summary). Those results, although still under debate (see Wittenmyer et al. 2013; Horner et al. 2014), suggest that a high fraction of the sdB stars might be orbited by such objects. Substellar companions in close orbit might therefore be frequent as well.

Here we report the discovery of a reflection effect, but no eclipses, in the light curves of two close sdB binaries. CPD-64°481 and PHL 457 have been reported to be close sdB binaries with small RV shifts by Edelmann et al. (2005). Furthermore, PHL 457 has been identified as long-period pulsator of V 1093 Her type (Blanchette et al. 2008). Those two

[★] Appendix A is available in electronic form at <http://www.aanda.org>

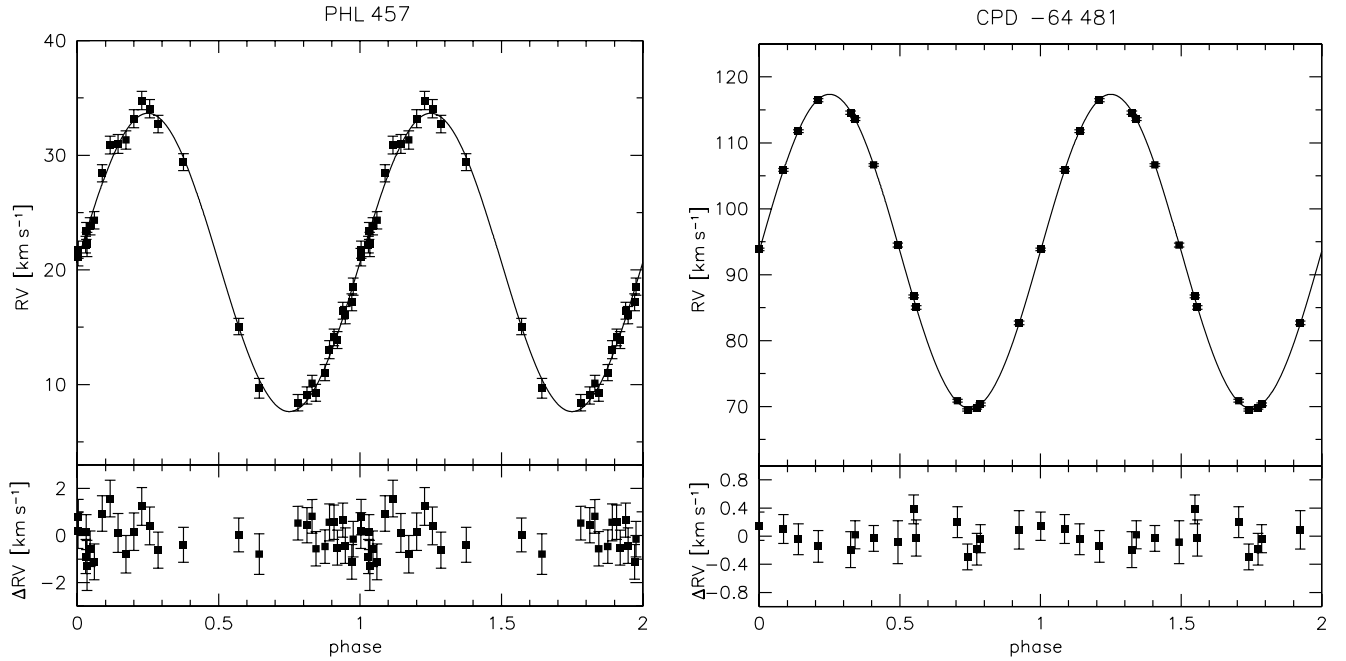


Fig. 1. Radial velocity plotted against orbital phase. The RV data were phase folded with the most likely orbital periods. The residuals are plotted below.

sdBs are among the best studied close sdB binaries. Detailed analyses showed that both are normal sdB binaries with typical atmospheric parameters (CPD-64°481: $T_{\text{eff}} = 27\,500 \pm 500$ K, $\log g = 5.60 \pm 0.05$, Geier et al. 2010; PHL 457: $T_{\text{eff}} = 26\,500 \pm 500$ K, $\log g = 5.38 \pm 0.05$, Geier et al. 2013a).

Geier et al. (2010) constrained the companion mass of CPD-64°481 to be as high as $0.62 M_{\odot}$ by measuring the projected rotational velocity of the sdB and assuming synchronised rotation. This assumption is reasonable, as the theoretical synchronisation timescales with stellar mass companions due to tidal interactions for binaries with periods of about 0.3 d are much smaller or comparable to the lifetime of the sdB on the EHB, depending on the theory (see Geier et al. 2010). The inclination angle was predicted to be as small as 7° . Because no traces of the companion are seen in the spectrum, they concluded that the companion must be a WD, as main sequence stars would be visible in the optical spectra, if their masses are higher than $\sim 0.45 M_{\odot}$ (Lisker et al. 2005). However, the detection of the reflection effect rules out such a compact companion.

Using the same method we constrained the companion mass of PHL 457. Although the companion mass assuming synchronisation ($\sim 0.26 M_{\odot}$) would still be consistent with observations, the derived inclination angle of 8° is very small and therefore unlikely.

Moreover, observational evidence, both from asteroseismic studies (Pablo et al. 2011, 2012) and spectroscopic measurements (Schaffenroth et al. 2014), indicates that synchronisation is not generally established in sdB binaries with low-mass companions (see also the discussion in Geier et al. 2010). Therefore, the rotation of the sdBs in CPD-64°481 and PHL 457 is most likely not synchronised with their orbital motion and the method described in Geier et al. (2010) not applicable.

2. Time-resolved spectroscopy and orbital parameters

In total, 45 spectra were taken with the FEROS spectrograph ($R \approx 48\,000$, $\lambda = 3800\text{--}9200$ Å) mounted at the

ESO/MPG-2.2 m telescope for studies of sdB stars at high resolution (Edelmann et al. 2005; Geier et al. 2010; Classen et al. 2011). The spectra were reduced with the FEROS pipeline available in the MIDAS package. The FEROS pipeline, moreover, performs the barycentric correction.

To measure the RVs with high accuracy, we chose a set of sharp, unblended metal lines situated between 3600 Å and 6600 Å. Accurate rest wavelengths were taken from the NIST database. Gaussian and Lorentzian profiles were fitted using the SPAS (Hirsch 2009) and FITSB2 routines (Napiwotzki et al. 2004b; for details see Classen et al. 2011). To check the wavelength calibration for systematic errors we used telluric features as well as night-sky emission lines. The FEROS instrument turned out to be very stable. Usually corrections of less than 0.5 km s^{-1} had to be applied. The RVs and formal 1σ -errors are given in Appendix A.

The orbital parameters and associated false-alarm probabilities are determined as described in Geier et al. (2011c). In order to estimate the significance of the orbital solutions and the contributions of systematic effects to the error budget, we normalised the χ^2 of the most probable solution by adding systematic errors e_{norm} in quadrature until the reduced χ^2 reached ≈ 1.0 . The hypothesis that both orbital periods are correct can be accepted with a high degree of confidence. The phased RV curves for the best solutions are of excellent quality (see Fig. 1). The derived orbital parameters are given in Table 1 and the orbital solution for CPD-64°481 is perfectly consistent with the result presented in Edelmann et al. (2005).

3. Photometry

Time-resolved differential photometry in BVR-filters for CPD-64°481 and VR filters for PHL 457 was obtained with the SAAO STE4 CCD on the 1.0 m telescope at the Sutherland site of the South African Astronomical Observatory (SAAO). Photometric reductions were performed using an automated version of DOPHOT (Schechter et al. 1993).

Table 1. Derived orbital solutions, mass functions and minimum companion masses.

Object	T_0^a [−2 450 000]	P^a [d]	γ^a [km s ^{−1}]	K^a [km s ^{−1}]	e_{norm} [km s ^{−1}]	$f(M)$ [M_\odot]	M_2^b [M_\odot]	i_{max}^c [°]
CPD-64°481	3431.5796 ± 0.0002	0.27726315 ± 0.00000008	93.54 ± 0.06	23.81 ± 0.08	0.16	0.0004	>0.048	70
PHL 457	5501.5961 ± 0.0009	0.3131 ± 0.0002	20.7 ± 0.2	13.0 ± 0.2	0.7	0.00007	>0.027	75

Notes. ^(a) The systematic error adopted to normalise the reduced χ^2 (e_{norm}) is given for each case. ^(b) The minimum companion masses take into account the highest possible inclination. ^(c) $i = 90$ is defined as an edge-on orbit.

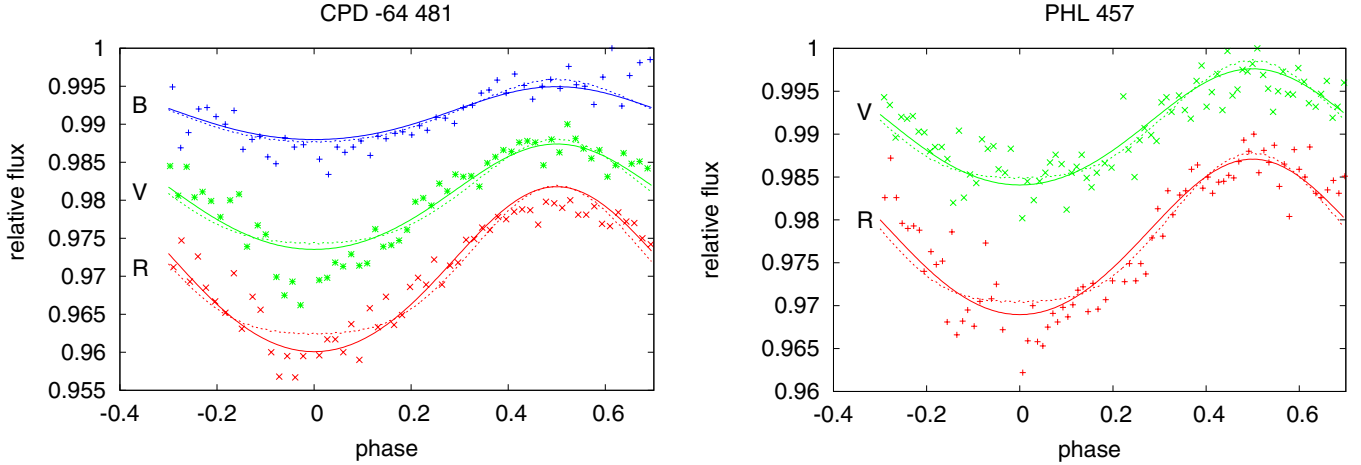


Fig. 2. Phased and binned light curves in *B*-, *V*- and *R*-bands in the case of CPD-64°481 (*left panel*) and *V*- and *R*-bands in the case of PHL 457 (*right panel*). Overplotted are two models for an inclination of 10° (solid) and 65° (dashed) for CPD-64°481 and 10° (solid) and 70° (dashed) for PHL 457. The lightcurve models with higher inclinations (dashed) have broader minima and shallower maxima.

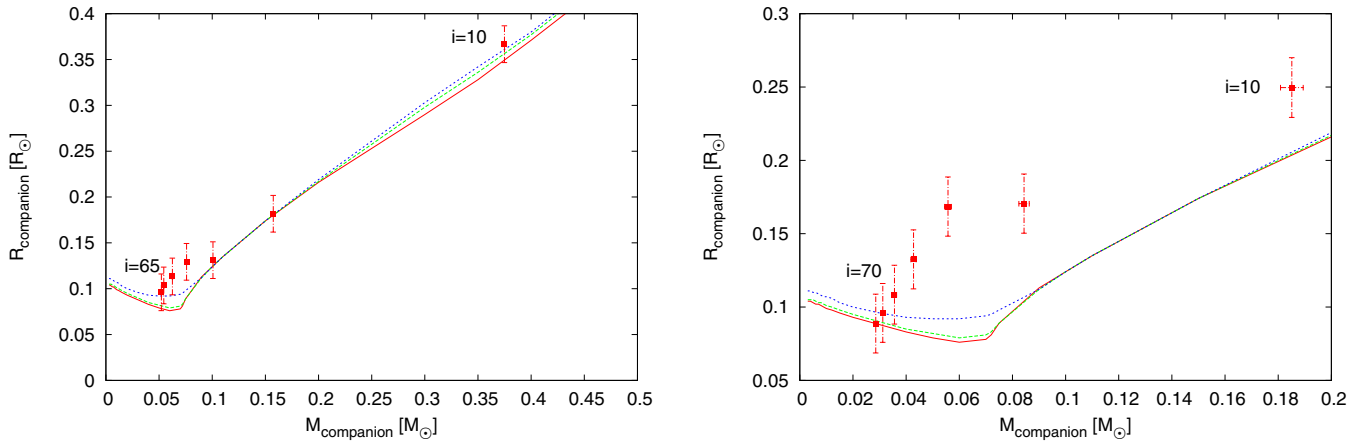


Fig. 3. Mass-radius relation of the companion of CPD-64°481 (*left panel*) and PHL 457 (*right panel*) for different inclinations (filled rectangles), compared to theoretical relations by Chabrier & Baraffe (1997) for an age of the system of 1 Gyr (short dashed line), 5 Gyr (long dashed line) and 10 Gyr (solid line). For all shown solutions mass and radius of the sdB are also consistent with the spectroscopic surface gravity measurement of $\log g = 5.60 \pm 0.05$ for CPD-64°481 (Geier et al. 2010) and $\log g = 5.38 \pm 0.05$ (Geier et al. 2013a) for PHL 457.

The differential light curves have been phased to the orbital periods derived from the RV-curves and binned to achieve higher signal-to-noise (S/N). The light curves show sinusoidal variations (~ 10 mmag) with orbital phase characteristic for a reflection effect (Fig. 2). It originates from the irradiation of a cool companion by the hot subdwarf primary. The projected area of the companion’s heated hemisphere changes while it orbits the primary. Compared to other reflection effect binaries the amplitude of the reflection effect in both systems is quite small. The amplitude of the reflection effect depends mostly on the separation of the system, the effective temperature of the subdwarf, and the visible irradiated area of the companion. Seen edge-on, the relative change of this area is the highest. However, for small

inclinations the derived mass of the companion becomes higher and because there is a strong correlation between mass and radius on the lower main sequence (see Fig. 3), the radius of the companion and the absolute irradiated area becomes larger as well. Due to this degeneracy it is therefore not straight forward to claim that small reflection effects can simply be explained by small inclination angles.

We fitted models calculated with MORO, which is based on the Wilson-Devinney code (MODified ROche model, Drechsel et al. 1995), to the light curves as described in Schaffenroth et al. (2013). As no eclipses are present, the inclination is difficult to determine and we fitted light curve solutions for different fixed inclinations. The mass ratio, which can be calculated from the

mass function for different inclinations, was also kept fixed, so that the mass of the sdB is equal to the canonical sdB mass $M_{\text{sdb}} = 0.47 M_{\odot}$ (see Fontaine et al. 2012, and references therein). Shape and amplitude of the variation mostly depends on the orbital inclination and the mass ratio, but also on the radius ratio of both components and the unknown albedo of the companion. Due to this high number of parameters, that are not independent from each other, we cannot find a unique solution.

Selecting only solutions for which the photometric radius is consistent with the spectroscopic radius derived from the surface gravity, we narrow down the number of solutions. Unfortunately, due to the degeneracy between the binary inclination and the radius of the companion we find equally good solutions for each inclination (see also Østensen et al. 2013). In the case of CPD-64°481, see Fig. 3, the derived mass and radius of the companion are in agreement with theoretical relations by Chabrier & Baraffe (1997) for the whole range of inclinations. In the case of PHL 457 the theoretical mass-radius relation is only consistent for an inclination of 50–70°. For lower inclinations the measured radius would be larger than expected by the models. However, due to the many assumptions used in the analysis, it is difficult to estimate the significance of this result, as a smaller mass for the sdB could solve this issue.

In Fig. 2 we show model light curves for high and low inclination. Although small differences are present, a much better quality light curve is needed to resolve them. The sum of the deviations between the measurements and the models are somewhat, but not significantly, smaller for low inclinations. Therefore, we cannot draw firm conclusions from our photometric data at hand.

4. Brown dwarf nature of the unseen companions

The two binaries are single-lined and their binary mass functions $f_m = M_{\text{comp}}^3 \sin^3 i / (M_{\text{comp}} + M_{\text{sdb}})^2 = PK^3 / 2\pi G$ can be determined. The RV semi-amplitude and the orbital period can be derived from the RV curve, but the sdB mass M_{sdb} , the companion mass M_{comp} and the inclination angle i remain free parameters. Adopting the canonical sdB mass $M_{\text{sdb}} = 0.47 M_{\odot}$ and the i_{max} , that can be constrained, because no eclipses are present in the lightcurve, we derive lower limits for the companion masses (see Table 1).

Those minimum masses of $0.048 M_{\odot}$ for CPD-64°481 and $0.027 M_{\odot}$ for PHL 457 – the smallest minimum companion mass measured in any sdB binary so far – are significantly below the hydrogen-burning limit ($\sim 0.07\text{--}0.08 M_{\odot}$, Chabrier et al. 2000). As no features of the companion are found in the spectrum, we also derive an upper mass limit of $\sim 0.45 M_{\odot}$ (Lisker et al. 2005).

The initial sample of Edelmann et al. (2005) consisted of known, bright hot subdwarf stars. Because no additional selection criteria were applied, it can be assumed that the inclination angles of the binaries found in this survey are randomly distributed. Due to the projection effect it is much more likely to find binary systems at high rather than low inclinations. The probability, that a binary has an inclination higher than a certain angle, can be calculated as described in Gray (1992), $P_{i>i_0} = 1 - (1 - \cos i_0)$. Since the companion mass scales with the inclination angle, we can derive the probability that the mass of the companion is smaller than the hydrogen-burning limit of $\sim 0.08 M_{\odot}$, which separates stars from brown dwarfs.

For CPD-64°481, the inclination angle must be higher than 38°, which translates into a probability of 79%. In the case of PHL 457, an inclination higher than 21° is required and the

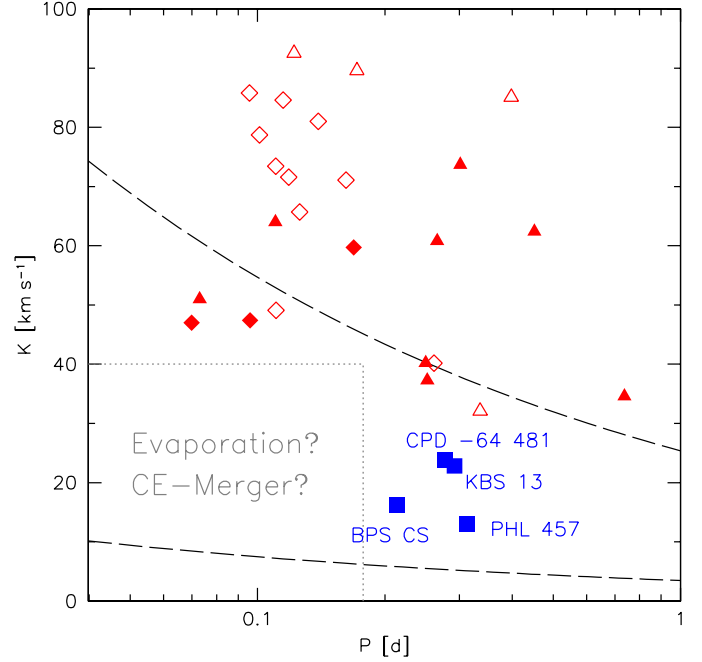


Fig. 4. The RV semi-amplitudes of all known sdB binaries with reflection effects and spectroscopic solutions plotted against their orbital periods (Kupfer et al., in prep.). Diamonds mark eclipsing sdB binaries of HW Vir type where the companion mass is well constrained, triangles systems without eclipses, where only lower limit can be derived for the companion masses. Squares mark CPD-64°481, PHL 457, KBS 13 and BPS CS 22169–0001. Open symbols mark systems that have been discovered based on photometry, filled symbols have been discovered based on spectroscopy. The dashed lines mark the regions to the right where the minimum companion masses derived from the binary mass function (assuming $0.47 M_{\odot}$ for the sdBs) exceed $0.01 M_{\odot}$ (lower curve) and $0.08 M_{\odot}$ (upper curve).

probability for the companion to be a brown dwarf is as high as 94%. We therefore conclude that the cool companions in those two binary systems are likely brown dwarfs.

The only chance to constrain the inclination better would be very high S/N lightcurves. Moreover, high resolution, high S/N spectra could help to constrain the mass ratio of the system. They could allow to discover emission lines from the irradiated hemisphere of the companion, as done for the sdOB+dM system AA Dor (Vučković et al. 2008). The strength of the emission lines should be independent of the inclination, depending only on the size of the companion, the separation of the system and the effective temperature of the primary. As the systems are very bright, it might be possible to find these emission lines despite the larger separation and lower effective temperature of our systems.

5. Discussion

Figure 4 gives an overview of the 29 sdB binaries with reflection effect and known orbital parameters (Kupfer et al., in prep.). While most companions are late M-dwarfs with masses close to $\sim 0.1 M_{\odot}$, there is no sharp drop below the hydrogen-burning limit. The fraction of close substellar companions is substantial. An obvious feature in Fig. 4 is the lack of binaries with periods shorter than ~ 0.2 d and $K < 50 \text{ km s}^{-1}$ corresponding to companion masses of less than $\sim 0.06 M_{\odot}$.

This feature could not be due to selection effects. About half of the known reflection effect binaries have been found based on RV-shifts detected in time-resolved spectra. As has been shown

in this work, RV-semiamplitudes of a few tens of km s^{-1} are easily measurable. Furthermore, short-period binaries are found and solved easier than long-period systems.

The other half of the sample has been discovered based on variations in their light curves. Shape and amplitude of the light curves depend mostly on the radius of the companion for similar orbital periods and separations. Since the radii of late M-dwarfs, brown dwarfs and also Jupiter-size planets are very similar ($\sim 0.1 R_{\odot}$), their light curves are expected to be very similar as well.

The most likely reason for this gap is the merger or evaporation of low-mass companions either before or after the CE-ejection corresponding to a population of single sdB stars. Other recent discoveries are perfectly consistent with this scenario. Charpinet et al. (2011) reported the discovery of two Earth-sized bodies orbiting a single pulsating sdB within a few hours. These might be the remnants of a more massive companion evaporated in the CE-phase (Bear & Soker 2012). Geier et al. (2011b, 2013b) found two fast rotating single sdBs, which might have formed in a CE-merger. Those discoveries provide further evidence that substellar companions play an important role in the formation of close binary and likely also single sdB stars.

We therefore conclude that the lack of short period systems with small RV variations $K < 50 \text{ km s}^{-1}$ is real. However, the probability that substellar companions are present in systems with longer periods ($> 0.2 \text{ d}$) is quite high. In addition to the two binaries discussed here, two more systems with similar orbital parameters and reflection effects have been found (KBS 13, For et al. 2008; BPS CS 22169–0001, Geier et al. 2012). Following the line of arguments outlined above, we calculate the probability for those two systems to host a stellar companion to be 9% for BPS CS 22169–0001 and 20% for KBS 13. Multiplying those numbers for all four binaries, we conclude that the probability that none of them has a substellar companions is less than 0.02%.

Acknowledgements. Based on observations at the La Silla Observatory of the European Southern Observatory for programmes number 073.D-0495(A), 074.B-455(A) and 086.D-0714(A). This paper uses observations made at the South African Astronomical Observatory (SAAO). V.S. acknowledges funding by the Deutsches Zentrum für Luft- und Raumfahrt (grant 50 OR 1110) and by the Erika-Giehl-Stiftung.

References

- Bear, E., & Soker, N. 2012, ApJ, 749, L14
 Blanchette, J.-P., Chayer, P., Wesemael, F., et al. 2008, ApJ, 678, 1329

- Chabrier, G., & Baraffe, I. 1997, A&A, 327, 1039
 Chabrier, G., Baraffe, I., Allard, F., & Hauschildt, P. 2000, ApJ, 542, 464
 Charpinet, S., Fontaine, G., Brassard, P., et al. 2011, Nature, 480, 496
 Classen, L., Geier, S., Heber, U., & O’Toole, S. J. 2011, AIP Conf. Ser., 1331, 297
 Drechsel, H., Haas, S., Lorenz, R., & Gayler, S. 1995, A&A, 294, 723
 Edelmann, H., Heber, U., Altmann, M., Karl, C., & Lisker, T. 2005, A&A, 442, 1023
 Fontaine, G., Brassard, P., Charpinet, S., et al. 2012, A&A, 539, A12
 For, B.-Q., Edelmann, H., Green, E. M., et al. 2008, ASP Conf. Ser., 392, 203
 Geier, S., Heber, U., Podsiadlowski, Ph., et al. 2010, A&A, 519, A25
 Geier, S., Hirsch, H., Tillich, A., et al. 2011a, A&A, 530, A28
 Geier, S., Classen, L., & Heber, U. 2011b, ApJ, 733, 13
 Geier, S., Maxted, P. F. L., Napiwotzki, R., et al. 2011c, A&A, 526, A39
 Geier, S., Schaffenroth, V., Drechsel, H., et al. 2011d, ApJ, 731, L22
 Geier, S., Classen, L., Brünner, P., et al. 2012, ASP Conf. Ser., 452, 153
 Geier, S., Heber, U., Edelmann, H., et al. 2013a, A&A, 557, A122
 Geier, S., Heber, U., Heuser, C., et al. 2013b, A&A, 551, A4
 Gray, D. F. 1992, The observation and analysis of stellar photospheres, 2nd edn. (Cambridge: University Press)
 Han Z., Podsiadlowski P., Maxted P. F. L., Marsh T. R., & Ivanova N. 2002, MNRAS, 336, 449
 Han, Z., Podsiadlowski, P., Maxted, P. F. L., & Marsh, T. R. 2003, MNRAS, 341, 669
 Heber, U. 1986, A&A, 155, 33
 Heber, U. 2009, ARA&A, 47, 211
 Hirsch, H. 2009, Ph.D. Thesis, Friedrich Alexander University Erlangen-Nuernberg
 Horner, J., Wittenmyer, R., Hinse, T. et al. 2014, The peer-reviewed proceedings of the 13th annual Australian Space Science Conf., accepted [[arXiv:1401.6742H](https://arxiv.org/abs/1401.6742H)]
 Ivanova, N., Justham, S., Chen, X., et al. 2013, A&ARv, 21, 59
 Lisker, T., Heber, U., Napiwotzki, R., et al. 2005, A&A, 430, 223
 Lutz, R., Schuh, S., & Silvotti, R. 2012, Astron. Nachr., 333, 1099
 Maxted, P. F. L., Heber, U., Marsh, T. R., & North, R. C. 2001, MNRAS, 326, 139
 Maxted, P. F. L., Napiwotzki, R., Dobbie, P. D., & Burleigh, M. R. 2006, Nature, 442, 543
 Napiwotzki, R., Karl, C., Lisker, T., et al. 2004a, Ap&SS, 291, 321
 Napiwotzki, R., Yungelson, L., Nelemans, G. et al. 2004b, ASP Conf. Ser., 318, 402
 Nelemans, G., & Tauris, T. M. 1998, A&A, 335, L85
 Østensen, R. H., Geier, S., Schaffenroth, V., et al. 2013, A&A, 559, A35
 Pablo, H., Kawaler, S. D., & Green, E. M. 2011, ApJ, 740, L47
 Pablo, H., Kawaler, S. D., Reed, M. D., et al. 2012, MNRAS, 422, 1343
 Schaffenroth, V., Geier, S., Drechsel, H., et al. 2013, A&A, 553, A18
 Schaffenroth, V., Geier, S., Heber, U., et al. 2014, A&A, 564, A98
 Schechter, P. L., Mateo, M., & Saha, A. 1993, PASP, 105, 1342
 Silvotti, R., Schuh, S., Janulis, R., et al. 2007, Nature, 449, 189
 Soker, N. 1998, AJ, 116, 1308
 Wittenmyer, Robert A., Horner, J., Marshall, J. P. 2013, MNRAS, 431, 2150
 Zorotovic, M., & Schreiber, M. R. 2013, A&A, 549, A95

Appendix A: Radial velocities

Table A.2. PHL 457.

Table A.1. CPD-64°481.

mid-HJD -2 450 000	RV [km s ⁻¹]
3249.89041	70.87 ± 0.15
3250.89408	114.58 ± 0.20
3251.85033	69.81 ± 0.16
3252.88158	94.51 ± 0.26
3252.89956	85.03 ± 0.20
3253.83281	82.69 ± 0.22
3253.87777	105.90 ± 0.13
3253.91205	116.47 ± 0.16
3425.51834	111.76 ± 0.15
3426.51685	69.48 ± 0.09
3427.53343	106.65 ± 0.09
3428.52983	93.84 ± 0.12
3429.51370	86.71 ± 0.13
3430.56510	113.59 ± 0.12
3431.52045	70.33 ± 0.12

Notes. All spectra were acquired with the FEROS instrument.

mid-HJD -2 450 000	RV [km s ⁻¹]
3249.64149	10.1 ± 0.2
3250.64322	22.2 ± 0.2
3251.58746	23.8 ± 0.3
3253.56948	29.4 ± 0.3
5500.52235	15.1 ± 0.2
5500.54504	9.7 ± 0.5
5501.52731	8.4 ± 0.2
5501.53727	9.1 ± 0.3
5501.54722	9.3 ± 0.2
5501.55718	11.0 ± 0.1
5501.56712	14.1 ± 0.2
5501.57705	16.4 ± 0.2
5501.58698	17.2 ± 0.2
5501.59692	21.1 ± 0.3
5501.60685	22.2 ± 0.8
5502.50148	13.0 ± 0.4
5502.51028	13.9 ± 0.2
5502.51908	16.1 ± 0.3
5502.52785	18.5 ± 0.3
5502.53663	21.8 ± 0.3
5502.54542	23.4 ± 0.3
5502.55420	24.3 ± 0.3
5502.56298	28.4 ± 0.3
5502.57175	30.9 ± 0.3
5502.58053	31.0 ± 0.4
5502.58932	31.3 ± 0.4
5502.59811	33.2 ± 0.4
5502.60688	34.8 ± 0.4
5502.61566	34.1 ± 0.4
5502.62502	32.7 ± 0.3

Notes. All spectra were acquired with the FEROS instrument.

Binaries discovered by the MUCHFUSS project

SDSS J162256.66+473051.1: An eclipsing subdwarf B binary with a brown dwarf companion[★]

V. Schaffenroth^{1,2}, S. Geier^{3,1}, U. Heber¹, T. Kupfer⁴, E. Ziegerer¹, C. Heuser¹, L. Classen¹, and O. Cordes⁵

¹ Dr. Remeis-Observatory & ECAP, Astronomical Institute, Friedrich-Alexander University Erlangen-Nürnberg, Sternwartstr. 7, 96049 Bamberg, Germany

e-mail: veronika.schaffenroth@sternwarte.uni-erlangen.de

² Institute for Astro- and Particle Physics, University of Innsbruck, Technikerstr. 25/8, 6020 Innsbruck, Austria

³ European Southern Observatory, Karl-Schwarzschild-Str. 2, 85748 Garching, Germany

⁴ Department of Astrophysics/IMAPP, Radboud University Nijmegen, PO Box 9010, 6500 GL Nijmegen, The Netherlands

⁵ Argelander Institute for Astronomy, Auf dem Hügel 71, 53121 Bonn, Germany

Received 7 January 2014 / Accepted 19 February 2014

ABSTRACT

Hot subdwarf B stars (sdBs) are core helium-burning stars located on the extreme horizontal branch. About half of the known sdB stars are found in close binaries. Their short orbital periods of 1.2 h to a few days suggest that they are post common-envelope systems. Eclipsing hot subdwarf binaries are rare but are important in determining the fundamental stellar parameters. Low-mass companions are identified by the reflection effect. In most cases, the companion is a main sequence star near the stellar mass limit.

Here, we report the discovery of an eclipsing hot subdwarf binary SDSS J162256.66+473051.1 (J1622) with very short orbital period (0.0697 d), which has been found in the course of the MUCHFUSS project. The lightcurve shows grazing eclipses and a prominent reflection effect. An analysis of the light- and radial velocity (RV) curves indicated a mass ratio of $q = 0.1325$, an RV semi-amplitude $K = 47.2 \text{ km s}^{-1}$, and an inclination of $i = 72.33^\circ$. We show that a companion mass of $0.064 M_\odot$, which is well below the hydrogen-burning limit, is the most plausible solution, which implies a mass close to the canonical mass ($0.47 M_\odot$) of the sdB star. Therefore, the companion is a brown dwarf, which has not only survived the engulfment by the red-giant envelope but also triggered its ejection and enabled the sdB star to form.

The rotation of J1622 is expected to be tidally locked to the orbit. However, J1622 rotates too slowly ($v_{\text{rot}} = 74.5 \pm 7 \text{ km s}^{-1}$) to be synchronized, challenging tidal interaction models.

Key words. subdwarfs – binaries: eclipsing – binaries: spectroscopic – brown dwarfs – stars: fundamental parameters – stars: individual: SDSS J162256.66+473051.1

1. Introduction

Hot subdwarfs (sdBs) are core helium-burning stars with very thin hydrogen envelopes that are not able to sustain hydrogen-shell burning (Heber 2009). To form such objects, the progenitor has to lose almost all of its hydrogen envelope. The high percentage of 50% of close binaries (Maxted et al. 2001; Napiwotzki et al. 2004) suggests that these sdBs are formed via binary evolution, which is responsible for the required large mass loss on the red giant branch (RGB). These sdB binaries are formed via a common envelope phase or by stable Roche lobe overflow. The other half of sdB stars, however, appears to be single. Hence, binary evolution seems to be irrelevant at first glance. Nevertheless, is it possible to form a single star through merging of the components of a binary star. To form a helium core burning object like an sdB star, two helium white dwarfs need to merge and ignite helium burning. The binary components are driven into a merger by gravitational wave radiation (Webbink 1984; Iben & Tutukov 1984). The merged object is expected to rotate rapidly. However, rotation velocities of single sdB stars

are very slow ($\leq 10 \text{ km s}^{-1}$, Geier & Heber 2012), which is in contradiction with the merger scenario. Therefore, the merger scenario may explain a few cases of exceptionally fast rotators (Geier et al. 2011a, 2013). Moreover, binary population synthesis predicts a wide mass distribution around $0.52 M_\odot$ for the sdBs, which result from the merger channel (Han et al. 2002, 2003). The empirical mass distribution derived by asteroseismology (Fontaine et al. 2012; Van Grootel et al. 2013b), however, shows a sharp peak at $0.47 M_\odot$ for single sdB stars, which is inconsistent with the prediction of the merger scenario.

An alternative scenario proposes the engulfment and possible destruction of a substellar object within a common envelope (CE) as formation channel for single sdB stars (Soker 1998; Nelemans & Tauris 1998). Close binary sdB stars with very low-mass stellar companions are known for decades (Kilkenny et al. 1978; Menzies & Marang 1986). When eclipsing, such systems are named HW Vir stars. Most of the dozen known HW Vir systems have periods as short as 0.1 days. Hence, they must have undergone a common envelope and spiral-in phase. Binary population synthesis shows that sdBs in these post-common envelope systems should have masses around $0.47 M_\odot$, also known as canonical mass (Han et al. 2002, 2003). The

[★] Appendix A is available in electronic form at <http://www.aanda.org>

companions in HW Vir type binaries have masses close to, but usually exceeding the nuclear-burning limit of $\approx 0.08 M_{\odot}$, and are, therefore, very late M-dwarf stars.

Whether a substellar companion would also be able to contribute enough energy and angular momentum to unbind a common envelope has been under debate. The discovery of a brown dwarf orbiting an sdB star in the HW Vir type binary SDSS J082053.53+000843.4 demonstrated that substellar companions are able to form an sdB (Geier et al. 2011d). The subsequent discoveries of two Earth-sized bodies orbiting a single pulsating sdB, which might be the remnants of one or two more massive companion evaporated in the CE-phase (Charpinet et al. 2011; Bear & Soker 2012), provide further evidence that substellar companions play an important role in the formation of close binary and single sdB stars alike. One of the open questions is, how massive the companion has to be to trigger the mass loss of the red giant to form an sdB star.

Here, we report on the discovery of a short period eclipsing hot subdwarf binary with a substellar companion in the course of the MUCHFUSS project. The project, Massive Unseen Companions to Hot Faint Underluminous Stars from SDSS (MUCHFUSS), aims to find sdBs with compact companions, such as massive white dwarfs ($M > 1.0 M_{\odot}$), neutron stars, or black holes. Details about target selection and the scope of the project can be found in Geier et al. (2011b). As one of two selection criteria, sdBs with radial velocity (RV) variations on timescales of half an hour or less were selected from the Sloan Digital Sky Survey (SDSS). These targets are either sdBs with compact, massive companions and comparatively long orbital periods, or short-period binaries with low-mass companions, such as the system described here.

To distinguish low-mass stellar or substellar companions from white dwarfs and other more compact objects, we also started a photometric follow-up. As HW Vir systems have characteristic lightcurves, this turned out to be the ideal approach to find such binaries. A low-mass, cool companion can be identified due to the so-called reflection effect, which results from the large difference in temperature of both components. The companion is heated up on one side, and, therefore, a sinusoidal variation of the flux with the phase can be observed, as the heated hemisphere emits more flux. This effect is also visible at rather low inclinations, where no eclipses are observed. If eclipses are present, a combined spectroscopic and photometric analysis allows us to put tight constraints on the binary parameters. In the course of the MUCHFUSS project, we already discovered three new HW Vir systems (Geier et al. 2011d; Schaffenroth et al. 2013a) and a pulsating sdB in a reflection-effect binary (Østensen et al. 2013).

In this paper, we present the observations and analysis of a HW Vir star, discovered by the MUCHFUSS project. We describe the spectroscopic and photometric observations in Sect. 2 and their analysis in Sects. 3 (spectroscopy) and 4 (photometry). Evidence for the brown dwarf nature of the companion is given in Sect. 5 and the lack of synchronisation of the sdB star is discussed in Sect. 6. Finally, we conclude and present suggestions on how to improve the mass determination.

2. Observations

2.1. Spectroscopy

The SDSS spectra of SDSS J162256.66+473051.1 (J1622 for short, also known as PG 1621+476, $g' = 15.96$ mag) showed a radial velocity shift of 100 km s^{-1} within 1.45 h. Therefore,

the star was selected as a high priority target for follow-up. The 18 spectra were taken with the ISIS instrument at the *William Herschel* Telescope on La Palma, from 24 to 27 August 2009 at medium resolution ($R \sim 4000$). Additional 64 spectra with the same resolution were obtained with the TWIN spectrograph at the 3.5 m telescope at the Calar Alto Observatory, Spain, from 25 to 28 May 2012. Moreover, ten higher resolution spectra ($R \sim 8000$) were observed with ESI at the Keck Telescope, Hawaii, on 13 July 2013. The TWIN and ISIS data were reduced with the MIDAS package distributed by the European Southern Observatory (ESO). The ESI data was reduced with the pipeline Makee¹.

2.2. Photometry

When the RV-curve from the ISIS spectra showed a short period of only 0.069 d, a photometric follow-up was started. The object J1622 was observed with the Bonn University Simultaneous Camera (BUSCA) at the 2.2 m telescope at the Calar Alto Observatory. The instrument BUSCA (Reif et al. 1999) can observe in four bands simultaneously. We did not use any filters but we used instead the intrinsic transmission curve given by the beam splitters, which divides the visible light into four bands U_B , B_B , R_B , and I_B (and means no light loss). Four sets of lightcurves, each covering one orbit of J1622, were obtained on 12 June 2010, 29 September 2010, 28 February 2011, and 1 June 2011. They were reduced by using the aperture photometry package of IRAF. As the comparison stars have different spectral types, we observed a long-term trend in the lightcurve with changing air mass due to the different wavelength dependency of atmospheric extinction, which cannot be corrected.

3. Spectroscopic analysis

3.1. Radial velocity curve

The radial velocities were measured by fitting a combination of Gaussians, Lorentzians, and polynomials to the Balmer and helium lines of all spectra and are given in Table A1. Since the phase-shift between primary and secondary eclipses in the phased lightcurve (see Fig. 1) is exactly 0.5, we know that the orbit of J1622 is circular. Therefore, sine curves were fitted to the RV data points in fine steps over a range of test periods. For each period, the χ^2 of the best-fit sine curve was determined (see Geier et al. 2011c). All three datasets were fit together. The orbit is well covered. Figure 2 shows the phased RV curve with the fit of the best solution. It gives a semi-amplitude of $K = 47.2 \pm 2.0 \text{ km s}^{-1}$, a system velocity of $\gamma = -54.7 \pm 1.5 \text{ km s}^{-1}$, and a period of 0.0696859 ± 0.00003 d. The period is consistent with the period from the photometry (see Sect. 4) and is the second shortest ever measured for an sdB binary.

3.2. Atmospheric parameters

The atmospheric parameters were determined by fitting synthetic spectra, which were calculated using local thermodynamical equilibrium model atmospheres with solar metallicity and metal line blanketing (Heber et al. 2000), to the Balmer and helium lines using SPAS (Hirsch 2009). For some of the HW Vir stars and similar non-eclipsing systems, it was found that the atmospheric parameters seemed to vary with the phase

¹ http://www.astro.caltech.edu/~tb/ipac_staff/tab/makee/

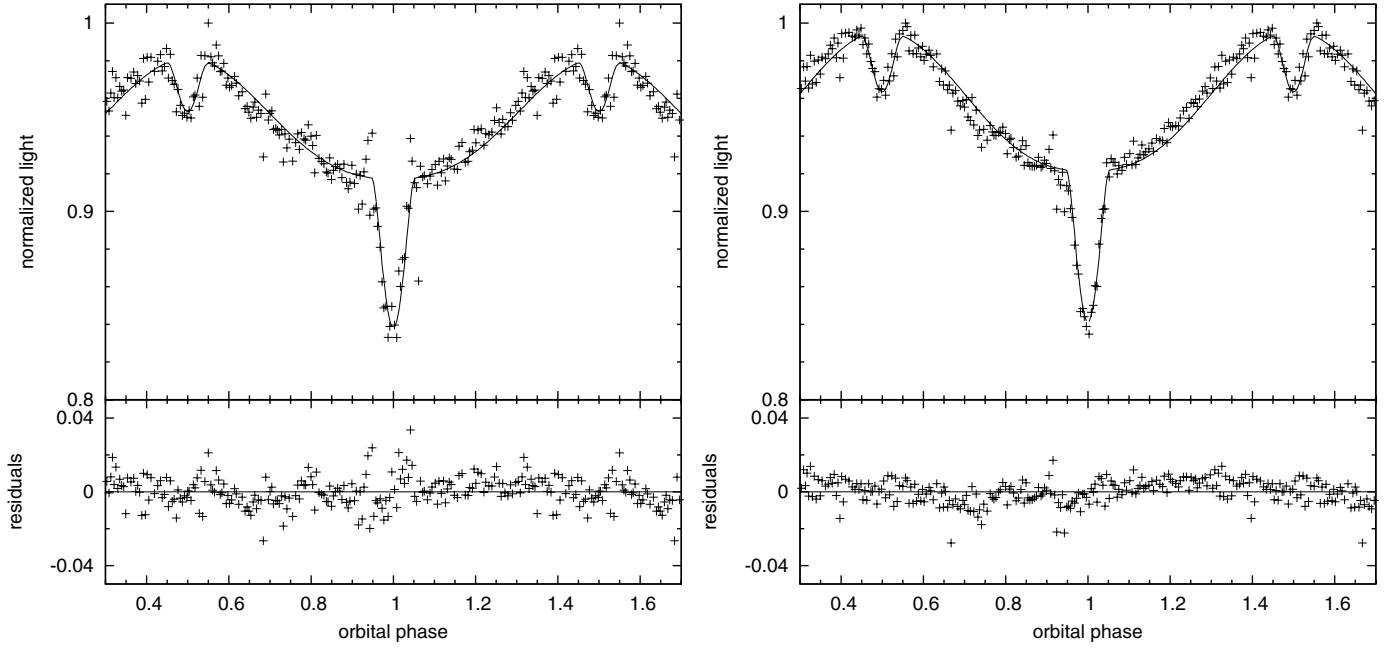


Fig. 1. Phased BUSCA lightcurve in B_B and R_B of J1622. The solid line demonstrates the best-fit model. In the *bottom panel*, the residuals can be seen.

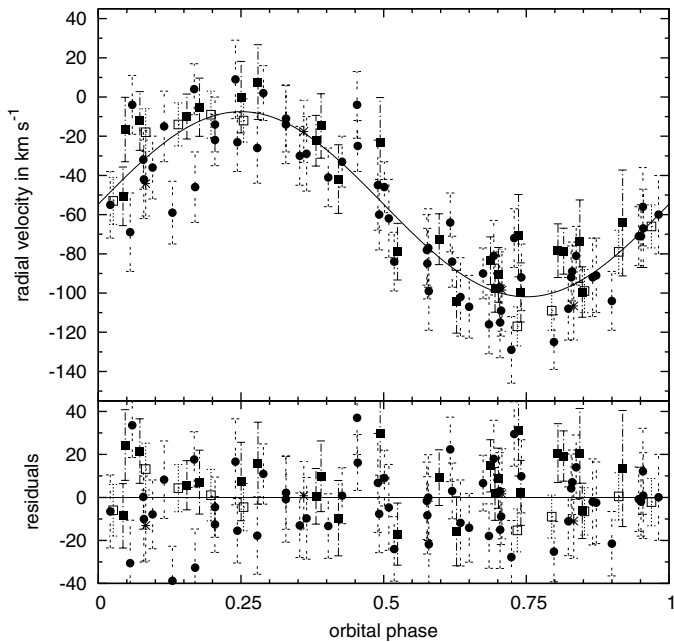


Fig. 2. Radial velocity plotted against orbital phase of J1622. The radial velocity was determined from the SDSS, ISIS, TWIN, and ESI spectra. All spectra were fitted together. The stars mark the SDSS spectra, the dots the TWIN spectra, the filled squares the ISIS spectra, and the open squares the ESI spectra. The errors are formal 1σ uncertainties. The lower panel shows the residuals.

(e.g. Schaffenroth et al. 2013b), as the contribution of the companion to the spectrum varies with the phase. Therefore, all spectra were fit separately. Figure 3 shows the effective temperature and the surface gravity determined from the TWIN spectra plotted against orbital phase. No change with the orbital phase can be seen. Therefore, we co-added all 64 TWIN spectra and derived the atmospheric parameters ($T_{\text{eff}} = 29\,000 \pm 600$ K, $\log g = 5.65 \pm 0.06$, $\log y = -1.87 \pm 0.05$). In Fig. 4 the best

fit to the Balmer and helium lines of the co-added spectrum is shown.

In Fig. 5, the position of J1622 in the $T_{\text{eff}}\text{-}\log g$ diagram is compared to those of the known HW Vir systems and other sdB binaries. It is worthwhile to note that all of the HW Vir systems, but two, which have evolved off the EHB, have very similar atmospheric parameters. Those systems cluster in a distinct region of the $T_{\text{eff}}\text{-}\log g$ diagram. Unlike the HW Vir stars, other sdB binaries are distributed more or less uniformly across the extreme horizontal branch (see Fig. 5). In this respect, J1622 turns out to be a typical HW Vir system.

Due to their higher resolution, the ESI spectra are suitable to measure the rotational broadening of spectral lines of the sdB. We co-added all 10 spectra and determined the projected rotational velocity of the sdB primary by adding a rotational profile to the fit of the Balmer and helium lines. The other atmospheric parameters were kept fixed to the values determined from the TWIN spectra. The best fit for $v_{\text{rot}} \sin i = 71 \pm 7$ km s $^{-1}$ is displayed in Fig. 6. Surprisingly, the projected rotational velocity is only about two thirds of the one expected for tidally locked rotation of the hot subdwarf primary. This issue is further discussed in Sect. 6.

4. Photometric analysis

The BUSCA lightcurves clearly show a strong reflection effect and grazing eclipses, as can be seen in Fig. 1. Unfortunately, the signal-to-noise of the U_B and I_B lightcurves is insufficient, so that only the B_B and R_B lightcurves are used for the analysis. The ephemeris was determined from the BUSCA lightcurves by fitting parabolas to the cores of the primary eclipses. The period was derived with the help of the Lomb-Scargle Algorithm (Press & Rybicki 1989).

The ephemeris of the primary minimum is given by $\text{HJD} = 2\,455\,359.58306(2) + 0.0697885(53) \cdot E$ (thereby E is the eclipse number, see Drechsel et al. 2001).

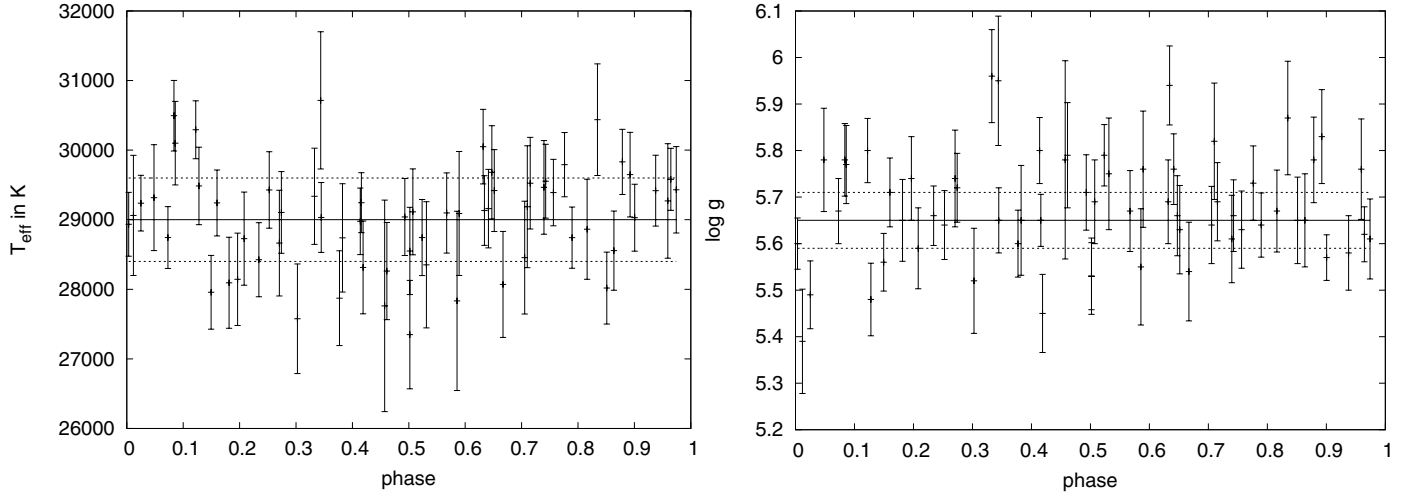


Fig. 3. Effective temperature and surface gravity plotted over the phase of J1622. T_{eff} and $\log g$ were determined from the TWIN spectra. The errors are statistical 1σ errors. The lines represent the parameters from the co-added spectrum with the errors.

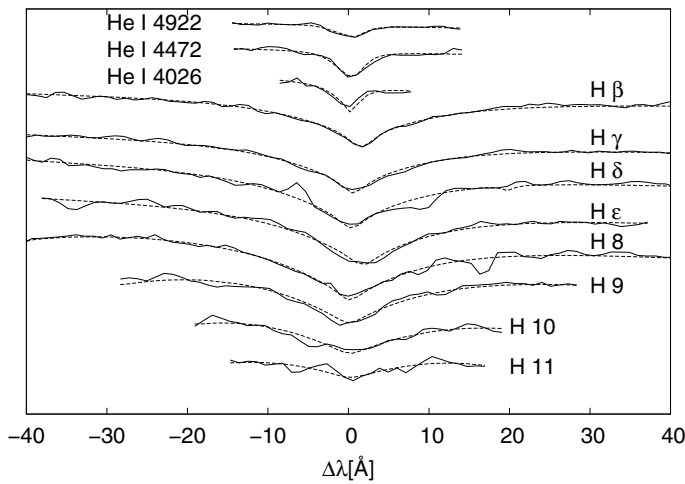


Fig. 4. Fit of the Balmer and helium lines in the co-added TWIN spectrum. The solid line shows the measurement, and the dashed line shows the best fitting synthetic spectrum.

The phased lightcurves are shown in Fig. 1. The lightcurve analysis was performed by using MORO (MODified ROche Program, see Drechsel et al. 1995), which calculates synthetic lightcurves, which were fitted to the observation. This lightcurve solution code is based on the Wilson-Devinney approach (Wilson & Devinney 1971) but uses a modified Roche model that considers the radiative pressure of hot binaries. More details of the analysis method are described in Schaffenroth et al. (2013b).

The main problem of the lightcurve analysis is the high number of parameters. To calculate the synthetic lightcurves, $12 + 5n$ (n is the number of lightcurves) parameters that are not independent are used. Therefore, strong degeneracies exist, in particular in the mass ratio, which is strongly correlated with the other parameters. The mass ratio is, therefore, fixed, and solutions for different mass ratios are calculated. To resolve this degeneracy, it is, moreover, important to constrain as many parameters as possible from the spectroscopic analysis or theory.

From the spectroscopic analysis, we derive the effective temperature and the surface gravity of the sdB primary. Due to the early spectral type of the primary star, the gravity darkening

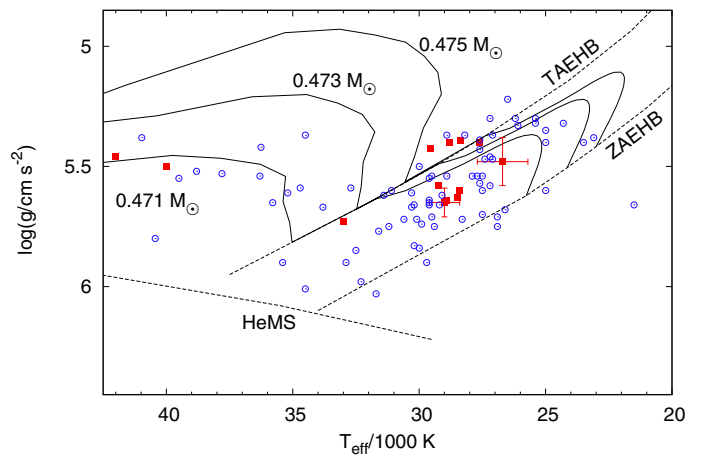


Fig. 5. $T_{\text{eff}} - \log g$ diagram of the HW Vir systems. The solid lines are evolutionary tracks by Dorman et al. (1993) for an sdB mass of 0.471, 0.473, and 0.475 M_{\odot} . The positions of J1622 and J0820 are indicated with crosses. The other squares mark the position of other HW Vir-like systems (Van Grootel et al. 2013a; Drechsel et al. 2001; For et al. 2010; Geier et al. 2011d; Maxted et al. 2002; Klepp & Rauch 2011; Østensen et al. 2008, 2010; Wood & Saffer 1999; Almeida et al. 2012; Barlow et al. 2013). The open dots represent other sdB binaries from the literature.

exponent can be fixed at $g_1 = 1$, as expected for radiative outer envelopes (von Zeipel 1924). For the cool convective companion, g_2 was set to 0.32 (Lucy 1967). The linear limb darkening coefficients were extrapolated from the table of Claret & Bloemen (2011).

To determine the quality of the lightcurve fit, the sum of the deviations from each point to the synthetic curve is calculated, and the solution with the smallest sum is supposed to be the best solution. The difference between the solutions for the different mass ratios is unfortunately small, as expected. Therefore, we cannot determine a unique solution from the lightcurve analysis alone and adopted the solution closest to the canonical mass for the sdB star. The corresponding results of the lightcurve analysis are given in Table 1 with errors determined with the bootstrapping method. The lightcurves in the B_B and R_B band are displayed in Fig. 1 with the best-fit models for these parameters. The apparent asymmetries of the observed lightcurve can not be

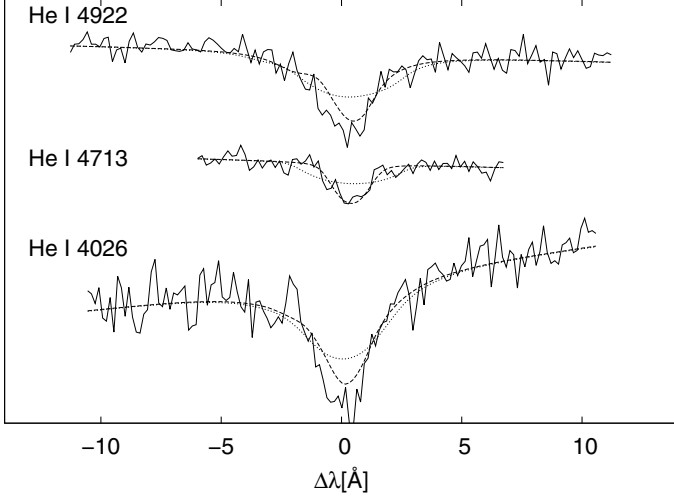


Fig. 6. Fit of the helium lines in the co-added ESI spectrum. The solid line shows the measurement and the dashed line shows the best fitting synthetic spectrum. The dotted line shows the line-broadening, if we assume synchronisation.

Table 1. Adopted lightcurve solution.

Fixed parameters:		
$q (=M_2/M_1)$		0.1325
$T_{\text{eff}}(1)$	[K]	29 000
g_1^b		1.0
g_2^b		0.32
$x_1(B_B)^c$		0.25
$x_1(R_B)^c$		0.20
δ_2^d		0.0
Adjusted parameters:		
i	[°]	72.33 ± 1.11
$T_{\text{eff}}(2)$	[K]	2500 ± 900
A_1^a		1.0 ± 0.03
A_2^a		0.9 ± 0.2
Ω_1^f		3.646 ± 0.17
Ω_2^f		2.359 ± 0.054
$\frac{L_1}{L_1+L_2}(B_B)^g$		0.99996 ± 0.00077
$\frac{L_1}{L_1+L_2}(R_B)^g$		0.99984 ± 0.00247
δ_1		0.001 ± 0.003
$x_2(B_B)$		1.0 ± 0.005
$x_2(R_B)$		1.0 ± 0.005
$l_3(B_B)^f$		0.0
$l_3(R_B)^f$		0.045 ± 0.008
Roche radii ^h :		
$r_1(\text{pole})$	[a]	0.284 ± 0.013
$r_1(\text{point})$	[a]	0.290 ± 0.015
$r_1(\text{side})$	[a]	0.290 ± 0.014
$r_1(\text{back})$	[a]	0.290 ± 0.014
$r_2(\text{pole})$	[a]	0.142 ± 0.009
$r_2(\text{point})$	[a]	0.150 ± 0.011
$r_2(\text{side})$	[a]	0.144 ± 0.009
$r_2(\text{back})$	[a]	0.149 ± 0.011

Notes. ^(a) Bolometric albedo. ^(b) Gravitational darkening exponent. ^(c) Linear limb darkening coefficient; taken from Claret & Bloemen (2011). ^(d) Radiation pressure parameter, see Drechsel et al. (1995). ^(e) Fraction of third light at maximum. ^(f) Roche potentials. ^(g) Relative luminosity; L_2 is not independently adjusted, but recomputed from r_2 and $T_{\text{eff}}(2)$. ^(h) Fractional Roche radii in units of separation of mass centres.

Table 2. Parameters of J1622.

SDSS J162256.66+473051.1		
i	[°]	72.33 ± 1.11
M_{sdB}	[M_{\odot}]	0.48 ± 0.03
M_{comp}	[M_{\odot}]	0.064 ± 0.004
a	[R_{\odot}]	0.58 ± 0.02
R_{sdB}	[R_{\odot}]	0.168 ± 0.007
R_{comp}	[R_{\odot}]	0.085 ± 0.004
$\log g(\text{sdB, phot})$		5.67 ± 0.02
$\log g(\text{sdB, spec})$		5.65 ± 0.06

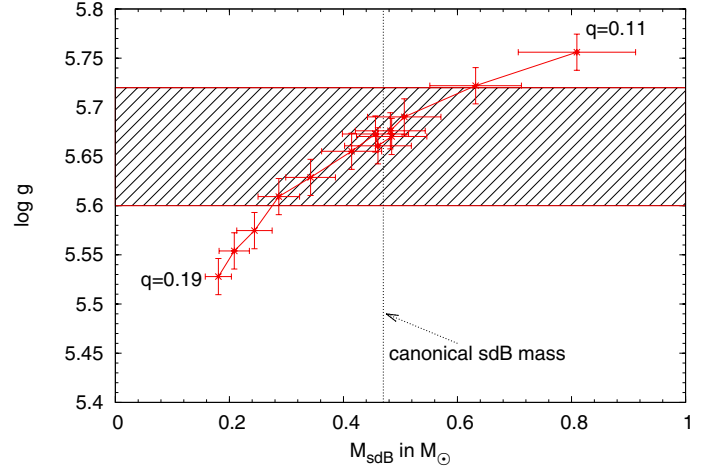


Fig. 7. Comparison of the photometric and spectroscopic surface gravity for the solutions with different mass ratio $q = 0.11$ – 0.19 (marked by the error cross). The spectroscopic surface gravity with uncertainty is given by the shaded area.

modelled, but we are not sure if this effect is real or is due to uncorrected long-term trends in the photometry (see Sect. 2.2). The parameters of the system resulting from the adopted solution with the mass function are summarised in Table 2. The errors result from error propagation of the errors of K , P , and i .

5. The brown dwarf nature of the companion

From the semi-amplitude of the radial velocity curve and the orbital period, we can derive the masses and the radii of both components for each mass ratio. To constrain the solutions further, we first compared the photometric surface gravity, which can be derived from the mass and the radius, to the spectroscopic surface gravity. This is displayed in Fig. 7. The spectroscopic surface gravity is consistent with the lightcurve solution for sdB masses from 0.25 to $0.6 M_{\odot}$. It is, therefore, possible to find a self-consistent solution. This is not at all a matter of course, because gravity derived from photometry was found to be inconsistent with the spectroscopic result in other cases, such as AA Dor (Vučković et al. 2008).

We also compared the radius of the companion to theoretical mass-radius relations for low-mass stars and brown dwarfs with ages of 1, 5, and 10 Gyr, respectively (Baraffe et al. 2003). As can be seen from Fig. 8, the measured mass-radius relation is well matched by theoretical predictions for stars $\gtrsim 3$ Gyr for companion masses between $0.055 M_{\odot}$ and $0.075 M_{\odot}$. The corresponding mass range for the sdB star is from $0.39 M_{\odot}$ to $0.63 M_{\odot}$, which is calculated from the mass ratio.

However, the companion is exposed to intense radiation of a luminous hot star that is only $0.58 R_{\odot}$ away, which could lead

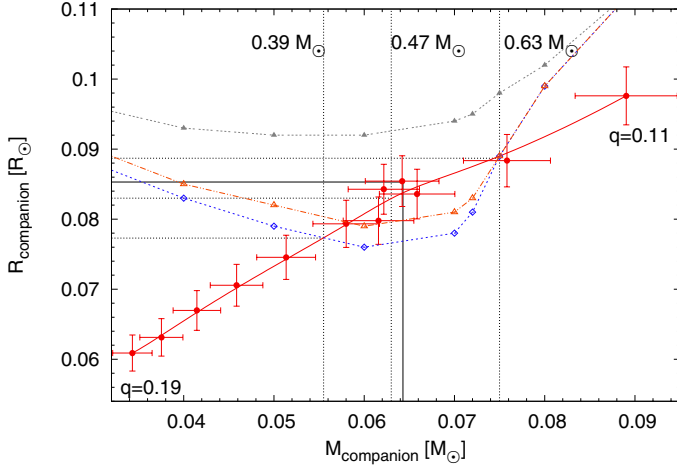


Fig. 8. Comparison of theoretical mass-radius relations of brown dwarfs by Baraffe et al. (2003) for an age of 1 Gyr (filled triangles), 5 Gyr (triangles) and 10 Gyr (diamond) to results from the lightcurve analysis. Each error cross represents a solution from the lightcurve analysis for a different mass ratio ($q = 0.11$ – 0.19). The dashed vertical lines mark different values of the corresponding sdB masses. The solid lines mark the solution closest to the canonical mass for the sdB star of $0.47 M_{\odot}$ that was adopted.

to an underestimate of the radius, if compared to non-irradiated models (Baraffe et al. 2003). Such inflation effects have been found in the case of hot Jupiter exoplanets (e.g. Udalski et al. 2008) but also in the MS+BD binary CoRoT-15b (Bouchy et al. 2011). We can estimate the maximum inflation effect from theoretical mass-radius relations shown in Fig. 8. As can be seen from Fig. 8, inflation by more than 10% can be excluded because none of the theoretical mass-radius relations otherwise would match the measured one, even if the star was as old as 10 Gyr (the age of the Galactic disk).

If we assume an inflation of 5–10%, the mass-radius relation for the companion would be in perfect agreement with the lightcurve solution for a companion with a mass of $0.064 M_{\odot}$ and a radius of $0.085 R_{\odot}$, and an age of ~ 5 – 10 Gyr. The corresponding mass of the sdB is close to the canonical sdB mass, which we therefore adopt for the sdB throughout the rest of the paper. As we calculated solutions for discrete q and, hence, discrete masses for the sdB and the companion, we adopted the solution closest to the canonical mass, which is also marked in Fig. 8.

6. Synchronisation

Most HW Vir systems have orbital separations as small as one solar radius. Hence, it is reasonable to expect that the rotation of both components is tidally locked to the orbit. Indeed the rotation rates of HW Vir and other objects of the class with similarly short periods (0.1d) are found to be synchronised. It is worthwhile to note that the system PG 1017–036, a reflection-effect binary with almost the same parameters as J1622 ($P = 0.072$ d, $K = 51$ km s $^{-1}$, $T_{\text{eff}} = 30\,300$ K, $\log g = 5.61$), has a measured $v_{\text{rot}} \sin i = 118$ km s $^{-1}$ (Maxted et al. 2002), which is fully consistent with synchronised rotation. However, J1622 ($P = 0.0698$ d, $K = 47$ km s $^{-1}$, $T_{\text{eff}} = 29\,000$ K, $\log g = 5.65$) rotates with $v_{\text{rot}} \sin i = 71$ km s $^{-1}$. With an inclination of 72.33° , this results in a rotational velocity of 74 km s $^{-1}$, which is only about two thirds of the rotational velocity expected for a synchronous rotation ($P_{\text{orbit}} = P_{\text{rot}} = \frac{2\pi R}{v_{\text{rot}}}$).

The physical processes leading to synchronisation are not well understood particularly for stars with radiative envelopes, such as sdB stars and rivalling theories (Zahn 1977; Tassoul & Tassoul 1992), predict very different synchronisation timescales (for details see Geier et al. 2010). The synchronisation timescales increase strongly with orbital separation, hence with the orbital period of the system. Actually the objects J1622 and PG 1017–036 have the shortest periods and the highest probability for tidally locked rotation amongst all known HW Vir systems. Therefore, it is surprising that J1622 apparently is not synchronised, while PG 1017–036 is. Calculations in the case of the less efficient mechanism (Zahn 1977) predict that the synchronisation should be established after 10^5 yr, a time span much shorter than the EHB lifetime of 10^8 yr.

Evidence for a non-synchronous rotation of sdB stars in reflection-effect binaries was presented recently by Pablo et al. (2011, 2012), who measured the rotational splittings of pulsation modes in three reflection-effect sdB binaries observed by the *Kepler* space mission, which reveals that the subdwarf primaries rotate more slowly than synchronised. However, those binaries have rather long periods (~ 0.5 d), and predicted synchronisation timescales are much longer than for J1622 and even exceed the EHB life time if the least efficient synchronisation process (see Fig. 19 in Geier et al. 2010) is adopted. Hence, unlike for J1622, the non-synchronisation of those systems is not in contradiction with synchronisation theory.

It is quite unlikely that J1622 is too young for its rotation to be tidally locked to the orbit. Hence, we need to look for an alternative explanation. Tidal forces leading to circularisation and synchronisation may lead to stable configurations, in which the rotational and the orbital periods are in resonance; that is, their ratio is that of integer numbers as observed for Mercury. Comparing the observed rotational period of J1622 to the orbital one, we find that the ratio is 0.607 ± 0.065 , hence close to a 2 to 3 resonance. However, J1622 must have undergone a spiral-in phase through the common-envelope phase and it must be investigated, whether such a resonant configuration can persist through that dynamical phase.

7. Conclusions

We performed a spectroscopic and photometric analysis of the eclipsing hot subdwarf binary J1622, which was found in the course of the MUCHFUSS project. The atmospheric parameters of the primary are typical for an sdB star in a HW Vir system. Mass-radius relations were derived for both components. The mass of the sdB star is constrained from spectroscopy (surface gravity) to $0.28 M_{\odot}$ to $0.64 M_{\odot}$. The mass of the companion can be constrained by theoretical mass-radius relations to lie between $0.055 M_{\odot}$ and $0.075 M_{\odot}$, which implies that the sdB mass is between $0.39 M_{\odot}$ and $0.63 M_{\odot}$.

Assuming small corrections of about 5–10% to the radius due to the inflation of the companion by the strong irradiation from the primary, a companion mass of $0.064 M_{\odot}$ appears to be the most plausible choice that results in a mass of the sdB close to the canonical mass of $0.47 M_{\odot}$ star. Accordingly, the companion is a substellar object. This is the second time that a brown dwarf is found as a close companion to an sdB star. The object J1622 provides further evidence that substellar objects are able to eject a common envelope and form an sdB star. Finding more of these systems helps to constrain theoretical models (Soker 1998; Nelemans & Tauris 1998).

An important result of the spectral analysis is that the sdB star is rotating slower than expected, if its rotation was

locked to its orbit, as observed for the very similar system PG 1017–036. The non-synchronous rotation of J1622 is in contradiction with the predictions of tidal interaction models unless the sdB star is very young. The ratio of the rotational to the orbital period is close to a resonance of 2 to 3. However, it has to be investigated further, if such a configuration can survive the common envelope phase.

Future investigations should aim at the detection of spectral lines from the secondary to measure its radial velocity, which turns the system into an double-lined spectroscopic binary that would allow to pin down the mass ratio. Emission lines of the companion's irradiated atmosphere have been detected in the sdOB system AA Dor (Vučković et al. 2008) and also for the prototype HW Vir (Vučković et al. 2013) most recently. Since J1622 is quite compact and the irradiation of the companion strong, such emission lines might be detectable in high-resolution spectra of sufficient quality. Accurate photometry is needed to confirm or disprove any asymmetries in its lightcurve, which hints at flows at the surface of the companion.

Acknowledgements. Based on observations collected at the Centro Astronómico Hispano Alemán (CAHA), operated jointly by the Max-Planck Institut für Astronomie and the Instituto de Astrofísica de Andalucía (CSIC) with BUSCA at 2.2 m telescope, and with TWIN at the 3.5 m telescope. Based on observations made with the *William Herschel* Telescope operated on the island of La Palma by the Isaac Newton Group in the Spanish Observatorio del Roque de los Muchachos of the Instituto de Astrofísica de Canarias. Based on observations obtained at the W.M. Keck Observatory, which is operated as a scientific partnership among the California Institute of Technology, the University of California, and the National Aeronautics and Space Administration. The Observatory was made possible by the generous financial support of the W.M. Keck Foundation. The authors wish to recognise and acknowledge the very significant cultural role and reverence that the summit of Mauna Kea has always had within the indigenous Hawaiian community. We are most fortunate to have the opportunity to conduct observations from this mountain. V.S. acknowledges funding by the Deutsches Zentrum für Luft- und Raumfahrt (grant 50 OR 1110) and by the Erika-Giehl-Stiftung. T.K. acknowledges support from the Netherlands Research School of Astronomy (NOVA).

References

- Almeida, L. A., Jablonski, F., Tello, J., & Rodrigues, C. V. 2012, *MNRAS*, 423, 478
- Baraffe, I., Chabrier, G., Barman, T. S., Allard, F., & Hauschildt, P. H. 2003, *A&A*, 402, 701
- Barlow, B. N., Kilkenny, D., Drechsel, H., et al. 2013, *MNRAS*, 430, 22
- Bear, E., & Soker, N. 2012, *ApJ*, 749, L14
- Bouchy, F., Deleuil, M., Guillot, T., et al. 2011, *A&A*, 525, A68
- Charpinet, S., Fontaine, G., Brassard, P., et al. 2011, *Nature*, 480, 496
- Claret, A., & Bloemen, S. 2011, *A&A*, 529, A75
- Dorman, B., Rood, R. T., & O'Connell, R. W. 1993, *ApJ*, 419, 596
- Drechsel, H., Haas, S., Lorenz, R., & Gayler, S. 1995, *A&A*, 294, 723
- Drechsel, H., Heber, U., Napiwotzki, R., et al. 2001, *A&A*, 379, 893
- Fontaine, G., Brassard, P., Charpinet, S., et al. 2012, *A&A*, 539, A12
- For, B.-Q., Green, E. M., Fontaine, G., et al. 2010, *ApJ*, 708, 253
- Geier, S., & Heber, U. 2012, *A&A*, 543, A149
- Geier, S., Heber, U., Podsiadlowski, P., et al. 2010, *A&A*, 519, A25
- Geier, S., Classen, L., & Heber, U. 2011a, *ApJ*, 733, L13
- Geier, S., Hirsch, H., Tillich, A., et al. 2011b, *A&A*, 530, A28
- Geier, S., Maxted, P. F. L., Napiwotzki, R., et al. 2011c, *A&A*, 526, A39
- Geier, S., Schaffenroth, V., Drechsel, H., et al. 2011d, *ApJ*, 731, L22
- Geier, S., Heber, U., Heuser, C., et al. 2013, *A&A*, 551, L4
- Han, Z., Podsiadlowski, P., Maxted, P. F. L., Marsh, T. R., & Ivanova, N. 2002, *MNRAS*, 336, 449
- Han, Z., Podsiadlowski, P., Maxted, P. F. L., & Marsh, T. R. 2003, *MNRAS*, 341, 669
- Heber, U. 2009, *ARA&A*, 47, 211
- Heber, U., Reid, I. N., & Werner, K. 2000, *A&A*, 363, 198
- Hirsch, H. 2009, Ph.D. Thesis, Friedrich Alexander Universität Erlangen Nürnberg
- Iben, Jr., I., & Tutukov, A. V. 1984, *ApJS*, 54, 335
- Kilkenny, D., Hilditch, R. W., & Penfold, J. E. 1978, *MNRAS*, 183, 523
- Klepp, S., & Rauch, T. 2011, *A&A*, 531, L7
- Lucy, L. B. 1967, *Zeitschrift für Astrophysik*, 65, 89
- Maxted, P. F. L., Heber, U., Marsh, T. R., & North, R. C. 2001, *MNRAS*, 326, 1391
- Maxted, P. F. L., Marsh, T. R., Heber, U., et al. 2002, *MNRAS*, 333, 231
- Menzies, J. W., & Marang, F. 1986, in *Instrumentation and Research Programmes for Small Telescopes*, eds. J. B. Hearnshaw, & P. L. Cottrell, IAU Symp., 118, 305
- Napiwotzki, R., Karl, C. A., Lisker, T., et al. 2004, *Ap&SS*, 291, 321
- Nelemans, G., & Tauris, T. M. 1998, *A&A*, 335, L85
- Østensen, R. H., Oreiro, R., Hu, H., Drechsel, H., & Heber, U. 2008, in *Hot Subdwarf Stars and Related Objects*, eds. U. Heber, C. S. Jeffery, & R. Napiwotzki, ASP Conf. Ser., 392, 221
- Østensen, R. H., Green, E. M., Bloemen, S., et al. 2010, *MNRAS*, 408, L51
- Østensen, R. H., Geier, S., Schaffenroth, V., et al. 2013, *A&A*, 559, A35
- Pablo, H., Kawaler, S. D., & Green, E. M. 2011, *ApJ*, 740, L47
- Pablo, H., Kawaler, S. D., Reed, M. D., et al. 2012, *MNRAS*, 422, 1343
- Press, W. H., & Rybicki, G. B. 1989, *ApJ*, 338, 277
- Reif, K., Bagnick, K., de Boer, K. S., et al. 1999, in *SPIE Conf. Ser.* 3649, eds. M. M. Blouke, & G. M. Williams, 109
- Schaffenroth, V., Geier, S., Barbu-Barna, I., et al. 2013a, ASP Conf. Ser., in press
- Schaffenroth, V., Geier, S., Drechsel, H., et al. 2013b, *A&A*, 553, A18
- Soker, N. 1998, *AJ*, 116, 1308
- Tassoul, M., & Tassoul, J.-L. 1992, *ApJ*, 395, 604
- Udalski, A., Pont, F., Naef, D., et al. 2008, *A&A*, 482, 299
- Van Grootel, V., Charpinet, S., Brassard, P., Fontaine, G., & Green, E. M. 2013a, *A&A*, 553, A97
- Van Grootel, V., Fontaine, G., Charpinet, S., Brassard, P., & Green, E. M. 2013b, in *Eur. Phys. J. Web Conf.*, 43, 4007
- von Zeipel, H. 1924, *MNRAS*, 84, 665
- Vučković, M., Østensen, R., Bloemen, S., Decoster, I., & Aerts, C. 2008, in *Hot Subdwarf Stars and Related Objects*, eds. U. Heber, C. S. Jeffery, & R. Napiwotzki, ASP Conf. Ser., 392, 199
- Vučković, M., et al. 2013, ASP Conf. Ser., in press
- Webbink, R. F. 1984, *ApJ*, 277, 355
- Wilson, R. E., & Devinney, E. J. 1971, *ApJ*, 166, 605
- Wood, J. H., & Saffer, R. 1999, *MNRAS*, 305, 820
- Zahn, J.-P. 1977, *A&A*, 57, 383

A new bright eclipsing hot subdwarf binary from the ASAS and SuperWASP surveys

V. Schaffenroth^{1,2}, S. Geier^{1,3}, H. Drechsel¹, U. Heber¹, P. Wils⁴, R. H. Østensen⁵, P. F. L. Maxted⁶, and G. di Scala⁷

¹ Dr. Reimis-Observatory & ECAP, Astronomical Institute, Friedrich-Alexander University Erlangen-Nürnberg, Sternwartstr. 7, 96049 Bamberg, Germany

e-mail: veronika.schaffenroth@sternwarte.uni-erlangen.de

² Institute for Astro- and Particle Physics, University of Innsbruck, Technikerstr. 25/8, 6020 Innsbruck, Austria

³ European Southern Observatory, Karl-Schwarzschild-Str. 2, 85748 Garching, Germany

⁴ Vereniging voor Sterrenkunde, Belgium

⁵ Institute of Astronomy, KU Leuven, Celestijnenlaan 200D, 3001 Heverlee, Belgium

⁶ Astrophysics Group, Keele University, Staffordshire, ST5 5BG, UK

⁷ Carnes Hill Observatory, 34 Perisher St., 2171 Horningsea Park, NSW, Sydney, Australia

Received 14 December 2012 / Accepted 1 March 2013

ABSTRACT

We report the discovery of a bright ($m_V = 11.6$ mag), eclipsing, hot subdwarf binary of spectral type B with a late main sequence companion from the All Sky Automated Survey (ASAS 102322-3737.0). Such systems are called HW Vir stars after the prototype. The lightcurve shows a grazing eclipse and a strong reflection effect. An orbital period of $P = 0.13927$ d, an inclination of $i = 65.86^\circ$, a mass ratio $q = 0.34$, a radial velocity semiamplitude $K_1 = 81.0$ km s⁻¹, and other parameters were derived from a combined spectroscopic and photometric analysis. The short period can only be explained by a common envelope origin of the system. The atmospheric parameters ($T_{\text{eff}} = 28\,400$ K, $\log g = 5.60$) are consistent with a core helium-burning star located on the extreme horizontal branch. In agreement with that we derived the most likely sdB mass to be $M_{\text{sdB}} = 0.46 M_\odot$, close to the canonical mass of such objects. The companion is a late M-dwarf with a mass of $M_{\text{comp}} = 0.16 M_\odot$. ASAS 102322-3737.0 is the third brightest of only 12 known HW Virginis systems, which makes it an ideal target for detailed spectroscopic studies and long-term photometric monitoring to search for period variations, e.g., those caused by a substellar companion.

Key words. subdwarfs – binaries: eclipsing – binaries: spectroscopic – stars: early-type – stars: fundamental parameters – stars: individual: ASAS 102322-3737.0

1. Introduction

Hot subdwarf stars (sdB) are evolved, compact stars found in the disk and halo of our Galaxy. They dominate the population of faint blue stars. Especially in the context of Galaxy evolution, sdBs are important because they are believed to be the dominant source of the “UV upturn phenomenon” which is observed in elliptical galaxies (Brown et al. 1997, 2000). Subdwarf B stars are core helium-burning stars on the extreme horizontal branch (EHB). They have very thin hydrogen envelopes (Saffer et al. 1994; Heber 1986) that avoid hydrogen shell-burning. Therefore they evolve from the EHB directly to white dwarfs (Dorman et al. 1993).

The formation of sdBs requires an extraordinarily high mass loss on the red-giant branch (RGB). About half of the sdB stars are found in close binaries with periods from ~ 0.05 to 30 d (e.g. Maxted et al. 2001; Napiwotzki et al. 2004; Geier et al. 2012; Vennes et al. 2012). Mass transfer must therefore play an important role in the formation of these stars. In their binary evolution studies, Han et al. (2002, 2003) found that common-envelope evolution, resulting from dynamically unstable mass transfer near the tip of the RGB, should produce such short-period binaries ($P = 0.1$ –10 d). The most probable mass for such sdBs is $0.47 M_\odot$ (Han et al. 2003), which is called the canonical mass.

Eclipsing post-common envelope binaries that consist of sdBs and late M star companions with periods of about 2–3 h are called HW Vir systems after the prototype. Such systems are of high value because it is possible to derive the mass of the sdB, as well as the mass and the nature of the companion, from a combined analysis of time-resolved spectra and the lightcurve. These systems are rare but can easily be recognized by the prominent reflection effect, which is the only contribution of the companion to the optical light. Until now only twelve such systems have been known. Interest in HW Virginis systems has been revived by the discovery of substellar companions to the prototype HW Virginis (Lee et al. 2009) and HS 0705 (Qian et al. 2009) via the light-travel time method (for an up-to-date census see Zorotovic & Schreiber 2013). For this method a long-term photometric monitoring for several years is necessary.

ASAS 102322-3737.0 (ASAS 10232 for short) was discovered as a variable star in the course of the All Sky Automated Survey by Pojmanski (2003), but misclassified as a δ Scuti star. In 2007 this system was found in the ASAS Survey by P. W. and recognized as an HW Virginis system. Another lightcurve was obtained at the Carnes Hill Observatory, Sydney, in March 2008. *BVRI* photometry was taken with the *Euler* telescope on La Silla in April 2008, confirming the presence of an eclipse. In the SuperWASP survey (Pollacco et al. 2006), this system was

also observed in several runs. ASAS 10232 is the third brightest HW Vir system with $m_V = 11.6$ mag, which makes it well suited for follow-up observations.

2. Observations

2.1. Photometry

Observations of ASAS 10232 were taken in the nights of the 10, 11, 12, 13, and 31 March 2008 in the B , V , and I band with a 12" LX200 GPS Schmidt-Cassegrain Telescope at the Carnes Hill Observatory in Sydney, Australia. More lightcurves in BVRI were taken with the 1.2-m *Leonhard Euler* Telescope at the La Silla Observatory, Chile, in the nights of the 23 and 25 April 2008. Moreover, a lightcurve of this system was observed with the robotic SuperWASP telescope at the South African Astronomical Observatory in three runs from May 2006 to January 2009. A broad band filter (400–800 nm) was used for this observation.

2.2. Spectroscopy

Fifteen medium-resolution spectra ($R = 3400$) of ASAS 10232 with exposure times of 70 s were obtained with the EMMI spectrograph at the ESO-NTT Telescope in La Silla, Chile, from the 11 to 14 January 2008. These spectra cover only a small part of the optical spectrum (3900–4360 Å) and are well suited to radial velocity work, but not to determining the atmospheric parameters. Another 33 spectra ($R \sim 1750$, 3800–6540 Å) were thus obtained on the 20 and 25 February 2010 with the GMOS spectrograph mounted at the 8.1 m Gemini South telescope at Cerro Pachón Observatory in service mode with an exposure time between 100 and 300 s. The EMMI data were reduced with the MIDAS package distributed by the European Southern Observatory (ESO). The GMOS data were reduced with the PAMELA¹ and MOLLY¹ packages.

3. Spectroscopic analysis

The optical EMMI and GMOS spectra offer good phase coverage of the radial velocity curve. The GMOS spectra enabled us to determine the atmospheric parameters covering about half of the orbit.

3.1. Radial velocity curve

The radial velocities were measured by fitting a combination of Gaussians, Lorentzians, and polynomials to the Balmer and helium lines of all spectra. Assuming a circular orbit, sine curves were fitted to the RV data points in fine steps over a range of test periods. For each period, the χ^2 of the best fitting sine curve was determined (see Geier et al. 2011a). At first the EMMI- and the GMOS-datasets were fitted separately. In each case the best solution had the same orbital period as derived from the lightcurve ($P \simeq 0.139$ d). Both datasets cover either the full phase (EMMI) or about half of the phase (GMOS). While the RV-semi-amplitudes are similar, the system velocities of the two datasets show a significant shift of about 27 km s^{-1} with respect to each other. This shift is probably an instrumental effect. More observations are needed to solve this issue.

¹ <http://www2.warwick.ac.uk/fac/sci/physics/research/astro/people/marsh/software>

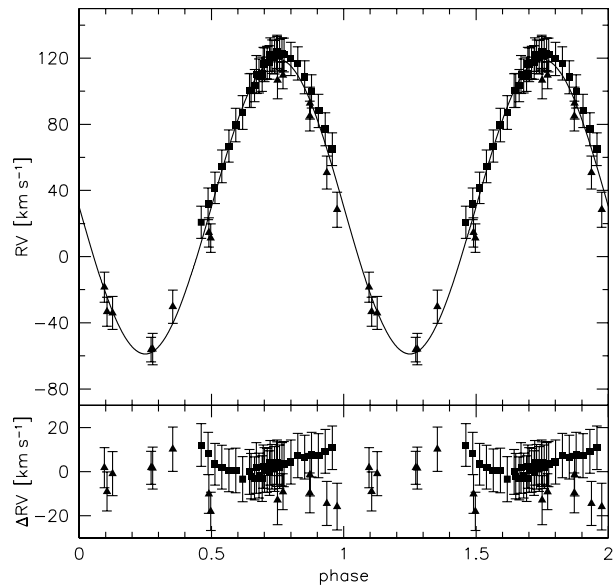


Fig. 1. Radial velocity plotted against orbital phase of ASAS 10232. The RV data was folded with the period measured from the SuperWASP lightcurve. The RVs were determined from ESO-NTT/EMMI spectra (triangle) and Gemini/GMOS spectra (rectangular). The errors are formal 1σ uncertainties. The GMOS-RVs were shifted systematically to fit to the EMMI results.

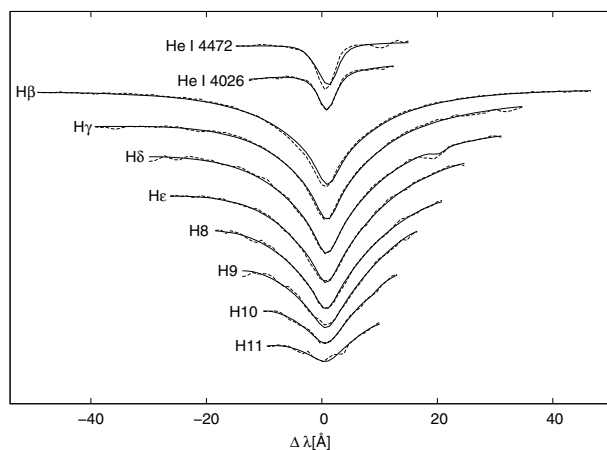


Fig. 2. Fit of the GMOS spectrum nearest to phase 0, the dashed line shows the measurement and the solid line shows the best fitting synthetic spectrum.

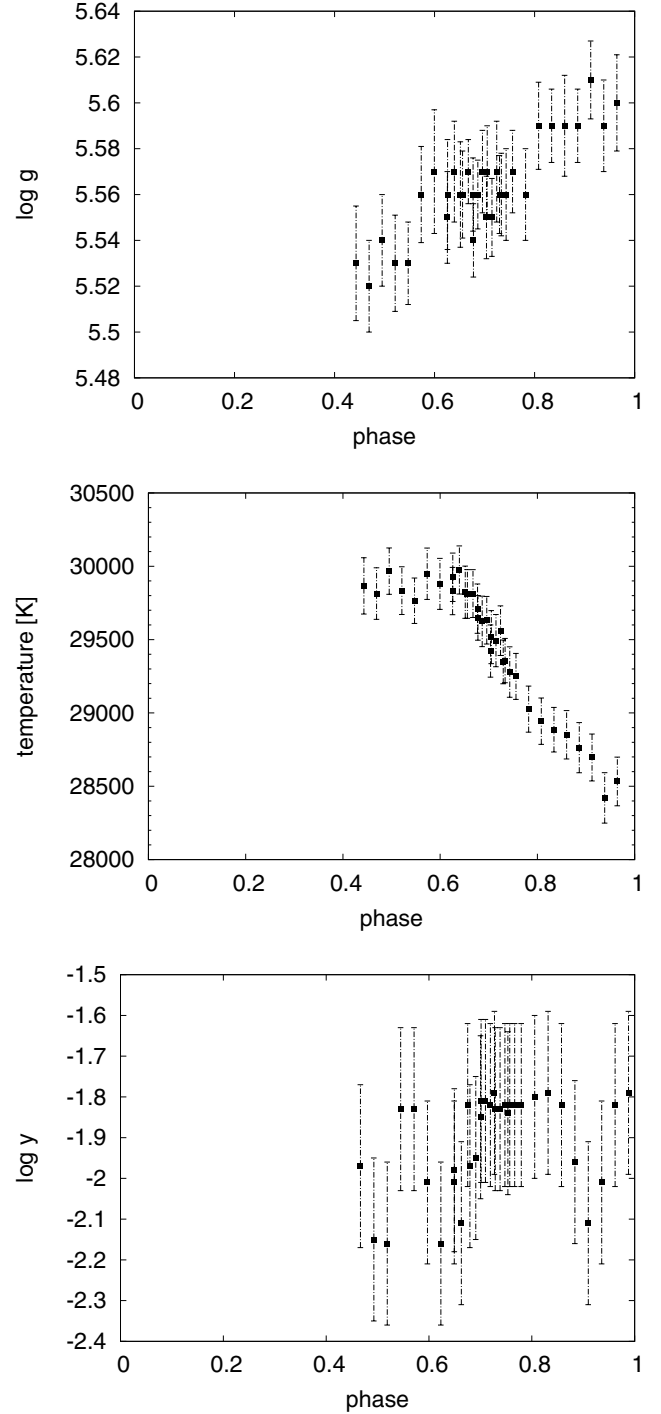
Taking the average value of the solutions derived from the two datasets, the semi-amplitude of the radial velocity curve was determined to $K_1 = 81.0 \pm 3 \text{ km s}^{-1}$. Figure 1 shows a phased RV-curve where the radial velocities derived from the GMOS spectra have been shifted by -27 km s^{-1} .

3.2. Atmospheric parameters

Atmospheric parameters were determined by fitting synthetic spectra to the observed Balmer and helium lines of each of the 33 GMOS spectra using SPAS (Hirsch 2009). A model grid of synthetic spectra was calculated by using LTE model atmospheres with solar metallicity and metal line blanketing (Heber et al. 2000). Because some HW Vir systems showed an apparent change in the atmospheric parameters over the orbital phase

Table 1. Radial velocities of ASAS 10232.

Mid-HJD	RV [km s ⁻¹]	Instrument
2 454 476.71277	109.7 ± 8.2	EMMI
2 454 476.72692	85.0 ± 9.0	
2 454 476.79412	-30.3 ± 10.0	
2 454 477.71635	28.4 ± 10.6	
2 454 477.73450	-33.3 ± 8.9	
2 454 477.75857	-55.8 ± 9.5	
2 454 477.84140	92.8 ± 9.7	
2 454 477.87249	-18.4 ± 9.1	
2 454 477.87674	-34.0 ± 10.0	
2 454 478.66009	106.6 ± 11.2	
2 454 478.68602	50.9 ± 10.0	
2 454 478.76423	11.2 ± 8.7	
2 454 478.87209	-56.2 ± 7.5	
2 454 479.73826	14.6 ± 8.9	
2 455 247.69381	127.4 ± 10.2	GMOS
2 455 247.69571	130.4 ± 9.8	
2 455 247.69801	136.2 ± 10.2	
2 455 247.69961	137.3 ± 10.4	
2 455 247.70092	143.0 ± 10.2	
2 455 247.70224	144.3 ± 9.9	
2 455 247.70355	144.3 ± 10.1	
2 455 247.70486	147.9 ± 10.1	
2 455 247.70618	147.5 ± 10.2	
2 455 247.70750	149.9 ± 10.2	
2 455 247.70881	148.6 ± 9.9	
2 455 247.71013	149.3 ± 9.8	
2 455 252.68221	47.8 ± 9.7	
2 455 252.68584	58.9 ± 9.6	
2 455 252.68947	68.6 ± 9.5	
2 455 252.69310	81.6 ± 9.9	
2 455 252.69673	93.9 ± 9.7	
2 455 252.70036	106.6 ± 10.2	
2 455 252.70399	114.2 ± 10.3	
2 455 252.70762	127.4 ± 10.2	
2 455 252.71125	137.2 ± 11.5	
2 455 252.71488	143.7 ± 9.9	
2 455 252.71851	149.1 ± 10.1	
2 455 252.72214	150.8 ± 10.1	
2 455 252.72577	148.9 ± 10.2	
2 455 252.72940	146.5 ± 10.0	
2 455 252.73303	143.8 ± 10.0	
2 455 252.73666	135.4 ± 10.0	
2 455 252.74029	126.9 ± 10.1	
2 455 252.74392	115.1 ± 10.0	
2 455 252.74755	104.0 ± 10.0	
2 455 252.75118	91.9 ± 9.9	
2 455 252.75481	76.7 ± 9.9	


Fig. 3. Apparent variation of the atmospheric parameters over the phase. Temperature, surface gravity and helium abundance were measured from the Gemini/GMOS spectra. The errors are statistical errors.

(e.g. Wood & Saffer 1999; Drechsel et al. 2001), all spectra were fitted separately. This effect is linked to the reflection effect since the contribution of the companion to the spectra is stronger the more the heated side is visible.

The variation in the parameters over the phase is likewise clearly visible for our star system. The temperature seems to change about 1500 K, and the surface gravity about 0.09 dex over the phase as can be seen in Fig. 3. The helium abundance shows a scatter of about 0.5 dex, which is not much more than the statistical error. For a grazing eclipse the least

contamination by the secondary, hence the most accurate, value is expected for phase 0. Unfortunately, the binary was not observed at this phase. We adopted the value closest to phase zero and therefore a temperature of $28\,400 \pm 500$ K, a surface gravity of $\log g = 5.60 \pm 0.05$ and a helium abundance of about 1.8 ± 0.2 . We considered bigger errors than the statistical errors, which can be seen in Fig. 3, to account for the change in the parameters over the phase and systematic errors. The helium abundance is sub-solar as in most sdBs. Such atmospheric parameters are typical of sdBs in HW Vir systems (see Fig. 4).

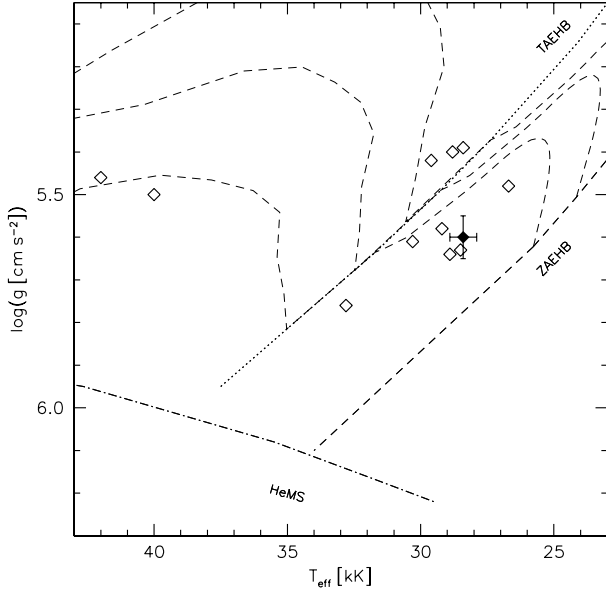


Fig. 4. $T_{\text{eff}} - \log g$ -diagram. The helium main sequence (HeMS) and the EHB band (limited by the zero-age EHB, ZAEHB, and the terminal-age EHB, TAEHB) are superimposed with EHB evolutionary tracks from Dorman et al. (1993). The position of ASAS 10232 is indicated with a solid diamond. Open diamonds mark the position of other HW Vir-like systems (Charpinet et al. 2008; Drechsel et al. 2001; For et al. 2010; Geier et al. 2011b; Maxted et al. 2002; Klepp & Rauch 2011; Østensen et al. 2008, 2010; Wood & Saffer 1999; Almeida et al. 2012; Barlow et al. 2013).

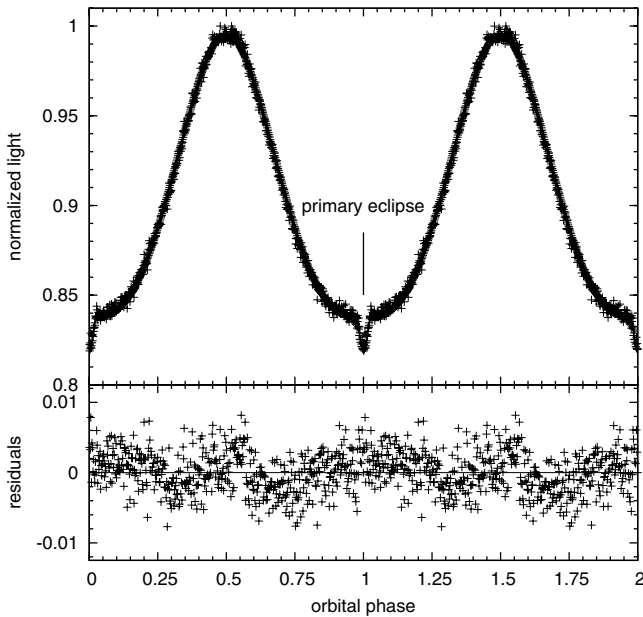


Fig. 5. Phased SuperWASP lightcurve. The solid line demonstrates the best-fitting model. In the bottom panel the residuals can be seen. The wave pattern that is seen in the residuals can be explained by the simplified treatment of the reflection effect. Better models of the reflection effect should remove this wave pattern.

4. Photometric analysis

4.1. Ephemeris

The SuperWASP lightcurve (see Fig. 5) clearly shows that ASAS 10232 is a short-period binary with a grazing eclipse. The

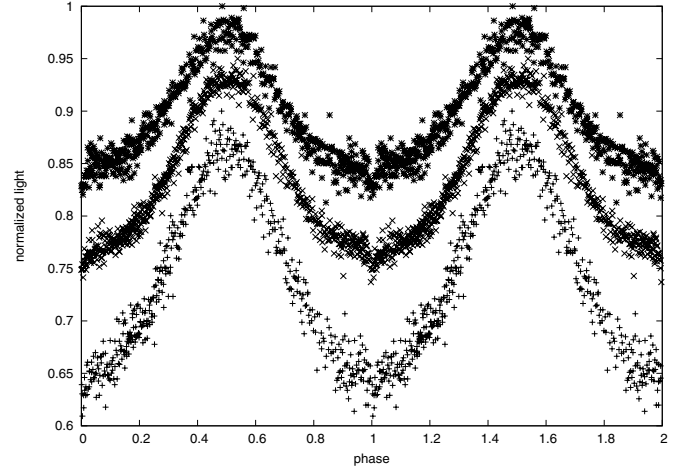


Fig. 6. Phased lightcurves of ASAS 10232 in the B (*), V (\times), and I (+) band taken from the Carnes Hill Observatory: V is shifted by 0.05, I is shifted by 0.1.

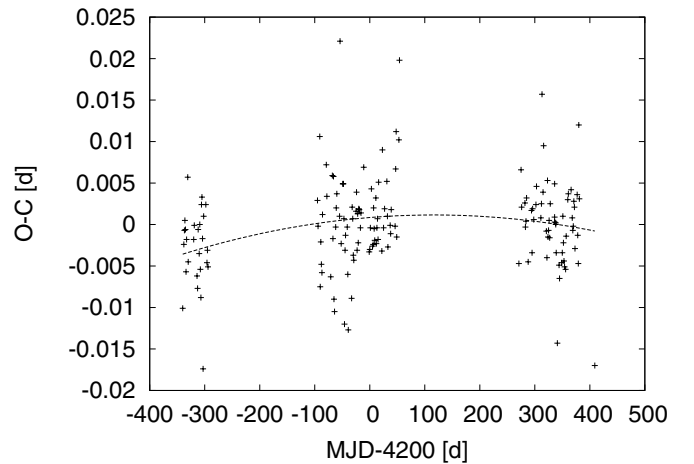


Fig. 7. O–C diagram of ASAS 10232 from the SuperWASP and ASAS observations with a fit of a parabola to determine a period derivative.

huge reflection effect indicates a cool main sequence star companion. The Carnes Hill Observatory lightcurves (see Fig. 6) in the three bands B , V , and I were used to determine the time of the primary minimum. Parabolas were fitted to the minimum obtained on the night of 13 March 2008, where the minimum was clearly visible in all bands. From the different measured times of the minima in the different bands, the standard deviation was calculated as the error in time. Since the SuperWASP lightcurve has much higher accuracy and covers a longer time span it was used to determine the orbital period of the system. The period derivative was found by a fit of a parabola to the O–C curve measured from the SuperWASP and BVI lightcurves, see Fig. 7:

$$\text{HJD} = 2\,454\,538^{\text{d}}99689 + 0^{\text{d}}.13926940 \times E - 6^{\text{d}} \times 10^{-11} \times E^2 \\ \pm 42 \quad \pm 4 \quad \pm 2.3$$

The period derivative is not yet a three-sigma detection, more observations are needed to confirm it.

4.2. Lightcurve solution

The phased B , V , I lightcurves along with the white-light SuperWASP lightcurve were analysed with the MORO code

Table 2. Parameters of ASAS 10232 (TYC 7709-376-1).

Coordinates	10 23 22 −37 37 00 (J2000.0)		
Proper motions	−28.9 −22.8 [2.4 2.4 35] mas/yr		
Mass of the sdB	M_{sdb}	$[M_{\odot}]$	0.461 ± 0.051
Mass of the companion	M_{comp}	$[M_{\odot}]$	0.157 ± 0.017
Separation	a	$[R_{\odot}]$	0.963 ± 0.036
Mean radius of the sdB	R_{sdb}	$[R_{\odot}]$	0.179 ± 0.011
Mean radius of the comp	R_{comp}	$[R_{\odot}]$	0.256 ± 0.015
Surface gravity (phot)	$\log g(\text{sdb})$		5.60 ± 0.02
Surface gravity (spec)	$\log g(\text{sdb})$		5.60 ± 0.05

(Drechsel et al. 1995). This lightcurve solution program is based on the Wilson-Devinney approach (Wilson & Devinney 1971), but uses a modified Roche model that considers the radiative pressure of hot binaries. For the analysis of the SuperWASP lightcurve normal points were formed by binning the fluxes of individual measurements over narrow time intervals. This is necessary because of the huge number of data points (13 816 data points were binned to 478 normal points) that would make the analysis very tedious.

We used the Wilson-Devinney mode 2, which does not restrict the system configuration and links the luminosity and the temperature of the second component on the basis of the Planck law. Since the luminosity ratio is very high and the companion contributes almost exclusively via the reflection effect, the measured temperature of the companion is not reliable. Because of the high number of parameters ($12 + 5N = 32$), some have to be deduced from spectral or theoretical constraints.

Owing the early spectral type of the primary star the gravity darkening exponent can be fixed at $g_1 = 1$ as expected for radiative outer envelopes (von Zeipel 1924). For the cool convective companion, g_2 was set to 0.32 (Lucy 1967). The linear limb darkening coefficients were interpolated from the tables of Wade & Rucinski (1985) and fixed at $x_1(B) = 0.26$, $x_1(V) = 0.22$, $x_1(I) = 0.165$, $x_1(\text{white}) = 0.20$. Since only monochromatic lightcurves are calculated in the lightcurve solution program, we used the central wavelengths of the band filters. The secondary's limb darkening coefficient x_2 was varied as the limb darkening of such heated objects cannot be predicted. The temperature of the hot component was taken from the spectral analysis ($T_{\text{eff,sdB}} = 28\,400$ K).

For the albedos of the companion values exceeding 1 were needed to model the reflection effect. This can be explained with processes in the stellar atmosphere that cause a spectral redistribution of the irradiated energy with wavelength. The third light that accounts for the disturbance by a potential third object in the system was first varied but then set to 0 because it did not deviate from this value. As the spectral type of the companion is very late, radiation pressure does not play a role, and the radiation pressure coefficient for the companion was fixed to zero (cf. Drechsel et al. 1995, 2001).

The rest of the parameters, such as the radiation pressure coefficient for the primary star, the inclination, the effective temperature of the companion, and the Roche potentials, were adjusted. A grid with different fixed mass ratios and different start parameters was calculated. All four lightcurves were analysed simultaneously. That there are so many correlated parameters means a unique solution cannot be found from the lightcurve alone, because of the degeneracy of mass ratio and radii of the components. In Table 3 the parameters of the lightcurve solution with the best standard deviation can be found.

Table 3. Best lightcurve solution of ASAS 10232.

Fixed parameters:		
$q(=M_2/M_1)$		0.34
$T_{\text{eff}}(1)$	[K]	28 400
g_1^b		1.0
g_2^b		0.32
$x_1(B)^c$		0.26
$x_1(V)^c$		0.22
$x_1(I)^c$		0.165
$x_1(\text{white})^c$		0.20
δ_2^d		0.0
l_3^f		0.0
Adjusted parameters:		
i	[°]	65.86 ± 0.69
$T_{\text{eff}}(2)$	[K]	3380 ± 561
A_1^a		0.94 ± 0.03
A_2^a		1.21 ± 0.13
Ω_1^f		5.700 ± 0.260
Ω_2^f		2.673 ± 0.052
$\frac{L_1}{L_1+L_2}(B)^g$		0.99954 ± 0.00077
$\frac{L_1}{L_1+L_2}(V)^g$		0.99804 ± 0.00247
$\frac{L_1}{L_1+L_2}(I)^g$		0.99036 ± 0.00845
$\frac{L_1}{L_1+L_2}(\text{white})^g$		0.99709 ± 0.00337
δ_1		0.0123 ± 0.0080
$x_2(B)$		0.638 ± 0.097
$x_2(V)$		0.548 ± 0.0630
$x_2(I)$		0.625 ± 0.087
$x_2(\text{white})$		0.238 ± 0.089
Roche radii ^h :		
$r_1(\text{pole})$	[a]	0.184 ± 0.009
$r_1(\text{point})$	[a]	0.186 ± 0.00
$r_1(\text{side})$	[a]	0.185 ± 0.009
$r_1(\text{back})$	[a]	0.186 ± 0.009
$r_2(\text{pole})$	[a]	0.248 ± 0.009
$r_2(\text{point})$	[a]	0.286 ± 0.017
$r_2(\text{side})$	[a]	0.256 ± 0.010
$r_2(\text{back})$	[a]	0.277 ± 0.014

Notes. ^(a) Bolometric albedo. ^(b) Gravitational darkening exponent. ^(c) Linear limb darkening coefficient; taken from Wade & Rucinski (1985). ^(d) Radiation pressure parameter, see Drechsel et al. (1995). ^(e) Fraction of third light at maximum. ^(f) Roche potentials. ^(g) Relative luminosity; L_2 is not independently adjusted, but recomputed from r_2 and $T_{\text{eff}}(2)$. ^(h) Fractional Roche radii in units of separation of mass centers.

The Euler lightcurves are consistent with this solution as can be seen in Fig. 8. The only difference is a higher albedo of 1.3 for the companion. Because the Euler lightcurves have a good signal-to-noise and four different colour bands are covered, the higher albedo is probably preferable.

Figure 9 shows the equipotential surfaces of both components for the case of the best solutions over the phase. It is clearly visible that ASAS 10232 is a detached system with a grazing eclipse since both components stay inside their Roche lobe. The companion is bigger than the primary star and is slightly distorted.

5. System parameters

Since the radial velocity amplitude of the companion is not known and a degeneracy in the mass ratio appears in the

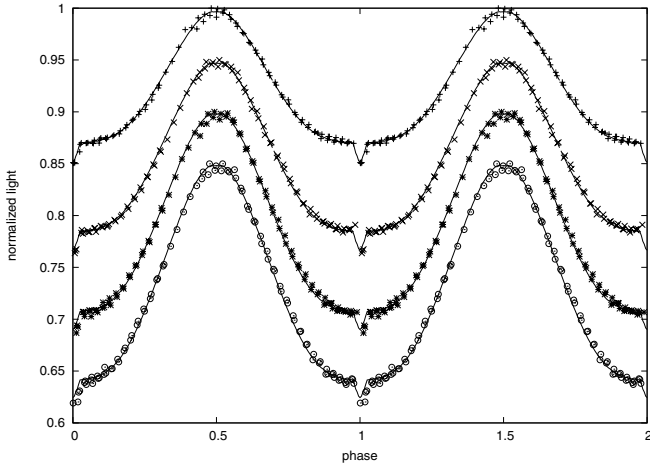


Fig. 8. *BVR I* Euler lightcurves with the model from the parameters of the best solution, but a higher $A_2 = 1.3$, every lightcurve is shifted by 0.05.

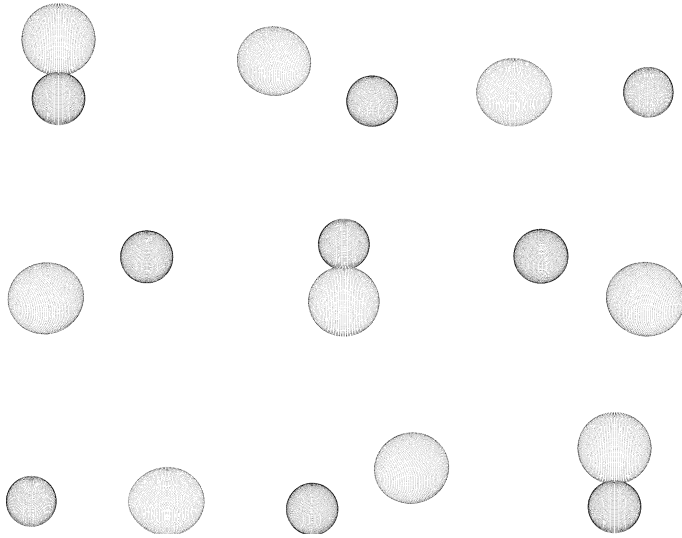


Fig. 9. Equipotential structure of ASAS 10232 corresponding to the best fit solution over the phase from 0.5 to 0.5 in steps of 0.125.

lightcurve solutions, we do not have a unique solution of the system yet. The solution with the smallest standard deviation from the lightcurve model to the measured values is found for a mass ratio $q = 0.34$. For this mass ratio we derive an inclination angle of $i = 65.9^\circ$ from the lightcurve analysis. Furthermore, the mean radii for the components could be determined: $R_1/a = 0.185$ and $R_2/a = 0.266$, where a is the separation of the mass centres. Together with the $K_1 = 81.0 \pm 3.0 \text{ km s}^{-1}$ measured from the radial velocity curve and the mass ratio q , the inclination i and the period $P = 0.13927 \text{ d}$, determined from the lightcurve, the masses of the components $M_1 = 0.461 \pm 0.051 M_\odot$ and $M_2 = 0.157 \pm 0.017 M_\odot$ were derived. Moreover, the separation $a = 0.963 \pm 0.036 R_\odot$, hence the absolute values for the radii of the stars $R_{\text{sdb}} = 0.179 \pm 0.011 R_\odot$ and $R_{\text{comp}} = 0.256 \pm 0.015 R_\odot$, could be calculated.

Radius and mass of the companion leads to the conclusion that the companion must be an M dwarf. The derived mass for the sdB is consistent with theoretical calculations for the formation of sdBs via the common envelope channel (Han et al. 2002, 2003).

To check this solution the surface gravity determined from the spectra can be compared to a photometric surface gravity. This surface gravity is derived via the mass–radius relation from the mass and radius calculated from the radial velocity curve together with the lightcurve analysis. The surface gravity determined in this way $\log g(\text{phot}) = 5.60 \pm 0.02$ is in perfect agreement to the spectroscopic surface gravity $\log g(\text{spec}) = 5.60 \pm 0.05$.

6. Conclusions

We discovered the new eclipsing sdB star ASAS 102322-3737.0, which shows a grazing eclipse and a huge reflection effect that is the only contribution of the companion to the optical light of the system. It has an orbital period of $P = 0.13927 \text{ d}$ and an inclination of $i = 65.9^\circ$. A unique solution cannot be found because of a degeneracy in the mass ratio. The best lightcurve solution was calculated for a mass ratio of $q = 0.34$. The masses of the components for this solution $M_{\text{sdb}} = 0.461 \pm 0.051 M_\odot$ and $M_{\text{comp}} = 0.157 \pm 0.017 M_\odot$ are typical of an sdB and a late main sequence star. Also the spectroscopic and the photometric surface gravity are in agreement. Since ASAS 10232 is very bright it is possible to apply rapid high-resolution time-series spectroscopy to search for spectral features and the RV semi-amplitude from the companion to resolve the degeneracy in the mass ratio, as done for AA Dor (Vučković et al. 2008).

Some of the sdBs were found to be pulsating. There are two classes of sdB pulsators, p-mode pulsators with periods of some minutes and g-mode pulsators with periods of 0.5 to 2 h, which are separated by their atmospheric parameters. Until now only one pulsating HW Virginis system was found, NY Virginis (Vučković et al. 2007). Such systems are very interesting since it is possible to compare the results from asteroseismology to the results from the lightcurve analysis of the eclipses. If it is pulsating, the parameters of ASAS 10232 would suggest that it is most likely a g-mode pulsator. However, the Euler lightcurve with the best signal-to-noise shows no sign of pulsation. But the strong reflection effect could hide the pulsations.

Period variations have been found for almost all of the HW Vir systems that have accurate eclipse timings covering more than five years, which may be attributed to the presence of a third body. In several cases the third bodies are likely to be one (or two) giant planet(s). These discoveries were unexpected, because it is considered to be difficult for giant planets to form around main sequence binaries owing to the short lifetime of circumbinary disks. In addition, such planets may not be able to survive common envelope (CE) evolution. Instead, it has been suggested that these circumbinary planets are second generation (Zorotovic & Schreiber 2013), which is formed from the instability of a post-CE disk. Zorotovic & Schreiber (2013) also proposed an alternative scenario for the period variations due to processes acting in deeply convective secondary stars.

HW Vir has been monitored for more than 28 years now and, Lee et al. (2009) found two sinusoidal variations of the light-travel time for HW Vir from 24 years of data, suggesting there are two substellar objects orbiting the close binary. New observations by Beuermann et al. (2012), however, deviate significantly from the prediction of Lee et al. (2009). The new solution involves one planet and a brown dwarf or low-mass star orbiting the HW Vir binary (Beuermann et al. 2012). The new solution was found to be stable in contrast to that of Lee et al. (2009).

These findings suggest that the probability of finding period variations in ASAS 10232 as well is high, whether due to substellar objects or the active secondary. The lesson learned

from HW Vir is that long-term and dense monitoring is a prerequisite (Beuermann et al. 2012). ASAS is the third brightest HW Vir system known: only one magnitude fainter than HW Vir, which allows us to use readily accessible small telescopes to obtain lightcurves. It is therefore a promising target for amateur and secondary school observatories to team up with professional astronomers (Backhaus et al. 2012).

Acknowledgements. Based on observations at the La Silla Observatory of the European Southern Observatory for programme number 080.D-0685(A) and on observations obtained at the Gemini Observatory (Program ID: GS-2009B-Q-98), which is operated by the Association of Universities for Research in Astronomy, Inc., under a cooperative agreement with the NSF on behalf of the Gemini partnership: the National Science Foundation (United States), the Science and Technology Facilities Council (United Kingdom), the National Research Council (Canada), CONICYT (Chile), the Australian Research Council (Australia), Ministério da Ciência e Tecnologia (Brazil) and Ministerio de Ciencia, Tecnología e Innovación Productiva (Argentina). S.G. is supported by the Deutsche Forschungsgemeinschaft (DFG) through grant HE1356/49-1. R.Ø. acknowledges funding from the European Research Council under the European Community's Seventh Framework Programme (FP7/2007–2013)/ERC grant agreement N^o227224 (PROSPERITY), as well as from the Research Council of K.U.Leuven grant agreement GOA/2008/04. V.S. acknowledges funding by the Deutsches Zentrum für Luft- und Raumfahrt (grant 50 OR 1110) and by the Erika-Giehl-Stiftung.

References

- Almeida, L. A., Jablonski, F., Tello, J., & Rodrigues, C. V. 2012, *MNRAS*, 423, 478
- Backhaus, U., Bauer, S., Beuermann, K., et al. 2012, *A&A*, 538, A84
- Barlow, B. N., Kilkenny, D., Drechsel, H., et al. 2013, *MNRAS*, 430, 22
- Beuermann, K., Dreizler, S., Hessman, F. V., & Deller, J. 2012, *A&A*, 543, A138
- Brown, T. M., Ferguson, H. C., Davidsen, A. F., & Dorman, B. 1997, *APJ*, 482, 685
- Brown, T. M., Bowers, C. W., Kimble, R. A., Sweigart, A. V., & Ferguson, H. C. 2000, *APJ*, 532, 308
- Charpinet, S., van Grootel, V., Reese, D., et al. 2008, *A&A*, 489, 377
- Dorman, B., Rood, R. T., & O'Connell, R. W. 1993, *APJ*, 419, 596
- Drechsel, H., Haas, S., Lorenz, R., & Gayler, S. 1995, *A&A*, 294, 723
- Drechsel, H., Heber, U., Napiwotzki, R., et al. 2001, *A&A*, 379, 893
- For, B.-Q., Green, E. M., Fontaine, G., et al. 2010, *APJ*, 708, 253
- Geier, S., Maxted, P. F. L., Napiwotzki, R., et al. 2011a, *A&A*, 526, A39
- Geier, S., Schaffenroth, V., Drechsel, H., et al. 2011b, *APJ*, 731, L22
- Geier, S., Marsh, T. R., Dunlap, B. H., et al. 2012 [[arXiv:1209.4740](https://arxiv.org/abs/1209.4740)]
- Han, Z., Podsiadlowski, P., Maxted, P. F. L., Marsh, T. R., & Ivanova, N. 2002, *MNRAS*, 336, 449
- Han, Z., Podsiadlowski, P., Maxted, P. F. L., & Marsh, T. R. 2003, *MNRAS*, 341, 669
- Heber, U. 1986, *A&A*, 155, 33
- Heber, U., Reid, I. N., & Werner, K. 2000, *A&A*, 363, 198
- Hirsch, H. 2009, Ph.D. Thesis, Friedrich Alexander Universität Erlangen Nürnberg
- Klepp, S., & Rauch, T. 2011, *A&A*, 531, L7
- Lee, J. W., Kim, S.-L., Kim, C.-H., et al. 2009, *AJ*, 137, 3181
- Lucy, L. B. 1967, *Z. Astrophysik*, 65, 89
- Maxted, P. F. L., Heber, U., Marsh, T. R., & North, R. C. 2001, *MNRAS*, 326, 1391
- Maxted, P. F. L., Marsh, T. R., Heber, U., et al. 2002, *MNRAS*, 333, 231
- Napiwotzki, R., Karl, C. A., Lisker, T., et al. 2004, *Ap&SS*, 291, 321
- Østensen, R. H., Oreiro, R., Hu, H., Drechsel, H., & Heber, U. 2008, in *Hot Subdwarf Stars and Related Objects*, eds. U. Heber, C. S. Jeffery, & R. Napiwotzki, *ASP Conf. Ser.*, 392, 221
- Østensen, R. H., Green, E. M., Bloemen, S., et al. 2010, *MNRAS*, 408, L51
- Pojmanski, G. 2003, *Acta Astron.*, 53, 341
- Pollacco, D. L., Skillen, I., Cameron, A. C., et al. 2006, *PASP*, 118, 1407
- Qian, S.-B., Zhu, L.-Y., Zola, S., et al. 2009, *APJ*, 695, L163
- Saffer, R. A., Bergeron, P., Koester, D., & Liebert, J. 1994, *APJ*, 432, 351
- Vennes, S., Kawka, A., O'Toole, S. J., Németh, P., & Burton, D. 2012, *ApJ*, 759, L25
- von Zeipel, H. 1924, *MNRAS*, 84, 665
- Vučković, M., Aerts, C., Østensen, R., et al. 2007, *A&A*, 471, 605
- Vučković, M., Østensen, R., Bloemen, S., Decoster, I., & Aerts, C. 2008, in *Hot Subdwarf Stars and Related Objects*, eds. U. Heber, C. S. Jeffery, & R. Napiwotzki, *ASP Conf. Ser.*, 392, 199
- Wade, R. A., & Rucinski, S. M. 1985, *A&AS*, 60, 471
- Wilson, R. E., & Devinnay, E. J. 1971, *APJ*, 166, 605
- Wood, J. H., & Saffer, R. 1999, *MNRAS*, 305, 820
- Zorotovic, M., & Schreiber, M. R. 2013, *A&A*, 549, A95

LETTER TO THE EDITOR

The subdwarf B star SB 290 – A fast rotator on the extreme horizontal branch[★]

S. Geier^{1,2}, U. Heber¹, C. Heuser¹, L. Classen¹, S. J. O’Toole³, and H. Edelmann¹

¹ Dr. Karl Remeis-Observatory & ECAP, Astronomical Institute, Friedrich-Alexander University Erlangen-Nuremberg, Sternwartstr. 7, 96049 Bamberg, Germany
e-mail: sgeier@eso.org

² European Southern Observatory, Karl-Schwarzschild-Str. 2, 85748 Garching, Germany

³ Australian Astronomical Observatory, PO Box 915, North Ryde NSW 1670, Australia

Received 20 December 2012 / Accepted 16 January 2013

ABSTRACT

Hot subdwarf B stars (sdBs) are evolved core helium-burning stars with very thin hydrogen envelopes. To form an sdB, the progenitor has to lose almost all of its hydrogen envelope right at the tip of the red giant branch. In close binary systems, mass transfer to the companion provides the extraordinary mass loss required for their formation. However, apparently single sdBs exist as well, and their formation has been unclear for decades. The merger of helium white dwarfs leading to an ignition of core helium-burning or the merger of a helium core and a low-mass star during the common envelope phase have been proposed. Here we report the discovery of SB 290 as the first apparently single, fast-rotating sdB star located on the extreme horizontal branch, indicating that those stars may form from mergers.

Key words. binaries: spectroscopic – subdwarfs – stars: rotation

1. Introduction

Hot subdwarf B stars (sdBs) are core helium-burning stars with thin hydrogen envelopes situated at the extreme end of the blue horizontal branch (Heber 2009). Horizontal branch stars are normally formed after the ignition of core helium-burning in the red-giant phase. However, the hydrogen envelopes of sdBs are extremely thin and strong mass loss just at the tip of the red-giant branch is needed to form them.

Ejection of a common envelope can be held responsible for the strong mass loss to form sdB stars in close binaries, which make up for half of the sdB population. While stable Roche lobe overflow explains the formation of sdB stars with main sequence companions in wider orbits, the existence of single sdB stars still remains a riddle. The most popular scenario invokes mergers of helium-core white dwarfs (Webbink 1984; Iben & Tutukov 1984). Politano et al. (2008) proposes the merger of a red giant and a low-mass main sequence star during the common envelope phase as another possible formation channel.

An important constraint for evolutionary scenarios is the distribution of the rotational properties of sdB stars. Geier et al. (2010) have studied a sample of close binary sdB stars and find that short-period systems (orbital periods $P < 1.2$ d) show significant rotation, while the longer period systems are slow rotators. Tidal interaction with the companion is thus important for the $v_{\text{rot}} \sin i$ -distribution of binary sdBs, and it has spun up the sdB stars in the closest systems.

To avoid tidal interaction effects, Geier & Heber (2012) extended their study to 105 apparently single and wide binary sdB stars and found all of them to be slowly rotating at $v_{\text{rot}} \sin i < 10 \text{ km s}^{-1}$. This result challenges merger scenarios because it

would require rapid loss of angular momentum after the merger event.

The only exception known is EC 22081–1916, which rotates at $v_{\text{rot}} \sin i = 163 \text{ km s}^{-1}$. There is no hint of any radial velocity variations, excluding a close companion and therefore tidal interactions. However, this star differs from typical sdB stars on the extreme horizontal branch (EHB) because its surface gravity is an order of magnitude lower. It must be an evolved object and may have formed quite differently from EHB stars (Geier et al. 2011a).

In the course of our studies of sdB stars at high spectral resolution (Geier et al. 2010, 2011a; Geier & Heber 2012; Geier 2013), the sdB star SB 290 caught our attention because of its unusual line shapes. SB 290 (CD–38 222) was discovered as a B-type star in the objective prism survey of the south Galactic pole region by Slettebak & Brundage (1971). Graham & Slettebak (1973) classified the spectrum of SB 290 as an sdB. Its atmospheric parameters were derived from the spectral energy distribution including IUE UV spectrophotometric data and optical spectra (Heber et al. 1984). The results ($T_{\text{eff}} = 28\,200 \pm 1300 \text{ K}$, $\log g = 5.5 \pm 0.2$, and helium abundance $\log y = -2.4$) place SB 290 on the EHB, as expected for a prototypical, core-helium burning, sdB star.

The first indication that SB 290 is not as typical as it seemed at first glance came from high-resolution optical spectra revealing a helium isotopic anomaly. Isotopic line shifts were found that indicate that the ^4He isotope in the atmosphere is almost completely replaced by ^3He due to gravitational settling (Heber 1987). Eventually, SB 290 became the prototype of a small class of sdBs showing this anomaly (Edelmann et al. 2001; Geier et al. 2012).

Kügler (1991) noted significant broadening of the Balmer line cores of SB 290. O’Toole (2004) analysed high-resolution

[★] Appendix A is available in electronic form at <http://www.aanda.org>

UV-spectra of SB 290 obtained with the IUE satellite and also found the metal lines to be significantly broadened compared to the other sdBs in his sample.

2. Possible line broadening mechanisms

Following the discussion in Geier et al. (2011a), there are different mechanisms that may cause this broadening. High magnetic fields that may cause a Zeeman-splitting of the lines as observed in magnetic white dwarfs can be excluded. Most recently, Mathys et al. (2012) have measured the magnetic field of SB 290 using the FORS2 instrument at ESO-VLT in spectropolarimetric mode. Although they report a marginal detection of a few hundred kG, this field strength is much too small to cause the observed line broadening.

A plausible explanation would be a close companion to SB 290. Hot subdwarfs with high measured projected rotational velocities ($v_{\text{rot}} \sin i > 100 \text{ km s}^{-1}$) mostly reside in very close binary systems with orbital periods of $\approx 0.1 \text{ d}$. Those sdBs were spun up by the tidal influence of their close companions, and their rotation became synchronised to their orbital motion (e.g. Geier et al. 2007, 2010).

The colours of SB 290 ($J - K_S \approx 0.06$, 2MASS, Skrutskie et al. 2006) do not show any signs of a cool companion (Stark & Wade 2003). A putative close companion, which is also not visible in the optical spectra, must therefore be either a low-mass main sequence star (with spectral type later than about M2), a compact object like a white dwarf, or a substellar object. While a close white dwarf or M-star companion would cause RV variations of tens or hundreds of km s^{-1} , any cool companion with a size similar to the sdB primary, no matter whether it is stellar or substellar, would be detectable in the light curve. Close sdB+dM or BD systems are often eclipsing, but they also show sinusoidal variations due to light originating at the irradiated surface of the cool companion (e.g. Geier et al. 2011c).

Furthermore, it can be premature to conclude that line broadening is due to rotation, since many sdB stars show multi-periodic pulsations with short periods (2–10 min), which can result in line broadening as high as 34 km s^{-1} in time-integrated spectra and extreme cases (Kuassivi et al. 2005).

Therefore we extracted photometric measurements from the SuperWASP archive and searched for short-period light variations. If the broadening were indeed due to rotation, we would expect that SB 290 had been spun up by tidal interaction with a close companion. Assuming spin-orbit synchronisation, we would expect an orbital period of $\approx 0.2 \text{ d}$. Therefore, we also obtained time-resolved spectroscopy to verify the existence of a nearby companion.

3. Observations, light curve, and radial velocity curve

3.1. Photometry

Thanks to its brightness, SB 290 has been monitored by planetary transit surveys. An excellent white light curve taken from May 2006 to December 2007 was downloaded from the SuperWASP Public archive¹ (Pollacco et al. 2006). The light curve consists of no fewer than 10 192 single measurements.

To search for periodic variations in the SuperWASP light curve, we performed a Fourier analysis using the FAMIAS routine developed by Zima (2008). No significant light variations

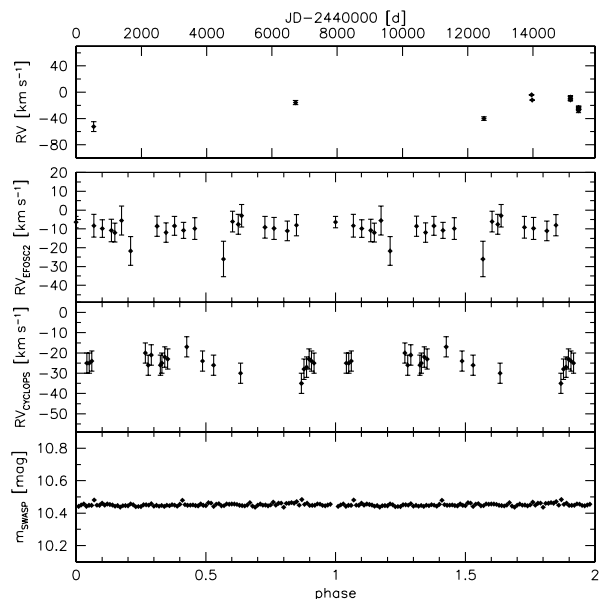


Fig. 1. Time resolved photometry (SWASP, *lower panel*) and radial velocities of the CYCLOPS and EFOSC2 spectra (*middle panels*) plotted against phase. The data has been folded to the upper limit for the orbital period of a putative close binary with synchronised rotation of the sdB ($P \approx 0.22 \text{ d}$, see Geier et al. 2011a). Two complete phases are plotted for better visualisation. Since no significant variations can be seen in the data, SB 290 is not in a close binary system. The nightly average values of the radial velocities measured from all spectra is plotted against the Julian Date (*upper panel*). The oldest RV point dates back to 1969 and is taken from Graham & Slettebak (1973).

have been detected (see Fig. 1, lower panel). A cool low-mass stellar or substellar companion in close orbit can therefore be excluded. Although the uneven sampling of the light curve does not allow a proper search for pulsations, strong variations causing significant line broadening can be excluded as well.

3.2. Time-resolved spectroscopy

Time-resolved medium-resolution spectroscopy ($R \approx 4000$, $\lambda = 3500\text{--}5100 \text{ \AA}$) was obtained in the course of the MUCHFUSS project (Geier et al. 2011b). One dataset consisting of 19 spectra was taken with the ISIS spectrograph mounted at the WHT in August 2009. Reduction was done with standard IRAF procedures. Another set of 20 single spectra ($R \approx 2200$, $\lambda = 4450\text{--}5110 \text{ \AA}$) was obtained with the EFOSC2 spectrograph mounted at the ESO-NTT in November 2009. Reduction was done with standard MIDAS procedures. Finally, 34 high-resolution spectra ($R \approx 70\,000$, $\lambda = 3900\text{--}5270 \text{ \AA}$) were obtained with the UCLES spectrograph equipped with the CYCLOPS fibre feed² and mounted at the AAT in July 2010.

Radial velocities were measured by fitting a set of mathematical functions (polynomial, Lorentzian, and Gaussian) to the Balmer and suitable helium lines of the spectra using the FITSB2 routine (Napiwotzki et al. 2004). No significant RV variations were measured within the EFOSC2 and CYCLOPS datasets³. The radial velocity of the CYCLOPS spectra is constant

² For some details on this instrument see http://www.phys.unsw.edu.au/~cgt/CYCLOPS/CYCLOPS_Classic.html

³ The ISIS spectra showed a linear trend in RV most likely caused by flexure of the instrument, because the target was observed at a very high zenith distance.

¹ <http://www.wasp.le.ac.uk/public/lc/index.php>

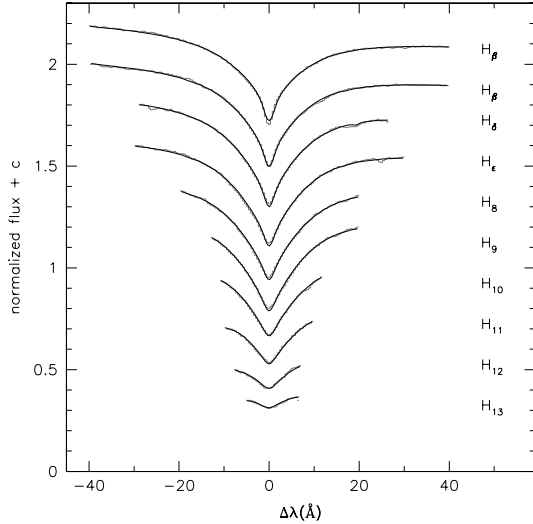


Fig. 2. Fit of synthetic LTE models to the hydrogen Balmer lines of the medium-resolution ISIS spectrum.

at $-25 \pm 4 \text{ km s}^{-1}$, the one of the EFOSC2 spectra at $-10 \pm 5 \text{ km s}^{-1}$, where the standard deviations of the respective single measurements are adopted as uncertainties (see Fig. 1, middle panels). Since no RV variations have been measured on timescales of a few hours, we can exclude any close stellar companion.

3.3. Long-term RV variations

While there is only a small discrepancy between the RVs measured from the CYCLOPS and EFOSC2 datasets, which might have come from zero-point shifts between the two instruments, Graham & Slettebak (1973) measured a significantly different RV of $-52.3 \pm 7.5 \text{ km s}^{-1}$. To investigate the possibility of an unseen companion in a wide orbit, we measured the RVs from spectra taken within the past 25 years (see Table A.1).

A high-resolution spectrum was taken back in 1986 with the CASPEC spectrograph ($R = 30\,000$, $\lambda = 3800\text{--}5000 \text{ \AA}$) mounted at the ESO 3.6 m telescope at La Silla. Two high-resolution spectra were taken in 2002 with the FEROS spectrograph ($R = 48\,000$, $\lambda = 3750\text{--}9200 \text{ \AA}$) mounted at the ESO 1.52 m telescope and another two spectra were taken with FEROS mounted at the ESO/MPG 2.2 m telescope at La Silla in 2006. The spectra have been reduced with the MIDAS package.

The spectra taken with CASPEC and FEROS indeed show a maximum RV-shift of $\approx 25 \text{ km s}^{-1}$ within 16 yr. SB 290 might therefore have an unseen companion in a wide orbit (see Fig. 1, upper panel), which is, however, not likely to be responsible for the observed line broadening of the sdB.

4. Atmospheric parameters and rotational broadening

Atmospheric parameters have been determined by fitting a grid of synthetic spectra, calculated from line-blanketed, solar-metallicity LTE model atmospheres (Heber et al. 2000), to the hydrogen Balmer ($H_\beta - H_{13}$) and helium lines (He I 4026, 4472, 4713, 4922, 5016 \AA) of the coadded ISIS spectrum using the SPAS routine developed by Hirsch (e.g. Geier et al. 2011b). Statistical errors are determined with a bootstrapping algorithm. The resulting effective temperature $T_{\text{eff}} = 26\,300 \pm 100 \text{ K}$, surface gravity $\log g = 5.31 \pm 0.01$ and helium abundance $\log y = -2.52 \pm 0.08$ are characteristic for sdB stars.

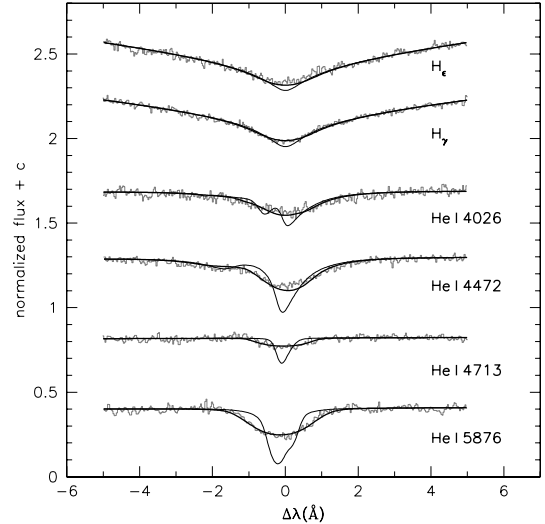


Fig. 3. Fit of synthetic LTE models to selected hydrogen Balmer and helium lines of the high-resolution FEROS spectrum. The thin solid line marks models without rotational broadening, the thick solid line the best-fitting model spectrum with $v_{\text{rot}} \sin i = 58 \text{ km s}^{-1}$. The significant rotational broadening of the lines is obvious.

To measure the projected rotational velocity, we used the coadded high-resolution FEROS spectrum, which is very well suited to this purpose (see Geier et al. 2010; Geier & Heber 2012). The atmospheric parameters have been fixed to the values derived from the ISIS spectrum, and only the $v_{\text{rot}} \sin i$ has been fitted. As can be seen in Fig. 3, the helium lines are significantly broadened. To fit those lines, as well as the Balmer line cores, a broadening of $58 \pm 1 \text{ km s}^{-1}$ is necessary. After excluding all alternative scenarios we conclude that this broadening is caused by rotation.

In addition to Balmer and helium lines, the spectrum shows several metal lines. The C II lines at 4267 \AA , as well as the Si III lines at 4552, 4567, 4574, and 5739 \AA , are strong enough to measure both the abundances and the rotational broadening in the way described in Geier (2013). The $v_{\text{rot}} \sin i = 48 \pm 2 \text{ km s}^{-1}$ measured from those lines is somewhat smaller than the one measured from the Balmer and helium lines.

Geier (2013) reports the discovery of C II and Si III lines with peculiar shapes in sdB stars, which also show the ^3He anomaly. The observed lines appeared narrower than the synthetic line profiles, even without any rotational broadening. Vertical stratification in the atmosphere may be responsible. Since SB 290 is the prototype for the ^3He -sDBs, it might also be affected. However, owing to the high line broadening, the effect might be less obvious and only lead to an underestimate of $v_{\text{rot}} \sin i$. In this special case, we therefore regard the rotational velocity derived from the Balmer and helium lines to be more reliable. The abundances of carbon ($\log \epsilon_{\text{C}} = 7.10 \pm 0.30$) and silicon ($\log \epsilon_{\text{Si}} = 7.28 \pm 0.15$) are typical of sDBs in this temperature range (Geier 2013).

By adopting typical systematic uncertainties of $\pm 500 \text{ K}$ in T_{eff} and $\pm 0.05 \text{ dex}$ in $\log g$, these results are also roughly consistent with the previous determination by Heber et al. (1984), although the effective temperature determined here is somewhat lower.

5. Discussion

That SB 290 is a fast-rotating sdB star might be an indication of a merger origin, although empirical evidence grows that the bulk of the known single sdB stars was not formed by merger

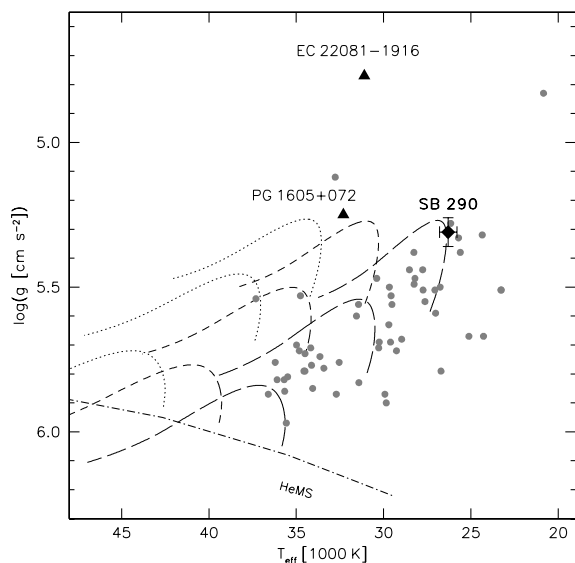


Fig. 4. $T_{\text{eff}} - \log g$ diagram. The grey circles mark sdBs from the SPY project (Lisker et al. 2005). The helium main sequence (HeMS) is plotted and evolutionary tracks have been calculated by Han et al. (2002) for EHB masses of $0.7 M_{\odot}$ (dotted lines), $0.6 M_{\odot}$ (short-dashed lines), and $0.5 M_{\odot}$ (long-dashed lines). The tracks to the lower left mark models without a hydrogen envelope, the tracks in the middle models with $0.001 M_{\odot}$ envelope mass, and the tracks to the upper right models with $0.005 M_{\odot}$ envelope mass.

events (e.g. Fontaine et al. 2012; Geier & Heber 2012). The fast rotator EC 22081–1916 on the other hand, might be the outcome of a rare common envelope merger proposed by Politano et al. (2008). Since the outcome of an He-WD merger should have no hydrogen envelope at all, while the atmosphere of SB 290 is hydrogen rich, the common envelope merger might be a possible formation channel for SB 290 as well.

Hot subdwarf stars formed by a merger event are predicted to have a broad mass distribution with possible masses of up to $\approx 0.7 M_{\odot}$. Han et al. (2002) calculated evolutionary tracks for EHB stars with different stellar and envelope masses. SB 290 should be situated close to the terminal-age EHB if its mass is close to the canonical value (Fig. 4). Looking at Fig. 4 one can see that the tracks for an EHB mass of $0.7 M_{\odot}$ hardly match the position of SB 290 in the $T_{\text{eff}} - \log g$ -diagram. With a mass of $0.6 M_{\odot}$, SB 290 would be situated close to the zero-age EHB.

However, it might still be premature to exclude a high mass right away. An object closely related to SB 290 might be the strong sdB pulsator PG 1605+072, which is known to be a single star with substantial line broadening ($v_{\text{rot}} \sin i = 39 \text{ km s}^{-1}$, Heber 1999). Although this broadening is most likely caused by unresolved pulsations rather than substantial rotation (Langfellner et al. 2012), asteroseismic analyses indicate a high mass of more than $0.7 M_{\odot}$ (van Spaandonk et al. 2008; van Grootel et al. 2010). These results are still under debate, but the tracks for stellar masses of $0.7 M_{\odot}$ and different masses of the hydrogen envelope are more or less consistent with the position of PG 1605+072 in the $T_{\text{eff}} - \log g$ -diagram.

The confirmation of a companion in a wide orbit might complicate the situation since it would require the progenitor to have been in a hierarchical triple system before. On the other hand, if SB 290 had originated in such a triple system, the putative outer companion may have accelerated the merger process by orbit shrinkage through Kozai cycles (Fabrycky & Tremaine 2007).

Acknowledgements. S. G. was supported by the Deutsche Forschungsgemeinschaft under grant He 1354/49-1. The authors thank L. Morales-Rueda for providing her data and Z. Han for providing his evolutionary tracks. We would also like to thank P. Butler for helping us with the reduction of the CYCLOPS data. Furthermore, we thank the referee P. Bergeron. Based on observations at the La Silla Observatory of the European Southern Observatory for programmes 077.D-0515(A) and 084.D-0348(A). Based on observations at the Australian Astronomical Observatory. Based on observations with the William Herschel Telescope operated by the Isaac Newton Group at the Observatorio del Roque de los Muchachos of the Instituto de Astrofísica de Canarias on the island of La Palma, Spain.

References

- Edelmann, H., Heber, U., & Napiwotzki, R. 2001, AN, 322, 401
 Fabrycky, D., & Tremaine, S. 2007, ApJ, 669, 1298
 Fontaine, G., Brassard, P., Charpinet, S., et al. 2012, A&A, 539, 12
 Geier, S. 2013, A&A, 549, A110
 Geier, S., & Heber, U. 2012, A&A, 543, A149
 Geier, S., Nesslinger, S., Heber, U., et al. 2007, A&A, 464, 299
 Geier, S., Heber, U., Podsiadlowski, Ph., et al. 2010, A&A, 519, A25
 Geier, S., Classen, L., & Heber, U. 2011a, ApJ, 733, L13
 Geier, S., Hirsch, H., Tillich, A., et al. 2011b, A&A, 530, A28
 Geier, S., Schaffenroth, V., Drechsel, H., et al. 2011c, ApJ, 731, L22
 Geier, S., Heber, U., Edelmann, H., et al. 2012, ASP Conf. Ser., 452, 57
 Graham, J. A., & Slettebak, A. 1973, AJ, 78, 295
 Han, Z., Podsiadlowski, Ph., Maxted, P. F. L., Marsh, T. R., & Ivanova, N. 2002, MNRAS, 336, 449
 Han, Z., Podsiadlowski, Ph., Maxted, P. F. L., & Marsh, T. R. 2003, MNRAS, 341, 669
 Heber, U. 1987, MitAG, 70, 79
 Heber, U. 2009, ARA&A, 47, 211
 Heber, U., Hunger, K., Jonas, G., & Kudritzki, R. P. 1984, A&A, 130, 119
 Heber, U., Reid, I. N., & Werner, K. 1999, A&A, 348, 25
 Heber, U., Reid, I. N., & Werner, K. 2000, A&A, 363, 198
 Heber, U., Edelmann, H., Lisker, T., & Napiwotzki, R. 2003, A&A, 411, 477
 Iben, I., Jr., & Tutukov, A. V. 1984, ApJS, 54, 335
 Kilkenny, D., van Wyk, F., Roberts, G., Marang, F., & Cooper, D. 1998, MNRAS, 294, 93
 Kuassivi, Bonanno, A., & Ferlet, R. 2005, A&A, 442, 1015
 Kügler, L. 1991, Diploma Thesis, Christian Albrechts Universität Kiel
 Langfellner, J., Schuh, S., et al. 2012, ASP Conf. Ser., 452, 203
 Lisker, T., Heber, U., Napiwotzki, R., et al. 2005, A&A, 430, 223
 Mathys, G., Hubrig, S., Mason, E., et al. 2012, AN, 333, 30
 Napiwotzki, R., Yungelson, L., Nelemans, G., et al. 2004, ASP Conf. Ser., 318, 402
 O’Toole, S. J. 2004, A&A, 423, 25
 Politano, M., Taam, R. E., van der Sluys, M., & Willems, B. 2008, ApJ, 687, 99
 Pollacco, D. L., Skillen, I., Collier Cameron, A., et al. 2006, PASP, 118, 1407
 Skrutskie, M. F., Cutri, R. M., Stiening, R., et al. 2006, AJ, 131, 1163
 Slettebak, A., & Brundage, R. K. 1971, AJ, 76, 338
 Stark, M. A., & Wade, R. 2003, AJ, 126, 1455
 van Grootel, V., Charpinet, S., Fontaine, G., & Brassard, P. 2010, Ap&SS, 329, 217
 van Spaandonk, L., Fontaine, G., Brassard, P., & Aerts, C. 2008, ASP Conf. Ser., 392, 387
 Webbink, R. F. 1984, ApJ, 277, 355
 Zima, W. 2008, CoAst, 157, 387

Appendix A

Table A.1. Radial velocities of SB 290.

Mid-HJD –2 400 000	RV [km s ^{–1}]	Instrument
40 539.50 ¹	–52.3 ± 7.5	Graham & Slettebak (1973)
46 724.57	–15.9 ± 3.2	CASPEC
52 495.66123	–40.4 ± 3.4	FEROS
52 495.70637	–39.5 ± 4.5	
53 953.84358	–4.1 ± 0.6	
53 974.88413	–12.0 ± 0.7	
55 144.62633	–6.4 ± 3.1	EFOSC2
55 144.66202	–12.0 ± 5.0	
55 145.62589	–8.5 ± 5.4	
55 145.62803	–11.9 ± 5.2	
55 145.63016	–9.1 ± 5.8	
55 145.63229	–9.7 ± 5.8	
55 145.63443	–11.0 ± 5.3	
55 145.63656	–8.0 ± 5.6	
55 145.66389	–8.3 ± 6.1	
55 145.66602	–9.8 ± 4.7	
55 145.66815	–10.8 ± 6.0	
55 145.72750	–5.5 ± 7.7	
55 145.72998	–21.7 ± 7.6	
55 145.73247	–26.0 ± 9.4	
55 146.59354	–6.1 ± 5.5	
55 146.59602	–3.0 ± 6.0	
55 146.59851	–8.4 ± 5.0	
55 146.62859	–10.8 ± 4.3	
55 146.65136	–9.8 ± 5.7	
55 146.67425	–7.5 ± 5.3	
55 393.22067	–26 ± 5	CYCLOPS ²
55 393.25356	–24 ± 5	
55 393.28933	–35 ± 5	
55 394.17695	–28 ± 5	
55 394.26083	–27 ± 5	
55 394.26853	–23 ± 5	
55 394.27977	–24 ± 5	
55 394.28749	–25 ± 5	
55 394.33581	–25 ± 5	
55 395.22288	–25 ± 5	
55 395.23057	–24 ± 5	
55 395.23918	–25 ± 5	
55 395.24687	–22 ± 5	
55 395.32561	–23 ± 5	
55 395.33330	–20 ± 5	
55 395.34099	–26 ± 5	
55 396.16408	–21 ± 5	
55 396.17177	–17 ± 5	
55 396.18130	–26 ± 5	
55 396.21822	–30 ± 5	

Notes. ⁽¹⁾ The observing time could only be reconstructed to within this night. ⁽²⁾ Due to the highly variable signal-to-noise ratio of the single spectra, consecutive spectra have been coadded until the quality was sufficient to measure the RV to within about the given uncertainty. In this way, 20 RV epochs have been obtained.

THE FAST-ROTATING, LOW-GRAVITY SUBDWARF B STAR EC 22081–1916: REMNANT OF A COMMON ENVELOPE MERGER EVENT

S. GEIER, L. CLASSEN, AND U. HEBER

Dr. Karl Remeis-Observatory & ECAP, Astronomical Institute, Friedrich-Alexander University Erlangen-Nuremberg,
Sternwartstr. 7, D 96049 Bamberg, Germany; geier@sternwarte.uni-erlangen.de
Received 2011 March 18; accepted 2011 April 14; published 2011 May 3

ABSTRACT

Hot subdwarf B stars (sdBs) are evolved core helium-burning stars with very thin hydrogen envelopes. In order to form an sdB, the progenitor has to lose almost all of its hydrogen envelope right at the tip of the red-giant branch. In binary systems, mass transfer to the companion provides the extraordinary mass loss required for their formation. However, apparently single sdBs exist as well and their formation has been unclear for decades. The merger of helium white dwarfs (He-WDs) leading to an ignition of core helium burning or the merger of a helium core and a low-mass star during the common envelope phase have been proposed as processes leading to sdB formation. Here we report the discovery of EC 22081–1916 as a fast-rotating, single sdB star of low gravity. Its atmospheric parameters indicate that the hydrogen envelope must be unusually thick, which is at variance with the He-WD merger scenario, but consistent with a common envelope merger of a low-mass, possibly substellar object with a red-giant core.

Key words: stars: horizontal-branch – stars: individual (EC 22081–1916)

1. INTRODUCTION

Hot subdwarf B stars (sdBs) are evolved core helium-burning stars with very thin hydrogen envelopes residing at the extreme end of the blue horizontal branch (Heber 2009). The formation of these stars remains unclear. Normal horizontal branch stars are formed after core helium burning is ignited in the red-giant phase. Since the hydrogen envelopes of sdBs are extraordinarily thin, large mass loss is necessary right at the tip of the red-giant branch. In the case of the close binaries among the hot subdwarfs—about half of the known sdB stars are members of short-period ($P \lesssim 10$ days) systems (Maxted et al. 2001; Napiwotzki et al. 2004a)—the required mass loss is triggered by the formation of a common envelope, which is finally ejected. The formation of sdBs with main-sequence companions in wide orbits on the other hand can be explained by stable Roche lobe overflow (Han et al. 2002, 2003).

The formation of single sdBs is less well understood. Several single star scenarios are currently under discussion (see Heber 2009, for a review), but all these scenarios require either a fine-tuning of parameters or extreme environmental conditions which are unlikely to be met for the bulk of the observed subdwarfs in the field. A particularly interesting scenario has been suggested by Soker (1998) and Nelemans & Tauris (1998): single sdB stars could be formed if a substellar companion in close orbit was engulfed by the red-giant progenitor and provided sufficient angular momentum to the common envelope before it was destroyed.

Alternative scenarios invoke stellar mergers to form single sdB stars. The merger of binary white dwarfs was investigated by Webbink (1984) as well as Iben & Tutukov (1984) who showed that an extreme horizontal branch (EHB) star can form when two helium core white dwarfs merge and the product is sufficiently massive to ignite helium. Politano et al. (2008) proposed the merger of a red-giant and a low-mass main-sequence star during the common envelope phase. However, the merger channel was under debate, because all single sdBs analyzed so far turned out to be slow rotators (Geier et al. 2009a), in contrast to the expectations. Here we report the discovery of the fast-rotating, single sdB EC 22081–1916.

2. OBSERVATIONS

EC 22081–1916 ($V = 12.9$ mag, $\alpha_{2000} = 22^{\text{h}}10^{\text{m}}52^{\text{s}}.9$, $\delta_{2000} = -19^{\circ}01'50''$) was discovered in the course of the Edinburgh-Cape blue object survey (Stobie et al. 1997) and classified as an sdB star by Copperwheat et al. (2011). Five high-resolution spectra were taken with the FEROS spectrograph ($R = 48,000$, $\lambda = 3750\text{--}9200$ Å) mounted at the ESO/MPG 2.2 m telescope at La Silla. The first spectrum was taken on 2006 June 14 followed by two exposures on August 9 and 11 in the same year. The last two spectra were taken consecutively on 2010 October 30. In total, the data points cover a timespan of 4.5 years. The spectra have been reduced with the FEROS-DRS pipeline in the context of the MIDAS package. A median filter was applied to correct for cosmics.

EC 22081–1916 has been monitored by planetary transit surveys. Due to its favorable declination it was observed by both the All Sky Automated Survey (ASAS; Pojmanski 1997) and the Northern Sky Variability Survey (NSVS; Woźniak et al. 2004). Both light curves have been downloaded from the data archives. The ASAS data set contains more than 450 data points of Johnson V photometry. We selected data extracted with smallest aperture and included only measurements of sufficient quality (flagged from A to C). The light curve was folded to a period of 0.15 days (see Section 4) and binned. The white light curve from NSVS contains 93 data points and was phased in the same way. No variations exceeding 2% (NSVS) and 1% (ASAS) were detected.

The VizieR database contains several consistent proper motion measurements of this object. Among them the PPMXL ($\mu_{\alpha} \cos \delta = 17.0$ mas yr $^{-1}$, $\mu_{\delta} = -13.5$ mas yr $^{-1}$; Roeser et al. 2010) and UCAC3 ($\mu_{\alpha} \cos \delta = 17.7$ mas yr $^{-1}$, $\mu_{\delta} = -12.1$ mas yr $^{-1}$; Zacharias et al. 2010) values are independently measured and perfectly consistent within the error bars. Taking the average values we obtain $\mu = 21.6$ mas yr $^{-1}$.

3. ATMOSPHERIC PARAMETERS AND ROTATIONAL BROADENING

Atmospheric parameters and projected rotational velocity (see Table 1) have been determined simultaneously by fitting a

Table 1
Parameters of EC 22081–1916

mid-HJD	RV (km s ⁻¹)	T_{eff} (K)	log g	log y	$v_{\text{rot}} \sin i$ (km s ⁻¹)
2453900.845477	-11.0 ± 1.0	$31,500 \pm 150$	4.74 ± 0.02	-1.91 ± 0.03	172 ± 4.0
2453956.798348 ^a	-18.6 ± 2.6	
2453958.634893	-13.4 ± 1.3	$31,500 \pm 190$	4.81 ± 0.03	-1.83 ± 0.04	150 ± 5.0
2455499.620294	-13.6 ± 1.0	$29,800 \pm 140$	4.67 ± 0.02	-2.01 ± 0.03	172 ± 4.0
2455499.639508	-9.0 ± 1.0	$31,200 \pm 170$	4.83 ± 0.03	-1.90 ± 0.04	170 ± 4.0
Co-added		$31,100 \pm 100$	4.77 ± 0.02	-1.97 ± 0.02	163 ± 3.0

Note. ^a Spectrum with low signal-to-noise ratio.

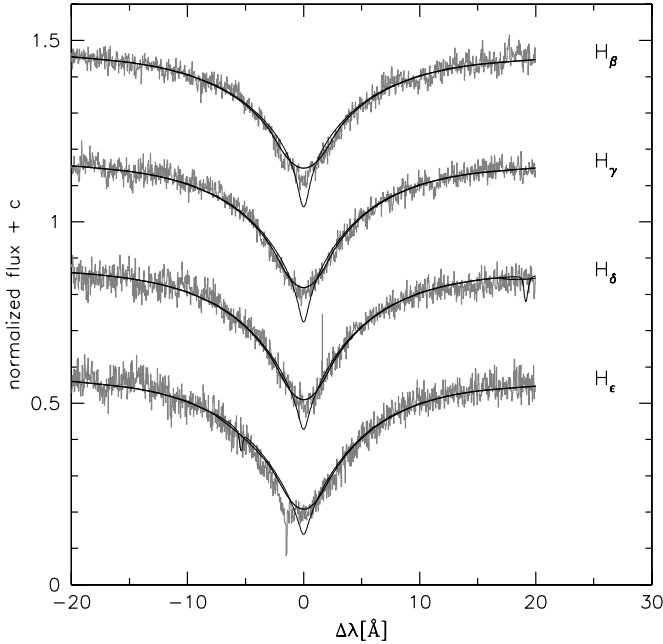


Figure 1. Fit of synthetic LTE models to some hydrogen Balmer lines. The thin solid line marks models without rotational broadening, the thick solid line the best fitting model spectrum with $v_{\text{rot}} \sin i = 163 \text{ km s}^{-1}$.

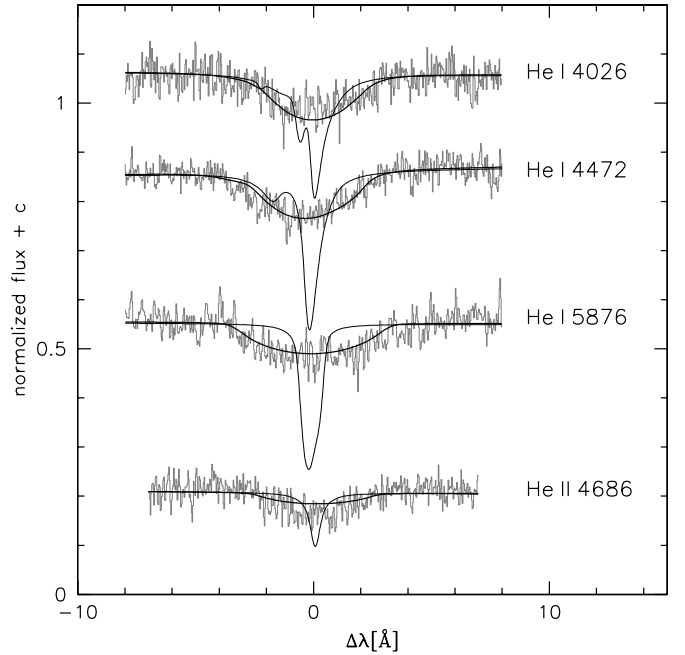


Figure 2. Fit of synthetic LTE models to helium lines (see Figure 1). The extreme rotational broadening of the lines is obvious.

grid of synthetic spectra, calculated from line-blanketed, solar-metallicity LTE model atmospheres (Heber et al. 2000), to the hydrogen Balmer lines (H_{β} – H_{10}) and helium lines (He I 4026, 4472, 4922, 5876 Å and He II 4686 Å) using the SPAS routine developed by H. Hirsch (e.g., Geier et al. 2011c). The single spectra have been corrected for their orbital motion and co-added. Statistical errors are determined with a bootstrapping algorithm.

As can be seen in Figures 1 and 2, the Balmer line cores and the helium lines are significantly broadened. In order to fit these lines, a very high rotational broadening of $v_{\text{rot}} \sin i = 163 \pm 3 \text{ km s}^{-1}$ is necessary. The fact that no metal lines have been found is consistent with this high broadening since weak features melt into the continuum in this case. The resulting effective temperature $T_{\text{eff}} = 31,100 \pm 1000 \text{ K}$ and helium abundance $\log y = -1.97 \pm 0.02$ are typical for sdB stars, whereas the surface gravity of $\log g = 4.77 \pm 0.10$ is unusually low for the effective temperature in question (see Figure 3).

The radial velocities (RVs) of the five single spectra were measured by fitting model spectra with fixed parameters derived from the spectral analysis to the Balmer and helium lines using the FITSB2 routine (Napiwotzki et al. 2004b; see Table 1). No significant RV variations were measured. The RV of the star is constant at $-13.1 \pm 3.6 \text{ km s}^{-1}$.

By adopting the canonical mass of sdB stars ($0.47 M_{\odot}$), we can derive the distance from the atmospheric parameters and the apparent magnitude following Ramspeck et al. (2001). The transversal velocity v_t of the star in km s^{-1} can then be calculated using the simple formula $v_t = 4.74 d \mu$, where the distance d is given in kpc and the proper motion μ in mas. The distance to the star is $\simeq 1.5 \text{ kpc}$ and the transversal velocity $\simeq 150 \text{ km s}^{-1}$ perfectly consistent with an evolved star in the thick disk or in the halo (e.g., Tillich et al. 2011).

4. CONSTRAINING THE NATURE OF EC 22081–1916

EC 22081–1916 has the highest $v_{\text{rot}} \sin i$ ever measured for an sdB star. All other single sdB stars analyzed so far have $v_{\text{rot}} \sin i < 10 \text{ km s}^{-1}$ (Geier et al. 2009a). In the following, we discuss and exclude several possible explanations for this finding.

Main-sequence star? Rotational velocities exceeding 100 km s^{-1} are quite common among main-sequence A and B stars. Since the surface gravity $\log g = 4.77$ is at the lower end of the hot subdwarf parameter range, the star may be regarded as a misclassified massive main-sequence star. This interpretation, however, can be ruled out because the surface gravity is too high (see Figure 3) and the helium abundance (1/10-solar) far too low. A double-lined binary consisting of two hot

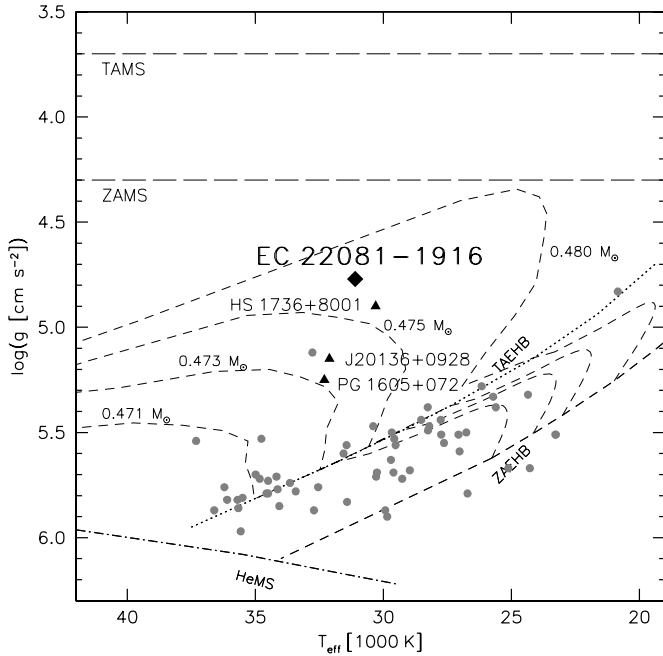


Figure 3. $T_{\text{eff}}-\log g$ diagram. The gray circles mark sdBs from the ESO Supernova Ia Progenitor Survey (Lisker et al. 2005). The low-gravity sdBs HS 1736+8001 (Edelmann et al. 2003), PG 1605+072 (Heber et al. 1999), and J20136+0928 (Østensen et al. 2011) are plotted as triangles. The helium main sequence (HeMS) and the EHB band (limited by the zero-age EHB, ZAEHB, and the terminal-age EHB, TAEHB) are superimposed with EHB evolutionary tracks for solar metallicity from Dorman et al. (1993). The location of the main sequence (MS, limited by the zero-age MS, ZAMS, and the terminal-age MS, TAMS) is indicated by the long-dashed horizontal lines.

main-sequence stars is another option. An unresolved, double-lined binary may explain the high measured surface gravity, which could be overestimated in this case. However, we cannot imagine a combination of main-sequence stars that would produce such an unusual spectrum.

Hot subdwarf with unresolved pulsations? Two kinds of sdB pulsators are known. The slow pulsations of the V 1093 Her stars (sdBV_s) are not expected to influence the line broadening significantly. In the case of the short-period pulsators (V 361 Hya type, sdBV_r), unresolved pulsations can severely affect the broadening of the lines and therefore mimic higher $v_{\text{rot}} \sin i$. Telting et al. (2008) showed that this happens in the case of the hybrid pulsator Balloon 090100001. Unresolved pulsations are also most likely responsible for the high $v_{\text{rot}} \sin i = 39 \text{ km s}^{-1}$ measured for the high-amplitude pulsator PG 1605+072 (Heber et al. 1999).

The five spectra of EC 22081–1916 have been taken with exposure times ranging from 900 s to 1500 s. The effective temperature of the sdB is consistent with the ones of short-period pulsating sdBs. The typical pulsation periods of sdBV_r stars are of the order of a few minutes and therefore shorter than the exposure times. However, the measured $v_{\text{rot}} \sin i = 163 \text{ km s}^{-1}$ is so high that very large photometric variations at periods of a few minutes would be inevitable. Therefore, the broadening cannot be caused by unresolved pulsations. The prominent mode of the strongest known sdB pulsator PG 1605+072 has a photometric amplitude of $\simeq 13\%$ (Koen et al. 1998) and an RV amplitude of $\simeq 15 \text{ km s}^{-1}$ (O’Toole et al. 2005b). In order to cause the line broadening necessary to fit EC 22081–1916, both values would have to be much higher. Due to the fact that we neither detect RV variations nor any features in the light

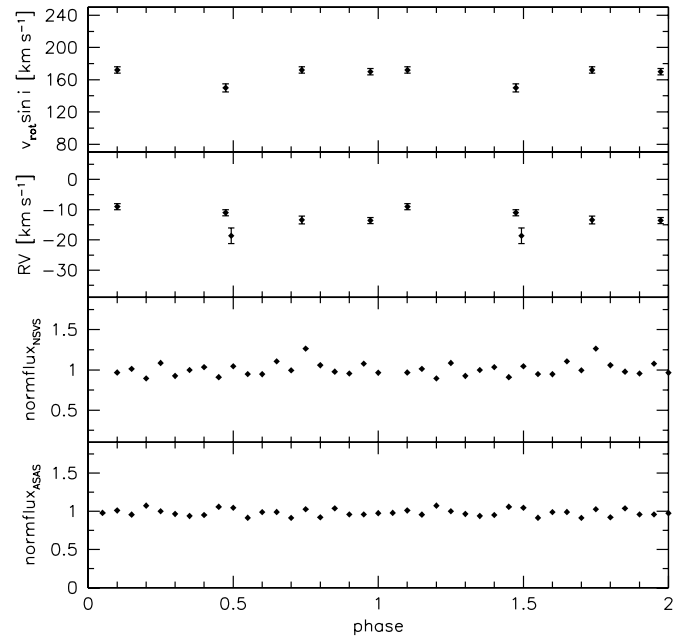


Figure 4. Time-resolved photometry (ASAS V band, NSVS white light, lower panels), radial and projected rotational velocities (with formal 1σ fitting errors, upper panels) plotted against phase. The data have been folded to the upper limit for the orbital period of a putative close binary with substellar companion ($P \simeq 0.15$ days; see Section 4). Two complete phases are plotted for better visualization. Since no significant variations can be seen in the data, EC 22081–1916 is neither a strong pulsator nor in a close binary system.

curves (see Figure 4) we conclude that EC 22081–1916 is not a high-amplitude pulsator.

Hot subdwarf with high magnetic fields? O’Toole et al. (2005a) discovered magnetic fields up to $\simeq 1.5 \text{ kG}$ in a small sample of sdB stars. From the analysis of magnetic white dwarfs with field strengths in the MG range, it is known that small Zeeman splitting can mimic a broadening of the spectral lines (see, e.g., Külebi et al. 2009). Could EC 22081–1916 be the prototype of a new sdB class with very strong magnetic fields? Looking at Figures 1 and 2, this explanation can be ruled out as well. Zeeman splitting affects every single spectral line in a different way. In contrast to that, the broadening of the lines is uniform. We therefore conclude that the line broadening of EC 22081–1916 is caused by rotation.

Close binary with large RV amplitude and orbital smearing? The hot subdwarfs with the highest measured projected rotational velocities ($v_{\text{rot}} \sin i > 100 \text{ km s}^{-1}$) all reside in very close binary systems with orbital periods of $\simeq 0.1$ days. These sdBs were spun up by the tidal influence of their close companions and their rotation became synchronized to their orbital motion (Geier et al. 2007, 2010).

A close companion would therefore be the most natural explanation for the high $v_{\text{rot}} \sin i$ of EC 22081–1916. The colors of this star ($J - K_S \simeq 0.0$, 2MASS; Skrutskie et al. 2006) do not show any signs of a cool companion (Stark & Wade 2003). A possible unseen companion must therefore be either a low-mass main-sequence star, a compact object like a white dwarf, or a substellar object.

White dwarf and main-sequence companions can be immediately ruled out because no significant RV variations are detected on timescales of years, days, and half an hour. This is also a strong argument against the hypothesis that the strong line broadening may be at least partly caused by orbital smearing. Since the exposure times of the FEROS spectra are rather long

(900–1500 s), the RV shift during the exposure would be large in a close binary with high RV amplitude (e.g., Geier et al. 2007). However, no RV variations are measured (see Figure 4, upper panel). Furthermore, a quantitative spectral analysis as outlined in Section 3 has been performed for a single FEROS spectrum and no significant variations in the atmospheric parameters or the $v_{\text{rot}} \sin i$ were detected (see Table 1). Orbital smearing can therefore be ruled out.

Close binary with small RV amplitude? The remaining option would be a substellar companion in a very close orbit similar to the sdB+brown dwarf (BD) binary SDSS J08205+0008 (Geier et al. 2011b). Assuming that the rotation of EC 22081–1916 is synchronized, an upper limit for the orbital period can be calculated. Adopting $M_{\text{sdB}} = 0.47 M_{\odot}$ and using the measured $\log g$, the radius of the star is $R_{\text{sdB}} = \sqrt{M_{\text{sdB}} G / g} \simeq 0.47 R_{\odot}$. Taking the inclination into account ($v_{\text{rot}} \geq v_{\text{rot}} \sin i$), we can calculate an upper limit for the orbital period $P \leq 2\pi R_{\text{sdB}} / v_{\text{rot}} \sin i \simeq 0.145$ days. Another strict constraint is set by the lack of significant RV variations. Taking the standard deviation of the RV measurements and multiplying it by 3 we end up with a conservative upper limit for the RV semi-amplitude $K < 12 \text{ km s}^{-1}$.

Adopting the upper limits for P and K , the companion would have to be a brown dwarf with $\simeq 20 M_{\text{J}}$ and a radius of $\simeq 0.1 R_{\odot}$. For inclinations lower than 90° the orbital period of the putative binary must be shorter, because the absolute rotational velocity of the sdB has to be higher to keep $v_{\text{rot}} \sin i$ fixed at the observed value.

However, other important constraints have to be met as well. Neither the sdB nor its putative companion is allowed to fill their Roche lobes, because in this case the system would exchange mass. Since no indicative features for ongoing mass transfer (e.g., emission lines) are present in the spectra, the system must be detached. Calculating the Roche radii of both components as outlined in Eggleton (1983) we derive a minimum orbital period for the system of $\simeq 0.11$ days and a minimum inclination of 47° . For shorter periods and hence lower inclinations the sdB would fill its Roche lobe. A similar limit ($\simeq 0.1$ days) is derived, if we allow K to be smaller than 12 km s^{-1} . For orbital periods shorter than that, a putative brown dwarf companion would fill its Roche lobe.

These simple calculations show that the possible parameter space of a close and synchronized binary would be extremely narrow ($P \simeq 0.1\text{--}0.15$ days, $K \simeq 4\text{--}12 \text{ km s}^{-1}$). Furthermore, all possible configurations would lead to photometric variabilities easily visible in the light curve. Close sdB+dM or BD systems are not only often eclipsing, but also show sinusoidal variations due to light from the irradiated surface of the cool companion (e.g., Østensen et al. 2010; For et al. 2010; Geier et al. 2011b). Due to its high temperature and low surface gravity EC 22081–1916 has a very high luminosity compared with other sdBs, which should lead to a very strong reflection effect at inclinations of $\simeq 50^{\circ}$ or higher. Since no variations were found in the ASAS and NSVS light curves (Figure 4), a nearby low-mass companion can be excluded as well.

5. CONCLUSION

After excluding all possible alternative scenarios we conclude that EC 22081–1916 is the first single sdB star which is rapidly rotating. Furthermore, the $\log g$ of EC 22081–1916 is the lowest one ever measured for an sdB (see Figure 3). Østensen et al. (2011) argued that the low gravity of the pulsating sdB J20163+0928 ($\log g = 5.15$) may be due to a rather thick layer

of hydrogen. In the model of Han et al. (2002, 2003) even the merger remnants with the highest masses would need a hydrogen layer of $\simeq 0.01 M_{\odot}$ to reach at such low surface gravities.

The formation of such an object through single star evolution is very hard to explain. EC 22081–1916 thus might have been formed by a merger event. Three merger scenarios have been proposed to explain the origin of hot subdwarfs. Webbink (1984) and Iben & Tutukov (1984) proposed the merger of two He-WDs as possible formation channel, which has been further explored by Saio & Jeffery (2002). Han et al. (2002, 2003) included this channel in their binary evolution calculations and were able to model both the UV excess in elliptical galaxies (Han et al. 2007) and the different close binary fractions of sdBs in populations of different age in a consistent way (Han 2008). He-WD mergers are believed to have very small envelope masses and are expected to be situated at the very blue end of the EHB. Both are at variance with the position of EC 22081–1916 in the $T_{\text{eff}}\text{--}\log g$ diagram (see Figure 3). Justham et al. (2010) proposed that the merger of a close binary system consisting of an sdB and an He-WD may form a single helium-enriched sdO. EC 22081–1916, however, is helium deficient.

EC 22081–1916 most likely belongs to an old stellar population, either thick disk or halo. Its position in the $T_{\text{eff}}\text{--}\log g$ diagram (see Figure 3) may indicate a mass higher than canonical, which would be consistent with the predictions by Han et al. (2002, 2003). If it should be the remnant of an He-WD merger, this would imply important constraints on the merger process itself. Since the helium abundance of EC 22081–1916 is 10 times below the solar value, enough hydrogen must have survived the merger and must have been enriched in the atmosphere by diffusion processes.

The third channel was suggested by Soker (1998) and further explored by Soker & Harpaz (2000, 2007). Politano et al. (2008) followed this idea and focused on the formation of hot subdwarfs. The merger of a red-giant core and a low-mass, main-sequence star or substellar object during a common envelope phase may lead to the formation of a rapidly rotating hot subdwarf star. This scenario fits particularly well with observations for several reasons.

First, the helium core of a red giant merges with an unevolved low-mass star or a brown dwarf. Both have hydrogen-rich envelopes. This provides a natural explanation for the low He abundance and surface gravity of the remnant. The hydrogen is provided by the merged companion. Furthermore, this companion also provides the energy required to eject the envelope and form the sdB. Several sdBs with low-mass stellar and substellar companions have been found most recently and the true number may be much higher due to selection effects (e.g., For et al. 2010; Østensen et al. 2010; Geier et al. 2009b, 2011a, 2011b).

A very important prediction made by Politano et al. (2008) is that sdBs formed via the CE-merger channel should be rare. EC 22081–1916 is unique among $\simeq 100$ slowly rotating sdB stars analyzed so far (Geier et al. 2009a). In contrast to that, Han et al. (2002, 2003) predict a large fraction if not all of the single sdBs to be formed by WD mergers. Unless there is a mechanism to get rid of all the angular momentum involved in a merger as suggested by Saio & Jeffery (2002), this observation is hard to explain.

Furthermore, Politano et al. (2008) predict that a large fraction of the sdBs formed after CE merger should rotate with a critical velocity v_{crit} , which is defined as the rotational velocity at which mass loss induced by centrifugal forces prevents the red-giant core to accrete more material from the secondary. Politano

et al. (2008) estimate this critical velocity to be about one-third of the breakup velocity $v_{br} = (GM/R)^{1/2}$. Using the parameters derived for EC 22081–1916, we calculate $v_{crit} \simeq 145 \text{ km s}^{-1}$ perfectly consistent with the projected rotational velocity measured from the spectrum.

In conclusion, the scenario proposed by Soker (1998) and Politano et al. (2008) fits best with the observational data obtained so far, although the He-WD+He-WD or sdB+He-WD merger scenarios cannot be ruled out. EC 22081–1916 is the first candidate for a merger remnant among the hot subdwarf stars. Similar objects are expected to be found in large spectroscopic databases like Sloan Digital Sky Survey (SDSS). Due to the high rotational broadening, the quality of these data should be sufficient to find them.

Based on observations at the La Silla Observatory of the European Southern Observatory for program numbers 082.D-0649 and 084.D-0348. S.G. is supported by the Deutsche Forschungsgemeinschaft (DFG) through grant HE1356/49-1. We thank L. Morales-Rueda for sharing her data with us. Furthermore, S.G. wants to thank Ph. Podsiadlowski, C. S. Jeffery, R. H. Østensen, and S. J. O’Toole for discussing and partly defending the merger channel as a possible formation scenario for hot subdwarfs. Special thanks go to the organizers of the 4th sdOB meeting in Shanghai where these and other problems were discussed.

REFERENCES

- Copperwheat, C. M., Morales-Rueda, L., Marsh, T. R., Maxted, P. F. L., & Heber, U. 2011, *MNRAS*, in press (arXiv:1103.4745)
- Dorman, B., Rood, R. T., & O’Connell, R. W. 1993, *ApJ*, 419, 596
- Edelmann, H., Heber, U., Hagen, H.-J., Lemke, M., Dreizler, S., Napiwotzki, R., & Engels, D. 2003, *A&A*, 400, 939
- Eggleton, P. P. 1983, *ApJ*, 268, 368
- For, B.-Q., et al. 2010, *ApJ*, 708, 253
- Geier, S., Heber, U., Edelmann, H., Kupfer, T., Napiwotzki, R., & Podsiadlowski, Ph. 2009a, *J. Phys. Conf. Ser.*, 172, 012008
- Geier, S., Heber, U., Edelmann, H., & Morales-Rueda, L. 2009b, *ApJ*, 702, L96
- Geier, S., Heber, U., Podsiadlowski, Ph., Edelmann, H., Napiwotzki, R., Kupfer, T., & Müller, S. 2010, *A&A*, 519, 25
- Geier, S., Napiwotzki, R., Heber, U., & Nelemans, G. 2011a, *A&A*, 528, L16
- Geier, S., Nesslinger, S., Heber, U., Przybilla, N., Napiwotzki, R., & Kudritzki, R.-P. 2007, *A&A*, 464, 299
- Geier, S., et al. 2011b, *ApJ*, 731, L22
- Geier, S., et al. 2011c, *A&A*, in press (arXiv:1103.4045)
- Han, Z. 2008, *A&A*, 484, 31
- Han, Z., Podsiadlowski, Ph., & Lynas-Gray, A. E. 2007, *MNRAS*, 380, 1098
- Han, Z., Podsiadlowski, Ph., Maxted, P. F. L., & Marsh, T. R. 2003, *MNRAS*, 341, 669
- Han, Z., Podsiadlowski, Ph., Maxted, P. F. L., Marsh, T. R., & Ivanova, N. 2002, *MNRAS*, 336, 449
- Heber, U. 2009, *ARA&A*, 47, 211
- Heber, U., Reid, I. N., & Werner, K. 1999, *A&A*, 348, 25
- Heber, U., Reid, I. N., & Werner, K. 2000, *A&A*, 363, 198
- Iben, I., Jr., & Tutukov, A. V. 1984, *ApJS*, 54, 335
- Justham, S., Podsiadlowski, Ph., Han, Z., & Wolf, C. 2010, *Ap&SS*, 329, 3
- Koen, C., O’Donoghue, D., Kilkenny, D., Lynas-Gray, A. E., Marang, F., & van Wyk, F. 1998, *MNRAS*, 296, 317
- Külebi, B., Jordan, S., Euchner, F., Gänsicke, B. T., & Hirsch, H. 2009, *A&A*, 506, 1341
- Lisker, T., Heber, U., Napiwotzki, R., Christlieb, N., Han, Z., Homeier, D., & Reimers, D. 2005, *A&A*, 430, 223
- Maxted, P. F. L., Heber, U., Marsh, T. R., & North, R. C. 2001, *MNRAS*, 326, 1391
- Napiwotzki, R., et al. 2004a, *Ap&SS*, 291, 321
- Napiwotzki, R., et al. 2004b, in ASP Conf. Ser. 318, Spectroscopically and Spatially Resolving the Components of the Close Binary Stars, ed. R. W. Hilditch, H. Hensberge, & K. Pavlovski (San Francisco, CA: ASP), 402
- Nelemans, G., & Tauris, T. M. 1998, *A&A*, 335, L85
- Østensen, R. H., et al. 2010, *MNRAS*, 408, 51
- Østensen, R. H., et al. 2011, *ApJ*, 731, L13
- O’Toole, S. J., Jordan, S., Friedrich, S., & Heber, U. 2005a, *A&A*, 437, 227
- O’Toole, S. J., et al. 2005b, *A&A*, 440, 667
- Pojmanski, G. 1997, *Acta Astron.*, 47, 467
- Politano, M., Taam, R. E., van der Sluys, M., & Willems, B. 2008, *ApJ*, 687, L99
- Ramspeck, M., Heber, U., & Edelmann, H. 2001, *A&A*, 379, 235
- Roeser, S., Demleitner, M., & Schilbach, E. 2010, *AJ*, 139, 2440
- Saio, H., & Jeffery, C. S. 2002, *MNRAS*, 333, 121
- Skrutskie, M. F., et al. 2006, *AJ*, 131, 1163
- Soker, N. 1998, *AJ*, 116, 1308
- Soker, N., & Harpaz, A. 2000, *MNRAS*, 317, 861
- Soker, N., & Harpaz, A. 2007, *ApJ*, 660, 699
- Stark, M. A., & Wade, R. 2003, *AJ*, 126, 1455
- Stobie, R. S., et al. 1997, *MNRAS*, 287, 848
- Telting, J. H., et al. 2008, *A&A*, 492, 815
- Tillich, et al. 2011, *A&A*, 527, 137
- Webbink, R. F. 1984, *ApJ*, 277, 355
- Woźniak, P. R., et al. 2004, *AJ*, 127, 2436
- Zacharias, N., et al. 2010, *AJ*, 139, 2184

BINARIES DISCOVERED BY THE MUCHFUSS PROJECT: SDSS J08205+0008—AN ECLIPSING SUBDWARF B BINARY WITH A BROWN DWARF COMPANION

S. GEIER¹, V. SCHAFFENROTH¹, H. DRECHSEL¹, U. HEBER¹, T. KUPFER¹, A. TILLICH¹, R. H. ØSTENSEN², K. SMOLDERS²,
P. DEGROOTE², P. F. L. MAXTED³, B. N. BARLOW⁴, B. T. GÄNSICKE⁵, T. R. MARSH⁵, AND R. NAPIWOTZKI⁶

¹ Dr. Reimis-Observatory & ECAP, Astronomical Institute, Friedrich-Alexander University Erlangen-Nürnberg, Sternwartstr. 7, 96049 Bamberg, Germany; geier@sternwarte.uni-erlangen.de

² Institute of Astronomy, K.U. Leuven, Celestijnenlaan 200D, B-3001 Heverlee, Belgium

³ Astrophysics Group, Keele University, Staffordshire, ST5 5BG, UK

⁴ Department of Physics and Astronomy, University of North Carolina, Chapel Hill, NC 27599-3255, USA

⁵ Department of Physics, University of Warwick, Coventry CV4 7AL, UK

⁶ Centre of Astrophysics Research, University of Hertfordshire, College Lane, Hatfield AL10 9AB, UK

Received 2010 December 14; accepted 2011 March 3; published 2011 March 24

ABSTRACT

Hot subdwarf B stars (sdBs) are extreme horizontal branch stars believed to originate from close binary evolution. Indeed about half of the known sdB stars are found in close binaries with periods ranging from a few hours to a few days. The enormous mass loss required to remove the hydrogen envelope of the red-giant progenitor almost entirely can be explained by common envelope ejection. A rare subclass of these binaries are the eclipsing HW Vir binaries where the sdB is orbited by a dwarf M star. Here, we report the discovery of an HW Vir system in the course of the MUCHFUSS project. A most likely substellar object ($\simeq 0.068 M_{\odot}$) was found to orbit the hot subdwarf J08205+0008 with a period of 0.096 days. Since the eclipses are total, the system parameters are very well constrained. J08205+0008 has the lowest unambiguously measured companion mass yet found in a subdwarf B binary. This implies that the most likely substellar companion has not only survived the engulfment by the red-giant envelope, but also triggered its ejection and enabled the sdB star to form. The system provides evidence that brown dwarfs may indeed be able to significantly affect late stellar evolution.

Key words: binaries: spectroscopic – brown dwarfs – stars: horizontal-branch – stars: individual (SDSS J082053.53+000843.4)

1. INTRODUCTION

Hot subdwarf B stars (sdBs) are core helium-burning stars with hydrogen envelopes too thin to sustain hydrogen shell burning and have masses of about $0.47 M_{\odot}$ (Heber 2009). The large fraction of close binaries—about half of the known sdB stars are members of short-period ($P \lesssim 10$ days) binaries (Maxted et al. 2001; Napiwotzki et al. 2004a)—can be explained by binary evolution models. The required extraordinarily large mass loss in the red-giant phase is triggered by the formation of a common envelope, which is finally ejected. Binary population synthesis models (Han et al. 2002, 2003) are successful in matching the observed properties of known systems qualitatively. The existence of apparently single sdB stars poses another problem. However, even in this case binary evolution comes to the rescue, because such stars may form from the merger of two helium white dwarfs (Webbink 1984; Iben & Tutukov 1984) or from the engulfment and possible destruction of a substellar object (Soker 1998; Nelemans & Tauris 1998).

The existence of eclipsing sdB+dM binaries of HW Vir type with very short orbital periods (0.1–0.26 days) and very low companion masses between $0.1 M_{\odot}$ and $0.2 M_{\odot}$ (e.g., For et al. 2010; Østensen et al. 2010) shows that stars close to the nuclear-burning limit of $\simeq 0.08 M_{\odot}$ are able to eject a common envelope and form an sdB. Claims have been made that the primaries of AA Dor (Rauch 2000; Rucinski 2009) and HS 2231+2441 (Østensen et al. 2008) are low-mass sdBs and the companions therefore substellar. However, in the former case this has been refuted by the measurement of the companion’s radial velocity (RV) curve (Vučković et al. 2008) and in the latter case by the gravity measurement (For et al. 2010). Substellar companions to sdB stars have been found using the light travel time technique

(Schuh 2010, and references therein). However, these systems have wide orbits and are therefore unlikely to have experienced a common envelope phase. None of these companions influenced the evolution of its host star, but the presence of such objects in wide orbits may be an indication of current or former close substellar companions to sdBs.

Here, we report the discovery of the short-period eclipsing HW Vir type binary J08205+0008 from the Massive Unseen Companions to Hot Faint Underluminous Stars from SDSS (MUCHFUSS) project. This system is regarded as the first one in which a close substellar companion to an sdB star has been detected unambiguously.

2. TARGET SELECTION AND RADIAL VELOCITY CURVE

The MUCHFUSS project aims at finding sdBs with compact companions such as massive white dwarfs (WDs; $M > 1.0 M_{\odot}$), neutron stars, or black holes. Details on the survey and target selection procedure are provided in Geier et al. (2011a), and an analysis of seven sdB binaries in Geier et al. (2011b). The same selection criteria that we applied to find such binaries are also well suited to single out hot subdwarf stars with constant high radial velocities in the Galactic halo and search for hypervelocity stars. First results of the search for hypervelocity stars are presented in Tillich et al. (2011).

The MUCHFUSS target selection strategy is tailored to single out RV variations on time scales of half an hour or less. Such variations may indicate the presence of short-period systems of relatively low RV amplitude or longer-period binaries with high RV amplitudes. The latter are the prime targets for the core program of MUCHFUSS. Obviously, the campaign is also

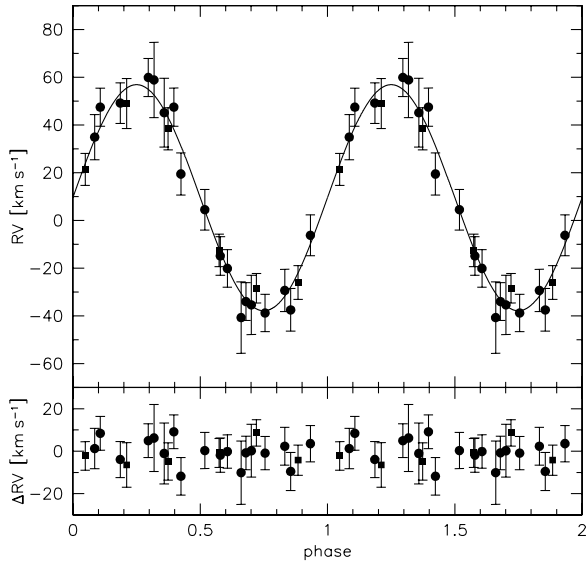


Figure 1. Radial velocity plotted against orbital phase of J08205+0008. The RV data were phase folded with the most likely orbital period. The residuals are plotted below. The RVs were measured from spectra obtained with SDSS (rectangles) and ESO-NTT/EFOSC2 (circles). The errors are formal 1σ uncertainties.

bound to find short-period, low RV amplitude systems with low-mass stellar or even substellar companions.

SDSS J082053.53+000843.4 (GALEX J082053.6+000843, in short J08205+0008, $g = 14.9$ mag) was classified as an sdB star by color selection and visual inspection of Sloan Digital Sky Survey (SDSS) spectra (Abazajian et al. 2009), which are flux calibrated and cover the wavelength range from 3800 Å to 9200 Å with a resolution of $R = 1800$. The six individual sub-spectra showed significant RV variability and the star became a high-priority target for the MUCHFUSS spectroscopic follow-up. Eighteen spectra were taken with the EFOSC2 spectrograph ($R \simeq 2200$, $\lambda = 4450\text{--}5110$ Å) mounted at the ESO NTT. Five additional spectra were taken with the Goodman spectrograph mounted at the Southern Astrophysical Research (SOAR) telescope ($R \simeq 2500$, $\lambda = 3500\text{--}6160$ Å).

The radial velocities were measured by fitting a set of mathematical functions to the hydrogen Balmer lines as well as He I lines using the FITSB2 routine (Napiwotzki et al. 2004b). The continuum is matched by a polynomial, line wings and line core by a Lorentzian and a Gaussian, respectively. The orbital solution (see Table 1) was derived based on the spectra from SDSS and the ones taken with EFOSC2 as described in Geier et al. (2011b). The phase coverage of the RV curve is very good (see Figure 1). The best fit orbital period is 0.096 ± 0.001 days. Two alias periods are possible at $P = 0.088$ days and 0.108 days, but can be rejected by the analysis of the light curve.

3. THE LIGHT CURVE

Photometric light curves were obtained on three separate nights between 2009 November 29 and 2010 January 13, with the Flemish 1.2 m Mercator Telescope on La Palma, Canary Islands. During the period that these observations were made, we were in the process of commissioning an upgrade to the Merope CCD camera, fitting it with a large E2V frame transfer CCD with 2048×3074 pixels (Østensen 2010). Although the upgraded camera suffered from some technical issues, and the observing conditions were far from perfect, the deep primary and

Table 1
Parameters of J08205+0008

Spectroscopic parameters		
T_0 (HJD)	2455147.8564 ± 0.0006	
P (days)	0.096 ± 0.001	
γ (km s^{-1})	9.5 ± 1.3	
K_1 (km s^{-1})	47.4 ± 1.9	
$f(M)$ (M_\odot)	0.0011 ± 0.0001	
T_{eff} (K)	26700 ± 1000	
$\log g$	5.48 ± 0.10	
$\log y$	-2.0 ± 0.07	
$M_{2, M_{\text{sdb}}=0.47}$ (M_\odot)	$0.068^{+0.003}_{-0.003}$	
$M_{2, M_{\text{sdb}}=0.25}$ (M_\odot)	$0.045^{+0.003}_{-0.002}$	
Light curve solution		
A_1	1.0	
$T_{\text{eff}}(1)$ (K)	26700	
g_1	1.0	
g_2	0.32	
$x_1(R)$	0.18	
$x_2(R)$	1.0	
	$M_{\text{sdb}} = 0.25 M_\odot$	$M_{\text{sdb}} = 0.47 M_\odot$
$q (= M_2/M_1)$	0.181	0.1438
i ($^\circ$)	85.87 ± 0.16	85.83 ± 0.19
$q (= M_2/M_1)$	0.181	0.1438
$T_{\text{eff}}(2)$ (K)	2958 ± 207	2484 ± 230
A_2	1.11 ± 0.05	1.09 ± 0.04
Ω_1	3.687 ± 0.026	3.621 ± 0.027
Ω_2	2.732 ± 0.009	2.470 ± 0.007
$\frac{L_1}{L_1+L_2}$ (R)	0.99983 ± 0.00008	0.99995 ± 0.00004
δ_1	0.0282 ± 0.002	0.030 ± 0.002
r_1 (pole) (a)	0.277 ± 0.002	0.278 ± 0.002
r_1 (point) (a)	0.283 ± 0.002	0.284 ± 0.002
r_1 (side) (a)	0.280 ± 0.002	0.282 ± 0.002
r_1 (back) (a)	0.282 ± 0.002	0.283 ± 0.002
r_2 (pole) (a)	0.136 ± 0.001	0.137 ± 0.001
r_2 (point) (a)	0.137 ± 0.001	0.138 ± 0.001
r_2 (side) (a)	0.137 ± 0.001	0.138 ± 0.001
r_2 (back) (a)	0.140 ± 0.001	0.142 ± 0.001

shallow secondary eclipses superimposed on a strong reflection effect are perfectly clear in all the light curves (see Figure 2). The data were obtained using the Geneva R -band filter and exposure times from 16 to 90 s.

The light curve was analyzed with the MORO code, which is based on the Wilson–Devinney approach (Wilson & Devinney 1971) but takes into account radiative interaction between the components of hot, close binaries (Drechsel et al. 1995).

The light curve was binned over narrow time intervals. The photometric period was determined by measuring the time spans between three consecutive primary eclipses. The result 0.096 ± 0.001 days is perfectly consistent with the best spectroscopic solution (see Section 2). We used Wilson–Devinney mode 2, which poses no restrictions to the system configuration and links the luminosity and the temperature of the second component by means of the Planck law. The gravity darkening exponents ($g_{1,2}$) and the linear limb darkening coefficient of the sdB primary ($x_1(R)$) were fixed at literature values (Drechsel et al. 2001, and references therein), whereas the linear limb darkening coefficient of the secondary ($x_2(R)$) was fixed to 1.0 because all light curve solutions converged at this value. The bolometric albedo of the primary was also fixed to 1.0. The temperature of the sdB was taken from the spectral analysis ($T_{\text{eff}}(1) = 26,000$ K).

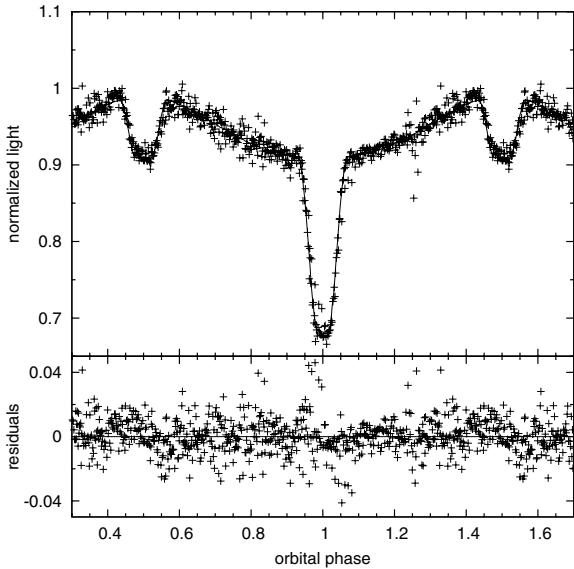


Figure 2. Phased *R*-band light curve of J08205+0008. The slight asymmetry in the secondary eclipse is most likely an artifact caused by the combination of the different data sets. The model light curve for the post-RGB case is overplotted as solid line. Fits of similar quality can be obtained for different mass ratios.

The remaining adjustable parameters are the inclination, the temperature of the second component ($T_{\text{eff}}(2)$), the Roche potentials ($\Omega_{1,2}$), the bolometric albedo of the secondary (A_2), the radiation pressure parameter (δ_1), and the luminosity of the hot component. The fractional Roche radii ($r_{1,2}$) in units of the orbital separation a were calculated using the Roche potentials and the mass ratio q . We used the binary mass function derived from spectroscopy to calculate possible mass ratios for a range of primary masses. A grid of light curve solutions with different mass ratios was calculated. In order to derive errors, we created 500 new data sets with a bootstrapping algorithm by random sampling with replacement from the original data set. In each case, a light curve solution was calculated in the way described above. The standard deviations of these results were adopted as the error estimates for the parameters.

The flat-bottomed eclipses, and the way the secondary eclipses reach down to the flux level just before and after primary eclipse, indicate that the secondary is totally eclipsed by the primary. The eclipses ensure that the inclination of the system and the relative radii of the components are very well constrained, but the usual degeneracy still remains in the mass ratio and the ratio of the components' radii and the size of the orbit. Table 1 shows light curve solutions for the most likely sdB masses after combining the photometric and spectroscopic analyses. Figure 2 shows an example model fit to the light curve.

4. ATMOSPHERIC AND STELLAR PARAMETERS OF THE SDB STAR

Atmospheric parameters have been determined by fitting a grid of synthetic spectra, calculated from line-blanketed, solar-metallicity LTE model atmospheres (Heber et al. 2000), to the hydrogen Balmer and helium lines of the SDSS and SOAR spectra in the way described in Geier et al. (2011a). The single spectra have been corrected for their orbital motion and co-added. In order to investigate systematic effects introduced by the individual instruments, especially the different resolutions and wavelength coverages, the parameters have been derived separately from spectra taken with SDSS ($S/N = 83$, $T_{\text{eff}} =$

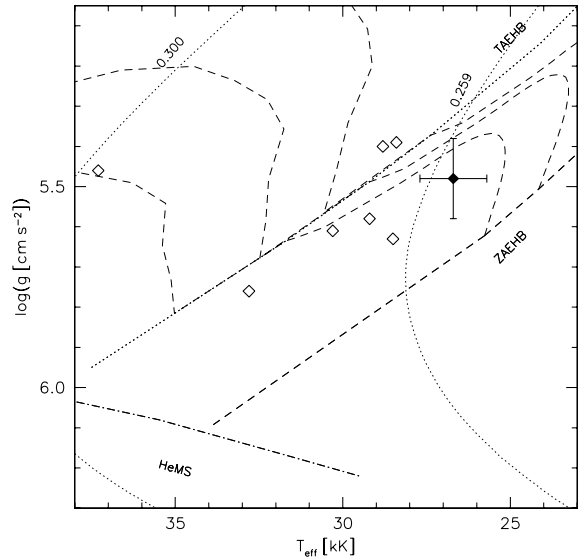


Figure 3. $T_{\text{eff}}-\log g$ diagram. The helium main sequence (HeMS) and the EHB band (limited by the zero-age EHB, ZAEHB, and the terminal-age EHB, TAEHB) are superimposed with EHB evolutionary tracks from Dorman et al. (1993) and a post-RGB track from Driebe et al. (1998). The position of J08205+0008 is indicated with a solid diamond. Open diamonds mark the position of other HW Vir like systems (Charpinet et al. 2008; Drechsel et al. 2001; For et al. 2010; Maxted et al. 2002; Müller et al. 2010; Østensen et al. 2008; Wood & Saffer 1999).

$26,000 \pm 1000$ K, $\log g = 5.37 \pm 0.14$) and SOAR ($S/N = 61$, $T_{\text{eff}} = 26,900 \pm 300$ K, $\log g = 5.51 \pm 0.04$), respectively. The weighted mean values have been calculated and adopted as final solutions (see Table 1).

The contribution of light from the irradiated surface of the cool companion in HW Vir type binaries can lead to systematic shifts in the atmospheric parameters (e.g., Heber et al. 2004; For et al. 2010; Müller et al. 2010). The quality of the individual SDSS spectra which cover most of the orbital phase is not good enough to resolve this effect. The statistical errors are higher than the expected modulations. Drechsel et al. (2001) adopted errors of 900 K in T_{eff} and 0.1 dex in $\log g$ to account for this effect in the case of the HW Vir type binary HS 0705+6700. Since the orbital period as well as the atmospheric parameters of this binary are similar to the ones of J08205+0008, we adopt similar uncertainties here. Systematic errors introduced by different model grids are typically smaller than that (Lisker et al. 2005; Geier et al. 2007).

While the inclination of the system is well constrained by the light curve analysis, there remains a degeneracy between the masses and the radii of the components. The surface gravity of the sdB determined in the quantitative spectroscopic analysis provides an additional constraint since it only depends on the mass and the radius of the subdwarf. To proceed, however, we need to constrain the sdB mass from evolutionary models.

In Figure 3, we compare the position of the star in the (T_{eff} , $\log g$)-plane to other HW Vir stars as well as to two sets of models. The first one represents the canonical picture of extreme horizontal branch (EHB) evolution, while the second one recalls post-RGB evolution, which means that the sdB star has left the red giant branch (RGB) early and did not ignite helium in the core at all.

According to Figure 3, the star is situated on the EHB consistent with being a core helium-burning star as are the other HW Vir stars (except AA Dor). Since the orbital period is short, it was formed via common envelope ejection. Population

synthesis models (Han et al. 2002, 2003) predict a mass range of $M_{\text{sdb}} = 0.37\text{--}0.48 M_{\odot}$ with a sharp peak at $0.47 M_{\odot}$ for sdBs in binaries formed in this way. Even lower sdB masses (down to $0.3 M_{\odot}$) are possible, when a more massive progenitor star ($2\text{--}3 M_{\odot}$) ignites core helium burning under non-degenerate conditions. Since this formation channel is predicted to be rare, the results of the quantitative spectroscopic analysis are fully consistent with an EHB model of the canonical mass. Hot subdwarf masses derived from asteroseismic analyses (e.g., van Grootel et al. 2010) or from analyses of eclipsing binaries are in general agreement with this picture.

In spite of the consistency discussed above, it may still be premature to adopt the canonical mass. It has been pointed out that the sdB stars in AA Dor, HS 2333+3927, and HD 188112 might not burn helium in their cores and may therefore be of lower mass (Rauch 2000; Heber et al. 2004, 2003). Such close binaries are expected to form whenever the RGB evolution is interrupted by the ejection of a common envelope before the core has reached the mass required for helium ignition.

Driebe et al. (1998) calculated evolutionary tracks of these so-called post-RGB objects. In Figure 3, we see that the evolutionary track for a $\simeq 0.25 M_{\odot}$ post-RGB star is also consistent with the atmospheric parameters of J08205+0008. The time it takes for such a low-mass star to cross the region of the $T_{\text{eff}}\text{--}\log g$ plane where canonical subdwarfs spend their time is only $\simeq 2$ Myr (for the model plotted in Figure 3), compared to 100–150 Myr for canonical EHB stars. Hence, such a low-mass solution is unlikely, but cannot be completely ruled out. In Table 1, we show solutions for both the canonical EHB and the post-RGB scenario.

To further constrain the mass of the sdB star, we can make use of the spectroscopic gravity determination. However, the $\log g$ derived from the spectra is fully consistent with both solutions within the uncertainties. To tighten this constraint, the gravity would need to be determined to better precision ($\Delta \log g \simeq 0.05$).

5. CONSTRAINING THE NATURE OF THE COMPANION

We now turn to the cool companion. Figure 4 shows its mass–radius relation derived from the light curve analysis. Theoretical mass–radius relations for low-mass stellar and substellar objects taken from Baraffe et al. (2003) are given for comparison. Since the normal progenitors of sdBs are expected to be stars around $1.0 M_{\odot}$, it seems reasonable to assume an age of a few Gyr for the system. The relations intersect at two very different mass ranges—a low mass one close to $0.25 M_{\odot}$ and a high mass one at $0.78 M_{\odot}$. The high-mass solution is very unlikely, because such high sdB masses are neither predicted by theory (Han et al. 2002, 2003; Zhang et al. 2009) nor have ever been measured empirically (e.g., van Grootel et al. 2010).

For the canonical sdB mass of $0.47 M_{\odot}$ and the corresponding companion mass of $0.068 M_{\odot}$, the radius of the companion would have to be $\simeq 20\%$ larger than expected from theory (see Figure 4). The irradiation by the sdB primary should influence the radius of the companion, which may be inflated. This effect has been measured in the case of hot Jupiter planets (e.g., Udalski et al. 2008), the accreting WD+BD binary SDSS 103533.03+055158.4 (Littlefair et al. 2006), and the eclipsing MS+BD binary CoRoT-15b (Bouchy et al. 2011). Baraffe et al. (2003) calculated mass–radius relations for planets including the influence of irradiation. The effect is of the order of up to 10% for hot Jupiters orbiting solar type stars. More massive objects should be less affected. On the other hand, the

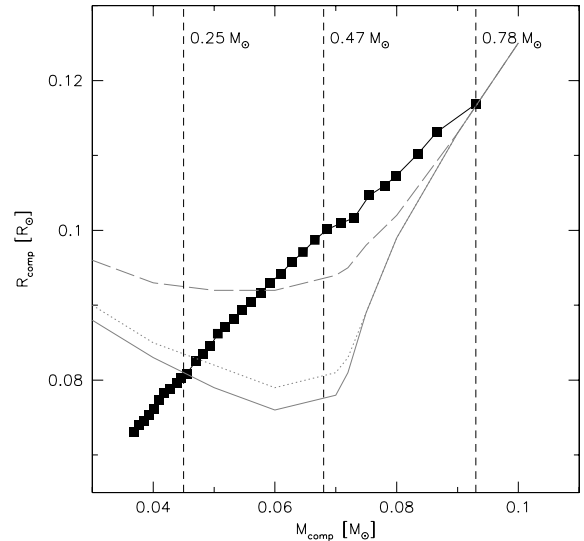


Figure 4. Radius of the cool companion plotted against the mass. The black symbols mark the relation derived from the spectroscopic and photometric analysis. The three curves mark theoretical relations for substellar objects with of 1 (dashed line), 5 (dotted line), and 10 Gyr (solid line) taken from Baraffe et al. (2003). The dashed vertical lines mark different values of the corresponding sdB masses.

sdB is more luminous than a solar type star and the separation of the system is less than one solar radius. Recently, Parsons et al. (2010) modeled the inflation of a late M star irradiated by a hot WD ($T_{\text{eff}} = 57,000$ K) in a 0.13 day orbit and showed that the measured 10% increase in radius compared to theoretical models can be reproduced in this way. For a discussion of other possible solutions to this issue (e.g., cold spots on the BD surface) see Bouchy et al. (2011).

For a low sdB mass of $\simeq 0.25 M_{\odot}$, the companion’s mass–radius relation is also consistent with theory. In this case, the companion mass would be $0.045 M_{\odot}$. A third possibility may be that the progenitor of the sdB was originally more massive. In this case, the sdB mass could be as low as $\simeq 0.3 M_{\odot}$ and the system as well as the substellar companion would be much younger. Since young BDs are considerably larger, this may also lead to a consistent solution (see Figure 4).

In the cases discussed above, the mass of the companion ranges between $0.045^{+0.003}_{-0.002} M_{\odot}$ and $0.068^{+0.003}_{-0.003} M_{\odot}$. The most conservative theoretical lower limit for core hydrogen burning ($\simeq 0.07 M_{\odot}$, Chabrier et al. 2000) is right at the border of this range. We therefore conclude that the companion is most likely a brown dwarf. However, given that the sdB mass is not strictly constrained, the companion may also be a star of extremely low mass.

6. DISCUSSION

We have presented a spectroscopic and photometric analysis of the HW Vir type eclipsing sdB star J08205+0008, discovered in the course of the MUCHFUSS project. The companion turns out to be a very low mass, most likely substellar object.

Although the mass of the sdB is not yet tightly constrained, it is important to stress that the companion remains below the core hydrogen-burning limit for reasonable subdwarf masses ranging from $0.25 M_{\odot}$ to $0.47 M_{\odot}$. The inclination constraint from eclipses means that J08205+0008 has the lowest unambiguously measured companion mass yet found in a subdwarf B binary.

The question of whether the sdB is burning helium in its core or not remains open for now. Time-resolved high-resolution

spectroscopy is necessary to measure both the $v_{\text{rot}} \sin i$ and the $\log g$ of the subdwarf with high accuracy. Combined with a high-quality multi-color light curve much tighter constraints could be put on this unique binary system. The fact that the sdB is situated on the EHB is a strong argument in favor of the EHB scenario, because post-RGB objects are very rare and not related to the EHB.

As witnessed by the HW Vir type systems, stellar companions with masses as low as $0.1 M_{\odot}$ are able to eject a common envelope and form an sdB star without being destroyed. The case of J08205+0008 demonstrates that even lower mass objects, i.e., substellar objects, are sufficient. This finding can be used to constrain theoretical models (Soker 1998; Nelemans & Tauris 1998) and learn more about the role of substellar companions for the formation of single and close binary sdBs.

The double-lined spectroscopic WD+BD system WD 0137–349 (Maxted et al. 2006) is a binary very similar to J0820+0008, but in a later stage of evolution. It consists of a He-core white dwarf of $0.39 M_{\odot}$ orbited by a $0.053 M_{\odot}$ brown dwarf in 0.0803 days. When evolving on the white dwarf cooling sequence J08205+0008 will therefore appear as a twin to WD 0137–349 once it is cooled down to the effective temperature of the latter (15,000 K).

This study is based on observations at the La Silla Observatory of the European Southern Observatory for program numbers 082.D-0649 and 084.D-0348 and on observations with the Southern Astrophysical Research (SOAR) telescope operated by the U.S. National Optical Astronomy Observatory (NOAO), the Ministério da Ciência e Tecnologia of the Federal Republic of Brazil (MCT), the University of North Carolina at Chapel Hill (UNC), and Michigan State University (MSU). Based on observations collected with the Flemish 1.2 m Mercator Telescope at the Roque de los Muchachos, La Palma, Spain. A.T. and S.G. are supported by the Deutsche Forschungsgemeinschaft (DFG) through grants HE1356/45-1 and HE1356/49-1. R.Ø. acknowledges funding from the European Research Council under the European Community's Seventh Framework Programme (FP7/2007–2013)/ERC grant agreement no. 227224 (PROSPERITY) as well as from the Research Council of K.U. Leuven grant agreement GOA/2008/04.

REFERENCES

- Abazajian, K. N., Adelman-McCarthy, J. K., & Agüeros, M. A. 2009, *ApJS*, **182**, 543
- Baraffe, I., Chabrier, G., Barman, T. S., Allard, F., & Hauschildt, P. H. 2003, *A&A*, **402**, 701
- Bouchy, F., et al. 2011, *A&A*, **525**, 68
- Chabrier, G., Baraffe, I., Allard, F., & Hauschildt, P. 2000, *ApJ*, **542**, 464
- Charpinet, S., et al. 2008, *A&A*, **489**, 377
- Dorman, B., Rood, R. T., & O'Connell, R. W. 1993, *ApJ*, **419**, 596
- Drechsel, H., Haas, S., Lorenz, R., & Gayler, S. 1995, *A&A*, **294**, 723
- Drechsel, H., et al. 2001, *A&A*, **379**, 893
- Driebe, T., Schönberner, D., Böcker, T., & Herwig, F. 1998, *A&A*, **339**, 123
- For, B.-Q., et al. 2010, *ApJ*, **708**, 253
- Geier, S., Nesslinger, S., Heber, U., Przybilla, N., Napiwotzki, R., & Kudritzki, R.-P. 2007, *A&A*, **464**, 299
- Geier, S., et al. 2011a, *A&A*, in press
- Geier, S., et al. 2011b, *A&A*, **526**, 39
- Han, Z., Podsiadlowski, Ph., Maxted, P. F. L., & Marsh, T. R. 2003, *MNRAS*, **341**, 669
- Han, Z., Podsiadlowski, Ph., Maxted, P. F. L., Marsh, T. R., & Ivanova, N. 2002, *MNRAS*, **336**, 449
- Heber, U. 2009, *ARA&A*, **47**, 211
- Heber, U., Edelmann, H., Lisker, T., & Napiwotzki, R. 2003, *A&A*, **411**, 477
- Heber, U., Reid, I. N., & Werner, K. 2000, *A&A*, **363**, 198
- Heber, U., et al. 2004, *A&A*, **420**, 251
- Iben, I., Jr., & Tutukov, A. V. 1984, *ApJS*, **54**, 335
- Lisker, T., Heber, U., Napiwotzki, R., Christlieb, N., Han, Z., Homeier, D., & Reimers, D. 2005, *A&A*, **430**, 223
- Littlefair, S. P., et al. 2006, *Science*, **314**, 1578
- Maxted, P. F. L., Heber, U., Marsh, T. R., & North, R. C. 2001, *MNRAS*, **326**, 1391
- Maxted, P. F. L., Napiwotzki, R., Dobbie, P. D., & Burleigh, M. R. 2006, *Nature*, **442**, 543
- Maxted, P. F. L., et al. 2002, *MNRAS*, **333**, 231
- Müller, S., Geier, S., & Heber, U. 2010, *Ap&SS*, **329**, 101
- Napiwotzki, R., Karl, C. A., Lisker, T., Heber, U., Christlieb, N., Reimers, D., Nelemans, G., & Homeier, D. 2004a, *Ap&SS*, **291**, 321
- Napiwotzki, R., et al. 2004b, in ASP Conf. Ser. 318, Spectroscopically and Spatially Resolving the Components of the Close Binary Stars, ed. R. W. Hilditch, H. Hensberge, & K. Pavlovski (San Francisco, CA: ASP), **402**
- Nelemans, G., & Tauris, T. M. 1998, *A&A*, **335**, L85
- Østensen, R. H., Oreiro, R., Hu, H., Drechsel, H., & Heber, U. 2008, in ASP Conf. Ser. 392, Hot Subdwarf Stars and Related Objects, ed. U. Heber, C. S. Jeffery, & R. Napiwotzki (San Francisco, CA: ASP), **221**
- Østensen, R. H. 2010, *Astron. Nachr.*, **331**, 1029
- Østensen, R. H., et al. 2010, *MNRAS*, **408**, 51
- Parsons, S. G., et al. 2010, *MNRAS*, **402**, 2591
- Rauch, T. 2000, *A&A*, **356**, 665
- Rucinski, S. M. 2009, *MNRAS*, **395**, 2299
- Schuh, S. 2010, *Astron. Nachr.*, **331**, 489
- Soker, N. 1998, *AJ*, **116**, 1308
- Tillich, A., et al. 2011, *A&A*, **527**, A137
- Udalski, A., et al. 2008, *A&A*, **482**, 299
- van Grootel, V., et al. 2010, *ApJ*, **718**, L97
- Vučković, M., Østensen, R., Bloemen, S., Decoster, I., & Aerts, C. 2008, in ASP Conf. Ser. 392, Hot Subdwarf Stars and Related Objects, ed. U. Heber, C. S. Jeffery, & R. Napiwotzki (San Francisco, CA: ASP), **199**
- Wilson, R. E., & Devinney, E. J. 1971, *ApJ*, **166**, 605
- Webbink, R. F. 1984, *ApJ*, **277**, 355
- Wood, J. H., & Saffer, R. 1999, *MNRAS*, **305**, 820
- Zhang, X., Chen, X., & Han, Z. 2009, *A&A*, **504**, L13

DISCOVERY OF A CLOSE SUBSTELLAR COMPANION TO THE HOT SUBDWARF STAR HD 149382—THE DECISIVE INFLUENCE OF SUBSTELLAR OBJECTS ON LATE STELLAR EVOLUTION

S. GEIER¹, H. EDELMANN^{1,3}, U. HEBER¹, AND L. MORALES-RUEDA²

¹ Dr. Remeis-Sternwarte, Institute for Astronomy, University Erlangen-Nürnberg, Sternwartstr. 7, 96049 Bamberg, Germany; geier@sternwarte.uni-erlangen.de

² Department of Astrophysics, Faculty of Science, Radboud University Nijmegen, P.O. Box 9010, 6500 GL Nijmegen, The Netherlands

³ McDonald Observatory, University of Texas at Austin, 1 University Station, C1402, Austin, TX 78712-0259, USA

Received 2009 April 29; accepted 2009 August 5; published 2009 August 17

ABSTRACT

Substellar objects, like planets and brown dwarfs orbiting stars, are by-products of the star formation process. The evolution of their host stars may have an enormous impact on these small companions. Vice versa a planet might also influence stellar evolution as has recently been argued. Here, we report the discovery of an 8–23 Jupiter-mass substellar object orbiting the hot subdwarf HD 149382 in 2.391 d at a distance of only about five solar radii. Obviously, the companion must have survived engulfment in the red giant envelope. Moreover, the substellar companion has triggered envelope ejection and enabled the sdB star to form. Hot subdwarf stars have been identified as the sources of the unexpected ultraviolet (UV) emission in elliptical galaxies, but the formation of these stars is not fully understood. Being the brightest star of its class, HD 149382 offers the best conditions to detect the substellar companion. Hence, undisclosed substellar companions offer a natural solution for the long-standing formation problem of apparently single hot subdwarf stars. Planets and brown dwarfs may therefore alter the evolution of old stellar populations and may also significantly affect the UV emission of elliptical galaxies.

Key words: binaries: spectroscopic – galaxies: evolution – planetary systems – stars: horizontal-branch – stars: individual (HD 149382) – stars: low-mass, brown dwarfs

1. INTRODUCTION

A long-standing problem in extragalactic astronomy is the ultraviolet (UV) excess observed in the spectra of elliptical galaxies. This phenomenon is caused by an old population of helium-burning stars, known as hot subdwarfs or sdBs (see review by Heber 2009). The origin of the UV excess can, hence, be traced back to that of the sdB stars themselves. The formation of such stars remains a mystery as it requires an extraordinarily high mass loss on the red giant branch. Hot subdwarfs often reside in close binaries, formed by ejection of the envelope of their red giant progenitors through interaction with the stellar companion. However, for half of the known sdBs no such companions could be found, requiring a yet unknown sdB formation channel.

After finishing core hydrogen burning, the progenitors of sdBs leave the main sequence and evolve to red giants before igniting helium and settling down on the extreme horizontal branch (EHB). Unlike normal stars, the sdB progenitors must have experienced a phase of extensive mass loss on the red giant branch, in order to explain the high temperatures and gravities observed at the surface of hot subdwarf stars. After consumption of the helium fuel, they evolve directly to white dwarfs avoiding a second red giant phase. What causes this extensive mass loss remains an open question.

The riddle of sdB formation is closely related to other long-standing problems regarding old stellar populations, which have been discussed for decades. The morphology of the horizontal branch in globular clusters, especially the existence and shape of its extreme hot part, is still far from understood (Catelan 2009). Hot subdwarfs are also regarded as the dominant source of the UV excess in early-type galaxies, where no active star formation is going on and hence no UV emission from young massive stars is expected. Hot subdwarf formation is the key to understanding the physics behind this phenomenon and a debate is going on whether single star (Yi 2008) or

binary evolution (Han et al. 2007) explains the observed UV excesses.

About half of the sdB stars reside in close binaries with periods as short as ~ 0.1 d (Maxted et al. 2001; Napiwotzki et al. 2004a). Because the components' separation in these systems is much less than the size of the subdwarf progenitor in its red giant phase, these systems must have experienced a common-envelope and spiral-in phase (Han et al. 2002, 2003). In such a scenario, two main-sequence stars of different masses evolve in a binary system. The more massive one will first reach the red giant phase and at some point fill its Roche lobe, where mass is transferred from the giant to the companion star. When mass transfer is unstable, the envelope of the giant will engulf the companion star and form a common envelope. Due to friction with the envelope, the two stellar cores lose orbital energy and spiral toward each other until enough orbital energy has been deposited within the envelope to eject it. The end product is a much closer system containing the core of the giant, which then may become an sdB star, and a main-sequence companion. This companion evolves to a white dwarf after another phase of unstable mass transfer.

The common-envelope ejection channel provides a reasonable explanation for the extra mass loss required to form sdB stars. But for about half of all analyzed subdwarfs, there is no evidence for close stellar companions as no radial velocity (RV) variations are found. Although in some cases, main-sequence companions are visible in the spectra, it remains unclear whether these stars are close enough to have interacted with the sdB progenitors. Among other formation scenarios, the merger of two helium white dwarfs has often been suggested to explain the origin of single sdB stars (Han et al. 2002, 2003). Merging should result in rapidly spinning stars, which is not consistent with observations. A recent analysis of single sdB stars revealed that their $v_{\text{rot}} \sin i$ distribution is consistent with a uniform rotational velocity $v_{\text{rot}} \approx 8 \text{ km s}^{-1}$ and randomly oriented polar axes (Geier et al. 2009).

Table 1
Radial Velocities of HD 149382

Mid-HJD	RV (km s ⁻¹)	Instrument
2452497.49150	27.0 ± 0.2	FEROS
2452497.51327	26.9 ± 0.2	FEROS
2452497.56524	26.9 ± 0.2	FEROS
2452891.30690	25.3 ± 0.2	FOCES
2452892.30170	25.7 ± 0.9	FOCES
2452893.32160	23.9 ± 0.6	FOCES
2453784.83294	23.8 ± 0.2	UVES
2453904.73904	22.9 ± 0.2	FEROS
2453931.76614	26.8 ± 0.2	Coudé
2453932.71806	26.1 ± 0.2	Coudé
2453932.72485	25.7 ± 0.2	Coudé
2453932.74337	25.9 ± 0.2	Coudé
2453932.74882	25.7 ± 0.2	Coudé
2453932.84790	24.8 ± 0.2	Coudé
2453932.85560	25.1 ± 0.2	Coudé
2453986.54830	24.8 ± 0.2	FEROS

The planet discovered to orbit the sdB pulsator V 931 Peg with a period of 1170 d and a separation of 1.7 AU was the first planet found to have survived the red giant phase of its host star (Silvotti et al. 2007). Serendipitous discoveries of two substellar companions around the eclipsing sdB binary HW Vir at distances of 3.6 AU and 5.3 AU with orbital periods of 3321 d and 5767 d (Lee et al. 2009) and one brown dwarf around the similar system HS 0705 + 6700 with a period of 2610 d and a separation of less than 3.6 AU (Qian et al. 2009) followed recently. These substellar companions to hot subdwarfs have rather wide orbits, were not engulfed by the red giant progenitor and therefore could not have influenced the evolution of their host stars.

2. OBSERVATIONS AND ANALYSIS

HD 149382 is the brightest core helium-burning subdwarf known. The first hint that this star could show very small RV variations was found during our survey aimed at finding sdBs in long-period binaries (Edelmann et al. 2005). We obtained 15 high-resolution spectra ($R = 30,000\text{--}48,000$) within four years with three different high-resolution spectrographs (ESO-2.2 m/ FEROS, McDonald-2.7 m/Coudé, CAHA-2.2 m/FOCES). One additional spectrum obtained with ESO-VLT/UVES at highest resolution ($R \approx 80,000$) was taken from the ESO archive.

In order to measure the RVs with highest possible accuracy, we fitted a set of mathematical functions (polynomial, Gaussian, and Lorentzian) to all suitable spectral lines with wavelengths from about 4000 Å to 6700 Å using the FITSB2 routine (Napiwotzki et al. 2004b). The formal deviation along the whole wavelength range was 0.2 km s⁻¹ at best. In order to check the accuracy of this measurements, we also obtained RVs from telluric and night sky lines and reached similar accuracies. Since telluric and night sky lines have zero RV, we used them to correct the measured RVs for calibration errors. The applied corrections were usually below 1.0 km s⁻¹. Since we used four entirely different instruments and obtained consistent results other systematic effects should be negligible. The RV measurements are given in Table 1.

The period search was carried out by means of a periodogram based on the singular value decomposition (SVD) method. A sine-shaped RV curve was fitted to the observations for a multitude of phases, which were calculated as a function of period. The difference between the observed RVs and the best-

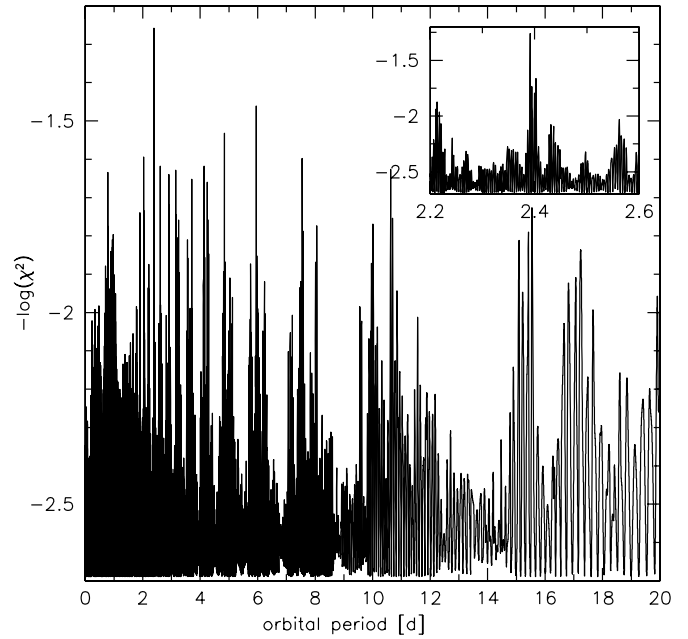


Figure 1. Power spectrum of HD 149382. $-\log \chi^2$ is plotted against the orbital period in days. The region around the most prominent period is plotted in the small window. The formal significance exceeds the 3σ -limit.

fitting theoretical RV curve for each phase set was evaluated in terms of the logarithm of the sum of the squared residuals (χ^2) as a function of period. This method finally results in the power spectrum of the data set which allows to determine the most probable period P of variability (Lorenz et al. 1998). The formal significance of the best orbital solution ($P = 2.391 \pm 0.002$ d, $K = 2.3 \pm 0.1$ km s⁻¹, $\gamma = 25.3 \pm 0.06$ km s⁻¹) exceeds the 3σ -limit (see Figure 1) and a very small mass function $f(M) = 3.8 \times 10^{-6}$ results. The RV curve is shown in Figure 2. The formal probability that the next best alias periods at about 4.8 d and 6.0 d are correct is less than 5%. Even if one of these longer periods should be the correct one, the mass function increases only by a factor of 1.5 at most and our conclusions still remain valid.

The atmospheric parameters effective temperature T_{eff} , surface gravity $\log g$, and helium abundance were determined by fitting simultaneously 17 hydrogen and helium lines in high-resolution, high-S/N FEROS and UVES spectra with NLTE model spectra (the method is described in Lisker et al. 2005; Geier et al. 2007). The parameters ($T_{\text{eff}} = 35,500 \pm 500$ K, $\log g = 5.80 \pm 0.05$) are in good agreement with the result of Saffer et al. (1994): $T_{\text{eff}} = 34,200 \pm 1500$ K, $\log g = 5.89 \pm 0.15$.

The mass of the unseen companion can be derived by solving the binary mass function $f_m = M_{\text{comp}}^3 \sin^3 i / (M_{\text{comp}} + M_{\text{sdb}})^2 = PK^3 / 2\pi G$. In order to obtain a unique solution, the mass of the sdB primary as well as the inclination of the system must be known. Due to the excellent quality of the data available for HD 149382, constraints can be put on both crucial parameters.

The distance to this star can be derived directly using a trigonometric parallax obtained with the *HIPPARCOS* satellite (van Leeuwen 2007). We derive the angular diameter by comparing the surface flux in the *V* band computed from a model atmosphere with the derived atmospheric parameters to the observed value (Mermilliod 1991). Using the trigonometric distance, we can derive the stellar radius, and from the surface gravity the mass of the sdB (Ramspeck et al. 2001).

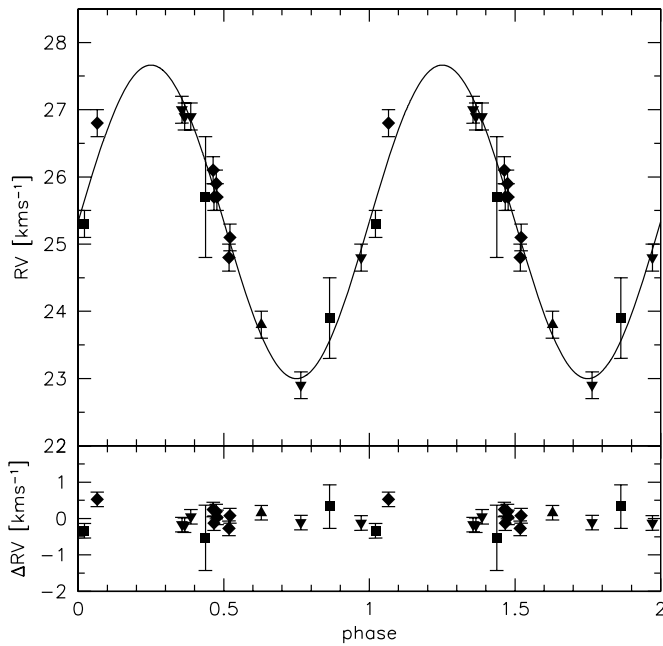


Figure 2. Radial velocity (RV) curve of HD 149382. The plot shows the RV plotted against orbital phase (diamonds: McDonald-2.7 m/Coudé, rectangles: CAHA-2.2 m/FOCES, upside down triangles: ESO-2.2 m/FEROS, triangle: ESO-VLT/UVES). The RV data were folded with the most likely orbital period. The residuals are plotted below.

Taking the uncertainties of all parameters into account (V magnitude, T_{eff} , $\log g$, parallax), the possible mass range for the sdB is $0.29\text{--}0.53 M_{\odot}$. This range is consistent with the canonical mass of $0.47 M_{\odot}$ derived from single and binary evolution calculations (Han et al. 2002, 2003). Without further constraints on the inclination only a lower limit to the mass of the unseen companion can be calculated.

The minimum companion mass lies between $0.006 M_{\odot}$ and $0.01 M_{\odot}$, well below the stellar limit of $0.075\text{--}0.083 M_{\odot}$ depending on the metallicity (Chabrier & Baraffe 1997), which is the lower limit where core hydrogen burning can be ignited and a star can be formed. The lower the inclination of the binary is, the higher is the mass of the unseen companion. Assuming a random distribution of orbital plane inclinations, the probability for a binary to fall below a certain inclination can be derived (Gray 1992). The probability for the companion to have a mass of more than $0.08 M_{\odot}$ is just 0.8%. The probability that the mass of the unseen companion exceeds the planetary limit of $0.012 M_{\odot}$ defined by the IAU⁴ is only 33%.

However, we can constrain the mass of HD 149382 b even further. Due to the very high resolution of the UVES spectrum, the broadening caused by the projected rotational velocity of the star could be measured from the metal lines although it turned out to be as small as $v_{\text{rot}} \sin i = 4.9 \pm 1.4 \text{ km s}^{-1}$. In order to derive $v_{\text{rot}} \sin i$, we compared the observed high-resolution ($R = 80,000$) UVES spectrum with rotationally broadened, synthetic line profiles. The profiles were computed using the LINFOR program (Lemke 1997). A simultaneous fit of elemental abundance, projected rotational velocity, and RV was then performed separately for every identified line using the FITSB2 routine (Napiwotzki et al. 2004b). The method is described in Geier et al. (2008).

⁴ Position statement on the definition of a “planet.” Working group on extrasolar planets of the International Astronomical Union, <http://www.dtm.ciw.edu/boss/definition.html>.

Table 2
Parameters of the HD 149382 System

Trigonometric parallax ^a	π	(mas)	13.53 ± 1.15
Distance	d	(pc)	74_{-8}^{+7}
Visual magnitude ^b	m_V	(mag)	8.947 ± 0.009
Atmospheric parameters			
Effective temperature	T_{eff}	(K)	$35\,500 \pm 500$
Surface gravity	$\log g$		5.80 ± 0.05
Helium abundance	$\log y$		-1.44 ± 0.01
Projected rotational velocity	$v_{\text{rot}} \sin i$	(km s^{-1})	4.9 ± 1.4
Orbital parameters			
Orbital period	P	(d)	2.391 ± 0.002
RV semiamplitude	K	(km s^{-1})	2.3 ± 0.1
System velocity	γ	(km s^{-1})	25.3 ± 0.06
Binary mass function	$f(M)$	(M_{\odot})	3.8×10^{-6}
Derived parameters			
Subdwarf mass	M_{sdb}	(M_{\odot})	$0.29\text{--}0.53$
Orbital inclination	i	($^{\circ}$)	$26\text{--}52$
Companion mass	M_{comp}	(M_J)	$8\text{--}23$
		(M_{\odot})	$0.008\text{--}0.022$
Separation	a	(R_{\odot})	$5.0\text{--}6.1$

Notes.

^a The trigonometric parallax was taken from the new reduction of the *HIPPARCOS* data (van Leeuwen 2007).

^b The visual magnitude is taken from Mermilliod (1991).

Assuming that HD 149382 rotates with the standard velocity of 8 km s^{-1} inferred for single sdBs (Geier et al. 2009), the inclination can be constrained to $i = 26^{\circ}\text{--}52^{\circ}$. The companion mass range is derived to be $M_2 = 0.008\text{--}0.022 M_{\odot} = 8\text{--}23 M_J$ consistent with a gas giant planet or a low-mass brown dwarf. Adopting the statistically most likely inclination $i = 52^{\circ}$ and the canonical sdB mass of $0.47 M_{\odot}$ (Han et al. 2002, 2003), the companion mass is $0.011 M_{\odot} = 12 M_J$, which places HD 149382 b just below the planetary limit. The separation of star and companion is $5\text{--}6 R_{\odot}$. All relevant measurements and parameters of the HD 149382 system are summarized in Table 2.

3. DISCUSSION

When the progenitor of HD 149382 evolved through the red giant phase, it expanded to a radius of 10 times the present orbital separation. The initial separation must have been larger (about 1 AU) and the companion spiralled-in due to interaction with the giant’s envelope until the envelope was ejected. Despite the very high local temperature inside the envelope ($300,000\text{--}400,000 \text{ K}$ at $5\text{--}6 R_{\odot}$ from the giant’s center; Soker 1998), the substellar companion survived. The companion of the sdB star AA Dor has also been suggested to be a brown dwarf in a 0.26 d orbit (Rauch 2000; Rucinski 2009). This conclusion, however, is rendered uncertain as Vucković et al. (2008) derive a higher mass indicating that the companion is a star.

Soker (1998) suggested that substellar objects like brown dwarfs and planets may also be swallowed by their host star and that common-envelope ejection could form hot subdwarfs. Substellar objects with masses higher than $\approx 10 M_J$ were predicted to survive the common-envelope phase and end up in a close orbit around the stellar remnant, while planets with lower masses would entirely evaporate. The stellar remnant is predicted to lose most of its envelope and evolve toward the EHB. The orbital period and mass we derived for HD 149382 b are in excellent agreement with the predictions made by Soker

(1998). A similar scenario has been proposed to explain the formation of apparently single low-mass white dwarfs (Nelemans & Tauris 1998). The discovery of a brown dwarf with a mass of $0.053 \pm 0.006 M_{\odot}$ in a 0.08 d orbit around such a white dwarf supports this scenario and shows that substellar companions can influence the outcome of stellar evolution (Maxted et al. 2006).

The discovery of planets and brown dwarfs around sdBs and especially the close-in substellar companion of HD 149382 may thus have important implications for the still open question of sdB formation. The extraordinary quality of the photometric data was a prerequisite for the detection of the substellar companions in V 931 Peg, HW Vir, and HS 0705 + 6700 (Silvotti et al. 2007; Lee et al. 2009; Qian et al. 2009). Finding such companions orbiting three of the best observed sdBs cannot be mere coincidence and leads to the conclusion that substellar objects may often be associated with sdBs. HD 149382 is the brightest sdB known. Hence, the quality of the spectroscopic data is also very high. It is not easy to detect such small RV variations even in high-resolution spectra. The fact that we found them in the case of HD 149382 leads to the conclusion that close-in planets or brown dwarfs may be common around apparently single sdB stars. They were just not detected up to now. Hence, all apparently single sdBs may have or had close brown dwarf or planetary companions, although those of lowest mass may have evaporated.

HD 149382 b provides evidence that substellar companions can decisively change the evolution of stars, as they trigger extensive mass loss. They could be responsible for the formation of the single hot subdwarf population. These stars are not only numerous in our Galaxy, but also make elliptical galaxies shine in UV light.

This Letter was based on observations at the La Silla Observatory of the European Southern Observatory for programme number 077.D-0515(A). Some of the data used in this work were obtained at the McDonald Observatory. Based on observations collected at the Centro Astronómico Hispano Alemán (CAHA) at Calar Alto, operated jointly by the Max-Planck Institut für Astronomie and the Instituto de Astrofísica de Andalucía (CSIC). Some of the data used in this work were downloaded from the ESO archive. S.G. gratefully acknowledges financial support from the Deutsche Forschungsgemeinschaft through grant He 1356/40-4. We thank Sebastian Müller for reducing the archival UVES spectrum.

REFERENCES

- Catelan, M. 2009, Ap&SS, in press (arXiv:astro-ph/0507464v2)
- Chabrier, G., & Baraffe, I. 1997, A&A, **327**, 1039
- Edelmann, H., Heber, U., Altmann, M., Karl, C., & Lisker, T. 2005, A&A, **442**, 1023
- Geier, S., Heber, U., Edelmann, H., Kupfer, T., Napiwotzki, R., & Podsiadlowski, Ph. 2009, J. Phys. Conf. Ser., in press (arXiv:0901.1777)
- Geier, S., Nesslinger, S., Heber, U., Przybilla, N., Napiwotzki, R., & Kudritzki, R.-P. 2007, A&A, **464**, 299
- Geier, S., Nesslinger, S., Heber, U., Randall, S. K., Edelmann, H., & Green, E. M. 2008, A&A, **477**, L13
- Gray, D. F. 1992, The Observation and Analysis of Stellar Photospheres (2nd ed.; Cambridge: Cambridge Univ. Press)
- Han, Z., Podsiadlowski, Ph., Maxted, P. F. L., & Marsh, T. R. 2003, MNRAS, **341**, 669
- Han, Z., Podsiadlowski, Ph., Maxted, P. F. L., Marsh, T. R., & Ivanova, N. 2002, MNRAS, **336**, 449
- Han, Z., Podsiadlowski, Ph., & Lynas-Gray, A. E. 2007, MNRAS, **380**, 1098
- Heber, U. 2009, ARA&A, **47**, 211
- Lee, J. W., Kim, S.-L., Kim, C.-H., Koch, R. H., Lee, C.-U., Kim, H. I., & Park, J.-H. 2009, AJ, **137**, 3181
- Lemke, M. 1997, A&AS, **122**, 285
- Lisker, T., Heber, U., Napiwotzki, R., Christlieb, N., Han, Z., Homeier, D., & Reimers, D. 2005, A&A, **430**, 223
- Lorenz, R., Mayer, P., & Drechsel, H. 1998, A&A, **332**, 909
- Maxted, P. F. L., Heber, U., Marsh, T. R., & North, R. C. 2001, MNRAS, **326**, 1391
- Maxted, P. F. L., Napiwotzki, R., Dobbie, P. D., & Burleigh, M. R. 2006, Nature, **442**, 543
- Mermilliod, J. C. 1991, Homogeneous Means in the UBVS System. VizieR Online Data Catalog: II/168 (Lausanne: Institut d'Astronomie, Université de Lausanne)
- Napiwotzki, R., Karl, C. A., Lisker, T., Heber, U., Christlieb, N., Reimers, D., Nelemans, G., & Homeier, D. 2004a, Ap&SS, **291**, 321
- Napiwotzki, R., et al. 2004b, in ASP Conf. Ser. 318, Spectroscopic and Spatially Resolving the Components of Close Binary Stars, ed. R. W. Hilditch, H. Hensberge, & K. Pavlovski (San Francisco, CA: ASP), **402**
- Nelemans, G., & Tauris, T. M. 1998, A&A, **335**, L85
- Qian, S., et al. 2009, ApJ, **695**, 163
- Ramspeck, M., Heber, U., & Moehler, S. 2001, A&A, **378**, 907
- Rauch, T. 2000, A&A, **356**, 665
- Rucinski, S. M. 2009, MNRAS, **395**, 2299
- Saffer, R. A., Bergeron, P., Koester, D., & Liebert, J. 1994, ApJ, **432**, 351
- Silvotti, R., et al. 2007, Nature, **449**, 189
- Soker, N. 1998, AJ, **116**, 1308
- van Leeuwen, F. 2007, Hipparcos, the New Reduction of the Raw Data (Dordrecht: Springer)
- Vučković, M., Østensen, R., Bloemen, S., Decoster, I., & Aerts, C. 2008, in ASP Conf. Ser. 392, Hot Subdwarf Stars and Related Objects, ed. U. Heber, C. S. Jeffery, & R. Napiwotzki (San Francisco, CA: ASP), **199**
- Yi, S. K. 2008, in ASP Conf. Ser. 392, Hot Subdwarf Stars and Related Objects, ed. U. Heber, C. S. Jeffery, & R. Napiwotzki (San Francisco, CA: ASP), **3**

A progenitor binary and an ejected mass donor remnant of faint type Ia supernovae

S. Geier^{1,2}, T. R. Marsh³, B. Wang⁴, B. Dunlap⁵, B. N. Barlow⁶, V. Schaffenroth^{2,7}, X. Chen⁴, A. Irrgang², P. F. L. Maxted⁸, E. Ziegerer², T. Kupfer⁹, B. Miszalski^{10,11}, U. Heber², Z. Han⁴, A. Shporer^{12,13,14}, J. H. Telting¹⁵, B. T. Gänsicke³, R. H. Østensen¹⁶, S. J. O’Toole¹⁷, and R. Napiwotzki¹⁸

¹ European Southern Observatory, Karl-Schwarzschild-Str. 2, 85748 Garching, Germany
e-mail: sgeier@eso.org

² Dr. Karl Remeis-Observatory & ECAP, Astronomical Institute, Friedrich-Alexander University Erlangen-Nürnberg, Sternwartstr. 7, 96049 Bamberg, Germany

³ Department of Physics, University of Warwick, Coventry CV4 7AL, UK

⁴ Key Laboratory of the Structure and Evolution of Celestial Objects, Yunnan Observatory, Chinese Academy of Sciences, 650011 Kunming, PR China

⁵ Department of Physics and Astronomy, University of North Carolina, Chapel Hill, NC 27599-3255, USA

⁶ The Pennsylvania State University, 525 Davey Lab, University Park, PA 16802, USA

⁷ Institute for Astro- and Particle Physics, University of Innsbruck, Technikerstr. 25/8, 6020 Innsbruck, Austria

⁸ Astrophysics Group, Keele University, Staffordshire, ST5 5BG, UK

⁹ Department of Astrophysics/IMAPP, Radboud University Nijmegen, PO Box 9010, 6500 GL Nijmegen, The Netherlands

¹⁰ South African Astronomical Observatory, PO Box 9, Observatory, 7935 Cape Town, South Africa

¹¹ Southern African Large Telescope Foundation, PO Box 9, Observatory, 7935 Cape Town, South Africa

¹² Las Cumbres Observatory Global Telescope Network, 6740 Cortona Drive, Suite 102, Santa Barbara, CA 93117, USA

¹³ Department of Physics, Broida Hall, University of California, Santa Barbara, CA 93106, USA

¹⁴ Division of Geological and Planetary Sciences, California Institute of Technology, Pasadena, CA 91125, USA

¹⁵ Nordic Optical Telescope, Apartado 474, 38700 Santa Cruz de La Palma, Spain

¹⁶ Institute of Astronomy, K.U. Leuven, Celestijnenlaan 200D, 3001 Heverlee, Belgium

¹⁷ Australian Astronomical Observatory, PO Box 915, North Ryde NSW 1670, Australia

¹⁸ Centre of Astrophysics Research, University of Hertfordshire, College Lane, Hatfield AL10 9AB, UK

Received 3 March 2013 / Accepted 16 April 2013

ABSTRACT

Type Ia supernovae (SN Ia) are the most important standard candles for measuring the expansion history of the universe. The thermonuclear explosion of a white dwarf can explain their observed properties, but neither the progenitor systems nor any stellar remnants have been conclusively identified. Underluminous SN Ia have been proposed to originate from a so-called double-detonation of a white dwarf. After a critical amount of helium is deposited on the surface through accretion from a close companion, the helium is ignited causing a detonation wave that triggers the explosion of the white dwarf itself. We have discovered both shallow transits and eclipses in the tight binary system CD-30° 11223 composed of a carbon/oxygen white dwarf and a hot helium star, allowing us to determine its component masses and fundamental parameters. In the future the system will transfer mass from the helium star to the white dwarf. Modelling this process we find that the detonation in the accreted helium layer is sufficiently strong to trigger the explosion of the core. The helium star will then be ejected at such high velocity that it will escape the Galaxy. The predicted properties of this remnant are an excellent match to the so-called hypervelocity star US 708, a hot, helium-rich star moving at more than 750 km s^{-1} , sufficient for it to leave the Galaxy. The identification of both progenitor and remnant provides a consistent picture of the formation and evolution of underluminous SNIa.

Key words. binaries: spectroscopic – subdwarfs – supernovae: general

1. Introduction

The search for the progenitors of type Ia supernovae (SN Ia) is ongoing, but the observational evidence remains inconclusive. In the standard single-degenerate scenarios, mass is transferred in a stable way by either a main sequence star or a red giant to a white dwarf (WD) companion. In the double-degenerate scenario, a close binary consisting of two white dwarfs shrinks because of angular momentum lost by the emission of gravitational waves and eventually merges. Possible progenitor systems have been proposed for both channels, but not conclusively identified

yet. Although most SN Ia form a homogeneous class, about one third of them differ significantly in their luminosities and other observational properties, and their proper classification is crucial when using such events as standard candles for cosmology (Wang & Han 2012).

It has been proposed that underluminous SN Ia originate from a so-called double-detonation of a white dwarf. After a critical amount of helium is deposited on the surface through accretion from a close companion, the helium is ignited causing a detonation wave that triggers the explosion of the white dwarf itself even if its mass is significantly lower than the Chandrasekhar

limit (Nomoto 1982; Woosley et al. 1986). Hydrodynamic simulations predict the explosion of a CO-WD with a minimum mass of only $\sim 0.8 M_{\odot}$ as underluminous SNIa triggered by the ignition of an He-shell of $\sim 0.1 M_{\odot}$ (Fink et al. 2010) in this so-called double-detonation scenario. Helium stars have already been proposed as possible donors for the single-degenerate scenario (Yoon & Langer 2003; Wang et al. 2009a,b) conveniently explaining the lack of hydrogen in the spectra of SNIa. Recent studies indicate that this scenario might also be consistent with the lack of helium in standard SNIa spectra as long as the accreted He-layer is thin (Sim et al. 2010; Kromer et al. 2010).

In the course of the MUCHFUSS project (Geier et al. 2011), which aims at finding hot subdwarf binary systems with massive companions, we have discovered a possible progenitor for such a supernova consisting of a hot subdwarf B star (sdB) and a white dwarf in an extremely compact binary (Heber et al. 2013; Geier et al. 2013). This system, CD-30°11223, was also independently discovered by Vennes et al. (2012).

Hot subdwarf stars are evolved, core helium-burning objects. About half of the sdB stars reside in close binaries with periods ranging from ~ 0.1 d to ~ 30 d (Maxted et al. 2001; Napiwotzki et al. 2004a). The sdB is the core of a former red giant star that has been stripped of almost all of its hydrogen envelope through interaction with a companion star. The mass of the emerging sdB star is constrained to about half a solar mass in order to allow central helium burning. After the helium-burning phase the sdB star will turn into a white dwarf.

Because the separation of the components in these systems is much less than the size of the subdwarf progenitor in its red-giant phase, these systems must have experienced a common-envelope (CE) and spiral-in phase (Han et al. 2002, 2003 and references therein). In this scenario, a star evolving to become a red giant swallows a nearby companion. Because of friction, the core of the giant and the more compact companion spiral towards each other in a common envelope. The orbital energy lost during this process is deposited in the envelope until the envelope is eventually ejected leaving a close binary system as a remnant.

Although most of the close companions to sdB stars are low-mass main sequence stars, brown dwarfs, or low-mass WDs ($\sim 0.5 M_{\odot}$), more massive compact companions like WDs, neutron stars, or black holes have been either observed or predicted by theory (Geier et al. 2007, 2010). The short-period sdB+WD binary KPD 1930+2752 is regarded as a progenitor candidate for an SNIa (Maxted et al. 2000; Geier et al. 2007).

Here we report the discovery of both shallow transits and eclipses in the tight binary system CD-30°11223 composed of a carbon/oxygen white dwarf and a hot helium star, allowing us to determine its component masses and fundamental parameters. This system turns out to be an excellent progenitor candidate for the double-detonation SNIa scenario and can be linked to the hypervelocity subdwarf US 708, the likely donor remnant of such an event.

2. Observations

The star CD-30°11223 ($\alpha_{2000} = 14^{\text{h}}11^{\text{m}}16^{\text{s}}.2$, $\delta_{2000} = -30^{\circ}53'03''$, $m_V = 12.3$ mag) was selected as a UV-excess object and spectroscopically identified to be an sdB star (Vennes et al. 2011; Németh et al. 2012). We selected this star as a bright backup target for our MUCHFUSS follow-up campaign. Because of unfavourable observing conditions, which prevented us from observing our main targets, two medium resolution

spectra ($R \sim 2200$, $\lambda = 4450\text{--}5110 \text{ \AA}$) were taken consecutively with the EFOSC2 spectrograph mounted at the ESO NTT on June 10, 2012. The radial velocity shift between those two spectra turned out to be as high as 600 km s^{-1} .

The first spectroscopic follow-up data was obtained with the grating spectrograph mounted on the SAAO-1.9 m telescope on July 2, 2012. The RV-curve derived from 18 single spectra confirmed the short orbital period of 0.0498 d and a high RV-semi-amplitude ($K = 370 \pm 14 \text{ km s}^{-1}$). In order to improve the orbital solution and minimize the effect of orbital smearing, we took another 105 spectra with the ISIS spectrograph ($R \sim 4000$, $\lambda = 3440\text{--}5270 \text{ \AA}$, $T_{\text{exp}} = 2$ min) mounted at the WHT during a dedicated MUCHFUSS follow-up run from July 9 to 12, 2012. Another 175 spectra were taken with the Goodman spectrograph mounted at the SOAR telescope ($R \sim 7700$, $\lambda = 3700\text{--}4400 \text{ \AA}$, $T_{\text{exp}} = 1$ min) on July 16, 2012.

CD-30°11223 was observed by the SuperWASP planetary transit survey (Pollacco et al. 2006). The light curve contains 23 678 measurements taken from May 4, 2006 to August 1, 2011. On July 6, 2012, 3.6 h of time-series photometry in the V-band ($T_{\text{exp}} = 3$ s) were taken with SOAR/Goodman under photometric conditions. The light curve was extracted using an aperture that minimizes the standard deviation of the two comparison stars used divided by each other at low airmass; a flat-field correction was also applied. The combination of short exposure times and bright stars makes scintillation the dominant noise source for our photometry. Another source of noise was likely caused by a small scatter in effective integration time of the order of a few ms.

3. Orbital and atmospheric parameters

The light curve shows variations caused by the ellipsoidal deformation of the sdB primary, which is triggered by the tidal influence of the compact companion. The light curve also shows Doppler boosting, caused by the extreme orbital motion of the sdB (Shakura & Postnov 1987; see also Bloemen et al. 2011, and references therein). The ephemeris has been derived from the SWASP data based on fitting a harmonic series. Because of the timebase of more than five years, the derived orbital period of $0.0489790724 \pm 0.0000000018$ d is very accurate and perfectly consistent with the independent determination ($P = 0.04897906 \pm 0.00000004$ d) by Vennes et al. (2012).

The radial velocities were measured by fitting a set of mathematical functions to the hydrogen Balmer lines as well as helium lines using the FITSB2 routine (Napiwotzki et al. 2004b). Three functions (Gaussians, Lorentzians, and polynomials) are used to match the continuum, the line and the line core, respectively and mimic the typical Voigt profile of spectral lines. The profiles are fitted to all suitable lines simultaneously using χ^2 -minimization, and the RV shift with respect to the rest wavelengths is measured. Assuming circular orbits, sine curves were fitted to the RV data points in fine steps over a range of test periods. The two datasets obtained with ISIS and Goodman are treated separately to investigate systematic errors. Details about the analysis method and error estimation are given in Geier et al. (2011). The derived orbital parameters from the ISIS dataset ($K = 378.6 \pm 1.0 \text{ km s}^{-1}$, $\gamma = 17.6 \pm 0.7 \text{ km s}^{-1}$, see Fig. 1, lower panel) and the Goodman dataset ($K = 374.5 \pm 1.1 \text{ km s}^{-1}$, $\gamma = 21.3 \pm 0.8 \text{ km s}^{-1}$, see Fig. 1, upper panel) are consistent, taking into account that systematic uncertainties are usually somewhat higher than the statistical 1σ errors given here. The deviation in system velocity is most likely caused by a slight systematic zero-point shift

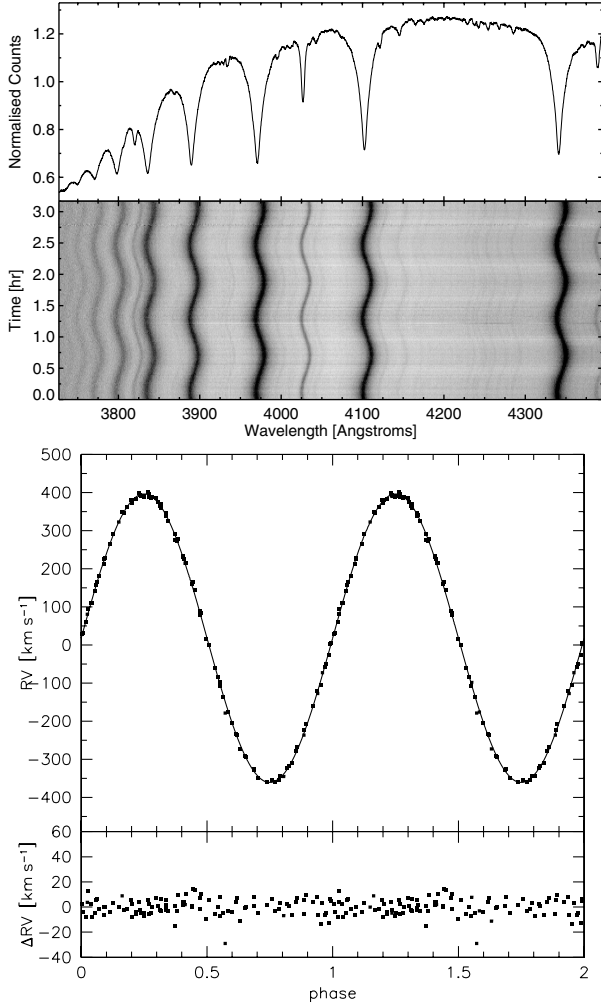


Fig. 1. *Upper panel:* spectrum of CD-30°11223 coadded from 175 RV-corrected spectra taken with SOAR/Goodman. The hydrogen Balmer series is clearly visible, as well as a prominent helium line at 4026 Å. The other features are rotationally broadened metal lines. Model spectra were matched to the hydrogen and helium lines to determine the atmospheric parameters of the hot subdwarf star. *Middle panel:* trailed spectra taken with SOAR/Goodman and showing the short-period sinusoidal variations of the Doppler-shifted spectral lines caused by the motion of the visible sdB star. The close and compact white-dwarf companion of the subdwarf star is not visible in this dataset. *Lower panel:* radial velocity curve of CD-30°11223 derived from 105 spectra taken with WHT/ISIS plotted twice against orbital phase for better visualisation.

between the two instruments. For further analysis we used the average values. Those values are in reasonable agreement with the results ($K = 386.9 \pm 1.9 \text{ km s}^{-1}$, $\gamma = 31.5 \pm 1.3 \text{ km s}^{-1}$) of Vennes et al. (2012), although somewhat discrepant.

The atmospheric parameters of effective temperature T_{eff} , surface gravity $\log g$, helium abundance, and projected rotational velocity were determined by fitting simultaneously the observed hydrogen and helium lines of the single spectra with metal-line-blanketed LTE model spectra (Heber et al. 2000) as described in Geier et al. (2007). No significant variations of the parameters with orbital phase have been detected. Average values and standard deviations have been calculated separately for the ISIS dataset ($T_{\text{eff}} = 28\,800 \pm 200 \text{ K}$, $\log g = 5.67 \pm 0.03$, $\log y = -1.50 \pm 0.07$, $v_{\text{rot}} \sin i = 180 \pm 8 \text{ km s}^{-1}$, see Figs. 2, 3) and the Goodman dataset ($T_{\text{eff}} = 29\,600 \pm 300 \text{ K}$,

$\log g = 5.65 \pm 0.05$, $\log y = -1.46 \pm 0.14$, $v_{\text{rot}} \sin i = 174 \pm 12 \text{ km s}^{-1}$). We adopt the average values from both datasets for further analysis. The final helium abundance is taken from the ISIS data because of the higher number of He-lines in the spectral range.

The derived parameters are consistent with literature values within the uncertainties (Vennes et al. 2011; Németh et al. 2012). More detailed information about the systematic errors of this method can be found in Geier et al. (2007, 2011). Table 1 shows the orbital and atmospheric parameters, Fig. 4 the position of CD-30°11223 in the $T_{\text{eff}} - \log g$ diagram.

4. Light curve analysis

The light curve obtained with SOAR/Goodman was analysed by fitting models calculated with the LCURVE code written by TRM (see Fig. 5, Copperwheat et al. 2010). The code uses grids of points modelling the two stars and takes into account limb darkening, gravity darkening, mutual illumination effects, Doppler boosting, and gravitational lensing. Since the masses and radii of both components are strongly correlated, those parameters have been constrained using Markov chain Monte Carlo simulations. A detailed description of the analysis method is given by Bloemen et al. (2011).

In order to determine masses and radii of both the sdB and the WD, we used two different prior constraints. In each case the K derived from spectroscopy is used. First, we assumed tidal synchronisation of the sdB primary (solution 1), which is a reasonable assumption given the short orbital period of the system. The $v_{\text{rot}} \sin i$ derived from spectroscopy is measured making the simplified assumption of a spherical, linear limb darkened star (limb darkening coefficient 0.3). To take into account the additional effects of limb darkening and gravitational darkening of the Roche-distorted star we calculated a correction factor of 0.963 by comparing the slightly different line profiles calculated under both assumptions (Claret & Bloemen 2011). This correction was applied to the $v_{\text{rot}} \sin i$ before deriving the binary parameters. The best fit is achieved for an sdB mass of $0.47 \pm 0.03 M_{\odot}$ and a WD mass of $0.74 \pm 0.02 M_{\odot}$. However, we found that the radius of the WD is about 10% smaller than predicted by the zero-temperature mass-radius relation for WDs, which provides a lower limit for the WD radius (see Fig. 6, second panel from top, Verbunt & Rappaport 1988).

To explore the influence of this discrepancy, we imposed the restriction that the white dwarf should be within 2% of the M - R -relation and allowed for deviations from corotation (solution 2). We determined an estimate for the temperature of the WD from our light curve analysis. Since we see a significant feature when the sdB occults the WD, we can derive a black-body temperature of $24\,700 \pm 1200 \text{ K}$ for the WD, which leads to a radius about 5% higher than expected from the zero-temperature relation. We adopt this more realistic value for our analysis. In this case the derived masses are somewhat higher ($M_{\text{sdB}} = 0.54 \pm 0.02 M_{\odot}$, $M_{\text{WD}} = 0.79 \pm 0.01 M_{\odot}$).

Although both solutions are consistent within their uncertainties, we refrain from favouring one over the other. To calculate the kinematics and the further evolution of the system, we adopt the average values for the component masses ($M_{\text{sdB}} = 0.51 M_{\odot}$, $M_{\text{WD}} = 0.76 M_{\odot}$, see Fig. 6).

Comparing the derived sdB masses with evolutionary tracks for core helium-burning objects (Fig. 4), it can be seen that the appropriate tracks are consistent with the position of CD-30°11223 in the $T_{\text{eff}} - \log g$ diagram. Furthermore, the effective temperature and surface gravity of the star tell us that the

Table 1. Parameters of the CD-30° 11223 system.

Visual magnitude [†]	m_V	[mag]	12.342 ± 0.003
Proper motion [‡]	$\mu_\alpha \cos \delta$	[mas/yr]	9.5 ± 2.2
	μ_δ	[mas/yr]	-5.6 ± 2.2
Atmospheric parameters of the subdwarf			
Effective temperature	T_{eff}	[K]	$29\,200 \pm 400$
Surface gravity	$\log g$		5.66 ± 0.05
Helium abundance	$\log y$		-1.50 ± 0.07
Projected rotational velocity	$v_{\text{rot}} \sin i$	[km s ⁻¹]	177 ± 10
Orbital parameters			
	T_0	[BJD UTC]	$2\,455\,113.205908 \pm 0.000363$
Orbital period	P	[d]	$0.0489790724 \pm 0.0000000018$
RV semi-amplitude	K	[km s ⁻¹]	376.6 ± 1.0
System velocity	γ	[km s ⁻¹]	19.5 ± 2.0
Binary mass function	$f(M)$	[M_\odot]	0.271 ± 0.002
Derived parameters			
Solution 1			
sdB mass	M_{sdB}	[M_\odot]	0.47 ± 0.03
sdB radius	R_{sdB}	[R_\odot]	0.169 ± 0.005
WD mass	M_{WD}	[M_\odot]	0.74 ± 0.02
WD radius	R_{WD}	[R_\odot]	0.0100 ± 0.0004
Orbital inclination	i	[°]	83.8 ± 0.6
Separation	a	[R_\odot]	0.599 ± 0.009
Mass ratio	q		0.63 ± 0.02
Solution 2			
sdB mass	M_{sdB}	[M_\odot]	0.54 ± 0.02
sdB radius	R_{sdB}	[R_\odot]	0.179 ± 0.003
WD mass	M_{WD}	[M_\odot]	0.79 ± 0.01
WD radius	R_{WD}	[R_\odot]	0.0106 ± 0.0002
Orbital inclination	i	[°]	82.9 ± 0.4
Separation	a	[R_\odot]	0.619 ± 0.005
Mass ratio	q		0.68 ± 0.01

Notes. ^(†) The visual magnitude is taken from Vennes et al. (2012). ^(‡) Proper motions taken from Roeser et al. (2010).

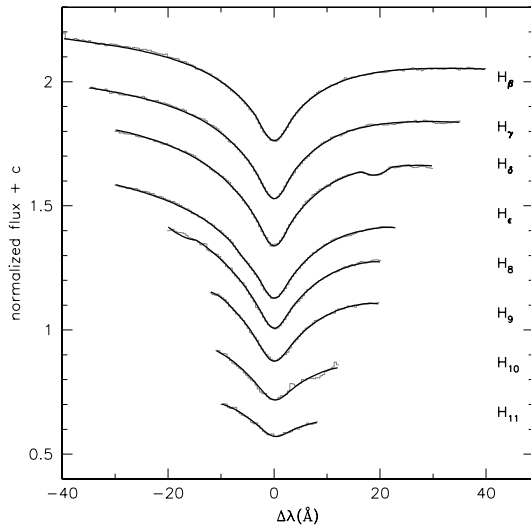


Fig. 2. Fit of synthetic LTE models to the hydrogen Balmer lines of a coadded ISIS spectrum. The normalized fluxes of the single lines are shifted for better visualisation.

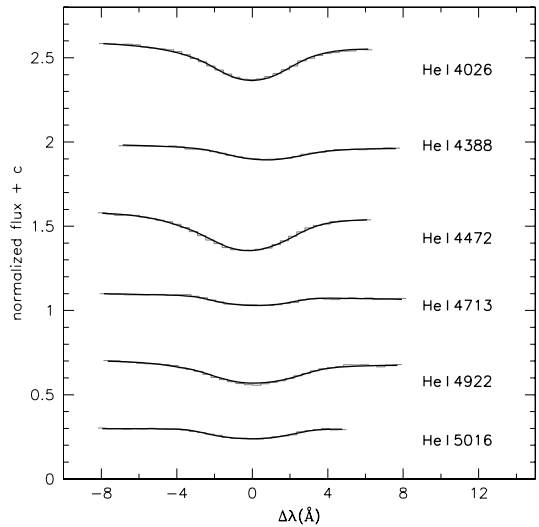


Fig. 3. Fit of synthetic LTE models to the helium lines (see Fig. 2).

sdB has just recently been formed and started the core helium-burning phase, which typically lasts for about 100 Myr.

5. Gravitational wave radiation

Because of its short orbital period, CD-30° 11223 is expected to be a strong source of gravitational waves. We

therefore calculated the current gravitational wave emission of CD-30° 11223. The gravitational wave strain amplitude h scales with the masses of both binary components, the binary inclination, the orbital period and the distance of the system.

We calculate it as described in Roelofs et al. (2007) to be as high as $\log h = -21.5 \pm 0.3$; CD-30° 11223 should therefore be one of the strongest gravitational wave sources detectable with missions like NGO/eLISA (Kilic et al. 2012; Nelemans 2009).

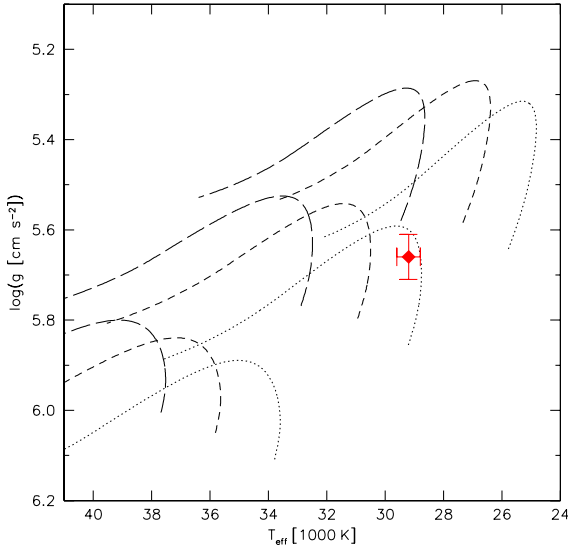


Fig. 4. $T_{\text{eff}} - \log g$ diagram. Evolutionary tracks (solar metallicity) of core helium-burning stars with masses of $0.45 M_{\odot}$ (dotted lines), $0.50 M_{\odot}$ (short-dashed lines) and $0.55 M_{\odot}$ (long-dashed lines) are plotted for different hydrogen envelope masses ($0.000 M_{\odot}$, $0.001 M_{\odot}$, $0.005 M_{\odot}$, $0.010 M_{\odot}$, from the lower left to the upper right). The diamond marks CD-30°11223.

It is even more noticeable, because the presence of eclipses allows us determine its binary parameters to very high accuracy. Therefore, this system can be used as a verification source for upcoming space missions.

No period change due to the orbital shrinkage caused by the emission of gravitational wave radiation has been detected in the SWASP data ($\dot{P} = 1.01 \times 10^{-12} \pm 3.38 \times 10^{-12} \text{ s s}^{-1}$). This non-detection is consistent with the theoretically expected value of $\dot{P} \sim 6 \times 10^{-13} \text{ s s}^{-1}$. However, within only a few more years the orbital shrinkage should become detectable.

6. Binary evolution calculations

More interesting than the present state of this system is its future evolution, which can now be studied in detail using theoretical models. Employing Eggleton’s stellar evolution code (Eggleton 1971, 1972, 1973), we calculated the evolution of the sdB star and its WD companion. The code has been updated with the latest input physics over the past four decades (Han et al. 1994; Pols et al. 1995, 1998). Roche lobe overflow (RLOF) is treated within the code described by Han et al. (2000). We set the ratio of mixing length to local pressure scale height, $\alpha = l/H_p$, to be 2.0. We assume that the binary model starts with a $0.51 M_{\odot}$ He star and a $0.76 M_{\odot}$ CO WD having a 0.049 d orbit period, similar to the initial model of the sdB star and its WD companion. Additionally, orbital angular momentum loss due to gravitational wave radiation is included by adopting a standard formula presented by Landau & Lifshitz (1971)

$$\frac{d \ln J_{\text{GR}}}{dt} = -\frac{32G^3}{5c^5} \frac{M_{\text{WD}}M_2(M_{\text{WD}} + M_2)}{a^4}, \quad (1)$$

where G , c , M_{WD} , and M_2 are the gravitational constant, vacuum speed of light, the mass of the accreting WD, and the mass of the companion sdB star, respectively.

In the He double-detonation model, if the mass-accretion rate is higher than $4 \times 10^{-8} M_{\odot} \text{ yr}^{-1}$, the WD can increase its

mass (Woosley et al. 1986; Wang et al. 2009a). However, for low mass-accretion rates ($1 \times 10^{-9} M_{\odot} \text{ yr}^{-1} \lesssim |\dot{M}_2| \lesssim 4 \times 10^{-8} M_{\odot} \text{ yr}^{-1}$), compressional heating at the base of the accreted He layer plays no significant role, and a layer of unburned He can be accumulated on the surface of the WD. If the mass-accretion rate is slower ($|\dot{M}_2| < 1 \times 10^{-9} M_{\odot} \text{ yr}^{-1}$), the He flash is strong enough to form a He detonation, but too weak to initiate a carbon detonation, and only a single He detonation wave propagates outward (Nomoto 1982).

We assume that if a CO WD accumulating He enters this “low” accretion rate regime and accumulates $0.1 M_{\odot}$ of He on its surface, a detonation is initiated at the base of the He shell layer (Fink et al. 2010). Consequently, a detonation in the core of the CO WD is presumed to follow, in which a sub- M_{Ch} SN Ia takes place. In this model, only accreting WDs with a total mass (CO core $0.8 M_{\odot}$ + helium shell $0.1 M_{\odot}$) $\geq 0.9 M_{\odot}$ are considered to result in potential sub- M_{Ch} SNe Ia, since the CO-core with lower mass may not detonate and it is unlikely to produce enough radioactive nickel observed in SNe Ia (Kromer et al. 2010).

The binary system starts with $(M_2^i, M_{\text{WD}}^i, \log(P^i/d)) = (0.510, 0.760, -1.310)$, where M_2^i and M_{WD}^i are the initial masses of the He star and of the CO WD in solar mass, and P^i is the initial orbital period in days. Figure 7 (left panel) shows the evolutionary track of the He star and the evolution of the orbital period. The right panel displays the mass-transfer rate and the mass of the WD envelope varying with time after the He star fills its Roche lobe.

Because of the short initial orbital period (0.049 d) of the system, angular momentum loss induced by gravitational wave radiation is large. This leads to the rapid shrinking of the orbital separation. After about 36 million years, the He star begins to fill its Roche lobe while it is still in the core helium-burning stage. The mass-transfer rate is stable and at a low rate between $1.6 \times 10^{-8} M_{\odot} \text{ yr}^{-1}$ and $2.2 \times 10^{-8} M_{\odot} \text{ yr}^{-1}$, resulting in the formation of a He shell on the surface of the CO WD. After about 6 million years, the mass of the He shell increases to $\sim 0.1 M_{\odot}$ in which a double-detonation may happen at the base of the He shell layer. At this moment, the mass of the He star is $M_2^{\text{SN}} = 0.41 M_{\odot}$ and the orbital period is $\log(P^{\text{SN}}/d) = -1.72$ ($P = 0.019$ d).

7. Hypervelocity sdO as donor remnant

Theoretical predictions about whether or not a progenitor candidate will explode as a SN Ia are useful, but in general difficult to test. Usually the theoretically predicted SN rates are compared to the observed rates, but these comparisons are often hampered by selection effects. A more direct proof would be the identification of the remnant objects. We therefore follow the future evolution of CD-30°11223. At the end of the He-accretion phase and just before the SN event, the orbital period of the binary is predicted to have shrunk to 0.019 d as a result of the further loss of orbital energy through the emission of gravitational waves. The sdB primary lost a fair amount of mass ($\sim 0.1 M_{\odot}$), which was transferred to the WD companion. The orbital velocity of the sdB will be about 600 km s^{-1} and therefore close to the Galactic escape velocity. As soon as the WD is disrupted, the sdB will be ejected. Depending on the ejection direction of such an object relative to its trajectory around the Galactic centre, the Galactic rest frame velocity could be even higher by up to 240 km s^{-1} . In this case the remnant star will leave the Galaxy.

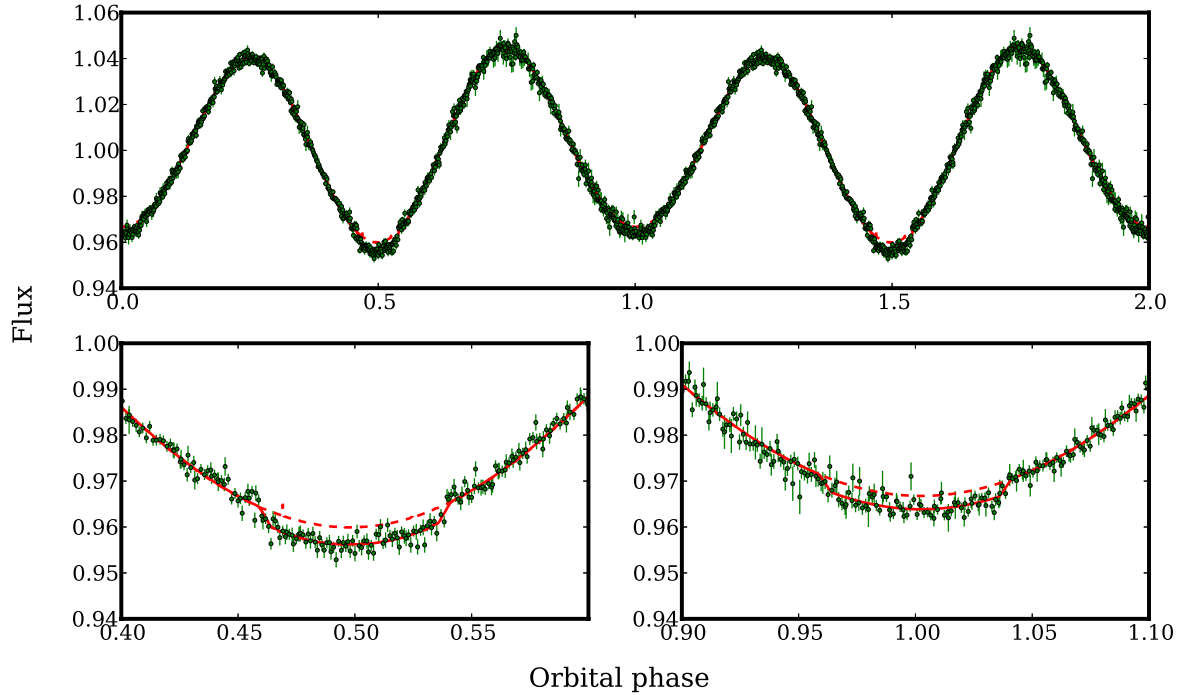


Fig. 5. *Upper panel:* V-band light curve of CD-30°11223 taken with SOAR/Goodman (green) with superimposed model (red) plotted twice against the orbital phase for better visualisation. The dashed red curve marks the same model without transits and eclipses. The sinusoidal variation is caused by the ellipsoidal deformation of the hot subdwarf as a result of the tidal influence of the compact white dwarf. The difference in the maxima between phase 0.25 and 0.75 originates from the relativistic Doppler boosting effect, which is usually not detectable with ground-based telescopes. *Lower panels:* close-up on the transit of the WD in front of the sdB (*left*). It is even possible to detect the eclipse of the WD by the sdB (*right*).

Such so-called hypervelocity stars have indeed been discovered (Brown et al. 2005; Hirsch et al. 2005; Edelmann et al. 2005). However, all but one of the known 22 objects are intermediate-mass main-sequence star. This enigmatic star (US 708) has been classified as a helium-rich hot subdwarf travelling at a Galactic rest frame velocity of at least 750 km s^{-1} (Hirsch et al. 2005), which matches the predicted ejection velocity of CD-30°11223 very well. It was proposed that this star might be the ejected He-donor after the WD companion exploded as a SN Ia (Justham et al. 2009; Wang & Han 2009).

In this scenario, the compact binary CD-30°11223 and the hypervelocity star US 708 represent two different stages of an evolutionary sequence linked by a SN Ia explosion. The existence of objects like US 708 thus provides evidence that binaries like CD-30°11223 are viable SN Ia progenitor candidates.

8. Age of the binary system

The analysis of our data also allows us to constrain the initial component masses and the age of the binary. Furthermore, we can constrain both its past and future trajectory.

8.1. Kinematic analysis

Using a standard Galactic gravitational potential with a Sun-Galactic centre distance of 8.4 kpc and a local standard of rest circular motion of 242 km s^{-1} (see Model I in Irrgang et al. 2013), we computed the past and future trajectory of CD-30°11223 (see Fig. 8). The orbit shows the typical characteristics of the local thin disc population, i.e. almost circular motion around the Galactic centre and small oscillations in direction perpendicular to the Galactic disc. The heliocentric distance to the

star increases during the next 42 Myr until the supernova is predicted to explode from its current value of $364 \pm 31 \text{ pc}$ to about $1920 \pm 160 \text{ pc}$.

The binary CD-30°11223 is by far the closest known SN Ia progenitor with respect to the Earth. The explosion will take place in a direction of the sky close to the current positions of the constellations Ara and Norma. Adopting an absolute visual magnitude of up to -19 mag for the SN Ia, the apparent magnitude seen from the Earth might be as high as $\sim -7.6 \text{ mag}$ or about as bright as SN 1006, the brightest stellar event in recorded history so far (Winkler et al. 2003).

8.2. Binary formation scenario

The system CD-30°11223 is the closest sdB binary known so far and the mass of its WD companion is higher than the average mass of CO WDs ($\sim 0.6 M_{\odot}$). To explore the formation of this exceptional system, we performed a binary population synthesis study in a similar way to the method described by Han et al. (2002, 2003). For given WD masses ranging from $0.6 M_{\odot}$ to $1.4 M_{\odot}$, an initial set of 10^6 WD+MS binaries was generated. For the main sequence stars the initial mass function of Salpeter was used. The orbital period distribution was assumed to be flat in $\log a$. The binaries were evolved through the common envelope phase for different values of the CE-efficiency parameters α_{CE} , which is the fraction of the available orbital energy used to eject the envelope, and α_{th} , the contributed fraction of internal energy.

In the standard scenario, which is called the 2nd CE channel, the progenitor of the sdB is a main sequence star of about solar mass and the common envelope is ejected right at the tip of the first giant branch (FGB, Han et al. 2002). However, this channel is not appropriate to form binaries as close as CD-30°11223, as

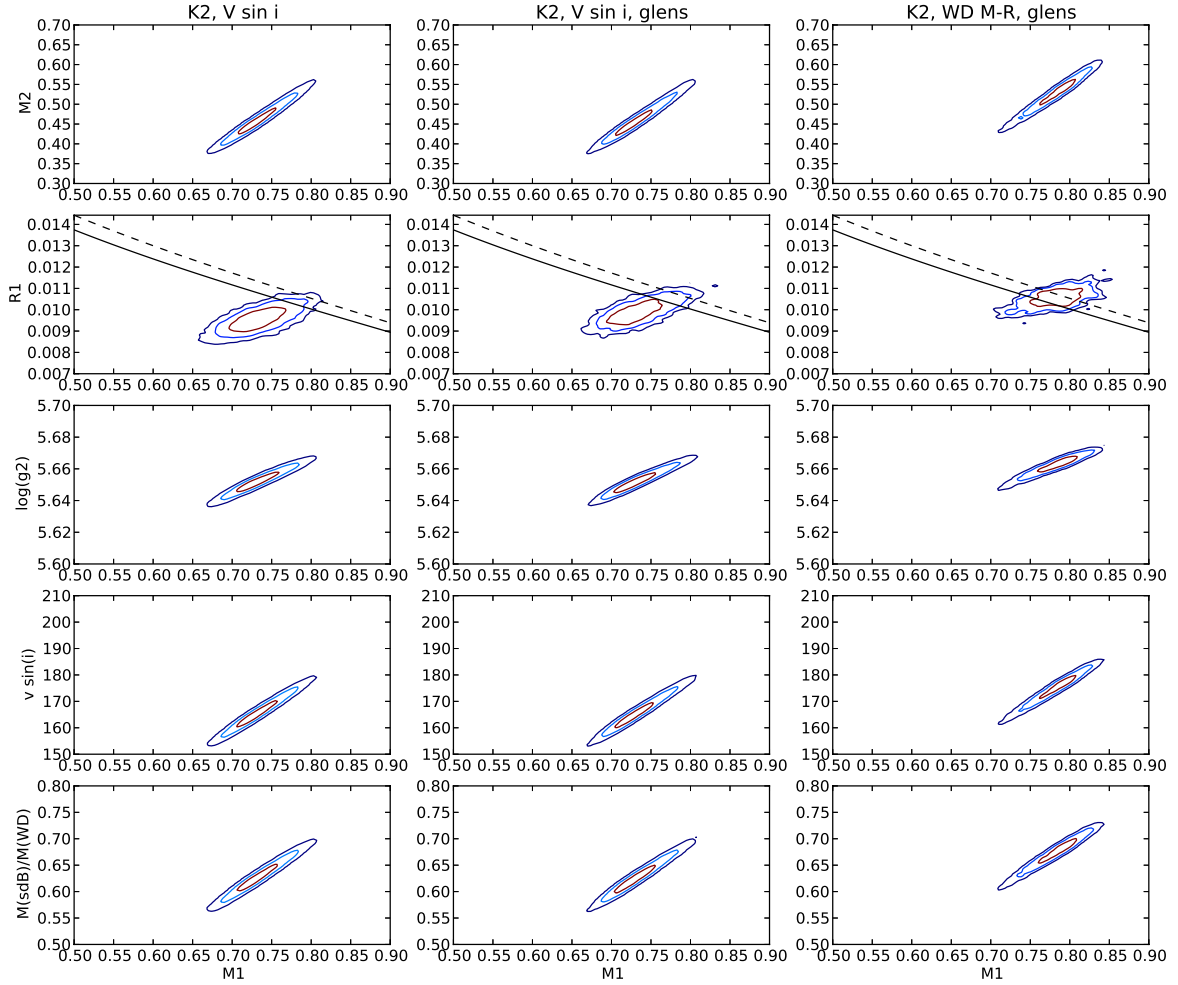


Fig. 6. Parameters of the CD-30° 11223 system plotted against the mass of the WD companion with contours marking the 1 σ (red), 2 σ (light blue), and 3 σ (dark blue) levels of confidence. In the *left column* tidal synchronisation of the sdB primary is assumed, while in the *middle column* the effect of microlensing has also been taken into account. Instead, in the *right column* the WD mass-radius relation has been used as an additional constraint. The solid lines in the mass-radius plots (*second panels from the top*) mark the zero-temperature mass-radius relation for WDs, the dashed lines more realistic models with 5% inflation. Note that both the $v_{\text{rot}} \sin i$ and the $\log g$ derived from the light curve are in agreement with the values derived from spectroscopy.

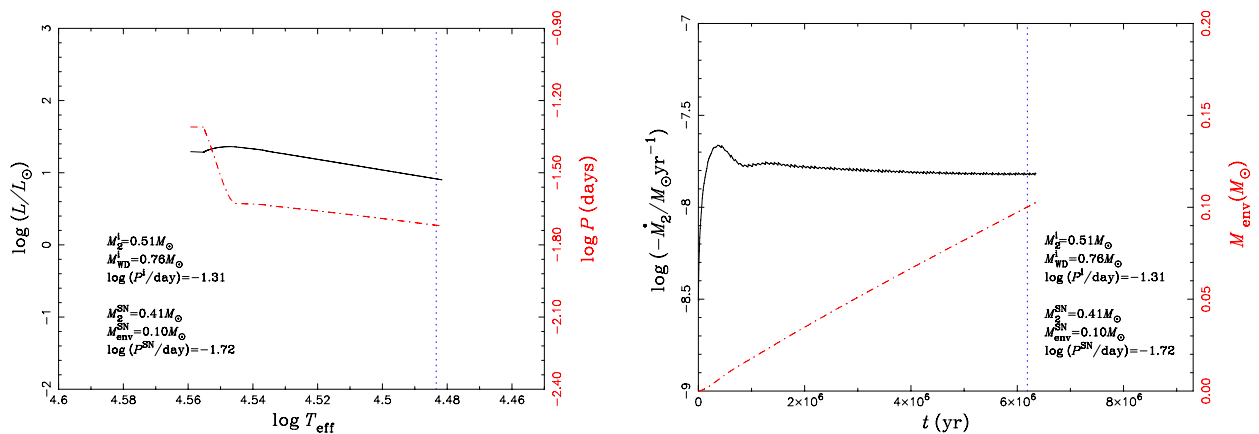


Fig. 7. Results of binary evolution calculations with initial masses of the two components and the orbital period similar to the sdB+WD binary system. *Left panel:* the evolutionary track of the He star is shown as a solid curve and the evolution of the orbital period as a dash-dotted curve. *Right panel:* the solid and dash-dotted curves show the mass-transfer rate and the mass of the WD envelope (He shell) varying with time after the He star fills its Roche lobe, respectively. Dotted vertical lines in both panels indicate the position where the double-detonation may happen (the mass of the He shell increases to $\sim 0.1 M_{\odot}$). The initial binary parameters and the parameters at the moment of the SN explosion are also given in the two panels.

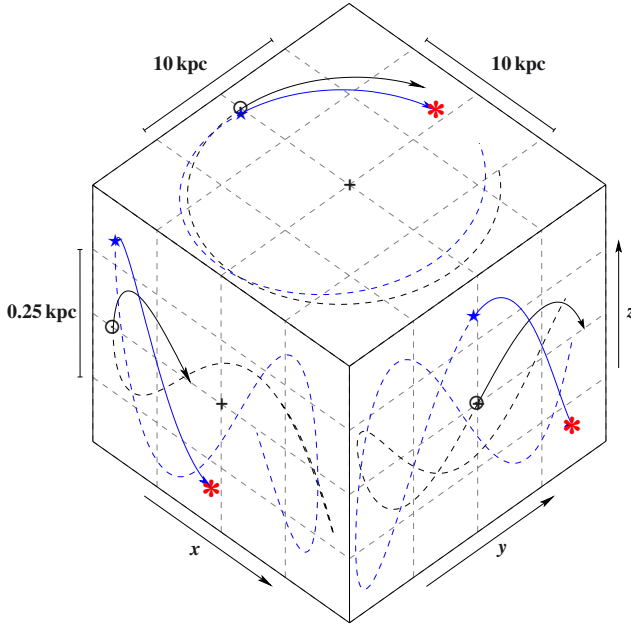


Fig. 8. Three-dimensional trajectory of CD-30°11223 in a Cartesian Galactic coordinate system with the z -axis pointing to the north Galactic pole. Current positions of CD-30°11223 (blue \star), Sun (black \odot), and Galactic centre (black $+$) are marked. The approximate point in time of the supernova explosion is symbolized by the red asterisk, while the arrow marks the position of the Sun at that time. Solid lines indicate the future 42 Myr, dashed lines the past 150 Myr. CD-30°11223's kinematic properties are obviously those of the local thin disc population.

shown in Fig. 9 (upper panel). The envelope at the tip of the FGB has a very low binding energy and can be ejected easily in the following CE. Thus, the orbital shrinkage during CE evolution is not significant and the produced sdB+WD system generally has an orbital period much longer than that of CD-30°11223. Only for a very small value of $\alpha_{\text{CE}} = 0.3$, which is very unlikely, some binaries reach the margin of 0.05 d. Indeed, the median period of the observed sdB binaries is as high as ~ 0.6 d (Geier et al. 2011). However, an sdB+WD binary can also be formed when the main-sequence progenitor of the subdwarf has an initial mass larger than $2 M_{\odot}$ and fills its Roche lobe during the Hertzsprung Gap or at the base of the FGB. In this case, the envelope is more tightly bound and the orbital shrinkage required to eject the CE becomes higher. In Fig. 9 (lower panel) the orbital period distribution is shown for this scenario when $\alpha_{\text{CE}} = \alpha_{\text{th}} = 0.75$, similar to the best fitting model of Han et al. (2003). As seen in the figure, short orbital periods, just as in the case of CD-30°11223, are expected.

We also investigated the distribution of sdB masses formed via this channel. While the standard CE-scenario predicts a mass distribution with a sharp peak at $0.47 M_{\odot}$, the sdB masses from more massive main-sequence stars (i.e. $>2 M_{\odot}$) show a significant scatter for higher values of α_{CE} , and even more so if we allow for a contribution of thermal energy in the CE-process by increasing the parameter α_{th} . The sdB mass for this channel largely depends on the mass of the progenitor, and can range from 0.3 to $1.0 M_{\odot}$ (see Fig. 10). This is consistent with the sdB mass of up to $0.54 M_{\odot}$ determined in the case of CD-30°11223.

We therefore conclude that CD-30°11223 was most likely formed via CE-ejection of a main sequence star with a mass larger than $2 M_{\odot}$, which means that it originated from a young stellar population.

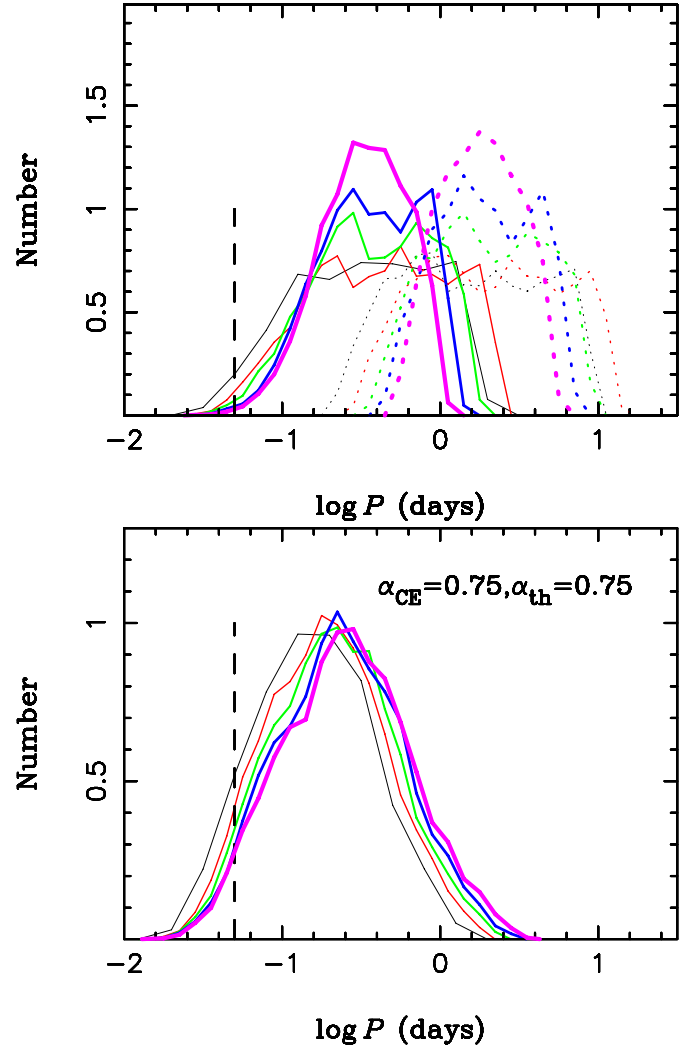


Fig. 9. *Top panel:* orbital period distribution of sdB+WD binaries from the 2nd CE channel. Different colours mark different WD masses (black $0.6 M_{\odot}$, red $0.8 M_{\odot}$, green $1.0 M_{\odot}$, blue $1.2 M_{\odot}$, purple $1.4 M_{\odot}$). The vertical dashed line marks $P = 0.05$ d. The contribution of thermal energy has not been included ($\alpha_{\text{th}} = 0$). The solid lines are for $\alpha_{\text{CE}} = 0.3$ and the dotted ones for $\alpha_{\text{CE}} = 1.0$. *Bottom panel:* orbital period distribution of sdB+WD binaries from the CE channel involving more massive main sequence stars (i.e. $>2 M_{\odot}$). The values of α_{CE} and α_{th} are indicated in the figure (see Fig. 9).

8.3. White dwarf cooling age and progenitor masses

We derived a mass of $0.76 M_{\odot}$ for the WD companion based on observations. Using an initial-to-final mass relation for isolated WDs the mass of the progenitor should have ranged from 3 to $4 M_{\odot}$ (see Fig. 7 in Kovetz et al. 2009, and references therein). Binary evolution is expected to lower the mass of the final WD and this progenitor mass estimate, therefore, has to be considered as lower limit.

Assuming a lifetime on the main sequence $\tau_{\text{MS}} = 10^{10} \text{ yr} \times [M/M_{\odot}]^{-2.5}$, the progenitor lived for a maximum of 640 Myr. We constrain the temperature of the WD in our light curve analysis to be ~ 25000 K. Therefore, its cooling age is $\sim 30\text{--}40$ Myr¹.

¹ Taken from cooling models for mixed C/O composition and for standard thick H and He layers, <http://www.astro.umontreal.ca/~bergeron/CoolingModels/>, Fontaine et al. (2001).

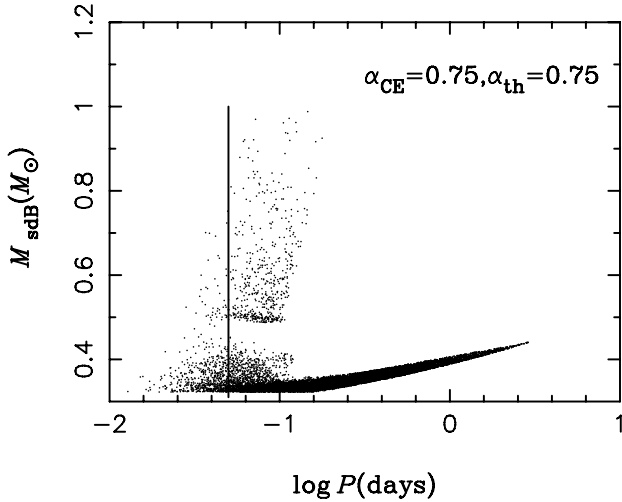


Fig. 10. sdB mass is plotted over the orbital period assuming the mass of the WD to be $1.2 M_{\odot}$. The main-sequence progenitors of the sdBs have initial masses larger than $2 M_{\odot}$. The values of α_{CE} and α_{th} are indicated in the figure.

The lifetime of the sdB on the extreme horizontal branch is of the same order as the one of the WD and we therefore derive a similar progenitor mass of more than $3 M_{\odot}$, consistent with the disc kinematics and the constraints from binary formation scenarios.

9. Conclusions

Systems like CD-30°11223 are young, which is consistent with the non-detection of objects with such high RV-shifts in the course of the MUCHFUSS project so far (Geier et al. 2011, 2011). Most targets of this survey are faint subdwarfs located in the old halo population. The sdB-donor double-detonation channel is therefore predicted to occur in young stellar populations and to contribute to the SN Ia population with short delay time (Ruiter et al. 2009).

Given that systems like CD-30°11223 are progenitors of some thermonuclear SN, a rough estimate can be made of the rate of such events. The system CD-30°11223 is one out of ~ 100 solved sdB binaries (Geier et al. 2011). About 50% of the known sdB stars are in close binary systems. So we can estimate the number fraction of systems like CD-30°11223 to be about 0.5% of the whole population of sdB stars. According to binary evolution calculations, the birthrate of such stars in our Galaxy is $\sim 5 \times 10^{-2} \text{ yr}^{-1}$ (Han et al. 2003). We therefore estimate the number of progenitor systems and the resulting SN Ia rate to be $\sim 2.5 \times 10^{-4} \text{ yr}^{-1}$. This is consistent with the theoretical birthrate predicted for the WD+He star channel ($\sim 3 \times 10^{-4} \text{ yr}^{-1}$, Wang et al. 2010), but more importantly, it is smaller than the SN Ia birthrate of $\sim 3 \times 10^{-3} \text{ yr}^{-1}$ and, therefore, consistent with observations (Capellaro & Turato 1997).

Although sub-Chandrasekhar scenarios in general have no well-defined explosion mass, the parameter space for the sdB binary progenitors turns out to be quite narrow. According to hydrodynamic simulations the minimum mass of the WD should be $\sim 0.8 M_{\odot}$, because carbon burning is not triggered for objects of much lower mass (Sim et al. 2012). On the other hand, the WD must consist of carbon and oxygen to be able to explode as a SN Ia. This limits the mass to values lower than $\sim 1.1 M_{\odot}$, because even more massive WDs consist of oxygen, neon, and

magnesium and tend to collapse rather than explode. This mass range is further narrowed down by binary evolution calculations. Very close sdB+WD systems with companion masses around $0.8 M_{\odot}$ are predicted to be formed in much higher numbers than binaries with more massive companions. Another important constraint is that the timespan from the binary formation after the CE to the SN Ia explosion must be shorter than the core helium-burning lifetime ($\sim 100 \text{ Myr}$). Otherwise the sdB will turn into a WD before helium can be transferred. This restricts the orbital periods of possible sdB+WD progenitors to less than $\sim 0.07 \text{ d}$.

The double-detonation scenario with a hot subdwarf donor is the only proposed SN Ia scenario where both progenitors and remnants have been identified. Analysing a larger sample of these objects will allow us to put tight constraints on their properties and evolution.

Acknowledgements. Based on observations obtained at the European Southern Observatory, La Silla for programme 089.D-0265(A). Based on observations with the *William Herschel* Telescope (WHT) operated by the Isaac Newton Group at the Observatorio del Roque de los Muchachos of the Instituto de Astrofísica de Canarias on the island of La Palma, Spain. Based on observations made at the South African Astronomical Observatory (SAAO). Based on observations with the Southern Astrophysical Research (SOAR) telescope operated by the US National Optical Astronomy Observatory (NOAO), the Ministério da Ciência e Tecnologia of the Federal Republic of Brazil (MCT), the University of North Carolina at Chapel Hill (UNC), and Michigan State University (MSU). We acknowledge the Director of SOAR for making the time for these observations during Technical and Engineering nights on the telescope. A.I. acknowledges support from a research scholarship by the Elite Network of Bavaria. V.S. acknowledges funding by the Deutsches Zentrum für Luft- und Raumfahrt (grant 50 OR 1110) and by the Erika-Giehl-Stiftung. S.G. and E.Z. are supported by the Deutsche Forschungsgemeinschaft (DFG) through grants HE1356/49-1 and HE1356/45-2, respectively. Finally, we want to thank the anonymous referee for helpful comments and suggestions.

References

- Bloemen, S., Marsh, T. R., Østensen, R. H., et al. 2011, *MNRAS*, 410, 1787
 Brown, W. R., Geller, M. J., Kenyon, S. J., & Kurtz M. J. 2005, *ApJ*, 622, L33
 Capellaro, E., & Turatto, M. 1997, *NATO ASI Series*, 486, 77
 Claret, A., & Bloemen, S. 2011, *A&A*, 529, 75
 Copperwheat, C., Marsh, T. R., Dhillon, V. S., et al. 2010, *MNRAS*, 402, 1824
 Edelmann, H., Napiwotzki, R., Heber, U., Christlieb, N., & Reimers, D. 2005, *ApJ*, 634, L181
 Eggleton, P. P. 1971, *MNRAS*, 151, 351
 Eggleton, P. P. 1972, *MNRAS*, 156, 361
 Eggleton, P. P. 1973, *MNRAS*, 163, 279
 Fink, M., Röpké, F. K., Hillebrandt, W., et al. 2010, *A&A*, 514, A53
 Fontaine, G., Brassard, P., & Bergeron, P. 2001, *PASP*, 113, 409
 Geier, S., Nesslinger, S., Heber, U., et al. 2007, *A&A*, 464, 299
 Geier, S., Heber, U., Podsiadlowski, Ph., et al. 2010, *A&A*, 519, A25
 Geier, S., Hirsch, H., Tillich, A., et al. 2011a, *A&A*, 530, A28
 Geier, S., Maxted, P. F. L., Napiwotzki, R., et al. 2011b, *A&A*, 526, A39
 Geier, S., Marsh, T. R., Dunlap, B. H., et al. 2013, *ASP Conf. Ser.*, in press [[arXiv:1209.4740](https://arxiv.org/abs/1209.4740)]
 Han, Z., Podsiadlowski, Ph., & Eggleton, P. P. 1994, *MNRAS*, 270, 121
 Han, Z., Tout, C. A., & Eggleton, P. P. 2000, *MNRAS*, 319, 215
 Han, Z., Podsiadlowski, Ph., Maxted, P. F. L., Marsh, T. R., & Ivanova, N. 2002, *MNRAS*, 336, 449
 Han, Z., Podsiadlowski, Ph., Maxted, P. F. L., & Marsh, T. R. 2003, *MNRAS*, 341, 669
 Heber, U., Reid, N., & Werner, K. 2000, *MNRAS*, 363, 198
 Heber, U., Geier, S., Gänsicke, B. 2013, *EPJ Web of Conferences*, 43, 04002
 Hirsch, H. A., Heber, U., O’Toole, S. J., & Bresolin, F. 2005, *A&A*, 444, L61
 Irgang, A., Wilcox, B., Tucker, E., & Schiefelbein, L. 2013, *A&A*, 549, A137
 Justham, S., Wolf, C., Podsiadlowski, Ph., & Han, Z. 2009, *A&A*, 493, 1081
 Kilic, M., Brown, W. R., Allende Prieto, C., et al. 2012, *ApJ*, 751, 141
 Kovetz, A., Yaron, O., & Prialnik, D. 2009, *MNRAS*, 395, 1857
 Kromer, M., Sim, S. A., Fink, M., et al. 2010, *ApJ*, 719, 1067
 Landau, L. D., & Lifshitz, E. M. 1971, *Classical theory of fields* (Oxford: Pergamon Press)
 Maxted, P. F. L., Marsh, T. R., & North, R. C. 2000, *MNRAS*, 317, L41
 Maxted, P. F. L., Heber, U., Marsh, T. R., & North, R. C. 2001, *MNRAS*, 326, 1391

- Napiwotzki, R., Karl, C. A., Lisker, T., et al. 2004a, *Ap&SS*, 291, 321
Napiwotzki, R., Yungelson, L., Nelemans, G., et al. 2004b, *ASP Conf. Ser.*, 318, 402
Nelemans, G. 2009, *Class. Quant. Grav.*, 26, 094030
Németh, P., Kawka, A., & Vennes, S. 2012, *MNRAS*, 427, 2180
Nomoto, K. 1982, *ApJ*, 257, 780
Pollacco, D. L., Skillen, I., Collier Cameron, A., et al. 2006, *PASP*, 118, 1407
Pols, O. R., Tout, C. A., Eggleton, P. P., & Han, Z. 1995, *MNRAS*, 274, 964
Pols, O. R., Schröder, K.-P., Hurley, J. R., Tout, C. A., & Eggleton, P. P. 1998, *MNRAS*, 298, 525
Roelofs, G. H. A., Groot, P. J., Benedict, G. F., et al. 2007, *ApJ*, 666, 1174
Roeser, S., Demleitner, M., & Schilbach, E. 2010, *AJ*, 139, 2440
Ruiter, A. J., Belczynski, K., & Fryer, C. 2009, *ApJ*, 699, 2026
Shakura, N. I., & Postnov, K. A. 1987, *A&A*, 183, L21
Sim, S., Röpké, F. K., Hillebrandt, W., et al. 2010, *ApJ*, 714, L52
Sim, S., Fink, M., Kromer, M., et al. 2012, *MNRAS*, 420, 3003
Vennes, S., Kawka, A., & Németh, P. 2011, *MNRAS*, 410, 2095
Vennes, S., Kawka, A., O'Toole, S. J., Németh, P., & Burton, D. 2012, *ApJ*, 759, L25
Verbunt, F., & Rappaport, S. 1988, *ApJ*, 332, 193
Wang, B., & Han, Z. 2009, *A&A*, 508, L27
Wang, B., & Han, Z. 2012, *New Astron. Rev.*, 56, 122
Wang, B., Chen, X., Meng, X., & Han, Z. 2009a, *ApJ*, 701, 1540
Wang, B., Meng, X., Chen, X., & Han, Z. 2009b, *MNRAS*, 395, 847
Wang, B., Liu, Z., Han, Y., et al. 2010, *Sci. China Ser. G*, 53, 586
Winkler, F. P., Gupta, G., & Long, K. S. 2003, *ApJ*, 585, 324
Woosley, S. E., Taam, R. E., & Weaver, T. A. 1986, *ApJ*, 301, 601
Yoon, S.-C., & Langer, N. 2003, *A&A*, 412, 53

11. L. V. E. Koopmans, T. Treu, C. D. Fassnacht, R. D. Blandford, G. Surpi, *Astrophys. J.* **599**, 70–85 (2003).
12. M. Tewes *et al.*, *Astron. Astrophys.* **556**, A22 (2013).
13. S. H. Suyu *et al.*, *Astrophys. J.* **766**, 70 (2013).
14. R. Chornock *et al.*, *Astrophys. J.* **767**, 162 (2013).
15. R. M. Quimby *et al.*, *Astrophys. J.* **768**, L20 (2013).
16. R. M. Quimby *et al.*, *Science* **344**, 396–399 (2014).
17. K. B. Schmidt *et al.*, *Astrophys. J.* **782**, L36 (2014).
18. T. Jones *et al.*, *arxiv.org/abs/1410.0967* (2014).
19. H. Ebeling *et al.*, *Astrophys. J.* **661**, L33–L36 (2007).
20. G. P. Smith *et al.*, *Astrophys. J.* **707**, L163–L168 (2009).
21. M. Ganeshalingam, W. Li, A. V. Filippenko, *Mon. Not. R. Astron. Soc.* **416**, 2607–2622 (2011).
22. S. Kaspi *et al.*, *Astrophys. J.* **659**, 997–1007 (2007).
23. M. C. Bentz *et al.*, *Astrophys. J.* **705**, 199–217 (2009).

ACKNOWLEDGMENTS

This work is based on data obtained with the NASA/ESA Hubble Space Telescope. We thank O. Fox, W. Zheng, J. Bloom, C. Keeton, J. Mauerhan, C. Steidel, and A. Strom for helpful discussions,

as well as the Space Telescope Science Institute (STScI) and Director Matt Mountain for supporting our proposal for follow-up observations. GLASS is supported by NASA through HST grant GO-13459. Support for S.A.R. was provided by NASA through Hubble Fellowship grant HST-HF-51312.01 awarded by STScI, which is operated by the Association of Universities for Research in Astronomy for NASA, under contract NAS 5-26555. Follow-up imaging through the FrontierSN program is supported by NASA through HST grant GO-13386. A.V.F.'s group at the University of California Berkeley has received generous financial assistance from the Christopher R. Redlich Fund, the TABASGO Foundation, Gary and Cynthia Bengier, and NSF grant AST-1211916. The Dark Cosmology Centre is funded by the Danish National Research Foundation. Support for A.Z. was provided by NASA through Hubble Fellowship grant HF2-51334.001-A awarded by STScI. SN research at Rutgers University is supported in part by NSF CAREER award AST-0847157 to S.W.J.. J.C.M. is supported by NSF grant AST-1313484 and by NASA HST grants GO-13343 and GO-13386; this research was carried out in part at the Jet Propulsion Laboratory, California Institute of Technology, under a contract with NASA. R.G. acknowledges the Centre National d'Etudes

Spatiales for financial support on the GLASS project. Some of the data presented here were obtained at the W. M. Keck Observatory, which is operated as a scientific partnership among the California Institute of Technology, the University of California, and NASA; the observatory was made possible by the generous financial support of the W. M. Keck Foundation. The HST imaging data used in this paper can be obtained from the Barbara A. Mikulski Archive for Space Telescopes at <https://archive.stsci.edu>, and the Keck-I LRIS spectra can be obtained at <http://hercules.berkeley.edu/database>.

SUPPLEMENTARY MATERIALS

www.sciencemag.org/content/347/6226/1123/suppl/DC1
Materials and Methods
Figs. S1 to S4
Tables S1 to S2
References (24–32)

21 November 2014; accepted 10 February 2015
10.1126/science.aaa3350

STELLAR DYNAMICS

The fastest unbound star in our Galaxy ejected by a thermonuclear supernova

S. Geier,^{1,2*} F. Fürst,³ E. Ziegerer,² T. Kupfer,⁴ U. Heber,² A. Irrgang,² B. Wang,⁵ Z. Liu,^{5,6} Z. Han,⁵ B. Sesar,^{7,8} D. Levitan,⁷ R. Kotak,⁹ E. Magnier,¹⁰ K. Smith,⁹ W. S. Burgett,¹⁰ K. Chambers,⁸ H. Flewelling,⁸ N. Kaiser,⁸ R. Wainscoat,⁸ C. Waters¹⁰

Hypervelocity stars (HVSs) travel with velocities so high that they exceed the escape velocity of the Galaxy. Several acceleration mechanisms have been discussed. Only one HVS (US 708, HVS 2) is a compact helium star. Here we present a spectroscopic and kinematic analysis of US 708. Traveling with a velocity of ~1200 kilometers per second, it is the fastest unbound star in our Galaxy. In reconstructing its trajectory, the Galactic center becomes very unlikely as an origin, which is hardly consistent with the most favored ejection mechanism for the other HVSs. Furthermore, we detected that US 708 is a fast rotator. According to our binary evolution model, it was spun-up by tidal interaction in a close binary and is likely to be the ejected donor remnant of a thermonuclear supernova.

According to the widely accepted theory for the acceleration of hypervelocity stars (HVSs) (1–3), a close binary is disrupted by the supermassive black hole (SMBH) in the center of our Galaxy, and one component is ejected as a HVS (4). In an alternative scenario, US 708 was proposed to be ejected from an ultracompact binary star by a thermonuclear supernova type Ia (SN Ia) (5). However, previous observational evidence was insufficient to put firm constraints on its past evolution. Here we show that US 708 is the fastest unbound star in our Galaxy, provide evidence for the SN ejection scenario, and identify a progenitor population of SN Ia.

In contrast to all other known HVSs, US 708 has been classified as a hot subdwarf star [subdwarf O- or B-type (sdO/B) star]. Those stars are evolved, core helium-burning objects with low masses around 0.5 times the mass of the Sun (M_{\odot}). About half of the sdB stars reside in close binaries with periods ranging from ~0.1 to ~30 days (6, 7). The hot subdwarf is regarded as

the core of a former red giant star that has been stripped of almost all of its hydrogen envelope through interaction with a close companion star (8, 9). However, single hot subdwarf stars like US 708 are known as well. Even in this case, binary evolution has been proposed, as the merger of two helium white dwarfs (He-WDs) is a possible formation channel for those objects (10).

The hot subdwarf nature of US708 poses a particular challenge for theories that aim to explain the acceleration of HVSs. Within the slingshot scenario proposed by Hills, a binary consisting of two main-sequence stars is disrupted by the close encounter with the SMBH in the center of our Galaxy. While one of the components remains in a bound orbit around the black hole, the other one is ejected with high velocity (4). This scenario explains the existence of the so-called S-stars orbiting the SMBH in the Galactic center and provides the most convincing evidence for the existence of this black hole (11). It is also consistent with the main properties of the known HVS population consisting of young main-sequence

stars (12, 13). However, more detailed analyses of some young HVSs challenge the Galactic center origin (14), and most recently, a new population of old main-sequence stars likely to be HVSs has been discovered. Most of those objects are also unlikely to originate from the Galactic center, but the acceleration mechanism remains unclear (15).

In the case of the helium-rich sdO (He-sdO) US 708, the situation is even more complicated. In contrast to all other known HVSs, which are normal main-sequence stars of different ages, this star is in the phase of shell helium burning, which lasts for only a few tens of millions of years. More importantly, it has been formed by close binary interaction. To accelerate a close binary star to such high velocity, the slingshot mechanism requires either a binary black hole (16) or the close encounter of a hierarchical triple system, where the distant component becomes bound to the black hole and the two close components are ejected (17). Similar constraints apply to the dynamical ejection out of a dense cluster, which is the second main scenario discussed to explain the HVSs.

Close binarity requires specific modifications of the canonical HVS scenarios. However, it is a necessary ingredient for an alternative scenario, in which US 708 is explained as the ejected donor

¹European Southern Observatory, Karl-Schwarzschild-Straße 2, 85748 Garching, Germany. ²Dr. Karl Remeis-Observatory and Erlangen Centre for Astroparticle Physics, Astronomical Institute, Friedrich-Alexander University Erlangen-Nuremberg, Sternwartstraße 7, 96049 Bamberg, Germany. ³Space Radiation Lab, MC 290-17 Cahill, California Institute of Technology, 1200 East California Boulevard, Pasadena, CA 91125, USA. ⁴Department of Astrophysics/Institute for Mathematics, Astrophysics and Particle Physics, Radboud University Nijmegen, P.O. Box 9010, 6500 GL Nijmegen, Netherlands. ⁵Key Laboratory of the Structure and Evolution of Celestial Objects, Yunnan Observatories, Chinese Academy of Sciences, Kunming 650011, China. ⁶Argelander-Institut für Astronomie, Universität Bonn, Auf dem Hügel 71, 53121 Bonn, Germany. ⁷Division of Physics, Mathematics, and Astronomy, California Institute of Technology, 1200 East California Boulevard, Pasadena, CA 91125, USA. ⁸Max-Planck-Institut für Astronomie, Königstuhl 17, 69117, Heidelberg, Germany. ⁹Astrophysics Research Center, School of Mathematics and Physics, Queen's University Belfast, Belfast BT7 1NN, UK. ¹⁰Institute for Astronomy, University of Hawaii at Manoa, Honolulu, HI 96822, USA.

*Corresponding author. E-mail: sgeier@eso.org

remnant of a thermonuclear SN Ia (18, 19). Underluminous SN Ia have been proposed to originate from a so-called “double detonation” of a white dwarf (WD) (20, 21). In this scenario, a massive WD is closely orbited by a low-mass helium star. Due to a tightening of the orbit, the helium star will start to transfer mass to its compact companion. After a critical amount of helium

is deposited on the surface of the WD through accretion, the helium is ignited, causing a detonation wave that triggers the explosion of the carbon-oxygen WD itself. The ultracompact sdB+WD binary CD -30° 11223 has recently been identified as progenitor candidate for such a scenario and has been linked to the putative ejected donor remnant US 708 (5, 22).

Fig. 1. Fit of model spectrum.

The fit of synthetic models to the helium and nitrogen lines of a Keck/ESI spectrum of US 708 is shown. The normalized fluxes of the single lines are shifted by constant values c for better visualization, and the most prominent lines are labeled. The weaker lines are from N III at 4634 and 4640 Å, He I at 4713 Å (spectral region in the middle), N III at 4379 Å, and He I at 4387 Å (spectral region at the bottom). The shift with respect to the rest wavelengths $\Delta\lambda$ (dashed vertical line) caused by the high radial velocity and the substantial broadening of the lines are clearly visible.

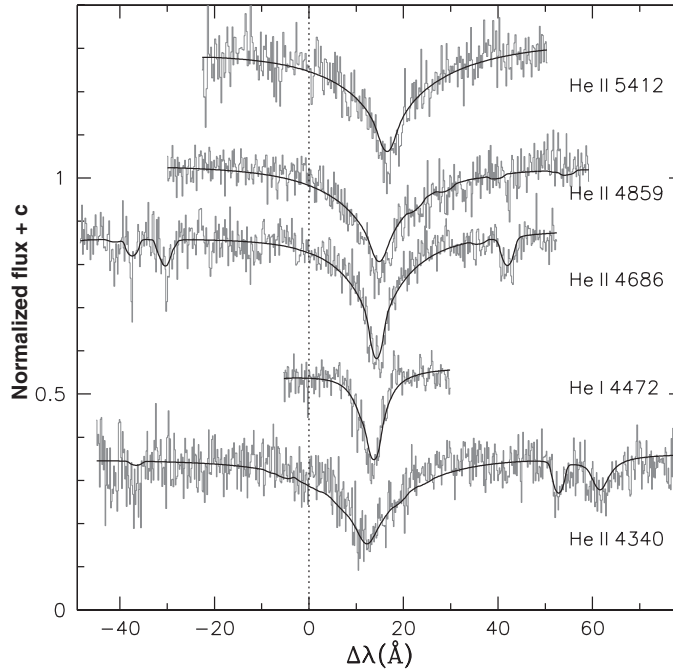


Table 1. Parameters of US 708. The uncertainty of the radial velocity is the 1σ error from a χ^2 fit, the uncertainties in the proper motion components have been propagated from the position errors by linear regression, and the uncertainties in the atmospheric parameters are bootstrap errors. The uncertainties of the other parameters have been propagated from the uncertainties of the input parameters. N/A, not applicable.

Parameter	Abbreviation	Unit	Value
Visual magnitude*	m_g	mag	18.668 ± 0.008
Proper motion	$\mu_\alpha \cos \delta$	milli-arc sec year $^{-1}$	-8.0 ± 1.8
	μ_δ	milli-arc sec year $^{-1}$	9.1 ± 1.6
Radial velocity	v_{helio}	km s $^{-1}$	917 ± 7
Galactic Cartesian coordinates	X	kpc	-14.2 ± 0.7
	Y	kpc	0.4 ± 0.1
	Z	kpc	6.2 ± 0.7
Galactic velocity components	v_X	km s $^{-1}$	-855 ± 61
	v_Y	km s $^{-1}$	643 ± 77
	v_Z	km s $^{-1}$	431 ± 58
Galactic rest-frame velocity	v_{grf}	km s $^{-1}$	1157 ± 53
Effective temperature	T_{eff}	K	47200 ± 400
Surface gravity	$\log g$	N/A	5.69 ± 0.09
Helium abundance	$\log y$	N/A	$+2.0$
Nitrogen abundance	$\log \frac{N(\text{N})}{N(\text{H})}$	N/A	-2.4 ± 0.2
Projected rotational velocity	$v_{\text{rot}} \sin i$	km s $^{-1}$	115 ± 8
Mass (adopted)	M_{sdb}	M_\odot	0.3
Distance	d	kpc	8.5 ± 1.0

*Taken from the Sloan Digital Sky Survey (SDSS) Data Server (das.sdss.org)

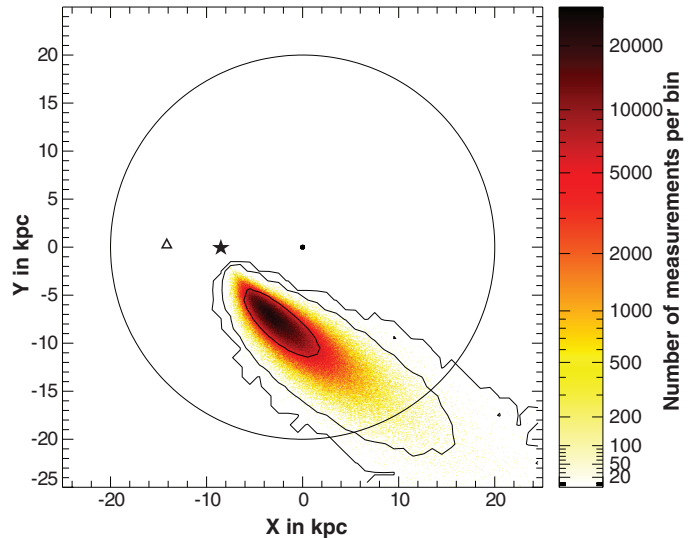
We performed a detailed spectroscopic and kinematic analysis of US 708 based on recently obtained and archival data to trace back its origin and constrain the ejection mechanism. To determine the three-dimensional motion of US 708, both the radial and tangential velocity components have to be determined. We measured the radial velocity from new spectra taken with the Keck and Palomar telescopes and compared it with archival data. We also derived atmospheric parameters and a spectroscopic distance from the new spectra (Fig. 1). In addition, we determined the proper motion by combining archival positions with new measurements from the PanSTARRS survey (fig. S2 and Table 1).

With a Galactic rest-frame velocity of 1157 ± 53 km s $^{-1}$, we find that US 708 is the fastest known unbound star in our Galaxy. Its current distance is 8.5 ± 1.0 kpc, and it is moving away from the Galactic plane into the halo. Tracing back its trajectory and assuming no further deviations, we deduced that it crossed the Galactic disc 14.0 ± 3.1 million years ago. In this way, an origin in the center of our Galaxy can be excluded with high confidence (Fig. 2), but the origin in the Galactic disc is fully consistent with the SN ejection scenario. In contrast to regular SN Ia, double-detonation SN Ia with hot subdwarf donors are predicted to happen in young stellar populations (5).

Both the current Galactic rest-frame velocity and the reconstructed ejection velocity from the Galactic disc (998 ± 68 km s $^{-1}$) are substantially higher than the value published before (~ 750 km s $^{-1}$, based on radial velocity alone) (2). This puts new constraints on the possible progenitor system, which can be derived from the observed parameters of US 708. To reach such a high ejection velocity, the progenitor binary must have been very compact and the WD companion rather massive. The likely progenitor system consists of a compact helium star with a mass of $\sim 0.3 M_\odot$ and a massive carbon-oxygen WD (1.0 to $1.2 M_\odot$) with an orbital period of ~ 10 min. We calculated the mass-transfer rate in such a binary and found that the helium is accreted by the WD at a rate suitable for the double-detonation scenario [10^{-9} to $10^{-8} M_\odot$ year $^{-1}$ (5)]. Such ultrashort-period systems with compact helium stars have indeed been observed. The eclipsing He-WD+CO-WD binary SDSS J065133+284423 has an orbital period of only 12 min (23). However, the mass of the CO-WD ($0.55 M_\odot$) is too low for a double-detonation SN Ia.

The ejection from such a close binary should leave another imprint on the remnant. We know that hot subdwarfs in compact binaries have been spun up by the tidal influence of the close companion (22, 24, 25) to projected rotational velocities ($v_{\text{rot}} \sin i$) that are substantially higher than the projected rotational velocities of single hot subdwarfs (26, 27). An ejected remnant is predicted to have a high $v_{\text{rot}} \sin i$ as well (28), and indeed we measured $v_{\text{rot}} \sin i = 115 \pm 8$ km s $^{-1}$, which is substantially higher than expected for a single He-sdO (Fig. 1) (27). However, assuming an ultracompact progenitor binary, the measured

Fig. 2. Origin of US 708. A Monte Carlo simulation (10^8 iterations) of the past trajectory of US 708 is shown. The color-coded bins mark the positions where the star crossed the Galactic disc, which is shown pole-on. The contours correspond to the 1σ , 3σ , and 5σ confidence limits. The position of the Galactic center is denoted by the black dot, the position of the Sun is given by the star symbol, and the current position of US 708 is marked by a triangle and given in Table 1.



$v_{\text{rot}} \sin i$ of the He-sdO is still slower than expected by about a factor of four. A high loss of mass and angular momentum caused by the SN impact is predicted for main-sequence companions in the standard single-degenerate SN Ia scenario, in which mass is transferred from such a companion to a WD (29–31). Though the loss of mass and angular momentum for a more compact companion like US 708 is expected to be smaller, our results indicate that it is still substantial. This puts important observational constraints on more detailed models.

Whereas the observed properties of US 708 are consistent with the SN ejection scenario, they are hardly compatible with the slingshot mechanism because an origin of the star in the center of the Galaxy is very unlikely (Fig. 2; see also the additional explanation in the supplementary materials). However, it must be stated that the SN ejection scenario is only applicable to such compact helium stars and cannot be invoked to explain the acceleration of the other HVSSs.

Depending on the pollution by SN material, the effect of the SN impact, and the subsequent stellar evolution, the surface abundances of US 708 might be substantially affected. Ultraviolet spectroscopy is necessary to measure the metal abundances of US 708 and put further constraints on the extreme history of this star, which witnessed a SN from a distance of less than 0.2 solar radii.

In providing evidence that US 708 is probably the donor remnant of a helium double-detonation SN Ia, we have shown an acceleration mechanism for the fastest unbound stars in our Galaxy. With that, we have also made an important step forward in understanding SN Ia explosions in general. Despite the fact that those bright events are used as standard candles to measure the expansion (and acceleration) of the universe, their progenitors are still unknown. Our results suggest that, due to the high WD masses derived for the progenitor binary, the double-detonation scenario might not only be applicable to some underluminous SN Ia (5, 21) but might also con-

tribute to the population of typical SNe Ia used as cosmic yardsticks (20).

REFERENCES AND NOTES

1. W. R. Brown, M. J. Geller, S. J. Kenyon, M. J. Kurtz, *Astrophys. J.* **622**, L33–L36 (2005).
2. H. A. Hirsch, U. Heber, S. J. O'Toole, F. Bresolin, *Astron. Astrophys.* **444**, L61–L64 (2005).
3. H. Edelmann, R. Napiwotzki, U. Heber, N. Christlieb, D. Reimers, *Astrophys. J.* **634**, L181–L184 (2005).
4. J. G. Hills, *Nature* **331**, 687–689 (1988).
5. S. Geier *et al.*, *Astron. Astrophys.* **554**, A54 (2013).
6. P. F. L. Maxted, U. Heber, T. R. Marsh, R. C. North, *Mon. Not. R. Astron. Soc.* **326**, 1391–1402 (2001).
7. R. Napiwotzki *et al.*, *Astrophys. Space Sci.* **291**, 321–328 (2004).
8. Z. Han, Ph. Podsiadlowski, P. F. L. Maxted, T. R. Marsh, N. Ivanova, *Mon. Not. R. Astron. Soc.* **336**, 449–466 (2002).
9. Z. Han, Ph. Podsiadlowski, P. F. L. Maxted, T. R. Marsh, *Mon. Not. R. Astron. Soc.* **341**, 669–691 (2003).
10. R. F. Webbink, *Astrophys. J.* **277**, 355–360 (1984).
11. S. Gillessen *et al.*, *Astrophys. J.* **692**, 1075–1109 (2009).
12. W. R. Brown, J. G. Cohen, M. J. Geller, S. J. Kenyon, *Astrophys. J.* **754**, L2 (2012).
13. B. C. Bromley, S. J. Kenyon, M. J. Geller, W. R. Brown, *Astrophys. J.* **749**, L42 (2012).
14. U. Heber, H. Edelmann, R. Napiwotzki, M. Altmann, R.-D. Scholz, *Astron. Astrophys.* **483**, L21–L24 (2008).
15. L. E. Palladino *et al.*, *Astrophys. J.* **780**, 7 (2014).
16. Y. Lu, Q. Yu, D. N. C. Lin, *Astrophys. J.* **666**, L89–L92 (2007).
17. H. P. Perets, *Astrophys. J.* **698**, 1330–1340 (2009).
18. B. Wang, X. Meng, X. Chen, Z. Han, *Mon. Not. R. Astron. Soc.* **395**, 847–854 (2009).
19. S. Justham, C. Wolf, Ph. Podsiadlowski, Z. Han, *Astron. Astrophys.* **493**, 1081–1091 (2009).
20. M. Fink *et al.*, *Astron. Astrophys.* **514**, A53 (2010).
21. R. Foley *et al.*, *Astrophys. J.* **767**, 57 (2013).
22. S. Vennes, A. Kawka, S. J. O'Toole, P. Németh, D. Burton, *Astrophys. J.* **759**, L25 (2012).
23. W. R. Brown *et al.*, *Astrophys. J.* **737**, L23 (2011).
24. S. Geier *et al.*, *Astron. Astrophys.* **464**, 299–307 (2007).
25. S. Geier *et al.*, *Astron. Astrophys.* **519**, A25 (2010).
26. S. Geier, U. Heber, *Astron. Astrophys.* **543**, A149 (2012).
27. H. Hirsch, U. Heber, *J. Phys. Conf. Ser.* **172**, 012015 (2009).
28. K.-C. Pan, P. M. Ricker, R. E. Taam, *Astrophys. J.* **773**, 49 (2013).
29. K.-C. Pan, P. M. Ricker, R. E. Taam, *Astrophys. J.* **750**, 151 (2012).

30. K.-C. Pan, P. M. Ricker, R. E. Taam, *Astrophys. J.* **760**, 21 (2012).

31. Z.-W. Liu *et al.*, *Astron. Astrophys.* **554**, A109 (2013).

ACKNOWLEDGMENTS

We thank H. Hirsch for providing us with the Low Resolution Imaging Spectrometer spectra. This work is based on observations obtained at the W.M. Keck Observatory, which is operated as a scientific partnership among the California Institute of Technology, the University of California, and NASA. The W. M. Keck Observatory was made possible by the generous financial support of the W. M. Keck Foundation. We wish to recognize the important cultural role and reverence that the summit of Mauna Kea has always had within the indigenous Hawaiian community. We are most fortunate to have the opportunity to conduct observations from this mountain. This work is also based on observations at the Palomar Observatory. The Pan-STARRS1 Surveys (PS1) have been made possible through contributions from the Institute for Astronomy, the University of Hawaii, the Pan-STARRS Project Office, the Max-Planck Society and its participating institutes (the Max Planck Institute for Astronomy, Heidelberg, and the Max Planck Institute for Extraterrestrial Physics, Garching), The Johns Hopkins University, Durham University, the University of Edinburgh, Queen's University Belfast, the Harvard-Smithsonian Center for Astrophysics, the Las Cumbres Observatory Global Telescope Network, the National Central University of Taiwan, the Space Telescope Science Institute, the NASA under grant no. NNX08AR22G issued through the Planetary Science Division of the NASA Science Mission Directorate, the NSF under grant no. AST-1238877, the University of Maryland, and Eotvos Lorand University (ELTE). Z.H. is supported by the Natural Science Foundation of China (grant nos. 11390374 and 11033008). E.Z. and A.I. are supported by the Deutsche Forschungsgemeinschaft through grant HE1356/45-2. T.K. acknowledges support from the Netherlands Research School for Astronomy (NOVA). A.I. acknowledges support from a research scholarship by the Elite Network of Bavaria. R.K. acknowledges support from Science and Technologies Council UK grant no. ST/L000709/1, Queen's University Belfast's contribution to the PanSTARRS1 science consortium. K.S. acknowledges support from European Union FP7 Programme ERC grant no. 291222. F.F. acknowledges NASA contract no. NNG08FD60C for the NuSTAR mission. The data observed with the SDSS and Keck telescope are published via the SDSS and Keck data archive; the PS1 data and catalog are available upon request.

SUPPLEMENTARY MATERIALS

www.sciencemag.org/content/347/6226/1126/suppl/DC1
Materials and Methods
Supplementary Text
Figs. S1 to S7
References (32–57)

22 July 2014; accepted 29 January 2015
10.1126/science.1259063

Supplementary Materials for

The fastest unbound star in our Galaxy ejected by a
thermonuclear supernova

S. Geier, F. Fürst, E. Ziegerer, T. Kupfer, U. Heber,
A. Irrgang, B. Wang, Z. Liu, Z. Han, B. Sesar, D. Levitan,
R. Kotak, E. Magnier, K. Smith, W. S. Burgett,
K. Chambers, H. Flewelling, N. Kaiser, R. Wainscoat,
C. Waters

correspondence to: sgeier@eso.org

This PDF file includes:

Materials and Methods

Supplementary Text

Figs. S1 to S7

Materials and Methods

Summary

Spectra of US 708 have been taken with the 10m Keck and the 5m Palomar telescopes. From the Doppler shift of the spectral lines we measured the radial ve-

locity using both new and archival data. The tangential velocity components have been determined by measuring the proper motion of the star from multi-epoch position measurements spanning 59 years and its spectroscopic distance performing a full quantitative spectral analysis using state-of-the-art model atmospheres. Using those informations we constrained the kinematics of this star and traced back its origin to the Galactic disk performing a Monte Carlo simulation. The properties of the progenitor binary have been determined mostly based on the derived ejection velocity from the Galactic disc. Binary evolution calculations have then been performed to check the consistency of those properties with theory. The current rotational properties of US 708 have been compared with hydrodynamical models of angular momentum-loss triggered by supernovae explosions.

Observations

US 708 ($\alpha_{2000} = 09^{\text{h}}33^{\text{m}}20^{\text{s}}.85$, $\delta_{2000} = +44^{\circ}17'05.8''$) was discovered to be a hypervelocity star by Hirsch et al. (2). A medium-resolution ($R \sim 1800$) spectrum was taken by the Sloan Digital Sky Survey (SDSS) on February 20, 2002 (32). Follow-up low-resolution ($R \sim 900$) spectroscopy was obtained with the LRIS instrument at the Keck telescope on May 13, 2005. The reduced spectra from the blue and red channel of the instrument were provided to us by H. Hirsch. A series of 11 consecutively taken medium-resolution ($R \sim 8000$) spectra was obtained with the ESI instrument at the Keck telescope on March 3, 2013. The spectra have been reduced with the ESI pipeline Makee.* One spectrum has been taken

*<http://www.astro.caltech.edu/~tb/makee/>

with the medium-resolution spectrograph at the 5.1 m Hale telescope on Mount Palomar on May 11, 2013 and another three spectra on June 1, 2013.

Revised radial velocity

Hirsch et al. measured the radial velocity (RV) of US 708 ($708 \pm 15 \text{ km s}^{-1}$) from the helium lines in the blue-channel LRIS spectrum. The measured RV exceeded the typical RVs of He-sdOs in the rest of the sample, which is characteristic for halo stars, considerably (see Fig. 5 in (35)). We obtained the RV of the SDSS, ESI and Palomar spectra by fitting a model spectrum (see below) to the helium lines using the FITSB2 routine (33). Surprisingly, the most accurate RV measured from the coadded ESI spectrum ($917 \pm 7 \text{ km s}^{-1}$) turned out to be significantly higher than the one published by Hirsch et al. (2). This velocity is consistent with the RVs measured both from the SDSS[†] ($898 \pm 30 \text{ km s}^{-1}$) and the Palomar spectra ($866 - 936 \text{ km s}^{-1}$). To investigate this issue, we performed a reanalysis of the LRIS spectra and measured an RV of $709 \pm 7 \text{ km s}^{-1}$ for the LRIS blue-channel spectrum perfectly consistent with the published value. However, when fitting the red-channel spectrum we found a significantly discrepant RV of $797 \pm 21 \text{ km s}^{-1}$. This was taken as first indication, that those spectra might be affected by systematics. We used the nightsky emission line of O I at 6300 \AA (red-channel) and the interstellar absorption line of Ca II at 3934 \AA (blue-channel) to quantify

[†]The RV of 793 km s^{-1} given by the SDSS Sky Server Object Explorer tool is based on the fit of an hydrogen rich template to the spectrum. The He II-lines of the Pickering series are misidentified as Balmer lines. This introduces the shift of $\sim -100 \text{ km s}^{-1}$ between our result and the template fit.

those systematic shifts (see Fig. S1, left panel). The nightsky emission line, which is supposed to be at zero RV, was blue-shifted by $-33 \pm 10 \text{ km s}^{-1}$. The interstellar line showed a significantly higher shift of $-128 \pm 22 \text{ km s}^{-1}$. Since the correct RV of the interstellar line is not known a priori, we measured it from a coadded Palomar spectrum to be $-9 \pm 28 \text{ km s}^{-1}$. Correcting the RVs for those shifts, the two RV values ($828 \pm 22 \text{ km s}^{-1}$ blue-channel, $830 \pm 21 \text{ km s}^{-1}$ red-channel) from the LRIS spectra are consistent with each other, but still smaller than the RVs measured from the ESI and Palomar spectra (see Fig. S1, right panel). Due to the low resolution of the LRIS spectra, the remaining shift corresponds to only about one pixel on the CCD and is therefore regarded as systematic as well. We conclude that the RV published by Hirsch et al. was affected by systematics and therefore underestimated. Going back to the original raw data, we performed an independent reduction. However, we were not able to resolve this issue. Given that the uncertainties are at the 1σ level of confidence and that the LRIS spectra are affected by systematics, no significant shifts in RV on both short and long timescales are detected (see Supplementary Fig. 1, right panel).

Proper motion

The proper motion of US 708 has been derived from multi-epoch position measurements of Schmidt plates obtained from the Digitised Sky Survey (DSS)[‡], the Sloan Digital Sky Survey (32) and the PanSTARRS survey (PS1) over a timebase of 59 years (see Fig. S2). The positions from the DSS and SDSS images have been

[‡]http://archive.stsci.edu/cgi-bin/dss_plate_finder

measured with respect to a set of compact background galaxies selected from the SDSS images as described in Tillich et al. (34). The positions of the background galaxies and the object are measured. For each image the measured positions of the background galaxies are compared to the reference values from the PS1 catalogue. The average of the deviations from these reference values is adopted as uncertainty of the object position. In the case of the 29 PS1 epochs, we took the calibrated positions from the PS1 catalogue and therefore use the same reference system for all our measurements. We obtained one position per epoch and used linear regression to derive the proper motion components with their uncertainties.

Atmospheric parameters

The atmospheric parameters effective temperature T_{eff} , surface gravity $\log g$, nitrogen abundance $\log N(\text{N})/N(\text{H})$ and projected rotational velocity $v_{\text{rot}} \sin i$ were determined by fitting simultaneously the observed helium and nitrogen lines of an ESI spectrum, constructed by coadding the 11 single exposures, with NLTE models taking into account line-blanketing of nitrogen (27) (see Fig. 1) as described in Geier et al. (35). Since no hydrogen lines are visible in the spectrum, we fixed the helium abundance to $\log y = \log N(\text{He})/N(\text{H}) = +2.0$. The atmospheric parameters ($T_{\text{eff}} = 47200 \pm 400$ K, $\log g = 5.69 \pm 0.09$) deviate significantly from the results by Hirsch et al. ($T_{\text{eff}} = 45600 \pm 700$ K, $\log g = 5.23 \pm 0.12$) especially in surface gravity. This is caused by the additional line-blanketing of nitrogen (27). The atmospheric parameters as well as the nitrogen abundance $\log N(\text{N})/N(\text{H}) = -2.4 \pm 0.2$ are typical for the nitrogen-rich subclass of He-sdOs

(36). The projected rotational velocity $v_{\text{rot}} \sin i = 115 \pm 8 \text{ km s}^{-1}$ on the other hand is significantly higher than the ones of both single sdB ($< 10 \text{ km s}^{-1}$) and He-sdO stars ($20 - 30 \text{ km s}^{-1}$) (26,27). Based on our analysis we can rule out objects with similar spectral features like DO-type white dwarfs ($\log g > 7.0$) or luminous He-stars ($\log g < 4.5$), which can be easily misclassified from visual inspection only.

Spectroscopic distance and kinematics

The spectroscopic distance is derived from the atmospheric parameters T_{eff} , $\log g$ and the apparent visual magnitude as described in Ramspeck et al. (40). The SDSS-g and r magnitudes have been converted to Johnson V magnitude[§], which has been corrected for interstellar reddening ($A_V = 0.07 \text{ mag}$) (41). Based on constraints provided by the supernova ejection scenario (see below) we adopted a mass of $0.3 M_{\odot}$ for the hot subdwarf. The spectroscopic distance in this case is $8.5 \pm 1.0 \text{ kpc}$. For this distance the proper motion components are converted to absolute transverse velocities and, combined with the radial velocity, the Galactic restframe velocity of US 708 is calculated to be $1157 \pm 53 \text{ km s}^{-1}$. This is the highest known restframe velocity of any unbound star in our Galaxy. The past trajectory of US 708 in the Galactic potential (42,43) has been reconstructed as outlined in Tillich et al. (34). Due to the high velocity of US 708 we found that the trajectory is not changed significantly if alternative model potentials are used (42). US 708 was ejected from the Galactic disc $14.0 \pm 3.1 \text{ Myr}$ ago and

[§]<http://www.sdss.org/dr6/algorithms/sdssUBVRITransform.html>

the ejection velocity, corrected for the motion of the Galactic disc, was calculated to be $998 \pm 68 \text{ km s}^{-1}$. We performed Monte Carlo simulations to trace back the trajectory of US 708 until it intersects with the Galactic disc. The uncertainty in the proper motion measurement dominates the error budget. Assuming no further perturbation of the trajectory an origin from the central kpc around the Galactic centre can be ruled out with a confidence of more than 6σ (see Fig. 2).

Properties of the progenitor binary. Geier et al. (5) proposed the ultra-compact sdB+WD binary CD-30°11223 to be a possible progenitor of the hypervelocity sdO US 708. However, based on the new results presented here, the ejection velocity is $\sim 250 \text{ km s}^{-1}$ higher than assumed by Geier et al. Hence, it is necessary to reexamine the supernova ejection scenario and to test its consistency with the newly derived parameters of US 708. Similar to the scenario discussed in Geier et al., we assume that the progenitor binary consisted of a compact helium star and a massive carbon-oxygen WD in close orbit. The ejection velocity of the He-star equals the radial velocity semiamplitude of the progenitor binary at the moment of the supernova explosion ($K = 998 \pm 68 \text{ km s}^{-1}$) modified by the additional perpendicular velocity component the star received through the SN explosion ($\sim 200 \text{ km s}^{-1}$). Since both velocities are added in quadrature, the kick velocity is negligible within the uncertainties. Assuming a mass for the He-star and a circular orbit, the orbital period of the progenitor binary as well as its separation can be calculated from the binary mass function:

$$f_m = \frac{M_{\text{WD}}^3 \sin^3 i}{(M_{\text{WD}} + M_{\text{He}})^2} = \frac{PK^3}{2\pi G} \quad (1)$$

Since we know the absolute space velocity, the inclination angle can be set to $\sin i = 1$, and the orbital period P of the progenitor binary can be calculated:

$$P = \frac{2\pi G}{K^3} \frac{M_{\text{WD}}^3}{(M_{\text{WD}} + M_{\text{He}})^2} \quad (2)$$

The binary separation a can be derived using Keplers laws:

$$a = \frac{G}{K^2} \frac{M_{\text{WD}}^2}{M_{\text{WD}} + M_{\text{He}}} \quad (3)$$

Another crucial assumption is that stable mass-transfer from the He-star to the WD triggered the SN, which means that the He-star must have filled its Roche lobe before ejection. To calculate the Roche lobe radius we used the equation given by Eggleton (44), where $q = M_{\text{He}}/M_{\text{MWD}}$:

$$R_{\text{L}} = \frac{0.49q^{2/3}a}{0.6q^{2/3} + \ln(1 + q^{1/2})} \quad (4)$$

The radius of the He-star can be calculated as a function of the mass and the surface gravity g :

$$R_{\text{He}} = \sqrt{\frac{M_{\text{He}}G}{g}} \quad (5)$$

To compare the Roche radius with the possible radius of the He-star we have to take into account that US 708 has already evolved away from the EHB (see Fig. S3), which led to an increase in radius. To calculate the radius at the time of ejection we therefore adopt the highest reasonable values for $\log g \simeq 6.1$ close to

the ZAEHB and the He-MS. Calculating Roche lobe and He-star radii for different He-star and WD masses, we explored the parameter space and put constraints on possible progenitor systems. Fig. S4 shows the Roche radii for WD masses from $1.0 M_{\odot}$ to $1.2 M_{\odot}$. The He-star radii for $\log g = 6.1$ are plotted for comparison. Consistent solutions are only found for low He-star masses ($\sim 0.3 - 0.35 M_{\odot}$) and high WD companion masses ($\sim 1.0 - 1.2 M_{\odot}$). The orbital period of the progenitor binary can be constrained to ~ 10 min. Following the method described in Geier et al. (5) we calculated the mass-transfer rates for binaries with similar orbital parameters and component masses. The rates of $\sim 10^{-8} M_{\odot}\text{yr}^{-1}$ are consistent with the helium double-detonation scenario. Figs. S5-S7 show as an example the evolution of a close binary ($P = 26$ min) that starts mass-transfer with an initial He-star mass of $0.45 M_{\odot}$ and a WD mass of $1.05 M_{\odot}$. After about 5 Myr the orbital period becomes as short as 13 min and the component masses change to $0.3 M_{\odot}$ and $1.2 M_{\odot}$, when the WD explodes as SN Ia. The helium donor has to be a helium-burning star rather than a He-WD without ongoing nuclear burning in its core, because those objects consist of degenerate matter and as soon as the small non-degenerate envelope is transferred, the mass-transfer rate becomes too high for the double-detonation scenario. Such systems will experience He-flashes on the surface of the WD companion without igniting the carbon in the core (45). This is consistent with the observational evidence. Since the ejection already happened ~ 14 Myr ago, we can also assume that US 708 is a helium-burning star. The minimum mass for such objects is $\sim 0.3 M_{\odot}$. Even less massive He-stars without nuclear burning, which are the progenitors of He-WDs, exist

(46). However, according to evolutionary tracks, their effective temperatures are much lower than the one of US 708. The most massive He-WD progenitors on the other hand, which can reach such temperatures, are cooling within a few Myr, too fast to be consistent with the position of US 708 in the $T_{\text{eff}} - \log g$ -diagram (see Fig. S3) (47). EHB-tracks for masses as low as $\sim 0.3 M_{\odot}$ are also not consistent with the position of US 708 in the $T_{\text{eff}} - \log g$ -diagram (6). However, since the He-star was significantly more massive before the mass-transfer started, its further evolution might not depend on its current total mass. Especially, if the helium in its core was already exhausted towards the end of the mass-transfer phase, the further evolution would depend on the core mass rather than the total mass. The position of US 708 in the $T_{\text{eff}} - \log g$ -diagram is, for example, perfectly consistent with post-EHB model tracks for an original mass of $0.45 M_{\odot}$ (see Fig. S3). Based on these simple calculations we can rule out the sdB+WD binary CD-30°11223 ($0.51 M_{\odot} + 0.76 M_{\odot}$, $P = 72$ min) as direct progenitor of US 708. However, systems like CD-30°11223 remain progenitor candidates of other high velocity sdB stars (34). There is no binary known yet, which fulfills all the criteria for a progenitor system to US 708. But evidence is growing, that such objects exist. A whole population of close binaries consisting of He-WDs and CO-WDs has been discovered recently (46). They form in almost exactly the same way as sdB+WD binaries. The only difference is that core helium-burning was not ignited before the hydrogen envelope has been stripped off in the common envelope phase of unstable mass-transfer. The ultracompact, eclipsing He-WD+CO-WD ($0.25 M_{\odot} + 0.55 M_{\odot}$) binary SDSS J065133+284423 with an orbital period of only

12 min sticks out (23). Its period is similar to the one expected for the progenitor of US 708, but the component masses are too small. In the double-lined WD+WD binary SDSS J125733+542850 ($0.2 M_{\odot} + 1.2 M_{\odot}$) on the other hand, the masses are very similar to the ones predicted, whereas the orbital period is much longer (274 min) (48). These discoveries as well as binary evolution calculations indicate the existence of binaries fulfilling the criteria for a progenitor of US 708 as well (18). We therefore conclude that the double-detonation supernova ejection scenario is still able to explain the observed properties of US 708 as ejected donor remnant.

Rotational velocity

Only two out of more than 100 single hot subdwarf stars are fast rotators. Both objects are sdB stars with hydrogen-rich atmospheres and might have been formed by a common-envelope merger (49,50). US 708 on the other hand belongs to the population of He-sdOs, which are hotter and show no or only some hydrogen in their atmospheres. They are regarded as a distinct group of stars, that might have been formed in different ways as the sdBs. US 708 is the only single He-sdO rotating faster than $20 - 30 \text{ km s}^{-1}$ indicating a close-binary origin (27). Due to the short orbital period and high companion mass, the rotation of the He-star in the proposed progenitor binary is expected to be synchronised to its orbital motion (22,24,25). Assuming the angular momentum is unchanged after the SN, the ejected donor remnant should remain a fast rotator. The rotational velocity can be calculated as follows:

$$v_{\text{rot}} = \frac{2\pi R_L}{P} \quad (6)$$

The expected rotational velocity of the ejected He-star is only weakly dependent on the masses of the binary components and of the order of 600 km s^{-1} . This is much higher than the measured $v_{\text{rot}} \sin i = 115 \pm 8 \text{ km s}^{-1}$. The significant difference between the expected rotational velocity and the measured $v_{\text{rot}} \sin i$ comes unexpected. In a synchronised binary system the rotational axes of both components are perpendicular to the orbital plane. As soon as the He-star is ejected, the rotation axis should be perpendicular to the flight trajectory, which means that $\sin i \simeq 1$. The impact of the supernova shockwave on main sequence (MS) companions in the standard single-degenerate scenario has recently been studied with hydrodynamic simulations. Due to stripping of matter, the star may lose up to $\sim 90\%$ of its initial angular momentum. A subsequent increase in radius due to stellar evolution is also predicted to lower the rotational velocity at the surface (28-31). However, simulations of more compact helium stars show that much less mass is stripped (28,51). The loss of angular momentum is also expected to be smaller in this case. Taking into account evolution on the extreme horizontal branch (EHB), the radius of the sdO increased by about a factor of ~ 1.6 since the ejection. Assuming conservation of angular momentum, the rotational velocity should now be of the order of 400 km s^{-1} . Whether the rest of the angular momentum was lost in the SN impact or later is still unclear. Pan et al. (28) predict an increase of the helium star's radius by a factor of up to four right after the

impact. This phase should last for a few tens of years. Due to the high initial rotational velocity of the star, another episode of mass and angular momentum loss may be possible in this phase. Another possibility might be a tilting of the stars rotation axis by the SN impact. The projected rotational velocity of the star measured from the line broadening would then be smaller than the true rotational velocity. However, simulations show that this effect is negligible for MS stars and most likely also for the more compact He stars studied here.

Supplementary Text

Discussing alternative acceleration scenarios

Any scenario for the acceleration of US 708 must explain four key properties of this star simultaneously: (I) US 708 is a compact He-sdO, which most likely formed via close binary interaction. Either it is the stripped core of a red giant or the result of a He-WD merger. (II) The star has the highest Galactic restframe velocity ($\sim 1200 \text{ km s}^{-1}$) ever measured for any unbound star in the Galaxy. (III) The past trajectory of the star is not consistent with an origin in the Galactic centre. (IV) In contrast to all other known single He-sdOs, US 708 has a projected rotational velocity exceeding $\sim 100 \text{ km s}^{-1}$. We now want to review other scenarios for the acceleration of hypervelocity stars in this way. In the classical runaway scenario a massive star in a binary system explodes as core-collapse supernova, while the companion is kicked out of the system (52). However, the ejection velocity scales with the binary separation and because a massive and hence large

star is involved, the binary separation cannot become small enough to reach an ejection velocity like the one of US 708. The disruption of a hierarchical triple system consisting of a normal star in wide orbit around a close He-WD binary by the SMBH is regarded as very unlikely as well, because an origin in the GC where the SMBH is located is very unlikely. The subsequent merger of a He-WD binary ejected in this way has been proposed as formation scenario for US 708 (2,16). The ejection of a He-WD binary star by a hypothetical binary black hole in the GC is very unlikely for the same reason (16). Other formation channels for hypervelocity stars invoke dynamical interactions in dense stellar clusters (53). Interactions of two close binaries can lead to the ejection of a star with the appropriate velocity. However, the binary-binary interaction is not affecting the angular momentum of the ejected star. We can therefore assume that the observed $v_{\text{rot}} \sin i = 115 \pm 8 \text{ km s}^{-1}$ resembles the rotational velocity in the tidally-locked progenitor binary. To reach such a high rotational velocity, the separation of this binary is constrained to $\sim 1 R_{\odot}$ (24). The interaction probability of two such binaries even in a very dense cluster is expected to be extremely small.

Another idea to explain HVS not originating from the GC is the origin in a nearby, low-mass galaxy (15). Since the escape velocities from those smaller galaxies are smaller as well, it is easier for stars to escape and travel through the intracluster medium. Some of those neighbouring galaxies also have quite high velocities with respect to our own Galaxy. However, this scenario is also unlikely for US 708. Although the star might have lived long enough on the main sequence ($\sim 10 \text{ Gyr}$) to travel all the way from a satellite or small neighbouring

galaxy, its current state of evolution is quite short compared to its total lifetime (only about 0.1%). Furthermore, only about 2% of all main sequence stars undergo an EHB phase. This means that for each single HVS sdO coming from the intracluster medium there should be about 50 000 HVS main sequence stars travelling through our Galactic halo. However, only a few tens of them have been reported so far. While faint, high proper motion objects are still not easy to identify, it is very easy to discover stars with high RVs in big survey like SDSS or RAVE. Palladino et al. (15) list more exotic mechanisms like interactions in globular clusters, with intermediate mass black holes or between galaxies (54). In addition to that, combinations of several scenarios are imaginable. If for example a hierarchical triple system would be disrupted by the SMBH and one component of the ejected binary would explode as core-collapse SN, the trajectory of the surviving companion would not point back to the GC. However, we also regard all those scenarios as very unlikely to explain the object presented here.

Estimating supernova rates

Another sanity check for our scenario is to provide a rough estimate of the double-detonation SNIa rates we would expect based on our observations and binary population synthesis models. So far US 708 is unique among the known He-sdO stars and this estimate is based on very small number statistics. The star was drawn from a sample of hot subdwarfs selected from SDSS. The full sample contains 1369 hot subdwarfs in total, 262 of them or roughly 20% are He-sdOs (55). Binary population synthesis models by Han et al. (9) predict a birthrate of $5 \times 10^{-2} \text{ yr}^{-1}$

for hot subdwarfs in general and therefore $1 \times 10^{-2} \text{ yr}^{-1}$ for He-sdOs. One of the observed He-sdOs (US 708) might be an ejected donor remnant ($\sim 0.4\%$). This translates into a double-detonation SN rate of roughly $4 \times 10^{-5} \text{ yr}^{-1}$. This has to be regarded as lower limit only, because a few He-sdOs with smaller RVs, but rather high proper motions might still be hidden in our sample.

The predicted rates of double-detonation SNIa are around $3 \times 10^{-4} \text{ yr}^{-1}$ and the observed rates of all types of SNIa around $3 \times 10^{-3} \text{ yr}^{-1}$ (56). Since all those numbers have quite significant uncertainties, they are regarded as broadly consistent. The most important point for this sanity check is, that our estimates from observations do not deviate from the predicted or observed rates by orders of magnitude.

Yu & Tremaine (57) calculated the ejection rates of hypervelocity stars expected from interactions with the Galactic centre black hole (or a binary black hole in the GC). The rates are of the order of $\sim 10^{-5} \text{ yr}^{-1}$ to $\sim 10^{-4} \text{ yr}^{-1}$. However, these numbers correspond to the simplest case, the ejection of single main sequence stars. Since stars as peculiar as US 708 and their progenitors are very rare compared to normal main sequence stars, the close encounter and ejection rates of such stars have to be orders of magnitude smaller. It is therefore very unlikely to find one He-sdO along with the about 20 other hypervelocity stars assuming that they are all accelerated in the GC.

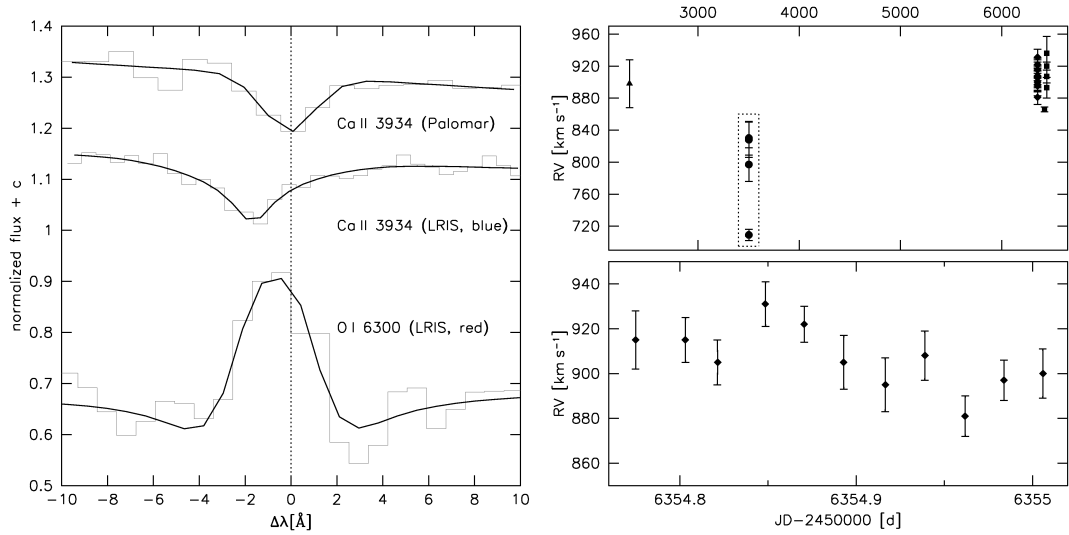


Fig. S1: Revised radial velocity. *Left panel*: Interstellar Ca II line of US 708 in the Palomar (upper plot) and blue-channel LRIS spectra (middle plot). In contrast to the Palomar spectrum, the LRIS spectrum is significantly blue-shifted. Night-sky emission line of O I in the LRIS red-channel spectrum (lower panel). The blue-shift is smaller than in the red-channel spectrum. *Right panel*: Radial velocities of US 708 plotted against Julian date. Upper panel: SDSS (triangle), LRIS blue- and red-channel uncorrected (grey circles), LRIS blue- and red-channel corrected (black circles), ESI (diamonds), Palomar (squares). The dotted box marks the LRIS RVs, which are affected by systematics. Lower panel: Close-up of the ESI RVs taken within one night.

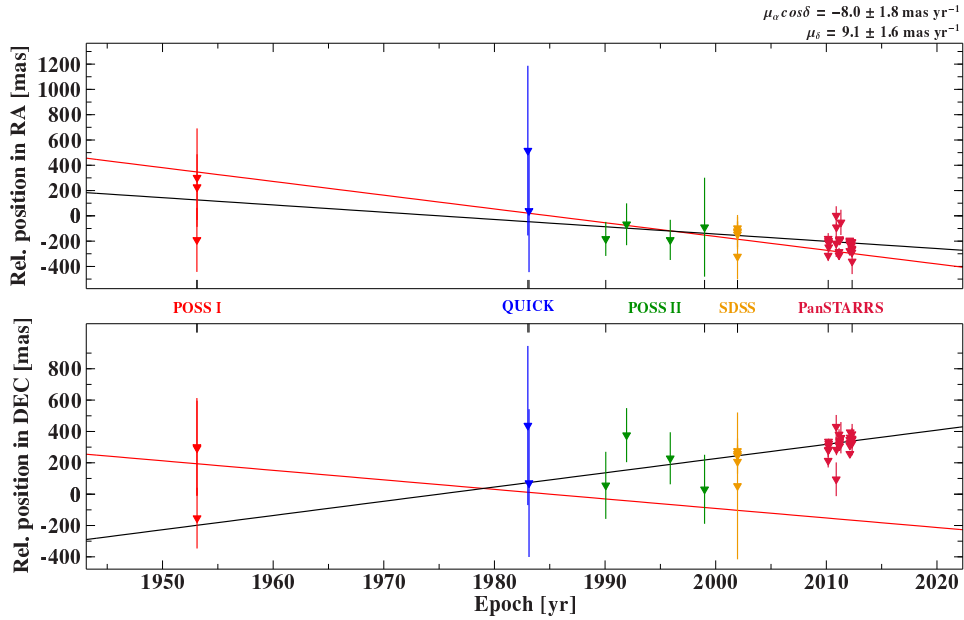


Fig. S2: Proper motion of US 708. Relative positions of US 708 in right ascension (upper panel) and declination (lower panel) plotted against time. The POSS I, QUICK and POSS II positions are measured from scanned photographic plates provided by the Digitised Sky Survey. SDSS and PanSTARRS positions are measured from CCD images. The black solid lines mark the best fits, from which we derive the proper motion components. The solid red lines mark the proper motion components required for the star to originate from the Galactic centre.

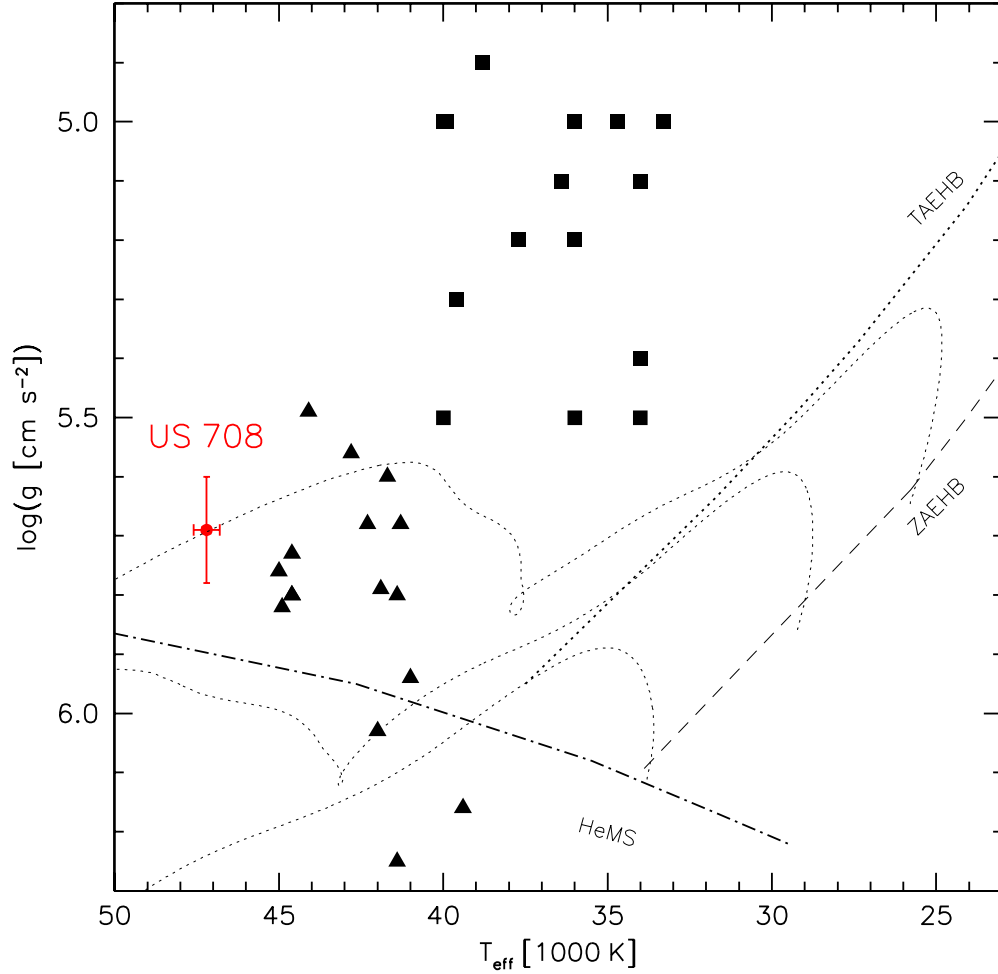


Fig. S3: Evolutionary status of US 708. $T_{\text{eff}} - \log g$ diagram. Evolutionary tracks (solar metallicity) of core helium-burning stars with a mass of $0.45 M_{\odot}$ and different masses of their hydrogen envelopes (for bottom to top, $0.0 M_{\odot}$, $0.001 M_{\odot}$, $0.005 M_{\odot}$) are plotted (6). The positions of both the Zero Age and the Terminal Age Extended Horizontal Branch (ZAEHB, TAEHB) are indicated as well as the helium main sequence (He-MS). The filled black symbols mark known He-sdBs

(37,38) (squares) and He-sdOs(39) (triangles) from the literature.

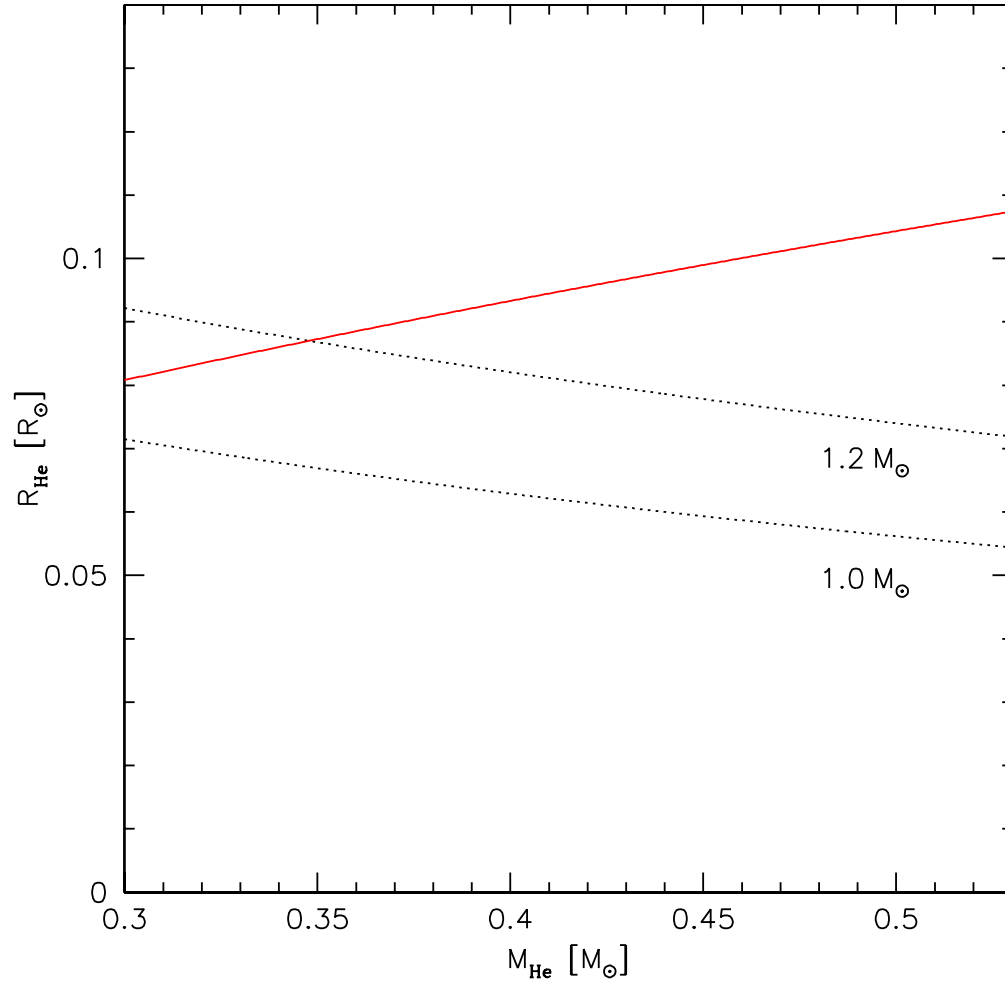


Fig. S4: Mass-radius relation of the compact He-star. The dotted black lines mark the Roche radii for WD companion masses of $1.0 M_{\odot}$ and $1.2 M_{\odot}$. The red solid line marks the He-star radius assuming $\log g = 6.1$.

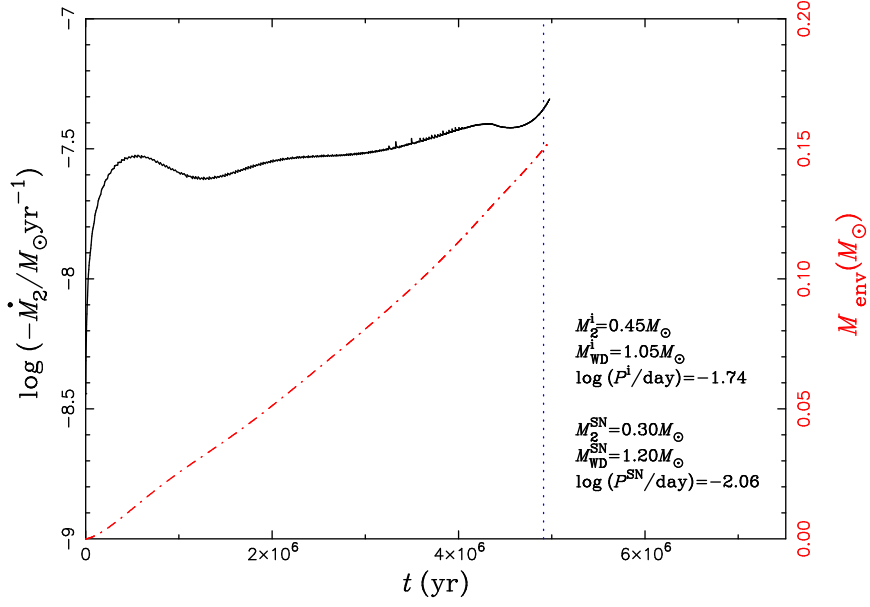


Fig. S5: Mass-transfer rate. The solid and dash-dotted curves show the mass-transfer rate and the mass of the WD envelope (He shell) varying with time after the He star fills its Roche lobe, respectively. The dotted vertical line indicates the position where the double-detonation may happen (the mass of the He shell increases to $\sim 0.15 M_\odot$). The initial binary parameters and the parameters at the moment of the SN explosion are also given.

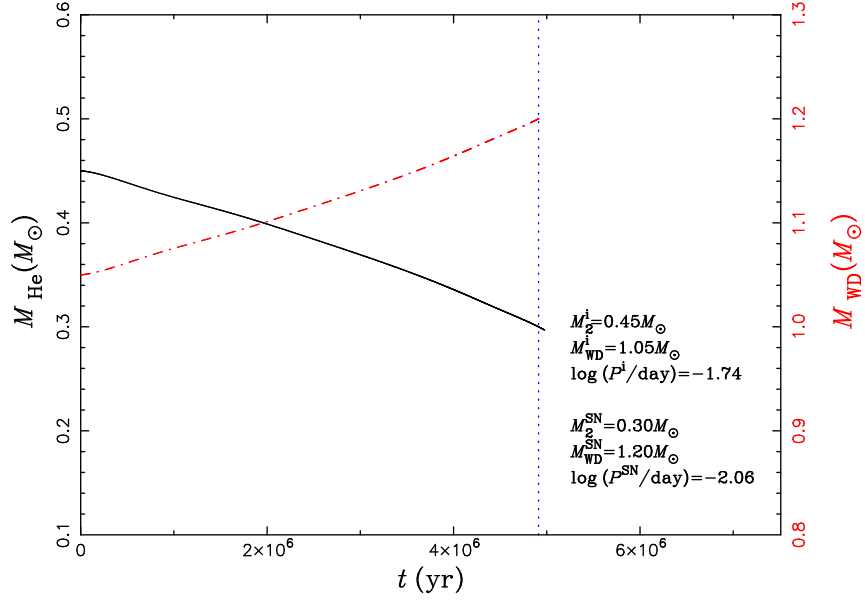


Fig. S6: Change of component masses. Change of He-star (solid line) and WD mass (dash-dotted line) with time. The dotted vertical line indicates the position where the double-detonation may happen (the mass of the He shell increases to $\sim 0.15 M_{\odot}$). The initial binary parameters and the parameters at the moment of the SN explosion are also given.

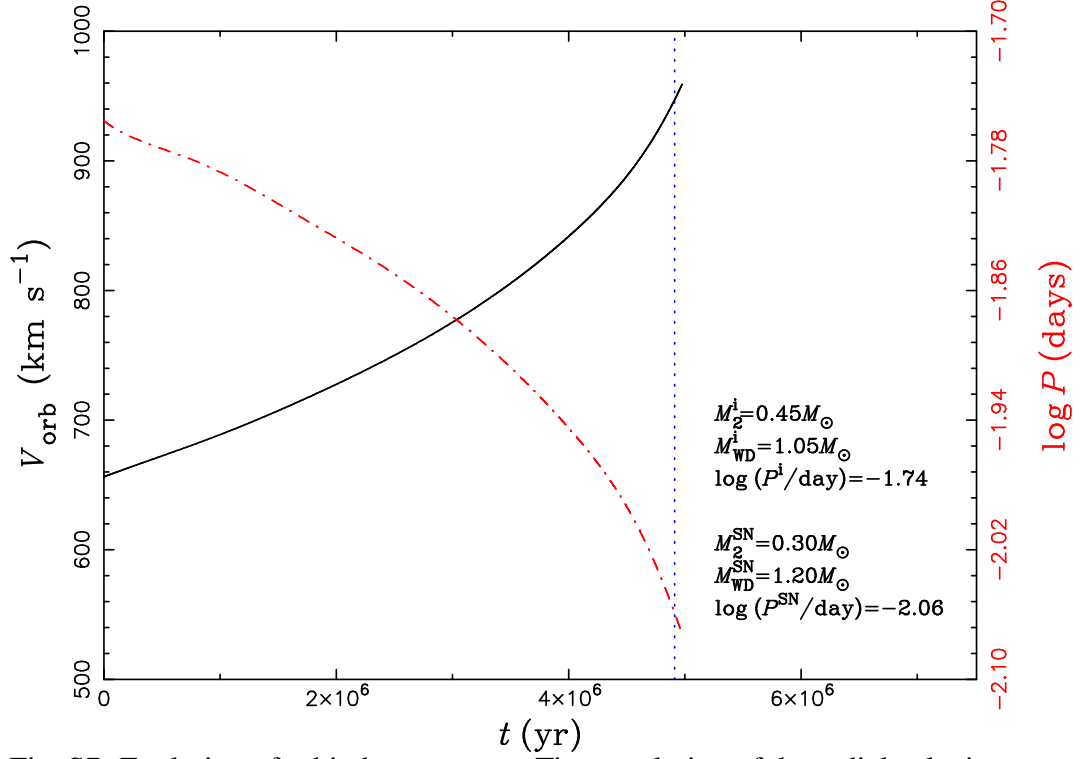


Fig. S7: Evolution of orbital parameters. Time evolution of the radial velocity semiamplitude (solid line) and the orbital period (dash-dotted line) of the binary. The dotted vertical line indicates the position where the double-detonation may happen (the mass of the He shell increases to $\sim 0.15 M_\odot$). The initial binary parameters and the parameters at the moment of the SN explosion are also given.

Hot subdwarf binaries from the MUCHFUSS project

Analysis of 12 new systems and a study of the short-period binary population

T. Kupfer¹, S. Geier², U. Heber³, R. H. Østensen⁴, B. N. Barlow⁵, P. F. L. Maxted⁶, C. Heuser³, V. Schaffenroth^{3, 7}, and B. T. Gänsicke⁸

¹ Department of Astrophysics/IMAPP, Radboud University Nijmegen, P.O. Box 9010, 6500 GL Nijmegen, The Netherlands

² European Southern Observatory, Karl-Schwarzschild-Str. 2, 85748 Garching, Germany

³ Dr. Karl Remeis-Observatory & ECAP, Astronomical Institute, Friedrich-Alexander University Erlangen-Nuremberg, Sternwartstr. 7, D 96049 Bamberg, Germany

⁴ Institute of Astronomy, KU Leuven, Celestijnenlaan 200D, B-3001 Heverlee, Belgium

⁵ Department of Physics, High Point University, 833 Montlieu Avenue, High Point, NC 27262, USA

⁶ Astrophysics Group, Keele University, Staffordshire, ST5 5BG, UK

⁷ Institute for Astro- and Particle Physics, University of Innsbruck, Technikerstr. 25/8, 6020 Innsbruck, Austria

⁸ Department of Physics, University of Warwick, Coventry CV4 7AL, UK

Received ; accepted

ABSTRACT

The project Massive Unseen Companions to Hot Faint Underluminous Stars from SDSS (MUCHFUSS) aims at finding hot subdwarf stars with massive compact companions like massive white dwarfs ($M > 1.0 M_{\odot}$), neutron stars, or stellar-mass black holes. The existence of such systems is predicted by binary evolution theory, and recent discoveries indicate that they exist in our Galaxy.

We present orbital and atmospheric parameters and put constraints on the nature of the companions of 12 close hot subdwarf B star (sdB) binaries found in the course of the MUCHFUSS project. The systems show periods between 0.14 and 7.4 days. In nine cases the nature of the companions cannot be constrained unambiguously whereas three systems most likely have white dwarf companions. We find that the companion to SDSS J083006.17+475150.3 is likely to be a rare example of a low-mass helium-core white dwarf. SDSS J095101.28+034757.0 shows an excess in the infrared that probably originates from a third companion in a wide orbit, which makes this system the second candidate hierarchical triple system containing an sdB star. SDSS J113241.58–063652.8 is the first helium deficient sdO star with a confirmed close companion.

This study brings to 142 the number of sdB binaries with orbital periods of less than 30 days and with measured mass functions. We present an analysis of the minimum companion mass distribution and show that it is bimodal. One peak around $0.1 M_{\odot}$ corresponds to the low-mass main sequence (dM) and substellar companions. The other peak around $0.4 M_{\odot}$ corresponds to the white dwarf companions. The derived masses for the white dwarf companions are significantly lower than the average mass for single carbon-oxygen white dwarfs. In a $T_{\text{eff}} - \log g$ diagram of sdB+dM companions, we find signs that the sdB components are more massive than the rest of the sample. The full sample was compared to the known population of extremely low-mass white dwarf binaries as well as short-period white dwarfs with main sequence companions. Both samples show a significantly different companion mass distribution indicating either different selection effects or different evolutionary paths. We identified 16 systems where the dM companion will fill its Roche Lobe within a Hubble time and will evolve into a cataclysmic variable; two of them will have a brown dwarf as donor star. Twelve systems with confirmed white dwarf companions will merge within a Hubble time, two of them having a mass ratio to evolve into a stable AM CVn-type binary and another two which are potential supernova Ia progenitor systems. The remaining eight systems will most likely merge and form RCrB stars or massive C/O white dwarfs depending on the structure of the white dwarf companion.

Key words. binaries: spectroscopic – stars: subdwarf

1. Introduction

Hot subdwarf B stars (sdBs) are hot core helium-burning stars with masses around $0.5 M_{\odot}$ and thin hydrogen layers (Heber 1986; for a recent review see Heber 2009). It has been shown that a large fraction of sdBs are members of short-period binaries with periods below ~ 10 days (Maxted et al. 2001; Napiwotzki et al. 2004a). For such short-period sdB binaries common envelope (CE) ejection is the only likely formation channel. One possible scenario is that two main sequence stars (MS) evolve in a binary system. The more massive one will

evolve faster to become a red giant. Unstable mass transfer from the red giant to the companion will lead to a CE phase. Because of the friction in this phase, the two stellar cores lose orbital energy and angular momentum, which leads to a shrinkage of the orbit. This energy is deposited in the envelope which will finally be ejected. If the core reaches the mass required for the core-helium flash before the envelope is lost, a binary consisting of a core-helium burning sdB star and a main sequence companion is formed. In another possible scenario the more massive star evolves to become a white dwarf (WD) either through a CE phase or stable mass transfer onto the less massive companion. The less massive star evolves then to become a red giant. Unstable mass transfer will lead to a CE and once the envelope is

Send offprint requests to: T. Kupfer,
e-mail: t.kupfer@astro.ru.nl

Table 1. Overview of the solved binary systems.

Short name	SDSS name	Other names
J01185−00254	SDSS J011857.20−002546.5	PB 6373
J03213+05384	SDSS J032138.67+053840.0	PG 0319+055
J08233+11364	SDSS J082332.08+113641.8	–
J08300+47515	SDSS J083006.17+475150.3	PG 0826+480
J09523+62581	SDSS J095238.93+625818.9	PG 0948+632
J09510+03475	SDSS J095101.28+034757.0	PG 0948+041
J10215+30101	SDSS J102151.64+301011.9	–
J11324+06365	SDSS J113241.58−063652.8	PG 1130−063
J13463+28172	SDSS J134632.65+281722.7	TON 168
J15082+49405	SDSS J150829.02+494050.9	SBSS 1506+498
J15222−01301	SDSS J152222.14−013018.3	–
J18324+63091	SDSS J183249.03+630910.5	FBS 1832+631

ejected the red giant remnant starts burning helium, and a system consisting of an sdB with a WD companion is formed (Han et al. 2002, 2003).

If the red giant loses enough mass that the remnant is not massive enough to ignite helium the star will evolve directly to become a helium-core white dwarf. Helium-core white dwarfs with masses below $0.3 M_{\odot}$ are called extremely low-mass (ELM) white dwarfs (Brown et al. 2010). According to single star evolution, ELM-WDs should not exist as the evolutionary timescale to form them is much longer than the age of the universe. Therefore, significant mass transfer during the evolution is needed and most of the observed ELM-WDs indeed reside in close binary systems, usually with WD companions. Those systems are formed through the same CE-ejection process as the short-period sdB binaries, except that the envelope is ejected before the core reaches the mass required to ignite helium (Brown et al. 2010). Recent studies have increased the number of known ELM-WDs significantly (Brown et al. 2013 and references therein). During their evolution they can spectroscopically appear as sdBs. However, they have lower masses compared to helium core-burning sdBs. Three low-mass sdBs, which evolve directly towards the ELM-WD phase are known so far. All have WD companions and lie below the Zero-Age Extreme Horizontal Branch (Heber et al. 2003; O’Toole et al. 2006; Silvotti et al. 2012). Furthermore, hot He-WD progenitors in an earlier stage of evolution have been recently found orbiting intermediate-mass main sequence stars (EL CVn systems, Maxted et al. 2013).

Hot subdwarf binaries, as well as WDs with massive WD companions, turned out to be good candidates for SN Ia progenitors. Because of gravitational wave radiation, the orbit will shrink further and mass transfer from the sdB onto the WD will start once the sdB fills its Roche lobe. The Chandrasekhar limit might be reached either through He accretion on the WD (e.g. Yoon & Langer 2004 and references therein) or a subsequent merger of the sdB+WD system (Tutukov & Yungelson 1981; Webbink 1984). Two sdBs with massive WD companions have been identified to be good candidates for being SN Ia progenitors. KPD 1930+2752 has a total mass of $1.47 M_{\odot}$ exceeding the Chandrasekhar limit and will merge within about 200 million years (Maxted et al. 2000a; Geier et al. 2007). CD−30° 11223 has the shortest known orbital period of all sdB binaries ($P_{\text{orb}} = 0.048979$ days) and is a good candidate to explode as an underluminous helium double-detonation SN Ia (Vennes et al. 2012; Geier et al. 2013b). The explosion of the massive WD companion in the eclipsing sdO+WD system HD 49798 on the other

hand may be triggered by stable mass transfer (Mereghetti et al. 2009).

Neutron star (NS) or even black hole (BH) companions are predicted by theory as well (Podsiadlowski et al. 2002; Pfahl et al. 2003). In this scenario two phases of unstable mass transfer are needed and the NS or the BH is formed in a supernova explosion. Yungelson & Tutukov (2005) predicted that about 0.8% of the short-period sdBs should have NS companions. In an independent study, Nelemans (2010) showed that about 1% of these systems should have NS companions whereas about 0.1% should have BH companions.

However, no NS/BH companion to an sdB has yet been detected unambiguously whereas a few candidates have been identified (Geier et al. 2010b). Follow-up observations have been conducted with radio and X-ray telescopes. Coenen et al. (2011) did not detect any radio signals of a pulsar companion at the positions of four candidate systems from Geier et al. (2010b). Mereghetti et al. (2011, 2014) searched for X-rays powered by wind accretion onto compact companions to sdBs using the *Swift* and *XMM* satellites, but did not detect any of those targets.

NS+WD systems have been discovered amongst pulsars. Ferdman et al. (2010) showed that the peculiar system PSR J1802-2124 contains a millisecond pulsar and a low-mass C/O WD. This system may have evolved from an sdB+NS system. Most recently, Kaplan et al. (2013) discovered the close companion to the pulsar PSR J1816+4510 to be a He-WD progenitor with atmospheric parameters close to an sdB star ($T_{\text{eff}} = 16\,000$ K, $\log g = 4.9$).

Many studies have been performed to identify short-period sdB binaries with periods from a few hours to more than ten days. Up to now, 142 short-period sdB binaries have measured radial velocity curves and mass functions with a peak in the period distribution between 0.5 to 1.0 days (e.g. Morales-Rueda et al. 2003; Geier et al. 2011; Copperwheat et al. 2011). In most cases it is hard to constrain the nature of the companion as most sdB binaries are single-lined systems. From the radial-velocity (RV) curve only lower mass limits can be derived. Most of the companions are either dMs or WDs. Only in a few examples could strong constraints be put on the nature of the companion.

SdBs with main sequence companions are potential progenitors of detached WD+dM binaries, which possibly further evolve to become cataclysmic variables (CVs). Hence, there should be correlations between those two types of systems, even though a compact WD+dM system can be formed directly and does not necessarily evolve from an sdB+dM binary. Recent studies have increased the number of known WD+dMs significantly and population studies have been carried out (Nebot Gómez-Morán et al. 2011 and references therein).

In addition to the short-period sdB binaries, long period sdBs formed via stable Roche lobe overflow have been postulated (Han et al. 2002, 2003). Between one third and half of sdB stars are found to show spectroscopic signature of a main sequence type F/G/K companion and associated infrared excess (Reed & Stiening 2004). Because of their long periods, these systems show only small radial velocity variations and radial velocity curves have not been measured for years. Just recently the first systems with orbits of several hundreds of days were discovered (Deca et al. 2012; Østensen & Van Winckel 2012; Vos et al. 2012, 2013). Eventually, these systems will evolve to become WD+main sequence binaries with periods of hundreds of days and might experience another phase of mass transfer, when the main sequence companion turns into a red giant.

Table 2. Summary of the follow-up observations in the course of the MUCHFUSS project.

Date	Telescope & Instrument	Resolution [$\lambda/\Delta\lambda$]	Coverage [\AA]	Observer
2009-May-27 – 2009-May-31	CAHA-3.5m+TWIN	4000	3460 – 5630	S. M. ^a
2009-Nov-08 – 2009-Nov-12	ESO-NTT+EFOSC2	2200	4450 – 5110	T. K.
2010-Feb-12 – 2010-Feb-15	SOAR+Goodman	7000	3500 – 6160	B. B.
2010-Aug-02 – 2010-Aug-03	SOAR+Goodman	7000	3500 – 6160	B. B.
February – July 2011	Gemini-North+GMOS-N	1200	3610 – 5000	Service
February – July 2011	Gemini-South+GMOS-S	1200	3610 – 5000	Service
2011-Nov-15 – 2011-Nov-19	CAHA-3.5m+TWIN	4000	3460 – 5630	S. G., P. B. ^a
February – July 2012	Gemini-North+GMOS-N	1200	3610 – 5000	Service
February – July 2012	Gemini-South+GMOS-S	1200	3610 – 5000	Service
2012-May-25 – 2012-May-27	CAHA-3.5m+TWIN	4000	3460 – 5630	C. H.
2012-Jul-09 – 2012-Jul-12	ING-WHT+ISIS	4000	3440 – 5270	V. S.
2012-Oct-21 – 2012-Oct-24	SOAR+Goodman	7000	3500 – 6160	B. B.
2012-Dec-14 – 2012-Dec-18	ING-WHT+ISIS	4000	3440 – 5270	T. K., A. F. ^a
2013-Jun-02 – 2013-Jun-05	ING-WHT+ISIS	4000	3440 – 5270	C. H.
2013-Aug-11 – 2013-Aug-13	ING-WHT+ISIS	4000	3440 – 5270	T. K., M. S. ^a
2014-Feb-01 – 2014-Feb-05	ESO-NTT+EFOSC2	2200	4450 – 5110	S. G., F. N. ^a

Notes. ^a see notes in the acknowledgements

Table 3. Derived orbital parameters.

Object	T_0 [−2 450 000]	P [d]	γ [km s ^{−1}]	K [km s ^{−1}]	e_{norm} [km s ^{−1}]	$\log p_{\text{false}}[10\%]$	$\log p_{\text{false}}[1\%]$
J08300+47515	6279.6067 ± 0.0004	0.14780 ± 0.00007	49.9 ± 0.9	77.0 ± 1.7	4.0	< −4.0	< −4.0
J08233+11364	6278.5729 ± 0.0007	0.20707 ± 0.00002	135.1 ± 2.0	169.4 ± 2.5	7.0	< −4.0	< −4.0
J10215+30101	6277.819 ± 0.003	0.2966 ± 0.0001	−28.4 ± 4.8	114.5 ± 5.2	6.4	−1.9	−1.9
J09510+03475	6693.666 ± 0.003	0.4159 ± 0.0007	111.1 ± 2.5	84.4 ± 4.2	2.8	−2.0	−0.8
J15222−01301	6516.632 ± 0.005	0.67162 ± 0.00003	−79.5 ± 2.7	80.1 ± 3.5	−	−1.2	−1.2
J15082−49405	6518.395 ± 0.02	0.967164 ± 0.000009	−60.0 ± 10.7	93.6 ± 5.8	6.0	−0.9	−0.9
J11324−06365	4583.06 ± 0.01	1.06 ± 0.02	8.3 ± 2.2	41.1 ± 4.0	8.6	−1.1	−0.2
J01185−00254	5882.000 ± 0.008	1.30 ± 0.02	37.7 ± 1.8	54.8 ± 2.9	6.9	< −4.0	−0.4
J13463+28172	6517.99 ± 0.01	1.96 ± 0.03	1.2 ± 1.2	85.6 ± 3.4	−	−0.4	−0.3
J18324−63091	6119.58 ± 0.03	5.4 ± 0.2	−32.5 ± 2.1	62.1 ± 3.3	2.7	−0.9	−0.1
J09523+62581	5210.23 ± 0.08	6.98 ± 0.04	−35.4 ± 3.6	62.5 ± 3.4	7.8	−0.7	−0.6
J03213+05384	6280.17 ± 0.05	7.4327 ± 0.0004	−16.7 ± 2.1	39.7 ± 2.8	4.7	−1.8	−1.8

PG 1253+284, the first triple system containing an sdB with a close companion and a wide main sequence companion was discovered by Heber et al. (2002). This system shows an infrared excess caused by the wide component. However, the wide component is not involved in the formation of the sdB. The unseen close companion expelled the envelope of the sdB progenitor.

Here we present orbital solutions for 12 new sdB binaries discovered in the course of the MUCHFUSS project. Sect. 2 describes the status of the MUCHFUSS project. Sect. 3 gives an overview of the observations and the data reduction. The derived orbital parameters, as well as the atmospheric parameters of the sdBs, are described in Sec. 4 and 5. In Sec. 6, we determine the minimum masses and put constraints on the nature of the unseen companions when no light variations were detected by searching for an infrared excess in a two-colour diagram. In addition, in Sec. 7 we study the full population of sdBs in close binaries, discuss the period distributions, the companion mass distributions, as well as selection effects of the whole sample of sdB binaries with derived mass function. Sect. 8 compares the full sample with the samples of known ELM-WD binaries and WD+dM bi-

naries to gain insight in the formation history of hot subdwarfs. Summary and conclusions are given in Sec. 9.

2. The MUCHFUSS project

The project Massive Unseen Companions to Hot Faint Underluminous Stars from SDSS (MUCHFUSS) aims at finding hot subdwarf stars with massive compact companions like massive white dwarfs ($M > 1.0 M_{\odot}$), neutron stars or stellar-mass black holes. Hot subdwarf stars were selected from the Sloan Digital Sky Survey by colour and visual inspection of the spectra. Objects with high radial velocity variations were selected as candidates for follow-up spectroscopy to derive the radial velocity curve and the mass function of the system.¹

Geier et al. (2011a, 2012b) discuss the target selection and the follow-up strategy. A detailed analysis of seven sdB binaries discovered in the course of this project is presented in Geier et al. (2011b). In addition, three eclipsing systems were

¹ Hot subdwarfs with a large but constant radial velocity were studied in the Hyper-MUCHFUSS project (Tillich et al. 2011).

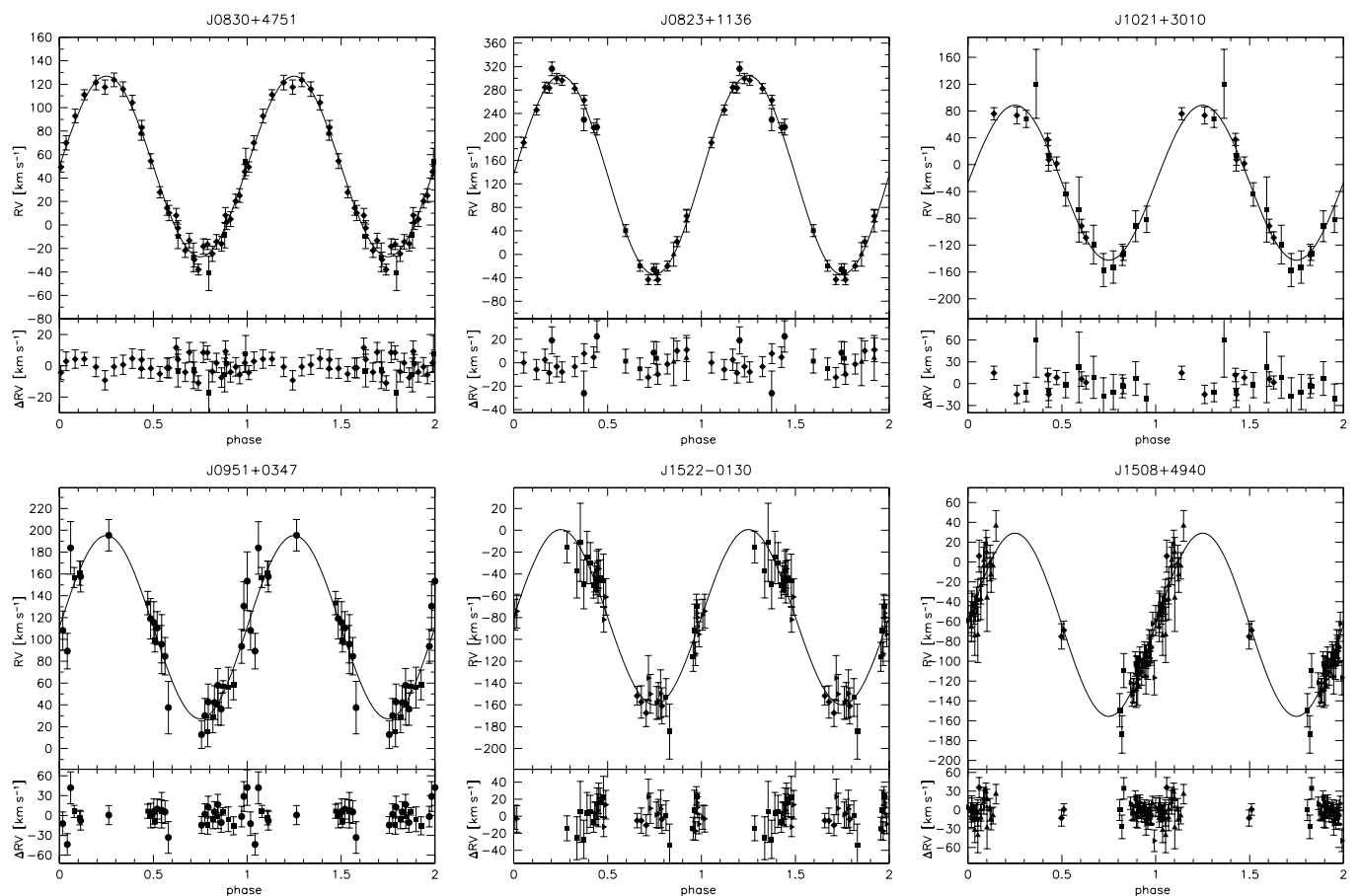


Fig. 1. Radial velocity plotted against orbital phase. The RV data were phase folded with the most likely orbital periods and are plotted twice for better visualisation. The residuals are plotted below. The RVs were measured from spectra obtained with SDSS (squares), CAHA.3.5m/TWIN (upward triangles), WHT/ISIS (diamonds), Gemini/GMOS (triangles turned to the right), ESO-NTT/EFOSC2 (circles), and SOAR/Goodman (pentagons).

detected, two of which host brown-dwarf companions. These are the first confirmed brown-dwarf companions to sdB stars (Geier et al. 2011d; Schaffenroth et al. 2014b). One sdB+dM system contains a hybrid pulsator and shows a strong reflection effect (Østensen et al. 2013). Results from a photometric follow-up campaign of the MUCHFUSS targets will be described in detail in Schaffenroth et al. (in prep). During dedicated spectroscopic MUCHFUSS follow-up runs with unfavourable weather conditions, bright sdB binary candidates were observed (Geier et al. 2013b, 2014). A full catalogue of all RV measurements is in preparation as well (Geier et al. in prep).

3. Observations and data reduction

Follow-up medium resolution spectroscopy of 12 sdB binaries (see Table 1 for an overview) was obtained using different instruments including the CAHA-3.5m telescope with the TWIN spectrograph, the ESO-NTT telescope with the EFOSC2 spectrograph, the SOAR telescope with the Goodman spectrograph, the Gemini-North/South telescopes with the GMOS-N/S spectrographs and the William Herschel telescope (WHT) with the ISIS spectrograph. Table 2 gives an overview of all follow-up runs and the instrumental set-ups.

All spectra were corrected with an average bias frame constructed from several individual bias frames as well as an average flat field constructed from several flat field lamps. Reduction

was done either with the MIDAS², IRAF³ or PAMELA⁴ and MOLLY⁴ packages.

4. Orbital parameters

The radial velocities (RVs) were measured by fitting a set of mathematical functions matching the individual line shapes to the hydrogen Balmer lines as well as helium lines if present using the FITSB2 routine (Napiwotzki et al. 2004b). Polynomials were used to match the continua and a combination of Lorentzian and Gaussian functions to match cores and wings of the lines.

The orbital parameter (orbital phase T_0 ⁵, period P , system velocity γ , and RV-semiamplitude K), as well as their un-

² The ESO-MIDAS system provides general tools for data reduction with emphasis on astronomical applications including imaging and special reduction packages for ESO instrumentation at La Silla and the VLT at Paranal

³ IRAF is distributed by the National Optical Astronomy Observatories, which are operated by the Association of Universities for Research in Astronomy, Inc., under cooperative agreement with the National Science Foundation

⁴ <http://www2.warwick.ac.uk/fac/sci/physics/research/astro/people/marsh/software>

⁵ T_0 corresponds to the minimum distance of the sdB star from our Solar System

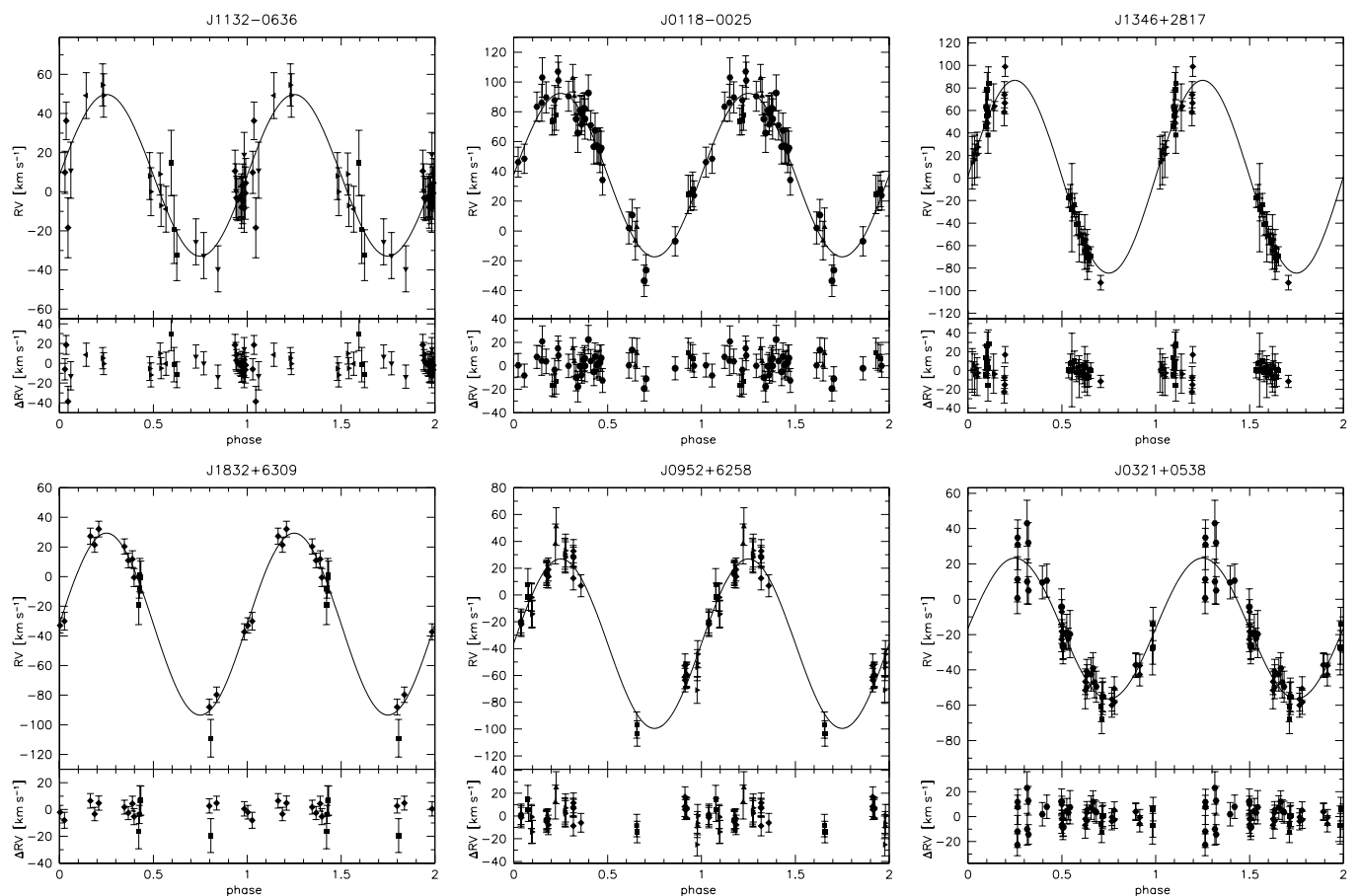


Fig. 2. Radial velocity plotted against orbital phase (see Fig 1).

certainties and associated false-alarm probabilities ($p_{\text{false}}[1\%]$, $p_{\text{false}}[10\%]$) are determined as described in Geier et al. (2011b, 2014). To calculate the significance of the orbital solutions and to estimate contribution of systematic effects to the error budget, we modified the χ^2 of the best solution by adding systematic errors e_{norm} in quadrature until the reduced χ^2 reached ~ 1.0 . The phased RV curves for the best solutions are given in Fig. 1 and 2, the χ^2 -values plotted against orbital period in Fig. 3. The minimum in χ^2 corresponds to the most likely solution. The adopted systematic errors and false-alarm probabilities are given in Table 3. The probabilities that the adopted orbital periods are correct to within 10% range from 80% to $> 99.99\%$.

5. Atmospheric parameters

Atmospheric parameters have been determined by fitting appropriate model spectra to the hydrogen Balmer and helium lines in the way described in Geier et al. (2007). For the hydrogen-rich and helium-poor ($\log y = \log(n(\text{He})/n(\text{H})) < -1.0$) sdBs with effective temperatures below 30 000 K, a grid of metal line blanketed LTE atmospheres with solar metallicity was used (Heber et al. 2000). Helium-poor sdBs and sdOBs with temperatures ranging from 30 000 K to 40 000 K were analysed using LTE models with enhanced metal line blanketing (O’Toole & Heber 2006). Metal-free NLTE models were used for the hydrogen-rich sdO J1132–0636 (Stroeer et al. 2007).

Each spectrum was velocity corrected according to the orbital solution and co-added for the atmospheric fit. To account

for systematic shifts introduced by the different instruments, atmospheric parameters for each star were derived separately from spectra taken with each instrument. Weighted means were calculated and adopted as the final solutions (see Table A.1).

6. The nature of the unseen companion

All our objects appear to be single-lined. Therefore, only the binary mass function can be calculated:

$$f_m = \frac{M_{\text{comp}}^3 \sin^3 i}{(M_{\text{comp}} + M_{\text{sdb}})^2} = \frac{PK^3}{2\pi G}. \quad (1)$$

From spectroscopy the orbital period P and the RV semi-amplitude K can be derived. Hence, the mass of the sdB (M_{sdb}) and the companion (M_{comp}) as well as the inclination angle i remain free parameters. Assuming a canonical mass for the sdB $M_{\text{sdb}} = 0.47 M_{\odot}$ (see Fontaine et al. 2012 and references therein) and an inclination angle $i < 90^\circ$, a minimum mass for the companion can be determined. If the derived minimum companion mass is higher than the Chandrasekhar limit, the NS/BH nature of the companion is proven without further constraints under the assumption that the sdB does not have a mass significantly lower than the canonical mass.

All spectra were checked for contamination by a cool stellar companion. Typically, the Mg I triplet around 5170 Å and the Ca II triplet around 8650 Å are the best indicators. None of our programme stars show obvious signs of a companion in the spectrum.

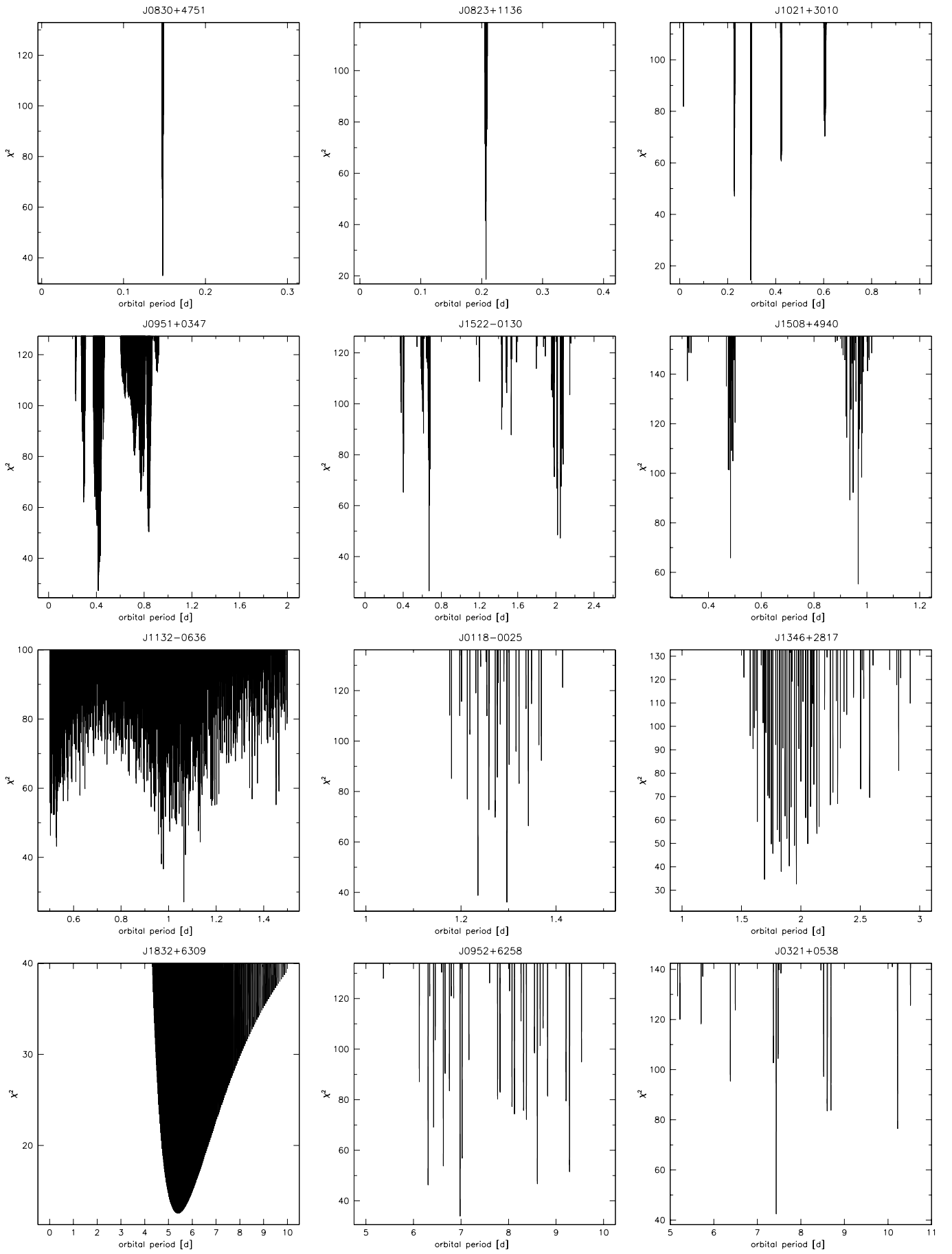


Fig. 3. χ^2 plotted against orbital period. The lowest peak corresponds to the most likely solution.

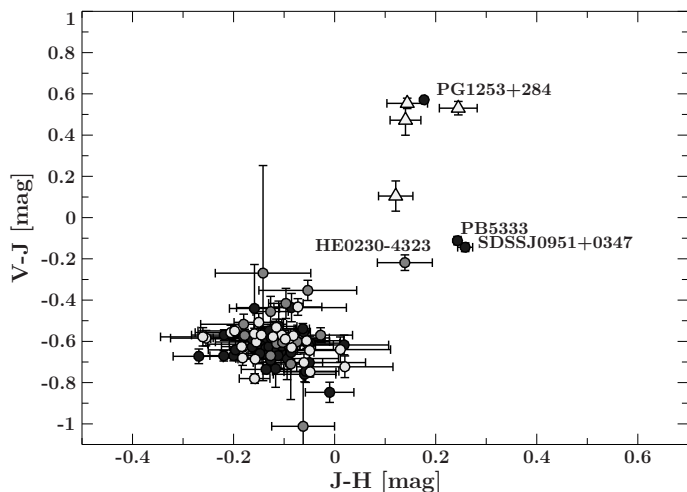


Fig. 4. Two-colour plots of $V-J$ vs. $J-H$ for all systems in our sample with 2MASS/UKIDSS colours, V magnitudes and low reddening ($E(B-V) < 0.1$; light grey circles: WD companion, grey circles: dM companion, dark grey circles: unknown companion type). Most of the systems show no excess from a companion. The systems showing an infrared excess which indicates a cool companion are named. For comparison, 4 sdB binaries with confirmed G/K-type companions (light grey triangles) are shown (Vos et al. 2012, 2013). All colours were corrected for reddening.

Table 4. Derived minimum masses and most probable nature of the companions.

Object	$f(M)$ [M_{\odot}]	$M_{2\min}$ [M_{\odot}]	Companion
J08300+47515	0.007	0.14	WD ^{lc}
J08233+11364	0.104	0.44	MS/WD
J09510+03475	0.025	0.23	MS/WD
J15222-01301	0.036	0.27	MS/WD
J10215+30101	0.046	0.30	MS/WD
J15082-49405	0.08	0.39	MS/WD
J11324-06365	0.008	0.14	MS/WD
J01185-00254	0.022	0.22	MS/WD
J13463+28172	0.13	0.49	WD
J18324-63091	0.13	0.50	MS/WD
J09523+62581	0.18	0.58	WD
J03213+05384	0.048	0.31	MS/WD

Notes. lc: companion type derived from the lightcurve

A cool companion of spectral type $\sim M1-M2$ or earlier is detectable from an infrared excess even if the spectra in the optical range are not contaminated with spectral lines from the cool companion. Stark & Wade (2003) showed that two-colour diagrams can be used to detect unresolved late-type stellar companions using optical colours (B and V) in combination with 2MASS colours (J and K_s). Reed & Stiening (2004) convolved Kurucz models with appropriate 2MASS (J , H and K_s) and B -filters and showed that companions of spectral type $M2$ and earlier would be separated from single sdBs in two-colour diagrams. Green et al. (2006, 2008) created two-colour plots from V band and 2MASS photometry (J and H) of single-lined and composite sdB spectra that showed a clear separation between the compos-

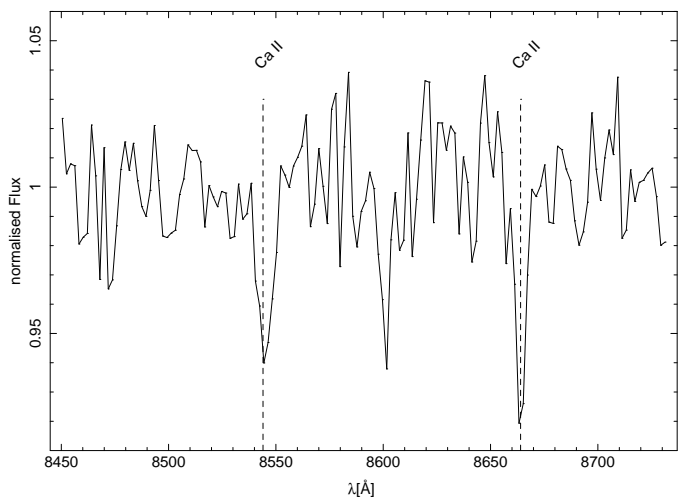


Fig. 5. Average SDSS spectrum of J09510+03475 showing evidence for weak absorption lines (two strongest components) of the infrared Ca II triplet originating very likely from a wide third component.

ites and the single-lined spectra. Hence, the presence of a cool companion can be inferred by its infrared excess.

We inspected each system with 2MASS/UKIDSS⁶ (J and H) and V band colour information for an infrared excess to put tighter constraints on the nature of the companions. Figure 4 shows the two-colour diagram of the whole sample for systems with colour information and small reddening ($E(B-V) < 0.1$). All colours were corrected for Galactic reddening using Table 6 with $R_v = 3.1$ from Schlafly & Finkbeiner (2011). However, if a system does not show an excess in the infrared a cool companion can be excluded only when the minimum companion mass derived from the RV-curve is higher than the mass of a stellar companion which would cause an excess. To calculate the mass of the companion needed to cause an excess we used the following approach.

First, we calculated the distance to each system using the reddening-corrected V magnitude, effective temperature and surface gravity as described in Ramspeck et al. (2001). The next step is to calculate the apparent magnitude in the J band for different subclasses of dMs using the distance modulus

$$m = 5 \log_{10}(d) - 5 + M, \quad (2)$$

where d is the distance in parsec and M the absolute magnitude of the dM taken from Table 5 in Kraus & Hillenbrand (2007). The calculated apparent magnitudes for each subclass in the J band can be compared to the measured J magnitudes of each individual system. Our assumption is that a cool companion would show up in the J band if the calculated magnitude is 3 sigma above the measured J magnitude. The calculated magnitude which would be visible in the J band can be converted to the corresponding mass of the dM from Table 5 in Kraus & Hillenbrand (2007) using linear interpolation. If the derived mass is lower than the minimum companion mass derived from the RV-curve, a cool companion can be excluded because it would cause an excess in the infrared. In these systems a compact companion is most likely. If an excess is detected a cool companion is likely.

If time resolved photometry for the short-period sdB binaries is available, further constraints can be put even if the companion mass is inconclusive. The hemisphere of a cool low-mass

⁶ for 2MASS; only colours flagged with quality A were used

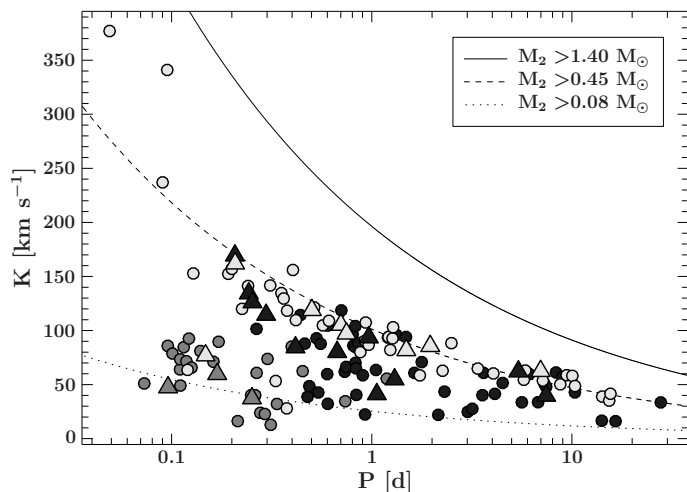


Fig. 6. The RV semi-amplitudes of all known short-period sdB binaries with spectroscopic solutions plotted against their orbital periods (light grey: WD companions, grey: dM companion, dark grey: unknown companion type). The binaries from the MUCHFUSS programme are marked with triangles, binaries taken from the literature with circles. The lines mark the regions to the right where the minimum companion masses derived from the binary mass function (assuming $0.47 M_{\odot}$ for the sdBs) exceed certain values.

main sequence companion facing the sdB is heated up by the significantly hotter sdB star. This causes a sinusoidal variation in the light curve. More(less) flux is emitted if the irradiated hemisphere of the cool companion is faced towards(away) from the observer. If this so-called reflection effect is detected, a compact companion can be excluded and a cool companion either a low-mass main sequence star of spectral type M or a brown dwarf is most likely. However, if the light curve of the short-period system shows no variation, a compact object like a WD is most likely to be the companion. Table 4 gives an overview on the most likely companions of our sample.

6.1. WD companions

J09523+62581 and J13463+28172 have minimum companion masses obtained from the radial velocity curve higher than dM masses which would cause an infrared excess. No sign of a companion is visible in the spectrum nor in the two-colour diagram. Therefore, the companion in both systems is most likely a WD.

6.2. J08300+47515 - a system with a possible ELM-WD companion

J08300+47515 is a remarkable system. The minimum companion mass is only $0.14 M_{\odot}$. Therefore, the nature of the companion cannot be constrained unambiguously from spectroscopy. The period of the system is 0.14780 ± 0.00007 days. This means that a cool main sequence companion would show a reflection effect in the light curve. However, a 2.14 h light curve of J08300+47515 obtained with the CAHA-2.2m telescope using BUSCA shows no light variation with a standard deviation of 0.0063 on the normalised lightcurve (see Schaffenroth et. al in prep). The companion might therefore be an ELM-WD. However, the inclination of the system cannot be constrained and it is still possible that the system is seen under low inclination. The maximum mass for an ELM-WD is $\sim 0.3 M_{\odot}$. If the sdB has the canonical mass of

$\sim 0.47 M_{\odot}$ and J08300+47515 is seen under an inclination angle of $i < 32.4^{\circ}$ the companion will be more massive than $\sim 0.3 M_{\odot}$ and not be a new ELM-WD companion. The probability of finding a system with $i < 32.4^{\circ}$ is $\sim 15\%$.

6.3. J11324–06365 - the first helium deficient sdO with a close companion

Stroer et al. (2007) studied the evolutionary status of 58 subdwarf O stars (sdOs) and concluded that the helium deficient sdOs are likely to be evolved sdBs. Indeed, evolution tracks by Han et al. (2002) and Dorman et al. (1993) show that sdBs will become helium deficient sdOs as they evolve to higher temperatures. Since a significant fraction of short-period sdBs is found in compact binaries, helium deficient sdOs should have a similar binary fraction. Although close companions to some helium deficient, evolved sdOBs have been found (Almeida et al. 2012; Klepp & Rauch 2011), J1132–0636 is the first helium deficient highly evolved sdO with a confirmed close companion. The minimum companion mass derived from the RV-curve is well below the mass which would cause an infrared excess if the companion were a dM. Therefore, the nature of the unseen companion remains unclear.

6.4. J09510+03475 - a hierarchical triple

J09510+03475 shows an excess in the J and H bands indicating a cool companion (see Fig. 4). In addition, a combination of 7 SDSS spectra from DR9 shows the two strongest components of the Ca II triplet at around 8600 \AA (Fig. 5). Radial velocity measurements of the hydrogen lines confirm that 4 SDSS spectra were taken when the sdB moved through the minimum of the radial velocity curve. This means that a close companion should be observed in anti-phase around its maximum velocity which is expected to be $\sim 250 \text{ km s}^{-1}$ depending on the mass ratio but certainly higher than the system velocity of $\gamma = 111.1 \pm 2.5 \text{ km s}^{-1}$. Using the same 4 SDSS spectra, an average velocity of $v_{\text{Ca}} = 86 \pm 16 \text{ km s}^{-1}$ for the calcium lines was measured which is just slightly below the system velocity ruling out a close companion. Therefore, the lines originate most likely from a third body in a wide orbit with a low RV amplitude. This makes this system the second candidate for a triple system after PG 1253+284 (Heber et al. 2002) which is an sdB star with one companion in a close orbit and another low-mass main sequence star in a wide orbit which causes the excess in the infrared and the Ca II lines. However, the nature of the close companion remains unclear.

6.5. Unconstrained companions

J18324–63091, J15222–01301, J01185–00254 and J03213+05384 have minimum companion masses derived from the RV-curve well below the mass which would cause an infrared excess. J10215+30101, J15082+49405 and J08233+11364 have no reliable infrared colours. Therefore, the nature of the unseen companion in those seven systems remains ambiguous.

6.6. The MUCHFUSS sample

Fig. 6 shows the RV semi-amplitudes of all known short-period sdB binaries with orbital solutions plotted against their orbital periods. The dotted, dashed and solid lines mark the regions to

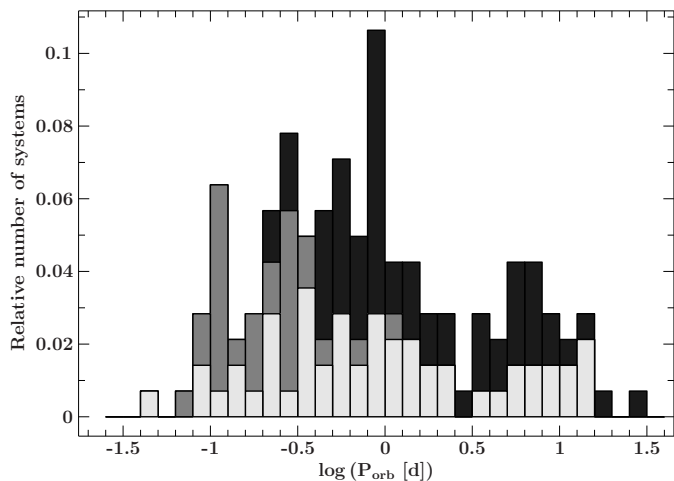


Fig. 7. Period histogram of the full sample. Light grey: WD companions, grey: dM companion, dark grey: unknown companion type.

the right where the minimum companion masses derived from the binary mass function (assuming $0.47 M_{\odot}$ for the sdBs) exceed $0.08 M_{\odot}$, $0.45 M_{\odot}$ and $1.40 M_{\odot}$.

The MUCHFUSS targets are marked with triangles. Most of the MUCHFUSS targets fall in the region with the highest minimum companion masses detected. However, the MUCHFUSS campaign discovered not only companions with the highest masses, but also detected the lowest-mass companions to sdBs (Geier et al. 2011d; Schaffenroth et al. 2014b). This shows that our target selection is efficient to find both the most massive companions known to sdB stars with periods of up to a few days and the least massive companions with short orbital periods of less than 3 hours. However, no NS or BH companion has been discovered yet.

7. The population of close hot subdwarf binaries

This study extends to 142, the sample of short-period sdB binaries that have measured mass functions. An overview is given in Tables A.2 and A.3.

In the following sections a canonical sdB mass of $0.47 M_{\odot}$ will be adopted. All systems have unseen companions, but masses could only be determined for the eclipsing ones. Hence only a minimum companion mass could be derived for most of them. Many systems were pre-selected either from high RV variations between several single exposures or from light variations such as reflection effects, ellipsoidal variations and/or eclipses. Consequently, the distribution is by no means random but biased towards high inclination, both for RV variables (large amplitudes preferred) and light variables (reflection effect and/or eclipses detected). Therefore, statistically, the derived minimum companion masses are expected to be not far from the real companion mass.

We collected orbital and atmospheric parameters as well as V-band and infrared photometry for the full sample from the literature (see Table A.3). Companion types for 82 systems were identified as described in Sec. 6. Thirty low-mass stellar or substellar companions were identified from a reflection effect in the lightcurve. Twenty-three systems show either ellipsoidal variation, eclipses with no additional reflection effect or no light variations at all. For these systems a WD companion is most likely. Additionally, 29 systems could be confirmed as WD companions because the minimum companion mass is higher than the

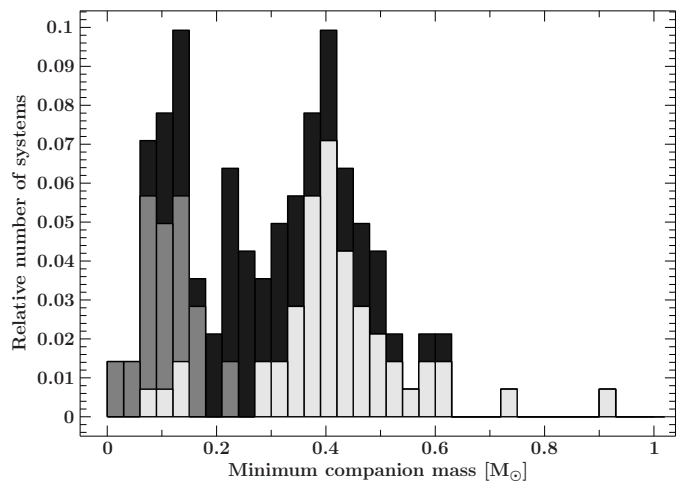


Fig. 8. Histogram of minimum companion masses (light grey: WD companions, grey: dM companion, dark grey: unknown companion type). Clearly visible are at least two separated populations. The first population peaks at around $0.1 M_{\odot}$ and consists mainly of low mass main sequence companions. The second population peaks at around $0.4 M_{\odot}$ and consists mainly of WD companions. The two high mass outliers belong to a population of massive WD companions.

mass for a non-degenerate companion which would cause an infrared excess. None of those show an excess in the *J* and *H* band (Fig. 4). Therefore, the companions are most likely WDs as well.

Four systems show an excess in the infrared and are good candidates for having a cool companion (see Fig. 4). Indeed, HE 0230-4323 shows a reflection effect and a low-mass stellar companion is confirmed.

Some systems may actually be triple as exemplified by PG1253+284, a radial velocity variable sdB with a dwarf companion which causes a strong infrared excess. The components were resolved by HST imaging (Heber et al. 2002), which indicated that the dwarf companion is on a wide orbit. Nevertheless, RV variations of the sdB star were observed, which must stem from another unresolved companion on a short-period orbit. Hence PG1253+284 is a triple system. Additional evidence of multiplicity (triples, quadruples) amongst sdB systems has recently been reported by Barlow et al. (2014). Hence it is worthwhile to search for triples amongst the four systems showing infrared excess. In fact, there is one, J09510+03475, which shows signs that the system actually may be triple (see Sec. 6.4 for a detailed discussion), while for HE 0230-4323 and PB5333 there is no hint for a third companion.

In the following we shall discuss the distribution of periods and companion masses, compare the stars' positions in the $T_{\text{eff}} - \log g$ plane to predictions from stellar evolution models, and discuss selection bias.

7.1. Distribution of orbital periods and minimum companion masses

Fig. 7 shows the period distribution of the full sample.

A wide peak near $P_{\text{orb}} = 0.3$ days is found in the full sample. The majority of systems in this group are dM companions detected from reflection effects in the lightcurves. Beyond half a day the contribution from the confirmed dM companions decreases significantly, most likely because a reflection effect is much weaker and not easy to detect. Another peak can be found at around $0.8 - 0.9$ days. Most of the systems here have uniden-

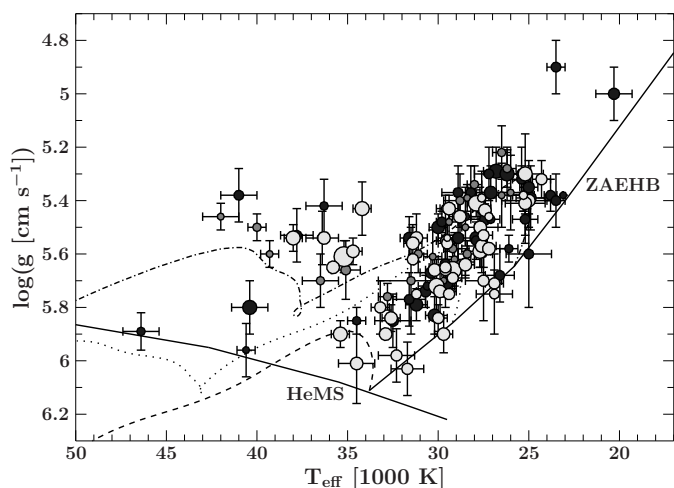


Fig. 9. $T_{\text{eff}} - \log g$ diagram of the full sample of binary sdB stars (light grey: WD companions, grey: M-dwarf companion, dark grey: unknown companion type). The size of the symbols corresponds to the minimum companion mass. The helium main sequence (HeMS) and the zero-age EHB (ZAEHB) are superimposed with EHB evolutionary tracks by Han et al. (2002) (dashed lines: $m_{\text{env}} = 0.000 M_{\odot}$, dotted lines: $m_{\text{env}} = 0.001 M_{\odot}$, dashed-dotted lines: $m_{\text{env}} = 0.005 M_{\odot}$ using $0.45 M_{\odot}$ models).

tified companion type. At longer periods the number of systems goes down, but in this region the selection effects are stronger.

Many of the WD companions were confirmed not only by the systems' lightcurves but also by the non-detection of an excess in the infrared (see Sec. 6) which is period independent. Therefore, in contrast to the dM companions, we find WD companions almost over the full period range. However, a gap near 3 days appears. We have no explanation for this but at the same time, with the present statistics, we cannot be sure that this gap is real.

The distribution of the minimum masses of the companions is displayed in Fig. 8. We identify three separate populations.

1) The first population has an average minimum companion mass around $0.1 M_{\odot}$, close to the hydrogen burning limit. Most of them were identified as either dMs or brown dwarfs from the observation of their reflection effect. Only four WDs were found in this period regime, which could be ELM-WDs ($M < 0.3 M_{\odot}$, see Sect. 8.1).

2) The second population peaks around $0.4 M_{\odot}$. Our analysis showed that the majority of this population are most likely WDs with an average minimum mass around $0.4 M_{\odot}$, lower than the average mass of single WDs (see discussion in Sec. 9.2).

3) The third group are the high mass WD companions ($M_{\text{WD}} > 0.7 M_{\odot}$). Systems with high companion masses stand out in radial velocity selected samples as they show higher RV variations compared to low-mass companions. However, only the eclipsing systems KPD1930+2752 and CPD-30° 11223 have confirmed companion masses above $0.7 M_{\odot}$. This means that in our sample less than 2% of the binaries with measured RV curves have such high mass WD companions.

7.2. $T_{\text{eff}} - \log g$ diagram

Fig. 9 shows the $T_{\text{eff}} - \log g$ diagram of the full sample with accurate atmospheric parameters. The size of the symbols represent the companion mass. Most of the stars populate the extreme horizontal branch (EHB) band all the way down to the helium main sequence while about 10% of the sdB sample has already

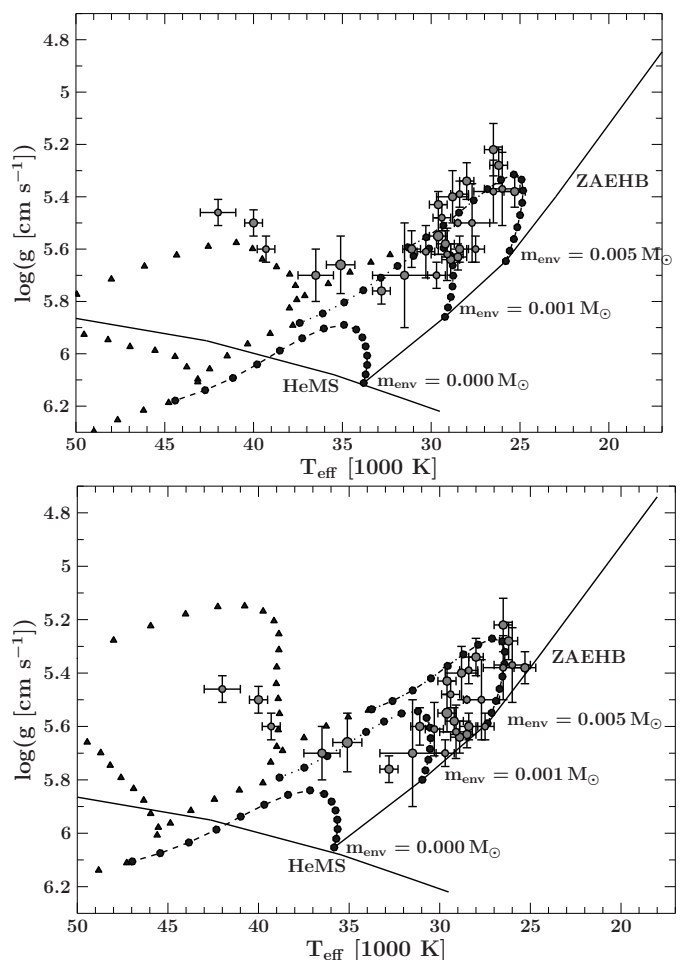


Fig. 10. $T_{\text{eff}} - \log g$ diagram of sdB stars with confirmed M-dwarf companions. The size of the symbols corresponds to the minimum companion mass. The helium main sequence (HeMS) and the zero-age EHB (ZAEHB) are superimposed with EHB evolutionary tracks by Han et al. (2002) using $0.45 M_{\odot}$ (upper panel) and $0.50 M_{\odot}$ (lower panel) models. The space between black symbols corresponds to equal times and shows that the sdB evolution speeds up once the sdB reaches its lowest gravity. Circles mark the region where the sdB star contains helium in the center of the core whereas triangles mark the region where the helium in the center of the core is completely burned.

evolved off the EHB. The total evolution time on the EHB is 100 Myr, whereas post-EHB evolutionary timescales are lower by a factor of about 10. The theoretical tracks show a linear time-luminosity-relation while the star is in the EHB strip until it comes close to the terminal age EHB (TAEHB), where evolution starts to speed up. Hence, we would expect a homogeneous coverage of the EHB band as it is indeed observed. A more detailed comparison can be made using the cumulative luminosity function (see Lisker et al. 2005, for details).

In the next step we concentrate on the systems for which the companions have been classified and separate the distribution according to companion type, that is dMs and WDs, respectively. For WD companions, the sdBs populate the full EHB band homogeneously with a small fraction of sdBs having evolved off the EHB. For sdB stars with dM companions the ratio of post-EHB to EHB stars is similar to that for sdB+WD systems. However, they appear not to cover the full EHB band. There is a lack of hot, high gravity sdBs close to the helium main sequence (Fig. 10).

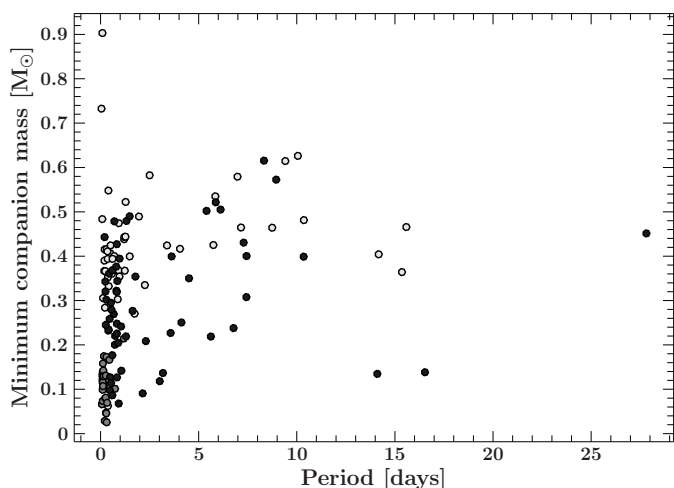


Fig. 11. Minimum companion masses plotted against the period of the systems (light grey: WD companions, grey: M-dwarf companion, dark grey: unknown companion type).

Most striking is that the width of the distribution of the sdB+dM systems is narrower than that of sdB+WD ones, in particular none of the sdB stars is found close to the zero age EHB (ZAEHB) if a sdB mass of $0.45 M_{\odot}$ is assumed. Because of the contamination of the sdB spectrum by light from the companion, their gravities could have been systematically overestimated and their effective temperatures could have been systematically underestimated, which would shift the systems away from the ZAEHB (Schaffenroth et al. 2013), which would shift them even further away from the ZAEHB. The location of the EHB band in the $T_{\text{eff}} - \log g$ diagram depends on the adopted core mass. By increasing it, the EHB stars become more luminous and therefore the EHB band is shifted to lower gravities. This is demonstrated in Fig. 10 by indicating the ZAEHB for a higher core mass of $0.5 M_{\odot}$ in addition to that of $0.45 M_{\odot}$ shown in all panels. The observed distribution of sdB stars is consistent with the $0.5 M_{\odot}$ ZAEHB, for which the EHB evolution timescales are shorter. Hence, adopting a higher core mass gives better agreement between observations and evolutionary tracks.

7.3. Separation of the systems

The details of the common envelope (CE) phase are still poorly understood (Ivanova et al. 2013). In a rather simplistic picture the orbital energy of the binary, which scales with the mass of the companion, is deposited in the envelope. If a more massive companion ejects the common envelope earlier, and therefore at a wider orbit than a less massive companion, a correlation between orbital period and minimum companion mass would be expected. Figure 11 shows the minimum companion masses plotted over the period of the systems: however, no obvious correlation can be seen in the sample with WD as well as dM companions (see Sec. 9.5 for further discussion).

We also note that, even if the core masses of the sdB progenitors were very similar, their total masses (core + envelope) might have been quite different, implying different energies to expel the envelope and different final orbital separations. This may partially explain why we do not see any correlation between minimum companion mass and orbital period in Fig. 11.

7.4. Selection effects

In order to compare the observed sample of close binary sdBs to population synthesis models (e.g. Han et al. 2002, 2003; Clausen et al. 2012) selection effects have to be taken into account. For the MUCHFUSS sample the target selection is well defined (Geier et al. 2011a). However, since the 142 solved binaries studied here are drawn from several different samples, it is impossible to come up with an unified description of selection bias.

All the sdBs studied here were initially discovered as faint blue stars from multi-band photometric survey data. However, spectral classification had to follow and the brighter limits of those spectroscopic observations have to be taken into account.

In the brightness distribution (V -band, Fig. 12) of the whole sample, we can identify two sub-samples. One peaks around 14 mag and consists of binaries mostly discovered in the Palomar Green (PG, Green et al. 1986), Edinburgh Cape (EC, Stobie et al. 1997), Kitt Peak Downes (KPD, Downes 1986) and some smaller scale surveys. The fainter subsample peaks around 15 mag and was selected mostly from the Hamburg/ESO (HE, Wisotzki et al. 1996), the Hamburg Schmidt (HS, Hagen et al. 1995) surveys and the SDSS (York et al. 2000).

For 127 binaries we calculated the z -distances from the Galactic plane⁷ assuming a canonical sdB mass of $0.47 M_{\odot}$ (Fig. 13) and for 118 systems with sufficient data we calculated also the spectroscopic distances.

Except for four distant stars (at 2 to 5 kpc above the Galactic plane) all stars lie within 2 kpc below or above the Galactic plane. Their distribution is asymmetric, with an excess of objects in the northern Galactic hemisphere. The deficit of near-Galactic plane stars, as well as those below the Galactic plane, is due to the insufficient depth of near-plane and southern surveys. The most distant systems are likely to be halo stars and may be considerably older than the bulk. A significant fraction belongs to the thick disc, which on average is older than the thin disc. Because the age of the progenitor population is an important ingredient for binary population synthesis, it is crucial to assign each system to one of the stellar populations via an investigation of its kinematic and thus derive age estimates.

The search for binarity of the targets has either been done by photometric or spectroscopic follow-up observations. Either the star shows light variations indicative of a close companion or the star RV shifts become apparent. Both discovery methods introduce different selection effects.

Only 20 of the binaries in the sample have been discovered photometrically (see Table A.3). Short-period sdB stars with cool dM or BD companions show a reflection effect and often also eclipses. 14 binaries with periods of less than 0.3–0.4 d and a peak period of 0.1 d have been discovered in this way. Close sdB+WD binaries can show ellipsoidal variations and sometimes very shallow eclipses. Of the six binaries discovered in this way, two have periods of less than 0.09 d and one has a period of 0.3 d. The remaining three long-period systems (> 3 d) have been discovered by the Kepler mission, which has a much higher sensitivity than ground-based telescopes. In general, photometric selection is clearly biased towards the shortest-period systems at high inclinations.

The remaining 122 systems have been discovered from RV shifts, most of them from medium-resolution spectra with an RV

⁷ We included near-Galactic plane objects neglecting reddening corrections as reddening is of little influence for calculating their z -distance.

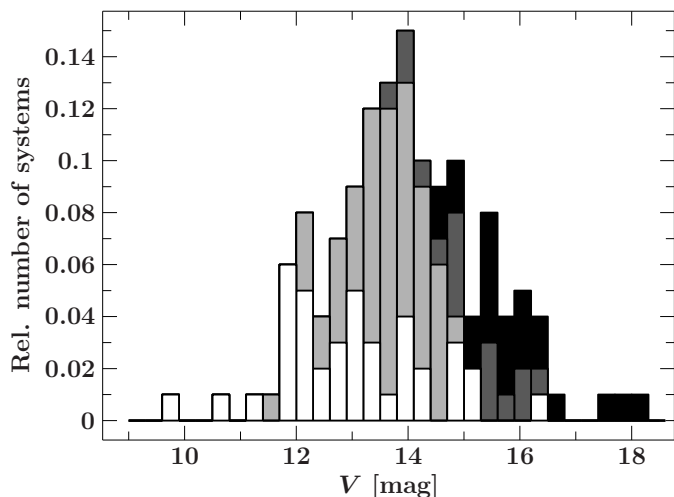


Fig. 12. Histogram of the magnitudes of the full sample. The systems selected from the SDSS surveys are marked in black and from the Hamburg/ESO (HE), Hamburg Schmidt (HS) are marked in dark grey. The systems selected from the Palomar Green (PG), Edinburgh Cape (EC) and Kitt Peak Downes (KPD) surveys are marked in light grey. The systems selected from smaller scale surveys (e.g. Feige...) are marked in white.

accuracy of $\sim 10 - 20 \text{ km s}^{-1}$ (e.g. Maxted et al. 2001). The binaries studied by Edelmann et al. (2005) and in the course of the ESO Supernova Ia Progenitor Survey (SPY, Napiwotzki et al. 2001a; Karl et al. 2006; Geier et al. 2010a, 2011c) have been discovered using high-resolution spectra with an RV accuracy better than 5 km s^{-1} .

To our knowledge, well-defined cuts of RV-shifts were only used in the MUCHFUSS target selection (see Geier et al. 2011a). In general, short-period systems with high RV shifts and therefore high inclinations are the easiest ones to solve within a few nights of observations. This introduces a selection in favour of such systems. It is unlikely that a significant population of binaries with periods longer than one day and RV semi-amplitudes higher than 100 km s^{-1} has been missed in the high-galactic latitude population of hot subdwarf stars covered by the SDSS. The missing population of close sdB binaries with periods from a few days to a few tens of days most likely consists of systems with small RV semi-amplitudes and rather low-mass companions ($< 0.5 M_{\odot}$).

8. Comparison with related binary populations

8.1. The population of helium-core WD binaries

The formation of helium-core WD binaries with masses $< 0.45 M_{\odot}$ is expected to occur in a similar way as the formation of sdB+WD binaries discussed in this paper. Both systems survive two phases of mass transfer with the second phase where the helium-core WD/sdB is formed being a common envelope phase. The helium-core WDs start transferring mass already when the progenitor evolves on the red giant branch (RGB) and lose so much mass that they are not able to ignite helium in the core. The sdBs start mass transfer on or near the tip of the RGB and are massive enough to ignite helium.

Orbital parameters of 55 helium-core WD binaries were selected from Gianninas et al. (2014). All the companions are WDs. Figure 14 shows the minimum companion mass histogram of the sample compared to the sdB sample. ELM companions cover a wider range of masses, extending to low as well as high

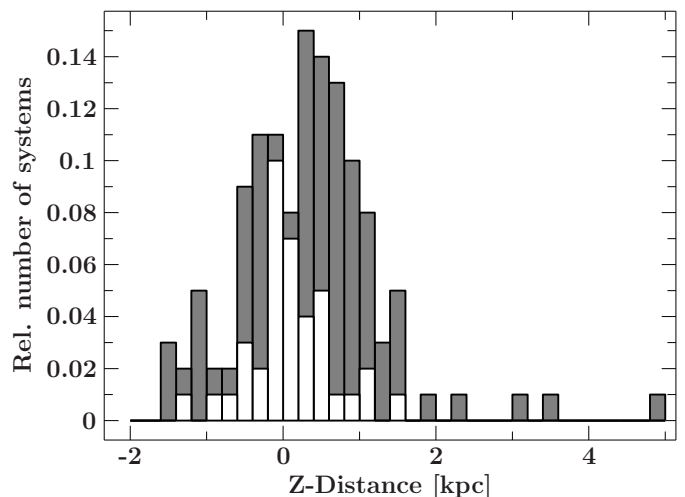


Fig. 13. Histogram of the spectroscopic z-distances above the Galactic plane. White are systems with a Galactic latitude $|b| < 30^{\circ}$. Grey marked are the systems with $|b| > 30^{\circ}$.

masses and indicating a different evolutionary path. The distribution does not show a clear separate population with a peak at $0.4 M_{\odot}$ like the confirmed WD companions to sdB stars.

Figure 15 shows the orbital period distribution of the helium-core WDs compared to our sample. Between an orbital period of 0.1 and 1.0 days both distributions look very similar. However, below 0.25 days helium-core WDs are more numerous compared to the sdB+WD systems. On the other hand at longer periods sdB+WD systems are more numerous which indicates that helium-core WD binaries are formed preferentially with shorter periods.

8.2. The population of compact WD+dM systems

Compact WD+dM binaries are also the product of CE evolution and so we might expect that the properties of these binaries are similar to the sdB+dM binaries. Indeed, some WD+dM systems may have been created as sdB stars with dM companions that have since evolved to become white dwarfs with masses close to $0.47 M_{\odot}$.

Orbital parameters of 68 post-common envelope binaries consisting of a WD+dM were selected from the literature (Zorotovic et al. 2011; Nebot Gómez-Morán et al. 2011; Pyrzas et al. 2012; Parsons et al. 2012). The systems cannot be compared in the same way as the ELM-WD binaries because all WD+dM systems have confirmed companion masses whereas, for sdB+dMs, only minimum companion masses are known. Figure 16 shows the orbital period vs. the companion masses of the dM companions to WDs compared to the confirmed dM companions to sdB stars. The plot shows dM companion masses larger than $\sim 0.2 M_{\odot}$ for the WD+dM systems, while the minimum masses of dM companions to sdBs peak well below, near $\sim 0.1 M_{\odot}$. To increase the companion masses of the sdB+dM systems to an sdB mass larger than $0.2 M_{\odot}$ the systems have to be observed with inclination angles below 30° . This is not very likely as the majority of the systems were selected from photometry by eclipses and/or reflection effects which are hardly detectable in systems with small inclinations.

The WD+dM systems show a wide spread in orbital period whereas the majority of the sdB+dM systems were found with periods below 0.3 days. A possible reason might be that WD+dM systems are usually identified spectroscopically be-

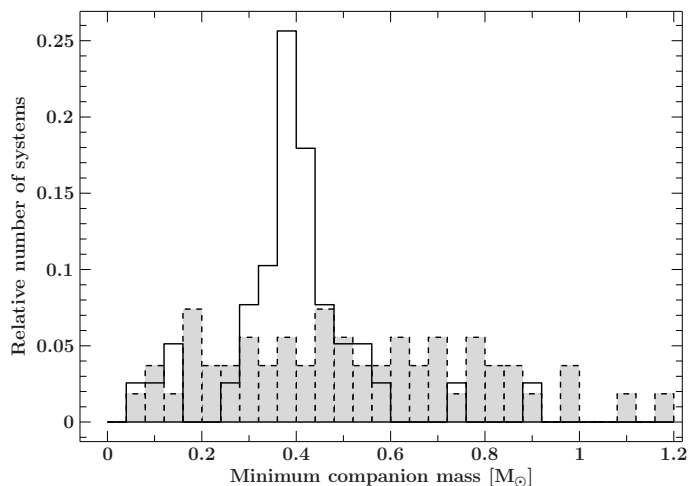


Fig. 14. Comparison of minimum companion masses of sdB binaries with confirmed WD companions to the ELM-WD binaries (grey shaded area) taken from Gianninas et al. (2014).

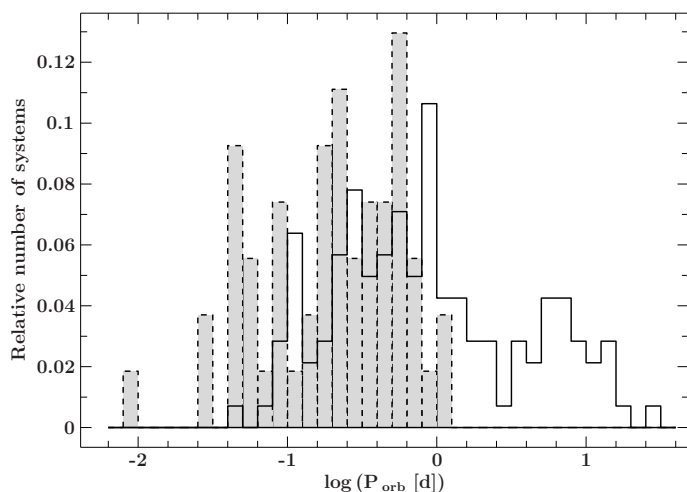


Fig. 15. Comparison of orbital periods of sdB binaries with confirmed WD companions to the known ELM-WD binaries with orbital solutions (grey shaded area) taken from Gianninas et al. (2014).

cause features of the dM dominate the red part of the composite spectra. In contrast to that, almost all sdB+dM systems were identified from the reflection effect in the lightcurves. Longer period systems show much weaker reflection effects and therefore are much harder to detect.

9. Discussion

9.1. Distribution of sdB masses

Several previous studies discussed the sdB mass distribution. Fontaine et al. (2012) collected sdB masses of a sample of 22 sdBs (15 derived from asteroseismology and 7 from resolved binaries), and found a sharp peak at $M_{\text{sdB}} = 0.47 M_{\odot}$. Han et al. (2003) discussed the sdB mass distribution formed via different phases of mass transfer. Figure 12 in Han et al. (2003) showed a sharp peak at $M_{\text{sdB}} = 0.46 M_{\odot}$ for sdBs formed after a common envelope phase.

In our analysis of the companion mass distribution shown in Fig. 8 we apply the assumption that the sdBs have all canoni-

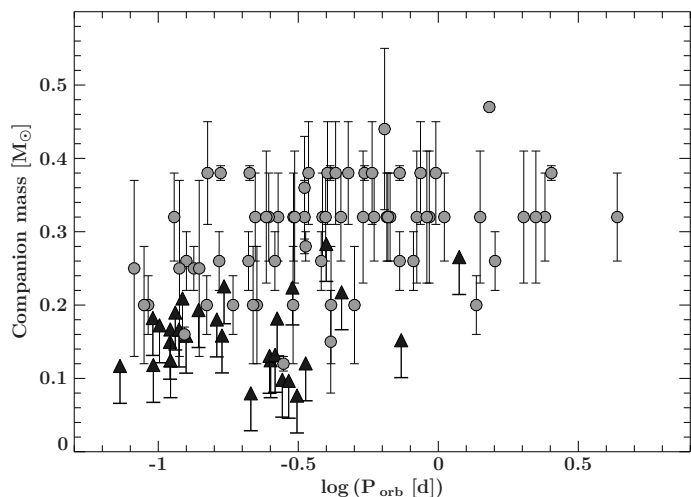


Fig. 16. Companion mass plotted against the orbital period. Grey circles mark derived companion masses of known WD+dM binaries with orbital solutions taken from Zorotovic et al. (2011), Nebot Gómez-Morán et al. (2011), Pyrzas et al. (2012) and Parsons et al. (2012). Black arrows mark minimum companion masses of the known sdB+dM binaries.

cal masses of $M_{\text{sdB}} = 0.47 M_{\odot}$ because of the results of previous studies (see Fontaine et al. 2012 and references therein). The distribution of the minimum companion masses (Fig. 8) shows two quite narrow peaks. If the distribution of the sdB masses would be much more smeared out than predicted, those two peaks would have to be smeared out as well. We therefore conclude that the width of the sdB mass distribution is of the order of $0.2 M_{\odot}$ at most, which is consistent with the prediction from theory. We note that from our analysis we cannot claim that $M_{\text{sdB}} = 0.47 M_{\odot}$ is the canonical mass for sdBs because adopting a higher (lower) average sdB mass would also increase (decrease) the companion masses but the distinct peaks in the companion mass distribution would persist.

9.2. WD companion masses

The majority of minimum companion masses of confirmed WD companions are located around $0.4 M_{\odot}$, which is significantly below the average mass for single (DA) WDs of $\sim 0.59 M_{\odot}$ (e.g. Kleinman et al. 2013). Because of projection effects and selection biases the detection of high inclination systems should be favoured, which means that the derived limits should be on average close to the companion masses. Since the minimum masses of the WD companions are significantly smaller than the average mass of single C/O-WDs, we test this hypothesis by computing the inclination angles for all sdB+WD binaries assuming that all companion WDs have an average mass of $0.6 M_{\odot}$.

Figure 17 shows a comparison between the computed distribution of inclination angles and the one expected for randomly distributed inclinations taking into account projection effects. We do not include any selection biases, but want to point out that they would in any case lead to even higher probabilities of seeing the systems at high inclinations. One can clearly see that the inclination distribution is not consistent with the one expected for a population of $0.6 M_{\odot}$ C/O-WD companions. Hence, it is likely that a significant fraction of the sdB binaries host WDs of masses below $0.6 M_{\odot}$.

Table 5. Derived times when the dM will fill its Roche Lobe and start accreting onto the primary to form a cataclysmic variable. The derived M_{Comp} are minimum companion masses which means that the time when the dM fills its Roche Lobe are upper limits

Object	Period [days]	M_{Comp} [M_{\odot}]	Time [Gyr]
HS 2333+3927	0.172	0.174	3.44
J192059+372220	0.169	0.107	6.09
2M1533+3759	0.162	0.129	4.21
ASAS102322–3737	0.139	0.142	2.15
2M1938+4603	0.126	0.107	2.38
BULSC16335	0.122	0.158	0.95
EC10246–2707	0.119	0.115	1.70
HW Vir	0.115	0.138	0.97
HS 2231+2441	0.111	0.073	3.05
NSVS14256825	0.110	0.115	1.27
UVEX 0328+5035	0.110	0.098	1.77
PG 1336–018	0.101	0.121	0.72
J082053+000843	0.096	0.067	2.22
HS 0705+6700	0.096	0.131	0.34
PG 1017–086	0.073	0.066	1.01
J162256+473051	0.069	0.060	0.95

Table 6. Derived merger timescales of the confirmed sdB+WD systems. The derived M_{Comp} are minimum companion masses which means that the merger timescales are upper limits to merger times.

Object	Period [days]	M_{Comp} [M_{\odot}]	Time [Gyr]	Merger result
PG 0941+280	0.311	0.415	10.27	WD/RCrB
PG 2345+318	0.241	0.366	5.78	WD/RCrB
PG 1432+159	0.225	0.283	6.01	WD/RCrB
J113840–003531	0.208	0.415	3.49	WD/RCrB
HS 1741+2133	0.20	0.389	3.34	WD/RCrB
HE 1414–0309	0.192	0.366	3.16	WD/RCrB
J083006+475150	0.148	0.137	3.77	AM CVn
EC00404–4429	0.128	0.305	1.26	WD/RCrB
PG 1043+760	0.120	0.101	2.88	AM CVn
KPD 1930+2752	0.095	0.903	0.23	SN Ia
KPD 0422+5421	0.090	0.483	0.33	WD/RCrB
CD–30°11223	0.049	0.732	0.05	SN Ia

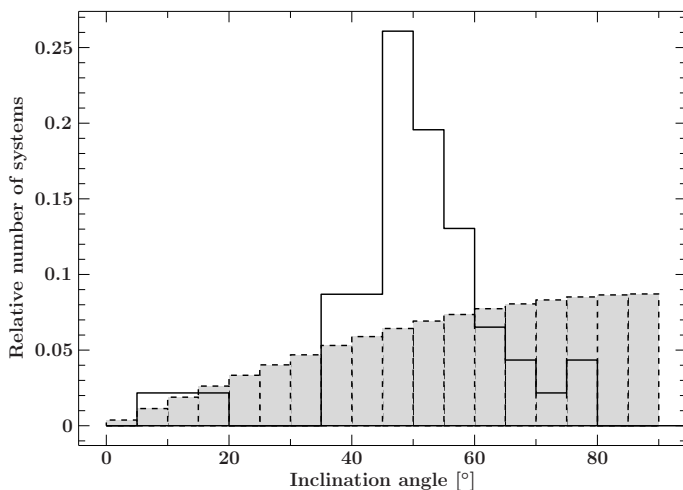


Fig. 17. Comparison of computed inclination angles of the confirmed sdB+WD systems to match companion masses of $0.6 M_{\odot}$ to a theoretical inclination angle distribution assuming randomly distributed inclination angles.

9.3. Triple systems

Only one sdB system was known to be triple up to recently. We found another sdB binary, J09510+03475, with a third component in a wide orbit. Barlow et al. (2014) studied 15 sdB binaries to detect long period companions. At least one has a visual companion well separated from the sdB. However, RV measurement show that the orbital period of the system is below 10 days, indicating a close companion in addition to the wide companion.

The properties of J09510+03475 also imply that a fraction of sdB binaries showing an excess in the infrared might be triples systems. If we assume all 3 systems to be triples we find a fraction of 2.1% in our sample. However, if the wide companion is too faint to show an excess in the infrared then it would be

hidden in our sample and the fraction of triple systems might be significantly higher. Some of the sdB triples might have formed from solar type triples. Raghavan et al. (2010) found a fraction of $9 \pm 2\%$ for solar type triples which is not in disagreement with our findings.

9.4. Massive companions

Hot subdwarf + WD binaries are potential supernova Ia progenitors if their masses are sufficiently large. However, only a very small fraction of massive WD companions ($< 2\%$) were detected. KPD1930+2752 and CD-30°11223 are the only systems with companion masses $> 0.7 M_{\odot}$. This implies that only a specific evolutionary path can form such systems. Wang et al. (2013) showed that a system like CD-30°11223 is formed from a young stellar population which can only be found in the Galactic disc. Indeed, CD-30°11223 is a confirmed member of the Galactic disc population (Geier et al. 2013b). No NS or BH was detected in our sample but previous studies concentrated on high Galactic latitudes. Based on the non-detection of a NS or BH in our sample with 142 systems, we find that $< 0.7\%$ of the close sdB binaries contain a NS or BH companion which is a small fraction but still consistent with the predictions from binary evolution calculations (Yungelson & Tutukov 2005; Nelemans 2010). We encourage a systematic search for compact sdB binaries at low Galactic latitudes.

9.5. Implications for the common envelope phase

A remarkable result of our analysis is that we find clearly distinct populations. The majority of confirmed WD companions have minimum companion masses strongly peaked at $\sim 0.4 M_{\odot}$. This is much lower than the average mass of single WDs and leads to the conclusion that the WDs need to lose a significant amount of mass during the evolution either during the first phase of mass transfer when the WD is formed or during the common envelope phase when the sdB is formed. The first phase can either be stable Roche lobe overflow or also a common envelope phase depending on the initial separation and the mass ratio of the system. White dwarf masses of $\sim 0.4 M_{\odot}$ are on the border between a WD with a helium core and a C/O core and a signif-

ificant fraction of white dwarf companions might be helium-core WDs.

In comparison, ELM-WD binaries show a much wider companion mass distribution starting at very low masses up to high masses close to the Chandrashekar limit. Either these systems form in a different way or sdB binaries need a special WD companion mass to lose the right amount of mass and form an sdB.

The dM companions were found to have minimum companion masses of $\sim 0.1 M_{\odot}$ close to the hydrogen burning limit. These systems have experienced one phase of mass transfer, namely the CE phase when the sdB was formed, and are direct progenitors of WD+dM systems. However, in comparison with the known population of WD+dM systems we find that the main sequence companions in WD systems are significantly more massive than the main sequence companions in sdB systems. This shows on the one hand that only a small number of WD+dM systems evolved from sdB+dM systems and on the other hand that sdBs might be formed preferentially by low mass main sequence companions whereas WD are preferably formed with higher mass main sequence companions. The other possible way to form a compact WD+dM system without forming an sdB first is the formation of the WD directly during a CE phase when the WD progenitor evolves on the asymptotic giant branch.

In addition we found no correlation of the orbital separation of the sdB binaries with companion mass (see Fig. 11) which means that the red giant progenitors of the sdB must have had different envelope masses. This could be tested, if we were able to identify systems that had similar envelope masses prior to envelope ejection. In this respect the halo population of sdB binaries would be of great interest because they are expected to form from systems where the sdB progenitor has a mass of $\sim 0.8 M_{\odot}$. A detailed kinematic analysis to identify the halo population of compact sdB binaries is crucial. The majority of the MUCHFUSS sample is faint and therefore they might be the best candidates to be member of the halo population and a good starting point for an extended kinematic analysis of the complete sample of compact sdB binaries.

9.6. Future evolution: Pre-CV vs. Merger

For systems with main sequence companions we calculate the time when the dM will fill its Roche Lobe and starts accretion. As approximation for the Roche radius the Eggleton equation was used (Eggleton 1983), with q being the mass ratio $q = M_{\text{comp}}/M_{\text{sdB}}$:

$$r_L = \frac{0.49q^{2/3}}{0.6q^{2/3} + \ln(1 + q^{1/3})}. \quad (3)$$

We used the minimum companion mass for the dM and calculated the corresponding radius using Table 1 in Kaltenegger & Traub (2009) by linear interpolation. Once the companion fills its Roche Lobe mass accretion starts and the systems becomes a cataclysmic variable (CV). We assumed that only gravitational wave radiation brings the two components closer. The time until the system starts accretions was calculated from the gravitational wave timescale, equation 7 from Piro (2011):

$$\tau_{\text{GW}} = P \left| \frac{dP}{dt} \right|^{-1} = \frac{5}{96} \frac{c^5}{G^{5/3}} \frac{M_{\text{total}}^{1/3}}{M_{\text{sdB}} M_{\text{dM}}} \left(\frac{P}{2\pi} \right)^{8/3}. \quad (4)$$

Table 5 shows the 16 systems which will become a CV and start accreting within a Hubble time. J0820+0008 and J1622+4730

have confirmed brown dwarf companions (Geier et al. 2011d; Schaffenroth et al. 2014b). Therefore at least two systems (J0820+0008 and J1622+4730) will have brown dwarf (BD) donor stars. The dM companion in HS0705+6700 will fill its Roche Lobe in about 340 Myr, being the first system of our sample. At this stage the sdB is already evolved and turned into a C/O-WD. Therefore, all 16 systems of our sample will appear as WD+dM/BD with a low-mass companion ($M_{\text{Comp}} < \sim 0.17 M_{\odot}$) before they become a CV. The currently known population of WD+dMs lacks such low-mass main sequence companions (see Fig. 16). However, our findings show that low mass dM companions to WDs should exist as well.

Merger timescales were calculated for systems of the full sample which have a confirmed WD companion and will merge within a Hubble time using equation 9 in Paczyński (1967):

$$T_0(\text{years}) = 3.22 \cdot 10^{-3} \frac{(M_{\text{sdB}} + M_{\text{Comp}})^{1/3}}{M_{\text{sdB}} M_{\text{Comp}}} P_{\text{orb}}^{8/3}. \quad (5)$$

We identified 12 systems of the full sample which will merge within a Hubble time. Only CD-30°11223 will merge before the sdB turns into a WD. Geier et al. (2013b) showed that this system will most likely explode as a subluminous SN Ia. All other systems will evolve and turn into a C/O WD before they merge. Depending on the mass ratio the systems either merge ($q > 2/3$) or form an AM CVn type binary ($q < 2/3$). For a helium-core white dwarf companion the merger might form an RCrB star, whereas a C/O-WD companion forms a massive single C/O-WD. If the system reaches the Chandrashekar mass it might explode as a SN Ia (e.g. Webbink 1984).

PG1043+760 and J0830+4751 have low minimum companion masses and a mass ratio $q < 2/3$. The companions in those systems are most likely helium-core white dwarfs. Both systems are therefore good candidates to have stable mass transfer and form an AM CVn type binary. KPD1930+2752 has a massive WD companion. The combined mass is close to the Chandrashekar limit. Thus, this is a good system to explode as a SN Ia. The other 8 systems have mass ratios $q > 2/3$ and therefore are potential progenitors for mergers. Depending on the structure of the companion, the merger with a helium-core white dwarf might form an RCrB star, whereas a C/O-WD companion might form a massive single C/O-WD.

This analysis shows that the majority of sdB binaries with white dwarf companions will not merge within a Hubble time and only a small number of systems have periods and companion masses to either merge, form an AM CVn type binary or explode as a supernova Ia.

10. Summary

In this paper we have presented atmospheric and orbital parameters of 12 new close sdB binaries discovered by the MUCHFUSS project. Three of them have most likely WD companions. We found the first helium deficient sdO with a compact companion, a good candidate for an ELM-WD companion and confirmed the second known hierarchical triple amongst the known sdBs.

This study increases the number of hot subdwarf binaries with orbital periods less than 30 days and measured mass functions to 142 systems. The companion mass distribution of the full sample shows two separate peaks. The confirmed dM/BD companions are concentrated around $0.1 M_{\odot}$ whereas the majority of the WD companions peak at around $0.4 M_{\odot}$ showing that WDs in compact hot subdwarf binaries have significantly lower masses

than single WDs. The $T_{\text{eff}} - \log g$ diagram of the sdB+dM systems indicates that in these systems the sdBs might have higher masses compared to the rest of the sample.

Close hot subdwarf binaries are expected to be formed in a similar way as the compact ELM-WD binaries or the WD+dM pre-CV systems. However, both samples show significantly different companion mass distributions indicating either selection biases or differences in their evolutionary paths.

We discussed possible implications for the common envelope phase, but also found that the progenitor stars of the sdB in our sample might have had a rather broad mass distribution. More insights in the formation process of field sdB stars can be gained, if they can be clearly assigned to their parent populations, either the thin disc, the thick disc or the Galactic halo. Accurate distances and kinematics are crucial for such an analysis. The *GAIA* space mission will provide accurate distances, luminosities and kinematics for most of the known sdB stars and will also cover the Galactic disc region, which has been avoided by previous surveys because of reddening.

This data will make it possible to derive sdB masses, identify different sdB populations and allow us to put constraints on the evolution history and the common envelope phase which forms the sdBs in close binaries.

Acknowledgements. TK acknowledges support by the Netherlands Research School of Astronomy (NOVA). The research leading to these results has received funding from the European Research Council under the European Union's Seventh Framework Programme (FP/2007-2013) / ERC Grant Agreement n. 320964 (WDTracer). BTG was supported in part by the UK's Science and Technology Facilities Council (ST/I001719/1). CH is supported by the Deutsche Forschungsgemeinschaft (DFG) through grant HE1356/62-1. VS is supported by Deutsches Zentrum für Luft- und Raumfahrt (DLR) under grant 50OR1110. We acknowledge that some observations used in this paper were carried out by Sebastian Müller, Patrick Brünner, Anna Faye McLeod, Markus Schindewolf and Florian Niederhofer.

Based on observations at the Paranal Observatory of the European Southern Observatory for programme number 165.H-0588(A). Based on observations at the La Silla Observatory of the European Southern Observatory for programmes number 079.D-0288(A), 080.D-0685(A), 084.D-0348(A) and 092.D-0040(A). Based on observations collected at the Centro Astronómico Hispano Alemán (CAHA) at Calar Alto, operated jointly by the Max-Planck Institut für Astronomie and the Instituto de Astrofísica de Andalucía (CSIC). Based on observations with the William Herschel Telescope operated by the Isaac Newton Group at the Observatorio del Roque de los Muchachos of the Instituto de Astrofísica de Canarias on the island of La Palma, Spain. Based on observations with the Southern Astrophysical Research (SOAR) telescope operated by the U.S. National Optical Astronomy Observatory (NOAO), the Ministério da Ciência e Tecnologia of the Federal Republic of Brazil (MCT), the University of North Carolina at Chapel Hill (UNC), and Michigan State University (MSU). Based on observations obtained at the Gemini Observatory, which is operated by the Association of Universities for Research in Astronomy, Inc., under a cooperative agreement with the NSF on behalf of the Gemini partnership: the National Science Foundation (United States), the Science and Technology Facilities Council (United Kingdom), the National Research Council (Canada), CONICYT (Chile), the Australian Research Council (Australia), Ministério da Ciência e Tecnologia (Brazil) and Ministerio de Ciencia, Tecnología e Innovación Productiva (Argentina).

References

Almeida, L. A., Jablonski, F., Tello, J., & Rodrigues, C. V. 2012, *MNRAS*, 423, 478
 Barlow, B., Wade, R., Liss, S., & Stark, M. 2014, in *Astronomical Society of the Pacific Conference Series*, Vol. 481, *Astronomical Society of the Pacific Conference Series*, ed. V. van Grootel, E. Green, G. Fontaine, & S. Charpinet, 301
 Barlow, B. N., Dunlap, B. H., & Clemens, J. C. 2011, *ApJ*, 737, L2
 Barlow, B. N., Kilkeny, D., Drechsel, H., et al. 2013, *MNRAS*, 430, 22
 Bloemen, S., Marsh, T. R., Østensen, R. H., et al. 2011, *MNRAS*, 410, 1787
 Brown, W. R., Kilic, M., Allende Prieto, C., Gianninas, A., & Kenyon, S. J. 2013, *ApJ*, 769, 66

Brown, W. R., Kilic, M., Allende Prieto, C., & Kenyon, S. J. 2010, *ApJ*, 723, 1072
 Charpinet, S., Van Grootel, V., Reese, D., et al. 2008, *A&A*, 489, 377
 Clausen, D., Wade, R. A., Kopparapu, R. K., & O'Shaughnessy, R. 2012, *ApJ*, 746, 186
 Coenen, T., van Leeuwen, J., & Stairs, I. H. 2011, *A&A*, 531, A125
 Copperwheat, C. M., Morales-Rueda, L., Marsh, T. R., Maxted, P. F. L., & Heber, U. 2011, *MNRAS*, 415, 1381
 Deca, J., Marsh, T. R., Østensen, R. H., et al. 2012, *MNRAS*, 421, 2798
 Dorman, B., Rood, R. T., & O'Connell, R. W. 1993, *ApJ*, 419, 596
 Downes, R. A. 1986, *ApJS*, 61, 569
 Drechsel, H., Heber, U., Napiwotzki, R., et al. 2001, *A&A*, 379, 893
 Edelmann, H. 2008, in *Astronomical Society of the Pacific Conference Series*, Vol. 392, *Hot Subdwarf Stars and Related Objects*, ed. U. Heber, C. S. Jeffery, & R. Napiwotzki, 187
 Edelmann, H., Heber, U., Altmann, M., Karl, C., & Lisker, T. 2005, *A&A*, 442, 1023
 Edelmann, H., Heber, U., Lisker, T., & Green, E. M. 2004, *Ap&SS*, 291, 315
 Edelmann, H., Heber, U., Napiwotzki, R., Reid, I. N., & Saffer, R. A. 1999, in *Astronomical Society of the Pacific Conference Series*, Vol. 169, *11th European Workshop on White Dwarfs*, ed. S.-E. Solheim & E. G. Meistas, 546
 Eggleton, P. P. 1983, *ApJ*, 268, 368
 Ferdman, R. D., Stairs, I. H., Kramer, M., et al. 2010, *ApJ*, 711, 764
 Fontaine, G., Brassard, P., Charpinet, S., et al. 2012, *A&A*, 539, A12
 For, B.-Q., Edelmann, H., Green, E. M., et al. 2008, in *Astronomical Society of the Pacific Conference Series*, Vol. 392, *Hot Subdwarf Stars and Related Objects*, ed. U. Heber, C. S. Jeffery, & R. Napiwotzki, 203
 For, B.-Q., Green, E. M., Fontaine, G., & Shaw, S. 2010, *Ap&SS*, 329, 87
 For, B.-Q., Green, E. M., O'Donoghue, D., et al. 2006, *ApJ*, 642, 1117
 Geier, S., Classen, L., Brünner, P., et al. 2012a, in *Astronomical Society of the Pacific Conference Series*, Vol. 452, *Fifth Meeting on Hot Subdwarf Stars and Related Objects*, ed. D. Kilkeny, C. S. Jeffery, & C. Koen, 153
 Geier, S., Heber, U., Edelmann, H., et al. 2013a, *A&A*, 557, A122
 Geier, S., Heber, U., Kupfer, T., & Napiwotzki, R. 2010a, *A&A*, 515, A37
 Geier, S., Heber, U., Podsiadlowski, P., et al. 2010b, *A&A*, 519, A25
 Geier, S., Hirsch, H., Tillich, A., et al. 2011a, *A&A*, 530, A28
 Geier, S., Karl, C., Edelmann, H., Heber, U., & Napiwotzki, R. 2006, in *International Symposium on Nuclear Astrophysics - Nuclei in the Cosmos*
 Geier, S., Marsh, T. R., Wang, B., et al. 2013b, *A&A*, 554, A54
 Geier, S., Maxted, P. F. L., Napiwotzki, R., et al. 2011b, *A&A*, 526, A39
 Geier, S., Napiwotzki, R., Heber, U., & Nelemans, G. 2011c, *A&A*, 528, L16
 Geier, S., Nesslinger, S., Heber, U., et al. 2007, *A&A*, 464, 299
 Geier, S., Nesslinger, S., Heber, U., et al. 2008, *A&A*, 477, L13
 Geier, S., Østensen, R. H., Heber, U., et al. 2014, *A&A*, 562, A95
 Geier, S., Schaffenroth, V., Drechsel, H., et al. 2011d, *ApJ*, 731, L22
 Geier, S., Schaffenroth, V., Hirsch, H., et al. 2012b, *Astronomische Nachrichten*, 333, 431
 Gianninas, A., Dufour, P., Kilic, M., et al. 2014, *ArXiv e-prints*
 Green, E. M., Fontaine, G., Hyde, E. A., Charpinet, S., & Chayer, P. 2006, *Baltic Astronomy*, 15, 167
 Green, E. M., Fontaine, G., Hyde, E. A., For, B.-Q., & Chayer, P. 2008, in *Astronomical Society of the Pacific Conference Series*, Vol. 392, *Hot Subdwarf Stars and Related Objects*, ed. U. Heber, C. S. Jeffery, & R. Napiwotzki, 75
 Green, E. M., For, B., Hyde, E. A., et al. 2004, *Ap&SS*, 291, 267
 Green, E. M., For, B.-Q., & Hyde, E. A. 2005, in *Astronomical Society of the Pacific Conference Series*, Vol. 334, *14th European Workshop on White Dwarfs*, ed. D. Koester & S. Moehler, 363
 Green, R. F., Schmidt, M., & Liebert, J. 1986, *ApJS*, 61, 305
 Hagen, H.-J., Groote, D., Engels, D., & Reimers, D. 1995, *A&AS*, 111, 195
 Han, Z., Podsiadlowski, P., Maxted, P. F. L., & Marsh, T. R. 2003, *MNRAS*, 341, 669
 Han, Z., Podsiadlowski, P., Maxted, P. F. L., Marsh, T. R., & Ivanova, N. 2002, *MNRAS*, 336, 449
 Heber, U. 1986, *A&A*, 155, 33
 Heber, U. 2009, *ARA&A*, 47, 211
 Heber, U., Drechsel, H., Østensen, R., et al. 2004, *A&A*, 420, 251
 Heber, U., Edelmann, H., Lisker, T., & Napiwotzki, R. 2003, *A&A*, 411, L477
 Heber, U., Moehler, S., Napiwotzki, R., Thejll, P., & Green, E. M. 2002, *A&A*, 383, 938
 Heber, U., Reid, I. N., & Werner, K. 2000, *A&A*, 363, 198
 Høg, E., Fabricius, C., Makarov, V. V., et al. 2000, *A&A*, 355, L27
 Ivanova, N., Justham, S., Chen, X., et al. 2013, *A&A Rev.*, 21, 59
 Jester, S., Schneider, D. P., Richards, G. T., et al. 2005, *AJ*, 130, 873
 Kaltenecker, L., & Traub, W. A. 2009, *ApJ*, 698, 519
 Kaplan, D. L., Bhallerao, V. B., van Kerkwijk, M. H., et al. 2013, *ApJ*, 765, 158
 Karl, C., Heber, U., Jeffery, S., Napiwotzki, R., & Geier, S. 2006, *Baltic Astronomy*, 15, 151
 Kawka, A., Pigulski, A., O'Toole, S., et al. 2012, in *Astronomical Society of the Pacific Conference Series*, Vol. 452, *Fifth Meeting on Hot Subdwarf Stars and Related Objects*, ed. D. Kilkeny, C. S. Jeffery, & C. Koen, 121

- Kilkenny, D., O'Donoghue, D., Koen, C., Stobie, R. S., & Chen, A. 1997, *MNRAS*, 287, 867
- Kleinman, S. J., Kepler, S. O., Koester, D., et al. 2013, *ApJS*, 204, 5
- Klepp, S. & Rauch, T. 2011, *A&A*, 531, L7
- Koen, C., Orosz, J. A., & Wade, R. A. 1998, *MNRAS*, 300, 695
- Kraus, A. L. & Hillenbrand, L. A. 2007, *AJ*, 134, 2340
- Kupfer, T., Geier, S., McLeod, A., et al. 2014, in *Astronomical Society of the Pacific Conference Series*, Vol. 481, *Astronomical Society of the Pacific Conference Series*, ed. V. van Grootel, E. Green, G. Fontaine, & S. Charpinet, 293
- Landolt, A. U. 2007, *AJ*, 133, 2502
- Landolt, A. U. 2009, *AJ*, 137, 4186
- Lisker, T., Heber, U., Napiwotzki, R., et al. 2005, *A&A*, 430, 223
- Maxted, P. F. L., Heber, U., Marsh, T. R., & North, R. C. 2001, *MNRAS*, 326, 1391
- Maxted, P. F. L., Marsh, T. R., Heber, U., et al. 2002, *MNRAS*, 333, 231
- Maxted, P. F. L., Marsh, T. R., & North, R. C. 2000a, *MNRAS*, 317, L41
- Maxted, P. F. L., Moran, C. K. J., Marsh, T. R., & Gatti, A. A. 2000b, *MNRAS*, 311, 877
- Mereghetti, S., Campana, S., Esposito, P., La Palombara, N., & Tiengo, A. 2011, *A&A*, 536, A69
- Mereghetti, S., La Palombara, N., Esposito, P., et al. 2014, *ArXiv e-prints*
- Mereghetti, S., Tiengo, A., Esposito, P., et al. 2009, *Science*, 325, 1222
- Mermilliod, J.-C. 1992, *Highlights of Astronomy*, 9, 725
- Morales-Rueda, L., Maxted, P. F. L., Marsh, T. R., North, R. C., & Heber, U. 2003, *MNRAS*, 338, 752
- Moran, C., Maxted, P., Marsh, T. R., Saffer, R. A., & Livio, M. 1999, *MNRAS*, 304, 535
- Müller, S., Geier, S., & Heber, U. 2010, *Ap&SS*, 329, 101
- Napiwotzki, R., Christlieb, N., Drechsel, H., et al. 2001a, *Astronomische Nachrichten*, 322, 411
- Napiwotzki, R., Edelmann, H., Heber, U., et al. 2001b, *A&A*, 378, L17
- Napiwotzki, R., Karl, C. A., Lisker, T., et al. 2004a, *Ap&SS*, 291, 321
- Napiwotzki, R., Yungelson, L., Nelemans, G., et al. 2004b, in *Astronomical Society of the Pacific Conference Series*, Vol. 318, *Spectroscopically and Spatially Resolving the Components of the Close Binary Stars*, ed. R. W. Hilditch, H. Hensberge, & K. Pavlovski, 402–410
- Naslim, N., Geier, S., Jeffery, C. S., et al. 2012, *MNRAS*, 423, 3031
- Nebot Gómez-Morán, A., Gänsicke, B. T., Schreiber, M. R., et al. 2011, *A&A*, 536, A43
- Nelemans, G. 2010, *Ap&SS*, 329, 25
- Németh, P., Kawka, A., & Vennes, S. 2012, *MNRAS*, 427, 2180
- O'Donoghue, D., Kilkenny, D., Koen, C., et al. 2013, *MNRAS*, 431, 240
- Orosz, J. A. & Wade, R. A. 1999, *MNRAS*, 310, 773
- Østensen, R., Oreiro, R., Drechsel, H., et al. 2007, in *Astronomical Society of the Pacific Conference Series*, Vol. 372, *15th European Workshop on White Dwarfs*, ed. R. Napiwotzki & M. R. Burleigh, 483
- Østensen, R. H., Geier, S., Schaffenroth, V., et al. 2013, *A&A*, 559, A35
- Østensen, R. H., Green, E. M., Bloemen, S., et al. 2010a, *MNRAS*, 408, L51
- Østensen, R. H., Silvotti, R., Charpinet, S., et al. 2010b, *MNRAS*, 409, 1470
- Østensen, R. H., Teltting, J. H., Reed, M. D., et al. 2014, *A&A*, 569, A15
- Østensen, R. H. & Van Winckel, H. 2012, in *Astronomical Society of the Pacific Conference Series*, Vol. 452, *Fifth Meeting on Hot Subdwarf Stars and Related Objects*, ed. D. Kilkenny, C. S. Jeffery, & C. Koen, 163
- O'Toole, S. J. & Heber, U. 2006, *A&A*, 452, 579
- O'Toole, S. J., Heber, U., & Benjamin, R. A. 2004, *A&A*, 422, 1053
- O'Toole, S. J., Napiwotzki, R., Heber, U., et al. 2006, *Baltic Astronomy*, 15, 61
- Paczynski, B. 1967, *Acta Astron.*, 17, 287
- Parsons, S. G., Marsh, T. R., Gänsicke, B. T., et al. 2012, *MNRAS*, 419, 304
- Pfahl, E., Rappaport, S., & Podsiadlowski, P. 2003, *ApJ*, 597, 1036
- Piro, A. L. 2011, *ApJ*, 740, L53
- Podsiadlowski, P., Rappaport, S., & Pfahl, E. D. 2002, *ApJ*, 565, 1107
- Pyrzas, S., Gänsicke, B. T., Brady, S., et al. 2012, *MNRAS*, 419, 817
- Raghavan, D., McAlister, H. A., Henry, T. J., et al. 2010, *ApJS*, 190, 1
- Ramspeck, M., Heber, U., & Edelmann, H. 2001, *A&A*, 379, 235
- Reed, M. D. & Stiening, R. 2004, *PASP*, 116, 506
- Saffer, R. A., Bergeron, P., Koester, D., & Liebert, J. 1994, *ApJ*, 432, 351
- Schaffenroth, V., Geier, S., Barbu-Barna, I., et al. 2014a, in *Astronomical Society of the Pacific Conference Series*, Vol. 481, *Astronomical Society of the Pacific Conference Series*, ed. V. van Grootel, E. Green, G. Fontaine, & S. Charpinet, 253
- Schaffenroth, V., Geier, S., Drechsel, H., et al. 2013, *A&A*, 553, A18
- Schaffenroth, V., Geier, S., Heber, U., et al. 2014b, *A&A*, 564, A98
- Schlafly, E. F. & Finkbeiner, D. P. 2011, *ApJ*, 737, 103
- Silvotti, R., Østensen, R. H., Bloemen, S., et al. 2012, *MNRAS*, 424, 1752
- Stark, M. A. & Wade, R. A. 2003, *AJ*, 126, 1455
- Stobie, R. S., Kilkenny, D., O'Donoghue, D., et al. 1997, *MNRAS*, 287, 848
- Stroerer, A., Heber, U., Lisker, T., et al. 2007, *A&A*, 462, 269
- Teltting, J. H., Baran, A. S., Németh, P., et al. 2014, *A&A* in press
- Teltting, J. H., Østensen, R. H., Baran, A. S., et al. 2012, *A&A*, 544, A1
- Tillich, A., Heber, U., Geier, S., et al. 2011, *A&A*, 527, A137
- Tutukov, A. V. & Yungelson, L. R. 1981, *Nauchnye Informatsii*, 49, 3
- Udalski, A., Szymanski, M., Kubiak, M., et al. 2002, *Acta Astron.*, 52, 217
- Vennes, S., Kawka, A., O'Toole, S. J., Németh, P., & Burton, D. 2012, *ApJ*, 759, L25
- Verbeek, K., Groot, P. J., Scaringi, S., et al. 2012, *MNRAS*, 426, 1235
- Vos, J., Østensen, R. H., Degroote, P., et al. 2012, *A&A*, 548, A6
- Vos, J., Østensen, R. H., Németh, P., et al. 2013, *A&A*, 559, A54
- Vučković, M., Aerts, C., Østensen, R., et al. 2007, *A&A*, 471, 605
- Wang, B., Justham, S., & Han, Z. 2013, *A&A*, 559, A94
- Webbink, R. F. 1984, *ApJ*, 277, 355
- Wesemael, F., Fontaine, G., Bergeron, P., Lamontagne, R., & Green, R. F. 1992, *AJ*, 104, 203
- Wisotzki, L., Koehler, T., Groote, D., & Reimers, D. 1996, *A&AS*, 115, 227
- Wood, J. H. & Saffer, R. 1999, *MNRAS*, 305, 820
- Yoon, S.-C. & Langer, N. 2004, *A&A*, 419, 645
- York, D. G., Adelman, J., Anderson, Jr., J. E., et al. 2000, *AJ*, 120, 1579
- Yungelson, L. R. & Tutukov, A. V. 2005, *Astronomy Reports*, 49, 871
- Zorotovic, M., Schreiber, M. R., & Gänsicke, B. T. 2011, *A&A*, 536, A42

Appendix A:

Table A.1. Atmospheric parameters

Object	T_{eff} [K]	$\log g$	$\log y$	Instrument
J01185–00254	26700 ± 1000	5.36 ± 0.15	-3.0	SDSS
	27700 ± 600	5.55 ± 0.09	< -3.0	TWIN
	28000 ± 350	5.55 ± 0.05	< -3.0	Goodman
	27900 ± 600	5.55 ± 0.07	< -3.0	adopted
J03213+05384	30200 ± 500	5.74 ± 0.11	-2.4	SDSS
	30700 ± 100	5.73 ± 0.02	-2.3	ISIS
	31200 ± 300	5.74 ± 0.05	-2.5	Goodman
	30700 ± 500	5.74 ± 0.06	-2.4 ± 0.1	adopted
J08233+11364	31300 ± 600	5.78 ± 0.12	-1.9	SDSS
	31100 ± 200	5.78 ± 0.03	-2.0	ISIS
	31200 ± 400	5.80 ± 0.06	-2.0	Goodman
	31200 ± 600	5.79 ± 0.06	-2.0 ± 0.1	adopted
J08300+47515	25200 ± 500	5.30 ± 0.05	-3.3 ± 0.7	SDSS†
	25400 ± 200	5.45 ± 0.02	< -3.0	ISIS
	25300 ± 600	5.38 ± 0.06	< -3.0	adopted
J09510+03475	29800 ± 300	5.48 ± 0.04	-2.8 ± 0.3	SDSS†
	29800 ± 300	5.48 ± 0.04	-2.8 ± 0.3	adopted
J09523+62581	27800 ± 500	5.61 ± 0.08	-2.6	SDSS†
	27600 ± 200	5.56 ± 0.02	-2.5	ISIS
	27700 ± 600	5.59 ± 0.06	-2.6 ± 0.1	adopted
J10215+30101	30700 ± 500	5.71 ± 0.06	< -3.0	SDSS†
	30000 ± 200	5.63 ± 0.02	-2.5	ISIS
	30400 ± 600	5.67 ± 0.06	-2.6 ± 0.1	adopted
J1132–0636	46400 ± 1900	5.83 ± 0.11	-2.7	SDSS
	46400 ± 500	5.94 ± 0.03	-3.0	ISIS
	46400 ± 1000	5.89 ± 0.07	-2.9 ± 0.2	adopted
J13463+28172	28000 ± 800	5.38 ± 0.12	-2.7	SDSS
	29500 ± 200	5.54 ± 0.02	-2.4	GMOS
	28800 ± 600	5.46 ± 0.07	-2.6 ± 0.2	adopted
J15082+49405	28200 ± 600	5.34 ± 0.09	-2.0 ± 0.2	SDSS†
	27000 ± 1100	5.28 ± 0.19	-2.2	GMOS
	29500 ± 600	5.76 ± 0.10	-2.3	TWIN
	29600 ± 300	5.70 ± 0.05	-2.3	ISIS
	29600 ± 600	5.73 ± 0.07	-2.3 ± 0.1	adopted
J15222–01301	24800 ± 1000	5.52 ± 0.15	-2.6 ± 0.5	SDSS†
	25600 ± 500	5.41 ± 0.07	< -3.0	ISIS
	25200 ± 700	5.47 ± 0.09	< -3.0	adopted
J18324+63091	26700 ± 1100	5.26 ± 0.17	-2.5	SDSS
	26900 ± 200	5.32 ± 0.03	-2.7	ISIS
	26800 ± 700	5.29 ± 0.09	-2.6 ± 0.1	adopted

Notes. † Parameters taken from Geier et al. (2011a)

Table A.2. Orbital parameters of all published helium burning hot subdwarf binaries

Object	T_{eff} [K]	$\log g$	Period [days]	γ [km s $^{-1}$]	K [km s $^{-1}$]	References
PG0850+170	27100±1000	5.37±0.10	27.815±0.005	32.2±2.8	33.5±3.3	[1,47]
EGB5	34500±500	5.85±0.05	16.532±0.003	68.5±0.7	16.1±0.8	[2]
PG0919+273	32900	5.90	15.5830±0.00005	-68.6±0.6	41.5±0.8	[3]
PG1619+522	32300±1000	5.98±0.10	15.3578±0.0008	-52.5±1.1	35.2±1.1	[1,47]
KIC7668647	27680±310	5.50±0.03	14.1742±0.0042	-27.4±1.3	38.9±1.9	[4]
CS1246	28500±700	5.46±0.11	14.105±0.011	67.2±1.7	16.6±0.6	[5]
LB1516	25200±1100	5.41±0.12	10.3598±0.00005	14.3±1.1	48.6±1.4	[6]
PG1558-007	20300±1000	5.00±0.10	10.3495±0.00006	-71.9±0.7	42.8±0.8	[3,48]
KIC11558725	27900±500	5.41±0.05	10.0545±0.0048	-66.1±1.4	58.1±1.7	[7]
PG1110+294	30100±1000	5.72±0.10	9.4152±0.0002	-15.2±0.9	58.7±1.2	[1,47]
EC20260-4757	-	-	8.952±0.0002	56.6±1.6	57.1±1.9	[3]
Feige108	34500±1000	6.01±0.15	8.74651±0.00001	45.8±0.6	50.2±1.0	[8,49]
PG0940+068	-	-	8.330±0.003	-16.7±1.4	61.2±1.4	[9]
PHL861	30000±500	5.50±0.05	7.44±0.015	-26.5±0.4	47.9±0.4	[10]
J032138+053840	30700±500	5.74±0.06	7.4327±0.0004	-16.7±2.1	39.7±2.8	This work
HE1448-0510	34700±500	5.59±0.05	7.159±0.005	-45.5±0.8	53.7±1.1	[10]
PG1439-013	-	-	7.2914±0.00005	-53.7±1.6	50.7±1.5	[3]
J095238+625818	27700±600	5.59±0.06	6.98±0.04	-35.4±3.6	62.5±3.4	This work
PG1032+406	31600±900	5.77±0.10	6.7791±0.0001	24.5±0.5	33.7±0.5	[1,47]
PG0907+123	26200±900	5.30±0.10	6.11636±0.00006	56.3±1.1	59.8±0.9	[1,47]
HE1115-0631	40400±1000	5.80±0.10	5.87±0.001	87.1±1.3	61.9±1.1	[11,50]
CD-24731	35400±500	5.90±0.05	5.85±0.003	20.0±5.0	63.0±3.0	[12,51]
PG1244+113	36300	5.54	5.75211±0.00009	7.4±0.8	54.4±1.4	[3]
PG0839+399	37800±900	5.53±0.10	5.6222±0.0002	23.2±1.1	33.6±1.5	[1]
J183249+630910	26800±700	5.29±0.09	5.4±0.2	-32.5±2.1	62.1±3.3	This work
EC20369-1804	-	-	4.5095±0.00004	7.2±1.6	51.5±2.3	[3]
TONS135	25000±1250	5.60±0.20	4.1228±0.0008	-3.7±1.1	41.4±1.5	[12,52]
PG0934+186	35800	5.65	4.051±0.001	7.7±3.2	60.3±2.4	[3]
PB7352	25000±500	5.35±0.10	3.62166±0.000005	-2.1±0.3	60.8±0.3	[12,53]
KPD0025+5402	28200±900	5.37±0.10	3.5711±0.0001	-7.8±0.7	40.2±1.1	[1]
KIC10553698	27423±293	5.436±0.024	3.387±0.014	52.1±1.5	64.8±2.2	[65]
PG0958-073	26100±500	5.58±0.05	3.18095±0.000007	90.5±0.8	27.6±1.4	[3,54]
PG1253+284	-	-	3.01634±0.000005	17.8±0.6	24.8±0.9	[3]
TON245	25200±1000	5.30±0.15	2.501±0.000	-	88.3	[1,49]
PG1300+279	29600±900	5.65±0.10	2.25931±0.0001	-3.1±0.9	62.8±1.6	[1,47]
CPD-201123	23500±500	4.90±0.10	2.3098±0.0003	-6.3±1.2	43.5±0.9	[13]
NGC188/II-91	-	-	2.15	-	22.0	[14]
J134632+281722	28800±600	5.46±0.07	1.96±0.03	1.2±1.2	85.6±3.4	This work
V1093Her	27400±800	5.47±0.10	1.77732±0.000005	-3.9±0.8	70.8±1.0	[1,47]
PG1403+316	31200	5.75	1.73846±0.000001	-2.1±0.9	58.5±1.8	[3]
HD171858	27200±800	5.30±0.10	1.63280±0.000005	62.5±0.1	60.8±0.3	[12,53]
J002323-002953	29200±500	5.69±0.05	1.4876±0.0001	16.4±2.1	81.8±2.9	[15]
KPD2040+3955	27900	5.54	1.482860±0.0000004	-16.4±1.0	94.0±1.5	[3]
HE2150-0238	30200±500	5.83±0.07	1.321±0.005	-32.5±0.9	96.3±1.4	[10,55]
J011857-002546	27900±600	5.55±0.07	1.30±0.02	37.7±1.8	54.8±2.9	This work
UVO1735+22	38000±500	5.54±0.05	1.278±0.001	20.6±0.4	103.0±1.5	[12,53]
PG1512+244	29900±900	5.74±0.10	1.26978±0.000002	-2.9±1.0	92.7±1.5	[1,47]
PG0133+114	29600±900	5.66±0.10	1.23787±0.000003	-0.3±0.2	82.0±0.3	[12,1]
HE1047-0436	30200±500	5.66±0.05	1.21325±0.00001	25.0±3.0	94.0±3.0	[16]
PG2331+038	27200	5.58	1.204964±0.0000003	-9.5±1.1	93.5±1.9	[3]
HE1421-1206	29600±500	5.55±0.07	1.188±0.001	-86.2±1.1	55.5±2.0	[17,55]
J113241-063652	46400±000	5.89±0.07	1.06±0.02	8.3±2.2	41.1±4.0	This work
PG1000+408	36400±900	5.54±0.10	1.049343±0.0000005	56.6±3.4	63.5±3.0	[3,47]
J150829+494050	29600±600	5.73±0.07	0.967164±0.000009	-60.0±10.7	93.6±5.8	This work
PG1452+198	29400	5.75	0.96498±0.000004	-9.1±2.1	86.8±1.9	[3]
HS2359+1942	31400±500	5.56±0.07	0.93261±0.00005	-96.1±6.0	107.4±6.8	[6,55]
PB5333	40600±500	5.96±0.10	0.92560±0.0000012	-95.3±1.3	22.4±0.8	[8,54]
HE2135-3749	30000±500	5.84±0.05	0.9240±0.0003	45.0±0.5	90.5±0.6	[10]
EC12408-1427	-	-	0.90243±0.000001	-52.2±1.2	58.6±1.5	[3]
PG0918+029	31700±900	6.03±0.10	0.87679±0.000002	104.4±1.7	80.0±2.6	[1,47]
PG1116+301	32500±1000	5.85±0.10	0.85621±0.000003	-0.2±1.1	88.5±2.1	[1,47]
PG1230+052	27100	5.47	0.837177±0.0000003	-43.1±0.7	40.4±1.2	[3]
EC21556-5552	-	-	0.8340±0.00007	31.4±2.0	65.0±3.4	[3]
V2579Oph	23500±500	5.40±0.10	0.8292056±0.0000014	-54.16±0.27	70.1±0.13	[18,53]
EC13332-1424	-	-	0.82794±0.000001	-53.2±1.8	104.1±3.0	[3]

Table A.2. continued.

Object	T_{eff}	$\log g$	Period [days]	γ [km s $^{-1}$]	K [km s $^{-1}$]	References
TONS183	27600±500	5.43±0.05	0.8277±0.00002	50.5±0.8	84.8±1.0	[12,53]
KPD2215+5037	29600	5.64	0.809146±0.0000002	-7.2±1.0	86.0±1.5	[3]
EC02200-2338	-	-	0.8022±0.00007	20.7±2.3	96.4±1.4	[3]
J150513+110836	33200±500	5.80±0.10	0.747773±0.00005	-77.1±1.2	97.2±1.8	[15]
PG0849+319	28900±900	5.37±0.10	0.74507±0.000001	64.0±1.5	66.3±2.1	[1,47]
JL82	26500±500	5.22±0.10	0.73710±0.00005	-1.6±0.8	34.6±1.0	[12,53]
PG1248+164	26600±800	5.68±0.10	0.73232±0.000002	-16.2±1.3	61.8±1.1	[1,47]
EC22202-1834	-	-	0.70471±0.000005	-5.5±3.9	118.6±5.8	[3]
J225638+065651	28500±500	5.64±0.05	0.7004±0.0001	-7.3±2.1	105.3±3.4	[15]
J152222-013018	25200±700	5.47±0.09	0.67162±0.00003	-79.5±2.7	80.1±3.5	This work
PG1648+536	31400	5.62	0.6109107±0.00000004	-69.9±0.9	109.0±1.3	[3]
PG1247+554	-	-	0.602740±0.000006	13.8±0.6	32.2±1.0	[9]
PG1725+252	28900±900	5.54±0.10	0.601507±0.0000003	-60.0±0.6	104.5±0.7	[1,47]
EC20182-6534	-	-	0.598819±0.0000006	13.5±1.9	59.7±3.2	[3]
PG0101+039	27500±500	5.53±0.07	0.569899±0.000001	7.3±0.2	104.7±0.4	[19]
HE1059-2735	41000±1000	5.38±0.10	0.555624	-44.7±0.6	87.7±0.8	[11,50]
PG1519+640	30600	5.72	0.54029143±0.0000000025	0.1±0.4	42.7±0.6	[8,3]
PG0001+275	25400±500	5.30±0.10	0.529842±0.0000005	-44.7±0.5	92.8±0.7	[12,53]
PG1743+477	27600±800	5.57±0.10	0.515561±0.0000001	-65.8±0.8	121.4±1.0	[1]
J172624+274419	32600±500	5.84±0.05	0.50198±0.00005	-36.7±4.8	118.9±3.7	[15]
HE1318-2111	36300±1000	5.42±0.10	0.487502±0.0000001	48.9±0.7	48.5±1.2	[11,50]
KUV16256+4034	23100	5.38	0.4776±0.00008	-90.9±0.9	38.7±1.2	[3]
GALEXJ2349+3844	23800±350	5.38±0.06	0.462516±0.000005	2.0±1.0	87.9±2.2	[20,56]
HE0230-4323	31100±500	5.60±0.07	0.45152±0.00002	16.6±1.0	62.4±1.6	[12,55]
HE0929-0424	29500±500	5.71±0.05	0.4400±0.0002	41.4±1.0	114.3±1.4	[10]
UVO1419-09	-	-	0.4178±0.00002	42.3±0.3	109.6±0.4	[12]
J095101+034757	29800±300	5.48±0.04	0.4159±0.0007	111.1±2.5	84.4±4.2	This work
KPD1946+4340	34200±500	5.43±0.10	0.403739±0.0000008	-5.5±1.0	156.0±2.0	[21,53]
V1405Ori	35100±800	5.66±0.11	0.398	-33.6±5.5	85.1±8.6	[6]
Feige48	29500±500	5.54±0.05	0.376±0.003	-47.9±0.1	28.0±0.2	[22,51]
GD687	24300±500	5.32±0.07	0.37765±0.00002	32.3±3.0	118.3±3.4	[23,55]
PG1232-136	26900±500	5.71±0.05	0.3630±0.0003	4.1±0.3	129.6±0.04	[12,53]
PG1101+249	29700±500	5.90±0.07	0.35386±0.00006	-0.8±0.9	134.6±1.3	[24,57]
PG1438-029	27700±1000	5.50±0.15	0.336	-	32.1	[25,49]
PG1528+104	27200	5.46	0.331±0.0001	-49.3±1.0	53.3±1.6	[3]
PHL457	26500±1100	5.38±0.12	0.3128±0.0007	-	12.8±0.08	[26,54]
PG0941+280	29400±500	5.43±0.05	0.311	73.7±4.3	141.7±6.3	[6]
HS2043+0615	26200±500	5.28±0.07	0.3015±0.0003	-43.5±3.4	73.7±4.3	[6,55]
J102151+301011	30400±600	5.67±0.06	0.2966±0.0001	-28.4±4.8	114.5±5.2	This work
KBS13	29700±500	5.70±0.05	0.2923±0.0004	7.53±0.08	22.82±0.23	[27,58]
CPD-64481	27500±500	5.60±0.05	0.277263±0.000005	94.1±0.3	23.9±0.05	[26,51]
GALEXJ0321+4727	28000±400	5.34±0.07	0.265856±0.000003	69.6±2.2	60.8±4.5	[20,56]
HE0532-4503	25400±500	5.32±0.05	0.2656±0.0001	8.5±0.1	101.5±0.2	[10]
AA Dor	42000±1000	5.46±0.05	0.2614±0.0002	1.57±0.09	40.15±0.11	[28,59]
J165404+303701	24900±800	5.39±0.12	0.25357±0.00001	40.5±2.2	126.1±2.6	[15]
J012022+395059	29400±500	5.48±0.05	0.252013±0.000013	-47.3±1.3	37.3±2.8	[44]
PG1329+159	29100±900	5.62±0.10	0.249699±0.0000002	-22.0±1.2	40.2±1.1	[1,47]
J204613-045418	31600±500	5.54±0.08	0.24311±0.00001	87.6±5.7	134.3±7.8	[15]
PG2345+318	27500±1000	5.70±0.15	0.2409458±0.0000008	-10.6±1.4	141.2±1.1	[24,49]
PG1432+159	26900±1000	5.75±0.15	0.22489±0.00032	-16.0±1.1	120.0±1.4	[24,49]
BPSCS22169-0001	39300±500	5.60±0.05	0.214	-	16.2	[26,53]
J113840-003531	31200±600	5.54±0.09	0.207536±0.000002	23.3±3.7	162.0±3.8	[15]
J082332+113641	31200±600	5.79±0.06	0.20707±0.00002	135.1±2.0	169.4±2.5	This work
HS1741+2133	-	-	0.20±0.01	-112.8±2.7	157.0±3.4	[29]
HE1414-0309	29500±500	5.56±0.07	0.192±0.004	104.7±9.5	152.4±1.2	[6,55]
HS2333+3927	36500±1000	5.70±0.10	0.1718023±0.0000009	-31.4±2.1	89.6±3.2	[30]
J192059+372220	27500±1000	5.4±0.1	0.168876±0.00035	16.8±2.0	59.7±2.5	[64]
2M1533+3759	29200±500	5.58±0.05	0.16177042±0.00000001	-3.4±5.2	71.1±1.0	[31]
J083006+475150	25300±600	5.38±0.06	0.14780±0.00007	49.9±0.9	77.0±1.7	This work
ASAS102322-3737	28400±500	5.60±0.05	0.13926940±0.00000004	-	81.0±3.0	[32]
EC00404-4429	-	-	0.12834±0.000004	33.0±2.9	152.8±3.4	[3]
2M1938+4603	29600±500	5.43±0.05	0.1257653±0.000000021	20.1±0.3	65.7±0.6	[33]
BULSC16335	31500±1800	5.70±0.2	0.122	36.4±19.6	92.5±6.2	[6]
PG1043+760	27600±800	5.39±0.1	0.1201506±0.00000003	24.8±1.4	63.6±1.4	[1,47]
EC10246-2707	28900±500	5.64±0.06	0.1185079935±0.00000000091	-	71.6±1.7	[34]
HWVir	28500±500	5.63±0.05	0.115±0.0008	-13.0±0.8	84.6±1.1	[35,60]
HS2231+2441	28400±500	5.39±0.05	0.1105880±0.0000005	-	49.1±3.2	[36]

Table A.2. continued.

Object	T_{eff}	$\log g$	Period [days]	γ [km s $^{-1}$]	K [km s $^{-1}$]	References
NSVS14256825	40000±500	5.50±0.05	0.110374230±0.000000002	12.1±1.5	73.4±2.0	[37]
UVEX0328+5035	28500	5.50	0.11017±0.00011	44.9±0.7	64.0±1.5	[29,61]
PG1336-018	32800±500	5.76±0.05	0.101015999±0.00000001	-25.0	78.7±0.6	[38,62]
J082053+000843	26000±1000	5.37±0.14	0.096±0.001	9.5±1.3	47.4±1.9	[45]
HS0705+6700	28800±900	5.40±0.10	0.09564665±0.00000039	-36.4±2.9	85.8±3.6	[39]
KPD1930+2752	35200±500	5.61±0.06	0.0950933±0.0000015	5.0±1.0	341.0±1.0	[40]
KPD0422+5421	25000±1500	5.40±0.10	0.09017945±0.00000012	-57.0±12.0	237.0±8.0	[41,63]
PG1017-086	30300±500	5.61±0.10	0.0729938±0.0000003	-9.1±1.3	51.0±1.7	[42]
J162256+473051	29000±600	5.65±0.06	0.069789	-54.7±1.5	47.0±2.0	[46]
CD-3011223	29200±400	5.66±0.05	0.0489790717±0.0000000038	16.5±0.3	377.0±0.4	[43]

References. 1: Morales-Rueda et al. (2003); 2: Geier et al. (2011c); 3: Copperwheat et al. (2011); 4: Telting et al. in press; 5: Barlow et al. (2011); 6: Geier et al. (2014) 7: Telting et al. (2012); 8: Edelmann et al. (2004); 9: Maxted et al. (2000b); 10: Karl et al. (2006); 11: Napiwotzki et al. (2004a); 12: Edelmann et al. (2005); 13: Naslim et al. (2012); 14: Green et al. (2004); 15: Geier et al. (2011b); 16: Napiwotzki et al. (2001b); 17: Geier et al. (2006); 18: For et al. (2006); 19: Geier et al. (2008); 20: Kawka et al. (2012); 21: Bloemen et al. (2011); 22: O'Toole et al. (2004); 23: Geier et al. (2010a); 24: Moran et al. (1999); 25: Green et al. (2005); 26: Geier et al. (2012a); 27: For et al. (2008); 28: Müller et al. (2010); 29: Kupfer et al. (2014); 30: Heber et al. (2004); 31: For et al. (2010); 32: Schaffenroth et al. (2013); 33: Østensen et al. (2010a); 34: Barlow et al. (2013); 35: Edelmann (2008); 36: Østensen et al. (2007); 37: Almeida et al. (2012); 38: Vučković et al. (2007); 39: Drechsel et al. (2001); 40: Geier et al. (2007); 41: Orosz & Wade (1999); 42: Maxted et al. (2002); 43: Geier et al. (2013b); 44: Østensen et al. (2013); 45: Geier et al. (2011d); 46: Schaffenroth et al. (2014b); 47: Maxted et al. (2001); 48: Heber et al. (2002); 49: Saffer et al. (1994); 50: Stroerer et al. (2007); 51: O'Toole & Heber (2006); 52: Heber (1986); 53: Geier et al. (2010b); 54: Geier et al. (2013a); 55: Lisker et al. (2005); 56: Németh et al. (2012); 57: Edelmann et al. (1999); 58: Østensen et al. (2010b); 59: Klepp & Rauch (2011); 60: Wood & Saffer (1999); 61: Verbeek et al. (2012); 62: Charpinet et al. (2008); 63: Koen et al. (1998); 64: Schaffenroth et al. (2014a); 65: Østensen et al. (2014)

Table A.3. Photometry, spectroscopic distances and companion types

Object	V [mag]	J [mag]	H [mag]	Distances [kPc]	Comp. Type	References
PG0850+170	13.977±0.000	14.531±0.043	14.624±0.066	1.04 $^{+0.16}_{-0.15}$	MS/WD	[1,13]
EGB5	13.808±0.04	14.482±0.036	14.530±0.055	0.68 $^{+0.07}_{-0.06}$	MS/WD	[2,13]
PG0919+273	12.765±0.009	13.303±0.021	13.420±0.030	0.39 $^{+0.00}_{-0.00}$	WD	[1,13]
PG1619+522	13.297±0.006	13.883±0.027	13.969±0.040	0.44 $^{+0.08}_{-0.06}$	WD	[1,13]
KIC7668647	15.218±0.07	15.815±0.066	16.056±0.201 ^C	1.54 $^{+0.12}_{-0.12}$	WD ^{lc}	[2,13]
CS1246	14.371±0.03	14.013±0.039	14.032±0.058	-	MS/WD ^{lc}	[2,13]
LB1516	12.967±0.003	13.520±0.035	13.663±0.054	0.59 $^{+0.11}_{-0.10}$	WD	[3,13]
PG1558-007	13.528±0.006	-	-	0.84 $^{+0.15}_{-0.12}$	MS/WD	[1]
KIC11558725	14.859±0.04	15.379±0.046	15.352±0.088	1.45 $^{+0.14}_{-0.13}$	WD ^{lc}	[2,13]
PG1110+294	14.086±0.006	14.626±0.037	14.674±0.063	0.79 $^{+0.13}_{-0.11}$	WD	[1,13]
EC20260-4757	13.735±0.01	14.424±0.023	14.465±0.046	-	MS/WD	[2,13]
Feige108	12.973±0.000	13.529±0.024	13.704±0.032	0.39 $^{+0.08}_{-0.07}$	WD	[4,13]
PG0940+068	-	14.151±0.027	14.147±0.049	-	MS/WD	[13]
PHL861	14.826±0.04	15.375±0.051	15.496±0.103	1.45 $^{+0.14}_{-0.13}$	MS/WD	[2,13]
J032138+053840	15.048±0.04	15.148±0.050	15.402±0.135 ^B	1.02 $^{+0.11}_{-0.10}$	MS/WD	[2,13]
HE1448-0510	14.611±0.04	15.199±0.056	15.234±0.096	1.30 $^{+0.12}_{-0.11}$	WD	[2,13]
PG1439-013	13.943±0.028	14.506±0.035	14.692±0.041	-	MS/WD	[1,13]
J095238+625818	14.693±0.09	15.420±0.067	15.609±0.147 ^B	1.13 $^{+0.16}_{-0.14}$	WD	[2,13]
PG1032+406	11.519±0.009	12.166±0.022	12.275±0.018	0.25 $^{+0.04}_{-0.04}$	MS/WD	[1,13]
PG0907+123	13.970±0.003	14.474±0.030	14.666±0.066	1.08 $^{+0.17}_{-0.15}$	MS/WD	[1,13]
HE1115-0631	-	15.623±0.079	15.580±0.129 ^B	-	MS/WD	[13]
CD-24731	11.748±0.024	12.404±0.027	12.583±0.027	0.26 $^{+0.02}_{-0.02}$	WD	[5,13]
PG1244+113	14.197±0.018	14.821±0.004	14.939±0.007	1.21 $^{+0.01}_{-0.01}$	WD	[1,14]
PG0839+399	14.389±0.000	14.885±0.035	15.080±0.064	1.36 $^{+0.19}_{-0.16}$	MS/WD	[1,13]
J183249+630910	15.695±0.01	16.236±0.096	16.068±0.176 ^C	2.41 $^{+0.34}_{-0.30}$	MS/WD	[2,13]
EC20369-1804	13.29 ±0.00	13.937±0.022	14.061±0.044	-	MS/WD	[6,13]
TONS135	13.302±0.042	13.868±0.029	14.017±0.047	0.54 $^{+0.19}_{-0.14}$	MS/WD	[5,13]
PG0934+186	13.138±0.001	13.759±0.025	13.972±0.038	0.66 $^{+0.00}_{-0.00}$	WD	[1,13]
PB7352	12.261±0.01	12.819±0.026	12.915±0.025	0.44 $^{+0.06}_{-0.06}$	MS/WD	[2,13]

Table A.3. continued.

Object	V[mag]	J [mag]	H [mag]	Distances [kPc]	Comp. Type	References
KPD0025+5402	13.919±0.015	14.259±0.031	14.361±0.047	-	MS/WD	[1,13]
KIC10553698	14.902±0.08	15.446±0.047	15.538±0.092	-	WD ^{lc}	[2,13]
PG0958-073	13.563±0.002	14.098±0.030	14.139±0.039	0.63 ^{+0.05} _{-0.05}	MS/WD	[4,13]
PG1253+284	12.769±0.000	12.182±0.001	12.003±0.001	-	MS/WD	[1,13]
TON245	13.859±0.04	14.312±0.002	14.417±0.005	0.97 ^{+0.24} _{-0.20}	WD	[2,14]
PG1300+279	14.266±0.023	14.894±0.004	15.006±0.007	0.94 ^{+0.16} _{-0.13}	WD	[1,14]
CPD-201123	12.173±0.12	12.565±0.024	12.658±0.027	0.64 ^{+0.13} _{-0.11}	MS/WD	[2,13]
NGC188/II-91	-	-	-	-	MS/WD	[]
J134632+281722	14.908±0.07	15.513±0.007	15.595±0.010	1.53 ^{+0.21} _{-0.19}	WD	[2,14]
V1093Her	13.967±0.008	14.518±0.034	14.677±0.074	0.93 ^{+0.14} _{-0.13}	MS/WD ^{lc}	[1,13]
PG1403+316	13.532±0.010	14.179±0.023	14.376±0.041	0.63 ^{+0.00} _{-0.00}	WD	[1,13]
HD171858	9.85±0.04	10.321±0.023	10.432±0.022	-	MS/WD	[7,13]
J002323-002953	15.577±0.02	16.153±0.013	16.275±0.026	1.60 ^{+0.14} _{-0.14}	WD	[2,14]
KPD2040+3955	14.472±0.049	14.560±0.036	14.560±0.065	-	MS/WD	[1,13]
HE2150-0238	-	-	-	-	MS/WD	[]
J011857-002546	14.804±0.05	15.184±0.047	15.262±0.098	1.25 ^{+0.16} _{-0.15}	MS/WD	[2,13]
UVO1735+22	11.861±0.01	12.509±0.021	12.650±0.022	0.37 ^{+0.04} _{-0.04}	WD	[2,13]
PG1512+244	13.185±0.04	13.957±0.028	13.957±0.039	0.50 ^{+0.09} _{-0.07}	WD	[2,13]
PG0133+114	12.345±0.000	12.801±0.001	12.918±0.002	0.37 ^{+0.05} _{-0.05}	WD	[1,14]
HE1047-0436	14.796±0.000	15.527±0.060	15.637±0.123 ^B	1.19 ^{+0.09} _{-0.09}	WD	[1,13]
PG2331+038	14.974±0.025	15.361±0.005	15.404±0.012	1.20 ^{+0.02} _{-0.01}	WD	[1,14]
HE1421-1206	15.510±0.0	15.891±0.073	15.872±0.165 ^C	1.72 ^{+0.18} _{-0.16}	MS	[8,13.15]
J113241-063652	16.273±0.005	16.684±0.142 ^B	-	2.39 ^{+0.24} _{-0.21}	MS/WD	[9,13]
PG1000+408	13.327±0.023	13.978±0.027	14.244±0.043	0.83 ^{+0.12} _{-0.10}	MS/WD	[1,13]
J150829+494050	17.516±0.005	-	-	3.83 ^{+0.41} _{-0.37}	MS/WD	[9]
PG1452+198	12.476±0.002	13.055±0.023	13.179±0.025	0.90 ^{+0.00} _{-0.00}	WD	[1,13]
HS2359+1942	15.639±0.06	16.234±0.092	16.227±0.212 ^C	2.02 ^{+0.26} _{-0.24}	WD	[2,13]
PB5333	12.874±0.020	12.879±0.001	12.622±0.001	0.42 ^{+0.05} _{-0.06}	MS/WD	[1,14]
HE2135-3749	13.896±0.01	14.598±0.035	14.650±0.051	0.63 ^{+0.05} _{-0.05}	WD	[2,13]
EC12408-1427	12.823±0.02	13.390±0.029	13.465±0.035	-	MS/WD	[2,13]
PG0918+029	13.415±0.080	13.995±0.002	14.092±0.004	0.43 ^{+0.08} _{-0.07}	WD	[1,14]
PG1116+301	14.337±0.019	-	-	0.84 ^{+0.14} _{-0.12}	MS/WD	[1]
PG1230+052	13.287±0.018	13.835±0.002	13.965±0.003	0.67 ^{+0.01} _{-0.01}	MS/WD	[1,14]
EC21556-5552	13.090±0.04	13.718±0.029	13.862±0.047	-	MS/WD	[2,13]
V2579Oph	12.930±0.025	13.369±0.026	13.476±0.030	0.52 ^{+0.08} _{-0.07}	MS/WD ^{lc}	[1,13]
EC13332-1424	13.380±0.03	13.895±0.030	13.990±0.035	-	MS/WD	[2,13]
TONS183	12.598±0.02	13.232±0.026	13.361±0.028	0.52 ^{+0.05} _{-0.04}	MS/WD	[2,13]
KPD2215+5037	13.739±0.022	14.218±0.040	14.313±0.042	-	MS/WD	[1,13]
EC02200-2338	12.014±0.01	12.616±0.026	12.748±0.021	-	MS/WD	[2,13]
J150513+110836	15.378±0.09	16.043±0.006	16.151±0.015	1.44 ^{+0.26} _{-0.23}	WD	[2,14]
PG0849+319	14.606±0.000	15.177±0.044	15.318±0.095	1.46 ^{+0.23} _{-0.19}	MS/WD	[1,13]
JL82	12.389±0.003	12.857±0.024	12.960±0.025	0.57 ^{+0.08} _{-0.07}	MS	[3,13]
PG1248+164	14.460±0.03	15.037±0.037	15.013±0.080	0.89 ^{+0.15} _{-0.13}	MS/WD	[2,13]
EC22202-1834	13.802±0.03	14.389±0.033	14.431±0.049	-	MS/WD	[2,13]
J225638+065651	15.314±0.01	15.744±0.006	15.789±0.012	1.39 ^{+0.12} _{-0.10}	WD	[2,14]
J152222-013018	17.813±0.02	18.424±0.098	18.202±0.131	-	MS/WD	[9,14]
PG1648+536	14.055±0.017	14.553±0.029	14.587±0.051	0.88 ^{+0.01} _{-0.01}	WD	[1,13]
PG1247+554	12.259±0.01	-	11.087±0.017	-	MS/WD	[2,13]
PG1725+252	13.008±0.018	13.496±0.026	13.641±0.037	0.54 ^{+0.09} _{-0.07}	MS/WD	[1,13]
EC20182-6534	13.29 ±0.0	13.782±0.029	13.877±0.021	-	MS/WD	[6,13]
PG0101+039	12.065±0.000	12.609±0.001	12.724±0.002	0.36 ^{+0.04} _{-0.03}	WD ^{lc}	[4,14]

Table A.3. continued.

Object	V[mag]	J [mag]	H [mag]	Distances [kPc]	Comp. Type	References
HE1059-2735	15.500±0.06	16.051±0.089	16.329±0.206 ^C	2.73 ^{+0.46} _{-0.43}	MS/WD	[2,13]
PG1519+640	12.458±0.001	13.007±0.023	13.185±0.026	0.39 ^{+0.00} _{-0.00}	MS/WD	[1,13]
PG0001+275	-	13.833±0.024	13.971±0.041	-	MS/WD	[13]
PG1743+477	13.787±0.009	14.313±0.024	14.526±0.060	0.76 ^{+0.12} _{-0.10}	WD	[1,13]
J172624+274419	15.994±0.01	16.467±0.101	-	1.76 ^{+0.15} _{-0.13}	WD	[2,13]
HE1318-2111	14.718±0.09	15.218±0.049	15.288±0.089	1.64 ^{+0.30} _{-0.26}	MS/WD	[2,13]
KUV16256+4034	12.64 ±0.21	13.067±0.035	13.224±0.035	0.49 ^{+0.04} _{-0.05}	MS/WD	[7,13]
GALEXJ2349+3844	11.73 ±0.13	12.040±0.024	12.156±0.031	-	MS/WD	[7,13]
HE0230-4323	13.768±0.02	13.948±0.032	13.804±0.044	0.82 ^{+0.09} _{-0.08}	MS	[2,13]
HE0929-0424	16.165±0.15	16.646±0.112 ^B	-	2.06 ^{+0.31} _{-0.28}	MS/WD	[2,13]
UVO1419-09	12.115±0.09	12.692±0.023	12.835±0.025	-	WD	[2,13]
J095101+034757	15.895±0.02	15.972±0.007	15.705±0.013	2.37 ^{+0.17} _{-0.15}	MS/WD	[2,14]
KPD1946+4340	14.299±0.002	14.683±0.031	14.836±0.055	-	WD	[1,13]
V1405Ori	15.142±0.09	14.574±0.031	14.677±0.045	-	MS ^{lc}	[2,13]
Feige48	13.456±0.000	13.983±0.027	14.137±0.043	0.73 ^{+0.05} _{-0.06}	WD ^{lc}	[1,13]
GD687	14.077±0.03	14.618±0.033	14.874±0.077	1.04 ^{+0.12} _{-0.11}	WD	[2,13]
PG1232-136	13.336±0.033	13.758±0.028	13.897±0.040	0.50 ^{+0.05} _{-0.04}	WD	[1,13]
PG1101+249	12.775±0.03	13.187±0.027	13.257±0.039	0.36 ^{+0.03} _{-0.04}	WD	[2,13]
PG1438-029	-	14.168±0.029	14.240±0.053	-	MS	[13]
PG1528+104	13.569±0.010	14.082±0.002	14.156±0.004	0.77 ^{+0.01} _{-0.01}	WD	[1,14]
PHL457	12.947±0.010	13.499±0.026	13.595±0.021	0.62 ^{+0.12} _{-0.11}	MS	[2,13]
PG0941+280	13.265±0.07	13.799±0.029	13.899±0.042	0.75 ^{+0.09} _{-0.07}	WD ^{lc}	[2,13]
HS2043+0615	15.420± 0	16.098±0.093	-	2.02 ^{+0.20} _{-0.19}	MS	[8,13]
J102151+301011	18.218±0.007	-	-	5.74 ^{+0.55} _{-0.51}	MS/WD	[9]
KBS13	13.633±0.01	14.018±0.024	14.063±0.032	-	MS ^{lc}	[2,13]
CPD-64481	11.291±0.01	11.878±0.022	11.994±0.028	0.23 ^{+0.02} _{-0.02}	MS	[2,13]
GALEXJ0321+4727	11.73 ±0.15	11.795±0.001	11.923±0.001	-	MS	[7,14]
HE0532-4503	15.98 ±0.0	16.563±0.146 ^C	-	2.55 ^{+0.20} _{-0.18}	MS/WD	[10,13]
AADor	11.90 ±0.0	11.795±0.028	11.965±0.029	-	MS ^{lc}	[2,13]
J165404+303701	15.409±0.04	15.938±0.008	16.030±0.016	1.78 ^{+0.37} _{-0.30}	MS/WD	[2,14]
J012022+395059	15.341±0.07	16.016±0.078	15.925±0.175 ^C	1.79 ^{+0.19} _{-0.18}	MS	[2,13]
PG1329+159	13.507±0.03	14.047±0.002	14.221±0.004	0.67 ^{+0.12} _{-0.10}	MS	[2,13]
J204613-045418	16.324±0.01	16.677±0.143 ^B	16.308±0.217 ^D	2.81 ^{+0.33} _{-0.30}	MS/WD	[2,13]
PG2345+318	14.178±0.005	14.690±0.039	14.833±0.071	0.19 ^{+0.05} _{-0.03}	WD	[1,13]
PG1432+159	13.896±0.013	14.445±0.028	14.530±0.050	0.64 ^{+0.15} _{-0.12}	WD	[1,13]
BPSCS22169-0001	12.848±0.01	13.456±0.023	13.551±0.024	-	MS	[2,13]
J113840-003531	14.467±0.03	15.161±0.043	15.137±0.085	1.23 ^{+0.17} _{-0.16}	WD	[2,13]
J082332+113641	16.658±0.005	-	-	2.48 ^{+0.22} _{-0.21}	MS/WD	[2]
HS1741+2133	13.990±0.01	14.386±0.036	14.616±0.060	-	WD	[2,13]
HE1415-0309	16.487±0.0	-	-	2.76 ^{+0.27} _{-0.26}	WD	[9]
HS2333+3927	14.794±0.01	14.986±0.048	15.018±0.084	1.25 ^{+0.17} _{-0.15}	MS ^{lc}	[2,13]
J192059+372220	15.745±0.01	16.186±0.083	16.272±0.224 ^D	-	MS	[2,13]
2M1533+3759	12.964±0.17	13.652±0.026	13.736±0.031	0.55 ^{+0.09} _{-0.08}	MS ^{lc}	[2,13]
J083006+475150	16.043±0.03	16.737±0.143 ^B	16.477±0.220 ^D	2.44 ^{+0.27} _{-0.24}	WD	[2,13]
ASAS102322-3737	11.707±0.07	12.028±0.021	12.112±0.027	0.28 ^{+0.03} _{-0.03}	MS ^{lc}	[2,13]
EC00404-4429	13.674±0.02	14.220±0.030	14.424±0.052	-	WD	[2,13]
2M1938+4603	12.063±0.01	12.757±0.022	12.889±0.020	-	MS ^{lc}	[2,13]
BULSC16335	16.395±0.028	12.868±0.022	12.072±0.021	-	MS ^{lc}	[11,13]
PG1043+760	13.768±0.016	14.278±0.030	14.359±0.049	0.89 ^{+0.14} _{-0.12}	WD	[1,13]
EC10246-2707	14.38 ±0.0	14.830±0.036	14.842±0.052	0.92 ^{+0.08} _{-0.07}	MS ^{lc}	[12,13]
HWVir	10.577±0.069	10.974±0.027	11.093±0.022	0.17 ^{+0.01} _{-0.02}	MS ^{lc}	[1,13]

Table A.3. continued.

Object	V[mag]	J [mag]	H [mag]	Distances [kPc]	Comp. Type	References
HS2231+2441	14.153±0.05	14.669±0.035	14.732±0.054	1.11 ^{+0.11} _{-0.10}	MS ^{lc}	[2,13]
NSVS14256825	13.389±0.25	13.658±0.026	13.797±0.026	-	MS ^{lc}	[2,13]
UVEX0328+5035	14.263±0.02	14.121±0.004	13.915±0.004	-	MS	[2,14]
PG1336-018	13.661±0.27	14.594±0.037	14.646±0.050	0.61 ^{+0.07} _{-0.07}	MS ^{lc}	[2,13]
J082053+000843	15.168±0.05	15.712±0.008	15.818±0.014	1.69 ^{+0.42} _{-0.33}	BD	[2,14]
HS0705+6700	14.923±0.52	15.103±0.039	15.233±0.086	1.58 ^{+0.74} _{-0.50}	MS ^{lc}	[2,13]
KPD1930+2752	13.833±0.035	13.983±0.029	13.968±0.045	-	WD ^{lc}	[1,13]
KPD0422+5421	14.682±0.018	14.425±0.031	14.421±0.046	-	WD ^{lc}	[1,13]
PG1017-086	14.426±0.025	14.866±0.042	15.036±0.074	1.05 ^{+0.16} _{-0.14}	MS	[1,13]
J162256+473051	16.188±0.02	16.732±0.136 ^B	-	2.25 ^{+0.23} _{-0.21}	BD	[2,13]
CD-3011223	12.296±0.03	12.886±0.029	12.932±0.023	0.35 ^{+0.03} _{-0.03}	WD	[2,13]

Notes. lc: identified photometrically; B,C,D: 2MASS colours of quality B, C or D which were excluded from the analysis

References. 1: Wesemael et al. (1992); 2: UCAC4; 3: Landolt (2007); 4: Landolt (2009); 5: Mermilliod (1992); 6: O'Donoghue et al. (2013) 7: Høg et al. (2000); 8: NOMAD; 9: SDSS, Jester et al. (2005); 10: SPM4.0; 11: Udalski et al. (2002); 12: Kilkeny et al. (1997); 13: 2MASS; 14: UKIDSS; 15: Koen priv. comment

The catalogue of radial velocity variable hot subluminous stars from the MUCHFUSS project

S. Geier¹, T. Kupfer², U. Heber³, V. Schaffenroth^{3,4}, B. N. Barlow⁵, R. H. Østensen⁶, S. J. O’Toole⁷, E. Ziegerer³, C. Heuser³, P. F. L. Maxted⁸, B. T. Gänsicke⁹, T. R. Marsh⁹, R. Napiwotzki¹⁰, P. Brünner³, M. Schindewolf³, and F. Niederhofer¹

¹ European Southern Observatory, Karl-Schwarzschild-Str. 2, 85748 Garching, Germany

² Department of Astrophysics/IMAPP, Radboud University Nijmegen, P.O. Box 9010, 6500 GL Nijmegen, The Netherlands

³ Dr. Karl Remeis-Observatory & ECAP, Astronomical Institute, Friedrich-Alexander University Erlangen-Nuremberg, Sternwartstr. 7, D 96049 Bamberg, Germany

⁴ Institute for Astro- and Particle Physics, University of Innsbruck, Technikerstr. 25/8, 6020 Innsbruck, Austria

⁵ Department of Physics, High Point University, 833 Montlieu Avenue, High Point, NC 27268, USA

⁶ Institute of Astronomy, KU Leuven, Celestijnenlaan 200D, B-3001 Heverlee, Belgium

⁷ Australian Astronomical Observatory, PO Box 915, North Ryde NSW 1670, Australia

⁸ Astrophysics Group, Keele University, Staffordshire, ST5 5BG, UK

⁹ Department of Physics, University of Warwick, Coventry CV4 7AL, UK

¹⁰ Centre of Astrophysics Research, University of Hertfordshire, College Lane, Hatfield AL10 9AB, UK

Received Accepted

ABSTRACT

The project Massive Unseen Companions to Hot Faint Underluminous Stars from SDSS (MUCHFUSS) aims to find sdBs with compact companions like massive white dwarfs, neutron stars or black holes. Here we provide classifications, atmospheric parameters and a complete radial velocity (RV) catalogue containing 1914 single measurements for an sample of 177 hot subluminous stars discovered based on SDSS DR7. 110 stars show significant RV variability, while 67 qualify as candidates. We constrain the fraction of close massive compact companions of hydrogen-rich hot subdwarfs in our sample to be smaller than $\sim 1.3\%$, which is already close to the theoretical predictions. However, the sample might still contain such binaries with longer periods exceeding ~ 8 d. We detect a mismatch between the ΔRV_{\max} -distribution of the sdB and the more evolved sdOB and sdO stars, which challenges our understanding of their evolutionary connection. Furthermore, irregular RV variations of unknown origin with amplitudes of up to ~ 180 km s⁻¹ on timescales of years, days and even hours have been detected in some He-sdO stars. They might be connected to irregular photometric variations in some cases.

Key words. binaries: spectroscopic – stars: subdwarfs – stars: horizontal branch – stars: atmospheres

1. Introduction

Hot subdwarf stars (sdO/Bs) show spectral features similar to hot main sequence stars, but are much less luminous and therefore more compact. Depending on their spectral appearance, hot subdwarf stars can be divided into subclasses (Moehler et al. 1990; see Drilling et al. 2013 for a more detailed classification scheme). While the observational classification seems straightforward, the formation and evolution of those objects is still unclear.

In the Hertzsprung-Russell diagram most hot subdwarf stars are situated at the blueward extension of the Horizontal Branch (HB), the so called Extreme or Extended Horizontal Branch (EHB, Heber et al. 1986). The most common class of hot subdwarfs, the sdB stars, are located on the EHB and are therefore considered to be core-helium burning stars. They have very thin hydrogen dominated atmospheres ($M_{\text{env}}/M_{\text{sdB}} \approx 10^{-3}$, $n_{\text{He}}/n_{\text{H}} \leq 0.01$), their effective temperatures (T_{eff}) range from 20 000 K to 40 000 K and their surface gravities ($\log g$) are one to two orders

of magnitude higher than those of main sequence stars of the same spectral type (usually between $\log g = 5.0$ and 6.0).

sdB stars are likely formed from stars that almost entirely lose their hydrogen envelopes after climbing up the red giant branch (RGB). The outer layer of hydrogen that remains does not have enough mass to sustain a hydrogen-burning shell, as is the case for cooler HB stars. Therefore the star can not evolve in the canonical way and ascend the Asymptotic Giant Branch (AGB). Instead the star remains on the EHB until core-helium burning stops, and after a short time of shell-helium burning eventually reaches the white dwarf (WD) cooling tracks. According to evolutionary calculations the average lifetime on the EHB is of the order of 10^8 yr (e.g. Dorman et al. 1993). In this canonical scenario the hotter ($T_{\text{eff}} = 40\,000 - 80\,000$ K) and much less numerous hydrogen rich sdOs can be explained as rather short-lived shell-helium burning stars evolving away from the EHB.

Systematic surveys for radial velocity (RV) variations revealed that a large fraction of the sdB stars (40 – 70 %) are members of close binaries with orbital periods ranging from ≈ 0.05 d to ≈ 30 d (Maxted et al. 2001; Morales-Rueda et al. 2003; Copperwheat et al. 2011). Most of the known companions of sdBs in radial velocity variable close binary systems are white

Send offprint requests to: S. Geier,
e-mail: sgeier@eso.org

Table 1. Telescopes and instrumental setups

Telescope	Instrument	R	$\Delta\lambda$ [Å]
Sloan	SDSS	1800	3800 – 9200
ESO-VLT	FORS1	1800	3730 – 5200
WHT	ISIS	4000	3440 – 5270
CAHA-3.5m	TWIN	4000	3460 – 5630
ESO-NTT	EFOSC2	2200	4450 – 5110
SOAR	Goodman	2500	3500 – 6160 ^a
	Goodman	7700	3700 – 4400
Gemini	GMOS-N/S	1200	3770 – 4240
INT	IDS	1400	3000 – 6800
	IDS	4000	3930 – 5100 ^b
SAAO-1.9m	Grating	4600	4170 – 5030

Notes. ^(a) Used until 2011. ^(b) Additional data taken in March 2003 and April 2004.

dwarfs or late type main sequence stars, but substellar companions like brown dwarfs have been found as well (see Kupfer et al. 2015 and references therein). Those systems were most likely formed after a common envelope (CE) and spiral-in phase, which also provides an explanation for the required mass-loss on the RGB. However, apparently single sdBs and wide binary systems (Vos et al. 2012, 2013; Barlow et al. 2013) exist as well. In those cases, it is less straightforward to explain the formation of the sdBs (see Geier 2013 for a review).

Hot subdwarf binaries with massive WD companions are good candidates for SN Ia progenitors. Due to gravitational wave radiation the orbit will shrink further and mass transfer from the sdB onto the WD will start once the sdB fills its Roche lobe. The Chandrasekhar limit might be reached either through He accretion on the WD (e.g. Yoon & Langer 2004 and references therein) or a subsequent merger of the system (Tutukov et al. 1981; Webbink 1984). Two sdBs with massive WD companions have been identified to be good candidates for being SN Ia progenitors (Maxted et al. 2000a; Geier et al. 2007; Vennes et al. 2012; Geier et al. 2013b). Neutron star (NS) or even black hole (BH) companions are predicted by theory as well (Podsiadlowski et al. 2002; Pfahl et al. 2003). In this scenario two phases of unstable mass transfer are needed and the NS or the BH is formed in a supernova explosion. Nelemans (2010) showed that about 1% of the short period sdBs should have NS companions whereas about 0.1% should have BH companions. In an independent study Yungelson et al. (2005) predicted the number of systems with NS companions to be about 0.8%. However, no NS/BH companion to an sdB has yet been detected unambiguously whereas a few candidates have been identified (Geier et al. 2010b). Most recently, Kaplan et al. (2013) discovered the close companion to the pulsar PSR J1816+4510 to be a He-WD progenitor with atmospheric parameters close to an sdB star ($T_{\text{eff}} = 16\,000$ K, $\log g = 4.9$).

The formation of the helium-rich classes of He-sdO/Bs is even more puzzling. Most (but not all) He-sdOs are concentrated in a very small region in the $T_{\text{eff}}\text{-}\log g$ plane, slightly blueward of the EHB at $T_{\text{eff}} = 40\,000 - 80\,000$ K and $\log g = 5.60 - 6.10$ (Ströer et al. 2007; Nemeth et al. 2012). The He-sdBs are scattered above the EHB. The late hot flasher scenario provides a possible channel to form these objects (Lanz et al. 2004; Miller Bertolami et al. 2008). After ejecting most of its envelope at the tip of the RGB, the stellar remnant evolves directly towards the WD cooling tracks and experiences a late core helium flash

there. Helium and other elements like carbon or nitrogen are mixed into the atmosphere and the star ends up close to the helium main sequence. Depending on the depth of the mixing, stars with more or less helium in the atmospheres and different atmospheric parameters can be formed in this way. Most recently, Latour et al. (2014) found a correlation between the carbon and helium abundances of the He-sdOB stars in the globular cluster ω Cen, which is predicted by late hot flasher models. Hirsch (2009) discovered a similar correlation for field helium-rich hot subdwarf (see also Heber & Hirsch 2010). Similar to the formation scenarios for sdB stars, the late hot flasher channel requires extreme mass-loss on the RGB probably triggered by binary interactions. However, the population of He-sdOs observed so far seems to consist mostly of single stars. Only one RV-variable He-sdO has been reported in the SPY sample, which corresponds to a fraction of only 3% (Napiwotzki 2008). However, higher fractions have been reported for the He-sdO populations in the PG sample (Green et al. 2008).

An alternative way of forming single hot subdwarfs is the merger of two helium white dwarfs in a close binary (Webbink 1984; Iben & Tutukov 1984). Loss of angular momentum through the emission of gravitational radiation will cause the system to shrink. Given the initial separation is small enough, the two white dwarfs eventually merge and if the mass of the merger is high enough, core-helium burning is ignited and a hot subdwarf is formed. Due to the strong mixing during the merger process, the atmospheres of the merger products are expected to be helium-rich (Zhang & Jeffery 2012).

Some hot subluminoous stars are not connected to EHB-evolution at all. Objects with spectra and atmospheric parameters similar to normal sdBs are known, which are situated below the EHB (e.g. Heber et al. 2003; Silvotti et al. 2012). These objects are considered to be direct progenitors of helium white dwarfs, which descend from the red giant branch. For these low-mass post-RGB objects, which cross the EHB, evolutionary tracks indicate masses of about $0.20 - 0.33 M_{\odot}$ (Driebe et al. 1998). In order to form such objects, the mass loss on the RGB has to be more extreme than in the case of EHB stars. Objects down to even lower masses are known as extremely low-mass (ELM) WDs, which are members of close binary systems (e.g. Brown et al. 2012). More massive He-stars, like the so-called low-gravity or luminous He-sdOs (Jeffery et al. 2008) also belong to the class of hot subdwarfs and are situated between the EHB and the main sequence.

2. The MUCHFUSS project

The project Massive Unseen Companions to Hot Faint Underluminoous Stars from SDSS (MUCHFUSS) aims to find hot subdwarf stars with massive compact companions like massive white dwarfs ($> 1.0 M_{\odot}$), neutron stars or stellar mass black holes. Hot subdwarf stars were selected from the Sloan Digital Sky Survey by colour and visual inspection of the spectra. Hot subdwarf stars with high radial velocity variations were selected as candidates for follow-up spectroscopy to derive the radial velocity curves and the binary mass functions of the systems.

Geier et al. (2011a) discussed the target selection and the follow-up strategy. Detailed analyses of sdB binaries discovered in the course of this project are given in Geier et al. (2011b) and Kupfer et al. (2015). Three eclipsing systems have been discovered, two of them being the first sdBs with brown dwarf companions (Geier et al. 2011c; Schaffenroth et al. 2014). One system turned out to be the first sdB hybrid pulsator showing a reflection effect (Østensen et al. 2013). The photometric follow-

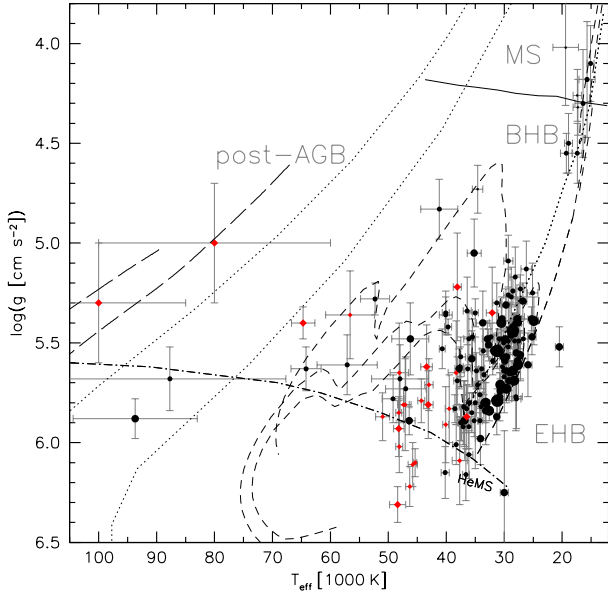


Fig. 1. $T_{\text{eff}} - \log g$ diagram of the full sample of hot, subluminous, RV-variable stars. The size of the symbols scales with ΔRV_{max} . The black circles mark stars with hydrogen dominated atmospheres ($\log y < 0$), while the red diamonds mark stars with helium dominated atmospheres. The helium main sequence (HeMS) and the HB band are superimposed with HB evolutionary tracks (dashed lines) for subsolar metallicity ($\log z = -1.48$) from Dorman et al. (1993). The three tracks in the high temperature range correspond to helium core masses of 0.488 , 0.490 and $0.495 M_{\odot}$ (from bottom-left to top-right). Those tracks mark the EHB evolution, since the stars do not reascend the giant branch in the helium shell-burning phase. The two tracks in the upper right correspond to core masses of 0.53 and $0.54 M_{\odot}$. BHB stars following those tracks are expected to experience a second giant phase. The solid line marks the relevant part of the zero-age main sequence for solar metallicity taken from Schaller et al. (1992). The two dotted lines are post-AGB tracks for hydrogen-rich stars with masses of 0.546 (lower line) and $0.565 M_{\odot}$ (upper line) taken from Schönberner (1983). The two long-dashed lines are post-AGB tracks for helium-rich stars with masses of 0.53 (lower line) and $0.609 M_{\odot}$ (upper line) taken from Althaus et al. (2009).

up campaign of the MUCHFUSS project will be described in detail in Schaffenroth et al. (in prep). During dedicated spectroscopic MUCHFUSS follow-up runs bright sdB binary candidates were observed in a supplementary programme (Geier et al. 2013b, 2014a). Hot subdwarfs with a high but constant radial velocity were studied in the Hyper-MUCHFUSS project (Tillich et al. 2011).

Here we present classifications, radial velocities and atmospheric parameters of the close binary candidates discovered in the MUCHFUSS project so far. In Sect. 3 we describe the observations, target selection, classification and quantitative spectral analysis of our sample as well as the radial velocity catalogue. In Sect. 4 the different populations of RV variable hot subluminous stars are presented and discussed. A summary is then given in Sect. 5.

3. Target selection, observations, spectroscopic analysis

3.1. Observations and sample selection

While the target selection presented in Geier et al. (2011a) includes SDSS up to Data Release 6 only, we have now applied the same selection criteria to Data Release 7 (Abazajian et al. 2009). Hot subdwarf candidates were selected by applying a colour cut to SDSS photometry. All point source spectra within the colours $u - g < 0.4$ and $g - r < 0.1$ were selected and downloaded from the SDSS Data Archive Server¹. By visual inspection we selected and classified $\approx 10\,000$ hot stars. Most objects much fainter than $g = 19$ mag have been excluded because of insufficient quality. The sample contains 1369 hot subdwarfs, consistent with the preliminary number of hot subdwarfs (1409) found by Kleinman et al. (2010) in SDSS-DR7.

The SDSS spectra are co-added from at least three individual integrations with typical exposure times of 15 min taken consecutively. We have obtained those individual spectra for stars brighter than $g = 18.5$ mag. In addition, second epoch medium resolution spectroscopy was obtained from SDSS as well as our own observations, using ESO-VLT/FORS1, WHT/ISIS, CAHA-3.5m/TWIN and ESO-NTT/EFOSC2 (see Table 1, Geier et al. 2011a). Typical exposure times ranged from 10 min to 20 min. The S/N of the individual spectra ranges from about 15 to about 100.

The radial velocities were measured by fitting a set of mathematical functions (Gaussians, Lorentzians and polynomials) to the spectral lines using the FITSB2 routine (Napiwotzki et al. 2004). Three functions are used to match the continuum, the line and the line core, respectively and mimic the typical Voigt profile of spectral lines. The profiles are fitted to all suitable lines simultaneously using χ^2 -minimization and the RV shift with respect to the rest wavelengths with the associated 1σ error is measured. For the hydrogen-rich stars the Balmer and helium lines of sufficient strength have been used. For the helium-rich stars we used appropriate lines of neutral and single ionized helium. Since some of those stars still have significant hydrogen contamination we avoided the helium lines from the Pickering series, because they can be blended by the weaker hydrogen Balmer lines. Each single fit has been inspected visually and outliers caused by cosmic rays and other artifacts have been excluded. Heliocentric corrections have been applied to the RVs and mid-JDs derived for the follow-up spectra, while the SDSS spectra available in the archive are already corrected.

The average 1σ RV error of all the measurements in the catalogue is $\sim 15 \text{ km s}^{-1}$, which is consistent with independent checks of the SDSS wavelength stability using SDSS observations of F-stars ($< 14.5 \text{ km s}^{-1}$, Rebassa-Mansergas et al. 2007). To correct for systematic shifts between different instruments we observed RV standards in our follow-up runs. The RMS scatter around the orbital fits of the solved binaries in our sample is also consistent with the formal uncertainties (for details, see Geier et al. 2011b; Kupfer et al. 2015). We selected all objects with maximum RV shifts discrepant at the formal 1σ -level and found 196 candidates for RV variability.

3.2. Visual classification

The basic classification of the hot subdwarf sample was done by visual inspection based on existence, width, and depth of

¹ das.sdss.org

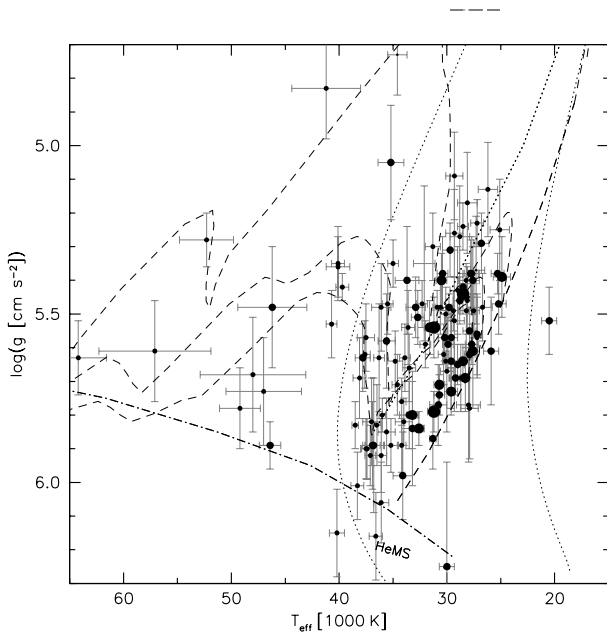


Fig. 2. $T_{\text{eff}} - \log g$ diagram of RV variable hydrogen-rich sdB and sdOB stars (see Fig. 1). The size of the symbols scales with ΔRV_{max} . The helium main sequence (HeMS) and the HB band are superimposed with HB evolutionary tracks (dashed lines) for subsolar metallicity ($\log z = -1.48$) from Dorman et al. (1993). The three tracks correspond to helium core masses of 0.488, 0.490 and 0.495 M_{\odot} (from bottom-left to top-right). The two dotted lines mark post-RGB tracks (Driebe et al. 1998) for core masses of 0.234 (left) and 0.259 M_{\odot} (right).

helium and hydrogen absorption lines as well as the flux distribution between 4000 and 6000 Å. Hot subdwarf B stars show strong and broad Balmer and weak (or no) He I lines. SdOB stars show strong and broad Balmer lines as well as weak lines from He I and He II, while sdO stars only display weak He II lines besides the Balmer lines. He-sdBs are dominated by strong He I and sometimes weaker He II lines. Hydrogen absorption lines are shallow or not present at all. He-sdOs show strong He II and sometimes weak He I lines. Balmer lines are not present or heavily blended by the strong He II lines of the Pickering series. A flux excess in the red compared to a reference spectrum as well as the presence of spectral features such as the Mg I triplet at 5170 Å or the Ca II triplet at 8650 Å were taken as indications of a late-type companion.

From the total number of 1369 hot subdwarfs, 983 belong to the class of single-lined sdBs and sdOBs. Features indicative of a cool companion were found for 98 of the sdBs and sdOBs. Nine sdOs show spectral features of cool companions, while 262 sdOs, most of which show helium enrichment, are single-lined.

Comparing the results from the visual classification with the more detailed quantitative spectral analysis for the RV variable subsample presented here (see Sect. 4), we conclude that our visual classification should be accurate to about 90%. A catalogue with classifications and atmospheric parameters of the full SDSS sample including more recent data releases is in preparation. Here we restrict ourselves to the RV-variable sample.

3.3. Atmospheric parameters and spectroscopic distances

To refine the visual classification and derive the atmospheric parameters a quantitative spectral analysis of the coadded SDSS

spectra (or follow-up spectra of higher quality, if available) was performed for all RV variable stars in our sample with data of sufficient quality. The method is described in Geier et al. (2011b). We used appropriate model grids for the different classes of hot stars. The hydrogen-rich and helium-poor ($\log y = \log n(\text{He})/n(\text{H}) < -1.0$) stars with effective temperatures below 30 000 K were fitted using a grid of metal line blanketed LTE atmospheres with solar metallicity. Helium-poor stars with temperatures ranging from 30 000 K to 40 000 K were analysed using LTE models with enhanced metal line blanketing (O’Toole & Heber 2006). Metal-free NLTE models (Ströer et al. 2007) were used for hydrogen-rich stars with temperatures below 40 000 K showing moderate He-enrichment ($\log y = -1.0 - 0.0$) and for hydrogen-rich sdOs. Finally, the He-sdOs were analysed with NLTE models taking into account the line-blanketing caused by nitrogen and carbon (Hirsch & Heber 2009).

Spectroscopic distances to our stars have been calculated as described in Ramspeck et al. (2001) assuming the canonical mass of 0.47 M_{\odot} for the subdwarfs and appropriate masses for objects of other classes (0.5 M_{\odot} for blue horizontal branch star candidates and 3.5 M_{\odot} for runaway main-sequence B star candidates, Geier et al. 2015; 0.6 M_{\odot} for post-AGB stars, Reindl et al. 2015) using the formula given by Lupton² to convert SDSS-g and r magnitudes to Johnson V magnitudes. Interstellar reddening was neglected in these calculations.

3.4. Spectroscopic follow-up, criterion for variability and radial velocity catalogue

During our follow-up campaign we obtained medium resolution ($R = 1200 - 7700$), time-resolved spectroscopy using WHT/ISIS, CAHA3.5m/TWIN, ESO-NTT/EFOSC2, SOAR/Goodman, Gemini/GMOS, INT/IDS and the grating spectrograph at the 1.9m telescope at SAAO (see Table 1, Geier et al. 2011b; Kupfer et al. 2015) and measured the RVs as described above.

To estimate the fraction of false detections produced by random fluctuations and calculate the significance of the measured RV variations we apply the method outlined in Maxted et al. (2001). For each star we calculate the inverse-variance weighted mean velocity from all measured epochs. Assuming this mean velocity to be constant, we calculate the χ^2 . Comparing this value with the χ^2 -distribution for the appropriate number of degrees of freedom we calculate the probability p of obtaining the observed value of χ^2 or higher from random fluctuations around a constant value. The maximum RV shifts (ΔRV_{max}), the average 1σ uncertainties of the two corresponding measurements, the timespan between those two epochs and the logarithm of the false-detection probability $\log p$ are given in Tables 3-5.

We consider the detection of RV variability to be significant, if the false-detection probability p is smaller than 0.01% ($\log p < -4.0$). The fraction of such significant detections in our initial sample of 196 is 56% (110 objects). Objects with false-detection probabilities between 0.01% and 5% ($\log p = -4.0$ to $\log p = -1.3$) are regarded as candidates for RV variability and constitute 34% of the initial sample (67 objects). About 10% ($\log p > -1.3$, 19 objects) are regarded as non-detections (the parameters of those stars can be found in Table A.1). Removing those non-detections we end up with a sample of 177 stars, which show RV variability with probabilities between 95% and 99.9% (see Table 2). Orbital solutions were already derived for

² <http://www.sdss.org/dr6/algorithms/sdssUBVRITransform.html>

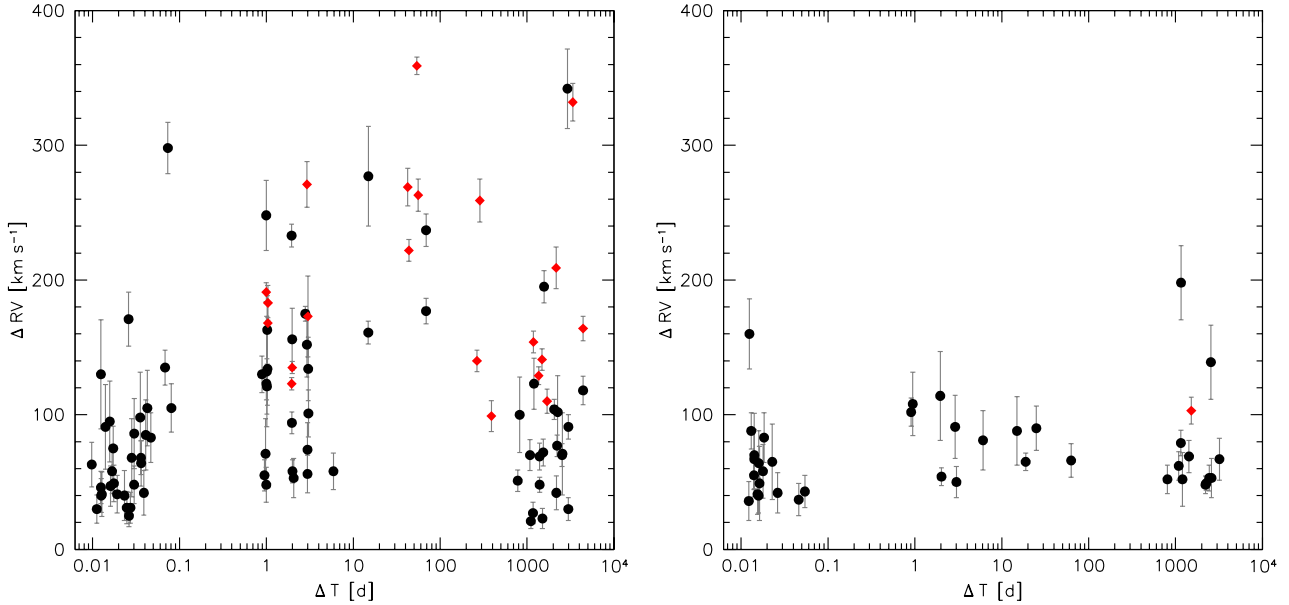


Fig. 3. *Left panel:* Highest radial velocity shift between individual spectra plotted against time difference between the corresponding observing epochs. The filled red diamonds mark sdB binaries with known orbital parameters (Kupfer et al. 2015), while the filled black circles mark the rest of the hydrogen-rich sdB sample of RV variable stars. *Right panel:* The same plot for the hydrogen-rich sdOB and sdO sample of RV variable stars.

Table 2. Sample statistics

Class	RV variable	RV variable candidates	non-detections
H-rich sdO/B	89	50	13
He-rich sdO/B	14	11	4
Others	7	6	2
Total	110	67	19

22 close binary sdB systems (see Kupfer et al. 2015 and references therein).

The catalogue contains 1914 epochs (mid-HJD), associated radial velocities and 1σ -RV-uncertainties of the RV variable stars as well as information about the instruments used to obtain the spectra. It can be accessed online from the VizieR database operated by CDS.

4. Radial velocity variable populations of hot subluminal stars

Since our sample has been preselected in the way outlined above it is not straightforward to derive the true fractions of RV variable stars for each class of hot subdwarfs. Most stars in our sample have been selected based on RV variations between the individual SDSS spectra, which have usually been taken within just 45 min. Only binaries with sufficiently short orbital periods and high RV amplitudes show significant variations on such short timescales, while binaries with smaller RV amplitudes and longer periods remain undetected.

Fig. 1 shows the $T_{\text{eff}} - \log g$ -diagram of the RV variable sample. Most of the stars are indeed associated with the EHB and therefore most likely core or shell-helium burning hot sub-

warfs. Four objects have higher temperatures and are more likely hydrogen and helium-rich post-AGB objects. Nine stars have temperatures below 20 000 K and most of them are likely associated with the blue horizontal branch (see Table 5). The B-type binary candidates are discussed separately in Geier et al. (2015), the hot post-AGB stars in Reindl et al. (2015).

Although only the orbits of 22 binaries from our sample have been solved, the distribution of ΔRV_{max} can be used as a diagnostic tool as well. The width of this distribution scales with the width of the companion mass distribution as well as the distribution of orbital periods.

4.1. Hydrogen-rich hot subdwarf stars and their evolutionary connection

The most common class of RV variable objects in our sample are sdB, sdOB and sdO stars with hydrogen-dominated atmospheres (see Table 3). Fig. 2 shows the $T_{\text{eff}} - \log g$ -diagram of this sub-sample. As expected, most objects are concentrated on the EHB and some objects follow the tracks of more evolved shell-helium burning stars. This distribution is consistent with other studies (e.g. Nemeth et al. 2012). However, it is not clear whether all objects situated above the EHB are really shell-helium burning stars that evolved along the predicted evolutionary tracks. Other objects like low-mass post-RGB stars evolve in a different way and might constitute a certain fraction of stars in this region of the $T_{\text{eff}} - \log g$ -diagram.

The detected RV-variability in those objects is very likely caused by binary motion. Up to now the orbital parameters of 142 close binaries have been measured. Most of the solved systems have hydrogen-rich sdB primaries, but this sample also contains 46 hydrogen-rich sdOB and sdO stars (see Kupfer et al. 2015 and references therein, but see also the discussion in Sect. 4.5). Another possible source of RV-variations are short-period p-mode pulsations. However, the fraction of pulsating hot

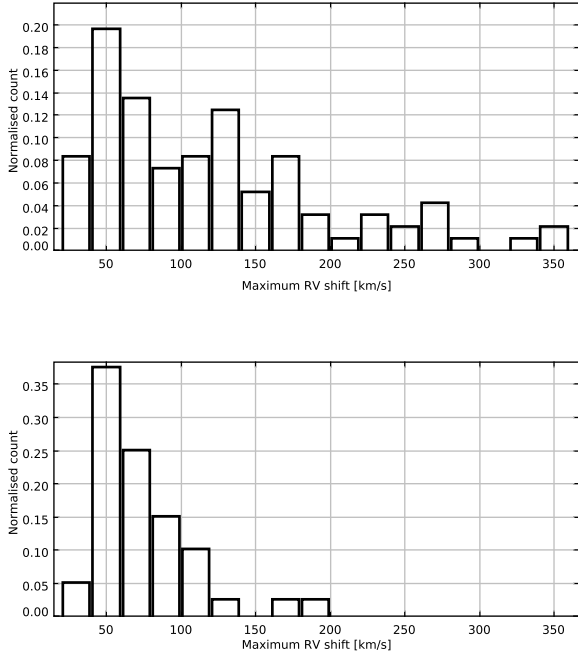


Fig. 4. ΔRV_{\max} distribution of RV-variable sdB stars (upper panel) as well as sdOB and sdO stars with hydrogen-rich atmospheres (lower panel).

subdwarf stars is quite small (about 5%) and the RV-variations are usually smaller than our detection limit. Even in the most extreme cases known, where those variations can reach amplitudes of $10 - 20 \text{ km s}^{-1}$ (e.g. O’Toole et al. 2005), we would most likely not resolve and detect them in our data, because our exposure times are usually longer than the typical periods (a few minutes) of those pulsations.

The additional information provided by the RV variability (Table 3, Fig. 3) allows us to probe the connection between objects on the EHB classified as sdBs (100 RV variable objects) with stars that are situated above the EHB classified as sdOB or sdO (40 RV-variable objects). While the internal structure and the atmospheric parameters of the hot subdwarf change with time, the orbital period and the companion mass are not predicted to change significantly within the lifetime of the sdB ($\sim 100 \text{ Myr}$). A significant shortening of the orbital period due to angular momentum lost by gravitational wave emission is only predicted for the most compact binaries with the most massive companions, which turned out to be quite rare (e.g. Geier et al. 2007, 2013b). Furthermore, the orbital evolution will always lead to shorter periods and therefore higher RV-amplitudes. If the sdBs on the EHB evolve to become hydrogen-rich sdOB and sdO stars, the ΔRV_{\max} -distribution should essentially remain the same.

Fig. 4 shows the ΔRV_{\max} -distribution of both subsamples. While the distribution below 100 km s^{-1} looks very similar as expected, the sdB sample shows a wider range of RV shifts (see also Fig. 3). This can only be partly explained by the smaller size of the sdOB/sdO sample. There are also no significant differences in data quality and temporal sampling between the two different groups. Essentially the same hydrogen Balmer lines have been used to measure the RVs. The reason for this mis-

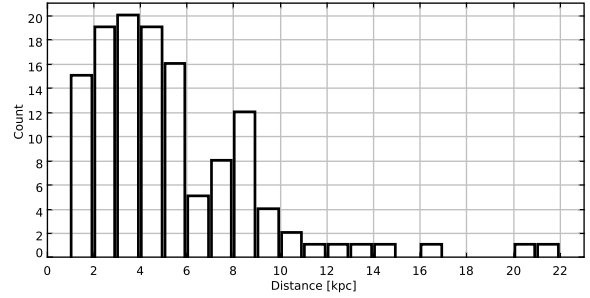


Fig. 5. Distribution of spectroscopic distances for the hydrogen-rich sdB, sdOB and sdO stars (see Table 3).

match, which challenges our understanding of EHB evolution, is unclear.

4.2. Low-mass post-RGB binaries

Our sample contains two sdBs that might be good candidates for low-mass post-RGB stars. With a low effective temperature of $20\,500 \text{ K}$ and a rather high surface gravity $\log g = 5.52$ J083334.76-045759.4 is situated well below the EHB. Such a location is inconsistent with core-helium burning. Furthermore, it shows a high $\Delta RV_{\max} = 161 \text{ km s}^{-1}$. J094750.71+162731.8 is hotter ($T_{\text{eff}} = 30000 \text{ K}$), but has a very high surface gravity $\log g = 6.25$. Also situated below the EHB it shows $\Delta RV_{\max} = 130 \text{ km s}^{-1}$. However, whether a significant contribution of low-mass post-RGB binaries leads to the wider distribution of RV-shifts, still needs to be studied in more detail (see also discussion in Geier et al. 2013a).

4.3. Hierarchical triple systems

One sdB in our sample is a double-lined system and shows weak spectral features of a main-sequence companion. J205101.72+011259.7 shows a shift of $91.0 \pm 31.5 \text{ km s}^{-1}$ within just 0.0141 d with a false-detection probability of only 0.05% . It is very unlikely that this variation is caused by the main-sequence companion. The solved orbits of sdB+MS binaries have long periods of the order of 1000 d (Vos et al. 2012, 2013; Barlow et al. 2012, 2013). We therefore conclude that J205101.72+011259.7 is another candidate for a hierarchical triple system consisting of an sdB in a short-period binary with unseen companion and a main sequence star orbiting this inner binary with a long period (e.g. Barlow et al. 2014, see also discussion in Kupfer et al. 2015).

4.4. The fraction of massive compact companions

The primary aim of the MUCHFUSS project is to find massive compact companions to sdB stars. However, only two known sdB binaries with periods shorter than 0.1 d and $\Delta RV_{\max} \sim 700 \text{ km s}^{-1}$ have WD companions with masses exceeding $0.7 M_{\odot}$ (Geier et al. 2007, 2013b). sdB+NS/BH binaries with similar periods would have $\Delta RV_{\max} > 1000 \text{ km s}^{-1}$.

However, the highest ΔRV_{\max} measured in our subsample of hydrogen-rich sdB, sdOB and sdO stars is just 359 km s^{-1} (see Table 3). Due to the RV sampling of our dataset provided by the individual SDSS spectra it is very unlikely that we have missed

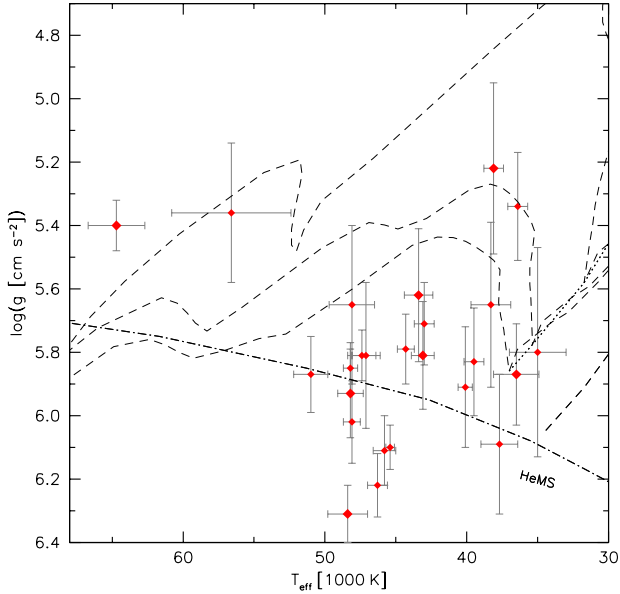


Fig. 6. $T_{\text{eff}} - \log g$ diagram of RV variable helium-rich sdOB and sdO stars (see Fig. 1). The size of the symbols scales with ΔRV_{max} . The helium main sequence (HeMS) and the HB band are superimposed with HB evolutionary tracks (dashed lines) for subsolar metallicity ($\log z = -1.48$) from Dorman et al. (1993). The three tracks correspond to helium core masses of 0.488 , 0.490 and $0.495 M_{\odot}$ (from bottom-left to top-right).

a short-period (0.1 d) binary with an $\Delta RV_{\text{max}} > 1000 \text{ km s}^{-1}$ by chance. To estimate an upper limit for the fraction of such extremely close binary sdB+NS/BH binaries in our sample we count the number of hydrogen-rich sdBs and sdOBs with significant RV variability ($\log p < -4.0$) in our sample (76 objects, see Table 3) and invert it. In this way we derive the fraction of those objects in our sample to be smaller than 1.3%. This fraction is still consistent with the theoretically predicted fractions of about 1% (Yungelson et al. 2005; Geier et al. 2010b; Nelemans 2010).

However, we would most likely not expect the most massive compact companions in our sample to have such short orbital periods anyway. To allow the massive companion to spiral in deep enough to form such compact binaries during the common envelope phase, the red-giant progenitors of the sdB stars are predicted to have tightly bound envelopes and to be rather massive ($2 - 3 M_{\odot}$, Geier et al. 2013b). Such stars are only found in young field populations like the Galactic thin disk and the two sdB binaries with the most massive WD companions known so far indeed belong to this population (Maxted et al. 2000a; Geier et al. 2007; Geier et al. 2013b).

Fig. 5 shows the distribution of spectroscopic distances for the sample. Those distances range from 1 to more than 20 kpc. Taking into account that the SDSS footprint mostly covers high Galactic latitudes and assuming a scale-height of $\sim 0.3 \text{ kpc}$ for the thin disk, we conclude that the vast majority of the stars in our sample do not belong to this young population. Most binary candidates exceeding $d \sim 3 \text{ kpc}$ should belong to the old Galactic halo population, the rest to the intermediate thick disk population. Since both populations do not contain intermediate mass main-sequence stars, which are the likely progenitors of short-period sdBs with massive compact companions, it is no surprise that we do not find them in our sample.

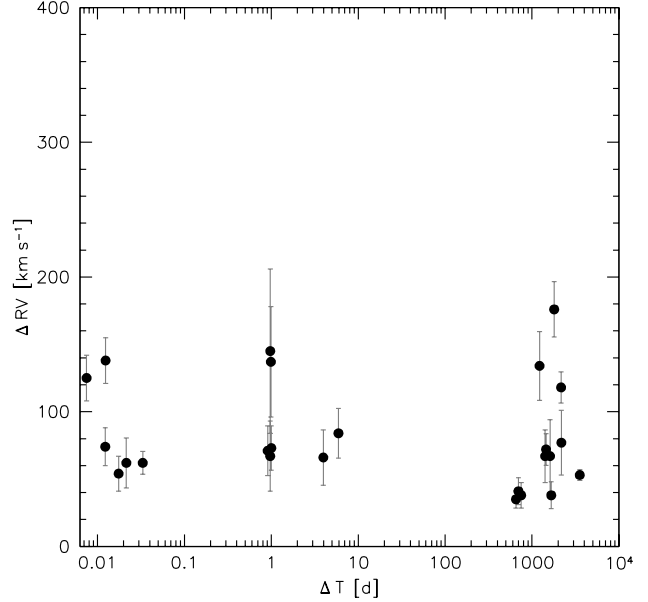


Fig. 7. Highest radial velocity shift between individual spectra plotted against time difference between the corresponding observing epochs for helium-rich sdO and sdOB stars (see Fig. 3).

While we can exclude sdB binaries with periods of a few hours and massive compact companions, our sample might still contain such objects with longer periods. Since more massive companions are expected to be quite efficient in ejecting the common envelope, such binaries might exist. Taking into account the ΔRV_{max} -distribution and the fraction of solved binary orbits (see Fig. 3), we estimate that a yet undetected population of long-period binaries with $K < 100 \text{ km s}^{-1}$ might be present. Assuming the canonical sdB mass of $0.47 M_{\odot}$ and a minimum companion mass at the Chandrasekhar limit ($1.4 M_{\odot}$) this translates into orbital periods longer than $\sim 8 \text{ d}$.

4.5. Irregular RV variations of helium-rich hot subdwarf stars

Our RV-variable sample contains 29 helium-rich hot subdwarf stars. 14 of them show significant RV variations while 15 qualify as candidates (see Table 4). Most of them are situated close to the He-MS in the $T_{\text{eff}} - \log g$ -diagram (see Fig. 6) and the atmospheric parameters are quite typical for the field population of He-sdOs ($T_{\text{eff}} = 40\,000 - 50\,000 \text{ K}$, Ströer et al. 2007; Nemeth et al. 2012). However, quite a number of stars have lower temperatures between $35\,000 \text{ K}$ and $40\,000 \text{ K}$. Those helium-rich sdOBs are rare in the field population, but quite dominant in the globular cluster $\omega \text{ Cen}$ (Latour et al. 2014). Following the discussion in Latour et al. (2014) this might be related to the age of the parent population, since most of the stars in our sample belong to the old thick disk or halo populations, while most of the bright stars studied by Nemeth et al. (2012) belong to the young thin disk population. The He-sdOs J232757.46+483755.2 and J110215.45+024034.1 seem to be more evolved than the rest of the sample and might also be associated to the helium-rich post-AGB stars.

J160450.44+051909.2 and J160623.21+363005.4 belong to the class of He-sdOBs with lower surface gravity (e.g. Naslim et

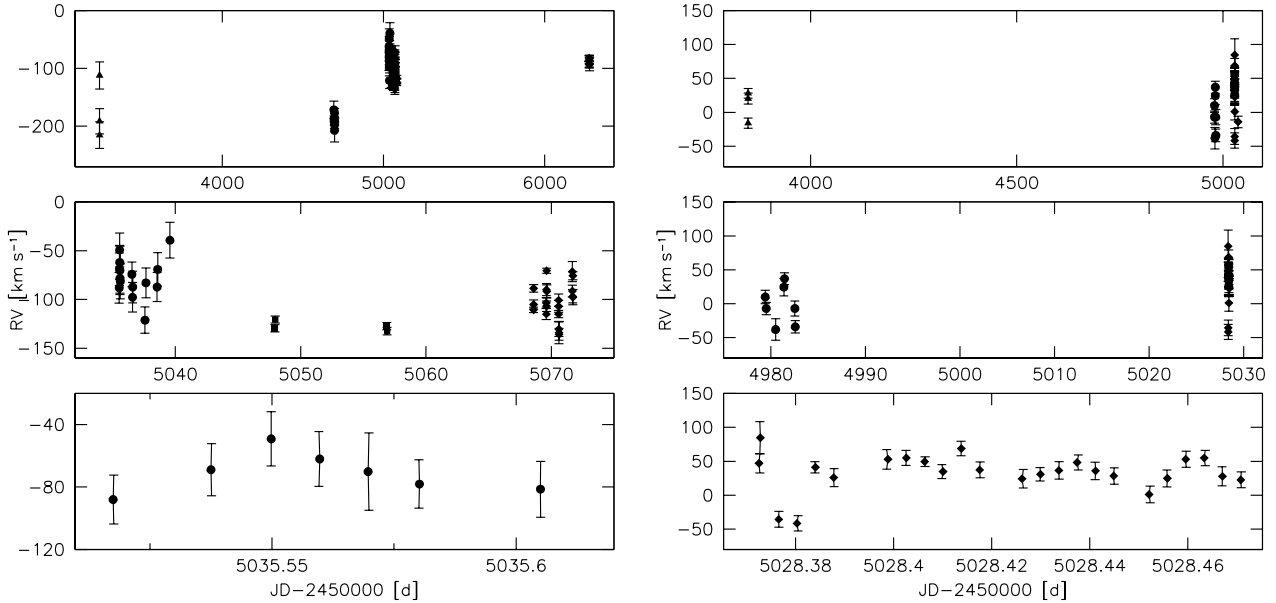


Fig. 8. Radial velocities of J232757.46+483755.2 (left panels) and J141549.05+111213.9 (right panels) against Julian date. Significant variations are present on timescales of years (upper panels), days (middle panels) and hours (lower panels).

al. 2010).³ Only one He-sdOB is known to be in a close double-lined, spectroscopic binary with an almost identical companion of the same type (Sener & Jeffery 2014). Another close binary contains an sdB with intermediate helium-enrichment (Naslim et al. 2012). Follow-up observations are needed to study the binary properties of those rare objects and compare them with the other hot subdwarf populations.

The discovery of RV variable He-sdOs (Green et al. 2008; Geier et al. 2011a) on the other hand seemed to be inconsistent with the idea, that those stars are formed by He-WD mergers (e.g. Webbink 1984), because merger products are expected to be single stars. Fig. 7 shows the maximum RV shifts between individual spectra plotted against the time difference between the corresponding epochs. When compared with Fig. 3 one can see that there are no stars with shifts higher than $\sim 200 \text{ km s}^{-1}$ and that the number of objects showing shifts at short timespans ($< 0.1 \text{ d}$) is smaller as well.

Because of the important implications for their formation, we were eager to solve the first He-sdO binaries and gave them high priority in our follow-up campaign. However, although we gathered up to 59 epochs for some of them, we were not able to find a single orbital solution. Adding more data in general degraded preliminary solutions that looked promising. Besides assuming circular orbits we also allowed for eccentricity and explored especially the parameter space of high orbital eccentricities (see Geier et al. 2011b). No periodic variations could be detected with sufficient significance.

Fig. 8 shows the radial velocities of the two He-sdO stars J141549.05+111213.9 and J232757.46+483755.2 for which we obtained the most data. Significant RV variations with amplitudes of up to $\sim 180 \text{ km s}^{-1}$ are seen on timescales of years, days and even hours. While J141549.05+111213.9 has atmospheric parameters typical for He-sdO stars, J232757.46+483755.2 has

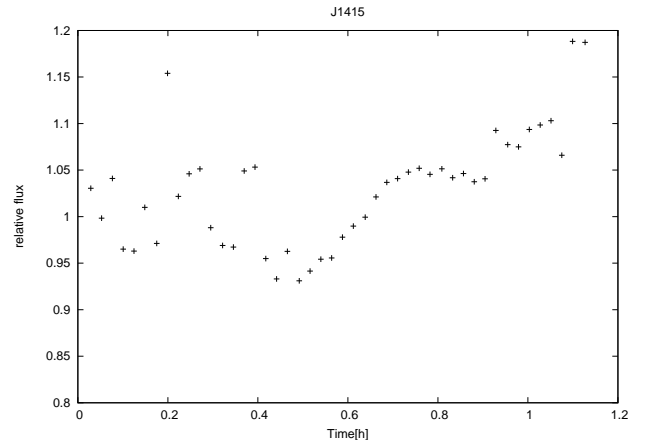


Fig. 9. V_B -band lightcurve of J141549.05+111213.9 taken with the BUSCA camera mounted at the 2.2m telescope at Calar Alto (Schaffenroth et al. in prep.).

a higher effective temperature and seems to be more evolved (see Table 3, Fig. 6).

The origin of these irregular RV variations remains unclear. Østensen et al. (2010) reported the discovery of irregular variations in the light curve of the He-sdOB star J19352+4555 observed by the Kepler mission. Jeffery et al. (2013) found another He-sdOB star with Kepler light curves (KIC 10449976) that shows a variation with a period of 3.9 d and variable amplitude. Radial velocity follow-up with time-resolved spectroscopy revealed a possible, but still marginal RV variability of $50 \pm 20 \text{ km s}^{-1}$. Most recently, Green et al. (2014) reported irregular variations in the lightcurves of two helium-rich and one hydrogen-rich sdO star. They also found RV variations of up to 20 km s^{-1} for some hydrogen- and helium-rich sdO stars.

³ In the literature those objects are usually called He-sdBs, but here we follow the more detailed spectroscopic classification outlined in Sect. 3.2.

During our photometric follow-up campaign (Schaffenroth et al. in prep.) we obtained a light curve of J141549.05+111213.9 (see Fig. 9) showing irregular variations very similar to the ones found by Green et al. (2014). There might therefore be a link between those two phenonema. A similar light curve of J232757.46+483755.2 showed no such variations, but this might also be an indication for their transient nature. It remains to be seen whether the high RV variations we found are really connected to the light curve variations observed in similar stars.

Whether this behaviour is restricted to helium-rich sdOs only or might also affect hydrogen-rich sdOs is unclear. The possibly connected photometric variations discovered by Green et al. (2014) affect both kinds of sdOs. Also the distributions of maximum RV-shifts for both populations look quite similar (see Fig. 3 right panel, Fig. 7). However, since we focused our follow-up mostly on hydrogen-rich sdBs and helium-rich sdOs, we did not obtain a sufficient number of RVs to check for irregular variations in one of the hydrogen-rich sdOs. An important difference between the two populations is that at least some hydrogen-rich sdOs are known to reside in close binaries (see Kupfer et al. 2015 and references therein), whereas not a single He-sdO in a close binary system has been found yet.

Some ideas have been put forward to explain the light curve variations. Jeffery et al. (2013) suggested that the variations might be due to star spots caused by magnetic fields. They also discuss the possibility of a shallow reflection effect originating from the irradiated hemisphere of a cool low-mass companion. Bear & Soker (2014) propose a heated planetary companion with strong weather to be responsible for the variability of KIC 10449976. Green et al. (2014) see strong similarities of the variations detected in their stars to the variations seen in some cataclysmic variables and attribute them to the presence of accretion disks. The high and irregular RV variations seen in our objects can be hardly explained in those ways. A reflection effect binary with a low-mass companion should show periodic variations with small RV amplitudes and the presence of an accretion disk would require a close companion as well.

Another possible reason might be magnetic activity of those stars. Heber et al. (2013) reported the discovery of a He-sdO star with significant Zeeman-splitting and a magnetic field of several hundred kG. More of those objects have been discovered recently (Nemeth priv. comm.). Variable magnetic fields might lead to distortions of the spectral lines, which are not resolved in the medium-resolution spectra we have and may mimic irregular RV shifts. However, the very high RV shifts observed are again hardly consistent with such a scenario. High-resolution, time-resolved follow-up photometry, spectroscopy, and maybe also spectropolarimetry are necessary to study those mysterious RV shifts.

5. Summary

In this paper we provide classifications, atmospheric parameters and a complete RV catalogue containing 1914 single measurements of the 177 most likely RV variable hot subluminoous stars discovered in the MUCHFUSS project from SDSS DR7.

We detect a mismatch between the ΔRV_{\max} -distribution of the sdB and the more evolved sdOB and sdO stars, which challenges our understanding of their evolutionary connection. Our sample contains two candidates for He-WD progenitors. Furthermore, one of the RV variable sdB binaries is double-lined and a candidate for a hierarchical triple system.

Based on the ΔRV_{\max} -distribution of the hydrogen-rich sdB and sdOB stars we constrain the fraction of close massive compact companions in our sample to be smaller than $\sim 1.3\%$. However, the sample might still contain such binaries with longer periods exceeding ~ 8 d. Future studies should therefore concentrate on this parameter range.

Irregular RV variations of unknown origin with amplitudes of up to $\sim 180 \text{ km s}^{-1}$ on timescales of years, days and even hours have been detected in some He-sdO stars. They might be connected to irregular photometric variations in some cases.

Acknowledgements. T.R.M. acknowledges support from the UK's Science and Technology Facilities Council, grant ST/L000733/1. E.Z. and C.H. are supported by the Deutsche Forschungsgemeinschaft (DFG) through grants HE1356/45-2 and HE1356/62-1. T.K. acknowledges support by the Netherlands Research School for Astronomy (NOVA). V.S. is supported by Deutsches Zentrum für Luft- und Raumfahrt (DLR) under grant 50 OR 1110.

Based on observations at the La Silla-Paranal Observatory of the European Southern Observatory for programmes number 165.H-0588(A), 079.D-0288(A), 080.D-0685(A), 081.D-0819, 082.D-0649, 084.D-0348, 089.D-0265(A), 090.D-0012(A), 091.D-0038(A) and 092.D-0040(A).

Based on observations collected at the Centro Astronómico Hispano Alemán (CAHA) at Calar Alto, operated jointly by the Max-Planck Institut für Astronomie and the Instituto de Astrofísica de Andalucía (CSIC).

Based on observations with the William Herschel and Isaac Newton Telescopes operated by the Isaac Newton Group at the Observatorio del Roque de los Muchachos of the Instituto de Astrofísica de Canarias on the island of La Palma, Spain.

Based on observations with the Southern Astrophysical Research (SOAR) telescope operated by the U.S. National Optical Astronomy Observatory (NOAO), the Ministério da Ciência e Tecnologia of the Federal Republic of Brazil (MCT), the University of North Carolina at Chapel Hill (UNC), and Michigan State University (MSU).

Based on observations obtained at the Gemini Observatory, which is operated by the Association of Universities for Research in Astronomy, Inc., under a cooperative agreement with the NSF on behalf of the Gemini partnership: the National Science Foundation (United States), the Science and Technology Facilities Council (United Kingdom), the National Research Council (Canada), CONICYT (Chile), the Australian Research Council (Australia), Ministério da Ciência e Tecnologia (Brazil) and Ministerio de Ciencia, Tecnología e Innovación Productiva (Argentina).

Funding for the SDSS and SDSS-II has been provided by the Alfred P. Sloan Foundation, the Participating Institutions, the National Science Foundation, the U.S. Department of Energy, the National Aeronautics and Space Administration, the Japanese Monbukagakusho, the Max Planck Society, and the Higher Education Funding Council for England. The SDSS Web Site is <http://www.sdss.org/>.

The SDSS is managed by the Astrophysical Research Consortium for the Participating Institutions. The Participating Institutions are the American Museum of Natural History, Astrophysical Institute Potsdam, University of Basel, University of Cambridge, Case Western Reserve University, University of Chicago, Drexel University, Fermilab, the Institute for Advanced Study, the Japan Participation Group, Johns Hopkins University, the Joint Institute for Nuclear Astrophysics, the Kavli Institute for Particle Astrophysics and Cosmology, the Korean Scientist Group, the Chinese Academy of Sciences (LAMOST), Los Alamos National Laboratory, the Max-Planck-Institute for Astronomy (MPIA), the Max-Planck-Institute for Astrophysics (MPA), New Mexico State University, Ohio State University, University of Pittsburgh, University of Portsmouth, Princeton University, the United States Naval Observatory, and the University of Washington.

References

- Abazajian, K., Adelman-McCarthy, J. K., Agüeros, M. A., et al. 2009, *ApJS*, 182, 543
- Ahmad, A., Jeffery, C. S., & Fullerton, A. W. 2004, *A&A*, 418, 275
- Althaus, L. G., Panei, J. A., Miller Bertolami, M. M., et al. 2009, *ApJ*, 704, 1605
- Barlow, B. N., Wade, R. A., Liss, S. E., Østensen, R. H., & van Winckel, H. 2012, *ApJ*, 758, 58
- Barlow, B. N., Liss, S. E., Wade, R. A., & Green, E. M. 2013, *ApJ*, 771, 23
- Barlow, B. N., Wade, R., Liss, S., & Stark, M. 2014, *ASP Conf. Ser.*, 481, 301
- Bear, E., & Soker, N. 2014, *MNRAS*, 437, 1400
- Brown, W. R., Kilic, M., Allende Prieto, C., Gianninas, A., & Kenyon, S. 2012, 744, 142

- Copperwheat, C., Morales-Rueda, L., Marsh, T. R., et al. 2011, *MNRAS*, 415, 1381
- Dorman, B., Rood, R. T., & O’Connell, R. W. 1993, *ApJ*, 419, 596
- Driebe, T., Schönberner, D., Bloeker, T., & Herwig, F. 1998, *A&A*, 339, 123
- Drilling, J. S., Jeffery, C. S., Heber, U., Moehler, S., & Napiwotzki, R. 2013, *A&A*, 551, 31
- Edelmann, H., Heber, U., Altmann, M., Karl, C., & Lisker, T. 2005, *A&A*, 442, 1023
- Edelmann, H., Heber, U., Hagen, H.-J., et al. 2003, *A&A*, 400, 939
- Fontaine, G., Brassard, P., Charpinet, S., et al. 2012, *A&A*, 539, 12
- Geier, S., Nesslinger, S., Heber, U., et al. 2007, *A&A*, 464, 2990
- Geier, S., Nesslinger, S., Heber, U., et al. 2008, *A&A*, 477, L13
- Geier, S., Heber, U., Kupfer, T., & Napiwotzki, R. 2010a, *A&A*, 515, 37
- Geier, S., Heber, U., Podsiadlowski, Ph., et al. 2010b, *A&A*, 519, 25
- Geier, S., Hirsch, H., Tillich, A., et al. 2011a, *A&A*, 530, 28
- Geier, S., Maxted, P. F. L., Napiwotzki, R., et al. 2011b, *A&A*, 526, 39
- Geier, S., Schaffenroth, V., Drechsel, H., et al. 2011c, *ApJ*, 731, L22
- Geier, S. 2013, *EPJ Web of Conferences*, 43, 04001
- Geier, S., Heber, U., Edelmann, H., et al. 2013a, *A&A*, 557, 122
- Geier, S., Marsh, T. R., Wang, B., et al. 2013b, *A&A*, 554, 54
- Geier, S., Østensen, R. H., Heber, U., et al. 2014, *A&A*, 562, 95
- Geier, S., Kupfer, T., Schaffenroth, V., et al. 2015, *A&A*, in prep.
- Green, E. M., Fontaine, G., Hyde, E. A., For, B.-Q., & Chayer, P. 2008, *ASP Conf. Ser.*, 392, 75
- Green, E. M., Johnson, C. B., Wallace, S. C., et al. 2014, *ASP Conf. Ser.*, 481, 161
- Han, Z. 2008, *A&A*, 484, L31
- Han Z., Podsiadlowski P., Maxted P. F. L., Marsh T. R., & Ivanova N. 2002, *MNRAS*, 336, 449
- Han, Z., Podsiadlowski, P., Maxted, P. F. L., & Marsh, T. R. 2003, *MNRAS*, 341, 669
- Heber, U. 1986, *A&A*, 155, 33
- Heber, U. 2009, *ARA&A*, 47, 211
- Heber, U., Edelmann, H., Lisker, T., & Napiwotzki, R. 2003, *A&A*, 411, 477
- Heber, U., Geier, S., & Gänsicke, B. T. 2013, *EPJ Web of Conferences*, 43, 04002
- Heber, U., & Hirsch, H. 2010, *AIP Conf. Ser.*, 1314, 79
- Hirsch, H. 2009, PhD thesis, Friedrich-Alexander University Erlangen-Nürnberg
- Hirsch, H., & Heber, U. 2009, *JPhCS*, 172, 2015
- Iben, I., & Tutukov, A. V. 1984, *ApJ*, 284, 719
- Jeffery, C. S. 2008, *ASP Conf. Ser.*, 391, 3
- Jeffery, C. S., Ramsay, G., Naslim, N., et al. 2013, *MNRAS*, 429, 3207
- Kaplan, D. L., Bhalerao, V. B., van Kerkwijk, M. H., et al. 2013, *ApJ*, 765, 158
- Kleinman, S. J. 2010, *AIP Conf. Ser.*, 1237, 156
- Kupfer, T., Geier, S., Schaffenroth, V., et al. 2015, *A&A*, in press (arXiv:1501.07760)
- Lanz, T., Brown, T. M., Sweigart, A. V., Hubeny, I., & Landsman, W. B. 2004, *ApJ*, 602, 342
- Latour, M., Randall, S. K., Fontaine, G., et al. 2014, *ApJ*, 795, 106
- Lisker, T., Heber, U., Napiwotzki, R., Christlieb, N., Han, Z., et al. 2005, *A&A*, 430, 223
- Maxted, P. F. L., Heber, U., Marsh, T. R., & North, R. C. 2001, *MNRAS*, 326, 139
- Maxted, P. F. L., Marsh, T. R., & North, R. C. 2000a, *MNRAS*, 317, L41
- Miller Bertolami, M. M., Althaus, L. G., Unglaub, K., & Weiss, A. 2008, *A&A*, 491, 253
- Moehler, S., Richtler, T., de Boer, K. S., Dettmar, R. J., & Heber, U. 1990, *A&AS*, 86, 53
- Morales-Rueda, L., Maxted, P. F. L., Marsh, T. R., North, R. C., & Heber, U. 2003a, *MNRAS*, 338, 752
- Napiwotzki, R., Yungelson, L., Nelemans, G. et al. 2004, *ASP Conf. Ser.*, 318, 402
- Napiwotzki, R. 2008, *ASP Conf. Ser.*, 392, 139
- Naslim, N., Jeffery, C. S., Ahmad, S., Behara, N. T., & Sahin, T. 2010, *MNRAS*, 409, 582
- Naslim, N., Geier, S., Jeffery, C. S., et al. 2012, *MNRAS*, 423, 3031
- Nelemans, G. 2010, *Ap&SS*, 329, 25
- Nemeth, P., Kawka, A., & Vennes, S. 2012, *MNRAS*, 427, 2180
- Østensen, R. H., Silvotti, R., Charpinet, S., et al. 2010, *MNRAS*, 409, 1470
- Østensen, R. H., Degroote, P., Telting, J. H., et al. 2012, *ApJ*, 753, L17
- Østensen, R. H., Geier, S., Schaffenroth, V., et al. 2013, *A&A*, 559, 35
- O’Toole, S. J., Heber, U., Jeffery, S. J., et al. 2005, *A&A*, 440, 667
- O’Toole, S. J., & Heber, U. 2006, *A&A*, 452, 579
- Pfahl, E., Rappaport, S., & Podsiadlowski, Ph. 2003, *ApJ*, 597, 1036
- Podsiadlowski, Ph., Rappaport, S., & Pfahl, E. D. 2002, *ApJ*, 565, 1107
- Ramspeck, M., Heber, U., & Edelmann, H. 2001, *A&A*, 379, 235
- Rebassa-Mansergas, A., Gänsicke, B. T., Rodríguez-Gil, P., Schreiber, M. R., & Koester, D. 2007, *MNRAS*, 382, 1377
- Reindl, N., Geier, S., Kupfer, T., et al. 2015, *A&A*, in prep.
- Schaffenroth, V., Geier, S., Heber, U., et al. 2014, *A&A*, 564, 98
- Schaller, G., Schaerer, D., Meynet, G., & Maeder, A. 1992, *A&AS*, 96, 269
- Schönberner, D. 1983, *ApJ*, 272, 708
- Sener, H. T., & Jeffery, C. S. 2014, *MNRAS*, 440, 2676
- Silvotti, R., Østensen, R. H., Bloemen, S., et al. 2012, *MNRAS*, 424, 1752
- Ströer, A., Heber, U., Lisker, T., et al. 2007, *A&A*, 462, 269
- Tillich, A., Heber, U., Geier, S., et al. 2011, *A&A*, 527, 137
- Tutukov, A. V., & Yungelson, L. R. 1981, *Nauchnye Informatsii*, 49, 3
- Vennes, S., Kawka, A., O’Toole, S. J., Németh, P., & Burton, D. 2012, *ApJ*, 759, L25
- Vos, J., Østensen, R. H., Degroote, P., et al. 2012, *A&A*, 548, 6
- Vos, J., Østensen, R. H., Nemeth, P., et al. 2013, *A&A*, 559, 54
- Webbink, R. F. 1984, *ApJ*, 277, 355
- Werner, K., Rauch, T., & Kepler, S. O. 2014, *A&A*, 564, 53
- Yoon, S.-C., & Langer, N. 2004, *A&A*, 419, 645
- Yungelson, L. R., & Tutukov, A. V. 2005, *ARep*, 49, 871
- Zhang, X., & Jeffery, C. S. 2012, *MNRAS*, 419, 452

Appendix A: Appendix

Table 3. Parameters of 139 hydrogen-rich hot subdwarfs (89 RV variable, 50 RV variable candidates). Solved binaries are marked in bold face and their orbital parameters can be found in Kupfer et al. (2015) and references therein.

Name	Class	m_V [mag]	T_{eff} [K]	$\log g$	$\log y$	d [kpc]	Δt [d]	ΔRV_{max} [km s $^{-1}$]	N	$\log p$
J082332.09+113641.9^b	sdB	16.7	31200 ± 600	5.79 ± 0.06	-2.0 ± 0.1	2.6 ^{+0.2} _{-0.2}	53.9447	359.0 ± 6.5	22	< -680
J113840.68-003531.7^c	sdB	14.5	31200 ± 600	5.54 ± 0.09	< -3.0	1.2 ^{+0.2} _{-0.2}	3361.5592	332.0 ± 14.0	31	< -680
J165404.26+303701.8^c	sdB	15.4	24900 ± 800	5.39 ± 0.12	-2.4 ± 0.1	1.8 ^{+0.3} _{-0.3}	2.9365	271.0 ± 17.0	38	< -680
J225638.34+065651.1^c	sdB	15.3	28500 ± 500	5.64 ± 0.05	-2.3 ± 0.2	1.5 ^{+0.1} _{-0.1}	42.3494	269.0 ± 14.0	50	< -680
J172624.10+274419.3^c	sdB	16.0	32600 ± 500	5.84 ± 0.05	-2.2 ± 0.1	1.9 ^{+0.1} _{-0.1}	55.9741	263.0 ± 12.0	38	< -680
J150513.52+110836.6^c	sdB	15.4	33200 ± 500	5.80 ± 0.10	-2.3 ± 0.1	1.5 ^{+0.2} _{-0.2}	43.6564	222.0 ± 8.0	42	< -680
J134632.66+281722.7^b	sdB	14.9	28800 ± 600	5.46 ± 0.07	-2.6 ± 0.2	1.6 ^{+0.2} _{-0.2}	0.9988	191.0 ± 7.0	41	< -680
J002323.99-002953.2^c	sdB	15.5	29200 ± 500	5.69 ± 0.05	-2.0 ± 0.1	1.6 ^{+0.1} _{-0.1}	1.0413	168.0 ± 4.0	47	< -680
J083006.17+475150.4^b	sdB	16.0	25300 ± 600	5.38 ± 0.06	< -3.0	2.5 ^{+0.2} _{-0.2}	4405.6747	164.0 ± 9.0	37	< -680
J095238.93+625818.9^b	sdB	14.8	27700 ± 600	5.59 ± 0.06	-2.6 ± 0.1	1.2 ^{+0.1} _{-0.1}	1183.7390	154.0 ± 8.0	34	< -680
J162256.66+473051.1^d	sdB	16.2	29000 ± 600	5.65 ± 0.06	-1.9 ± 0.1	2.3 ^{+0.2} _{-0.2}	1.9832	135.0 ± 4.5	34	< -680
J012022.10+395059.4^e	sdB	15.4	28500 ± 100	5.42 ± 0.01	-3.0 ± 0.1	2.1 ^{+0.0} _{-0.0}	1358.9782	129.0 ± 6.5	22	< -680
J173606.25+315842.7	sdB	17.0	31300 ± 300	5.87 ± 0.09	-2.5 ± 0.2	2.8 ^{+0.3} _{-0.3}	1567.7104	195.0 ± 12.0	12	-537.49
J032138.67+053840.0^b	sdB	15.0	30700 ± 500	5.74 ± 0.06	-2.4 ± 0.1	1.3 ^{+0.1} _{-0.1}	1699.1435	110.0 ± 9.0	46	-536.46
J191908.76+371423.9	sdB	17.2	28300 ± 400	5.69 ± 0.10	-2.7 ± 0.3	3.4 ^{+0.5} _{-0.4}	68.8608	237.0 ± 12.0	15	-526.21
J102151.64+301011.9^a	sdB	18.3	30700 ± 500	5.71 ± 0.06	< -3.0	5.8 ^{+0.5} _{-0.5}	14.9363	277.0 ± 37.0	19	-508.16
J204613.40-045418.7^c	sdB	16.2	31600 ± 500	5.54 ± 0.08	< -3.0	2.8 ^{+0.3} _{-0.3}	286.2265	259.0 ± 16.0	22	-480.28
J173806.51+451701.7	sdB	17.4	30500 ± 500	5.40 ± 0.08	< -3.0	5.5 ^{+0.6} _{-0.6}	1.9536	233.0 ± 8.5	13	-461.58
J183249.04+630910.7^b	sdB	15.8	26800 ± 700	5.29 ± 0.09	-2.6 ± 0.1	2.7 ^{+0.4} _{-0.3}	1487.7733	141.0 ± 8.0	17	-453.62
J164326.04+330113.1 ^a	sdB	16.3	27900 ± 500	5.62 ± 0.07	-2.3 ± 0.2	2.4 ^{+0.2} _{-0.2}	2.8085	175.0 ± 5.5	10	-452.26
J011857.19-002546.5^b	sdB	14.9	27900 ± 600	5.55 ± 0.07	< -3.0	1.3 ^{+0.1} _{-0.1}	265.2187	140.0 ± 8.0	43	-386.44
J192059.78+372220.0 ^f	sdB	15.8	27600 ± 600	5.40 ± 0.10	-2.5 ± 0.3	2.4 ^{+0.3} _{-0.3}	1.9589	123.0 ± 4.5	15	-319.72
J150829.02+494050.9^b	sdB	17.7	29600 ± 600	5.73 ± 0.07	-2.3 ± 0.1	4.3 ^{+0.5} _{-0.4}	2161.9292	209.0 ± 15.5	58	-269.10
J180940.41+234328.4	sdB	16.5	28500 ± 300	5.44 ± 0.06	-2.9 ± 0.2	3.3 ^{+0.4} _{-0.3}	2909.9029	342.0 ± 29.5	36	-215.11
J183349.79+652056.3	sdB	17.4	27200 ± 500	5.56 ± 0.12	-2.6 ± 0.1	4.1 ^{+0.7} _{-0.7}	68.8591	177.0 ± 9.5	16	-190.20
J095101.28+034757.0^b	sdB	15.9	29800 ± 300	5.48 ± 0.04	-2.8 ± 0.3	2.5 ^{+0.1} _{-0.1}	1.0425	183.0 ± 13.0	31	-170.79
J082053.53+000843.4^g	sdB	15.2	26700 ± 900	5.48 ± 0.10	-2.0 ± 0.1	1.6 ^{+0.1} _{-0.1}	388.9794	99.0 ± 11.5	24	-153.08
J080738.96-083322.6	sdB	17.2	27600 ± 600	5.61 ± 0.17	-2.7 ± 0.3	3.6 ^{+0.9} _{-0.7}	0.0736	298.0 ± 19.0	27	-136.25
J152222.15-013018.3^b	sdB	17.8	25200 ± 700	5.47 ± 0.09	< -3.0	5.2 ^{+0.7} _{-0.6}	3.0055	173.0 ± 30.0	26	-126.07
J155628.34+011335.0 ^a	sdB	16.2	32700 ± 600	5.51 ± 0.08	-2.9 ± 0.2	3.1 ^{+0.4} _{-0.2}	4412.8910	118.0 ± 10.5	15	-121.64
J113241.58-063652.8^b	sdO	16.2	46400 ± 1000	5.89 ± 0.07	-2.9 ± 0.2	2.4 ^{+0.2} _{-0.2}	1517.8240	103.0 ± 10.0	32	-108.89
J222850.00+391917.4	sdB	16.4	33500 ± 900	5.80 ± 0.10	-1.7 ± 0.1	2.4 ^{+0.4} _{-0.3}	2051.8410	104.0 ± 7.5	40	-85.63
J173057.94+320737.0	sdB	16.2	28200 ± 700	5.40 ± 0.05	-2.9 ± 0.2	3.0 ^{+0.2} _{-0.2}	1.9680	94.0 ± 8.0	6	-69.42
J083334.76-045759.4	sdB	18.2	20500 ± 700	5.52 ± 0.10	< -3.0	5.0 ^{+0.8} _{-0.7}	14.8908	161.0 ± 8.5	11	-66.11
J164853.26+121703.0	sdB	18.5	30400 ± 500	5.38 ± 0.11	< -3.0	9.3 ^{+1.4} _{-1.2}	0.0684	135.0 ± 13.0	11	-64.89
J072245.27+305233.4	sdB	18.0	25900 ± 700	5.61 ± 0.16	-2.6 ± 0.2	5.0 ^{+1.2} _{-0.9}	1.0019	123.0 ± 12.0	7	-62.09
J093059.63+025032.3	sdB	15.0	30000 ± 600	5.67 ± 0.18	-2.7 ± 0.2	1.3 ^{+0.3} _{-0.3}	2986.7695	91.0 ± 9.0	10	-49.22
J203526.46+141948.4	sdB	18.7	30200 ± 600	5.57 ± 0.07	-2.9 ± 0.2	8.3 ^{+0.9} _{-0.8}	1.0235	163.0 ± 25.5	12	-33.12
J203843.97+141706.0	sdOB	18.7	36800 ± 1000	5.89 ± 0.20	-2.4 ± 0.3	6.8 ^{+1.9} _{-1.5}	0.9067	102.0 ± 10.5	12	-32.22
J095229.62+301553.6 ^a	sdOB	18.5	35200 ± 1200	5.05 ± 0.17	< -3.0	16.0 ^{+3.8} _{-3.3}	1155.7612	198.0 ± 27.5	5	-28.52
J154531.01+563944.7	sdB	17.0	26200 ± 900	5.13 ± 0.14	-2.0 ± 0.2	5.5 ^{+1.3} _{-1.0}	2527.7769	70.0 ± 8.5	9	-27.76
J200959.27-115519.9	sdB	18.7	29700 ± 700	5.31 ± 0.08	< -3.0	10.7 ^{+1.3} _{-1.2}	1.9832	156.0 ± 23.0	8	-27.48
J005107.01+004232.5	sdOB	15.9	38500 ± 300	5.83 ± 0.07	-1.0 ± 0.1	2.0 ^{+0.2} _{-0.2}	2.0256	54.0 ± 6.5	7	-24.96
J104248.94+033355.3	sdO	17.6	41200 ± 3200	4.83 ± 0.15	-2.1 ± 0.4	14.5 ^{+3.4} _{-2.8}	2246.6948	49.0 ± 5.0	2	-24.34
J181141.86+241902.7	sdB	18.7	-	-	-	-	0.9972	248.0 ± 26.0	7	-23.56
J071424.12+401645.9	sdB	18.2	27700 ± 700	5.38 ± 0.11	-2.6 ± 0.1	7.6 ^{+1.2} _{-1.1}	2.9312	152.0 ± 24.0	9	-23.37
J204300.90+002145.0 ^a	sdO	17.9	40200 ± 700	6.15 ± 0.13	-1.3 ± 0.4	3.6 ^{+0.6} _{-0.5}	18.8480	65.0 ± 6.5	9	-22.54
J191645.87+371224.5	sdB	18.3	33200 ± 1000	5.84 ± 0.17	-2.7 ± 0.2	5.6 ^{+1.1} _{-1.1}	3.0338	134.0 ± 23.5	19	-22.15
J094750.71+162731.8	sdB	17.4	30000 ± 700	6.25 ± 0.31	-2.2 ± 0.3	2.1 ^{+1.0} _{-0.7}	0.8902	130.0 ± 13.5	5	-20.08
J115358.81+353929.0 ^a	sdOB	16.6	29400 ± 500	5.49 ± 0.06	-2.5 ± 0.3	3.3 ^{+0.3} _{-0.3}	1151.6544	79.0 ± 9.5	5	-19.15
J175125.67+255003.5 ^a	sdB	17.4	30600 ± 500	5.48 ± 0.08	< -3.8	5.0 ^{+0.6} _{-0.5}	1533.6229	72.0 ± 10.0	8	-16.50
J125702.30+435245.8 ^a	sdB	18.2	28000 ± 1100	5.77 ± 0.17	< -3.0	4.9 ^{+1.3} _{-1.0}	0.0098	63.0 ± 16.5	3	-16.32
J165446.26+182224.6	sdB	18.6	30100 ± 500	5.50 ± 0.08	-1.7 ± 0.1	8.5 ^{+1.0} _{-0.9}	1396.0335	48.0 ± 5.5	3	-15.27
J120855.51+403716.1	sdB	18.6	34100 ± 900	5.98 ± 0.13	-1.5 ± 0.1	5.4 ^{+1.0} _{-0.9}	0.0260	171.0 ± 20.0	7	-14.61
J164122.32+334452.0	sdB	15.5	28200 ± 500	5.49 ± 0.11	-2.5 ± 0.3	1.9 ^{+0.3} _{-0.3}	2213.5393	77.0 ± 8.0	8	-14.60
J211421.39+100411.4	sdOB	18.4	36100 ± 900	5.48 ± 0.13	-2.5 ± 0.3	9.2 ^{+1.6} _{-1.4}	1427.1132	69.0 ± 12.0	7	-14.02
J170810.97+244341.6 ^a	sdOB	18.5	35600 ± 800	5.58 ± 0.14	-0.8 ± 0.1	8.5 ^{+1.6} _{-1.4}	0.0125	160.0 ± 26.0	3	-13.73
J153411.10+543345.2 ^a	sdOB	16.9	34800 ± 700	5.64 ± 0.09	-2.6 ± 0.3	3.8 ^{+0.5} _{-0.3}	0.0184	83.0 ± 18.5	8	-12.52
J224518.65+220746.5	sdB	16.6	34000 ± 800	5.82 ± 0.07	-2.2 ± 0.1	2.6 ^{+0.3} _{-0.3}	1080.8857	70.0 ± 11.5	9	-12.28
J120613.40+205523.1	sdOB	18.4	35000 ± 500	5.35 ± 0.07	< -3.0	10.5 ^{+1.0} _{-0.9}	2.9112	91.0 ± 23.5	10	-11.37
J204247.51+001913.9 ^b	sdB	19.6	34200 ± 400	5.89 ± 0.08	-1.3 ± 0.1	9.6 ^{+1.1} _{-1.0}	1393.1941	69.0 ± 10.0	3	-10.83
J151314.23+234248.8	sdB	17.1	28700 ± 300	5.69 ± 0.10	-2.3 ± 0.2	3.3 ^{+0.4} _{-0.4}	2.0006	58.0 ± 8.5	3	-10.83
J082944.75+132302.5	sdOB	17.2	39700 ± 600	5.42 ± 0.04	< -3.0	6.1 ^{+0.3} _{-0.3}	24.9992	90.0 ± 16.5	5	-10.40

Name	Class	m_V [mag]	T_{eff} [K]	$\log g$	$\log y$	d [kpc]	Δt [d]	ΔRV_{max} [km s $^{-1}$]	N	$\log p$
J074534.16+372718.5 ^a	sdB	17.9	37500 ± 500	5.90 ± 0.09	< -3.0	4.6 ^{+0.5} _{-0.7}	0.0363	64.0 ± 17.0	8	-9.74
J202313.83+131254.9 ^a	sdB	17.2	29600 ± 600	5.64 ± 0.14	-2.1 ± 0.1	3.8 ^{+0.7} _{-0.6}	1201.7981	123.0 ± 19.0	5	-9.20
J162610.34+130401.6	sdB	19.4	33900 ± 500	5.63 ± 0.10	-1.0 ± 0.1	12.1 ^{+1.7} _{-1.5}	780.7541	51.0 ± 8.0	3	-9.16
J030607.95+382335.7 ⁱ	sdO	16.8	30100 ± 300	5.64 ± 0.03	-2.1 ± 0.1	3.2 ^{+0.1} _{-0.1}	2210.7452	48.0 ± 6.5	8	-8.85
J204451.08-062753.8	sdO	20.0	57100 ± 5200	5.61 ± 0.15	-2.2 ± 0.4	21.4 ^{+5.1} _{-4.2}	1087.0571	62.0 ± 10.5	3	-7.88
J091615.49+132833.1	sdB	17.5	30900 ± 400	5.48 ± 0.05	< -3.0	5.4 ^{+0.4} _{-0.4}	0.9512	55.0 ± 11.5	3	-7.58
J163413.09+153109.5	sdB	18.3	34600 ± 900	4.73 ± 0.12	-2.0 ± 0.5	20.7 ^{+3.5} _{-3.1}	1105.3751	21.0 ± 5.5	3	-7.44
J123220.09+260913.3	sdB	18.1	33700 ± 1100	5.40 ± 0.16	-1.3 ± 0.2	8.5 ^{+2.7} _{-1.7}	1.0302	134.0 ± 27.0	5	-7.36
J185129.02+182358.8	sdB	16.8	27800 ± 700	5.38 ± 0.10	< -3.0	3.9 ^{+0.6} _{-0.5}	0.0808	105.0 ± 18.0	22	-7.33
J220048.67+123612.4 ^h	sdO	18.6	64200 ± 2600	5.63 ± 0.11	-1.3 ± 0.1	11.4 ^{+1.8} _{-1.6}	2437.2535	53.0 ± 9.5	3	-7.04
J153752.95+160201.8	sdB	18.4	32300 ± 500	5.47 ± 0.07	< -3.0	8.5 ^{+0.9} _{-0.8}	0.0361	68.0 ± 12.5	3	-7.03
J183229.22+402418.4	sdO	15.7	40100 ± 600	5.35 ± 0.11	-2.0 ± 0.2	3.3 ^{+0.8} _{-0.4}	3.0098	50.0 ± 11.5	5	-6.82
J181126.83+233413.7	sdB	18.4	—	—	—	—	1.0156	121.0 ± 20.5	7	-6.47
J204448.63+153638.8 ^a	sdB	17.9	29600 ± 600	5.57 ± 0.09	-2.2 ± 0.1	5.7 ^{+0.7} _{-0.7}	3.0489	101.0 ± 17.5	7	-6.41
J185414.11+175200.2	sdOB	16.9	35200 ± 700	5.89 ± 0.08	-1.4 ± 0.1	2.9 ^{+0.3} _{-0.3}	6.0874	81.0 ± 22.0	10	-6.25
J171629.92+575121.2 ^a	sdOB	18.2	37500 ± 800	5.57 ± 0.10	< -0.7	7.8 ^{+1.0} _{-0.9}	3195.9096	67.0 ± 15.5	12	-6.14
J184434.74+412158.7	sdB	17.3	27200 ± 500	5.57 ± 0.12	-2.6 ± 0.1	4.0 ^{+0.7} _{-0.6}	2.9795	56.0 ± 14.0	5	-5.72
J091136.73+124015.2	sdB	18.2	—	—	—	—	0.0173	75.0 ± 16.5	3	-5.31
J151337.80+195012.5	sdB	18.9	—	—	—	—	0.0354	98.0 ± 33.5	4	-5.16
J172727.55+091215.5 ⁱ	sdO	17.5	40100 ± 1100	5.36 ± 0.09	< -2.1	7.4 ^{+0.9} _{-0.8}	0.0141	55.0 ± 10.5	6	-5.10
J112242.69+613758.5 ^a	sdB	15.4	29300 ± 500	5.69 ± 0.10	-2.3 ± 0.3	1.5 ^{+0.2} _{-0.2}	0.0469	83.0 ± 18.5	6	-5.08
J161140.50+201857.0 ^a	sdOB	18.5	36900 ± 700	5.89 ± 0.13	-1.2 ± 0.1	6.1 ^{+1.7} _{-0.9}	0.9472	108.0 ± 23.5	5	-4.77
J065044.30+383133.7	sdOB	17.3	34200 ± 400	5.76 ± 0.07	-2.9 ± 0.2	3.9 ^{+0.4} _{-0.3}	0.0131	88.0 ± 13.5	14	-4.63
J170645.57+243208.6 ^a	sdB	17.8	32000 ± 500	5.59 ± 0.07	< -4.0	5.5 ^{+0.6} _{-0.5}	0.0125	46.0 ± 12.0	3	-4.41
J083359.65-043521.9	sdOB	18.3	36100 ± 500	5.92 ± 0.11	-1.9 ± 0.2	5.5 ^{+0.8} _{-0.7}	14.9765	88.0 ± 25.5	11	-4.39
J140545.25+014419.0 ^a	sdB	15.8	27300 ± 800	5.37 ± 0.16	-1.9 ± 0.2	2.5 ^{+0.6} _{-0.5}	0.0263	25.0 ± 8.0	3	-4.12
J160534.96+062733.5	sdB	19.3	—	—	—	—	1.0113	132.0 ± 41.0	8	-3.97
J221920.67+394603.5	sdO	17.3	47000 ± 3500	5.73 ± 0.16	< -3.0	4.7 ^{+1.2} _{-0.9}	62.8679	66.0 ± 12.5	8	-3.93
J183840.52+400226.8	sdB	17.8	29300 ± 900	5.52 ± 0.13	-1.6 ± 0.2	5.5 ^{+1.1} _{-0.9}	2.9795	74.0 ± 20.0	5	-3.89
J115716.37+612410.7 ^a	sdB	17.2	29900 ± 500	5.59 ± 0.08	-3.2 ± 0.8	4.0 ^{+0.5} _{-0.4}	2250.6902	102.0 ± 27.0	7	-3.63
J113303.70+290223.0 ^a	sdB/DA	18.9	—	—	—	—	0.0158	95.0 ± 30.0	3	-3.39
J161817.65+120159.6 ^a	sdB	18.0	32100 ± 1000	5.35 ± 0.23	< 0.0	8.1 ^{+2.8} _{-2.1}	0.0427	105.0 ± 28.0	4	-3.35
J205101.72+011259.7	sdB+X	17.6	—	—	—	—	0.0141	91.0 ± 31.5	8	-3.28
J133638.81+111949.4 ^a	sdB	17.3	27500 ± 500	5.49 ± 0.08	-2.7 ± 0.2	4.4 ^{+0.5} _{-0.5}	0.0301	48.0 ± 14.0	3	-3.25
J094044.07+004759.6 ^h	sdB	19.1	37000 ± 800	5.82 ± 0.13	-0.1 ± 0.1	8.8 ^{+1.5} _{-1.3}	2982.7971	30.0 ± 8.5	2	-3.24
J210454.89+110645.5 ^a	sdOB	17.3	37800 ± 700	5.63 ± 0.10	-2.4 ± 0.2	4.9 ^{+0.6} _{-0.6}	2548.0064	139.0 ± 27.5	9	-3.14
J211651.96+003328.5 ^a	sdB	18.0	27900 ± 800	5.78 ± 0.15	-3.9 ± 0.7	4.3 ^{+0.9} _{-0.8}	0.0161	47.0 ± 15.0	3	-3.08
J091428.87+125023.8	sdB	18.0	33600 ± 600	5.54 ± 0.11	< -3.0	7.0 ^{+1.1} _{-0.9}	0.0176	49.0 ± 13.5	3	-3.07
J112014.86+412127.3	sdB	18.1	—	—	—	—	1503.8023	23.0 ± 7.5	2	-2.98
J173614.19+335249.5	sdB	18.8	—	—	—	—	0.0410	85.0 ± 26.0	5	-2.97
J092520.70+470330.6 ^a	sdB	17.7	28100 ± 900	5.17 ± 0.15	-2.5 ± 0.2	7.5 ^{+1.7} _{-1.4}	0.0126	40.0 ± 12.5	3	-2.88
J171617.33+553446.7 ^a	sdB	17.2	32900 ± 900	5.48 ± 0.09	< -3.0	4.9 ^{+0.7} _{-0.6}	0.0125	130.0 ± 40.5	9	-2.85
J064809.54+380850.1	sdB	18.4	29300 ± 800	5.26 ± 0.13	-2.8 ± 0.3	9.8 ^{+1.9} _{-1.6}	0.9989	48.0 ± 13.0	5	-2.85
J075937.15+541022.2 ^a	sdB	17.8	31300 ± 700	5.30 ± 0.10	-3.3 ± 0.3	7.6 ^{+1.1} _{-1.0}	0.0233	40.0 ± 18.5	3	-2.75
J001844.33-093855.0	sdB	18.8	—	—	—	—	1169.8455	27.0 ± 8.0	3	-2.75
J130439.57+312904.8 ^a	sdOB	17.1	38100 ± 600	5.69 ± 0.12	-0.4 ± 0.1	4.1 ^{+0.6} _{-0.6}	0.0163	49.0 ± 27.5	3	-2.63
J143347.59+075416.9	sdOB	16.7	36600 ± 600	6.16 ± 0.13	< -0.5	1.9 ^{+0.3} _{-0.3}	805.7659	52.0 ± 10.5	11	-2.61
J153540.30+173458.8	sdB	18.0	—	—	—	—	0.0168	58.0 ± 16.5	3	-2.57
J202758.63+773924.5 ^a	sdO	17.9	46200 ± 3200	5.48 ± 0.18	-2.8 ± 0.9	8.2 ^{+2.2} _{-1.8}	1.9601	114.0 ± 33.0	3	-2.48
J215648.71+003620.7 ^a	sdB	18.0	30800 ± 800	5.77 ± 0.12	-2.2 ± 0.3	4.7 ^{+0.8} _{-0.7}	822.1114	100.0 ± 28.0	6	-2.38
J073701.45+225637.6	sdB	16.8	28100 ± 300	5.45 ± 0.04	< -3.0	3.7 ^{+0.2} _{-0.2}	2.0639	53.0 ± 14.5	5	-2.36
J220810.05+115913.9	sdB	17.4	27200 ± 600	5.23 ± 0.07	-2.3 ± 0.3	6.1 ^{+0.6} _{-0.6}	2172.7020	42.0 ± 12.5	5	-2.31
J172919.04+072204.5	sdO	17.3	49200 ± 1900	5.78 ± 0.12	-3.0 ± 0.4	4.6 ^{+0.8} _{-0.7}	0.0179	58.0 ± 20.0	5	-2.22
J031226.01+001018.2	sdB	19.2	—	—	—	—	2552.8670	71.0 ± 30.5	2	-2.17
J204546.81-054355.6 ^a	sdB	17.9	35500 ± 500	5.47 ± 0.09	-1.4 ± 0.2	7.3 ^{+0.9} _{-0.8}	0.0128	41.0 ± 16.5	4	-2.15
J133200.95+673325.7	sdOB	17.2	37400 ± 500	5.90 ± 0.09	-1.5 ± 0.1	3.4 ^{+0.4} _{-0.4}	2584.9083	53.0 ± 14.5	7	-2.09
J120427.94+172745.3	sdB	18.3	25100 ± 900	5.25 ± 0.15	-2.6 ± 0.4	8.2 ^{+1.9} _{-1.5}	0.0282	68.0 ± 29.0	3	-2.05
J204550.97+153536.3	sdB	18.2	30300 ± 500	5.62 ± 0.09	< -3.0	6.3 ^{+0.8} _{-0.7}	5.9148	58.0 ± 13.5	7	-1.98
J135807.96+261215.5 ^a	sdB	17.9	33500 ± 600	5.66 ± 0.10	> +2.0	5.8 ^{+0.8} _{-0.7}	0.0302	86.0 ± 26.0	6	-1.89
J113935.45+614953.9 ^a	sdB	16.9	28800 ± 900	5.27 ± 0.15	-2.8 ± 0.3	4.9 ^{+1.1} _{-0.9}	0.0112	30.0 ± 10.5	3	-1.86
J155343.39+131330.4	sdOB	18.5	36300 ± 500	5.63 ± 0.16	-0.8 ± 0.1	8.1 ^{+1.7} _{-1.4}	0.0160	64.0 ± 24.0	3	-1.77

Name	Class	m_V [mag]	T_{eff} [K]	$\log g$	$\log y$	d [kpc]	Δt [d]	ΔRV_{max} [km s $^{-1}$]	N	$\log p$
J082657.29+122818.1	sdOB	17.1	36500 ± 400	5.83 ± 0.12	-1.4 ± 0.1	3.4 $^{+0.5}_{-0.5}$	0.0142	67.0 ± 22.0	4	-1.73
J152705.03+110843.9 ^a	sdOB	17.3	37600 ± 500	5.62 ± 0.10	-0.5 ± 0.1	4.8 $^{+0.6}_{-0.5}$	0.0543	43.0 ± 12.0	5	-1.73
J052544.93+630726.0 ^a	sdOB	17.7	35600 ± 800	5.85 ± 0.10	-1.6 ± 0.2	4.3 $^{+0.6}_{-0.5}$	0.0264	42.0 ± 15.0	5	-1.73
J100535.76+223952.1 ^a	sdB	18.4	29000 ± 700	5.43 ± 0.13	-2.7 ± 0.2	7.9 $^{+1.5}_{-1.3}$	0.0192	41.0 ± 14.0	4	-1.71
J164204.37+440303.2	sdB	16.8	29300 ± 800	5.09 ± 0.13	-2.5 ± 0.3	5.7 $^{+1.3}_{-0.9}$	0.0273	31.0 ± 11.5	4	-1.68
J090957.82+622927.0	sdO	16.4	48000 ± 4900	5.68 ± 0.17	-1.7 ± 0.6	3.4 $^{+1.0}_{-0.8}$	0.0461	37.0 ± 12.0	4	-1.64
J152458.81+181940.5	sdO	18.3	52300 ± 2500	5.28 ± 0.08	-2.8 ± 0.3	13.5 $^{+1.7}_{-1.5}$	0.0155	41.0 ± 15.0	3	-1.60
J112140.20+183613.7	sdB	18.6	28100 ± 500	5.46 ± 0.10	-1.8 ± 0.1	8.3 $^{+1.2}_{-1.1}$	0.9796	71.0 ± 26.0	4	-1.57
J151254.55+150447.0	sdOB	17.8	38300 ± 600	6.01 ± 0.10	-1.5 ± 0.2	4.0 $^{+0.3}_{-0.5}$	0.0229	65.0 ± 28.0	3	-1.54
J233406.11+462249.3 ^a	sdB	17.7	34600 ± 500	5.71 ± 0.09	-1.3 ± 0.1	4.9 $^{+0.6}_{-0.6}$	0.0248	31.0 ± 12.0	3	-1.53
J095054.97+460405.2	sdB	18.0	28500 ± 500	5.24 ± 0.07	-2.3 ± 0.3	8.1 $^{+0.8}_{-1.0}$	0.0390	42.0 ± 16.5	3	-1.52
J112526.95+112902.6	sdOB	17.4	36100 ± 700	6.06 ± 0.12	-0.8 ± 0.1	2.9 $^{+0.8}_{-0.4}$	0.0142	70.0 ± 31.0	4	-1.50
J163834.68+265110.2	sdOB	17.0	36000 ± 300	5.80 ± 0.05	-1.6 ± 0.1	3.4 $^{+0.2}_{-0.2}$	0.0159	40.0 ± 13.0	4	-1.50
J203017.81+131849.2	sdOB	16.8	37100 ± 500	5.92 ± 0.09	-1.4 ± 0.1	2.7 $^{+0.3}_{-0.3}$	1200.7860	52.0 ± 20.0	5	-1.47
J130059.20+005711.7 ^a	sdOB	16.5	40700 ± 500	5.53 ± 0.10	-0.6 ± 0.1	3.9 $^{+0.5}_{-0.4}$	0.0123	36.0 ± 14.5	3	-1.43

Notes. ^(a) Atmospheric parameters taken from Geier et al. (2011a). ^(b) Atmospheric parameters taken from Kupfer et al. (2015). ^(c) Atmospheric parameters taken from Geier et al. (2011b). ^(d) Atmospheric parameters taken from Schaffenroth et al. (2014). ^(e) Atmospheric parameters taken from Østensen et al. (2013). ^(f) Atmospheric parameters taken from Schaffenroth et al. in prep. ^(g) Atmospheric parameters taken from Geier et al. (2011c). ^(h) Atmospheric parameters derived from a spectrum taken with ESO-VLT/FORS1. ⁽ⁱ⁾ Atmospheric parameters derived from a spectrum taken with WHT/ISIS.

Table 4. Parameters of 25 helium-rich hot subdwarfs (14 RV variable, 11 RV variable candidates).

Name	Class	m_V [mag]	T_{eff} [K]	$\log g$	$\log y$	d [kpc]	Δt [d]	ΔRV_{max} [km s $^{-1}$]	N	$\log p$
J232757.46+483755.2 ^a	He-sdO	15.8	64700 ± 2000	5.40 ± 0.08	> +2.0	4.2 $^{+0.5}_{-0.4}$	1799.6136	176.0 ± 20.5	59	-680.31
J141549.05+111213.9 ^a	He-sdO	16.1	43100 ± 800	5.81 ± 0.17	> +2.0	2.4 $^{+0.5}_{-0.4}$	0.0075	125.0 ± 17.0	35	-86.42
J103549.68+092551.9 ^a	He-sdO	16.3	48100 ± 600	6.02 ± 0.13	> +2.0	2.2 $^{+0.4}_{-0.3}$	3541.9636	53.0 ± 4.0	6	-54.25
J170045.09+391830.3	He-sdOB	18.2	36500 ± 1600	5.87 ± 0.16	+0.1 ± 0.1	5.5 $^{+1.2}_{-1.0}$	2160.0414	118.0 ± 11.5	10	-44.76
J161014.87+045046.6	He-sdO	17.3	48400 ± 1400	6.31 ± 0.09	> +2.0	2.5 $^{+0.3}_{-0.3}$	0.0124	138.0 ± 17.0	14	-31.77
J110215.45+024034.1 ^a	He-sdO	17.5	56600 ± 4200	5.36 ± 0.22	> +2.0	8.9 $^{+3.0}_{-2.2}$	0.0332	62.0 ± 8.5	3	-10.91
J174516.32+244348.3 ^a	He-sdO	17.7	43400 ± 1000	5.62 ± 0.21	> +2.0	6.2 $^{+1.8}_{-1.4}$	1220.5806	134.0 ± 25.5	13	-8.81
J160304.07+165953.8 ^b	He-sdO	16.9	45400 ± 300	6.10 ± 0.07	> +2.0	2.5 $^{+0.2}_{-0.2}$	0.9087	71.0 ± 18.5	5	-8.11
J094856.95+334151.0 ^a	He-sdO	17.7	51000 ± 1200	5.87 ± 0.12	+1.8 ± 0.5	5.1 $^{+0.7}_{-0.7}$	0.0123	74.0 ± 14.0	3	-7.73
J152136.25+162150.3	He-sdO	17.1	47400 ± 1000	5.81 ± 0.08	+1.6 ± 0.4	4.0 $^{+0.4}_{-0.4}$	2175.9687	77.0 ± 24.0	9	-5.94
J163416.08+221141.0	He-sdOB	15.5	38300 ± 1400	5.65 ± 0.26	> +2.0	2.0 $^{+0.8}_{-0.6}$	653.3309	35.0 ± 6.5	6	-5.55
J153237.94+275636.9	He-sdO	18.5	37700 ± 1300	6.09 ± 0.22	+0.0 ± 0.2	5.0 $^{+1.5}_{-0.6}$	1.0012	73.0 ± 16.5	3	-5.52
J233914.00+134214.3	He-sdO	17.6	48100 ± 1600	5.65 ± 0.25	> +2.0	6.0 $^{+1.1}_{-1.6}$	1451.6391	72.0 ± 11.8	12	-5.11
J173034.09+272139.8 ^c	He-sdO	18.9	39500 ± 700	5.83 ± 0.17	+0.1 ± 0.1	8.1 $^{+1.8}_{-1.5}$	698.7112	41.0 ± 10.0	2	-5.00
J170214.00+194255.1 ^b	He-sdO	15.8	44300 ± 600	5.79 ± 0.11	> +2.0	2.1 $^{+0.3}_{-0.3}$	1665.2088	38.0 ± 10.0	5	-3.76
J081329.81+383326.9	He-sdO	17.5	45800 ± 800	6.11 ± 0.11	+1.8 ± 0.4	3.3 $^{+0.5}_{-0.5}$	0.0175	54.0 ± 13.0	6	-3.35
J204940.85+165003.6 ^a	He-sdO	17.9	43000 ± 700	5.71 ± 0.13	> +2.0	6.2 $^{+1.1}_{-0.9}$	5.9325	84.0 ± 18.5	7	-3.13
J160623.21+363005.4	He-sdOB	18.5	36400 ± 700	5.34 ± 0.17	-0.5 ± 0.1	11.3 $^{+2.6}_{-2.1}$	1414.9811	67.0 ± 19.5	2	-3.04
J112414.45+402637.1 ^a	He-sdO	18.0	47100 ± 1000	5.81 ± 0.23	> +1.7	5.9 $^{+1.9}_{-1.4}$	0.0215	62.0 ± 18.5	3	-2.65
J161059.80+053625.2 ^b	He-sdO	17.2	46300 ± 700	6.22 ± 0.10	+1.0 ± 0.6	2.6 $^{+0.3}_{-0.3}$	751.7674	38.0 ± 9.5	4	-2.64
J151415.66-012925.2 ^a	He-sdO	17.0	48200 ± 500	5.85 ± 0.08	+1.7 ± 0.4	3.6 $^{+0.4}_{-0.3}$	3.9687	66.0 ± 20.5	5	-2.58
J161938.64+252122.4	He-sdOB	17.5	35000 ± 2000	5.80 ± 0.33	-0.4 ± 0.2	4.3 $^{+2.1}_{-1.5}$	0.9716	67.0 ± 26.0	3	-1.81
J160450.44+051909.2	He-sdOB	18.5	38100 ± 700	5.22 ± 0.27	+1.2 ± 0.2	13.7 $^{+3.2}_{-3.8}$	0.9736	145.0 ± 61.0	8	-1.75
J090252.99+073533.9	He-sdO	17.4	40100 ± 500	5.91 ± 0.19	> +2.0	3.7 $^{+0.9}_{-0.7}$	1612.4334	67.0 ± 27.0	5	-1.65
J081304.04-071306.5	He-sdO	18.6	48200 ± 900	5.93 ± 0.14	+1.8 ± 0.5	7.0 $^{+1.3}_{-1.1}$	0.9897	137.0 ± 41.0	7	-1.50

Notes. ^(a) Atmospheric parameters taken from Geier et al. (2011a). ^(b) Atmospheric parameters derived from a spectrum taken with ESO-VLT/FORS1. ^(c) Atmospheric parameters derived from a spectrum taken with WHT/ISIS.

Table 5. Parameters of 13 other types of hot stars (7 RV variable, 6 RV variable candidates).

Name	Class	m_V [mag]	T_{eff} [K]	$\log g$	$\log y$	d [kpc]	Δt [d]	ΔRV_{max} [km s $^{-1}$]	N	$\log p$
J131916.15-011404.9	BHB	16.4	17400 \pm 800	4.55 \pm 0.15	-1.9 \pm 0.2	5.9 $^{+1.4}_{-1.1}$	2888.0925	46.0 \pm 9.0	8	-42.10
J164121.22+363542.7	BHB	17.4	19300 \pm 1000	4.55 \pm 0.10	-1.9 \pm 0.2	9.9 $^{+1.7}_{-1.4}$	1035.9093	99.0 \pm 9.0	8	-39.13
J075732.18+184329.3 ^a	O(He)	18.6	80000 \pm 2000	5.00 \pm 0.30	> +2.0	29.6 $^{+12.7}_{-9.0}$	0.0216	107.0 \pm 22.0	6	-30.13
J155610.40+254640.3 ^b	PG 1159	17.9	100000 $^{+15000}_{-10000}$	5.3 \pm 0.3	> +2.0	16.9 $^{+5.6}_{-5.6}$	231.1694	116.0 \pm 21.0	10	-17.98
J201302.58-105826.1	MS-B	18.5	16400 \pm 1400	4.30 \pm 0.27	-1.3 \pm 0.2	51.8 $^{+23.6}_{-16.4}$	2.0155	61.0 \pm 11.5	8	-13.42
J093521.39+482432.4	O(H)	18.5	87700 \pm 20000	5.68 \pm 0.16	-1.0 \pm 0.3	12.0 $^{+3.7}_{-3.3}$	2269.7542	38.0 \pm 7.5	2	-6.97
J161253.21+060538.7	MS-B	15.5	15700 \pm 1400	4.18 \pm 0.29	-1.0 \pm 0.2	14.4 $^{+7.2}_{-4.8}$	811.5968	38.0 \pm 7.0	10	-6.84
J020531.40+134739.8 ^c	BHB	18.4	17400 \pm 700	4.26 \pm 0.13	-1.7 \pm 0.2	20.3 $^{+4.0}_{-3.4}$	2781.1087	28.0 \pm 7.0	3	-3.64
J144023.58+135454.7	BHB	18.3	18900 \pm 700	4.50 \pm 0.15	-1.9 \pm 0.3	16.1 $^{+3.6}_{-3.0}$	0.0528	78.0 \pm 24.0	4	-3.15
J171947.87+591604.2	MS-B	16.9	15100 \pm 600	4.10 \pm 0.19	-0.9 \pm 0.2	29.2 $^{+8.3}_{-6.5}$	2568.7218	32.0 \pm 6.5	10	-3.11
J100019.98-003413.3	O(H)	17.8	93700 \pm 10700	5.88 \pm 0.10	-0.6 \pm 0.2	7.3 $^{+1.3}_{-1.3}$	3.0114	135.0 \pm 28.0	16	-2.20
J110256.32+010012.3 ^c	BHB	18.5	17300 \pm 800	4.32 \pm 0.14	-2.1 \pm 0.2	19.5 $^{+4.3}_{-3.5}$	2735.5338	24.0 \pm 9.0	3	-1.77
J204149.38+003555.8 ^c	BHB	19.0	19400 \pm 2200	4.02 \pm 0.29	-2.1 \pm 0.4	38.3 $^{+20.3}_{-13.4}$	38.0700	26.0 \pm 10.5	3	-1.71

Notes. ^(a) Atmospheric parameters taken from Werner et al. (2014). ^(b) Atmospheric parameters taken from Reindl et al. (2015). ^(c) Atmospheric parameters derived from a spectrum taken with ESO-VLT/FORS1.

Table A.1. Parameters of 19 stars with non-significant RV variations.

Name	Class	m_V [mag]	T_{eff} [K]	$\log g$	$\log y$	d [kpc]	Δt [d]	ΔRV_{max} [km s $^{-1}$]	N	$\log p$
J085727.65+424215.4 ^a	He-sdO	18.5	39500 \pm 1900	5.63 \pm 0.24	+0.2 \pm 0.2	8.7 $^{+3.0}_{-2.2}$	0.0657	111.0 \pm 39.5	4	-1.26
J074551.13+170600.3	sdOB	17.1	35600 \pm 400	5.54 \pm 0.05	-2.8 \pm 0.1	4.7 $^{+0.3}_{-0.3}$	9.9390	65.0 \pm 12.0	18	-1.26
J110445.01+092530.9 ^a	sdOB	16.3	35900 \pm 800	5.41 \pm 0.07	-2.1 \pm 0.4	3.8 $^{+0.4}_{-0.3}$	0.0396	34.0 \pm 12.0	4	-1.25
J012739.35+404357.8 ^a	sdO	16.8	48300 \pm 3200	5.67 \pm 0.10	-1.3 \pm 0.2	4.1 $^{+0.7}_{-0.6}$	0.0369	45.0 \pm 17.0	8	-1.23
J172816.87+074839.0	sdB	18.4	30700 \pm 700	5.37 \pm 0.09	-2.5 \pm 0.4	9.0 $^{+1.2}_{-1.1}$	1.9962	75.0 \pm 34.0	7	-1.11
J143153.05-002824.3 ^a	sdOB	18.1	37300 \pm 800	6.02 \pm 0.16	-0.8 \pm 0.1	4.4 $^{+0.9}_{-0.8}$	0.0120	64.0 \pm 20.5	8	-1.05
J225150.80-082612.7 ^b	BHB	18.4	19000 \pm 500	4.98 \pm 0.09	-1.8 \pm 0.3	9.5 $^{+1.3}_{-1.1}$	2411.2964	20.0 \pm 7.0	5	-1.04
J074806.15+342927.7	sdOB	17.3	35100 \pm 800	5.72 \pm 0.08	-1.7 \pm 0.1	4.3 $^{+0.5}_{-0.5}$	5.9453	42.0 \pm 12.5	12	-0.95
J111225.70+392332.7	sdOB	17.6	37800 \pm 500	5.76 \pm 0.11	-0.6 \pm 0.1	4.9 $^{+0.7}_{-0.6}$	0.0563	104.0 \pm 28.0	13	-0.92
J134352.14+394008.3 ^a	He-sdOB	18.2	36000 \pm 2100	4.78 \pm 0.30	-0.2 \pm 0.2	18.8 $^{+8.5}_{-6.1}$	0.0224	53.0 \pm 27.0	3	-0.89
J163702.78-011351.7 ^a	He-sdO	17.3	46100 \pm 700	5.92 \pm 0.22	> +2.0	3.8 $^{+1.1}_{-0.9}$	0.0853	100.0 \pm 42.5	12	-0.85
J174442.35+263829.9	sdOB	17.9	-	-	-	-	0.0384	88.0 \pm 44.0	7	-0.84
J180757.08+230133.0	He-sdO	17.1	42700 \pm 1000	6.04 \pm 0.21	> +2.0	2.9 $^{+0.8}_{-0.7}$	0.9992	39.0 \pm 19.0	4	-0.83
J204623.12-065926.8	O(H)	17.7	79500 \pm 12500	5.74 \pm 0.13	-1.1 \pm 0.2	7.6 $^{+1.9}_{-1.6}$	1376.1081	47.0 \pm 18.0	5	-0.64
J075818.49+102742.5	sdOB	16.4	37400 \pm 600	5.51 \pm 0.05	< -3.0	3.6 $^{+0.6}_{-0.2}$	0.0596	32.0 \pm 12.5	6	-0.57
J215053.84+131650.5	sdB+X	17.0	-	-	-	-	0.0154	24.0 \pm 13.5	4	-0.56
J215307.34-071948.3	sdB	17.1	33100 \pm 1300	5.74 \pm 0.15	-2.0 \pm 0.2	3.6 $^{+0.8}_{-0.7}$	24.9831	50.0 \pm 27.5	13	-0.42
J113418.00+015322.1 ^a	sdB	17.7	29700 \pm 1200	4.83 \pm 0.16	< -4.0	11.8 $^{+2.9}_{-2.4}$	0.0757	46.0 \pm 20.0	6	-0.42
J170716.53+275410.4	sdB	16.7	30200 \pm 1400	5.62 \pm 0.16	< -3.0	3.1 $^{+0.8}_{-0.6}$	0.0124	52.0 \pm 23.0	9	-0.21

Notes. ^(a) Atmospheric parameters taken from Geier et al. (2011a). ^(b) Atmospheric parameters derived from a spectrum taken with ESO-VLT/FORS1.